frontiers | Research Topics

Underlying mechanisms and treatment for intervertebral disc disease

Edited by
Baoshan Xu, Shibao Lu, Hong Zhang and Meifeng Zhu

Published in
Frontiers in Endocrinology

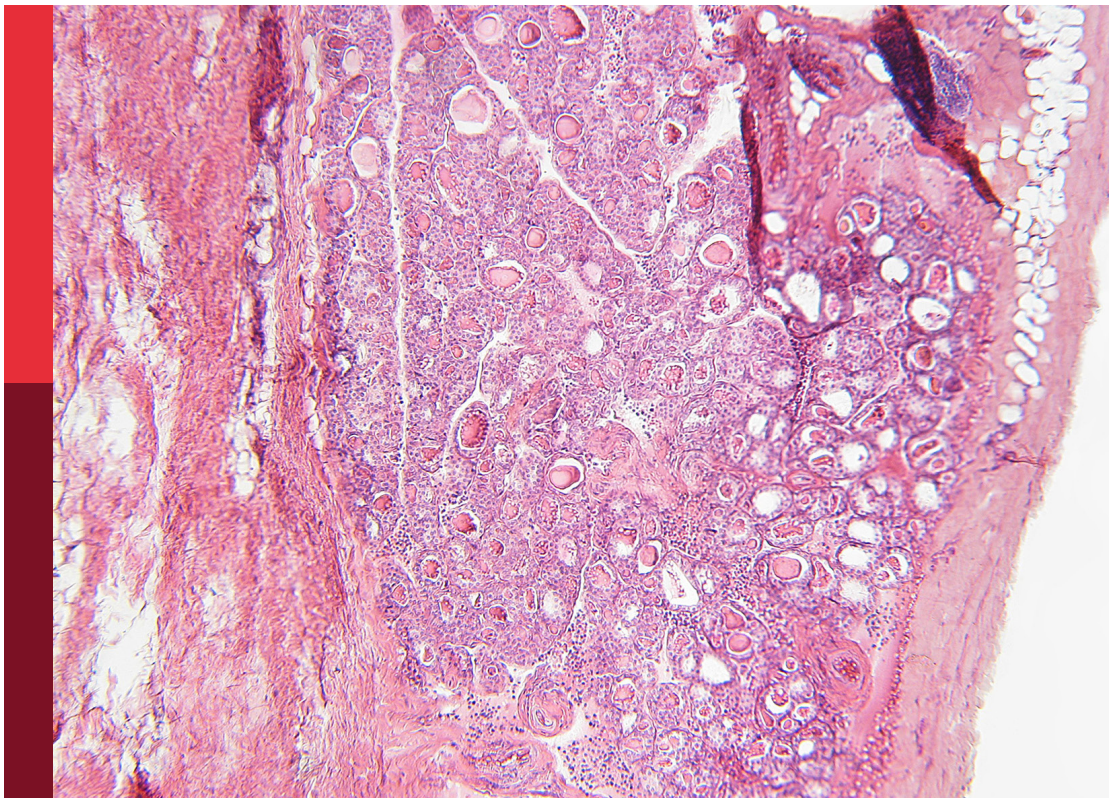

ISSN 1664-8714
ISBN 978-2-8325-3300-0
DOI 10.3389/978-2-8325-3300-0

About Frontiers

Frontiers is more than just an open access publisher of scholarly articles: it is a pioneering approach to the world of academia, radically improving the way scholarly research is managed. The grand vision of Frontiers is a world where all people have an equal opportunity to seek, share and generate knowledge. Frontiers provides immediate and permanent online open access to all its publications, but this alone is not enough to realize our grand goals.

Frontiers journal series

The Frontiers journal series is a multi-tier and interdisciplinary set of open-access, online journals, promising a paradigm shift from the current review, selection and dissemination processes in academic publishing. All Frontiers journals are driven by researchers for researchers; therefore, they constitute a service to the scholarly community. At the same time, the *Frontiers journal series* operates on a revolutionary invention, the tiered publishing system, initially addressing specific communities of scholars, and gradually climbing up to broader public understanding, thus serving the interests of the lay society, too.

Dedication to quality

Each Frontiers article is a landmark of the highest quality, thanks to genuinely collaborative interactions between authors and review editors, who include some of the world's best academicians. Research must be certified by peers before entering a stream of knowledge that may eventually reach the public - and shape society; therefore, Frontiers only applies the most rigorous and unbiased reviews. Frontiers revolutionizes research publishing by freely delivering the most outstanding research, evaluated with no bias from both the academic and social point of view. By applying the most advanced information technologies, Frontiers is catapulting scholarly publishing into a new generation.

What are Frontiers Research Topics?

Frontiers Research Topics are very popular trademarks of the *Frontiers journals series*: they are collections of at least ten articles, all centered on a particular subject. With their unique mix of varied contributions from Original Research to Review Articles, Frontiers Research Topics unify the most influential researchers, the latest key findings and historical advances in a hot research area.

Find out more on how to host your own Frontiers Research Topic or contribute to one as an author by contacting the Frontiers editorial office: frontiersin.org/about/contact

Underlying mechanisms and treatment for intervertebral disc disease

Topic editors

Baoshan Xu — Tianjin Hospital, China

Shibao Lu — Capital Medical University, China

Hong Zhang — SRH Hochschule für Logistik und Wirtschaft, Germany

Meifeng Zhu — Nankai University, China

Citation

Xu, B., Lu, S., Zhang, H., Zhu, M., eds. (2023). *Underlying mechanisms and treatment for intervertebral disc disease*. Lausanne: Frontiers Media SA.

doi: 10.3389/978-2-8325-3300-0

Table of contents

frontiers | Frontiers in Endocrinology

TYPE Original Research
PUBLISHED 21 September 2022
DOI 10.3389/fendo.2022.994307

OPEN ACCESS

EDITED BY
Shibao Lu,
Xuanwu Hospital, Capital Medical University, China

REVIEWED BY
Yukun Zhang,
Huazhong University of Science and Technology, China
Bo Li,
Sun Yat-sen Memorial Hospital, China

*CORRESPONDENCE
Hao Yang
yanghao.71_99@yahoo.com
Ding-Jun Hao
haodingjun@126.com;
haodingjun@mail.xjtu.edu.cn

†These authors have contributed equally to this work

SPECIALTY SECTION
This article was submitted to Bone Research, a section of the journal Frontiers in Endocrinology

RECEIVED 14 July 2022
ACCEPTED 07 September 2022
PUBLISHED 21 September 2022

CITATION
Fan H, Chen Z, Tang H-B, Shan L-Q, Chen Z-Y, Liu S-C, Zhang Y-Y, Guo X-Y, Yang H and Hao D-J (2022) Necroptosis of nucleus pulposus cells involved in intervertebral disc degeneration through MyD88 signaling. *Front. Endocrinol.* 13:994307. doi: 10.3389/fendo.2022.994307

Necroptosis of nucleus pulposus cells involved in intervertebral disc degeneration through MyD88 signaling

Hong Fan[1,2†], Zhe Chen[1†], Hai-Bin Tang[3†], Le-Qun Shan[1], Zi-Yi Chen[4], Shi-Chang Liu[1], Yong-Yuan Zhang[1], Xin-Yu Guo[1], Hao Yang[1*] and Ding-Jun Hao[1*]

[1]Shaanxi Spine Medicine Research Center, Translational Medicine Center, Department of Spine Surgery, Hong Hui Hospital, Xi'an Jiaotong University, Xi'an, China, [2]Department of Neurology, The Second Affiliated Hospital of Xi'an Jiaotong University, Xi'an, China, [3]Department of Laboratory Medicine, Xi'an Central Hospital, Xi'an Jiaotong University, Xi'an, China, [4]Department of Endocrinology, The First Affiliated Hospital of Xi'an Jiaotong University, Xi'an, China

Background context: Low back pain, affecting nearly 40% of adults, mainly results from intervertebral disc degeneration (IVDD), while the pathogenesis of IVDD is still not fully elucidated. Recently, some researches have revealed that necroptosis, a programmed necrosis, participated in the progression of IVDD, nevertheless, the underlying mechanism remains unclear.

Purpose: To study the mechanism of necroptosis of Nucleus Pulposus (NP) cells in IVDD, focusing on the role of MyD88 signaling.

Study design: The expression and co-localization of necroptotic indicators and MyD88 were examined *in vivo*, and MyD88 inhibitor was applied to determine the role of MyD88 signaling in necroptosis of NP cells *in vitro*.

Methods: Human disc specimens were collected from patients receiving diskectomy for lumbar disc herniation (LDH) or traumatic lumbar fractures after MRI scanning. According to the Pfirrmann grades, they were divided into normal (Grades 1, 2) and degenerated groups (4, 5). Tissue slides were prepared for immunofluorescence to assess the co-localization of necroptotic indicators (RIP3, MLKL, p-MLKL) and MyD88 histologically. The combination of TNFα, LPS and Z-VAD-FMK was applied to induce necroptosis of NP cells. Level of ATP, reactive oxygen species (ROS), live-cell staining and electron microscope study were employed to study the role of MyD88 signaling in necroptosis of NP cells.

Results: *In vivo*, the increased expression and co-localization of necroptotic indicators (RIP3, MLKL, p-MLKL) and MyD88 were found in NP cells of degenerated disc, while very l low fluorescence intensity in tissue of traumatic lumbar fractures. *In vitro*, the MyD88 inhibitor effectively rescued the necroptosis of NP cells, accompanied by increased viability, ATP level, and decreased ROS level. The effect of MyD88 inhibition on necroptosis of NP cells

was further confirmed by ultrastructure of mitochondria shown by Transmission Electron Microscope (TEM).

Conclusion: Our results indicated that the involvement of MyD88 signaling in the necroptosis of NP cells in IVDD, which will replenish the pathogenesis of IVDD and provide a novel potential therapeutic target for IVDD.

KEYWORDS

IVDD, necroptosis, nucleus pulposus cells, MyD88 signaling, low back pain

Introduction

Low back pain, affecting nearly 40% of adults in the world, mainly results from intervertebral disc degeneration (IVDD) (1, 2). Although discectomy could relief the pain for patients with surgical indications, there are no strategy could suppress the progression of the degeneration, partially due to un-fully elucidated pathogenesis of IVDD (3–6). Therefore, further clarification of the underlying mechanisms of IVDD is needed for developing novel and specific treatment to inhibit degeneration.

It is widely accepted that the death of nucleus pulposus (NP) cells plays important role in the progress of intervertebral disc degeneration (IVDD) (7, 8). Apoptosis has been considered as the main way of death of NP cells in IVDD, but the results were not very satisfactory from the treatment strategies based on apoptosis inhibition (9, 10), indicating that other types of cell death contribute to the IVDD.

Necroptosis, a form of programmed necrotic cell death, which is regulated by receptor-interacting protein kinase 3 (RIPK3) and mixed lineage kinase domain-like (MLKL), has been demonstrated to participate in the loss of NP cells in IVDD (11–14). It has been reported that compression could induce necroptosis of NP cells through mitochondrial dysfunction and endoplasmic reticulum stress *in vitro* (15–17). In addition, Ding and his colleagues found that RIP3and MLKL markedly increased in severely degenerated disc tissues (14). Nevertheless, less attention has been paid to the mechanism of necroptosis of NP cells in degenerated disc. In our previous study, we have demonstrated that astrocytes underwent necroptosis partially *via* TLR/MyD88 signaling after spinal cord injury (18). MyD88 pathway was indeed participated in the progression of IVDD (19–22), however, whether that it involved in RIP3/MLKL mediated necroptosis of NP cells has never been studied.

To identify the role of MyD88 signaling in necroptosis of NP cells in IVDD, we extracted the degenerated and normal disc from patients by discectomy, and confirmed the necroptosis of NP cells and annulus fibrosus (AF) cells on the degenerated disc. We further demonstrated that inhibition of MyD88 could rescue the necroptosis of NP cells shown by increased viability, ATP level, ultrastructure of mitochondria, as well as the decreased ROS level.

In conclusion, our present study provides novel insights into the mechanism of necroptosis of NP cells in IVDD, which might be a potential target for the further therapy.

Method and materials

Clinical specimens

This study has been approved by the Ethics Committee of HongHui Hospital, Xi'an Jiaotong University. All participants in our study have signed written informed consent before surgery. All patients were evaluated by the magnetic resonance imaging (MRI) scans before surgery according to the Pfirrmann grades, and they were divided into normal (Grades I, II) and degenerated groups (IV, V) (23, 24). A total of 29 human lumber disc tissues (9 normal lumber disc samples were from patients of traumatic lumbar fractures, and the other 20 degenerated samples were from LDH patients) were harvested after discectomy. In the morphological analysis, 6 normal discs were included and 6 degenerated discs were randomly selected from the 17 degenerated samples. For western-blot analysis, another 3 normal discs and 3 degenerated discs were collected.

Immunofluorescence

The discs were fixed by 4% paraformaldehyde (PFA) for 24h at 4°C, followed by dehydration in 25% sucrose solution for 48 h. The tissues were then implanted into optimal cutting temperature compound (Sakura), and serial 12-μm-thick sections were cut on freezing microtome (Leica). All sections were placed on slides and stored at -20°C for immunostaining.

After blocking with 0.01M PBS solution containing 3% BSA and 0.3% Triton X-100 for 30 min, the sections were incubated with primary antibodies in a humid chamber at 4°C overnight.

Anti-RIP3(1:300, Santa Cruz Biotechnology, sc-374639), anti-MLKL(1:200, Milipore, MABC 604), anti- p-MLKL(1:200, Abcam, ab187091), and anti-MyD88(1:400, R&D, MAB2928) antibodies were used in this study. The slides were then washed by 0.01M PBS three times, and incubated with corresponding secondary antibodies. The nuclei were stained with Hoechst 33342. The images were photographed by confocal microscope (LSM 800, Zeiss).

Western-blot analysis

Normal and degenerated discs were obtained to detect the expression of MyD88. Ice-cold radioimmunoprecipitation assay (RIPA, Boster) buffer containing 1% phenylmethylsulfonyl fluoride (PMSF, Boster) were applied to extract total protein. Sodium dodecyl sulfate-polyacrylamide gel (SDS-PAGE,10%) was utilized to separate proteins, which was then transferred to polyvinylidene fluoride (PVDF, Milipore) membrane. The membranes were then incubated with primary antibodies anti-MyD88 (R&D, MAB2928, 1:2000), β-actin (Cell Signaling Technology, 4970, 1:3500) at 4°C for 12h, followed by incubation with correspondence secondary antibodies at room temperature for 1.5h. The bands were visualized and analyzed by Bio-Rad Image Lab System.

Microarray data collection and processing

Microarray data set (GSE70362) was obtained from NCBI Gene Expression Omnibus (GEO), which was used to analyze the correlation between MyD88 and different grade of IVDD. The GSE70362 data set was generated utilizing the GPL17810. The normalization and quality control of GSE70362 was processed with the 'limma' R package (version 3.42.2). The correlation between the expression of MyD88 and different grades of IVDD were performed by spearman method.

Animal samples

All animals utilized in experiments were purchased form the Animal Center of Xi'an Jiaotong University. Animal procedures were approved by Animal Care and Use Committee of Xi'an Jiaotong University.

Isolation, culture and treatment of rat NP cells

Sprague-Dawley rats (about 200g) were applied to obtain NP cells in this study. After removing the lumber spine, lumber discs were cut to get the NP tissues. Then tissues were chopped and digested for 15min in 0.25% type II collagenase (Sigma) at 37°C and gently shaken every 5 minutes during the digestion. After centrifuged at 1000 rpm for 5min, samples were suspended and cultured in DF12 (Gibco) containing 20% FBS (Gibco). Medium was changed every three days. When cells reached a confluence of 80-90%, they were digested and reseeded for further experiments.

According to our previous studies (18, 25), necroptosis of NP cells was induced by TLZ treatment (100 ng/ml of TNFα + 4 μg/ml of LPS + 20 μM of z-VAD) for 48 h. To explore the role of MyD88 in necroptosis, NP cells were treated with 100 μM of MyD88 inhibitory peptide (Novas, NBP2-29328) 8 h before TLZ challenge.

Cell viability assay

NP cells were seeded into a 96-well plate (3×10^3 cells/well) and treated by TLZ or TLZ + MyD88 inhibitor. The cell viability of NP cells were tested by Cell Counting Kit-8 (CCK-8, Sangon Biotech) according to the manual.

ROS level measurement

For testing reactive oxygen species (ROS) levels, 10 μM of DCFH-DA probe (Sigma) was added into NP cells and incubated at 37°C for 30min. The fluorescence intensities were measured by a microplate reader (TECAN, Infinite M200).

ATP examination

Cell Titer-Glo assay Kit (Promega) was used to examine ATP level according to the manual and our previous studies (26).

Propidium iodide staining

After NP cells were treated with TLZ, TLZ + MyD88 inhibitor or MyD88 inhibitor, propidium iodide (PI) (Sigma) and Hoechst 33342 were supplied into the cells and incubated at 37°C for 20min. Then, cells were washed three times by PBS and fixed by 4% PFA for 15min at RT. Cells were photographed by confocal microscope (LSM 800, Zeiss).

Ultrastructure of NP cells detection

The ultrastructure of NP cells was detected by transmission electron microscope. Briefly, NP cells were harvested and fixed in 4% PFA containing 0.05% glutaraldehyde for 20 min, and

50-μm sections were prepared with vibratome (VT 1000S, Leica). After immersed in 0.5% osmium tetroxide, the sections were dehydrated with graded ethanol series, and incubated with propylene oxide and embedded in Epon812. After contrasted in uranyl acetate, the sections were detected by electron microscope (JEM-1230).

Statistical analysis

Quantification was performed by a person who is blind to this study. GraphPad prism 8.0 was used for statistical analysis. For multiple group comparisons, significance was assessed by one-way analysis of variance followed by *post hoc* Tukey's analysis. All data were showed as mean ± standard deviation (SEM). P values of less than 0.05 were regarded as statistically significant.

Results

Detection of necroptosis in human disc tissues

Double-immunostaining of RIP3/MLKL and RIP3/p-MLKL was performed to examine the necroptosis in degenerated and normal disc from patients undergoing discectomy. Our data showed that the expression levels of RIP3 and MLKL were significantly increased in NP cells of the degenerated disc, compared to normal (Figures 1A, B). The increased expression of RIP3 and p-MLKL was also found in NP cells of the degenerated disc (Figures 2A, B). Besides the NP cells, higher levels of RIP3, MLKL and p-MLKL were also detected in the annulus fibrosus (AF) cells in degenerated disc (Figures 1C, D, 2C, D). The above results indicated that necroptosis could be found in both of AF cells and NP cells

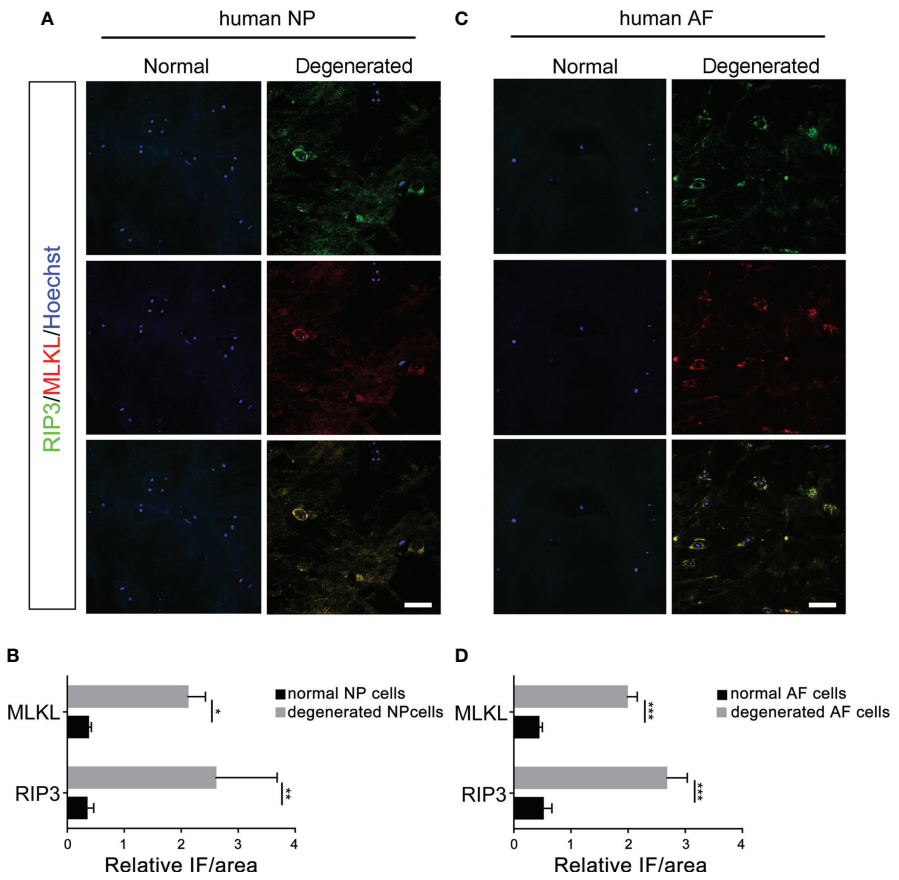

FIGURE 1
Analysis of necroptosis of NP cells and AF cells in the normal and degenerated disc. **(A)** Double-staining of RIP3 with MLKL was performed to detect necroptotic NP cells in normal and degenerated disc. **(B)** Relative IF intensity of MLKL and RIP3 in NP cells. **(C)** Double-staining of RIP3 with MLKL was performed to detect necroptotic AF cells in disc. **(D)** Relative IF intensity of MLKL and RIP3 in AF cells. *P < 0.05, **P < 0.01, ***P < 0.001. N = 6. Bars = 50μm.

10.3389/fendo.2022.994307

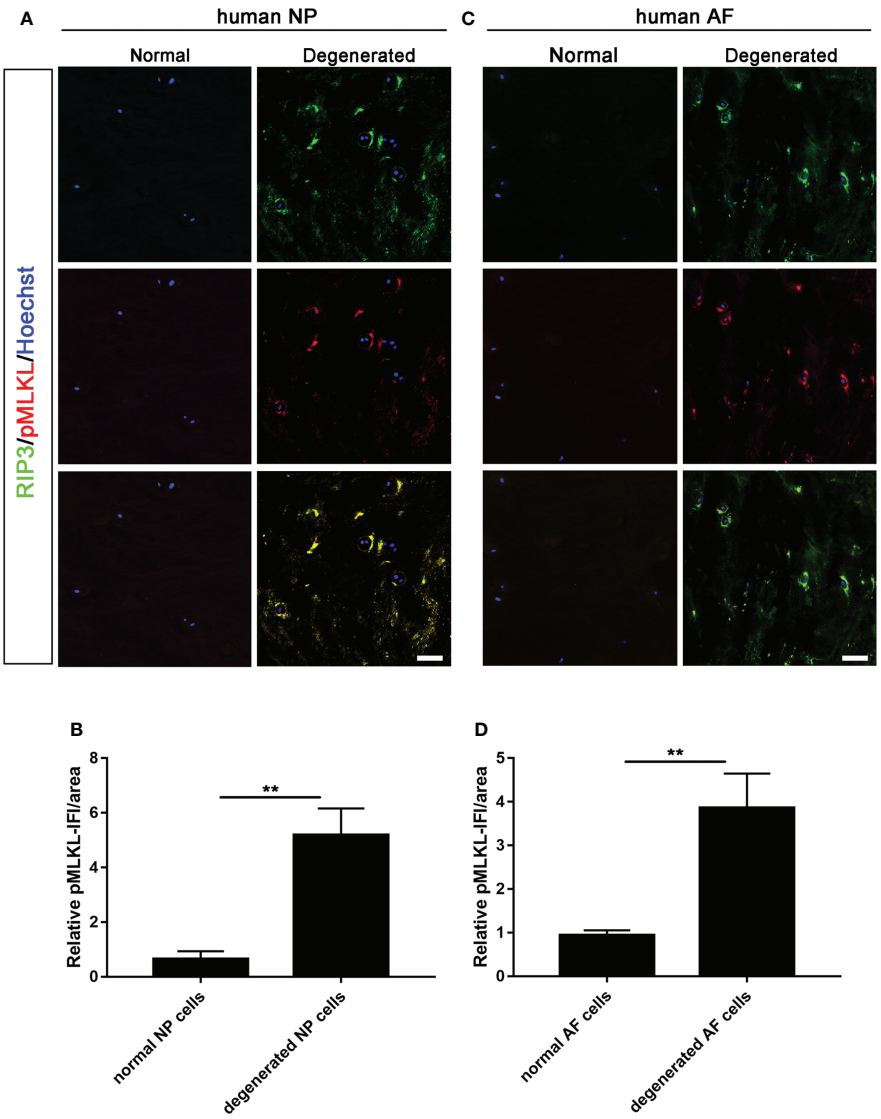

FIGURE 2
Analysis of necroptosis of NP cells and AF cells in the normal and degenerated disc. **(A)** Double-staining of RIP3 with p-MLKL was performed to detect necroptotic NP cells in normal and degenerated disc. **(B)** Relative IF intensity of p-MLKL in NP cells. **(C)** Double-staining of RIP3 with p-MLKL was performed to detect necroptotic AF cells in disc. **(D)** Relative IF intensity of p-MLKL in AF cells. **P < 0.01. N = 6. Bars = 50μm.

in degenerated disc. Considering that the important role of NP cells in progress of IVDD, we focused on the necroptosis of NP cells in the following study.

The role of MyD88 signal in necroptosis of NP cells

We first conducted spearman test to determine the correlation between MyD88 and IVDD grades. Our data showed that MyD88 gene was positively correlated with the progression of IVD (MyD88: p = 0.04837, Figure 3A). Our data of western blot further showed that the expression of MyD88 was significantly increased degenerated discs, compared to normal discs (Figure 3B).

To further study the role of MyD88 in RIP3/MLKL-mediated necroptosis of NP cells, double-immunostaining of RIP3/MyD88 was performed. The co-localization of RIP3 and MyD88and higher expression level of MyD88 were found in NP cells of the degenerated disc (Figures 3C, D), indicating that MyD88 signal might participate in necroptosis of NP cells.

To further define the role of MyD88 signal in necroptosis of NP cells, MyD88 inhibitor was applied. The *in vitro* necroptosis of NP cells was established by TLZ treatment

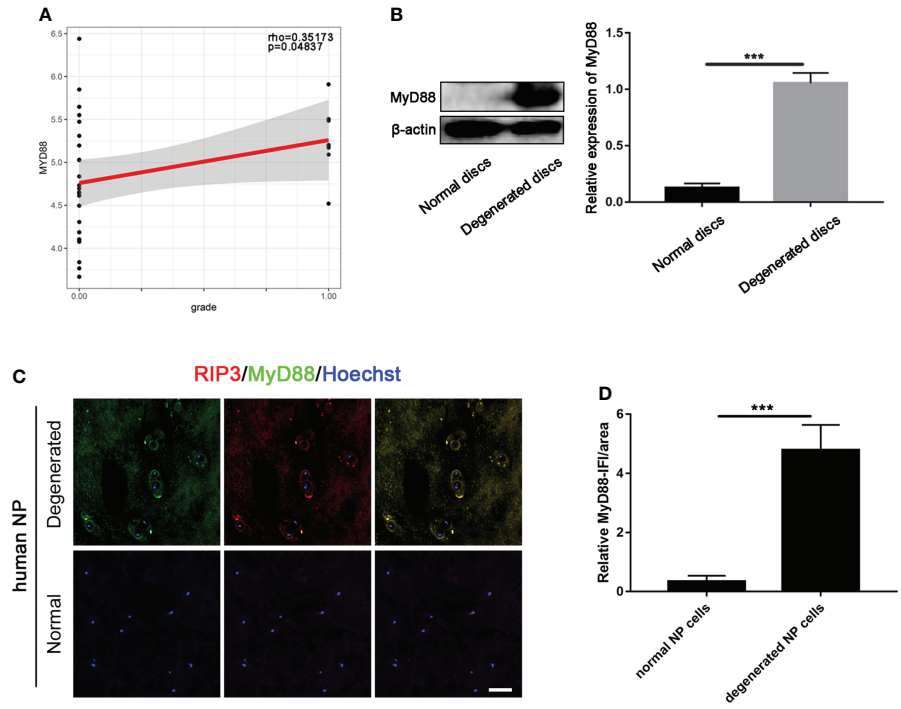

FIGURE 3
Expression of MyD88 in normal and degenerated disc. **(A)** The correlations of the expression of the MyD88 with IVDD grades by linear regression analysis. ("0.00" means early stage-thompson grade III, IV, "1.00" means advanced stage-thompson grade V). **(B)** Detection of MyD88 levels in normal and degenerated disc by western blot. ***P < 0.001. **(C)** Double-staining of RIP3 with MyD88 in NP cells in normal and degenerated disc. **(D)** Relative IF intensity of MyD88 in NP cells. ***P < 0.001. N = 6. Bar = 50μm.

according to our previous study (18, 25). The data of CCK-8 assays showed that inhibiting MyD88 could significantly rescue decreased cell viability, ATP level and increased ROS level in NP cells upon TLZ treatment, while MyD88 inhibitor alone did not influence the viability, ATP level and ROS level of NP cells (Figures 4A–C). Besides these indicators of necroptosis, data of PI staining directly showed that MyD88 inhibitor could decrease TLZ-induced necrosis of NP cells (Figures 4D, E). The above data suggested that MyD88 signaling played a pivotal role in necroptosis of NP cells.

Detection of the change of mitochondrial ultrastructure

Considering that necroptosis was related to mitochondrial dysfunction, mitochondrial ultrastructure was detected by transmission electron microscope (TEM). The data showed that MyD88 inhibitor could significantly decrease the TLZ-induced mitochondria destruction, indicating that MyD88 inhibitor suppressed the necroptosis of NP cells partially *via* protecting mitochondria (Figures 5A–D).

Discussion

Necroptosis has been demonstrated to play pivotal roles in diverse conditions, including traumatic and degenerative diseases (12, 18, 25). Recently, although necroptosis of NP cells has been reported *in vitro* (15, 17), there still lacks of evidence that necroptosis of NP cells could occur in degenerated disc. In the present study, we confirmed the necroptosis of NP cells in degenerated human disc and demonstrated that necroptosis of NP cells involved in IVDD through MyD88 signaling. Our study referring to NP cells necroptosis may provide a promising target for IVDD therapy.

Although ferroptosis and apoptosis of AF cells had been investigated in IVDD (27–29), there is no reported study on necroptosis of AF cells in IVDD. In this study, increased expression levels of RIP3, MLKL and p-MLKL were also been found in AF cells, which indicated that AF cells also underwent necroptosis in degenerated disc. Considering that the loss of AF cells contributed to the degeneration of AF tissue, we speculate that necroptosis of AF cells might also participate in IVDD. The mechanism of AF cells necroptosis and its

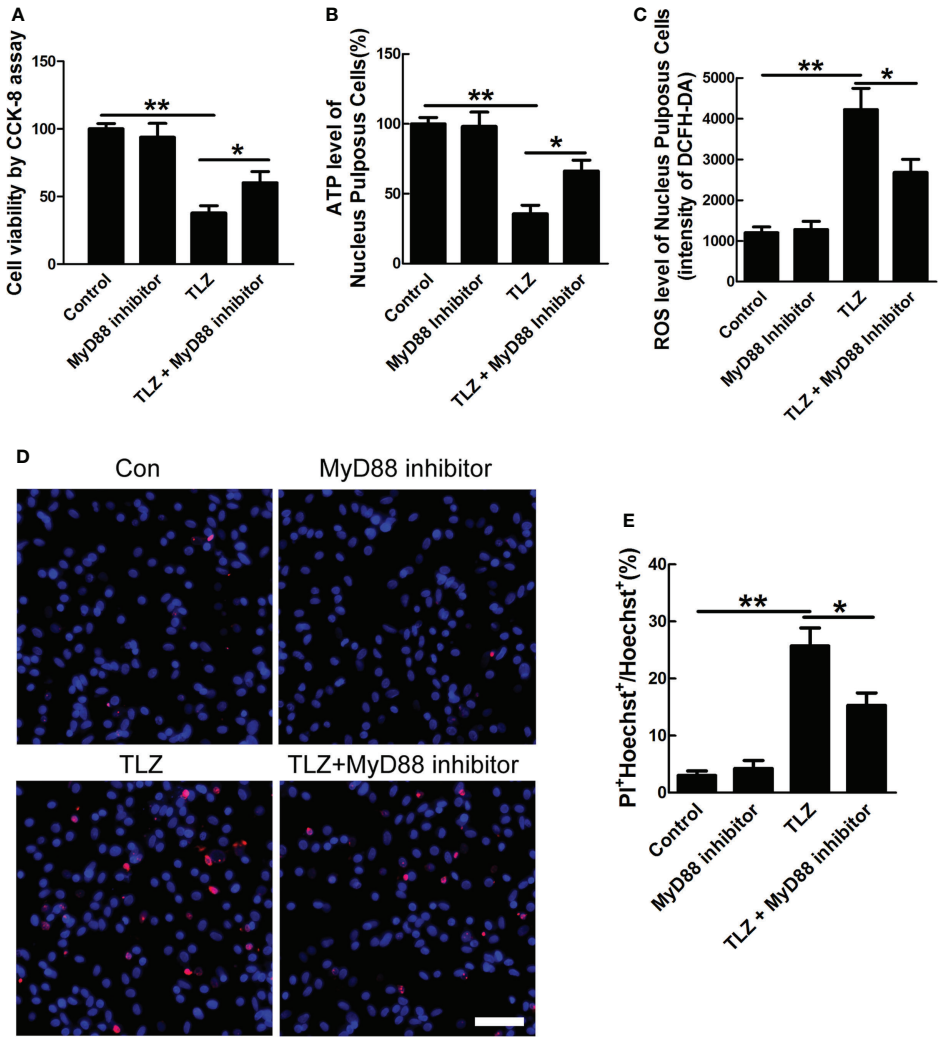

FIGURE 4
Effects of MyD88 signaling on necroptotic NP cells. **(A)** NP cells viability under TLZ with MyD88 inhibitor condition. **(B)** ATP level of necroptotic NP cells with blocking MyD88 signaling. **(C)** ROS level of NP cells with different conditions. **(D)** PI-positive cells under TLZ condition with or without MyD88 inhibitor. **(E)** Relative percentage of PI+ NP cells. *P < 0.05, **P < 0.01. N= 3 independent replicates. Bar = 50μm.

interaction with the death of NP cells in IVDD is worth to be explored in future.

Multiple Toll-like receptors(TLRs) are activated upon inflammatory stimulus. Each TLR selectively recruits specific adaptor proteins, and MyD88 is a common adapter shared by all known TLRs (30). Considering that Toll-like receptors activate necroptosis through RIP3 pathway (31), we then focused on the role of MyD88 in necroptosis of NP cells. MyD88 signaling has been demonstrated to contribute to necroptosis in spinal cord injury, colitis and acute pancreatitis (18, 32, 33). In the present study, we demonstrated that MyD88 signaling also participate in necroptosis of NP cells, shown by the changed levels of ROS, ATP and mitochondrial structure. One of the limitations of this study is that rat NP cells was applied to investigate the role of MyD88 signaling in necroptosis, human NP cells will be utilized to clarify the role of MyD88 signaling in necroptosis of NP cells.

Although the role of MyD88 signaling in necroptosis of NP cells has been explored in the present study, the mechanism of necroptosis of NP cells in IVDD was still not fully clarified. Previously, we demonstrated that necroptotic astrocytes could release high mobility group box 1(HMGB1), which driven downstream inflammation in spinal cord injury (34). It was reported that HMGB1 was crucial in the progression of IVDD (19, 35–38). Therefore, we speculated that HMGB1 might be released from necroptotic NP cells and might be a participant in the progression of IVDD. The further clarification of

10.3389/fendo.2022.994307

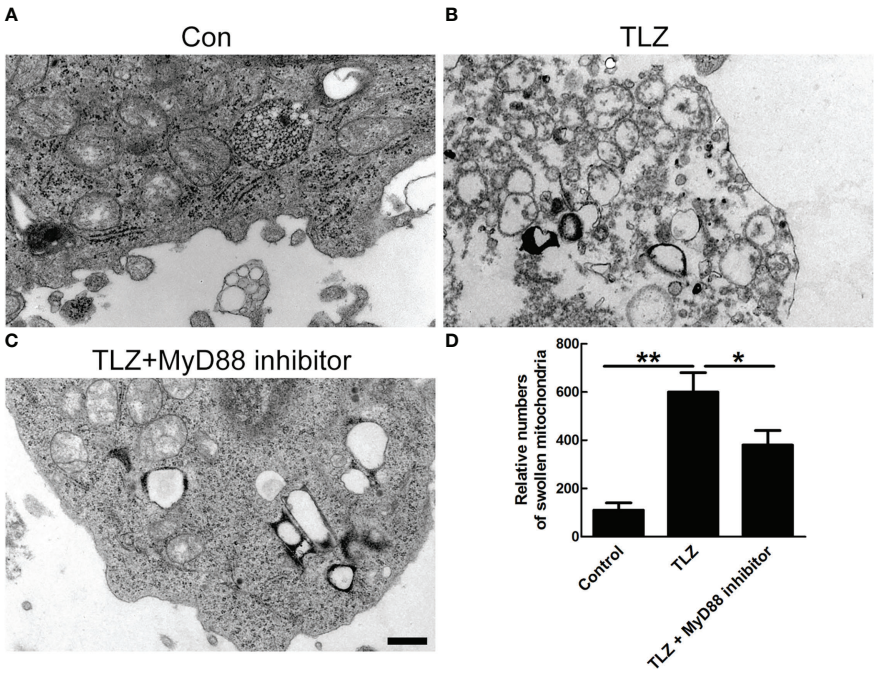

FIGURE 5
TEM photographs of ultrastructure of NP cells showing mitochondria. **(A)** Normal NP cells. **(B, C)** Normal NP cells under TLZ condition with or without MyD88 inhibitor. **(D)** Relative numbers of swollen mitochondria. *P < 0.05, **P < 0.01. N= 3 independent replicates. Bar = 1μm.

the how necroptotic NP cells participate in IVDD needs to be explored in future.

Conclusion

Necroptosis of Nucleus Pulposus Cells involved in intervertebral disc degeneration through MyD88 signaling.

Data availability statement

The raw data supporting the conclusions of this article will be made available by the authors, without undue reservation.

Ethics statement

The studies involving human participants were reviewed and approved by Ethics Committee of HongHui Hospital, Xi'an Jiaotong University. Written informed consent to participate in this study was provided by the participants' legal guardian/ next of kin. The animal study was reviewed and approved by Animal Care and Use Committee of Xi'an Jiaotong University.

Author contributions

HF, HY, and D-JH conceived and designed the study. HF and D-JH screened participants for study entry. HF, ZC, H-BT and Z-YC processed the data. HF, ZC, L-QS, S-CL, Y-YZ, and X-YG collected samples and data. HF, ZC, H-BT and Z-YC performed experiments and analysis. HF, ZC, HY, and D-JH prepared the manuscript. All authors contributed to the article and approved the submitted version.

Funding

This work was supported by grants from the National Natural Science Foundation of China (NSFC, Grant code: 81830077) to D-JH, NSFC (Grant code: 82171471) to HF, NSFC (Grant code: 82101551) to H-BT, NFSC (Grant code: 82071551) to HY, Shaanxi Natural Science Basic Research Program (2021JZ-39) and ShaanXi Nova Program (2022KJXX-54) to HF, Shaanxi Natural Science Basic Research Program (2021JQ-932) to H-BT, and China Postdoctoral Science Foundation (Grant code: 2018M643703, 2020T130526) to HF.

Acknowledgments

We thank the support from Translational Medicine Center and Department of Spine Surgery of Hong Hui Hospital, and Department of Neurology, The Second Affiliated Hospital, Xi'an Jiaotong University.

Conflict of interest

The authors declare that the research was conducted in the absence of any commercial or financial relationships that could be construed as a potential conflict of interest.

Publisher's note

Supplementary material

The Supplementary Material for this article can be found online at: https://www.frontiersin.org/articles/10.3389/fendo.2022.994307/full#supplementary-material

References

1. Colella F, Garcia JP, Sorbona M, Lolli A, Antunes B, D'atri D, et al. Drug delivery in intervertebral disc degeneration and osteoarthritis: Selecting the optimal platform for the delivery of disease-modifying agents. *J Control Release* (2020) 328:985–99. doi: 10.1016/j.jconrel.2020.08.041

2. Yang S, Zhang F, Ma J, Ding W. Intervertebral disc ageing and degeneration: The antiapoptotic effect of oestrogen. *Ageing Res Rev* (2020) 57:100978. doi: 10.1016/j.arr.2019.100978

3. Liu C, Liu L, Yang M, Li B, Yi J, Ai X, et al. A positive feedback loop between EZH2 and NOX4 regulates nucleus pulposus cell senescence in age-related intervertebral disc degeneratio. *Cell Div* (2020) 15:2. doi: 10.1186/s13008-020-0060-x

4. Wang F, Cai F, Shi R, Wang XH, Wu XT. Aging and age related stresses: a senescence mechanism of intervertebral disc degeneration. *Osteoarthritis Cartilage* (2016) 24:398–408. doi: 10.1016/j.joca.2015.09.019

5. Ravichandran D, Pillai J, Krishnamurthy K. Genetics of intervertebral disc disease: A review. *Clin Anat* (2022) 35:116–20. doi: 10.1002/ca.23803

6. Sampara P, Banala RR, Vemuri SK, Av GR, Gpv S. Understanding the molecular biology of intervertebral disc degeneration and potential gene therapy strategies for regeneration: a review. *Gene Ther* (2018) 25:67–82. doi: 10.1038/s41434-018-0004-0

7. Li S, Hua W, Wang K, Gao Y, Chen S, Liu W, et al. Autophagy attenuates compression-induced apoptosis of human nucleus pulposus cells *via* MEK/ERK/NRF1/Atg7 signaling pathways during intervertebral disc degeneration. *Exp Cell Res* (2018) 370:87–97. doi: 10.1016/j.yexcr.2018.06.012

8. Yu H, Hou G, Cao J, Yin Y, Zhao Y, Cheng L. Mangiferin alleviates mitochondrial ROS in nucleus pulposus cells and protects against intervertebral disc degeneration *via* suppression of NF-kappaB signaling pathway. *Oxid Med Cell Longev* (2021) 2021:663278. doi: 10.1155/2021/6632786

9. Xie L, Huang W, Fang Z, Ding F, Zou F, Ma X, et al. CircERCC2 ameliorated intervertebral disc degeneration by regulating mitophagy and apoptosis through miR-182-5p/SIRT1 axis. *Cell Death Dis* (2019) 10:751. doi: 10.1038/s41419-019-1978-2

10. Yu ZH, Ji YC, Li K, Liang T, Liu B, Chen HL, et al. Stiffness of the extracellular matrix affects apoptosis of nucleus pulposus cells by regulating the cytoskeleton and activating the TRPV2 channel protein. *Cell Signal* (2021) 84:110005. doi: 10.1016/j.cellsig.2021.110005

11. Galluzzi L, Kroemer G. Necroptosis: A specialized pathway of programmed necrosis. *Cell* (2008) 135:1161–3. doi: 10.1016/j.cell.2008.12.004

12. Newton K, Manning G. Necroptosis and inflammation. *Annu Rev Biochem* (2016) 85:743–63. doi: 10.1146/annurev-biochem-060815-014830

13. Galluzzi L, Kepp O, Chan FK, Kroemer G. Necroptosis: Mechanisms and relevance to disease. *Annu Rev Pathol* (2017) 12:103–30. doi: 10.1146/annurev-pathol-052016-100247

14. Zhang QX, Guo D, Wang FC, Ding WY. Necrosulfonamide (NSA) protects intervertebral disc degeneration *via* necroptosis and apoptosis inhibition. *Eur Rev Med Pharmacol Sci* (2020) 24:. 2683–2691. doi: 10.26355/eurrev_202003_20538

15. Chen S, Lv X, Hu B, Shao Z, Wang B, Ma K, et al. RIPK1/RIPK3/MLKL-mediated necroptosis contributes to compression-induced rat nucleus pulposus cells death. *Apoptosis* (2017) 22:626–38. doi: 10.1007/s10495-017-1358-2

16. Chen S, Lv X, Hu B, Zhao L, Li S, Li Z, et al. Critical contribution of RIPK1 mediated mitochondrial dysfunction and oxidative stress to compression-induced rat nucleus pulposus cells necroptosis and apoptosis. *Apoptosis* (2018) 23:299–313. doi: 10.1007/s10495-018-1455-x

17. Wang W, Qing X, Wang B, Ma K, Wei Y, Shao Z. Tauroursodeoxycholic acid protects nucleus pulposus cells from compression-induced apoptosis and necroptosis *via* inhibiting endoplasmic reticulum stress. *Evid Based Complement Alternat Med* (2018) 2018:6719460. doi: 10.1155/2018/6719460

18. Fan H, Zhang K, Shan L, Kuang F, Chen K, Zhu K, et al. Reactive astrocytes undergo M1 microglia/macrohpages-induced necroptosis in spinal cord injury. *Mol Neurodegener* (2016) 11:14. doi: 10.1186/s13024-016-0081-8

19. Zhao F, Guo Z, Hou F, Fan W, Wu B, Qian Z. Magnoflorine alleviates "M1" polarized macrophage-induced intervertebral disc degeneration through repressing the HMGB1/Myd88/NF-kappaB pathway and NLRP3 inflammasome. *Front Pharmacol* (2021) 12701087:701087. doi: 10.3389/fphar.2021.701087

20. Qin C, Zhang B, Zhang L, Zhang Z, Wang L, Tang L, et al. MyD88-dependent toll-like receptor 4 signal pathway in intervertebral disc degeneration. *Exp Ther Med* (2016) 12:611–8. doi: 10.3892/etm.2016.3425

21. Zhang L, Chen Q, Wang H, Yang J, Sheng S. Andrographolide mitigates IL1betainduced human nucleus pulposus cells degeneration through the TLR4/MyD88/NFkappaB signaling pathway. *Mol Med Rep* (2018) 18:5427–36. doi: 10.3892/mmr.2018.9599

22. Qin C, Lv Y, Zhao H, Yang B, Zhang P. MicroRNA-149 suppresses inflammation in nucleus pulposus cells of intervertebral discs by regulating MyD88. *Med Sci Moni* (2019) 25:4892–900. doi: 10.12659/MSM.915858

23. Pfirrmann CW, Metzdorf A, Zanetti M, Hodler J, Boos N. Magnetic resonance classification of lumbar intervertebral disc degeneration. *Spine (Phila Pa 1976)* (2001) 26:1873–8. doi: 10.1097/00007632-200109010-00011

24. Griffith JF, Wang YX, Antonio GE, Choi KC, Yu A, Ahuja AT, et al. Modified pfirrmann grading system for lumbar intervertebral disc degeneration. *Spine (Phila Pa 1976* (2007) 32:E708–12. doi: 10.1097/BRS.0b013e31815a59a0

25. Chen Z, Tang HB, Kang JJ, Chen ZY, Li YL, Fan, Q. Y, et al. Necroptotic astrocytes induced neuronal apoptosis partially through EVs-derived pro-BDNF. *Brain Res Bull* (2021) 177:73–80. doi: 10.1016/j.brainresbull.2021.09.014

26. Fan H, Tang HB, Shan LQ, Liu SC, Huang DG, Chen X, et al. Quercetin prevents necroptosis of oligodendrocytes by inhibiting macrophages/microglia polarization to M1 phenotype after spinal cord injury in rats. *J Neuroinflamm* (2019) 16:. 206. doi: 10.1186/s12974-019-1613-2

27. Yang RZ, Xu WN, Zheng HL, Zheng XF, Li B, Jiang LS, et al. Involvement of oxidative stress-induced annulus fibrosus cell and nucleus pulposus cell ferroptosis in intervertebral disc degeneration pathogenesis. *J Cell Physiol* (2021) 236:2725–39. doi: 10.1002/jcp.30039

28. Jing D, Wu W, Deng X, Peng Y, Yang W, Huang D, et al. FoxO1a mediated cadmium-induced annulus fibrosus cells apoptosis contributes to intervertebral disc degeneration in smoking". *J Cell Physiol* (2021) 236:677–87. doi: 10.1002/jcp.29895

29. Xu WN, Yang RZ, Zheng HL, Yu W, Zheng XF, Li B, et al. PGC-1alpha acts as an mediator of Sirtuin2 to protect annulus fibrosus from apoptosis induced by oxidative stress through restraining mitophagy. *Int J Biol Macromol* (2019) 136:1007–17. doi: 10.1016/j.ijbiomac.2019.06.163

30. Deguine J, Barton GM. MyD88: a central player in innate immune signaling. *F1000Prime Rep* (2014) 6:97. doi: 10.12703/P6-97

31. He S, Liang Y, Shao F, Wang X. Toll-like receptors activate programmed necrosis in macrophages through a receptor-interacting kinase-3-mediated pathway. *Proc Natl Acad Sci USA* (2011) 108:20054–9. doi: 10.1073/pnas.1116302108

32. Hong YP, Yu J, Su YR, Mei FC, Li M, Zhao KL, et al. High-fat diet aggravates acute pancreatitis *via* TLR4-mediated necroptosis and inflammation in rats. *Oxid Med Cell Longev* (2020) 2020:8172714. doi: 10.1155/2020/8172714

33. Duan C, Xu X, Lu X, Wang L, Lu Z. RIP3 knockdown inhibits necroptosis of human intestinal epithelial cells *via* TLR4/MyD88/NF-kappaB signaling and ameliorates murine colitis. *BMC Gastroenterol* (2022) 22:137. doi: 10.1186/s12876-022-02208-x

34. Fan H, Tang HB, Chen Z, Wang HQ, Zhang L, Jiang Y, et al. Inhibiting HMGB1-RAGE axis prevents pro-inflammatory macrophages/microglia polarization and affords neuroprotection after spinal cord injury. *J Neuroinflamm* (2020) 17:295. doi: 10.1186/s12974-020-01973-4

35. Han Y, Yuan F, Deng C, He F, Zhang Y, Shen H, et al. Metformin decreases LPS-induced inflammatory response in rabbit annulus fibrosus stem/progenitor cells by blocking HMGB1 release. *Aging (Albany NY)* (2019) 11:10252–65. doi: 10.18632/aging.102453

36. Tang N, Dong Y, Xiao T, Zhao H. LncRNA TUG1 promotes the intervertebral disc degeneration and nucleus pulposus cell apoptosis though modulating miR-26a/HMGB1 axis and regulating NF-kappaB activation. *Am J Transl Res* (2020) 12:5449–64.

37. Fu B, Lu X, Zhao EY, Wang JX, Peng SM. HMGB1-induced autophagy promotes extracellular matrix degradation leading to intervertebral disc degeneration. *Int J Clin Exp Pathol* (2020) 13:2240–8.

38. Liu X, Zhuang J, Wang D, Lv L, Zhu F, Yao A, et al. Glycyrrhizin suppresses inflammation and cell apoptosis by inhibition of HMGB1 *via* p38/p-JUK signaling pathway in attenuating intervertebral disc degeneration. *Am J Transl Res* (2019) 11:5105–13.

frontiers | Frontiers in Endocrinology

TYPE Original Research
PUBLISHED 30 September 2022
DOI 10.3389/fendo.2022.1031616

OPEN ACCESS

EDITED BY
Baoshan Xu,
Tianjin Hospital, China

REVIEWED BY
Xiaozhong Zhou,
Second Affiliated Hospital of Soochow University, China
Xueyu Hu,
Fourth Military Medical University, China

*CORRESPONDENCE
Yinlian Pan
panyinlian@126.com
Xing Du
duxing92@yeah.net

†These authors have contributed equally to this work

SPECIALTY SECTION
This article was submitted to Bone Research, a section of the journal Frontiers in Endocrinology

RECEIVED 30 August 2022
ACCEPTED 16 September 2022
PUBLISHED 30 September 2022

CITATION
Chen X, Li X, Gan Y, Lu Y, Tian Y, Fu Y, Yang H, Liu K, Pan Y and Du X (2022) Is depression the contraindication of anterior cervical decompression and fusion for cervical spondylosis? *Front. Endocrinol.* 13:1031616. doi: 10.3389/fendo.2022.1031616

Is depression the contraindication of anterior cervical decompression and fusion for cervical spondylosis?

Xiaolu Chen[1†], Xiao Li[2†], Yu Gan[3], Ying Lu[4], Yu Tian[4], Yixiao Fu[2], Hanjie Yang[5], Ke Liu[6], Yinlian Pan[7*] and Xing Du[8*]

[1]Department of Psychiatry, The First Branch, The First Affiliated Hospital of Chongqing Medical University, Chongqing, China, [2]Department of Psychiatry, The First Affiliated Hospital of Chongqing Medical University, Chongqing, China, [3]Department of Psychiatry, Chongqing Eleventh People's Hospital, Chongqing, China, [4]Department of the First Clinical Medicine, Chongqing Medical University, Chongqing, China, [5]Department of Neurology, The Thirteenth People's Hospital of Chongqing, Chongqing, China, [6]Department of Emergency, The Second Affiliated Hospital of Chongqing Medical University, Chongqing, China, [7]Department of Medical Oncology, The First Affiliated Hospital of Hainan Medical University, Haikou, China, [8]Department of Orthopedics, The First Affiliated Hospital of Chongqing Medical University, Chongqing, China

Objective: To evaluate whether depression is the contraindication of anterior cervical decompression and fusion (ACDF) for cervical spondylosis.

Material and methods: Patients with single-segment cervical spondylosis who underwent ACDF from January 2015 to December 2018 in our department were retrospectively included in this study and divided into two groups. Patients who were diagnosed of depression and prescribed with antidepressant drugs for at least 6 months before surgery were included in the intervention group. Patients without depression were included in the control group. The Beck Depression Inventory (BDI) score was used to evaluate the severity of depression. Visual Analogue Scale (VAS) score, Japanese Orthopeadic Association (JOA) score, Neck Disability Index (NDI), and the 36-Item Short-Form Health Survey (SF-36) were recorded as indexes to assess the pain, cervical spine function, degree of cervical spine injury, and life quality, respectively. The operative time, operative blood loss, hospital stay and complications were also recorded and compared.

Results: A total of 117 patients were included in this study, involving 32 patients in the intervention group and 85 patients in the control group. No significant differences were found in operative time, operative blood loss, hospital stay and complications between the two groups (P>0.05). The BDI score, VAS score, JOA score, NDI, SF-36 physical component score (SF-36 PCS) and SF-36 mental component score (SF-36 MCS) were all significantly improved at last follow-up in both the two groups. The intervention group showed higher BDI score and SF-36 MCS than the control group at both preoperative and the last follow-up (P<0.05), and the improvements of BDI score and SF-36 MCS were also higher in the intervention group (P<0.05). Although the intervention group showed higher VAS score, NDI, SF-36 PCS and lower JOA score at preoperative

and last follow-up, respectively (P<0.05), there were no significant differences in the improvements of these indexes between the two group (P>0.05).

Conclusions: Depression is not the contraindication of ACDF for cervical spondylosis. Depression patients who received preoperative antidepressants can achieve similar improvement of clinical symptoms from ACDF with non-depression patients.

KEYWORDS

depression, anterior cervical decompression and fusion, cervical spondylosis, clinical efficacy, safety

Introduction

Anterior cervical decompression and fusion (ACDF) is a common surgical method and has been regarded as the the gold standard treatment for cervical spondylosis (1). However, in recent years, clinical reports showed that the improvements of pain and life quality were not as satisfactory as preoperative expected in some cervical spondylosis patients undergoing ACDF (2, 3). These variable surgical outcomes prompted us to seek for the preoperative factors that may affect the clinical efficacy of ACDF.

Cervical spondylosis patients are often complicated with psychological disorders (4, 5). It is reported that more than 30% of cervical spondylosis patients suffer from depression or anxiety (6). Prior studies have identified that preoperative psychological disorders, such as anxiety and depression, are negatively correlated with the improvement of functional outcomes and life quality in cervical spondylosis patients undergoing cervical spine surgery (7, 8). It was reported that in the US patients undergoing ACDF, pre-surgical clinical depression predicts post-surgical acute or chronic pain, a slightly prolonged length of hospital stay and the presence of any complication (9). Harris et al. found that patients with preoperative diagnoses of depression or anxiety had a greater likelihood of adverse outcomes, increased opioid consumption, and increased cumulative health care payments after ACDF compared with patients without depression or anxiety (10). Since depression had a negative impact on the efficacy of ACDF surgery, antidepressant treatment may improve the efficacy of ACDF for depression patients.

However, little data so far had assessed the efficacy and safety of antidepressant medications in ACDF. Elsamadicy et al. found that preoperative antidepressant treatment could significantly improve postoperative pain and dysfunction in patients with depression after cervical surgery (11). However, Sayadipour et al. concluded that preoperative antidepressants treatment increased the total cost of medical treatment and prolonged the hospital stay in patients with depression undergoing elective lumbar surgery (12). Moreover, it was reported that the use of antidepressants may lead to an increased risk of abnormal bleeding in orthopedic surgery (13). Therefore, the safety and efficacy of antidepressant therapy before ACDF in patients with depression are remain controversial.

Therefore, we conducted this retrospective study to compare the pain relief and functional outcomes improvement of ACDF between the normal patients and depression patients to evaluate whether depression is the contraindication of ACDF. The main hypothesis was that, depression is not the contraindication of ACDF for cervical spondylosis, and depression patients who received preoperative standard antidepressants can achieve similar improvement of clinical symptoms from ACDF with non-depression patients.

Materials and methods

This study was approved by the Ethics Committee of The First Affiliated hospital of Chongqing Medical University (No: 2017-98). All of the participants provided their written informed consent to participate in this study before their data were stored in the hospital database and used for research purposes. This work was reported in line with the STROCSS criteria (14).

Patients selection

From January 2015 to December 2018, patients who underwent ACDF for cervical spondylosis were retrospectively included in our study.

Inclusion criteria: (1) patients with symptoms and signs of cervical spondylotic radiculopathy (unilateral/bilateral upper limb pain, numbness or weakness, negative pathological signs); (2) preoperative MRI of the cervical spine revealed compression of a single segment of the nerve root; (3) patients with

progressive neurological deficit; (4) patients undergoing conservative therapy for at least 3 months without improvement; (5) patients without depression (control group) or was diagnosed as depression by a psychiatrist and took antidepressants for at least 6 months before surgery (intervention group).

Exclusion criteria: (1) patients who took drugs that may affect the antidepressant medications efficacy assessment within 1 month before surgery (e.g., calcium channel blockers, corticosteroids, methotrexate, a vitamin K antagonist, or an antiplatelet medication; (2) patients with a previous history of spine surgery; (3) patients with recurrent cervical spondylosis or re-hospitalization due to a revision cervical surgery.

Preoperative management

All patients received X-ray in cervical flexion and extension position, CT and MRI. Surgery was conducted after the patients' basic diseases such as diabetes, coronary heart disease and hypertension, were controlled and stabilized.

Surgical method

All patients underwent ACDF *via* the anterior Smith–Robinson approach. The procedures were similar with previous article (15). Two types of cages were used: PEEK cage (Medtronic, USA) and nHA-PA66 cages (Guona, China).

Postoperative management

Prophylactic use of antibiotics for the first 3 days after surgery. Incision drainage was removed when drainage volume was less than 10 ml/d, and then an X-ray examination was checked. A neck collar fixation was applied for postoperative 3 months. X-ray and MRI (if necessary) were followed up to 1, 3, 6, 12, 24 months postoperatively.

Assessment measures

Patients basic demographics: age, gender, duration of symptoms, body mass index (BMI), employment status, smoking history, radiculopathy laterality, and disease level.

Clinical outcomes: (1) Surgery-related outcomes: operative time, operative blood loss, hospital stay and complications. (2) Pain: visual analogue scale (VAS) score. (3) Depression: the Beck Depression Inventory (BDI) score. (4) Cervical spine function: Japanese Orthopeadic Association (JOA) score and neck disability index (NDI). (5) Life quality: the 36-Item Short-Form Health Survey (SF-36).

Statistical analysis

Matched *t* test was used to compare VAS score, BDI score and SF-36 score between preoperative and postoperative period. Independent samples *t* test and Chi-square test were used for the comparison of quantitative data (e.g. operative time, operative blood loss) and disordered qualitative data (e.g. postoperative complications) between the intervention group and the control group, respectively. SPSS 17.0.1 (Chicago, USA) was used for statistical analysis. $P<0.05$ was considered to be the significant difference.

Results

A total of 117 patients were included in this study, involving 32 patients in the intervention group and 85 patients in the control group (Figure 1). No significant differences were found in age (P=0.373), gender (P=0.061), duration of symptoms (P=0.243), BMI (P=0.317), employment status (P=0.385), smoking history (P=0.342), radiculopathy laterality (P=0.542), disease level (P=0.507), and follow-up time (P=0.373) between the two groups. (Table 1)

In both the two groups, the BDI score, VAS, JOA score, NDI, SF-36 physical component score (SF-36 PCS) and SF-36 mental component score (SF-36 MCS) were all significantly improved at last follow-up compared with preoperative (all $P<0.05$). The intervention group showed higher BDI score (both $P<0.001$) and higher SF-36 MCS (P=0.002 and $P<0.001$, respectively) than the control group at both preoperative and the last follow-up, and the changes of BDI score (P=0.014) and SF-36 MCS (P=0.031) were also higher in the intervention group. Although the intervention group showed higher VAS (P=0.020 and P=0.011, respectively), lower JOA score (P=0.014 and $P<0.001$, respectively), higher NDI (both $P<0.001$), and higher SF-36 PCS (P=0.002 and $P<0.001$, respectively) at preoperative and last follow-up, there were no significant differences in the changes of these indexes between the two group (P=0.087, 0.067, 0.060, and 0.067, respectively). (Table 2)

No significant differences were found in operative time (P=0.074), operative blood loss (P=0.060), hospital stay (P=0.083) and complications (P=0.542) between the two groups. (Table 3)

Discussion

In this study, the preoperative BDI score of the intervention group was higher than that in the control group, suggesting that although depression patients received standard antidepressant therapy before surgery, taking anti-depression drugs could not control the symptoms of depression to the same level as normal

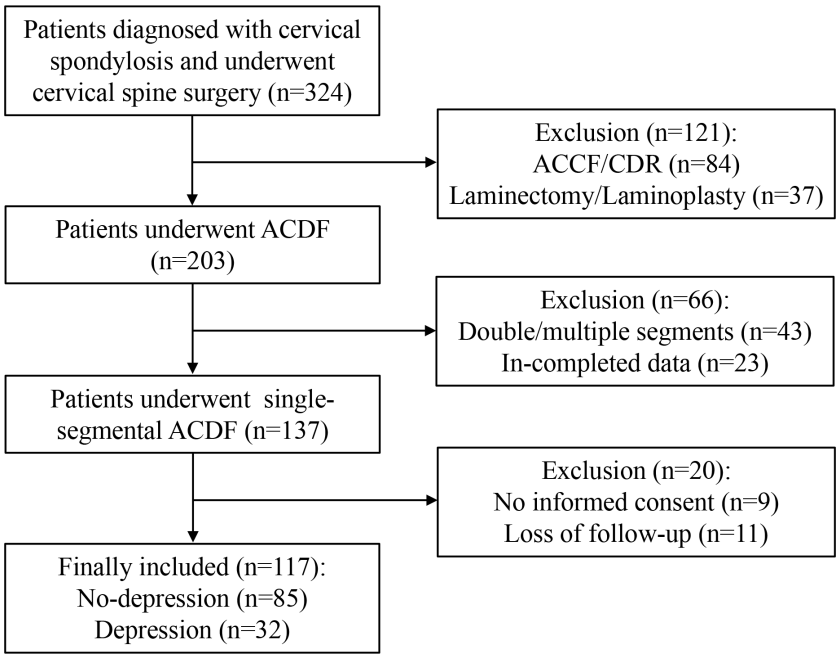

FIGURE 1
Flow chart of the inclusion and exclusion of patients.

TABLE 1 Comparison of clinical basic characteristics between the two groups.

	Control group (N = 85)	Intervention group (N = 32)	*P* value
Age, yr	60.3 ± 10.5	58.5 ± 9.4	0.373
Gender, n			0.061
Male	18	12	
Female	67	20	
Duration of symptoms, month	12.5 ± 4.1	13.6 ± 5.5	0.243
BMI, kg/m^2	28.6 ± 6.7	30.1 ± 8.4	0.317
Employment status, n			0.385
Working/studying	15	4	
Unemployed or retiree	70	28	
Smoking history, n			0.342
Yes	19	8	
No	66	24	
Radiculopathy laterality, n			0.542
Bilateral	25	9	
Unilateral	60	23	
Disease Level, n			0.507
C3/4	14	5	
C4/5	34	13	
C5/6	27	10	
C6/7	10	4	

10.3389/fendo.2022.1031616

TABLE 2 Comparison of depression, pain, cervical spine function and quality of life between the two groups.

	Control group (N = 85)	Intervention group (N = 32)	*P* value
BDI, score			
Preoperative	5.3 ± 2.1	12.6 ± 7.8	<0.001
Last follow-up	2.1 ± 1.5*	10.5 ± 7.2*	<0.001
Change	3.3 ± 1.9	2.4 ± 1.2	0.014
VAS, score			
Preoperative	3.4 ± 2.3	4.5 ± 2.1	0.020
Last follow-up	1.1 ± 0.9*	1.6 ± 1.0*	0.011
Change	2.2 ± 1.9	2.9 ± 2.1	0.087
JOA, score			
Preoperative	7.4 ± 3.6	5.6 ± 3.1	0.014
Last follow-up	15.1 ± 2.9*	11.9 ± 5.5*	<0.001
Change	7.6 ± 3.1	6.3 ± 3.2	0.067
NDI, %			
Preoperative	40.4 ± 10.2	48.2 ± 9.1	<0.001
Last follow-up	19.0 ± 9.1*	30.5 ± 10.3*	<0.001
Change	21.1 ± 11.4	16.8 ± 9.5	0.060
SF-36 PCS, score			
Preoperative PCS	35.3 ± 7.5	40.8 ± 9.8	0.002
Last follow-up PCS	27.6 ± 5.4*	33.3 ± 8.7*	<0.001
Change	7.4 ± 2.1	6.5 ± 2.9	0.067
SF-36 MCS, score			
Preoperative MCS	38.2 ± 8.3	44.2 ± 9.5	0.002
Last follow-up MCS	28.1 ± 7.2*	36.4 ± 8.4*	<0.001
Change	8.6 ± 4.3	7.1 ± 2.9	0.031

*Compared with preoperative, P < 0.05.

people (16). However, after antidepressant therapy, the BDI scores of depression patients before ACDF were all at a low level, that was to say, most patients were in the so-called mild or moderate depression state (BDI score<15) before surgery, and almost none of patients with severe depression (17). This also indirectly supports the effectiveness of preoperative antidepressant therapy. Since the SF-36 MCS is a patient's mental condition score, it has some similarities with the BDI score (depression score), that is, the preoperative SF-36 MCS of depression patients are higher than that of the normal group.

The preoperative clinical symptoms of cervical spondylosis patients complicated with depression were more obvious than those of the normal group, mainly reflected in high VAS score, low JOA score and high NDI score, which may be related to the higher preoperative BDI score in the intervention group and the more sensitive experience of uncomfortable feelings, such as pain and cervical dysfunction, in the depressed state (18, 19). This conclusion was similar to that of previous studies, that was, depression was an independent risk factor for obvious symptoms and poor treatment effect in cervical spondylosis patients (20).

TABLE 3 Comparison of surgery-related outcomes between the two groups.

	Control group (N = 85)	Intervention group (N = 32)	*P* value
Operative time, min	78.4 ± 12.5	83.3 ± 14.6	0.074
Operative blood loss, ml	32.5 ± 5.1	34.8 ± 7.5	0.060
Hospital stay, d	5.8 ± 1.4	6.4 ± 2.2	0.083
Complications, n			0.542
PE/DVT	3	1	
UTI	7	3	
Pneumonia	5	2	

PE, pulmonary embolism; DVT, deep venous thrombosis; UTI, urinary tract Infection.

This was also the reason why we discussed whether depression is the contraindication of ACDF for cervical spondylosis.

In this study, the BDI score, VAS, JOA score, NDI, and SF-36 score were all significantly improved after ACDF, which means that cervical spondylosis patients with or without preoperative depression can all achieve good clinical outcomes from ACDF (21). There may be the following reasons: (1) The diseased intervertebral disc, marginal osteophyte and posterior longitudinal ligament were all removed during ACDF, which reduced the compression of spinal cord and nerve root, and thus provided good conditions for the recovery of neurological function (22); (2) ACDF alleviates neck pain and dysfunction which has a positive impact on the quality of life of patients (23); (3) ACDF was a mature surgical technique with short operative time and little operative blood loss, which greatly alleviates the pain of patients and has a positive impact on the psychological state of patients (24). The results showed that the long-term clinical efficacy of ACDF in patients with depression undergoing antidepressant treatment was similar to that in non-depression patients. This suggests that the previous view that depression is a contraindication of spinal surgery may need to be reassessed (7, 8). After antidepressant treatment, patients with depression can also obtain satisfactory long-term pain and life quality improvement from ACDF. Moreover, this result indicated that the relief of pain and disability after ACDF was also associated with the relief of depression (25). It was predicted that antidepressants after ACDF may also improve the relief of the pain and functional outcomes. Therefore, we don't think depression is a contraindication for ACDF surgery, and preoperative and postoperative antidepressant therapy are helpful to relieve postoperative pain and improve life quality.

Antidepressants include selective serotonin reuptake inhibitors (SSRIs), serotonin norepinephrine reuptake inhibitors (SNRIs), tricyclic and tetracycline antidepressants, MAO inhibitors, 5-HT2 antagonists and so on (26). At present, studies have shown that SSRIs may result in abnormal bleeding in patients undergoing orthopedic surgery (13, 27). Mago et al. reported that the operative blood loss in patients taking SSRIs drugs was 2.5 times higher than that in the control group during lumbar fusion surgery (28), so it was suggested that preoperative platelet function test be conducted in patients with SSRIs taking, especially in elderly undergoing elective surgery, although there is no data indicating the benefits of this test (29). In this study, we found that the operative blood loss of patients taking antidepressants was similar to that of the control group. There may be the following reasons: (1) The baseline bleeding risk of patients included in our study maybe different from that of previous studies (30); (2) It was reported that, for complex spinal surgery, antidepressants may cause a significant increase in intraoperative bleeding, but a relative simple spinal surgery (such as ACDF) only had a small amount of blood loss (31); (3) There may be differences in the methods used in each study to record intraoperative blood loss (32); (4) In our study, we avoided using NSAIDs in patients taking SSRIs, which may reduce the risk of abnormal bleeding caused by SSRIs (33). In addition, there was no significant difference in the risk of postoperative complications related to platelet function, such as deep venous thrombosis and pulmonary embolism. These results confirmed that it was safe for patients with depression to use antidepressants before ACDF.

Our study has several limitations. First, we did not include some demographic and medical data (such as education level, platelet function test, etc.), which may affect the study results. Second, patients were not randomly divided. The decision of taking antidepressants and the type of antidepressants is entirely made by psychiatrists. Third, the duration of preoperative pain, depression and other symptoms could not be assessed, which may affect the results of the study.

Depression is not the contraindication of ACDF for cervical spondylosis. Depression patients who received preoperative antidepressants can achieve similar improvement of clinical symptoms from ACDF with non-depression patients.

Data availability statement

The raw data supporting the conclusions of this article will be made available by the authors, without undue reservation.

Ethics statement

The studies involving human participants were reviewed and approved by the Ethics Committee of the First Affiliated Hospital of Chongqing Medical University. The patients/participants provided their written informed consent to participate in this study.

Author contributions

Conception and design: XD, YP, XC, and XL. Data analysis and interpretation: XD, YP, XC, YG, YL, and YT. Data collection and management: XD, XL, YF, HY, and KL. Manuscript writing and critical revisions: all authors. Overall responsibility: YP and XD. All authors have read and approved the manuscript.

Conflict of interest

The authors declare that the research was conducted in the absence of any commercial or financial relationships that could be construed as a potential conflict of interest.

Publisher's note

References

1. Theodore N. Degenerative cervical spondylosis. *N Engl J Med* (2020) 383 (2):159–68. doi: 10.1056/NEJMra2003558

2. Scholz C, Masalha W, Naseri Y, Hohenhaus M, Klingler JH, Hubbe U. Subjective and objective change in cervical spine mobility after single-level anterior cervical decompression and fusion. *Spine (Phila Pa 1976)* (2021) 46(18):1241–8. doi: 10.1097/BRS.0000000000003987

3. Inose H, Yoshii T, Kimura A, Takeshita K, Inoue H, Maekawa A, et al. Comparison of clinical and radiographic outcomes of laminoplasty, anterior decompression with fusion, and posterior decompression with fusion for degenerative cervical myelopathy: A prospective multicenter study. *Spine (Phila Pa 1976)* (2020) 45(20):E1342–8. doi: 10.1097/BRS.0000000000003592

4. Menendez ME, Neuhaus V, Bot AG, Ring D, Cha TD. Psychiatric disorders and major spine surgery: Epidemiology and perioperative outcomes. *Spine (Phila Pa 1976)* (2014) 39(2):E111–22. doi: 10.1097/BRS.0000000000000064

5. Lin SY, Sung FC, Lin CL, Chou LW, Hsu CY, Kao CH. Association of depression and cervical spondylosis: A nationwide retrospective propensity score-matched cohort study. *J Clin Med* (2018) 7(11):387. doi: 10.3390/jcm7110387

6. Stoffman MR, Roberts MS, King JTJr. Cervical spondylotic myelopathy, depression, and anxiety: A cohort analysis of 89 patients. *Neurosurgery* (2005) 57 (2):307–13; discussion 307-13. doi: 10.1227/01.NEU.0000166664.19662.43

7. Li S, Qi M, Yuan W, Chen H. The impact of the depression and anxiety on prognosis of cervical total disc replacement. *Spine (Phila Pa 1976)* (2015) 40(5): E266–71. doi: 10.1097/BRS.0000000000000743

8. Alcocer GF, Moheno-Gallardo AJ, Elizalde-Martínez E, Rojano-Mejía D, López-Martínez E, González-Andrade KG, et al. Association of depression and functional outcomes in patients treated surgically for cervical spondylotic myelopathy through an anterior approach. *Cir Cir* (2021) 89(5):657–63. doi: 10.24875/CIRU.20000915

9. Chen J, Li JY, Tian GH, Qiu RJ, Zhao XQ, Di XS, et al. A national snapshot of the impact of clinical depression on post-surgical pain and adverse outcomes after anterior cervical discectomy and fusion for cervical myelopathy and radiculopathy: 10-year results from the US nationwide inpatient sample. *PloS One* (2021) 16(10): e0258517. doi: 10.1371/journal.pone.0258517

10. Harris AB, Marrache M, Puvanesarajah V, Raad M, Jain A, Kebaish KM, et al. Are preoperative depression and anxiety associated with patient-reported outcomes, health care payments, and opioid use after anterior discectomy and fusion? *Spine J* (2020) 20(8):1167–75. doi: 10.1016/j.spinee.2020.03.004

11. Elsamadicy AA, Adogwa O, Cheng J, Bagley C. Pretreatment of depression before cervical spine surgery improves patients' perception of postoperative health status: A retrospective, single institutional experience. *World Neurosurg* (2016) 87:214–9. doi: 10.1016/j.wneu.2015.11.067

12. Sayadipour A, Kepler CK, Mago R, Certa KM, Rasouli MR, Vaccaro AR, et al. Economic effects of anti-depressant usage on elective lumbar fusion surgery. *Arch Bone Jt Surg* (2016) 4(3):231–5. doi: 10.22038/ABJS.2016.6697

13. Sayadipour A, Mago R, Kepler CK, Chambliss RB, Certa KM, Vaccaro AR, et al. Antidepressants and the risk of abnormal bleeding during spinal surgery: A case–control study. *Eur Spine J* (2012) 21(10):2070–8. doi: 10.1007/s00586-011-2132-8

14. Mathew G, Agha RSTROCSS Group. STROCSS 2021: Strengthening the reporting of cohort, cross-sectional and case-control studies in surgery. *Int J Surg* (2021) 96:106165. doi: 10.1016/j.ijsu.2021.106165

15. Rhee JM, Ju KL. Anterior cervical discectomy and fusion. *JBJS Essent Surg Tech* (2016) 6(4):e37. doi: 10.2106/JBJS.ST.15.00056

16. Ogle NR, Akkerman SR. Guidance for the discontinuation or switching of antidepressant therapies in adults. *J Pharm Pract* (2013) 26(4):389–96. doi: 10.1177/0897190012467210

17. Wang YP, Gorenstein C. Psychometric properties of the beck depression inventory-II: A comprehensive review. *Braz J Psychiatry* (2013) 35(4):416–31. doi: 10.1590/1516-4446-2012-1048

18. Cha EDK, Lynch CP, Jadczak CN, Mohan S, Geoghegan CE, Singh K. Impact of depression severity on patient-reported outcome measures following multilevel anterior cervical discectomy and fusion. *Int J Spine Surg* (2022) 16 (1):81–7. doi: 10.14444/8180

19. Phan K, Moran D, Kostowski T, Xu R, Goodwin R, Elder B, et al. Relationship between depression and clinical outcome following anterior cervical discectomy and fusion. *J Spine Surg* (2017) 3(2):133–40. doi: 10.21037/jss.2017.05.02

20. Mangan JJ3rd, Tadley M, Divi SN, Stull JD, Goyal DKC, McKenzie JC, et al. The impact of multiple comorbid mental health disorders on health-related quality of life following ACDF. *Clin Spine Surg* (2020) 33(10):E472–7. doi: 10.1097/BSD.0000000000000957

21. Divi SN, Goyal DKC, Mangan JJ, Galetta MS, Nicholson KJ, Fang T, et al. Are outcomes of anterior cervical discectomy and fusion influenced by presurgical depression symptoms on the mental component score of the short form-12 survey? *Spine (Phila Pa 1976)* (2020) 45(3):201–7. doi: 10.1097/BRS.0000000000003231

22. Schroeder GD, Kurd MF, Millhouse PW, Vaccaro AR, Hilibrand AS. Performing an anterior cervical discectomy and fusion. *Clin Spine Surg* (2016) 29(5):186–90. doi: 10.1097/BSD.0000000000000383

23. Schroeder GD, Kurd MF, Millhouse PW, Vaccaro AR, Hilibrand AS. Comparing health-related quality of life outcomes in patients undergoing either primary or revision anterior cervical discectomy and fusion. *Spine (Phila Pa 1976)* (2018) 43(13):E752–7. doi: 10.1097/BRS.0000000000002511

24. Tamai K, Suzuki A, Terai H, Hoshino M, Toyoda H, Takahashi S, et al. Improvement in patient mental well-being after surgery for cervical spondylotic myelopathy. *Spine (Phila Pa 1976)* (2020) 45(10):E568–75. doi: 10.1097/BRS.0000000000003337

25. MacDowall A, Robinson Y, Skeppholm M, Olerud C, Toyoda H. Anxiety and depression affect pain drawings in cervical degenerative disc disease. *Ups J Med Sci* (2017) 122(2):99–107. doi: 10.1080/03009734.2017.1319441

26. Faquih AE, Memon RI, Hafeez H, Zeshan M, Naveed S. A review of novel antidepressants: A guide for clinicians. *Cureus* (2019) 11(3):e4185. doi: 10.7759/cureus.4185

27. van Haelst IM, Egberts TC, Doodeman HJ, Traast HS, Burger BJ, Kalkman CJ, et al. Use of serotonergic antidepressants and bleeding risk in orthopedic patients. *Anesthesiology* (2010) 112(3):631–6. doi: 10.1097/ALN.0b013e3181cf8fdf

28. Mago R, Mahajan R, Thase ME. Medically serious adverse effects of newer antidepressants. *Curr Psychiatry Rep* (2008) 10(3):249–57. doi: 10.1007/s11920-008-0041-2

29. de Abajo FJ. Effects of selective serotonin reuptake inhibitors on platelet function: mechanisms, clinical outcomes and implications for use in elderly patients. *Drugs Aging* (2011) 28(5):345–67. doi: 10.2165/11589340-000000000-00000

30. Meijer WE, Heerdink ER, Nolen WA, Herings RM, Leufkens HG, Egberts AC. Association of risk of abnormal bleeding with degree of serotonin reuptake inhibition by antidepressants. *Arch Intern Med* (2004) 164(21):2367–70. doi: 10.1001/archinte.164.21.2367

31. Tavakoli HR, DeMaio M, Wingert NC, Rieg TS, Cohn JA, Balmer RP, et al. Serotonin reuptake inhibitors and bleeding risks in major orthopedic procedures. *Psychosomatics* (2012) 53(6):559–65. doi: 10.1016/j.psym.2012.05.001

32. Movig KL, Janssen MW, de Waal Malefijt J, Kabel PJ, Leufkens HG, Egberts AC. Relationship of serotonergic antidepressants and need for blood transfusion in orthopedic surgical patients. *Arch Intern Med* (2003) 163(19):2354–8. doi: 10.1001/archinte.163.19.2354

33. Helin-Salmivaara A, Huttunen T, Grönroos JM, Klaukka T, Huupponen R. Risk of serious upper gastrointestinal events with concurrent use of NSAIDs and SSRIs: A case-control study in the general population. *Eur J Clin Pharmacol* (2007) 63(4):403–8. doi: 10.1007/s00228-007-0263-y

frontiers | Frontiers in Endocrinology

TYPE Original Research
PUBLISHED 07 October 2022
DOI 10.3389/fendo.2022.1015198

OPEN ACCESS

EDITED BY
Meifeng Zhu,
Nankai University, China

REVIEWED BY
Baoshan Xu,
Tianjin Hospital, China
Lichen Wang,
Stevens Institute of Technology, United States

*CORRESPONDENCE
Tao Zhang
zhtyzx2019@163.com
Zhaoyang Li
zyli@tju.edu.cn

SPECIALTY SECTION
This article was submitted to Bone Research, a section of the journal Frontiers in Endocrinology

RECEIVED 09 August 2022
ACCEPTED 20 September 2022
PUBLISHED 07 October 2022

CITATION
Wang Z, Xue T, Zhang T, Wang X, Zhang H, Gao Z, Zhou Q, Gao E, Zhang T and Li Z (2022) Identification of compositional and structural changes in the nucleus pulposus of patients with cervical disc herniation by Raman spectroscopy. *Front. Endocrinol.* 13:1015198. doi: 10.3389/fendo.2022.1015198

Identification of compositional and structural changes in the nucleus pulposus of patients with cervical disc herniation by Raman spectroscopy

Zhiqi Wang[1], Tao Xue[2], Tongxing Zhang[3], Xuehui Wang[4], Hui Zhang[1], Zhongyu Gao[1], Qiang Zhou[1], Erke Gao[5], Tao Zhang[1]* and Zhaoyang Li[2]*

[1]Department of Orthopedic, Tianjin First Central Hospital, Tianjin, China, [2]School of Materials Science and Engineering, Tianjin University, Tianjin, China, [3]Department of Minimally Invasive Spine Surgery, Tianjin Hospital, Tianjin University, Tianjin, China, [4]Department of Orthopedic and Joint Sports Medicine, The First Affiliated Hospital of Baotou Medical College, Baotou, China, [5]First Central Clinical College, Tianjin Medical University, Tianjin, China

Purpose: Cervical disc herniation (CDH) is one of the most common spinal diseases in modern society; intervertebral disc degeneration (IVDD) has long been considered as its primary cause. However, the mechanism of intervertebral disc degeneration is still unclear. The aim of the study is to examine the components and structures of proteoglycan and collagen in cervical disc herniated nucleus pulposus (NP) using a validated and convenient Raman spectra technique and histological methods to further elucidate the mechanism of IVDD at the microscopic level.

Methods: Our study used a burgeoning technique of Raman spectroscopy combined with *in vitro* intervertebral disc NP to characterize the above mentioned research purposes. Firstly, we collected cervical disc NP samples and imaging data by certain inclusion and exclusion criteria. Then, we graded the NP of the responsible segment according to the patient's preoperative cervical magnetic resonance imaging (MRI) T2-weighted images by Pfirrmann grading criteria while measuring the T2 signal intensity value of NP. In addition, the structure of the NP samples was evaluated by histological staining (H&E staining and Safranin-O staining). Finally, the samples were scanned and analyzed by Raman spectroscopy.

Results: A total of 28 NP tissues from 26 patients (two of these patients were cases that involved two segments) with CDH were included in this study. According to the Raman spectroscopy scan, the relative content of proteoglycans which is characterized by the ratio of the two peaks ($I_{1,064}/I_{1,004}$) in the NP showed a significantly negative correlation with Pfirrmann grade ($P < 0.001$), while the collagen content and the NP intensity value showed a positive correlation ($P < 0.001$). For the microstructural characterization of collagen, we found that it may have an essential role in the degenerative

process of the intervertebral disc. Moreover, histological staining (H&E staining and Safranin-O staining) showed the general structure of the NP and the distribution of macromolecules.

Conclusion: The present study demonstrated the possibility of characterizing the macromolecular substances inside the cervical disc NP tissue by Raman spectroscopy. It also confirmed that macromolecular substances such as proteoglycans and collagen have some degree of alteration in content and structure during degeneration, which has a further positive significance for the elucidation of CDH's mechanism.

KEYWORDS

intervertebral disc degeneration, cervical disc herniation, Raman spectroscopy, nucleus pulposus, proteoglycan

Introduction

Cervical disc herniation (CDH), as one of the most prevalent spinal diseases, is characterized by radicular symptoms and spinal cord compression symptoms such as neck and shoulder pain, muscle tone changes, and so on. CDH is considered to be a highly prevalent disease in middle-aged and elderly people (1), but with the popularization of social lifestyles and electronic devices, it is gradually showing a trend of rejuvenation (2). A review of the global burden of neck pain estimated that more than one-third of the world's population experience persistent neck and shoulder pain malaising for more than 3 months (3), further emphasizing the magnitude of CDH's impact on global health. The occurrence of degenerative diseases such as CDH and depression-related psychiatric disorders has been well documented (4), causing physical pain as well as mental health risks to patients. As the earliest and most susceptible of the body's tissues to succumb to degeneration with age, the intervertebral discs also lose water and corresponding elasticity in the NP (5). Intervertebral disc degeneration (IVDD) is also considered to be an influential risk factor for the development of CDH (6). Although there are a fair number of theories and related animal studies in the exploration of IVDD, the internal composition and microstructural changes of the human intervertebral disc NP remain a significant challenge for scientific research.

The high sensitivity of MRI to water and proteoglycan content has made it widely used in the diagnosis of intervertebral disc- and cartilage-related diseases (7). However, MRI is more of an adjunctive diagnostic tool for clinically relevant diseases and is still limited in its ability to characterize the macromolecular substances within the NP during IVDD. In the maturation of MRI-related technologies, there has been no shortage of approaches to improve the accuracy of diagnosis through dynamic magnetic resonance imaging, functional magnetic resonance imaging, diffusion imaging, *etc.* (8). Nevertheless, there are still several restrictions of MRI in evaluating microstructural changes within the NP.

Raman spectroscopy, being a new generation of non-destructive molecular spectroscopy, has been widely used in recent years for the study of structural and compositional changes of biomolecules in diseased tissues and in the early diagnosis of related diseases (9). It has the advantages of real-time rapid detection, simple sample processing, low biological interference, and high sensitivity and specificity (10, 11); most importantly, it can indirectly reflect the structural composition and content changes of macromolecules at the microscopic level (12), which makes it one of the hot spots for the early diagnosis of related diseases (13). It has also been reported in the literature that it is used in the study of articular cartilage and lumbar intervertebral disc degeneration.

We analyzed the NP tissue of cervical discs with different degrees of degeneration by Raman spectroscopy to further investigate the mechanism of disc degeneration and the feasibility of early clinical diagnosis.

Materials and methods

Patient data and sample collection

Our study was endorsed by the Ethics Committee of Tianjin First Central Hospital, and the consent of patients with CDH treated by surgery was obtained. All procedures were carried out in strict compliance with relevant domestic and international policies. A total of 28 NP samples from 26 patients (15 male and 11 female; age, 20–78 years; mean age, 51.4 years) with CDH treated by anterior cervical spine surgery in the Department of Orthopedics, Tianjin First Central Hospital, were enrolled in this study from June 2020 to September 2021. All patients included

in the group were diagnosed with CDH by MRI and had relevant clinical symptoms and corresponding syndromes, among whom conservative treatment was found ineffective after 3 months of application.

Preoperative Pfirrmann grade

All patients' cervical MRI profiles were scanned at the Siemens Magnetom Trio 3.0T superconducting MR scanner (Magnetom, Trio, Siemens Healthcare, Erlangen, Germany) in the imaging department of the First Central Hospital of Tianjin. The cervical MR scan parameters were as follows: sagittal T2-weighted: repetition time, 3,270 ms; echo time, 112 ms; field of view, 260 × 260 mm; slice thickness, 3.0 mm; scanning slice number, 12; and voxel size, 320 × 224 mm. The samples were graded and evaluated on MRI sagittal T2-weighted images by the clinically used Pfirrmann grading (14), an intervertebral disc degeneration classification standard. The images were evaluated by a radiologist and a spine surgeon who were both unaware of the experiment, and the observers graded the sample strictly according to the Pfirrmann grading in the median sagittal position of the cervical MRI T2-weighted term. To increase the accuracy of the grading results, the cervical spine images of all patients were randomly evaluated by both observers again 2 months later (the two observers were unaware of the homogeneity of the two evaluations).

NP signal intensity value measurement

We used Siemens post-processing software to measure the signal intensity of NP on MRI sagittal T2-weighted images. The study randomly selected a range area (20–40 mm^2) of anterior, middle, and posterior positions on the targeted NP and then measured three times continuously at the respectively selected position to obtain the average brightness value. The brightness value of the cerebrospinal fluid on the cervical segment was measured by a similar method. Then, the NP signal intensity value was defined as the ratio of NP to the cerebrospinal fluid brightness value (15).

Preparation of sample

All samples were obtained through anterior cervical surgery in strict accordance with the surgical procedure, then placed in sterile sample boxes, and labeled with patient-related information under the premise of sample freezing. The samples were repeatedly washed with sterile saline in clean petri dishes. The loose NP tissues were blended into ellipsoidal spheres with a radius of 3 mm (for better embedding and section staining) and placed in optimal cutting temperature (OCT) media for embedded freezing treatment. All samples were processed by frozen sectioning to a thickness of 30 μm on stripping-resistant slides, and the samples were collected in a slide box and stored in a refrigerator at -20°C.

Assessments of histological staining

The obtained frozen section samples were removed from -20 °C inside the refrigerator and thawed to room temperature for histological staining (1). Hematoxylin and eosin (H&E) staining was carried out as follows: the OCT-embedded frozen sections were washed in running water at room temperature for 5 min. Subsequently, the frozen sections were stained with hematoxylin (H&E staining kit; Beijing Solarbio Science and Technology Co., Ltd.) for 10 min, followed by fractionation in 1% hydrochloric acid alcohol for 2 s. Then, the sections were incubated in 1% ammonia for 2 min and stained with 1% eosin for 1 min. After each step, the sections were rinsed under running water for 3 min. Lastly, the sections were dehydrated with graded ethanol and vitrified with dimethylbenzene. Then, the sections were sealed with neutral resin. After that, the upper layer of each group of sample tissue was stained, dried, and observed under a microscope, with the position of the corresponding NP tissue being marked. The corresponding position of the lower layer of the sections was marked as well. All processes were performed under sterile conditions (2). On the other hand, Safranin-O-Fast Green staining (Modified Safranine O-Fast Green FCF Cartilage Stain Kit; Beijing Solarbio Science and Technology Co., Ltd.) was performed as follows: OCT-embedded frozen sections were washed in running water at room temperature for 5 min, and then the sections were stained with freshly prepared Weigert iron hematoxylin stain for 5 min before being washed under running water for 3 min. Then, the sections were partitioned in acidic partitioning solution for 15 s and rinsed in distilled water for 10 min. After immersing the sections in Fast Green solution for 5 min, the sections were quickly washed with a weak acid solution for 15 s. The sections were dried before being stained in Safranin-O solution for 3 min. Finally, the sections were dehydrated, vitrified, and mounted with neutral gum.

All staining procedures were performed according to the kit manufacturer's instructions. The images of the stained sections were obtained using an optical microscope (Nikon Eclipse 600, Nikon Corporation) mounted with a digital camera (Nikon DXM1200F, Nikon Corporation).

Sample Raman spectroscopy detection

All frozen samples were defrosted to room temperature, and the samples were rinsed with sterile saline to wash off the OCT reagent for Raman spectroscopy. Sterile saline was added dropwise to keep the samples moist during the testing process (the characteristic peaks of saline on the Raman spectra were negligible). The Raman

spectroscopy test parameters were as follows: laser wavelength, 532 nm; sample magnification, ×500; laser power, 10.0 mW; spot size, 1.1 μm; spectral range, 800–1,800 cm^{-1}; grating, 900 line/mm; and resolution, 5 cm^{-1}. For each NP sample, a total of 10 randomly selected positions were scanned by the spectrometer to obtain the corresponding spectra (16), with a single exposure time of 16 s and number of scans of 5. Confocal correction was needed before scanning at different positions.

The acquired Raman spectral data were processed and analyzed by OMNIC software (Thermo Fisher Scientific, Inc.), and the peak shapes and peak positions were calculated by fitting the Raman spectra with Gaussian/Lorentzian functions after baseline correction. Then, the intensity and the area of the different peaks of the obtained Raman spectra were imported into Microsoft Excel software to calculate the relative ratios of intensity and area of different characteristic peaks.

Statistical analysis

Statistical analysis was performed using SPSS 26.0 software (SPSS, Chicago), and all data were expressed as mean ± standard deviation. κ statistics was used to evaluate the consistency and reliability of Pfirrmann grade results. The association between the NP T2-weighted intensity values and the relative content of proteoglycans was assessed by a bivariate correlation. Statistical differences between groups were statistically analyzed using one-way ANOVA, followed by Tukey's test for variability between the Raman spectral data of different Pfirrmann grades. The correlation between the acquired Raman spectral data and Pfirrmann grade was assessed by Spearman's correlation analysis. P <0.05 was defined as statistically significant.

Results

Pfirrmann classification

By κ statistics analysis, the first grading results were in great agreement between the two observers (κ = 0.620, P < 0.001), and the second observation grading results were in excellent agreement likewise (κ = 0.614, P < 0.001). The grading results of patients with CDH included in this study did not have Pfirrmann grade I (Table 1). The imaging performance of patients with a different grading is shown in Figure 1A.

Analysis of the NP T2 signal intensity value

The present study demonstrated that the NP T2 signal intensity value in Pfirrmann III, IV, and V was significantly lower compared with Pfirrmann II (P < 0.001), but the NP T2 signal intensity value was not significantly different between grade IV and grade V (P > 0.05). In terms of Spearman's correlation analysis, there was a significantly negative correlation between NP T2 signal intensity value and Pfirrmann grade (ρ = -0.9196, P < 0.001, Figure 1B).

Histological staining of NP in different Pfirrmann grades

H&E staining

In the normal macroscopic assessment, the annulus fibrosus (AF) tissue was dense and showed the typical several layers of concentric fibrous sheets, whereas since our study used a surgically obtained sample, it was possible to see the presence of partial AF tissues presenting as red striated structures, but there were more pale blue NP tissues in the field of view, which appeared spongy and had a soft and loose appearance. In addition, scattered nuclei could be seen in the extracellular matrix of the NP (Figure 2).

Safranin-O-Fast green staining

All grade samples were stained as shown in Figure 3; we observed the structural components of the NP proteoglycan to be showing a reddish tone as well as the fibrous ring tissue in pale blue color. The proteoglycan structure was fluffy and more abundantly distributed in the extracellular matrix than the AF tissue. Furthermore, Safranin-O staining was also used to appropriately express the distribution of proteoglycans in the extracellular matrix. Another reason for these procedures was to make sure that all locations tested were NP tissue, and the same position was accurately detected by subsequent Raman spectroscopy.

TABLE 1 Grading results of patients with Pfirrmann grade.

Pfirrmanngrade	Sex		Intervertebral disc level				Total
	Male	Female	C3/4	C4/5	C5/6	C6/7	
II	2	4	1	1	3	1	6
III	5	1	1	1	3	3	8
IV	5	3	4	1	3	0	8
V	3	3	3	1	2	0	6
Total	15	11	9	4	11	4	28

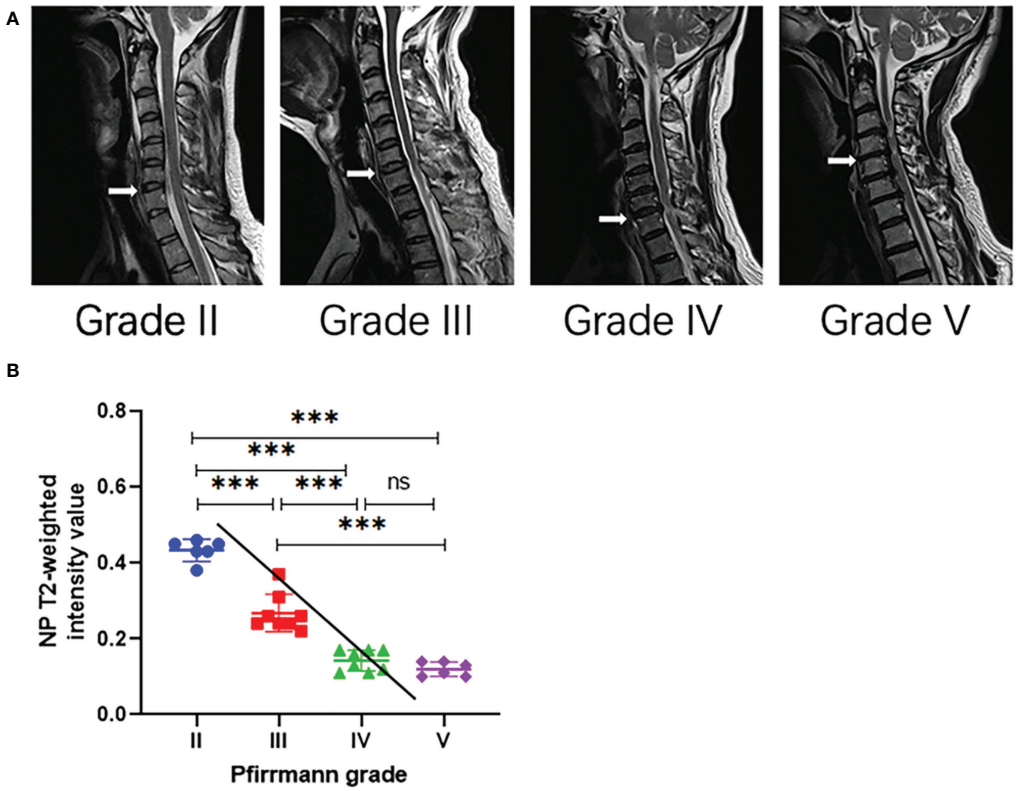

FIGURE 1
(A) Representative T2-weighted median sagittal MRI scans of the cervical spine with intervertebral disc degeneration at different Pfirrmann grades. The segments responsible for the lesion are indicated by the white arrow. **(B)** Analysis of NP T2 signal intensity values with Pfirrmann grade by Spearman's correlation analysis. $^{***}P < 0.001$; ns, no significance.

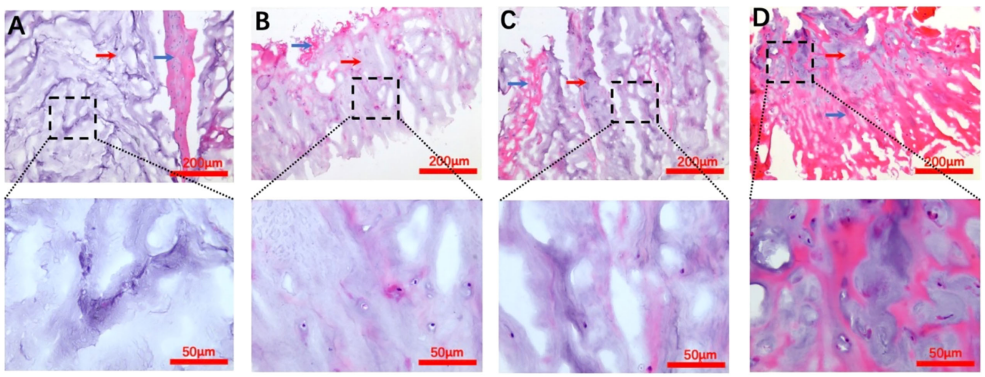

FIGURE 2
H&E staining images for each Pfirrmann grade. **(A–D)** Representative Pfirrmann grade II, III, IV, and V images, respectively. The blue arrows in each figure point to the annulus fibrosus tissue, and the nucleus pulposus tissue structure is indicated by the red arrows. The scale bar of each figure is shown at the lower righthand corner of the figure.

Raman spectroscopy peak distribution

Proteoglycans and collagens play a major role in the extracellular matrix of NP (17), and macromolecules like these all have their own characteristic peaks in Raman spectroscopy. Proteoglycans are often characterized in Raman spectroscopy by their special glycosaminoglycan complex structure, which has been previously identified by scholars, and their characteristic

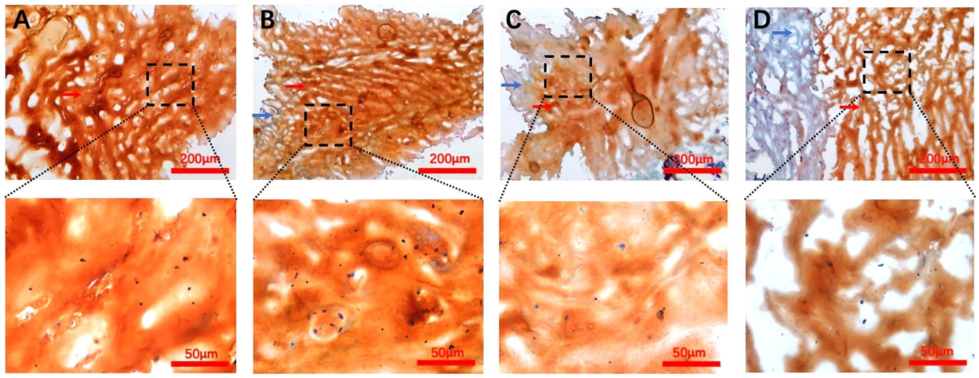

FIGURE 3
Safranin-O-Fast Green staining images for each Pfirrmann grade. **(A–D)** Representative Pfirrmann grade II, III, IV, and V images, respectively. The blue arrows in each figure point to the annulus fibrosus tissue, and the nucleus pulposus tissue structure is indicated by the red arrows. The scale bar of each figure is shown at the lower righthand corner of the figure.

peaks are mainly located at 1,064–1,065 cm^{-1} (18); phenylalanine is often used as a reference internal standard to measure the relative content due to its insensitivity to the surrounding environment, and its characteristic peak position on the Raman spectrum is mainly in the range of 1,003–1,004 cm^{-1} (19). Because of the possibility of individual differences in the proteoglycan content within the sample, the measured proteoglycan Raman spectral peak intensities are usually corrected by the ratio for further comparison. Therefore, the ratio of the two ($I_{1,064}/I_{1,004}$) was taken as the relative content of proteoglycan.

Collagen, as an internal mesh-mounted scaffold structure for intervertebral disc, has its peak characterization on Raman spectra mainly depending on two amide groups: amide I and amide III. The identification of the peak positions of the two Raman spectra has been demonstrated in the last century: the peak position of amide I is mainly located at 1,600–1,700 cm^{-1} (20, 21), while amide III is at 1,200–1,300 cm^{-1} (20, 22).

In contrast, the collagen secondary structure changes are mainly characterized by correlated Raman spectroscopy peaks within both, and the ratio of the correlated peaks is usually used to assess the relative variation in disordered collagen (random coil) *versus* ordered collagen (α-helix) (20, 23, 24). The peak positions of the Raman spectra of various macromolecules in the samples are provided in Table 2, and the fitted and calculated images of different Pfriimann-graded Raman spectra are shown in Figure 4.

Analysis of proteoglycan and collagen content in samples

The relative proteoglycan content was found to be significantly reduced in Pfirrmann grades III, IV, and V compared with grade II ($P < 0.001$). According to Spearman's correlation analysis, the relative proteoglycan content showed a dramatically negative correlation with the Pfirrmann grade (ρ = -0.9654, $P < 0.001$, Figure 5A).

As for the collagen content, the amide I group as well as the amide III group within it were analyzed separately. The amide I content was significantly higher in Pfirrmann grades III, IV, and V compared with grade II ($P < 0.05$, $P < 0.001$, and $P < 0.001$, respectively). Spearman's correlation analysis indicated a highly positive correlation between amide I content and Pfirrmann grade (ρ = 0.9629, $P < 0.001$, Figure 5B). The content of amide III in Pfirrmann grades III, IV, and V was significantly increased

TABLE 2 Raman spectroscopy peak distribution and affiliated compounds.

Peak position(cm^{-1})	Affiliated compounds	References
1,004	Phenylalanine	(19)
1,064	Glycoaminoglycan	(18)
1,200–1,300	Amide III, major collagen band	(20, 22)
1,640	Amide I, ordered coil, α-helix	(20, 23, 24)
1,670	Amide I, disordered coil, random coil	(20, 23, 24)
1,600–1,700	Amide I, major collagen band	(20, 22)

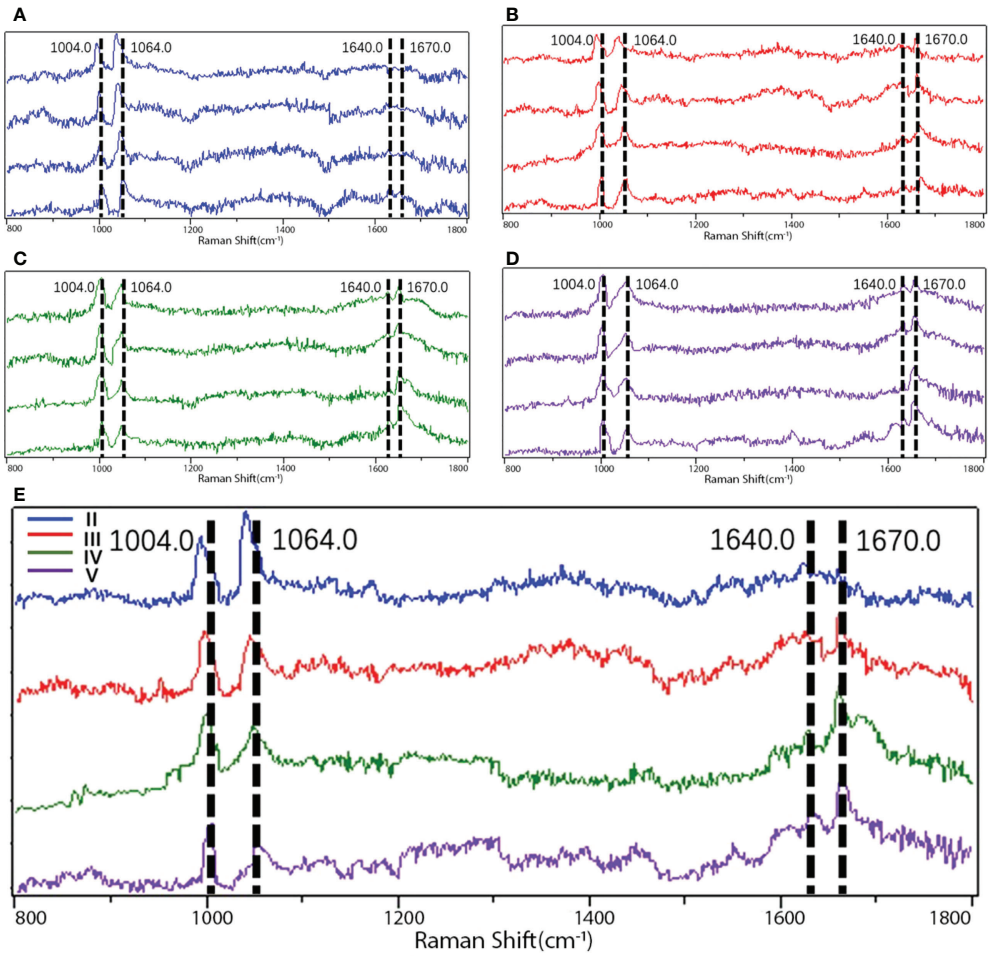

FIGURE 4
Raman spectra images of different Pfirrmann grades. **(A)** Images detected by Raman spectroscopy in Pfirrmann grade II. **(B)** Images detected by Raman spectroscopy in Pfirrmann grade III. **(C)** Images detected by Raman spectroscopy in Pfirrmann grade IV. **(D)** Images detected by Raman spectroscopy in Pfirrmann grade V. **(E)** Comparison among the images in different Pfirrmann grades detected by Raman spectroscopy. $I_{1,004.0}$, peak position of phenylalanine; $I_{1,064.0}$, peak position of proteoglycan; $I_{1640.0}$, peak position of α-helix in amide I; $I_{1670.0}$, peak position of random coil in amide I; *I*, relative intensity.

compared with that in grade II ($P < 0.05$, $P < 0.001$, and $P < 0.001$, respectively). Spearman's correlation analysis demonstrated that the content of amide III was also significantly positively correlated with the Pfirrmann grade ($\rho = 0.9312$, $P < 0.001$, Figure 5C).

Analysis of collagen structure in the samples

We found that the intensity ratio of the two peaks ($I_{1,670}$/$I_{1,640}$; amide I) in grades III, IV, and V was significantly higher compared with that in grade II ($P < 0.05$, $P < 0.001$, and $P < 0.001$, respectively), and the intensity ratio of the two peaks ($I_{1,670}$/$I_{1,640}$; amide I) had shown a significantly positive correlation with the Pfirrmann grade by Spearman's correlation analysis ($\rho = 0.8598$, $P < 0.001$, Figure 5D).

Discussion

To the extent of our knowledge, the present study was the first to characterize the composition and structure of the NP in patients with CDH by Raman spectroscopy, an emerging optical instrument. The Pfirrmann grade was proposed as an early semi-quantitative clinical assessment method to classify IVDD by disc structure, MRI signal intensity, height of disc, and the distinction between NP and AF. The Miyazaki grade (25) was introduced as a subsequent grading system for cervical degeneration since its grading criteria were similar to the Pfirrmann grading, and in view of our team's previous study on lumbar disc degeneration according to the Pfirrmann grade, we choose this grading criteria as a standard reference. Due to the shortcoming of imprecise quantitative analysis of Pfirrmann, the IVDD grading results

10.3389/fendo.2022.1015198

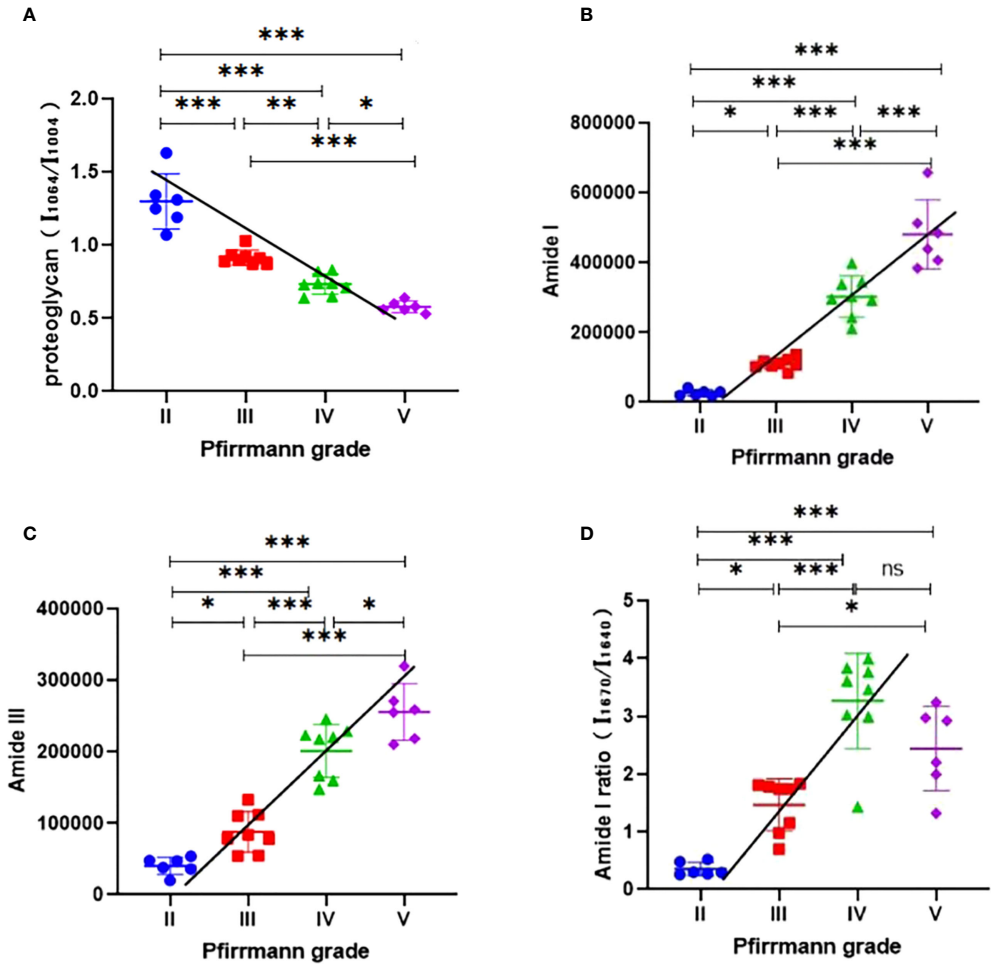

FIGURE 5
(A) Analysis of the relative proteoglycan content ($I_{1,064}/I_{1,004}$) in different Pfirrmann grades; the Spearman's correlation analysis indicated that the relative proteoglycan content ($I_{1,064}/I_{1,004}$) decreased with the increase of Pfirrmann grades. **(B)** Analysis of the content of collagen (amide I) in different Pfirrmann grades; the Spearman's correlation analysis showed that the content of collagen (Amide I) increased with the development of Pfirrmann grades. **(C)** Analysis of the content of collagen (amide III) in different Pfirrmann grades, the Spearman's correlation analysis determined that the content of collagen (amide III) increased with the progression of the Pfirrmann grades. **(D)** Analysis of the intensity ratio of two peaks (I_{1670}/I_{1640}; amide I) in different Pfirrmann grades; the Spearman's correlation analysis found that the intensity ratio of two peaks (I_{1670}/I_{1640}; Amide I) was significantly positively correlated with the Pfirrmann grade. $^{*}P < 0.05$; $^{**}P < 0.01$; $^{***}P < 0.001$; ns, no significance; *I*, relative intensity.

were assessed by κ statistics analysis ($\kappa 1 = 0.620$ and $\kappa 2 = 0.614$); therefore, the grading result is indeed credible. With MRI as one of the common clinical diagnostic techniques for intervertebral disc degeneration, it is more likely to determine disc degeneration in terms of some coefficients such as apparent diffusion coefficient and diffusion-weighted imaging. A previous study has also shown that segmental quantitative T2 grading was able to assess the degree of IVDD (26). However, the connection between these imaging parameters and extracellular matrix changes in IVDD has not been exactly elucidated. We analyzed the correlations between NP T2 signal intensity value and proteoglycan relative content using the bivariate correlation analysis and found that there was a significant correlation between them ($P = 0.912$ and $P < 0.01$) at the 0.01 level (two-tailed). The property of proteoglycans to maintain disc hydration further explains the changes in the MRI T2-weighted signal. Regrettably, it is still not yet possible to characterize the content and structure of the macromolecules within NP through MRI.

Raman spectroscopy is used to determine the composition of a substance by collecting the light scattered from the irradiated substance compared with the characteristic peaks and indirectly reflects the substance content by detecting the intensity of these peaks (27). Proteoglycans, as the main component of NP, form the network of polysaccharide polymers by binding multiple glycosaminoglycan chains in order to maintain intervertebral

disc infiltration and hydration properties (28). A pilot study demonstrated that higher AF/NP glycosaminoglycan ratios tended to associate with higher MRI T2 grades (29). Moreover, we observed that the relative content of proteoglycans ($I_{1,064}/I_{1,004}$) measured by Raman spectroscopy was comparable with the NP T2 signal intensity value. It is worthwhile to mention that both studies illustrated the decrease in proteoglycan content. The previous study found that proteoglycan content was negatively correlated with Pfirrmann grade by light microscopy examination (30). In terms of experimental protocol, this study applied more advanced microscopic techniques to carry out experiments based on changing the animal model to the isolated NP. This is somewhat consistent with the data that we have tested; the relative content of proteoglycans in NP was significantly correlated with Pfirrmann grade. In our previous study, Raman spectroscopy of proteoglycans ($I_{1,064}/I_{1,004}$) in the NP of lumbar disc herniation revealed a significant correlation between Pfirrmann grades IV, V, and III, while no significant differences were found between grades IV and V (31). This is somewhat inconsistent with the results of this study. We consider this because of the uniquely anatomical characteristic of the cervical vertebrae; the cervical intervertebral discs have more probability to degenerate. In the present study, we demonstrated that the proteoglycan content decreased during the progression of the Pfirrmann grade. This also provides some statistical support for the MRI T2-weighted signal intensity change results in our study.

Another significant component within the NP, type II collagen, provides a meshwork for the proteoglycans to attach to while enabling the proteoglycans to be wound more tightly to cope with the corresponding compression and tension forces (32). In the present study, we assayed the major amide moieties of collagen to characterize itself by Raman peak position, respectively. The Raman spectroscopy analysis indicated that the content of amide I and III in grades III, IV, and V was significantly higher compared with that in grade II. As for the Spearman's correlation coefficient, we found that both amide I and amide III contents had a significantly positive correlation with Pfirrmann grade. Our team found similar changes in the NP with lumbar disc herniation; the content of amide I in grades IV and V was higher than in grade III. With regards to amide III, there was no correlation between Pfirrmann grades III and V (31). The interpretation that we think is such that the composition of the disc also varies with level in the spine, with the collagen content of the NP being highest in the cervical discs and lowest in the lumbar discs (33), so the amide III content may be slightly different. We also hypothesized that this may be due to a decrease in the proteoglycan content of the NP and a relative compensatory proliferation of collagen in response to this degenerative condition. In addition, it is also not excluded that the structure of the NP may be further disturbed, and there is the possibility of the outer fibrous ring to break through to the inner layer. The structural disorders of the NP may further lead to the intervertebral disc being dehydrated, deflated, and hardened, which may make the process of herniation more susceptible to happen.

Raman spectroscopy could not only detect changes in NP collagen content but also characterize its secondary structure including α-helices, β-sheets, and random coils (34, 35). Amide I and III groups are the main expressive groups on the Raman spectrum; therefore, the secondary structures of both are usually characterized separately. A previous study indicated that the intensity ratio of the two peaks (I_{1245}/I_{1270}) provides information about the relative content of random *versus* ordered coils in the protein structure and the progression of cartilage dysregulation (36). In our study, we compared the relative contents of disordered coils *vs.* ordered coils to further determine the degree of disorder in the secondary structure of collagen. It was found that the intensity ratio of the two peaks ($I_{1,670}/I_{1,640}$; amide I) was significantly positively correlated with the Pfirrmann grade. Compared with the previous study that we have conducted (31), the present study results include additional Pfirrmann grade II samples and show the comparable results with before. The increase in disordered collagen components further aggravated the degree of structural disorder in NP. These results characterize the secondary structure of disordered collagen by Raman spectroscopy and further have the potential to elucidate the microstructural mechanism of IVDD.

It should be emphasized that this study has several limitations. First, the number of samples that we included was relatively limited, and there was still a lack of some degree of classical histological basis. In future studies, a larger sample composition and experiments like IHC will be applied to further investigate the mechanism of IVDD. Second, the irregularities on the surface of biological materials can significantly affect the peak intensity and background, making the high background expression inherent to the Raman spectroscopy detection process unavoidable. Furthermore, the study was designed for *in vitro* NP samples; thus, the comparative effectiveness of Raman spectroscopy in detecting the composition and structure of macromolecules still needs to be elucidated by *in vivo* studies.

In summary, our results demonstrated that content of macromolecules like proteoglycan and collagen during IVDD and, most importantly, provided a certain elaboration of this process at the microscopic level. The higher relative intensity of the two peak ratios ($I_{1,670}/I_{1,640}$; amide I) detected by Raman spectroscopy may have the potential to become an early effective indicator for the detection of IVDD.

Data availability statement

The raw data supporting the conclusions of this article will be made available by the authors without undue reservation.

Ethics statement

This study was reviewed and approved by the Ethics Committee of Tianjin First Central Hospital. The patients/participants provided their written informed consent to participate in this study.

Author contributions

TZ and ZL conceptualized and designed the study. ZW, XW, TX Z, and EG contributed to the collection and preparation of the samples. TX, ZL, and ZW performed the Raman spectroscopy measurement. ZW and HZ contributed to the acquisition of data. ZW and XW performed the data analysis. ZG and QZ supervised and directed the project. All authors contributed to the article and approved the submitted version.

Funding

This work was supported by a research grant from the Science and Technology Project of the Tianjin Municipal Health Commission (project number MS20020).

Acknowledgments

Thanks to all the teachers and students at the Department of Orthopedics, Tianjin First Central Hospital and the School of Materials Engineering Science and Engineering, Tianjin University.

Conflict of interest

The authors declare that the research was conducted in the absence of any commercial or financial relationships that could be construed as a potential conflict of interest.

Publisher's note

All claims expressed in this article are solely those of the authors and do not necessarily represent those of their affiliated organizations, or those of the publisher, the editors and the reviewers. Any product that may be evaluated in this article, or claim that may be made by its manufacturer, is not guaranteed or endorsed by the publisher.

References

1. Northover JR, Wild JB, Braybrooke J, Blanco J. The epidemiology of cervical spondylotic myelopathy. *Skeletal Radiol* (2012) 41:1543–6. doi: 10.1007/s00256-012-1388-3

2. Zhuang L, Wang L, Xu D, Wang Z, Liang R. Association between excessive smartphone use and cervical disc degeneration in young patients suffering from chronic neck pain. *J Orthop. Sci* (2021) 26:110–5. doi: 10.1016/j.jos.2020.02.009

3. Haldeman S, Nordin M, Chou R, Côté P, Hurwitz EL, Johnson CD, et al. The global spine care initiative: World spine care executive summary on reducing spine-related disability in low- and middle-income communities. *Eur Spine J* (2018) 27:776–85. doi: 10.1007/s00586-018-5722-x

4. Linton SJ. A review of psychological risk factors in back and neck pain. *Spine (Phila Pa 1976)* (2000) 25:1148–56. doi: 10.1097/00007632-200005010-00017

5. Benoist M. Natural history of the aging spine. *Eur Spine J* (2003) 12(Suppl 2): S86–9. doi: 10.1007/s00586-003-0593-0

6. Kepler CK, Ponnappan RK, Tannoury CA, Risbud MV, Anderson DG. The molecular basis of intervertebral disc degeneration. *Spine J* (2013) 13:318–30. doi: 10.1016/j.spinee.2012.12.003

7. Ogon I, Takebayashi T, Takashima H, Morita T, Terashima Y, Yoshimoto M, et al. Imaging diagnosis for intervertebral disc. *JOR Spine* (2020) 3:e1066. doi: 10.1002/jsp2.1066

8. Haughton V. Medical imaging of intervertebral disc degeneration: current status of imaging. *Spine (Phila Pa 1976)* (2004) 29:2751–6. doi: 10.1097/01.brs.0000148475.04738.73

9. Kong K, Kendall C, Stone N, Notingher I. Raman spectroscopy for medical diagnostics–from in-vitro biofluid assays to in-vivo cancer detection. *Adv Drug Delivery Rev* (2015) 89:121–34. doi: 10.1016/j.addr.2015.03.009

10. Keating ME, Byrne HJ. Raman spectroscopy in nanomedicine: current status and future perspective. *Nanomed. (Lond)* (2013) 8:1335–51. doi: 10.2217/nnm.13.108

11. Nima ZA, Biswas A, Bayer IS, Hardcastle FD, Perry D, Ghosh A, et al. Applications of surface-enhanced raman scattering in advanced bio-medical technologies and diagnostics. *Drug Metab Rev* (2014) 46:155–75. doi: 10.3109/03602532.2013.873451

12. Gong B, Oest ME, Mann KA, Damron TA, Morris MD. Raman spectroscopy demonstrates prolonged alteration of bone chemical composition following extremity localized irradiation. *Bone* (2013) 57:252–8. doi: 10.1016/j.bone.2013.08.014

13. Coda S, Siersema PD, Stamp GW, Thillainayagam AV. Biophotonic endoscopy: a review of clinical research techniques for optical imaging and sensing of early gastrointestinal cancer. *Endosc Int Open* (2015) 3:E380–92. doi: 10.1055/s-0034-1392513

14. Pfirrmann CW, Metzdorf A, Zanetti M, Hodler J, Boos N. Magnetic resonance classification of lumbar intervertebral disc degeneration. *Spine (Phila Pa 1976)* (2001) 26:1873–8. doi: 10.1097/00007632-200109010-00011

15. Luoma EK, Raininko R, Nummi PJ, Luukkonen R, Manninen HI, Riihimäki HA. Suitability of cerebrospinal fluid as a signal-intensity reference on MRI: evaluation of signal-intensity variations in the lumbosacral dural sac. *Neuroradiology* (1997) 39:728–32. doi: 10.1007/s002340050496

16. Tsao YT, Huang YJ, Wu HH, Liu YA, Liu YS, Lee OK. Osteocalcin mediates biomineralization during osteogenic maturation in human mesenchymal stromal cells. *Int J Mol Sci* (2017) 18(1):159. doi: 10.3390/ijms18010159

17. Roberts S, Evans H, Trivedi J, Menage J. Histology and pathology of the human intervertebral disc. *J Bone Joint Surg Am* (2006) 88(Suppl 2):10–4. doi: 10.2106/jbjs.F.00019

18. Pudlas M, Brauchle E, Klein TJ, Hutmacher DW, Schenke-Layland K. Non-invasive identification of proteoglycans and chondrocyte differentiation state by raman microspectroscopy. *J Biophotonics* (2013) 6:205–11. doi: 10.1002/jbio.201200064

19. Tuma R, Tsuruta H, Benevides JM, Prevelige PEJr., Thomas GJJr. Characterization of subunit structural changes accompanying assembly of the bacteriophage P22 procapsid. *Biochemistry* (2001) 40:665–74. doi: 10.1021/bi001965y

20. Benevides JM, Overman SA, Thomas GJJr. Raman spectroscopy of proteins. *Curr Protoc Protein Sci* (2004) 17:17.8. doi: 10.1002/0471140864.ps1708s33

21. Nemecek D, Stepanek J, Thomas GJJr. Raman spectroscopy of proteins and nucleoproteins. *Curr Protoc Protein Sci* (2013) 17:7.8. doi: 10.1002/0471140864.ps1708s71

22. Zhang Q, Andrew Chan KL, Zhang G, Gillece T, Senak L, Moore DJ, et al. Raman microspectroscopic and dynamic vapor sorption characterization of

hydration in collagen and dermal tissue. *Biopolymers* (2011) 95:607–15. doi: 10.1002/bip.21618

23. Roach CA, Simpson JV, JiJi RD. Evolution of quantitative methods in protein secondary structure determination *via* deep-ultraviolet resonance raman spectroscopy. *Analyst* (2012) 137:555–62. doi: 10.1039/c1an15755h

24. Galvis L, Dunlop JW, Duda G, Fratzl P, Masic A. Polarized raman anisotropic response of collagen in tendon: towards 3D orientation mapping of collagen in tissues. *PloS One* (2013) 8:e63518. doi: 10.1371/journal.pone.0063518

25. Miyazaki M, Hong SW, Yoon SH, Morishita Y, Wang JC. Reliability of a magnetic resonance imaging-based grading system for cervical intervertebral disc degeneration. *J Spinal Disord Tech.* (2008) 21:288–92. doi: 10.1097/BSD.0b013e31813c0e59

26. Chen C, Huang M, Han Z, Shao L, Xie Y, Wu J, et al. Quantitative T2 magnetic resonance imaging compared to morphological grading of the early cervical intervertebral disc degeneration: an evaluation approach in asymptomatic young adults. *PloS One* (2014) 9:e87856. doi: 10.1371/journal.pone.0087856

27. Mulvaney SP, Keating CD. Raman spectroscopy. *Anal Chem* (2000) 72:145R–57R. doi: 10.1021/a10000155

28. Johnstone B, Bayliss MT. The large proteoglycans of the human intervertebral disc. changes in their biosynthesis and structure with age, topography, and pathology. *Spine (Phila Pa 1976)* (1995) 20:674–84. doi: 10.1097/00007632-199503150-00008

29. Bostelmann R, Bostelmann T, Nasaca A, Steiger HJ, Zaucke F, Schleich C. Biochemical validity of imaging techniques (X-ray, MRI, and dGEMRIC) in degenerative disc disease of the human cervical spine-an in vivo study. *Spine J* (2017) 17:196–202. doi: 10.1016/j.spinee.2016.08.031

30. Che YJ, Guo JB, Liang T, Chen X, Zhang W, Yang HL, et al. Assessment of changes in the micro-nano environment of intervertebral disc degeneration based on pfirrmann grade. *Spine J* (2019) 19:1242–53. doi: 10.1016/j.spinee.2019.01.008

31. Wang X, Meng J, Zhang T, Weijia Lv W, Liang Z, Shi Q, et al. Identifying compositional and structural changes in the nucleus pulposus from patients with lumbar disc herniation using raman spectroscopy. *Exp Ther Med* (2020) 20:447–53. doi: 10.3892/etm.2020.8729

32. Sivan SS, Hayes AJ, Wachtel E, Caterson B, Merkher Y, Maroudas A, et al. Biochemical composition and turnover of the extracellular matrix of the normal and degenerate intervertebral disc. *Eur Spine J* (2014) 23(Suppl 3):S344–53. doi: 10.1007/s00586-013-2767-8

33. Scott JE, Bosworth TR, Cribb AM, Taylor JR. The chemical morphology of age-related changes in human intervertebral disc glycosaminoglycans from cervical, thoracic and lumbar nucleus pulposus and annulus fibrosus. *J Anat* (1994) 184(Pt 1):73–82.

34. Choi S, Jung GB, Kim KS, Lee GJ, Park HK. Medical applications of atomic force microscopy and raman spectroscopy. *J Nanosci. Nanotechnol.* (2014) 14:71–97. doi: 10.1166/jnn.2014.9112

35. Takahashi Y, Sugano N, Takao M, Sakai T, Nishii T, Pezzotti G. Raman spectroscopy investigation of load-assisted microstructural alterations in human knee cartilage: Preliminary study into diagnostic potential for osteoarthritis. *J Mech Behav BioMed Mater* (2014) 31:77–85. doi: 10.1016/j.jmbbm.2013.02.014

36. Kumar R, Singh GP, Grønhaug KM, Afseth NK, de Lange Davies C, Drogset JO, et al. Single cell confocal raman spectroscopy of human osteoarthritic chondrocytes: a preliminary study. *Int J Mol Sci* (2015) 16:9341–53. doi: 10.3390/ijms16059341

frontiers | Frontiers in Endocrinology

TYPE Original Research
PUBLISHED 13 October 2022
DOI 10.3389/fendo.2022.1020743

OPEN ACCESS

EDITED BY
Wu Zhou,
Huazhong University of Science and Technology, China

REVIEWED BY
Yukun Zhang,
Huazhong University of Science and Technology, China
Xinhua Li,
Shanghai General Hospital, China
Weihua Cai,
The First Affiliated Hospital of Nanjing Medical University, China

*CORRESPONDENCE
Shibao Lu
spinelu@163.com

SPECIALTY SECTION
This article was submitted to Bone Research, a section of the journal Frontiers in Endocrinology

RECEIVED 16 August 2022
ACCEPTED 21 September 2022
PUBLISHED 13 October 2022

CITATION
Li Y, Kong C, Wang B, Sun W, Chen X, Zhu W, Ding J and Lu S (2022) Identification of differentially expressed genes in mouse paraspinal muscle in response to microgravity. *Front. Endocrinol.* 13:1020743. doi: 10.3389/fendo.2022.1020743

Identification of differentially expressed genes in mouse paraspinal muscle in response to microgravity

Yongjin Li[1,2], Chao Kong[1,2], Baobao Wang[1,2], Wenzhi Sun[1,2], Xiaolong Chen[1,2], Weiguo Zhu[1,2], Junzhe Ding[1,2] and Shibao Lu[1,2]*

[1]Department of Orthopedics, Xuanwu Hospital, Capital Medical University, Beijing, China, [2]National Clinical Research Center for Geriatric Diseases, Xuanwu Hospital, Capital Medical University, Beijing, China

Lower back pain (LBP) is the primary reason leading to dyskinesia in patients, which can be experienced by people of all ages. Increasing evidence have revealed that paraspinal muscle (PSM) degeneration (PSMD) is a causative contributor to LBP. Current research revealed that fatty infiltration, tissue fibrosis, and muscle atrophy are the characteristic pathological alterations of PSMD, and muscle atrophy is associated with abnormally elevated oxidative stress, reactive oxygen species (ROS) and inflammation. Interestingly, microgravity can induce PSMD and LBP. However, studies on the molecular mechanism of microgravity in the induction of PSMD are strongly limited. This study identified 23 differentially expressed genes (DEGs) in the PSM (longissimus dorsi) of mice which were flown aboard the Bion M1 biosatellite in microgravity by bioinformatics analysis. Then, we performed protein–protein interaction, Gene Ontology function, and Kyoto Encyclopedia of Genes and Genomes pathway enrichment analysis for the DEGs. We found that Il6ra, Tnfaip2, Myo5a, Sesn1, Lcn2, Lrg1, and Pik3r1 were inflammatory genes; Fbox32, Cdkn1a, Sesn1, and Mafb were associated with muscle atrophy; Cdkn1a, Sesn1, Lcn2, and Net1 were associated with ROS; and Sesn1 and Net1 were linked to oxidative stress. Furthermore, Lcn2, Fbxo32, Cdkn1a, Pik3r1, Sesn1, Net1, Il6ra, Myo5a, Lrg1, and Pfkfb3 were remarkably upregulated, whereas Tnfaip2 and Mafb were remarkably downregulated in PSMD, suggesting that they might play a significant role in regulating the occurrence and development of PSMD. These findings provide theoretical basis and therapeutic targets for the treatment of PSMD.

KEYWORDS

paraspinal muscle, differentially expressed genes, microgravity, muscle atrophy, paraspinal muscle degeneration

Introduction

Lower back pain (LBP), including nociceptive, neuropathic, nociplastic, or non-specific pain, is one of the most common musculoskeletal disorders and might be experienced by people of all ages (1–3). As a global public health problem, LBP is known to impose a huge socioeconomic burden worldwide each year (3, 4). The maintenance of spinal stability depends on the coordinated movement of the active subsystem [paraspinal muscles (PSM) and tendons], the passive subsystem (vertebrae, intervertebral discs, and ligaments), and the nervous system (5, 6). The structure and the function disorder of any of the above components might contribute to LBP. The psoas major, multifidus, and erector spinae are the most important muscle groups of the PSM, which exert a critical role in maintaining the upright posture and the sagittal balance of the spine (5, 7, 8). In recent years, increasing evidence have revealed that paraspinal muscle (PSM) degeneration (PSMD) is closely correlated with LBP and spine degenerative diseases, such as intervertebral disc degeneration and scoliosis (9–13). Microgravity is caused by factors such as the residual atmosphere in space, which is reported to affect the metabolism of human muscles and bones by regulating the gene expression and the molecular signaling pathways. The space environment is a microgravity environment; this environment can induce PSMD and intervertebral disc degeneration. Thus, microgravity is also a key contributor to LBP (14–16). Nevertheless, the role and the molecular regulatory mechanisms of microgravity in the induction of PSMD remain largely unknown.

Up to now, most studies focused on multifidus degeneration and spine pathophysiology (9, 10, 17–20). Notably, the degeneration of the erector spinae usually occurs earlier, and the degree of degeneration is more serious than that of the multifidus (5, 21). The erector spinae consists of the iliocostalis lumborum, longissimus dorsi, and spinous muscles. The developing fatty infiltration, tissue fibrosis, and muscle atrophy have long been considered as characteristic pathological alterations of PSMD (9). Muscle atrophy is associated with abnormally elevated oxidative stress, reactive oxygen species (ROS), and inflammation (15, 22). Altered gene expression appears to be a hallmark pathological feature of PSMD. Yang et al. (23) found that the serum CXC chemokine ligand 10 concentrations were significantly increased in patients with PSMD compared with patients without PSMD. Kudo et al. (19) observed that anti-muscular dystrophy gene peroxisome proliferator-activated receptor gamma coactivator 1 alpha (PGC-1α) as well as pro-inflammatory cytokines TNF-α and IL-6 were significantly increased in multifidus from patients with lumbar kyphosis (a reduced lumbar lordosis) compared with normal lumbar lordosis. The genes of the PSM were also differentially expressed in microgravity. Yamakuchi et al. (24) found that 42 genes were differentially expressed in the PSM of rats after 14 days of space flight, among which the heat shock protein 70 and t complex polypeptide 1 were increased, whereas myocyte-specific enhancer binding factor 2C, aldolase A, and muscle ankyrin were decreased. Mirzoev et al. (25) found that ubiquitin ligase MURF-1 was upregulated in the longissimus dorsi of mice after a flight of 30 days. Ogneva et al. (26) found that the content of α-actinin-1/4 and β-actin, respectively, were decreased in the skeletal muscle of mice after a space flight on board the BION-M1 biosatellite for 30 days. However, the effects of microgravity on the gene expression of the longissimus dorsi (erector spinae) remain unclear.

Gambler and colleagues studied the global gene expression profile in the longissimus dorsi of C57BL/N6 male mice after a space flight of 30 days and reported that several genes were associated with insulin resistance and PSM metabolism (27). In this study, we re-analyzed this microarray dataset (GSE94381) downloaded from the public open Gene Expression Omnibus (GEO) database (http://www.ncbi.nlm.nih.gov/geo) (28). R software was used to identify the differentially expressed genes (DEGs). Gene Ontology (GO) and Kyoto Encyclopedia of Genes and Genomes (KEGG) enrichment analysis were performed to predict the potential biological functions of the DEGs.

Materials and methods

Analysis of the mRNA microarray dataset

The GSE94381 microarray dataset was downloaded from GEO database through R software GEOquery package (29). The probes corresponding to multiple molecules for one probe were removed, and we kept only the probes with the largest signal value when encountering probes corresponding to the same molecule. The data was then standardized using the normalizeBetweenArrays function of the limma package in R software. Limma package was also used to identify the DEGs according to the following criteria: $-\log_{10}$ (*P*-value) > $\log_{10}$ 20 and $|\log_2$ fold-change (FC)| > 1. The Ggplot2 package in R software was used to analyze and visualize the clustering situation between the different groups (30). The Ggplot2 package was also used to visualize the principal component analysis (PCA), uniform manifold approximation and projection (UMAP), and volcano plots. The heat map was visualized using the complexheatmap package (31).

Venn diagram analysis

In the GSE94381 microarray dataset, the mice were divided into three groups: Bion-flown (BF), Bion ground (BG), and flight

control (FC) group (28). The DEGs between the BG and BF groups, the FC and BF groups, as well as the FC and BG groups were intersected to select overlapping genes using http://www.bioinformatics.com.cn, a free online platform for data analysis.

GO and KEGG pathway enrichment analysis

The potential biological functions of the DEGs were predicted through GO and KEGG enrichment analysis. The GO database divides the gene functions into three parts: cellular component (CC), molecular function (MF), and biological process (BP). CC is used to describe the location of gene products in cells, such as endoplasmic reticulum or nucleus; MF mostly refers to the functions of individual gene products, such as binding activity or catalytic activity; while BP mostly refers to an orderly biological process with multiple steps, such as cell growth, apoptosis, and signal transduction. The KEGG pathway analysis is a comprehensive database that integrates genomic, chemical, and systemic functional information. KEGG has four major categories and 17 sub-databases, one of which is called the KEGG pathway. The results of the GO and KEGG analyses were visualized using an online tool (http://www.bioinformatics.com.cn).

Identification of oxidative stress-related genes and ferroptosis-related genes

The ferroptosis-related genes (FRGs) were obtained from the FerrDb V2 database (http://www.zhounan.org/ferrdb/) (32), including ferroptosis driver, suppressor, marker, and unclassified regulator, which is shown in Supplementary Table S1. The oxidative stress-related genes (OSRGs) were obtained from the molecular signature database (https://www.gsea-msigdb.org/gsea/msigdb/index.jsp) (33) and are listed in Supplementary Table S2.

Protein–protein interaction network construction

The Search Tool for the Retrieval of Interacting Genes (STRING) database (https://cn.string-db.org/) was widely utilized to assess protein–protein interactions (PPIs) in functional protein association networks (34). Then, we input the DEGs into the multiple protein section of the STRING database and set the organisms as "Mus musculus" to construct the PPI network. The "required score" was set at >0.4. Finally, we generated and downloaded the results of the PPI network analysis.

Statistical analysis

The expression data of several key genes in the GSE94381 dataset were analyzed and visualized using GraphPad Prism software. The statistical significance between the two groups was compared by an unpaired Student's *t*-test, whereas the differences among more than two groups were evaluated by one-way analysis of variance followed by Turkey's multiple-comparisons test. The results were expressed as mean ± standard deviation. *P*-value <0.05 was determined to statistical significance (** represents $p < 0.01$ and *** represents $p < 0.001$).

Results

Evaluation of the reasonableness of the sample and grouping

To explore the DEGs that can regulate PSMD in microgravity, we analyzed the microarray dataset GSE94381. The basic information of GSE94381 is shown in Table 1. Given that the BF group of mice (experimental group) was flown aboard the Bion M1 biosatellite in microgravity, the authors designed the BG group wherein mice were housed in the same condition but exposed to Earth's gravity and the FC group wherein mice were housed in a standard animal facility to rule out the effect of housing conditions. We analyzed the transcriptome of the BG–BF group, the FC–BF group, and the FC–BG group, respectively.

PCA is a technique for simplifying datasets, which reflects the difference and the distance between different samples by presenting multiple sets of data on the coordinate axis. The closer the distance in the PCA diagram, the more similar the sample composition. As shown in Figures 1A–C, the distance between the same group of samples was closer, while the samples between the BG and BF groups, the FC and BF groups, as well as the FC and BG groups were separated, suggesting that the within-group differences were smaller, while the differences between groups were obvious, and there may be more meaningful results in the subsequent difference analysis. The UMAP plot could clearly distinguish the different groups, which further supported the rationality of sample grouping (Figures 1D–F). The box plot was utilized to confirm the distribution trends of the hybridization data and the degree of dispersion. As shown in Figures 1G–I, we did not observe

TABLE 1 Basic information on GSE94381.

Dataset	Platform	Samples	RNA	Year	Organism	Region
GSE94381	GPL8321	5/5/5	mRNA	2017	*Mus musculus*	China

10.3389/fendo.2022.1020743

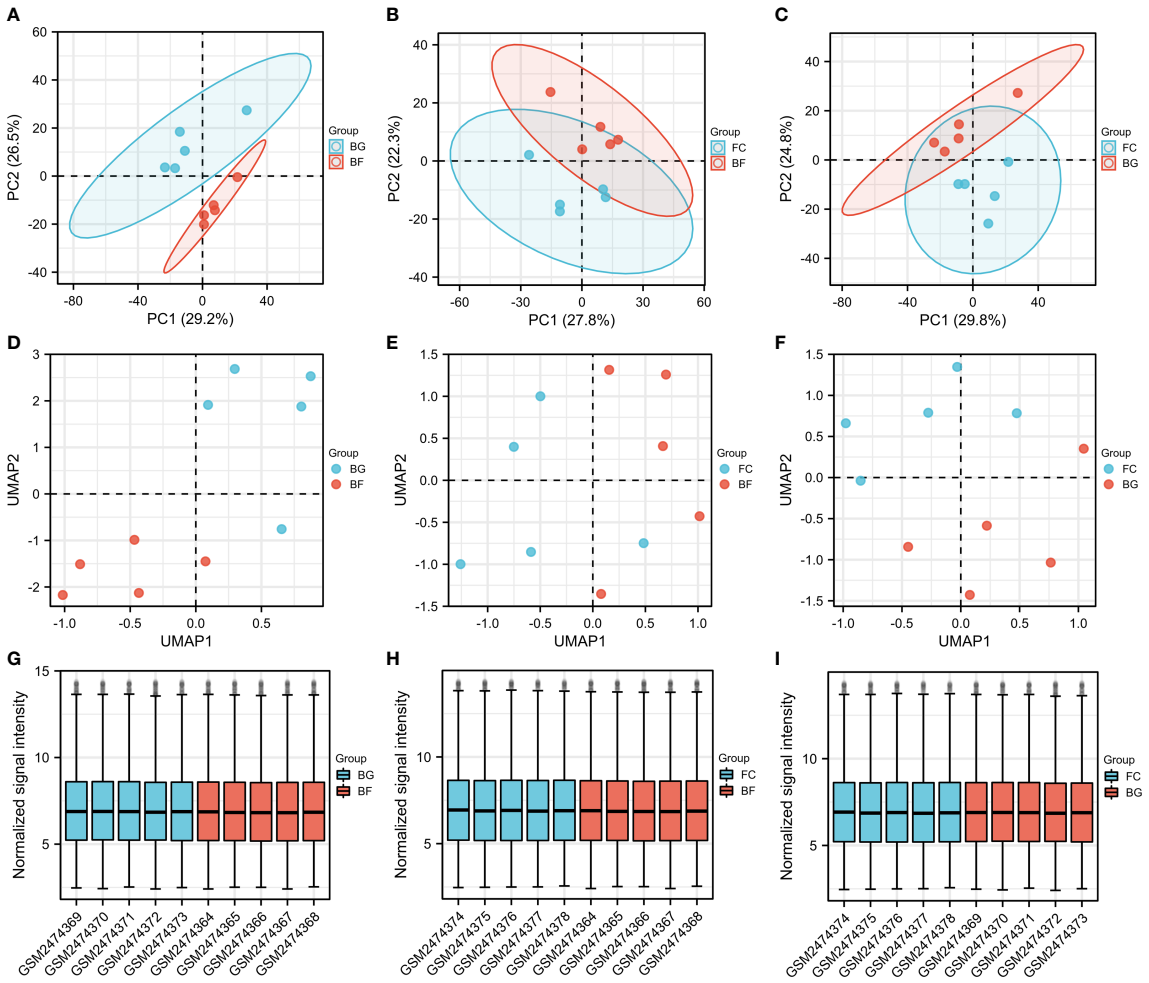

FIGURE 1
Evaluation of the reasonableness of the sample and grouping. **(A–C)** Principal component analysis diagrams. The horizontal and vertical coordinates show the relative distance among different samples. **(D–F)** Uniform manifold approximation and projection diagrams. **(G–I)** Box plots of samples—normalized. The X-axis represents samples, and the Y-axis represents normalized signal intensity.

abnormal distributions of data in the six different samples, revealing that the data have already been standardized.

Identification of the DEGs

In our study, the thresholds of $-\log_{10}$ (*P*-value) > $\log_{10}$ 20 and | log2 (FC)| > 1 were used to select the DEGs. The volcano plots were used to evaluate the gene expression variation among different groups. The cluster heat map showed the first 20 DEGs. A total of 27 DEGs were downregulated and 40 DEGs were upregulated between the BG and BF groups (Figures 2A, D), 16 DEGs were downregulated and 30 DEGs were upregulated between the FC and BF groups (Figures 2B, E), and 11 DEGs were downregulated and 21 DEGs were upregulated between the FC and BG groups (Figures 2C, F).

First, a total of 32 DEGs were identified between two control groups. Second, we observed that there were only five overlapping DEGs by intersecting BG–BF and FC–BG as well as 10 DEGs by intersecting FC–BF and FC–BG through Venn analysis (Figure 3A), suggesting that the BION-M1 biosatellite, on its own, hardly affected the alteration of gene expression in flown mice muscle compared with the ground control (BG). We also found 23 overlapping DEGs by intersecting BG–BF and FC–BF (Figure 3A); then, we determined to study the functions of these DEGs.

KEGG pathway enrichment analysis

Functional enrichment analysis is critical for elucidating high-throughput omics data in life science. The KEGG

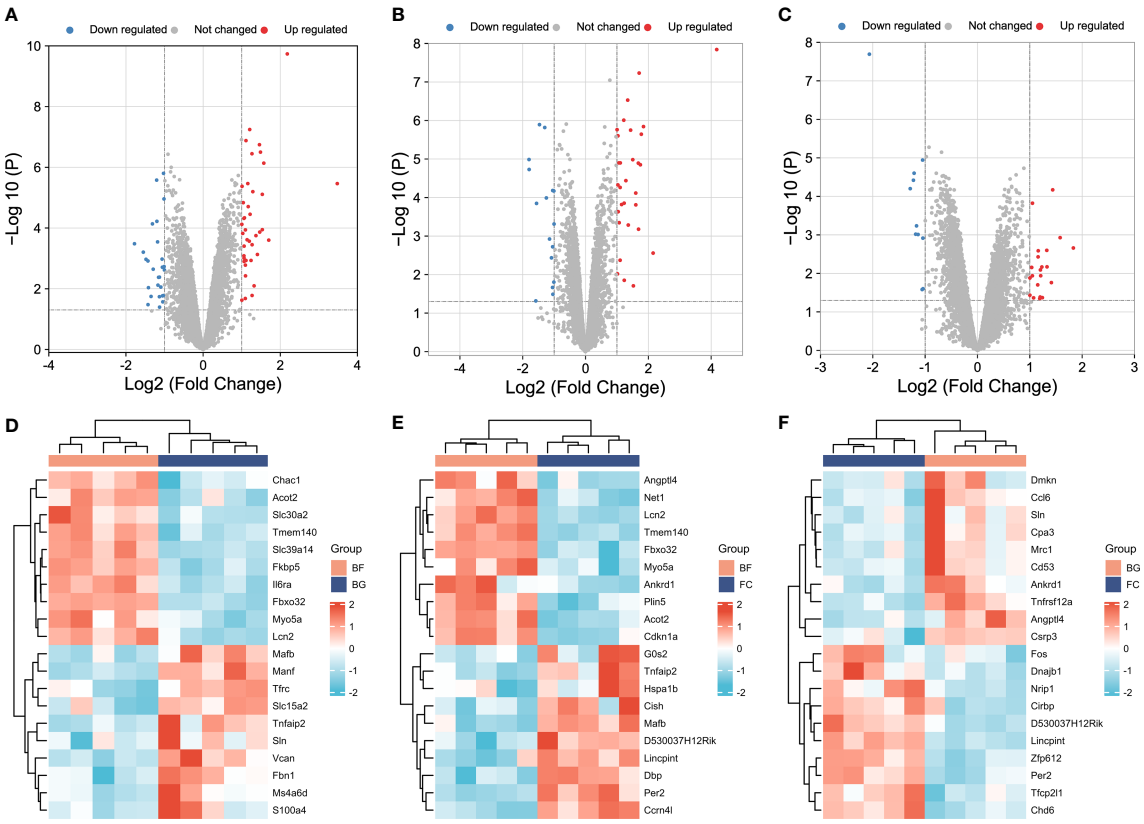

FIGURE 2
Identification of differentially expressed genes (DEGs) among different groups. **(A–C)** Volcano plots showing the gene expression variation among different groups. **(D–F)** Hierarchical clustering of the first 20 DEGs [-$\log_{10}$ (*P*-value) > $\log_{10}$ 20]. In the heat map, the red color indicates the upregulated DEGs, and the green color indicates the downregulated DEGs. In the volcano plot, the X-axis is fold change ($\log_2$), and the Y-axis is *P* (–$\log_{10}$). The red points indicate the upregulated DEGs, the blue points indicate the downregulated DEGs, and the gray points indicate the genes that are not differentially expressed.

pathway enrichment analysis showed that the 23 DEGs were enriched in the HIF-1 signaling pathway, FoxO signaling pathway, bladder cancer, JAK-STAT signaling pathway, endometrial cancer, renal cell carcinoma, p53 signaling pathway, melanoma, non-small cell lung cancer, and glioma (Figure 3B). Furthermore, Il6ra, pik3r1, and Cdkn1a were involved in the regulation of JAK-STAT signaling pathway and HIF-1 signaling pathway, thereby mediating cell cycle, proliferation, apoptosis, inflammatory response, *etc.* (Figures 3C, D, F). Sesn1 and Cdkn1a might regulate DNA repair and damage prevention and cell cycle arrest through mediating the p53 signaling pathway (Figures 3C, E). Additionally, Fbox32, pik3r1, and Cdkn1a were involved in the regulation of FoxO signaling pathway, which can regulate muscle atrophy, cell cycle, *etc.* (Figures 3C, G).

GO functional enrichment analysis

To further predict the functions of DEGs, we conducted GO functional enrichment analysis. GO function annotations included BP, MF, and CC. As shown in Figures 4A, B, the top 10 BP terms were enriched in the negative regulation of osteoclast differentiation, cellular response to radiation, regulation of smooth muscle cell proliferation, response to reactive oxygen species, negative regulation of myeloid leukocyte differentiation, response to steroid hormone, *etc.*, of which lipocalin-2 (Lcn2), sestrin 1 (Sesn1), and neuroepithelial cell transforming 1 (Net1) were involved in the regulation of cell response to reactive oxygen species, interleukin 6 receptor alpha (Il6ra), phosphatidylinositol 3-kinase, regulatory subunit polypeptide 1 (Pik3r1), and cyclin-dependent kinase inhibitor p21 (Cdkn1a) were involved in the

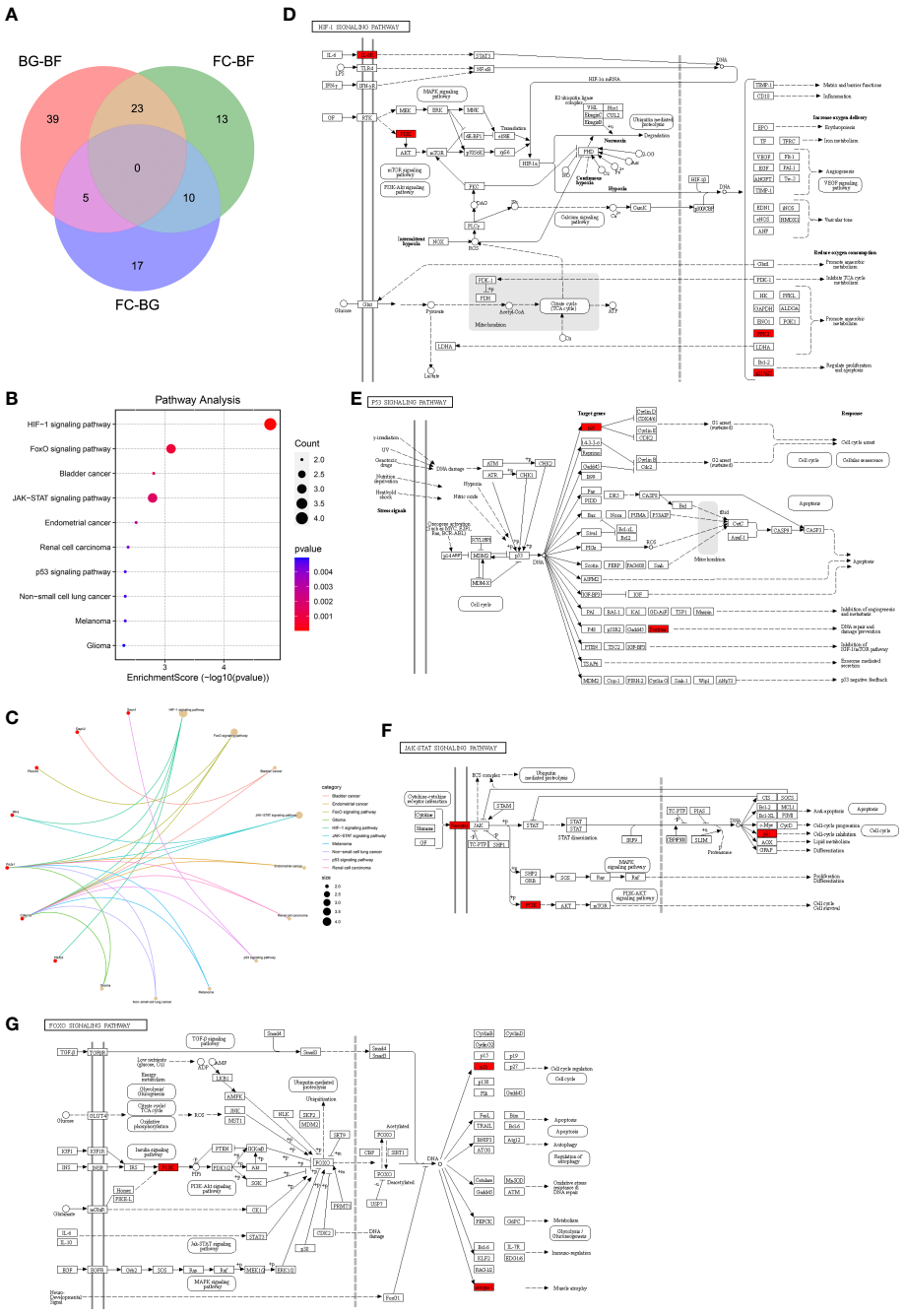

FIGURE 3
Kyoto Encyclopedia of Genes and Genomes (KEGG) pathway enrichment analysis. **(A)** The 23 overlapping differentially expressed genes (DEGs) between the BG–BF group and the FC–BF group were selected using Venn analysis. **(B, C)** KEGG pathway enrichment analysis of the 23 DEGs. **(D)** KEGG analysis of the HIF signaling pathway. **(E)** KEGG analysis of the p53 signaling pathway. **(F)** KEGG analysis of the JAK-STAT signaling pathway. **(G)** KEGG analysis of the FOXO signaling pathway.

regulation of smooth muscle cell proliferation, and muscle atrophy F-box32 (Fbxo32), Pik3r1, and Niemann-Pick C1 protein (Npc1) were related to "response to steroid hormone". Mafb was involved in the negative regulation of osteoclast and myeloid leukocyte differentiation. The CC were predicted to be predominantly enriched in the following terms: insulin-responsive compartment, GATOR2 complex, TORC2 complex, postsynaptic actin cytoskeleton, TOR complex, Seh1-associated complex, filopodium tip, exocyst, postsynaptic cytoskeleton, and transferase complex—transferring phosphorus-containing

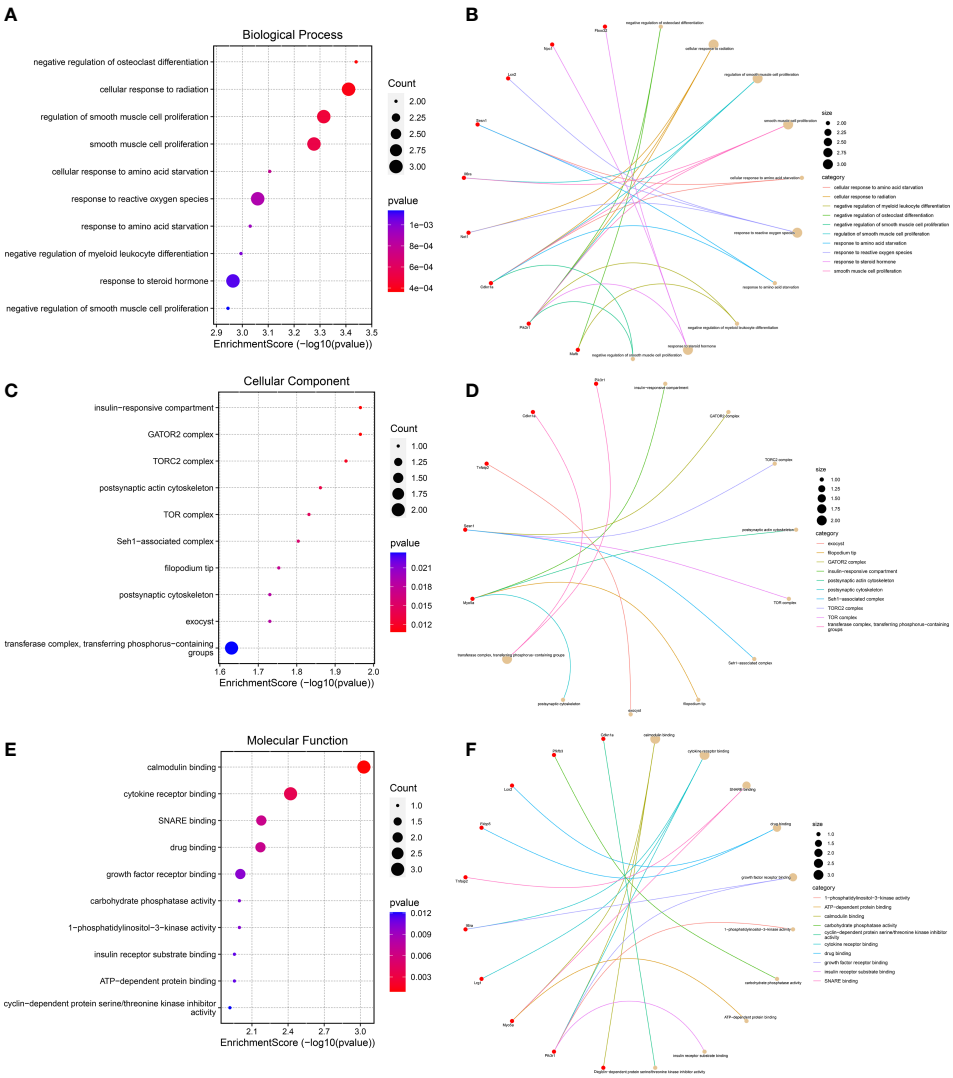

FIGURE 4
Gene Ontology functional enrichment analysis. **(A, B)** Top 10 biological processes in which the 23 genes may be involved. **(C, D)** The top 10 cellular components were displayed as bubble diagram and cnetplot. **(E, F)** The enrichment of the top 10 molecular functions was displayed by a bubble diagram and cnetplot.

groups, of which sesn1 was related to "GATOR2 complex, TORC2 complex, TOR complex, and Seh1-associated complex", and Pik3r1 and Cdkn1a were related to "transferase complex, transferring phosphorus-containing groups" (Figures 4C, D). The genes involved in MF are as follows: calmodulin binding, cytokine receptor binding, SNARE binding, growth factor receptor binding, 1-phosphatidylinositol-3-kinase activity, carbohydrate phosphatase activity, insulin receptor substrate binding, and cyclin-dependent protein serine/threonine kinase inhibitor activity—of which Il6ra was involved in cytokine receptor binding and growth factor receptor binding, and Pik3r1 was related to "calmodulin binding, cytokine receptor binding, growth factor receptor binding, 1-phosphatidylinositol-3-kinase activity, and insulin receptor substrate binding" (Figures 4E, F).

Identification of PSMD-related DEGs

Given that the abnormally increased oxidative stress, ROS, and inflammation and muscle atrophy are the important pathological mechanism of PSMD, the aim of this study was to explore the relevant genes. Ferroptosis is iron-dependent cell death, and the production of a large number of ROS is its hallmark pathological feature (35). A total of 567 FRGs were identified from the FerrDb database *via* intersecting ferroptosis

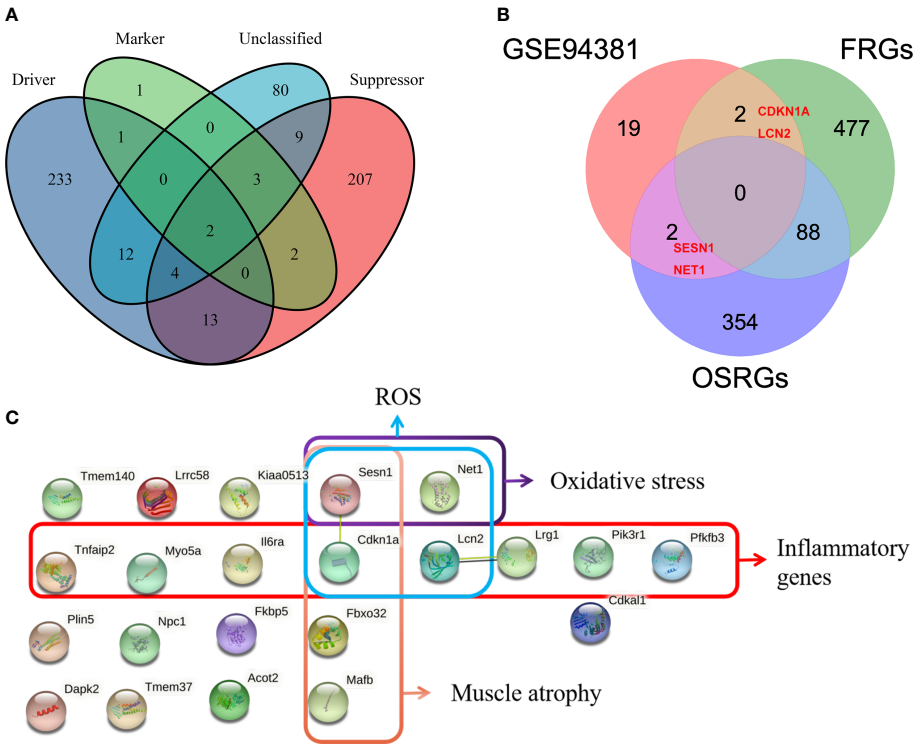

FIGURE 5
Identification of paraspinal muscles (PSM) degeneration-related differentially expressed genes (DEGs). **(A)** Venn diagram showing that a total of 567 different ferroptosis-related genes (FRGs) were obtained from the FerrDb V2 database. **(B)** Venn analysis was used to identify FRG- and oxidative stress-related genes from 23 DEGs. **(C)** Protein–protein interaction network analysis of the 23 DEGs, of which muscle atrophy-, ROS-, oxidative stress-, and inflammation-related genes were checked.

driver, suppressor, marker, and unclassified regulator (Figure 5A). Thus, we merged FRGs, OSRGs, and DEGs to determine the PSMD-related DEGs. The result unveiled that Cdkn1a and Lcn2 were related to ROS and that Sesn1 and Net1 were associated with oxidative stress as well (Figure 5B). Using the STRING database, we constructed a PPI network of 23 DEGs and visualized them (Figure 5C). Combining literature reports and the results of functional enrichment analysis, we determined that Il6ra, TNF-α-inducible protein 2 (Tnfaip2), myosin Va (Myo5a), Sesn1, Lcn2, leucine-rich α-2 glycoprotein1 (Lrg1), and Pik3r1 were inflammatory genes; Fbox32, Cdkn1a, Sesn1, and musculoaponeurotic fibrosarcoma oncogene (MAF)/MAF family B (Mafb) were associated with muscle atrophy; Cdkn1a, Sesn1, Lcn2, and Net1 were associated with ROS; and Sesn1 and Net1 were linked to oxidative stress (Figure 5C).

The expression of PSMD-related DEGs in GSE94381

Through the abovementioned analysis, we found that Lcn2, Fbxo32, Cdkn1a, Pik3r1, Sesn1, Net1, Il6ra, Myo5a, Lrg1, and phosphofructo-2-kinase/fructose-2,6- biophosphatase 3 (Pfkfb3), Tnfaip2, and Mafb might play a significant role in regulating the development of longissimus dorsi muscle in mice. Subsequently, we analyzed their expression in different groups. Compared with the FC and BG groups, Lcn2, Fbxo32, Cdkn1a, Pik3r1, Sesn1, Net1, Il6ra, Myo5a, Lrg1, and Pfkfb3 were significantly upregulated, whereas Mafb and Tnfaip2 were significantly downregulated in the BF group (Figures 6A–N).

Discussion

Spinal degeneration and instability are not only due to changes in bone and intervertebral disc structure and function but also to PSMD. The limitation of the current research on the PSM is that they only measure the morphological parameters of PSM on T2-weighted magnetic resonance imaging, including cross-sectional area, fat infiltration rate, *etc.* The understanding of the molecular pathological mechanism of PSMD is very limited. This year, Anderson et al. (36) collected multifidus muscle for biopsy and confirmed that pro-fibrogenic and pro-atrophic genes were upregulated and that anti-fibrogenic and

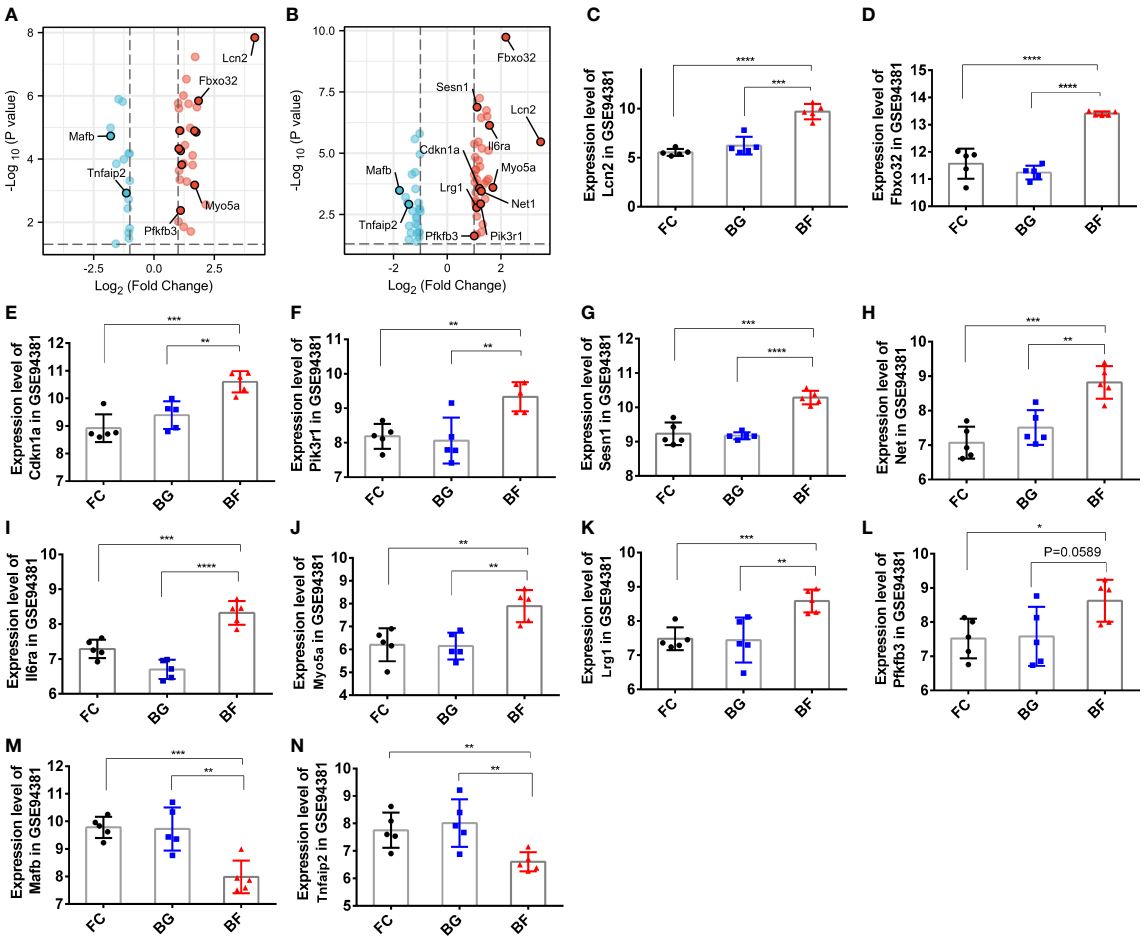

FIGURE 6
Expression of paraspinal muscles degeneration (PSMD)-related differentially expressed genes (DEGs) in the GSE94381 dataset. **(A)** Volcano plot visualizing the differential expression of PSMD-related DEGs between the flight control (FC) group and the Bion-flown (BF) group in the GSE94381 dataset. **(B)** Volcano plot visualizing the differential expression of PSMD-related DEGs between Bion ground (BG) and BF groups in the GSE94381 dataset. **(C–N)** Expression of Lcn2, Fbox32, Cdkn1a, Pik3r1, Sesn1, Net1, Mafb, Il6ra, Myo5a, Tnfaip2, Lrg1, and Pfkfb3 in the FC, BG, and BF groups. * represents p<0.05, ** represents p<0.01 and *** represents p<0.001.

inflammatory genes were downregulated in patients with lumbar spine pathology. Nevertheless, the research on the molecular mechanism of longissimus dorsi muscle is still a blank. Gambler et al. (27) observed moderate signs of longissimus dorsi atrophy in mice after a space flight of 30 days by performing hematoxylin–eosin, immunohistochemical, and immunofluorescence analyses of longissimus dorsi in mice. This study re-analyzed the gene expression profile of the longissimus dorsi of mice exposed to microgravity for 30 days and found that several DEGs were correlated to oxidative stress, ROS, inflammation, and muscle atrophy, which are the pathogenesis of PSMD.

PSM atrophy is a health problem that is currently receiving increasing attention. Identifying the relevant molecular mechanisms and blocking or alleviating PSM atrophy is therefore of utmost importance, yet the mechanisms leading to muscle atrophy are largely unclear. PSM atrophy may be driven by changes in molecules linked to oxidative stress, ROS, and inflammation (9, 15, 22, 37). Growing evidence has revealed that microgravity can alter the expression levels of muscle atrophy-related genes (15, 24–26). To further study the molecular mechanisms of muscle atrophy in response to microgravity, we performed bioinformatics analysis. Muscle-specific ubiquitin E3 ligase Fbox32 (atrogin-1) was reported to be highly expressed in muscle atrophy and inflammation (38). Anderson *et al.* (36) demonstrated that FBXO32 was found to be remarkably increased in multifidus muscle from 59 patients with lumbar spine pathology by quantitative polymerase chain reaction. Our study also predicted that Fbox32 was upregulated under microgravity, which was consistent with Gambler's result (27). Another E3 ligase muscle atrophy F-Box (MAFb) was downregulated under microgravity (22, 27). Mahmassani *et al.*

(39) demonstrated that the expression of MAFB was downregulated in older adults and associated with the change in leg muscle mass. These findings are consistent with the results of our analysis. Additionally, the cyclin-dependent kinase inhibitor P21 (Cdkn1a) is an inducer of cell cycle arrest and senescence-associated gene, which also serves as a mediator in controlling muscle atrophy (40, 41) and inflammation (42). Kumar et al. (37) demonstrated that microgravity can substantially induce Cdkn1a expression, which is in agreement with our data. Sestrin 1 (Sesn1) was verified to be significantly downregulated in several models of muscle atrophy, including sarcopenia, and protect muscles against aging-induced atrophy (43). However, Sesn1 was significantly upregulated in mouse PSM in response to microgravity, but its roles and mechanism deserve further study. Thus, Sesn1, Cdkn1a, Fbox32, and Mafb might play a pivotal role in muscle atrophy under microgravity.

Chronic muscle inflammation may contribute to the rapid loss of muscle mass, function, and myofibrillar proteins. Our study observed that Il6ra, Pik3r1, and Lrg1 were involved in cytokine receptor binding; Cdkn1a, Il6ra, Pik3r1, and Pfkfb3 were found as well to belong to the HIF-1 signaling pathway *via* GO and KEGG pathway enrichment analysis. Furthermore, Li et al. (44) reported that the inflammatory gene PIK3R1 was remarkably overexpressed in the total T cells in COVID-19 patients. Liu et al. (45) demonstrated that leucine-rich α-2 glycoprotein 1 (LRG1) may prevent renal fibrosis by inhibiting the inflammatory response and pro-fibrotic cytokines. Interleukin (IL)-6 is a common pro-inflammatory cytokine that regulates many inflammatory pathways. IL6RA is an IL6 receptor. Frempah et al. (46) demonstrated that the absence of IL6RA in keratinocytes can promote an inflammatory response. Wang et al. (47) confirmed that the inhibition of PFKFB3 significantly attenuated the inflammatory response in human valve interstitial cell. Faust et al. (42) found that the decrease in Cdkn1a expression paralleled the reduction in cartilage tissue inflammation, suggesting that Cdkn1a may be associated with cartilage inflammation in osteoarthritis. TNFAIP2, a TNF-α-induced protein, which was an inflammatory-responsive molecule for TNF-α and was upregulated in spinal cord ischemia/reperfusion injury patients (48). Additionally, the expression of protease-activated receptors (PAR) is associated with inflammation, and MYO5A is a PAR1-dependent transcript, which has been implicated in the inflammatory process (49). LCN2, an inflammation-related factor with elevated expression in the skeletal muscle of ob/ob mice with sarcopenia, is associated with muscle atrophy-related inflammation and oxidative stress (50). Keping et al. (51) demonstrated that SESN1 inhibited oxidized low-density lipoprotein-induced activation of NK-κB signaling and reduced the expression of pro-inflammatory cytokines in macrophages. Collectively, the abovementioned studies unveiled that Pfkfb3, Il6ra, Tnfaip2, Myo5a, Sesn1, Lcn2, Irg1, and Pik3r1 were inflammatory genes, suggesting that they might exert a key role in the pathogenesis of PSMD.

Other causes of inducing muscle atrophy are oxidative stress and ROS, which were confirmed to promote muscle protein catabolism and inhibit protein synthesis signaling pathways (52–54). In addition to mediating inflammation and muscle atrophy, Cdkn1a was also involved in the regulation of oxidative stress and ROS under microgravity (37). Sesn1 belongs to the family of stress-inducible proteins that regulate oxidative stress and ROS, thus protecting the cells from various stimuli (55). Additionally, Lcn2 was confirmed to promote mitochondrial ROS production and alleviate mitochondrial oxidative phosphorylation in rat primary cardiomyocytes (56). However, whether they mediate PSMD *via* regulating ROS and oxidative stress is an interesting problem which needs future experiments to be verified.

Our study recognizes some limitations. First, the data was downloaded from GEO database, and we did not perform RNA sequencing. Second, we did not perform molecular biology and animal experiments to demonstrate the expression and the roles of the 12 key DEGs in longissimus dorsi muscle in mice. Lastly, there are inherent differences between mice and humans, so the generalization of mouse findings to humans is limited.

Conclusion

In conclusion, a total of 23 DEGs were observed to be remarkably dysregulated in the PSM of mice in microgravity by bioinformatics analysis. Moreover, we found that Il6ra, Tnfaip2, Myo5a, Sesn1, Lcn2, Lrg1, and Pik3r1 were linked to inflammatory response; Fbox32, Cdkn1a, Sesn1, and Mafb were associated with muscle atrophy; Cdkn1a, Sesn1, Lcn2, and Net1 were associated with ROS; and Sesn1 and Net1 were linked to oxidative stress. Notably, Sesn1 was involved in the regulation of inflammatory response, muscle atrophy, ROS, and oxidative stress. These results suggest that they might be a therapeutic candidate target for PSMD treatment.

Data availability statement

The original contributions presented in the study are included in the article/Supplementary Material. Further inquiries can be directed to the corresponding author.

Author contributions

SL and YL: conceived and designed this study. YL: wrote the manuscript. SL: critically reviewed and revised the manuscript.

CK, BW, and WS: helped with the bioinformatics analysis. WZ, XC, and JD: created the figures and tables. YL is the only first author. All authors contributed to the article and approved the submitted version.

Funding

This research was funded by the R&D Program of Beijing Municipal Education Commission (KZ/KM/SZ/SM2022100250**) and Beijing Municipal Medical Science Institute—Public Welfare Development Reform Pilot Project (Capital Medical Research no. 2019-2).

Conflict of interest

The authors declare that the research was conducted in the absence of any commercial or financial relationships that could be construed as a potential conflict of interest.

Publisher's note

Supplementary material

The Supplementary Material for this article can be found online at: https://www.frontiersin.org/articles/10.3389/fendo.2022.1020743/full#supplementary-material

SUPPLEMENTARY TABLE 1
Detailed information on ferroptosis-related genes.

SUPPLEMENTARY TABLE 2
Detailed information on oxidative stress-related genes.

References

1. Vos T, Lim SS, Abbafati C, Abbas KM, Abbasi M, Abbasifard M, et al. Global burden of 369 diseases and injuries in 204 countries and territories, 1990-2019: A systematic analysis for the global burden of disease study 2019. *Lancet (London England)* (2020) 396(10258):1204–22. doi: 10.1016/s0140-6736(20)30925-9

2. Hartvigsen J, Hancock MJ, Kongsted A, Louw Q, Ferreira ML, Genevay S, et al. What low back pain is and why we need to pay attention. *Lancet (London England)* (2018) 391(10137):2356–67. doi: 10.1016/s0140-6736(18)30480-x

3. Knezevic NN, Candido KD, Vlaeyen JWS, Van Zundert J, Cohen SP. Low back pain. *Lancet (London England)* (2021) 398(10294):78–92. doi: 10.1016/s0140-6736(21)00733-9

4. Dieleman JL, Cao J, Chapin A, Chen C, Li Z, Liu A, et al. Us health care spending by payer and health condition, 1996-2016. *Jama* (2020) 323(9):863–84. doi: 10.1001/jama.2020.0734

5. Panjabi MM. The stabilizing system of the spine. part i. function, dysfunction, adaptation, and enhancement. *J Spinal Disord* (1992) 5(4):383–9. doi: 10.1097/00002517-199212000-00001

6. Panjabi MM. The stabilizing system of the spine. part ii. neutral zone and instability hypothesis. *J Spinal Disord* (1992) 5(4):390–6. doi: 10.1097/00002517-199212000-00002

7. Jun HS, Kim JH, Ahn JH, Chang IB, Song JH, Kim TH, et al. The effect of lumbar spinal muscle on spinal sagittal alignment: Evaluating muscle quantity and quality. *Neurosurgery* (2016) 79(6):847–55. doi: 10.1227/neu.0000000000001269

8. Masaki M, Ikezoe T, Fukumoto Y, Minami S, Tsukagoshi R, Sakuma K, et al. Association of sagittal spinal alignment with thickness and echo intensity of lumbar back muscles in middle-aged and elderly women. *Arch Gerontology Geriatrics* (2015) 61(2):197–201. doi: 10.1016/j.archger.2015.05.010

9. Noonan AM, Brown SHM. Paraspinal muscle pathophysiology associated with low back pain and spine degenerative disorders. *JOR Spine* (2021) 4(3):e1171. doi: 10.1002/jsp2.1171

10. Cho TG, Park SW, Kim YB. Chronic paraspinal muscle injury model in rat. *J Kor Neurosurgical Soc* (2016) 59(5):430–6. doi: 10.3340/jkns.2016.59.5.430

11. Hey HWD, Lam WMR, Chan CX, Zhuo WH, Crombie EM, Tan TC, et al. Paraspinal myopathy-induced intervertebral disc degeneration and thoracolumbar kyphosis in Tsc1mko mice model-a preliminary study. *Spine J Off J North Am Spine Soc* (2022) 22(3):483–94. doi: 10.1016/j.spinee.2021.09.003

12. Özcan-Ekşi EE, Ekşi M, Turgut VU, Canbolat Ç, Pamir MN. Reciprocal relationship between multifidus and psoas at L4-L5 level in women with low back pain. *Br J Neurosurg* (2021) 35(2):220–8. doi: 10.1080/02688697.2020.1783434

13. Kalichman L, Carmeli E, Been E. The association between imaging parameters of the paraspinal muscles, spinal degeneration, and low back pain. *BioMed Res Int* (2017) 2017:2562957. doi: 10.1155/2017/2562957

14. Sayson JV, Hargens AR. Pathophysiology of low back pain during exposure to microgravity. *Aviation space Environ Med* (2008) 79(4):365–73. doi: 10.3357/asem.1994.2008

15. Hides JA, Lambrecht G, Sexton CT, Pruett C, Petersen N, Jaekel P, et al. The effects of exposure to microgravity and reconditioning of the lumbar multifidus and anterolateral abdominal muscles: Implications for people with lbp. *Spine journal: Off J North Am Spine Soc* (2021) 21(3):477–91. doi: 10.1016/j.spinee.2020.09.006

16. Bailey JF, Nyayapati P, Johnson GTA, Dziesinski L, Scheffler AW, Crawford R, et al. Biomechanical changes in the lumbar spine following spaceflight and factors associated with postspaceflight disc herniation. *Spine journal: Off J North Am Spine Soc* (2022) 22(2):197–206. doi: 10.1016/j.spinee.2021.07.021

17. Wang X, Jia R, Li J, Zhu Y, Liu H, Wang W, et al. Research progress on the mechanism of lumbarmultifidus injury and degeneration. *Oxid Med Cell Longevity* (2021) 2021:6629037. doi: 10.1155/2021/6629037

18. Shahidi B, Hubbard JC, Gibbons MC, Ruoss S, Zlomislic V, Allen RT, et al. Lumbar multifidus muscle degenerates in individuals with chronic degenerative lumbar spine pathology. *J orthopaedic research: Off Publ Orthopaedic Res Soc* (2017) 35(12):2700–6. doi: 10.1002/jor.23597

19. Kudo D, Miyakoshi N, Hongo M, Kasukawa Y, Ishikawa Y, Fujii M, et al. Mrna expressions of peroxisome proliferator-activated receptor gamma coactivator 1α, tumor necrosis factor-A, and interleukin-6 in paraspinal muscles of patients with lumbar kyphosis: A preliminary study. *Clin Interventions Aging* (2018) 13:1633–8. doi: 10.2147/cia.S172952

20. Shahidi B, Fisch KM, Gibbons MC, Ward SR. Increased fibrogenic gene expression in multifidus muscles of patients with chronic versus acute lumbar spine pathology. *Spine (Phila Pa 1976)* (2020) 45(4):E189–e95. doi: 10.1097/brs.0000000000003243

21. Lerer A, Nykamp SG, Harriss AB, Gibson TW, Koch TG, Brown SH. Mri-based relationships between spine pathology, intervertebral disc degeneration, and muscle fatty infiltration in chondrodystrophic and non-chondrodystrophic dogs. *Spine journal: Off J North Am Spine Soc* (2015) 15(11):2433–9. doi: 10.1016/j.spinee.2015.08.014

22. Olaso-Gonzalez G, Ferrando B, Derbre F, Salvador-Pascual A, Cabo H, Pareja-Galeano H, et al. Redox regulation of E3 ubiquitin ligases and their role in skeletal muscle atrophy. *Free Radical Biol Med* (2014) 75 Suppl 1:S43–4. doi: 10.1016/j.freeradbiomed.2014.10.799

23. Yang JE, Zhao KH, Qu Y, Zou YC. Increased serum Cxcl10 levels are associated with clinical severity and radiographic progression in patients with lumbar disc degeneration. *Clinica chimica acta; Int J Clin Chem* (2022) 525:15–22. doi: 10.1016/j.cca.2021.12.006

24. Yamakuchi M, Higuchi I, Masuda S, Ohira Y, Kubo T, Kato Y, et al. Type I muscle atrophy caused by microgravity-induced decrease of myocyte enhancer factor 2c (Mef2c) protein expression. *FEBS Lett* (2000) 477(1-2):135–40. doi: 10.1016/s0014-5793(00)01715-4

25. Mirzoev TM, Vil'chinskaia NA, Lomonosova Iu N, Nemirovskaia TL, Shenkman BS. [Effect of 30-day space flight and subsequent readaptation on the signaling processes in m. longissimus dorsi of mice]. *Aviakosmicheskaia i ekologicheskaia meditsina = Aerospace Environ Med* (2014) 48(2):12–5.

26. Ogneva IV, Maximova MV, Larina IM. Structure of cortical cytoskeleton in fibers of mouse muscle cells after being exposed to a 30-day space flight on board the bion-M1 biosatellite. *J Appl Physiol (Bethesda Md: 1985)* (2014) 116(10):1315–23. doi: 10.1152/japplphysiol.00134.2014

27. Gambara G, Salanova M, Ciciliot S, Furlan S, Gutsmann M, Schiffl G, et al. Microgravity-induced transcriptome adaptation in mouse paraspinal longissimus dorsi muscle highlights insulin resistance-linked genes. *Front Physiol* (2017) 8:279. doi: 10.3389/fphys.2017.00279

28. Barrett T, Wilhite SE, Ledoux P, Evangelista C, Kim IF, Tomashevsky M, et al. Ncbi geo: Archive for functional genomics data sets–update. *Nucleic Acids Res* (2013) 41:D991–5. doi: 10.1093/nar/gks1193

29. Davis S, Meltzer PS. Geoquery: A bridge between the gene expression omnibus (Geo) and bioconductor. *Bioinf (Oxford England)* (2007) 23(14):1846–7. doi: 10.1093/bioinformatics/btm254

30. Wu T, Hu E, Xu S, Chen M, Guo P, Dai Z, et al. Clusterprofiler 4.0: A universal enrichment tool for interpreting omics data. *Innovation (Cambridge (Mass)* (2021) 2(3):100141. doi: 10.1016/j.xinn.2021.100141

31. Gu Z, Eils R, Schlesner M. Complex heatmaps reveal patterns and correlations in multidimensional genomic data. *Bioinf (Oxford England)* (2016) 32(18):2847–9. doi: 10.1093/bioinformatics/btw313

32. Zhou N, Bao J. Ferrdb: A manually curated resource for regulators and markers of ferroptosis and ferroptosis-disease associations. *Database: J Biol Database Curation* (2020) 2020:1–8. doi: 10.1093/database/baaa021

33. Liberzon A, Birger C, Thorvaldsdóttir H, Ghandi M, Mesirov JP, Tamayo P. The molecular signatures database (Msigdb) hallmark gene set collection. *Cell Syst* (2015) 1(6):417–25. doi: 10.1016/j.cels.2015.12.004

34. Szklarczyk D, Gable AL, Lyon D, Junge A, Wyder S, Huerta-Cepas J, et al. String V11: Protein-protein association networks with increased coverage, supporting functional discovery in genome-wide experimental datasets. *Nucleic Acids Res* (2019) 47(D1):D607–d13. doi: 10.1093/nar/gky1131

35. Dixon SJ, Lemberg KM, Lamprecht MR, Skouta R, Zaitsev EM, Gleason CE, et al. Ferroptosis: An iron-dependent form of nonapoptotic cell death. *Cell* (2012) 149(5):1060–72. doi: 10.1016/j.cell.2012.03.042

36. Anderson B, Ordaz A, Zlomislic V, Allen RT, Garfin SR, Schuepbach R, et al. Paraspinal muscle health is related to fibrogenic, adipogenic, and myogenic gene expression in patients with lumbar spine pathology. *BMC musculoskeletal Disord* (2022) 23(1):608. doi: 10.1186/s12891-022-05572-7

37. Kumar A, Tahimic CGT, Almeida EAC, Globus RK. Spaceflight modulates the expression of key oxidative stress and cell cycle related genes in heart. *Int J Mol Sci* (2021) 22(16):9088. doi: 10.3390/ijms22169088

38. Bodine SC, Baehr LM. Skeletal muscle atrophy and the E3 ubiquitin ligases Murf1 and Mafbx/Atrogin-1. *Am J Physiol Endocrinol Metab* (2014) 307(6):E469–84. doi: 10.1152/ajpendo.00204.2014

39. Mahmassani ZS, Reidy PT, McKenzie AI, Stubben C, Howard MT, Drummond MJ. Age-dependent skeletal muscle transcriptome response to bed rest-induced atrophy. *J Appl Physiol (Bethesda Md 1985)* (2019) 126(4):894–902. doi: 10.1152/japplphysiol.00811.2018

40. Bongers KS, Fox DK, Kunkel SD, Stebounova LV, Murry DJ, Pufall MA, et al. Spermine oxidase maintains basal skeletal muscle gene expression and fiber size and is strongly repressed by conditions that cause skeletal muscle atrophy. *Am J Physiol Endocrinol Metab* (2015) 308(2):E144–58. doi: 10.1152/ajpendo.00472.2014

41. Fox DK, Ebert SM, Bongers KS, Dyle MC, Bullard SA, Dierdorff JM, et al. P53 and Atf4 mediate distinct and additive pathways to skeletal muscle atrophy during limb immobilization. *Am J Physiol Endocrinol Metab* (2014) 307(3):E245–61. doi: 10.1152/ajpendo.00010.2014

42. Faust HJ, Zhang H, Han J, Wolf MT, Jeon OH, Sadtler K, et al. Il-17 and immunologically induced senescence regulate response to injury in osteoarthritis. *J Clin Invest* (2020) 130(10):5493–507. doi: 10.1172/jci134091

43. Segalés J, Perdiguero E, Serrano AL, Sousa-Victor P, Ortet L, Jardí M, et al. Sestrin prevents atrophy of disused and aging muscles by integrating anabolic and catabolic signals. *Nat Commun* (2020) 11(1):189. doi: 10.1038/s41467-019-13832-9

44. Li S, Wu B, Ling Y, Guo M, Qin B, Ren X, et al. Epigenetic landscapes of single-cell chromatin accessibility and transcriptomic immune profiles of T cells in covid-19 patients. *Front Immunol* (2021) 12:625881. doi: 10.3389/fimmu.2021.625881

45. Liu TT, Luo R, Yang Y, Cheng YC, Chang D, Dai W, et al. Lrg1 mitigates renal interstitial fibrosis through alleviating capillary rarefaction and inhibiting inflammatory and pro-fibrotic cytokines. *Am J Nephrol* (2021) 52(3):228–38. doi: 10.1159/000514167

46. Frempah B, Luckett-Chastain LR, Calhoun KN, Gallucci RM. Keratinocyte-specific deletion of the il-6rα exacerbates the inflammatory response during irritant contact dermatitis. *Toxicology* (2019) 423:123–31. doi: 10.1016/j.tox.2019.05.015

47. Wang S, Yu H, Gao J, Chen J, He P, Zhong H, et al. Palmd regulates aortic valve calcification *Via* altered glycolysis and nf-Kb-Mediated inflammation. *J Biol Chem* (2022) 298(5):101887. doi: 10.1016/j.jbc.2022.101887

48. Zhao D, Deng SC, Ma Y, Hao YH, Jia ZH. Mir-221 alleviates the inflammatory response and cell apoptosis of neuronal cell through targeting Tnfaip2 in spinal cord ischemia-reperfusion. *Neuroreport* (2018) 29(8):655–60. doi: 10.1097/wnr.0000000000001013

49. Saban R, D'Andrea MR, Andrade-Gordon P, Derian CK, Dozmorov I, Ihnat MA, et al. Regulatory network of inflammation downstream of proteinase-activated receptors. *BMC Physiol* (2007) 7:3. doi: 10.1186/1472-6793-7-3

50. Choi EB, Jeong JH, Jang HM, Ahn YJ, Kim KH, An HS, et al. Skeletal lipocalin-2 is associated with iron-related oxidative stress in Ob/Ob mice with sarcopenia. *Antioxidants (Basel Switzerland)* (2021) 10(5):758. doi: 10.3390/antiox10050758

51. Keping Y, Yunfeng S, Pengzhuo X, Liang L, Chenhong X, Jinghua M. Sestrin1 inhibits oxidized low-density lipoprotein-induced activation of Nlrp3 inflammasome in macrophages in a murine atherosclerosis model. *Eur J Immunol* (2020) 50(8):1154–66. doi: 10.1002/eji.201948427

52. Li YP, Chen Y, Li AS, Reid MB. Hydrogen peroxide stimulates ubiquitin-conjugating activity and expression of genes for specific E2 and E3 proteins in skeletal muscle myotubes. *Am J Physiol.-Cell Physiol* (2003) 285:C806–12. doi: 10.1152/ajpcell.00129.2003

53. Powers SK, Smuder AJ, Criswell DS. Mechanistic links between oxidative stress and disuse muscle atrophy. *Antioxid Redox Signal* (2011) 15:2519–28. doi: 10.1089/ars.2011.3973

54. Smuder AJ, Kavazis AN, Hudson MB, Nelson WB, Powers SK. Oxidation enhances myofibrillar protein degradation *via* calpain and caspase-3. *Free Radic Biol Med* (2010) 49:1152–60. doi: 10.1016/j.freeradbiomed.2010.06.025

55. Sun G, Xue R, Yao F, Liu D, Huang H, Chen C, et al. The critical role of sestrin 1 in regulating the proliferation of cardiac fibroblasts. *Arch Biochem Biophys* (2014) 542:1–6. doi: 10.1016/j.abb.2013.11.011

56. Song E, Ramos SV, Huang X, Liu Y, Botta A, Sung HK, et al. Holo-lipocalin-2-derived siderophores increase mitochondrial ROS and impair oxidative phosphorylation in rat cardiomyocytes. *Proc Natl Acad Sci U S A* (2018) 115 (7):1576–81. doi: 10.1073/pnas.1720570115

frontiers | Frontiers in Endocrinology

TYPE Review
PUBLISHED 20 October 2022
DOI 10.3389/fendo.2022.1042060

OPEN ACCESS

EDITED BY
Baoshan Xu,
Tianjin Hospital, China

REVIEWED BY
Changwing Li,
Xinqiao Hospital, China
Lei Cheng,
Qilu Hospital, Shandong University, China

*CORRESPONDENCE
Cai-Liang Shen
shencailiang@ahmu.edu.cn

†These authors have contributed equally to this work and share first authorship

SPECIALTY SECTION
This article was submitted to Bone Research, a section of the journal Frontiers in Endocrinology

RECEIVED 12 September 2022
ACCEPTED 04 October 2022
PUBLISHED 20 October 2022

CITATION
Zhou L-P, Zhang R-J, Jia C-Y, Kang L, Zhang Z-G, Zhang H-Q, Wang J-Q, Zhang B and Shen C-L (2022) Ferroptosis: A potential target for the intervention of intervertebral disc degeneration.
Front. Endocrinol. 13:1042060.
doi: 10.3389/fendo.2022.1042060

Ferroptosis: A potential target for the intervention of intervertebral disc degeneration

Lu-Ping Zhou†, Ren-Jie Zhang†, Chong-Yu Jia†, Liang Kang, Zhi-Gang Zhang, Hua-Qing Zhang, Jia-Qi Wang, Bo Zhang and Cai-Liang Shen*

Department of Orthopedics, The First Affiliated Hospital of Anhui Medical University, Hefei, Anhui, China

Ferroptosis, an iron-dependent form of programmed cell death marked by phospholipid peroxidation, is regulated by complex cellular metabolic pathways including lipid metabolism, iron balance, redox homeostasis, and mitochondrial activity. Initial research regarding the mechanism of ferroptosis mainly focused on the solute carrier family 7 member 11/glutathione/glutathione peroxidase 4 (GPX4) signal pathway. Recently, novel mechanisms of ferroptosis, independent of GPX4, have been discovered. Numerous pathologies associated with extensive lipid peroxidation, such as drug-resistant cancers, ischemic organ injuries, and neurodegenerative diseases, are driven by ferroptosis. Ferroptosis is a new therapeutic target for the intervention of IVDD. The role of ferroptosis in the modulation of intervertebral disc degeneration (IVDD) is a significant topic of interest. This is a novel research topic, and research on the mechanisms of IVDD and ferroptosis is ongoing. Herein, we aim to review and discuss the literature to explore the mechanisms of ferroptosis, the relationship between IVDD and ferroptosis, and the regulatory networks in the cells of the nucleus pulposus, annulus fibrosus, and cartilage endplate to provide references for future basic research and clinical translation for IVDD treatment.

KEYWORDS

ferroptosis, intervertebral disc degeneration, iron, lipid peroxidation, therapeutic implication

Introduction

Low back pain (LBP) is a common musculoskeletal disease in the world, and its prevention and treatment are the major challenges in public health programs, which contribute to severe socioeconomic and health burdens (1). Intervertebral disc (IVD) degeneration (IVDD) has been considered as the leading cause of LBP, thereby resulting

in a series of structural changes, such as the decrease of intervertebral height, breakage of the existing nucleus pulposus (NP), fissure of annulus fibrosus (AF), calcification of cartilage endplate (CEP), and imbalance of extracellular matrix (ECM) metabolism (2). In recent years, many new ways of programmed cell death have been reported in studies on IVDD. In contrast to apoptosis, necroptosis, pyroptosis, autophagy, and other types of death procedures, ferroptosis is characterized by the iron-mediated accumulation of lipid peroxides, morphologically manifested as mitochondrial shrinkage, reduction of mitochondrial cristae, and rupture of the mitochondrial outer membrane, and it has been regarded as a new target for the treatment of IVDD (3).

The overload of cellular iron content, particularly ferrous iron, can induce lipid peroxidation of fatty acids (4). The abnormal mitochondrial oxidative phosphorylation pathway results from iron overload, which produces a large amount of reactive oxygen species (ROS) and ATP. When the ROS content exceeds the scavenging level of the antioxidant system, polyunsaturated fatty acids (PUFAs) on the cell membranes and organelle membranes are oxidized to form lipid peroxides, which directly or indirectly destroy cell structure and function, thereby resulting in cell damage or death. Initial research on the mechanism of ferroptosis primarily focuses on the solute carrier family 7 member 11 (SLC7A11)–glutathione (GSH)–glutathione peroxidase 4 (GPX4) signaling pathway. Recently, novel mechanisms of ferroptosis independent of GPX4 have been discovered, which are closely related to lipid metabolism, iron balance, and redox reactions.

Although ferroptosis has been extensively investigated in various physiological and pathological processes, such as tumors, injuries, viral infection, immune response, and metabolic disorders since the item was coined by Dixon et al. (5) in 2012, research regarding the relationship between ferroptosis and IVDD started relatively lately (6–9). To date, a growing number of studies have investigated the relationship between ferroptosis and IVDD. Herein, we aimed to review recent literature to explore the underlying mechanism of ferroptosis and its role in IVDD and to investigate new therapeutic targets for the treatment of IVDD.

Iron metabolism

Systemic iron homeostasis

Iron homeostasis is essential for various metabolic processes in mammalian organ systems (Figure 1). Iron absorption mainly has two sources (heme iron primarily from animal products, including beef, fish, chicken, and liver, and non-heme iron primarily from fruit, vegetables, eggs, and grains) in the intestine, depending on different receptors (10). The heme iron is transported through the intestinal epithelium by heme carrier protein 1 (11). For the non-heme iron, ferric iron is reduced to be ferrous iron by cytochrome b reductase 1, which is then transported by divalent metal transporter 1 (DMT1), a carrier protein, into the enterocytes (12). Ferrous iron is exported through the iron exporter, ferroportin 1 (FPN1) (12, 13). The ferrous iron is oxidized from +2 to +3 state by hephaestin, subsequently loading ferric iron onto transferrin (TF) for systematic transport in the bloodstream (14). Moreover, the systematic iron homeostasis is complemented by serum ferritin and non-TF bound iron and regulated by the hepcidin–FPN1–regulatory axis (15).

For intracellular iron homeostasis, ferric iron binding to the TF in the serum can be taken up by a transferrin receptor (TFRC) on the cell membrane (16). The ferric iron is released from the TF in the endosome because of the rapid drop of pH and then reduced by six transmembrane epithelial antigens of prostate 3 (STEAP3) to ferrous iron, which is subsequently transported into the cytoplasm through the solute carrier family 11 member 2 (SLC11A2)/DMT1 (17). The transported ferrous iron stored in ferritin or labile iron pool for further utilization is essential for metabolic and biochemical processes, such as the regulation of the iron-requiring enzymatic activity, iron–sulfur protein production, and oxygen transport (18). Excess iron can be extruded into the extracellular space *via* the iron-efflux protein metal transporter protein-1/FPN1/iron-regulated transporter-1, which is the product of the solute carrier family 40 member 1 (SLC40A1) gene (19). Moreover, the intracellular iron homeostasis is regulated by iron-responsive element binding protein 2, heme oxygenase 1 (HO-1), and iron regulatory proteins (20, 21).

Iron overload in the blood circulation

Hematological disorders, such as hereditary hemochromatosis associated with gene mutations of HFE, hepcidin hormone, and TFRC, can contribute to a high serum ferritin level (22, 23). In addition, chronic renal failure receiving repeated hemodialysis and other chronic diseases receiving repeated blood transfusions, including myelodysplastic syndrome and thalassemias, can saturate the iron-binding capacity of TF in the cytoplasm, leading to chronic iron overload (24, 25).

Intracellular iron overload

Restrictive export and excessive import of iron result in intracellular iron overload. Genetic defects in SLC40A1 and STEAP3 mutations restrict iron export, but they have no effect on iron import (26, 27). Genetic mutations in SLC11A2 accelerate iron import, leading to intracellular iron overload (28).

Iron overload in IVD

Iron accumulation in IVD is commonly observed in aging patients suffering from diseases because of the lack of effective

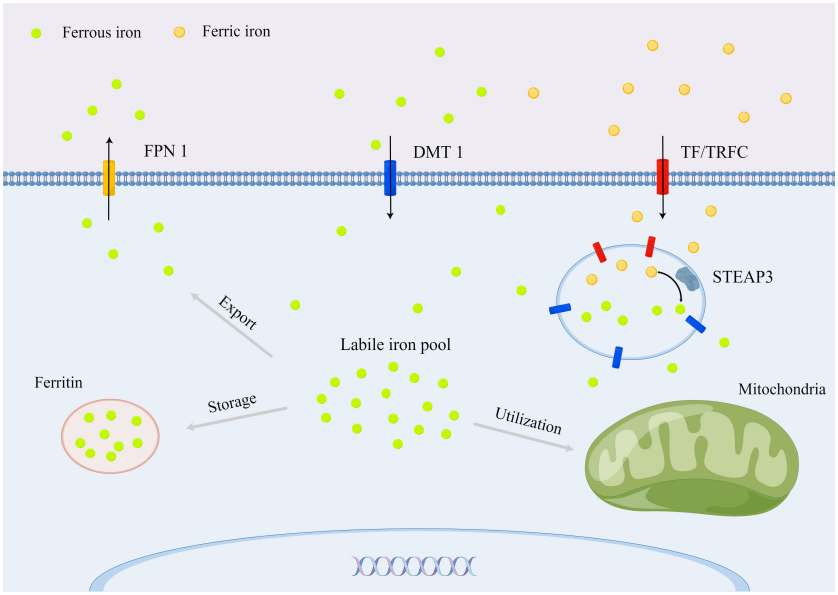

FIGURE 1
Cellular iron metabolism in mammals.

mechanisms to exert excess iron, including hereditary hemochromatosis and thalassemia (29, 30). Meanwhile, iron overload in IVD may result from neovascularization within the disc, which exposes tissues to high levels of heme, a major source of intracellular iron (31, 32). Neovascularization was initially reported in herniated NP using histological staining in 1993, and Shan et al. (31) found that the immature vessels during neovascularization in herniated IVD lead to the extravasation of red blood cells and the deposition of iron in this tissue.

Signaling pathways of ferroptosis

SLC7A11/GSH/GPX4 signaling pathway

System X_C^-, consisting of SLC7A11 and solute carrier family 3 member 2 (SLC3A2), is a Na^+-dependent amino acid antiporter that is widely distributed in the plasma membrane and is responsible for the import of extracellular cystine and the export of intracellular glycine (33). Intracellular cystine is immediately reduced back to cysteine by depleting NADPH, which is a rate-limiting precursor amino acid for the synthesis of GSH, a tripeptide consisting of cysteine, glutamate, and glycine (34). GSH plays an important role in anti-oxidative stress, reduction of lipid peroxidation, and protection of tissue cells, which is a necessary cofactor of GPX4 for normal function (35). Compared with other members of the GPXs family, GPX4 can directly convert phospholipid hydroperoxides (PLOOHs), a form of lipid-based ROS, on cell membranes to nontoxic lipid alcohols (PLOHs) with sufficient cellular GSH, whereas the depletion of GSH results in the inactivation of GPX4 (36, 37) (Figure 2).

GPX4 is the major neutralizing enzyme for PLOOHs, which protects the structure and function of cell membranes, and it has been regarded as a specific marker of ferroptosis, which plays an essential role in limiting lipid peroxidation (36, 38). Selenocysteine is the key group for the catalytic function of GPX4. PLOOH is reduced to PLOH, whereas the selenocysteine is oxidized to selenic acid intermediate (GPX4-SeOH). Subsequently, the selenium–glutathione adduct is produced after the reaction between GPX4-SeOH and GSH. Then, the selenium–glutathione adduct is converted back to selenocysteine by reacting with the equivalent of GSH. Similarly, the oxidized glutathione (GSSG) is produced from GSH, which is then reduced to GSH by glutathione reductase for recycling and utilization (35). Apart from ferroptosis, GPX4 plays a role in pyroptosis (39), apoptosis (40), necroptosis (41), and autophagy (42, 43), indicating that the regulation of PLOOHs may be a hallmark in the signaling pathway for the induction of regulated cell death.

Recently, the regulation of ferroptosis through the SLC7A11/GSH/GPX4 signaling pathway has been explored for the intervention of IVDD. Zhang et al. (44) demonstrated that the promotion of methylase expression upregulated GPX4 methylation in patients with hyperhomocysteinemia (HHcy), thereby inducing ferroptosis in NP cells (NPCs). In addition, the

level of GPX4 protein was reduced after treatment with heme by simulating neovascularization in a heme-induced ferroptosis model (31). Moreover, ferroptosis in cartilage cells was modulated *via* the IL-6/miR-10a-5p/IL-6R axis in the inflammatory microenvironment (45), and the IL-6/STAT3/GPX4 signaling pathway might be implicated in this procedure (46).

Signaling pathways independent of GPX4

GPX4 has been regarded as the primary enzyme that prevents ferroptosis through the conversion of lipid hydroperoxides into non-toxic lipid alcohols (36). However, the sensitivity of GPX4 inhibitors differs in cancer cell lines, indicating that additional independent pathways govern the regulation of ferroptosis (47). Therefore, current mechanisms of intracellular defense against ferroptosis can be divided into the SLC7A11-GSH-GPX4 signaling pathway and other signaling pathways independent of GPX4 (Figure 3).

Bersuker et al. (48) and Doll et al. (49) identified that ferroptosis suppressor protein 1 (FSP1), also known as apoptosis-inducing factor mitochondrial 2, acts parallel to the GSH-dependent GPX4 pathway with regard to the inhibition of phospholipid (PL) peroxidation and ferroptosis. FSP1 on the membrane reduces coenzyme Q (CoQ) by using NAD(P)H to ubiquinol (CoQH2), which serves as a lipophilic radical-trapping antioxidant (RTA), suppressing the propagation of lipid peroxides (50, 51). The loss of FPS1 improves PL peroxidation with the normal function of GPX4, indicating an independent mechanism of the FSP1/CoQH2/NAD(P)H pathway during ferroptosis.

The GTP cyclohydrolase-1 (GCH1)/6(R)-L-erythro5,6,7,8-tetrahydrobiopterin (BH4)/dihydrofolate reductase (DHFR) axis is another unique protective mechanism for ferroptosis, which is independent of the GSH-GPX4 system. Kraft et al. (52) identified GCH1 as a potent antagonist of ferroptosis using a whole-genome activation screen. The endogenous antioxidant BH4 on the membrane generated by the enzyme GCH1 also serves as a lipophilic RTA to selectively neutralize PUFA-PL-OOH, which alleviates sensitivity to ferroptosis. Moreover, BH4 also participates in the synthesis of CoQ to leverage oxidative damage under oxidative stress (52). Furthermore, DHFR serves as an essential regulator of ferroptosis by regenerating BH4 from dihydrobiopterin (BH2). The genetic or pharmacological loss of DHFR's function can also induce ferroptosis (53).

Metabolism and ferroptosis

Lipid metabolism and ferroptosis

Lipid peroxidation is an important process in ferroptosis. PUFA-containing PLs on the cell membrane are easily oxidized because of the highly active hydrogen atoms in the methylene bridge, destroying the structure and stability of the lipid bilayer,

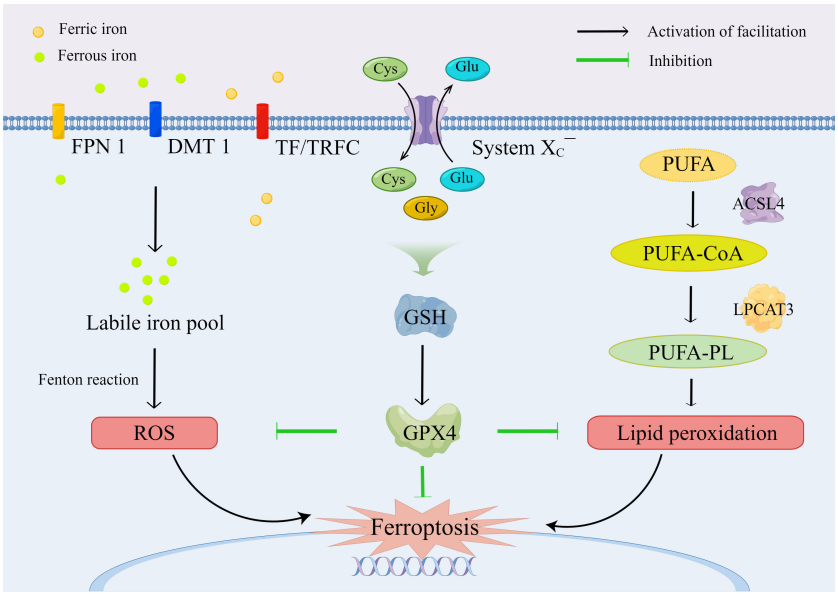

FIGURE 2
The molecular mechanism and regulation of ferroptosis.

10.3389/fendo.2022.1042060

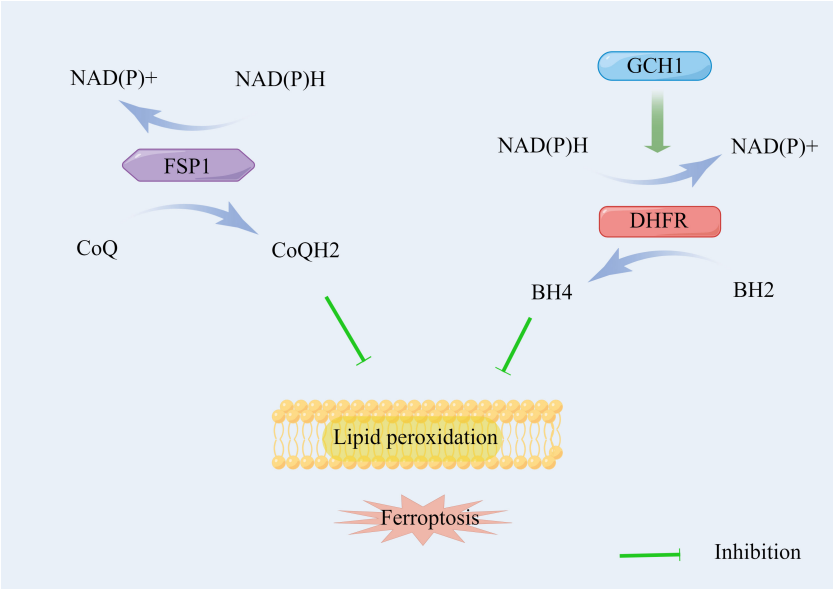

FIGURE 3
The signaling pathways of ferroptosis independent of SLC7A11/GSH/GPX4 axis.

and disintegration of the cell membrane. Free PUFAs, such as adrenal acid and arachidonic acid, are catalyzed by acyl-CoA synthetase long-chain family member 4 (ACSL4) to generate PUFA-CoA, which is then transported to the cell membrane through lysophosphatidylcholine acyltransferase 3 (LPCAT3) by inserting acyl groups into lysophospholipids and synthesizing PUFA-PLs with PLs (54–56). PUFA oxidation mainly has two forms. First, PUFA can be oxidized through an enzymatic reaction. PUFA-PL is catalyzed by arachidonate lipoxygenase (ALOX) into PUFA-PL-OOH (57). Zou et al. (58) found that cytochrome P450 oxidoreductase (POR) promotes lipid peroxidation during ferroptosis in an ALOX-independent manner using systematic lipidomic profiling and suggested that POR is an essential mediator of ferroptosis. In addition, PUFAs are oxidized by other oxygenases, including NADPH oxidases (NOXs) and prostaglandin-endoperoxide synthase 2 (PTGS2/COX) (59, 60). Despite being upregulated during ferroptosis, PTGS2 might not be involved in the production of lipid peroxidation. Whether PTGS2 affects the procedure of ferroptosis still needs further investigation (61). Second, PUFA oxidation occurs through Fenton reaction in a non-enzymatic way. Ferric iron, hydroxyl radicals (HO ·), and OH- are generated during the reaction between ferrous iron and hydrogen peroxide (H_2O_2). Thus, free radical ions further cause oxidative damage to membrane lipids, particularly PUFAs. The inhibition of key molecules, such as ACSL4, LPCAT3, ALOX, POR, and NOXs, is of great significance to the reduction of lipid peroxidation, thereby counteracting ferroptosis.

Iron metabolism and ferroptosis

The main mechanism of the biological toxicity of iron ions is the classical Fenton reaction, where ferrous iron reacts with hydrogen peroxide (H_2O_2). Among the products of the Fenton reaction, the hydroxyl radicals are largely destroyed, which can not only cause oxidative damage to cells by unspecifically attacking biomolecules, but also promote the peroxidation of lipid components to generate various oxidation products, the main products of which are lipid hydroperoxides (LOOHs) (57). LOOHs can be converted to oxygen radical intermediates, including lipid peroxyl radical (LOO ·) or alkoxyl (LO ·) (62). Given the high proportion of PUFAs on cell and plasma membranes, the oxygen radical intermediates cause cascade reactions, which further aggravate the destruction of the membranes, contributing to the disturbance of cellular homeostasis and activation of serious biochemical reactions. Furthermore, many different aldehydes that can be formed as secondary products, including 4-hydroxynonenal, malondialdehyde, hexanal, and propanal, can continuously react with PUFAs, destroy cells, and eventually lead to irreversible disruption of the structure and function of the cell membranes (63–65). Finally, the free radical ions and hydroxyl radicals generated from intracellular free ferrous ions through the Fenton reaction oxidize PUFA on the cell membrane and damage the protein in the cytoplasm and DNA in the nucleus (66). Moreover, iron ions are considered as the key components of various metabolic enzymes, including ALOX and POR.

Therefore, homeostasis of iron ions is important for the normal functioning of organisms and cells.

The regulation of iron homeostasis can affect the sensitivity of cells to ferroptosis with regard to the uptake, storage, and efflux of iron. The knockdown of TF can suppress lapatinib-induced ferroptosis in SKBR3 cancer cell line, and the loss of TFRC can also decrease cystine starvation- or erastin-induced ferroptosis (67–69). Ferritin, composed of H and L subtypes, is the main iron storage protein primarily located in the cytoplasm, which stores around 70%–80% newly imported iron (35). The H subtype, ferritin heavy chain 1 (FTH1), can oxidize ferrous iron to ferric iron and combine with it to reduce free ferrous iron and subsequent Fenton reaction. SLC40A1, the only known iron exporter in mammalian cells, can influence ferroptosis by mediating iron output. Studies have shown that ferroptosis is promoted by the knockdown of SLC40A1, whereas this procedure is ameliorated by the overexpression of SLC40A1 (68, 70). In response to different types of ferroptosis inducers, the level of intracellular ferric ions will increase, and various protein transporters related to iron metabolism, such as TF, TFRC, ferritin, and SLC40A1, will be rearranged under the ferroptosis program.

In the oxidative stress microenvironment of IVDD simulated by the tert-butyl hydroperoxide (TBHP), Lu et al. (71) indicated that the intercellular iron overload resulted from FPN dysregulation that was regulated by metal-regulatory transcription factor 1 (MTF1), and the TBHP-indued ferroptosis was aggravated through the JNK/MTF1/FPN signal pathway. In addition, the levels of intercellular iron in AF cells (AFCs) and NPCs were increased by nuclear receptor coactivator 4 (NCOA4)-mediated ferritin selective autophagy during TBHP-indued ferroptosis (72).

Animo acid metabolism and ferroptosis

Amino acid metabolism is an important part of the metabolic loop of organisms, and imbalances in intracellular and extracellular cysteine, cystine, glutamate, and GSH can induce ferroptosis. Intracellular cysteine is primarily used to synthesize antioxidant enzymes, including GSH and thioredoxin. When cysteine is deficient, cystathionine-β-synthase (CBS) and cystathionine gamma-lyase are activated under oxidative stress conditions, and cysteine is biosynthesized from methionine through the transsulfuration pathway, thereby reducing oxidative stress–induced ferroptosis (73). Liu et al. (74) demonstrated that the overexpression of CBS can confer ferroptosis resistance in ovarian cancer cells, and CBS has been identified as a new negative regulator of ferroptosis. By contrast, cysteinyl-tRNA synthetase (CARS) positively regulates ferroptosis by limiting the transsulfuration pathway. Hayano et al. (75) found that the loss of CARS contributed to the accumulation of cystathionine, induction of the transsulfuration pathway, and upregulation of genes associated with serine biosynthesis and transsulfuration.

The glutaminolysis pathway, in which glutamine is catabolized to glutamate, has also been implicated in the regulation of ferroptosis. Gao et al. (67) indicated that α-ketoglutarate converted from glutamine can cause cysteine deprivation and promote ferroptosis, and the limitation of glutaminolysis can reduce the heart triggered by ischemia–reperfusion injury through the inhibition of ferroptosis. Moreover, glutaminolysis is catalyzed by cytosolic glutaminase (GLS1) and mitochondrial glutaminase (GLS2); however, GLS2, instead of GLS1, is required for ferroptosis (67, 76, 77). Mitochondria play a crucial role in cysteine deprivation-induced ferroptosis, instead of GPX4 inhibition-induced ferroptosis, which is mediated by the potential hyperpolarization, mitochondrial tricarboxylic acid cycle, and electron transport chain of the mitochondrial membrane (78).

Glucose metabolism and ferroptosis

Glucose is the principal nutrient for biosynthesis and the main source of acetyl-CoA for the synthesis of fatty acids. Under nutritional deficiency, energy stress is induced by the depletion of intracellular ATP and subsequent improvement of intracellular AMP levels. In short-term and slight energy stress, the AMP-activated protein kinase (AMPK), a sensor of cellular energy status, participates in the adaptive response by promoting ATP-generating catabolism and maintaining cell survival (79). Lee et al. (80) found that the energy stress caused by glucose starvation can partly reduce ferroptosis by AMPK, and the activation of AMPK inhibits ferroptosis by the phosphorylation of acetyl-CoA carboxylase and restrains PUFA biosynthesis. In type 2 diabetic osteoporosis, high glucose levels can induce ferroptosis *via* increased ROS/lipid peroxidation/GSH depletion (81).

Transcriptional regulation of ferroptosis

The transcription factors regulate ferroptosis-related target genes that serve as promoters or blockers, thereby affecting the sensitivity of ferroptosis through multiple roles in transcription-dependent or transcription-independent mechanisms (82). Many transcription factors, such as tumor protein 53, nuclear factor-erythroid 2 like 2 (NRF2), Yes 1-associated transcriptional regulator, MTF1, activating transcription factor 3 (ATF3), transcription factor AP-2 gamma, specificity protein 1, hypoxia-inducible factor 1 alpha, and egl-9 family hypoxia-inducible factor 2, have been found to be involved in a ferroptotic network, which has been a new potential treatment target (83–89).

Epigenetic regulation of ferroptosis

DNA methylation and histone modification can regulate ferroptosis. Helicase can inhibit ferroptosis by DNA methylation through the induction of sterol-CoA desaturase 1 and fatty acid desaturase 2, epigenetic silencing of cytosolic long non-coding RNAs (lncRNA) LINC00472, and promotion of nuclear lncRNA 00336 (35, 90–92). Histone 2A ubiquitination (H2Aub) and histone 2 B ubiquitination (H2Bub) can induce SLC7A11 expression by histone modification to reduce sensitivity to ferroptosis. Bromodomain containing 4 (BRD4) epigenetically prevents ferroptosis by recognizing acetylated lysine residues on histones, and demethylase 3 B (KDM3B), a histone H3 lysine 9 demethylase, can activate the expression of SLC7A11 to reduce erastin-induced ferroptosis (93, 94).

Inducers and inhibitors of ferroptosis

The ferroptosis inducer (FINs) can be divided into four categories: The first category is the inhibiting activity of SCL7A11. The FINs inhibit the function of System X_C^- to reduce the uptake of cystine and the synthesis of GHS, including erastin, sulfasalazine, and sorafenib (5, 36). The second category refers to the FINs inhibiting GPX4. The FINs, including RSL3, ML162/DP17, and ML210/DP110, covalently react with selenocysteine to inhibit the activity of GPX4 (36, 95). The third category refers to organic peroxides that cause oxidative damage, including TBHP, artemisinin, and FINO2 (96, 97). The fourth category refers to the FINs resulting in iron overload, including exogenous hemin and hemoglobin (31, 98, 99). The inhibitors of ferroptosis include antioxidants (e.g., butylated hydroxytoluene, butylated hydroxyanisole, tetrahydronaphthyridinols, ferrostatin-1, liproxstain-1, vitamin E, and vitamin K), iron chelators (e.g., deferoxamine [DFO], deferasirox [DFP], deferiprone [DFX], and ciclopirox), ferroptosis-related enzyme inhibitors (e.g., ALOX inhibitors, including baicalein, zileuton, and cinnamyl-3,4-dihydroxya-cyanocinnamate; ACSL4 inhibitors, including thiazolidinediones and triacsin C; and NOX inhibitors, including diphenylene iodonium and 2-acetylphenothiazine), and protein degradation inhibitors (5, 35, 100–103) (Figure 4).

Ferroptosis and IVDD

The IVD is a special structure without blood vessels in an ischemic and hypoxic microenvironment under normal physiological conditions, the steady balance of which is the basis for the maintenance of normal function. IVDD is a chronic process that commonly causes LBP; however, the specific cause of IVDD remains unclear. Published studies have demonstrated that IVDD is a complex process with multifactorial interactions, which is primarily characterized by ECM destruction and cell phenotype changes, as well as apoptosis, autophagy, pyroptosis, necroptosis, and ferroptosis of IVD (31, 104–107). The term ferroptosis was first coined in 2012. Since then the molecular mechanism and regulatory network of ferroptosis have been exponentially investigated in

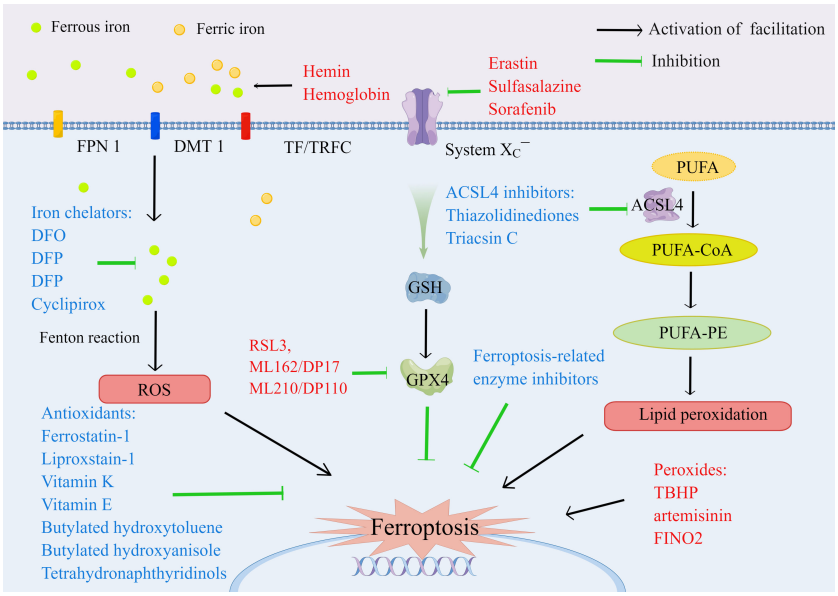

FIGURE 4
The inducers (marked red) and inhibitors (marked blue) of ferroptosis.

many degenerative diseases, such as Parkinson's disease, Alzheimer's disease, kidney degeneration, atherosclerosis, osteoporosis, and osteoarthritis (OA) (108–113). Although studies on ferroptosis in IVDD have been conducted in recent years, increasing evidence has shown that ferroptosis is associated with IVDD and is involved in degenerative processes of NP, AF, CEP, and ECM (Table 1).

Ferroptosis in NP

The property of resident progenitor cells in NP is altered by IVDD (117). The healthy NP primarily consists of chondrocyte-like cells, whereas the degenerative NP is primarily composed of chondrocyte-like cells, inflammatory cells, and fibroblast-like cells, which shrank extensively and became yellowish and fibrous (118). Zhang et al. (119) performed single-cell RNA sequencing analysis of NPCs isolated from normal controls and from patients with IVDD. Gene Ontology and Kyoto Encyclopedia of Genes and Genomes analyses revealed that ferroptosis pathways were enriched in mild IVDD. The pathways identified by scRNA-Seq were validated using a rat model of IVDD, and the levels of iron (a sign of ferroptosis), FTL, and HO-1 (two important regulators of ferroptosis) were assessed. They found that NP in the degenerative group was associated with remarkably higher iron levels and lower levels of ferritin light chain and HO-1 than in the control group, indicating that ferroptosis played a role in the progression of IVDD. Shan et al. (31) found that the increased level of iron primarily resulted from the high level of heme caused by neovascularization in degenerative NP, thereby inducing cytotoxicity and ferroptosis and accelerating the progression of IVDD. This result is also supported by scRNA-Seq analysis reporting endothelial cells only in IVDD samples, and the proportion of endothelial cells increased with the severity of IVDD (119).

Ferroptosis is regulated by multiple pathways during IVDD. Lu et al. (71) detected a decreased expression of FPN and the occurrence of ferroptosis under oxidative stress conditions simulated using TBHP in human NPCs *in vitro* and *in vivo*. They found that the downregulation of FPN, but not TFRC and DMT1, primarily accounted for the intercellular iron overload and ferroptosis in TBHP-induced human NPCs, whereas the overexpression of FPN inhibited ferroptosis through the JNK/MTF1/FPN signaling pathway. Therefore, the decreased nuclear

TABLE 1 Mechanism and intervention methods of ferroptosis in IVDD.

Study	Induction of ferroptosis	Mechanism	Effects on cells	Intervention method
Zhang et al. (44)	Hcy to simulate the pathological condition of HHcy	Promotion of methylase expression and the upregulation of the GPX4 methylation.	Inducing ferroptosis in NPCs	Folic acid reducing the ability of HHcy to promote IVDD
Bin et al. (45)	IL-6 to simulate inflammatory condition	IL-6/miR-10a-5p/IL-6R axis	Inducing ferroptosis in cartilage cells	Inhibiting miR-10a-5p and subsequently derepressing IL-6R signaling pathway
Lu et al. (71)	TBHP to simulate oxidative stress condition	FPN downregulation and intercellular iron overload	Inducing ferroptosis in NPCs.	Enhancing the nuclear translocation of MTF1 by suppressing the JNK pathway and ameliorating the progression of IVDD
Shan et al. (31)	Heme to simulate neovascularization condition	Increased heme catabolism, downregulation of GPX4, and intercellular iron overload, which might be mediated by the Notch pathway	Inducing ferroptosis in NPCs.	Inhibiting of the Notch signaling pathway
Yang et al. (72)	TBHP to simulate oxidative stress condition	NCOA4-mediated ferritinophagy and intercellular iron overload	Inducing ferroptosis in NPCs and AFCs.	Silencing NCOA4 to alleviate ferroptosis
Li et al. (114)	TBHP to simulate oxidative stress condition	Upregulation of ATF3 and ROS products	Inducing ferroptosis in NPCs.	Silencing ATF3 by miR-874-3p and alleviating IVDD
Wang et al. (115)	FAC to simulate iron overload condition	Mineralization of endplate chondrocytes and oxidative stress	Inducing ferroptosis in endplate chondrocytes.	DFO, NAC and ferrostatin-1 rescuing high dose iron-induced IVDD and cartilage endplate calcification
Yu et al. (116)	IL-1β to simulate inflammatory condition	Decreased NRF2 expression and upregulation of ROS products	Inducing ferroptosis in NPCs.	circ_0072464 shuttled by BMSC-secreted EVs inhibiting NPC ferroptosis by downregulation of miR-431 and upregulation of NRF2.

IVDD, Intervertebral disc degeneration; Hcy, homocysteine; HHcy, hyperhomocysteinemia; NPCs, nucleus pulposus cells; TBHP, tert-butyl hydroperoxide; FPN, ferroportin; MTF1, metal-regulatory transcription factor 1; GPX4, glutathione peroxidase 4; NCOA4, nuclear receptor coactivator 4; AFCs, annulus fibrosus cells; ATF3, activation transcription factor 3; ROS, reactive oxygen species; FAC, ferric ammonium citrate; DFO, deferoxamine; NAC, N-acetyl-cysteine; NRF2, nuclear factor-erythroid 2 like 2; BMSC, bone marrow mesenchymal stem cells; EV, extracellular vesicle.

translocation of MTF1 under TBHP treatment contributes to the reduced expression of FPN and ferroptosis in human NPCs. Meanwhile, hinokitiol, a natural tropolone derivative, can increase the nuclear translocation of MTF1, restore FPN, and attenuate TBHP-induced ferroptosis by suppressing the JNK pathway in human NPCs, as well as in the NP tissue of IVDD. Moreover, ferritinophagy is involved in TBHP-induced ferroptosis of NPCs through NCOA4-mediated ferritin-selective autophagy in an autophagy-dependent manner (72). NCOA4, a selective cargo receptor mutually combining with ferritin, transports ferritin to the autophagosomes with the occurrence of oxidative stress in IVD cells, thereby releasing free iron to induce ferroptosis (72, 120, 121). A newly published clinical study also proved that serum ferritin was negatively correlated with the degree of IVDD, which can be used as a clinical predictor of IVDD severity (122). Furthermore, Shan et al. (31) showed that heme-induced ferroptosis of human NPCs by the inhibition of the GPX4 protein can be rescued by DFO treatment. In addition, heme-induced ferroptosis might be mediated by the Notch signaling pathway, with substantial changes in the mRNA and protein levels of Notch1, Notch2, Jag1, Jag2, Hes1, Hes2, and Hey1.

MicroRNAs (miRNAs) and short non-coding RNAs (ncRNAs) primarily downregulate the expression of target genes and modulate the related downstream pathways by directly binding to the 3′-untranslated regions of the target genes, thereby regulating ferroptosis in human NPCs and IVDD. Li et al. (114) established a rat model of IVDD with TBHP and found that the overexpression of ATF3 induced ROS production and ferroptosis by suppressing SLC7A11. In addition, bioinformatics analysis and molecular experiments demonstrated that ATF3 is a direct target of miR-874-3p, indicating that the upregulation of ATF3 partially results from the downregulation of miR-874-3p in IVDD. Extracellular vesicles (EVs) derived from most cell types have been increasingly considered as important mediators of cell-to-cell communication and biomarkers of diseases, and they are involved in pathophysiological processes of IVDD (123, 124). Exosome-transported circular RNAs (circRNAs) have also been confirmed to exert effects on the regulation of IVDD (125). CircRNAs serve as miRNA sponges, contributing to the downregulation of miRNA and upregulation of miRNA downstream targets (126). Yu et al. (116) found that the uptake of EVs extracted from mouse bone marrow mesenchymal stem cells (BMSCs) by NPCs alleviated IVDD. *In vitro* and *in vivo* experiments showed that circ_0072464 shuttled by BMSC-derived EVs reduced ferroptosis in NPCs through the inhibition of miR-431 and upregulation of miR-431-mediated NRF2, indicating a potential biotherapeutic target for the treatment of IVDD.

Ferroptosis of NPCs and IVDD is also regulated by DNA methylation. HHcy, characterized by increased total homocysteine in plasma and its close relation to DNA methylation, results from the high concentration of homocysteine (Hcy) in serum caused by the deficiency of folic acid or the excessive intake of methionine (127–129). Zhang et al. (44) demonstrated that Hcy aggravates oxidative stress and induces ferroptosis in NPCs through the promotion of methylase expression and upregulation of GPX4 methylation. They also confirmed that HHcy is an independent risk factor for IVDD and that HHcy accelerates IVDD *in vivo*, which can be rescued by folic acid and the methylase inhibitor 5-AZA.

Ferroptosis in AF

AF, which is divided into the inner (proteoglycan and collagen II rich) and outer regions (collagen I rich), has strong resistance to traction and compression, preventing the NP from protruding outwards (130). The AFCs in the outer region tend to be fibroblast-like and parallel to collagen fibers, whereas the AFCs in the inner region can be more oval (131). Yang et al. (72) investigated the expression of ferroptosis marker proteins in the AFCs of a rat model exposed to TBHP at different concentrations. They found decreased expression of FTH and GPX4 and increased expression of PTGS2 and ACSL4 with an increase in TBHP concentration in AFCs, indicating the existence of oxidative stress–induced ferroptosis in rat APCs. Moreover, ferroptosis in AFCs is upregulated by NCOA4-mediated ferritinophagy in response to TBHP treatment, indicating new insights into the treatment of IVDD. The composition and structure of AF are unique and critical for the maintenance of disc anisotropy, elastic mechanical loading, and homeostasis. However, most published research focuses on NPCs, and studies on the effects of ferroptosis on AFCs are rare. Therefore, further studies on the relationship between AFCs must be conducted in the future.

Ferroptosis in CEP

CEP interfaces the disc and vertebral body with a thin horizontal layer of semi-porous thickened cancellous bone and hyaline cartilage, serving as the predominant route for nutrition supply and waste product exchange within the IVD (131, 132). The degeneration of CEP has been regarded as the primary predictor of IVDD, which reduces tissue diffusivity and changes the biochemical microenvironment of IVD, leading to reduced glucose and oxygen concentrations, increased lactate levels, and decreased PH within the disc, thereby initiating IVDD (133–135). The overload of iron and ferroptosis plays a role in the degeneration and calcification of CEP. Wang et al. (115) explored the connection between iron overload and degeneration of CEP and found that oxidative stress mediated by iron overload induced endplate chondrocyte ferroptosis, which can be reversed by iron chelation, antioxidants, and ferroptosis inhibition, indicating that ferroptosis plays an important role in endplate chondrocyte degeneration. Bin

et al. (45) demonstrated aberrant expression of interleukin (IL) 6 (IL-6) and its receptor in cartilage specimens obtained from patients with IVDD. Furthermore, they showed that cartilage cell ferroptosis is induced by IL-6 through oxidative stress and iron homeostasis. Furthermore, miR-10a-5p partially inhibited IL-6-induced ferroptosis by suppressing IL-6R expression, indicating that the IL-6/miR-10a-5p/IL-6R axis is a potential target for IVDD treatment.

Chondrocytes are the predominant cell type in ECP and articular cartilage. Thus, studies reporting the mechanisms of articular cartilage degeneration caused by ferroptosis in OA are inspiring and learnable for the intervention of IVDD. Jing et al. (136) indicated that iron overload in chondrocytes induced by pro-inflammatory cytokines contributes to oxidative stress and mitochondrial dysfunction through the upregulation of TRF1 and downregulation of FPN. In a study by Yao et al. (137), lipid ROS and ferroptosis in chondrocytes were induced by IL-1β and ferric ammonium citrate (FAC), but they were attenuated by Ferrostatin-1 that activated the NRF2 antioxidant system. The overexpression of NRF2 upregulated the level of GPX4 expression and ameliorated ferroptosis.

Ferroptosis and ECM

Under normal circumstances, the components of the ECM in the IVD are continuously updated through anabolism and catabolism, and the cells in the IVD associated with ECM form a coordinated functional system (138). However, the imbalance of anabolic and catabolic activities might result in ECM degradation, which is a pathological characteristic of IVDD (139). ECM metabolism is modulated by iron overload and ferroptosis.

The ECM of NP primarily consists of collagen II, proteoglycan, and chondroitin sulfate (140). In NPCs, the levels of collagen II, proteoglycan, matrix metalloproteinases (MMPs, particularly MMP13), disintegrin, and metalloproteinase with thrombospondin motifs (ADAMTSs, particularly ADAMTS4 and ADAMTS5) can reflect the degree of ECM degradation during the progression of IVDD (141, 142). The overexpression of circ_0072464 can promote the levels of collagen II and proteoglycan and reduce the levels of MMP13 and ADAMTS5 by sponging miR-431, upregulating NRF2, and suppressing ferroptosis (116). Meanwhile, the overexpression of ATF3 in NPCs not only aggravates TBHP-induced ferroptosis, apoptosis, and ROS production by suppressing SLC7A11 and superoxide dismutase 2, but also enhances ECM degradation by reducing the levels of proteoglycan and collagen II (114).

In endplate chondrocytes, the iron overload induced by FAC treatment enhanced the expression of MMP3 and MMP13 and reduced the expression of collagen II, thereby accelerating the degeneration of CEP and ECM (115). The study conducted by Camacho et al. (143) also demonstrated that iron overload was involved in chondrocyte-mediated ECM degradation. Meanwhile, erastin, an inducer of ferroptosis, reduces the expression of collagen II and increases the expression of MMP13 in chondrocytes (137). Furthermore, the inflammatory factor IL-1β accelerated iron uptake in chondrocytes, which was then promoted after co-treatment with FAC, because IL-1β can promote the expression of TFRC and DMT1 but downregulate the expression of FPN1, thereby aggravating iron accumulation in chondrocytes (136). Finally, co-treatment with IL-1β and FAC upregulated the expression of ECM-degrading enzymes, including MMPs and ADAMTS5.

Ferroptosis and IVDD treatment

Ferroptosis, characterized by iron-dependent lipid peroxidation and the accumulation of ROS within the IVD, is implicated in the pathogenesis of IVDD. Thus, ferroptosis opens a new therapeutic target for the intervention of IVDD with regard to the regulation of iron metabolism, chelation of iron, and antioxidants (113). Moreover, the key components in the signaling pathways are essential regulators of ferroptosis inhibition.

Classical iron chelators such as DFO, DFP, and DFX have been used for the clinical treatment of iron overload in thalassemia major (144). However, there is no clinical evidence of iron chelation therapy for the treatment of IVDD. Nevertheless, iron chelators have shown promising results in the inhibition of ferroptosis *in vivo* and *in vitro* in IVDD models. In addition, antioxidants, including Ferrostatin-1 and N-acetyl-cysteine (NAC), can exert protective effects against iron-induced abnormalities in IVDD. DFO and Fer-1 reversed the decreased expression of FTH and GPX4 and the upward levels of autophagy and ferritinophagy induced by TBHP treatment in NPCs and AFCs (71, 72). In the tissue of CEP, the administration of DFO, NAC, and Ferrostatin-1 substantially inhibited iron overload-induced IVDD by alleviating endplate calcification and IVD collapse in a mouse model (115). Meanwhile, the FAC-induced ECM degradation and the decrease of mitochondrial membrane potential can be reversed by DFO or NAC (136). Furthermore, DFO partially reduced the inhibition of IL-6 on miR10a-5p in cartilage cell ferroptosis through the promotion of GPX4 and FPN1 and suppression of DMT1 expression (45). However, the long-term use of iron chelators may lead to iron deficiency in cells, which is detrimental to cellular metabolism. Thus, the safe application of iron chelators needs further investigation.

EVs, exosomes, and ncRNAs are involved in the regulation of gene expression related to ferroptosis, which has emerged as a potential therapeutic strategy for IVDD (116, 145, 146). The

upregulation of miR-10a-5p inhibited IL-6R expression, thereby partially reducing IL-6-induced ferroptosis in chondrocytes (45). In addition, circ_0072464 shuttled by BMSC-secreted EVs suppresses ferroptosis in NPCs through the upregulation of miR-431-mediated NRF2 (116). At present, considerable research is needed to identify new ncRNAs and related mechanisms for the treatment of IVDD. Furthermore, the exact route of administration, safe dosing, and related dose toxicity of EVs, exosomes, and ncRNAs remain major problems in the application of regenerative medicine in clinical practice.

In addition, previous studies have demonstrated that hinokitiol ameliorates the activation of protein kinase B and mitogen-activated protein kinase to inhibit platelet activation and alleviate ferroptosis-related neurotoxicity through iron chelation and regulation of the NRF2 pathway (147, 148). Recently, Lu et al. (71) indicated that hinokitiol alleviates IVDD by upregulating MTF1, restoring FPN, and suppressing the JNK pathway, thereby attenuating TBHP-induced NPC ferroptosis. Furthermore, folic acid, a coenzyme in the methionine cycle, has been regarded as another ferroptosis-related therapeutic drug for IVDD caused by Hcy through the downregulation of GPX4 methylation and oxidative stress, thereby rescuing ferroptosis-induced NPC degeneration (44). In addition, other antioxidants and drugs, such as vitamin E, vitamin K, and curcumin, have exerted protective effects on ferroptosis (149–152). Moreover, the essential regulators of ferroptosis, such as ferritin, FPN1, NRF2, GPX4, GSH, HO-1, and TFRC, can be selected as the regulation targets for the treatment of IVDD. However, studies concerning the therapeutic effects of new bioactive compounds on ferroptosis-induced IVDD are rare and worthy of further studies.

The therapeutic efficacy of regulating iron homeostasis and ferroptosis to alleviate osteoporosis and OA was regarded as a potential option and reference for the treatment of IVDD. Icariin, the main active ingredient of Herba Epimedii, has antioxidant and antiosteoporosis functions by preventing iron overload-induced bone loss and regulating iron accumulation *in vitro* and *in vivo* (153). Icariin also attenuated IL-1β-induced degeneration of ECM and ROS in human OA cartilage *via* the activation of the Nrf2/ARE signaling pathway (154). Resveratrol, a member of the stilbene family of phenolic compounds, can reverse iron overload-induced bone loss by upregulating the levels of FOXO1 in osteoporotic mice (155). In addition, Tian et al. (156) demonstrated that NAC exerted protective effects against iron-mediated mitochondrial dysfunction and protected osteoblasts from iron overload-induced apoptosis. Moreover, melatonin (N-acetyl-5-methoxytryptamine), an effective endogenous antioxidant, can suppress high-glucose-induced ferroptosis by activating the Nrf2/HO-1 signaling pathway to improve bone microstructure in individuals with type 2 diabetes and osteoporosis (81). Furthermore, the upregulation of mitochondrial ferritin reduced osteoblastic ferroptosis under a high-glucose environment, whereas the deficiency of mitochondrial ferritin induced mitophagy *via* the ROS/PINK1/Parkin pathway in individuals with type 2 diabetes and osteoporosis (157). Therefore, mitochondrial ferritin might be another potential target for the treatment of type 2 diabetes and osteoporosis. Moreover, the endothelial cell-secreted exosomes antagonized glucocorticoid-induced osteoporosis *in vitro* and *in vivo via* the suppression of ferritinophagy-dependent ferroptosis (158). Lu et al. (159) also indicated that EVs from endothelial progenitor cells suppressed the ferroptotic pathway of osteoblasts by restoring levels of GPX4 and System X_C^-. Collectively, the pathophysiological progression of osteoporosis and OA is associated with iron metabolism disorder, ROS, and lipid peroxidation, which might provide potential therapeutic strategies for IVDD.

Conclusions and perspectives

As a highly disabling disease, IVDD has attracted increasing attention worldwide. Growing evidence has shown that ferroptosis is involved in the pathophysiological processes of IVDD; thus, regulation of ferroptosis has become a new therapeutic target for IVDD. In this review, we summarized the pathogenesis and mechanisms of ferroptosis, the relationship between ferroptosis and IVDD, and the choice of IVDD treatment by inhibiting ferroptosis. Recent studies have demonstrated that ferroptosis is mainly regulated by SLC7A11/GSH/GPX4, FSP1/CoQH2/NAD(P)H, and GCH1/BH4/DHFR pathways. Ferroptosis is accompanied by metabolic imbalances of lipids, iron, amino acids, and glucose and is modulated by transcriptional and epigenetic regulation. The interaction and crosstalk between ferroptosis and IVD components in terms of NP, AF, CEP, and ECM provide remarkable insights into the prevention and treatment of IVDD. However, studies on ferroptosis in IVDD are still at a relatively early stage, and simulations of ferroptosis in IVDD are mainly induced by oxidative stress and inflammation. Other factors, such as hypoxia, acidic microenvironments, and compression, are needed to confirm the universality of ferroptosis in IVDD. Therefore, further research is required to investigate the specific mechanisms, molecular targets, and associated signaling pathways of ferroptosis to develop further understanding and effective options for intervention in IVDD.

Author contributions

L-PZ, R-JZ and C-LS conceptualized the review. L-PZ and R-JZ drafted the manuscript. L-PZ, R-JZ, C-YJ, LK, Z-GZ, H-

QZ, J-QW, BZ, and C-LS revised the manuscript. All authors have read and approved the final manuscript.

Funding

This work was supported by the National Natural Science Foundation of China (No. 81772408).

Acknowledgments

Figures were created by Figdraw (www.figdraw.com). We would like to thank Figdraw for its help in creating the figures.

Conflict of interest

The authors declare that the research was conducted in the absence of any commercial or financial relationships that could be construed as a potential conflict of interest.

Publisher's note

References

1. Yang S, Zhang F, Ma J, Ding W. Intervertebral disc ageing and degeneration: The antiapoptotic effect of oestrogen. *Ageing Res Rev* (2020) 57:100978. doi: 10.1016/j.arr.2019.100978

2. Millecamps M, Stone LS. Delayed onset of persistent discogenic axial and radiating pain after a single-level lumbar intervertebral disc injury in mice. *Pain* (2018) 159(9):1843–55. doi: 10.1097/j.pain.0000000000001284

3. Xiong Y, Chen L, Lin Z, Hu Y, Panayi AC, Zhou W, et al. The regulatory role of ferroptosis in bone homeostasis. *Stem Cells Int* (2022) 2022:3568597. doi: 10.1155/2022/3568597

4. Hassan W, Noreen H, Khalil S, Hussain A, Rehman S, Sajjad S, et al. Ethanolic extract of nigella sativa protects Fe(II) induced lipid peroxidation in rat's brain, kidney and liver homogenates. *Pak J Pharm Sci* (2016) 29(1):231–7.

5. Dixon SJ, Lemberg KM, Lamprecht MR, Skouta R, Zaitsev EM, Gleason CE, et al. Ferroptosis: an iron-dependent form of nonapoptotic cell death. *Cell* (2012) 149(5):1060–72. doi: 10.1016/j.cell.2012.03.042

6. Chen X, Kang R, Kroemer G, Tang D. Broadening horizons: the role of ferroptosis in cancer. *Nat Rev Clin Oncol* (2021) 18(5):280–96. doi: 10.1038/s41571-020-00462-0

7. Jiang X, Stockwell BR, Conrad M. Ferroptosis: mechanisms, biology and role in disease. *Nat Rev Mol Cell Biol* (2021) 22(4):266–82. doi: 10.1038/s41580-020-00324-8

8. Zhang HL, Hu BX, Li ZL, Du T, Shan JL, Ye ZP, et al. PKCbetaII phosphorylates ACSL4 to amplify lipid peroxidation to induce ferroptosis. *Nat Cell Biol* (2022) 24(1):88–98. doi: 10.1038/s41556-021-00818-3

9. Liu P, Wang W, Li Z, Li Y, Yu X, Tu J, et al. Ferroptosis: A new regulatory mechanism in osteoporosis. *Oxid Med Cell Longev* (2022) 2022:2634431. doi: 10.1155/2022/2634431

10. Saboor M, Zehra A, Hamali HA, Mobarki AA. Revisiting iron metabolism, iron homeostasis and iron deficiency anemia. *Clin Lab* (2021) 67(3). doi: 10.7754/Clin.Lab.2020.200742

11. Shayeghi M, Latunde-Dada GO, Oakhill JS, Laftah AH, Takeuchi K, Halliday N, et al. Identification of an intestinal heme transporter. *Cell* (2005) 122(5):789–801. doi: 10.1016/j.cell.2005.06.025

12. Muckenthaler MU, Rivella S, Hentze MW, Galy B. A red carpet for iron metabolism. *Cell* (2017) 168(3):344–61. doi: 10.1016/j.cell.2016.12.034

13. Canonne-Hergaux F, Donovan A, Delaby C, Wang HJ, Gros P. Comparative studies of duodenal and macrophage ferroportin proteins. *Am J Physiol Gastrointest Liver Physiol* (2006) 290(1):G156–63. doi: 10.1152/ajpgi.00227.2005

14. Chaston T, Chung B, Mascarenhas M, Marks J, Patel B, Srai SK, et al. Evidence for differential effects of hepcidin in macrophages and intestinal epithelial cells. *Gut* (2008) 57(3):374–82. doi: 10.1136/gut.2007.131722

15. Ganz T, Nemeth E. Hepcidin and iron homeostasis. *Biochim Biophys Acta* (2012) 1823(9):1434–43. doi: 10.1016/j.bbamcr.2012.01.014

16. Anderson GJ, Frazer DM. Current understanding of iron homeostasis. *Am J Clin Nutr* (2017) 106(Suppl 6):1559s–66s. doi: 10.3945/ajcn.117.155804

17. Montalbetti N, Simonin A, Simonin C, Awale M, Reymond JL, Hediger MA. Discovery and characterization of a novel non-competitive inhibitor of the divalent metal transporter DMT1/SLC11A2. *Biochem Pharmacol* (2015) 96(3):216–24. doi: 10.1016/j.bcp.2015.05.002

18. Lin L, Wang S, Deng H, Yang W, Rao L, Tian R, et al. Endogenous labile iron pool-mediated free radical generation for cancer chemodynamic therapy. *J Am Chem Soc* (2020) 142(36):15320–30. doi: 10.1021/jacs.0c05604

19. Lymboussaki A, Pignatti E, Montosi G, Garuti C, Haile DJ, Pietrangelo A. The role of the iron responsive element in the control of ferroportin1/IREG1/MTP1 gene expression. *J Hepatol* (2003) 39(5):710–5. doi: 10.1016/s0168-8278(03)00408-2

20. Rouault TA. The role of iron regulatory proteins in mammalian iron homeostasis and disease. *Nat Chem Biol* (2006) 2(8):406–14. doi: 10.1038/nchembio807

21. Menon AV, Liu J, Tsai HP, Zeng L, Yang S, Asnani A, et al. Excess heme upregulates heme oxygenase 1 and promotes cardiac ferroptosis in mice with sickle cell disease. *Blood* (2022) 139(6):936–41. doi: 10.1182/blood.2020008455

22. Adams PC, Barton JC. Haemochromatosis. *Lancet* (2007) 370(9602):1855–60. doi: 10.1016/s0140-6736(07)61782-6

23. Rostoker G. The changing landscape of iron overload disorders at the beginning of the 21st century. *Presse Med* (2017) 46(12 Pt 2):e269–71. doi: 10.1016/j.lpm.2017.10.011

24. Taher AT, Saliba AN. Iron overload in thalassemia: different organs at different rates. *Hematol Am Soc Hematol Educ Program* (2017) 2017(1):265–71. doi: 10.1182/asheducation-2017.1.265

25. Gattermann N, Muckenthaler MU, Kulozik AE, Metzgeroth G, Hastka J. The evaluation of iron deficiency and iron overload. *Dtsch Arztebl Int* (2021) 118(49):847–56. doi: 10.3238/arztebl.m2021.0290

26. Grandchamp B, Hetet G, Kannengiesser C, Oudin C, Beaumont C, Rodrigues-Ferreira S, et al. A novel type of congenital hypochromic anemia associated with a nonsense mutation in the STEAP3/TSAP6 gene. *Blood* (2011) 118(25):6660–6. doi: 10.1182/blood-2011-01-329011

27. Le Lan C, Mosser A, Ropert M, Detivaud L, Loustaud-Ratti V, Vital-Durand D, et al. Sex and acquired cofactors determine phenotypes of ferroportin disease. *Gastroenterology* (2011) 140(4):1199–1207.e1-2. doi: 10.1053/j.gastro.2010.12.049

28. Bardou-Jacquet E, Island ML, Jouanolle AM, Détivaud L, Fatih N, Ropert M, et al. A novel N491S mutation in the human SLC11A2 gene impairs protein trafficking and in association with the G212V mutation leads to microcytic anemia and liver iron overload. *Blood Cells Mol Dis* (2011) 47(4):243–8. doi: 10.1016/j.bcmd.2011.07.004

29. Li J, Wang S, Duan J, Le P, Li C, Ding Y, et al. The protective mechanism of resveratrol against hepatic injury induced by iron overload in mice. *Toxicol Appl Pharmacol* (2021) 424:115596. doi: 10.1016/j.taap.2021.115596

30. Haidar R, Mhaidli H, Musallam KM, Taher AT. The spine in β-thalassemia syndromes. *Spine (Phila Pa 1976)* (2012) 37(4):334–9. doi: 10.1097/BRS.0b013e31821bd095

31. Shan L, Xu X, Zhang J, Cai P, Gao H, Lu Y, et al. Increased hemoglobin and heme in MALDI-TOF MS analysis induce ferroptosis and promote degeneration of herniated human nucleus pulposus. *Mol Med* (2021) 27(1):103. doi: 10.1186/s10020-021-00368-2

32. Chifman J, Laubenbacher R, Torti SV. A systems biology approach to iron metabolism. *Adv Exp Med Biol* (2014) 844:201–25. doi: 10.1007/978-1-4939-2095-2_10

33. Dixon SJ, Patel DN, Welsch M, Skouta R, Lee ED, Hayano M, et al. Pharmacological inhibition of cystine-glutamate exchange induces endoplasmic reticulum stress and ferroptosis. *Elife* (2014) 3:e02523. doi: 10.7554/eLife.02523

34. Maiorino M, Conrad M, Ursini F. GPx4, lipid peroxidation, and cell death: Discoveries, rediscoveries, and open issues. *Antioxid Redox Signal* (2018) 29(1):61–74. doi: 10.1089/ars.2017.7115

35. Chen X, Li J, Kang R, Klionsky DJ, Tang D. Ferroptosis: machinery and regulation. *Autophagy* (2021) 17(9):2054–81. doi: 10.1080/15548627.2020.1810918

36. Yang WS, SriRamaratnam R, Welsch ME, Shimada K, Skouta R, Viswanathan VS, et al. Regulation of ferroptotic cancer cell death by GPX4. *Cell* (2014) 156(1-2):317–31. doi: 10.1016/j.cell.2013.12.010

37. Ursini F, Maiorino M, Gregolin C. The selenoenzyme phospholipid hydroperoxide glutathione peroxidase. *Biochim Biophys Acta* (1985) 839(1):62–70. doi: 10.1016/0304-4165(85)90182-5

38. Brandes RP, Weissmann N, Schröder K. Nox family NADPH oxidases: Molecular mechanisms of activation. *Free Radic Biol Med* (2014) 76:208–26. doi: 10.1016/j.freeradbiomed.2014.07.046

39. Fan R, Sui J, Dong X, Jing B, Gao Z. Wedelolactone alleviates acute pancreatitis and associated lung injury *via* GPX4 mediated suppression of pyroptosis and ferroptosis. *Free Radic Biol Med* (2021) 173:29–40. doi: 10.1016/j.freeradbiomed.2021.07.009

40. Ding Y, Chen X, Liu C, Ge W, Wang Q, Hao X, et al. Identification of a small molecule as inducer of ferroptosis and apoptosis through ubiquitination of GPX4 in triple negative breast cancer cells. *J Hematol Oncol* (2021) 14(1):19. doi: 10.1186/s13045-020-01016-8

41. Basit F, van Oppen LM, Schöckel L, Bossenbroek HM, van Emst-de Vries SE, Hermeling JC, et al. Mitochondrial complex I inhibition triggers a mitophagy-dependent ROS increase leading to necroptosis and ferroptosis in melanoma cells. *Cell Death Dis* (2017) 8(3):e2716. doi: 10.1038/cddis.2017.133

42. Liu Y, Wang Y, Liu J, Kang R, Tang D. Interplay between MTOR and GPX4 signaling modulates autophagy-dependent ferroptotic cancer cell death. *Cancer Gene Ther* (2021) 28(1-2):55–63. doi: 10.1038/s41417-020-0182-y

43. Han D, Jiang L, Gu X, Huang S, Pang J, Wu Y, et al. SIRT3 deficiency is resistant to autophagy-dependent ferroptosis by inhibiting the AMPK/mTOR pathway and promoting GPX4 levels. *J Cell Physiol* (2020) 235(11):8839–51. doi: 10.1002/jcp.29727

44. Zhang X, Huang Z, Xie Z, Chen Y, Zheng Z, Wei X, et al. Homocysteine induces oxidative stress and ferroptosis of nucleus pulposus *via* enhancing methylation of GPX4. *Free Radic Biol Med* (2020) 160:552–65. doi: 10.1016/j.freeradbiomed.2020.08.029

45. Bin S, Xin L, Lin Z, Jinhua Z, Rui G, Xiang Z. Targeting miR-10a-5p/IL-6R axis for reducing IL-6-induced cartilage cell ferroptosis. *Exp Mol Pathol* (2021) 118:104570. doi: 10.1016/j.yexmp.2020.104570

46. Zhang Z, Tang J, Song J, Xie M, Liu Y, Dong Z, et al. Elabela alleviates ferroptosis, myocardial remodeling, fibrosis and heart dysfunction in hypertensive mice by modulating the IL-6/STAT3/GPX4 signaling. *Free Radic Biol Med* (2022) 181:130–42. doi: 10.1016/j.freeradbiomed.2022.01.020

47. Zou Y, Palte MJ, Deik AA, Li H, Eaton JK, Wang W, et al. A GPX4-dependent cancer cell state underlies the clear-cell morphology and confers sensitivity to ferroptosis. *Nat Commun* (2019) 10(1):1617. doi: 10.1038/s41467-019-09277-9

48. Bersuker K, Hendricks JM, Li Z, Magtanong L, Ford B, Tang PH, et al. The CoQ oxidoreductase FSP1 acts parallel to GPX4 to inhibit ferroptosis. *Nature* (2019) 575(7784):688–92. doi: 10.1038/s41586-019-1705-2

49. Doll S, Freitas FP, Shah R, Aldrovandi M, da Silva MC, Ingold I, et al. FSP1 is a glutathione-independent ferroptosis suppressor. *Nature* (2019) 575(7784):693–8. doi: 10.1038/s41586-019-1707-0

50. Marshall KR, Gong M, Wodke L, Lamb JH, Jones DJ, Farmer PB, et al. The human apoptosis-inducing protein AMID is an oxidoreductase with a modified flavin cofactor and DNA binding activity. *J Biol Chem* (2005) 280(35):30735–40. doi: 10.1074/jbc.M414018200

51. Shimada K, Skouta R, Kaplan A, Yang WS, Hayano M, Dixon SJ, et al. Global survey of cell death mechanisms reveals metabolic regulation of ferroptosis. *Nat Chem Biol* (2016) 12(7):497–503. doi: 10.1038/nchembio.2079

52. Kraft VAN, Bezjian CT, Pfeiffer S, Ringelstetter L, Muller C, Zandkarimi F, et al. GTP cyclohydrolase 1/Tetrahydrobiopterin counteract ferroptosis through lipid remodeling. *ACS Cent Sci* (2020) 6(1):41–53. doi: 10.1021/acscentsci.9b01063

53. Soula M, Weber RA, Zilka O, Alwaseem H, La K, Yen F, et al. Metabolic determinants of cancer cell sensitivity to canonical ferroptosis inducers. *Nat Chem Biol* (2020) 16(12):1351–60. doi: 10.1038/s41589-020-0613-y

54. Kagan VE, Mao G, Qu F, Angeli JP, Doll S, Croix CS, et al. Oxidized arachidonic and adrenic PEs navigate cells to ferroptosis. *Nat Chem Biol* (2017) 13(1):81–90. doi: 10.1038/nchembio.2238

55. Yuan H, Li X, Zhang X, Kang R, Tang D. Identification of ACSL4 as a biomarker and contributor of ferroptosis. *Biochem Biophys Res Commun* (2016) 478(3):1338–43. doi: 10.1016/j.bbrc.2016.08.124

56. Dixon SJ, Winter GE, Musavi LS, Lee ED, Snijder B, Rebsamen M, et al. Human haploid cell genetics reveals roles for lipid metabolism genes in nonapoptotic cell death. *ACS Chem Biol* (2015) 10(7):1604–9. doi: 10.1021/acschembio.5b00245

57. Yang WS, Kim KJ, Gaschler MM, Patel M, Shchepinov MS, Stockwell BR. Peroxidation of polyunsaturated fatty acids by lipoxygenases drives ferroptosis. *Proc Natl Acad Sci USA* (2016) 113(34):E4966–75. doi: 10.1073/pnas.1603244113

58. Zou Y, Li H, Graham ET, Deik AA, Eaton JK, Wang W, et al. Cytochrome P450 oxidoreductase contributes to phospholipid peroxidation in ferroptosis. *Nat Chem Biol* (2020) 16(3):302–9. doi: 10.1038/s41589-020-0472-6

59. Yang WH, Huang Z, Wu J, Ding CC, Murphy SK, Chi JT. A TAZ-ANGPTL4-NOX2 axis regulates ferroptotic cell death and chemoresistance in epithelial ovarian cancer. *Mol Cancer Res* (2020) 18(1):79–90. doi: 10.1158/1541-7786.Mcr-19-0691

60. Li Y, Wang J, Chen S, Wu P, Xu S, Wang C, et al. miR-137 boosts the neuroprotective effect of endothelial progenitor cell-derived exosomes in oxyhemoglobin-treated SH-SY5Y cells partially *via* COX2/PGE2 pathway. *Stem Cell Res Ther* (2020) 11(1):330. doi: 10.1186/s13287-020-01836-y

61. Xu Y, Liu Y, Li K, Yuan D, Yang S, Zhou L, et al. COX-2/PGE2 pathway inhibits the ferroptosis induced by cerebral ischemia reperfusion. *Mol Neurobiol* (2022) 59(3):1619–31. doi: 10.1007/s12035-021-02706-1

62. Valko M, Morris H, Cronin MT. Metals, toxicity and oxidative stress. *Curr Med Chem* (2005) 12(10):1161–208. doi: 10.2174/0929867053764635

63. Benedetti A, Comporti M, Esterbauer H. Identification of 4-hydroxynonenal as a cytotoxic product originating from the peroxidation of liver microsomal lipids. *Biochim Biophys Acta* (1980) 620(2):281–96. doi: 10.1016/0005-2760(80)90209-x

64. Cheeseman KH, Beavis A, Esterbauer H. Hydroxyl-radical-induced iron-catalysed degradation of 2-deoxyribose. *Quantit deter malondialdehyde. Biochem J* (1988) 252(3):649–53. doi: 10.1042/bj2520649

65. Esterbauer H, Zollner H. Methods for determination of aldehydic lipid peroxidation products. *Free Radic Biol Med* (1989) 7(2):197–203. doi: 10.1016/0891-5849(89)90015-4

66. Ayala A, Munoz MF, Arguelles S. Lipid peroxidation: production, metabolism, and signaling mechanisms of malondialdehyde and 4-hydroxy-2-nonenal. *Oxid Med Cell Longev* (2014) 2014:360438. doi: 10.1155/2014/360438

67. Gao M, Monian P, Quadri N, Ramasamy R, Jiang X. Glutaminolysis and transferrin regulate ferroptosis. *Mol Cell* (2015) 59(2):298–308. doi: 10.1016/j.molcel.2015.06.011

68. Ma S, Henson ES, Chen Y, Gibson SB. Ferroptosis is induced following siramesine and lapatinib treatment of breast cancer cells. *Cell Death Dis* (2016) 7(7):e2307. doi: 10.1038/cddis.2016.208

69. Yang WS, Stockwell BR. Synthetic lethal screening identifies compounds activating iron-dependent, nonapoptotic cell death in oncogenic-RAS-harboring cancer cells. *Chem Biol* (2008) 15(3):234–45. doi: 10.1016/j.chembiol.2008.02.010

70. Geng N, Shi BJ, Li SL, Zhong ZY, Li YC, Xua WL, et al. Knockdown of ferroportin accelerates erastin-induced ferroptosis in neuroblastoma cells. *Eur Rev Med Pharmacol Sci* (2018) 22(12):3826–36. doi: 10.26355/eurrev_201806_15267

71. Lu S, Song Y, Luo R, Li S, Li G, Wang K, et al. Ferroportin-dependent iron homeostasis protects against oxidative stress-induced nucleus pulposus cell ferroptosis and ameliorates intervertebral disc degeneration in vivo. *Oxid Med Cell Longev* (2021) 2021:6670497. doi: 10.1155/2021/6670497

72. Yang RZ, Xu WN, Zheng HL, Zheng XF, Li B, Jiang LS, et al. Involvement of oxidative stress-induced annulus fibrosus cell and nucleus pulposus cell ferroptosis in intervertebral disc degeneration pathogenesis. *J Cell Physiol* (2021) 236(4):2725–39. doi: 10.1002/jcp.30039

73. McBean GJ. The transsulfuration pathway: a source of cysteine for glutathione in astrocytes. *Amino Acids* (2012) 42(1):199–205. doi: 10.1007/s00726-011-0864-8

74. Liu N, Lin X, Huang C. Activation of the reverse transsulfuration pathway through NRF2/CBS confers erastin-induced ferroptosis resistance. *Br J Cancer* (2020) 122(2):279–92. doi: 10.1038/s41416-019-0660-x

75. Hayano M, Yang WS, Corn CK, Pagano NC, Stockwell BR. Loss of cysteinyl-tRNA synthetase (CARS) induces the transsulfuration pathway and inhibits ferroptosis induced by cystine deprivation. *Cell Death Differ* (2016) 23(2):270–8. doi: 10.1038/cdd.2015.93

76. Cassago A, Ferreira AP, Ferreira IM, Fornezari C, Gomes ER, Greene KS, et al. Mitochondrial localization and structure-based phosphate activation mechanism of glutaminase c with implications for cancer metabolism. *Proc Natl Acad Sci USA* (2012) 109(4):1092–7. doi: 10.1073/pnas.1112495109

77. Jennis M, Kung CP, Basu S, Budina-Kolomets A, Leu JI, Khaku S, et al. An African-specific polymorphism in the TP53 gene impairs p53 tumor suppressor function in a mouse model. *Genes Dev* (2016) 30(8):918–30. doi: 10.1101/gad.275891.115

78. Gao M, Yi J, Zhu J, Minikes AM, Monian P, Thompson CB, et al. Role of mitochondria in ferroptosis. *Mol Cell* (2019) 73(2):354–63.e3. doi: 10.1016/j.molcel.2018.10.042

79. Neumann D, Viollet B. AMP-activated protein kinase signalling. *Int J Mol Sci* (2019) 20(3):766. doi: 10.3390/ijms20030766

80. Lee H, Zandkarimi F, Zhang Y, Meena JK, Kim J, Zhuang L, et al. Energy-stress-mediated AMPK activation inhibits ferroptosis. *Nat Cell Biol* (2020) 22 (2):225–34. doi: 10.1038/s41556-020-0461-8

81. Ma H, Wang X, Zhang W, Li H, Zhao W, Sun J, et al. Melatonin suppresses ferroptosis induced by high glucose *via* activation of the Nrf2/HO-1 signaling pathway in type 2 diabetic osteoporosis. *Oxid Med Cell Longev* (2020) 2020:9067610. doi: 10.1155/2020/9067610

82. Dai C, Chen X, Li J, Comish P, Kang R, Tang D. Transcription factors in ferroptotic cell death. *Cancer Gene Ther* (2020) 27(9):645–56. doi: 10.1038/s41417-020-0170-2

83. Bieging KT, Mello SS, Attardi LD. Unravelling mechanisms of p53-mediated tumour suppression. *Nat Rev Cancer* (2014) 14(5):359–70. doi: 10.1038/nrc3711

84. Ma Q. Role of nrf2 in oxidative stress and toxicity. *Annu Rev Pharmacol Toxicol* (2013) 53:401–26. doi: 10.1146/annurev-pharmtox-011112-140320

85. Wang L, Liu Y, Du T, Yang H, Lei L, Guo M, et al. ATF3 promotes erastin-induced ferroptosis by suppressing system xc(). *Cell Death Differ* (2020) 27(2):662–75. doi: 10.1038/s41418-019-0380-z

86. Wu J, Minikes AM, Gao M, Bian H, Li Y, Stockwell BR, et al. Intercellular interaction dictates cancer cell ferroptosis *via* NF2-YAP signalling. *Nature* (2019) 572(7769):402–6. doi: 10.1038/s41586-019-1426-6

87. Wang X, Sun D, Tai J, Chen S, Yu M, Ren D, et al. TFAP2C promotes stemness and chemotherapeutic resistance in colorectal cancer *via* inactivating hippo signaling pathway. *J Exp Clin Cancer Res* (2018) 37(1):27. doi: 10.1186/s13046-018-0683-9

88. Liu J, Yang M, Kang R, Klionsky DJ, Tang D. Autophagic degradation of the circadian clock regulator promotes ferroptosis. *Autophagy* (2019) 15(11):2033–5. doi: 10.1080/15548627.2019.1659623

89. Yang M, Chen P, Liu J, Zhu S, Kroemer G, Klionsky DJ, et al. Clockophagy is a novel selective autophagy process favoring ferroptosis. *Sci Adv* (2019) 5(7): eaaw2238. doi: 10.1126/sciadv.aaw2238

90. Wang M, Mao C, Ouyang L, Liu Y, Lai W, Liu N, et al. Long noncoding RNA LINC00336 inhibits ferroptosis in lung cancer by functioning as a competing endogenous RNA. *Cell Death Differ* (2019) 26(11):2329–43. doi: 10.1038/s41418-019-0304-y

91. Jiang Y, Mao C, Yang R, Yan B, Shi Y, Liu X, et al. EGLN1/c-myc induced lymphoid-specific helicase inhibits ferroptosis through lipid metabolic gene expression changes. *Theranostics* (2017) 7(13):3293–305. doi: 10.7150/thno.19988

92. Mao C, Wang X, Liu Y, Wang M, Yan B, Jiang Y, et al. A G3BP1-interacting lncRNA promotes ferroptosis and apoptosis in cancer *via* nuclear sequestration of p53. *Cancer Res* (2018) 78(13):3484–96. doi: 10.1158/0008-5472.Can-17-3454

93. Sui S, Zhang J, Xu S, Wang Q, Wang P, Pang D. Ferritinophagy is required for the induction of ferroptosis by the bromodomain protein BRD4 inhibitor (+)-JQ1 in cancer cells. *Cell Death Dis* (2019) 10(5):331. doi: 10.1038/s41419-019-1564-7

94. Wang Y, Zhao Y, Wang H, Zhang C, Wang M, Yang Y, et al. Histone demethylase KDM3B protects against ferroptosis by upregulating SLC7A11. *FEBS Open Bio* (2020) 10(4):637–43. doi: 10.1002/2211-5463.12823

95. Eaton JK, Furst L, Ruberto RA, Moosmayer D, Hilpmann A, Ryan MJ, et al. Selective covalent targeting of GPX4 using masked nitrile-oxide electrophiles. *Nat Chem Biol* (2020) 16(5):497–506. doi: 10.1038/s41589-020-0501-5

96. Gaschler MM, Andia AA, Liu H, Csuka JM, Hurlocker B, Vaiana CA, et al. FINO(2) initiates ferroptosis through GPX4 inactivation and iron oxidation. *Nat Chem Biol* (2018) 14(5):507–15. doi: 10.1038/s41589-018-0031-6

97. Wenz C, Faust D, Linz B, Turmann C, Nikolova T, Bertin J, et al. T-BuOOH induces ferroptosis in human and murine cell lines. *Arch Toxicol* (2018) 92(2):759–75. doi: 10.1007/s00204-017-2066-y

98. Baba Y, Higa JK, Shimada BK, Horiuchi KM, Suhara T, Kobayashi M, et al. Protective effects of the mechanistic target of rapamycin against excess iron and ferroptosis in cardiomyocytes. *Am J Physiol Heart Circ Physiol* (2018) 314(3): H659–h668. doi: 10.1152/ajpheart.00452.2017

99. Li Q, Han X, Lan X, Gao Y, Wan J, Durham F, et al. Inhibition of neuronal ferroptosis protects hemorrhagic brain. *JCI Insight* (2017) 2(7):e90777. doi: 10.1172/jci.insight.90777

100. Li L, Wang K, Jia R, Xie J, Ma L, Hao Z, et al. Ferroportin-dependent ferroptosis induced by ellagic acid retards liver fibrosis by impairing the SNARE complexes formation. *Redox Biol* (2022) 56:102435. doi: 10.1016/j.redox.2022.102435

101. Doll S, Proneth B, Tyurina YY, Panzilius E, Kobayashi S, Ingold I, et al. ACSL4 dictates ferroptosis sensitivity by shaping cellular lipid composition. *Nat Chem Biol* (2017) 13(1):91–8. doi: 10.1038/nchembio.2239

102. Xie Y, Zhu S, Song X, Sun X, Fan Y, Liu J, et al. Tang: The tumor suppressor p53 limits ferroptosis by blocking DPP4 activity. *Cell Rep* (2017) 20 (7):1692–704. doi: 10.1016/j.celrep.2017.07.055

103. Wu Z, Geng Y, Lu X, Shi Y, Wu G, Zhang M, et al. Chaperone-mediated autophagy is involved in the execution of ferroptosis. *Proc Natl Acad Sci USA* (2019) 116(8):2996–3005. doi: 10.1073/pnas.1819728116

104. Zhou W, Shi Y, Wang H, Chen L, Yu C, Zhang X, et al. Exercise-induced FNDC5/irisin protects nucleus pulposus cells against senescence and apoptosis by activating autophagy. *Exp Mol Med* (2022) 54(7):1038–48. doi: 10.1038/s12276-022-00811-2

105. Bahar ME, Hwang JS, Ahmed M, Lai TH, Pham TM, Elashkar O, et al. Targeting autophagy for developing new therapeutic strategy in intervertebral disc degeneration. *Antioxid (Basel)* (2022) 11(8):1571. doi: 10.3390/antiox11081571

106. Li F, Xie W, Chen Z, Zhou Z, Wang Z, Xiao J, et al. Neuropeptide y and receptors are associated with the pyroptosis of nucleus pulposus in aging and degenerative intervertebral discs of rats. *Neuropeptides* (2022) 96:102284. doi: 10.1016/j.npep.2022.102284

107. Cao C, Chen S, Song Z, Liu Z, Zhang M, Ma Z, et al. Inflammatory stimulation mediates nucleus pulposus cell necroptosis through mitochondrial function disfunction and oxidative stress pathway. *Front Biosci (Landmark Ed)* (2022) 27(4):111. doi: 10.31083/j.fbl2704111

108. Ma J, Li X, Fan Y, Yang D, Gu Q, Li D, et al. miR-494-3p promotes erastin-induced ferroptosis by targeting REST to activate the interplay between SP1 and ACSL4 in parkinson's disease. *Oxid Med Cell Longev* (2022) 2022:7671324. doi: 10.1155/2022/7671324

109. He DL, Fan YG, Wang ZY. Energy crisis links to autophagy and ferroptosis in alzheimer's disease: current evidence and future avenues. *Curr Neuropharmacol* (2022). doi: 10.2174/1570159x20666220817140737

110. Fan X, Zhang X, Liu LC, Zhang S, Pelger CB, Lughmani HY, et al. Hemopexin accumulates in kidneys and worsens acute kidney injury by causing hemoglobin deposition and exacerbation of iron toxicity in proximal tubules. *Kidney Int* (2022). doi: 10.1016/j.kint.2022.07.024

111. Li M, Xin S, Gu R, Zheng L, Hu J, Zhang R, et al. Novel diagnostic biomarkers related to oxidative stress and macrophage ferroptosis in atherosclerosis. *Oxid Med Cell Longev* (2022) 2022:8917947. doi: 10.1155/2022/8917947

112. Li M, Yang N, Hao L, Zhou W, Li L, Liu L, et al. Melatonin inhibits the ferroptosis pathway in rat bone marrow mesenchymal stem cells by activating the PI3K/AKT/mTOR signaling axis to attenuate steroid-induced osteoporosis. *Oxid Med Cell Longev* (2022) 2022:8223737. doi: 10.1155/2022/8223737

113. Sun K, Guo Z, Hou L, Xu J, Du T, Xu T, et al. Iron homeostasis in arthropathies: From pathogenesis to therapeutic potential. *Ageing Res Rev* (2021) 72:101481. doi: 10.1016/j.arr.2021.101481

114. Li Y, Pan D, Wang X, Huo Z, Wu X, Li J, et al. Silencing ATF3 might delay TBHP-induced intervertebral disc degeneration by repressing NPC ferroptosis, apoptosis, and ECM degradation. *Oxid Med Cell Longev* (2022) 2022:4235126. doi: 10.1155/2022/4235126

115. Wang W, Jing X, Du T, Ren J, Liu X, Chen F, et al. Iron overload promotes intervertebral disc degeneration *via* inducing oxidative stress and ferroptosis in endplate chondrocytes. *Free Radic Biol Med* (2022) 190:234–46. doi: 10.1016/j.freeradbiomed.2022.08.018

116. Yu X, Xu H, Liu Q, Wang Y, Wang S, Lu R, et al. circ_0072464 shuttled by bone mesenchymal stem cell-secreted extracellular vesicles inhibits nucleus pulposus cell ferroptosis to relieve intervertebral disc degeneration. *Oxid Med Cell Longev* (2022) 2022:2948090. doi: 10.1155/2022/2948090

117. Mizrahi O, Sheyn D, Tawackoli W, Ben-David S, Su S, Li N, et al. Nucleus pulposus degeneration alters properties of resident progenitor cells. *Spine J* (2013) 13(7):803–14. doi: 10.1016/j.spinee.2013.02.065

118. Peng B, Chen J, Kuang Z, Li D, Pang X, Zhang X. Expression and role of connective tissue growth factor in painful disc fibrosis and degeneration. *Spine (Phila Pa 1976)* (2009) 34(5):E178–82. doi: 10.1097/BRS.0b013e3181908ab3

119. Zhang Y, Han S, Kong M, Tu Q, Zhang L, Ma X. Single-cell RNA-seq analysis identifies unique chondrocyte subsets and reveals involvement of

ferroptosis in human intervertebral disc degeneration. *Osteoarthritis Cartilage* (2021) 29(9):1324–34. doi: 10.1016/j.joca.2021.06.010

120. Masaldan S, Clatworthy SAS, Gamell C, Meggyesy PM, Rigopoulos AT, Haupt S, et al. Iron accumulation in senescent cells is coupled with impaired ferritinophagy and inhibition of ferroptosis. *Redox Biol* (2018) 14:100–15. doi: 10.1016/j.redox.2017.08.015

121. Kang R, Kroemer G, Tang D. The tumor suppressor protein p53 and the ferroptosis network. *Free Radic Biol Med* (2019) 133:162–8. doi: 10.1016/j.freeradbiomed.2018.05.074

122. Guo Y, Li C, Shen B, Chen X, Hu T, Wu D. Is intervertebral disc degeneration associated with reduction in serum ferritin? *Eur Spine J* (2022). doi: 10.1007/s00586-022-07361-1

123. Li Y, Zhao J, Yu S, Wang Z, He X, Su Y, et al. Extracellular vesicles long RNA sequencing reveals abundant mRNA, circRNA, and lncRNA in human blood as potential biomarkers for cancer diagnosis. *Clin Chem* (2019) 65(6):798–808. doi: 10.1373/clinchem.2018.301291

124. DiStefano TJ, Vaso K, Danias G, Chionuma HN, Weiser JR, Iatridis JC. Extracellular vesicles as an emerging treatment option for intervertebral disc degeneration: Therapeutic potential, translational pathways, and regulatory considerations. *Adv Healthc Mater* (2022) 11(5):e2100596. doi: 10.1002/adhm.202100596

125. Song J, Chen ZH, Zheng CJ, Song KH, Xu GY, Xu S, et al. Exosome-transported circRNA_0000253 competitively adsorbs MicroRNA-141-5p and increases IDD. *Mol Ther Nucleic Acids* (2020) 21:1087–99. doi: 10.1016/j.omtn.2020.07.039

126. Du WW, Zhang C, Yang W, Yong T, Awan FM, Yang BB. Identifying and characterizing circRNA-protein interaction. *Theranostics* (2017) 7(17):4183–91. doi: 10.7150/thno.21299

127. Shen W, Gao C, Cueto R, Liu L, Fu H, Shao Y, et al. Homocysteine-methionine cycle is a metabolic sensor system controlling methylation-regulated pathological signaling. *Redox Biol* (2020) 28:101322. doi: 10.1016/j.redox.2019.101322

128. Sonkar SK, Kumar S, Singh NK, Tandon R. Hyperhomocysteinemia induced locked-in syndrome in a young adult due to folic acid deficiency. *Nutr Neurosci* (2021) 24(10):781–3. doi: 10.1080/1028415x.2019.1681064

129. Komorniak N, Szczuko M, Kowalewski B, Stachowska E. Nutritional deficiencies, bariatric surgery, and serum homocysteine level: Review of current literature. *Obes Surg* (2019) 29(11):3735–42. doi: 10.1007/s11695-019-04100-2

130. van den Akker GGH, Koenders MI, van de Loo FAJ, van Lent P, Blaney Davidson E, van der Kraan PM. Transcriptional profiling distinguishes inner and outer annulus fibrosus from nucleus pulposus in the bovine intervertebral disc. *Eur Spine J* (2017) 26(8):2053–62. doi: 10.1007/s00586-017-5150-3

131. Raj PP. Intervertebral disc: anatomy-physiology-pathophysiology-treatment. *Pain Pract* (2008) 8(1):18–44. doi: 10.1111/j.1533-2500.2007.00171.x

132. Ashinsky BG, Bonnevie ED, Mandalapu SA, Pickup S, Wang C, Han L, et al. Intervertebral disc degeneration is associated with aberrant endplate remodeling and reduced small molecule transport. *J Bone Miner Res* (2020) 35(8):1572–81. doi: 10.1002/jbmr.4009

133. van der Werf M, Lezuo P, Maissen O, van Donkelaar CC, Ito K. Inhibition of vertebral endplate perfusion results in decreased intervertebral disc intranuclear diffusive transport. *J Anat* (2007) 211(6):769–74. doi: 10.1111/j.1469-7580.2007.00816.x

134. Grunhagen T, Wilde G, Soukane DM, Shirazi-Adl SA, Urban JP. Nutrient supply and intervertebral disc metabolism. *J Bone Joint Surg Am* (2006) 88 Suppl:2, 30–5. doi: 10.2106/jbjs.E.01290

135. Wong J, Sampson SL, Bell-Briones H, Ouyang A, Lazar AA, Lotz JC, et al. Nutrient supply and nucleus pulposus cell function: effects of the transport properties of the cartilage endplate and potential implications for intradiscal biologic therapy. *Osteoarthritis Cartilage* (2019) 27(6):956–64. doi: 10.1016/j.joca.2019.01.013

136. Jing X, Du T, Li T, Yang X, Wang G, Liu X, et al. The detrimental effect of iron on OA chondrocytes: Importance of pro-inflammatory cytokines induced iron influx and oxidative stress. *J Cell Mol Med* (2021) 25(12):5671–80. doi: 10.1111/jcmm.16581

137. Yao X, Sun K, Yu S, Luo J, Guo J, Lin J, et al. Chondrocyte ferroptosis contribute to the progression of osteoarthritis. *J Orthop Translat* (2021) 27:33–43. doi: 10.1016/j.jot.2020.09.006

138. Zhang S, Liu W, Chen S, Wang B, Wang P, Hu B, et al. Extracellular matrix in intervertebral disc: basic and translational implications. *Cell Tissue Res* (2022), 390(1):1–22. doi: 10.1007/s00441-022-03662-5

139. Hu B, Lv X, Wei L, Wang Y, Zheng G, Yang C, et al. Sensory nerve maintains intervertebral disc extracellular matrix homeostasis *Via* CGRP/CHSY1 axis. *Adv Sci (Weinh)* (2022) e2202620. doi: 10.1002/advs.202202620

140. Francisco V, Pino J, González-Gay M, Lago F, Karppinen J, Tervonen O, et al. A new immunometabolic perspective of intervertebral disc degeneration. *Nat Rev Rheumatol* (2022) 18(1):47–60. doi: 10.1038/s41584-021-00713-z

141. Choi H, Tessier S, Silagi ES, Kyada R, Yousefi F, Pleshko N, et al. A novel mouse model of intervertebral disc degeneration shows altered cell fate and matrix homeostasis. *Matrix Biol* (2018) 70:102–22. doi: 10.1016/j.matbio.2018.03.019

142. Liu W, Xia P, Feng J, Kang L, Huang M, Wang K, et al. MicroRNA-132 upregulation promotes matrix degradation in intervertebral disc degeneration. *Exp Cell Res* (2017) 359(1):39–49. doi: 10.1016/j.yexcr.2017.08.011

143. Camacho A, Simao M, Ea HK, Cohen-Solal M, Richette P, Branco J, et al. Iron overload in a murine model of hereditary hemochromatosis is associated with accelerated progression of osteoarthritis under mechanical stress. *Osteoarthritis Cartilage* (2016) 24(3):494–502. doi: 10.1016/j.joca.2015.09.007

144. Di Maggio R, Maggio A. The new era of chelation treatments: effectiveness and safety of 10 different regimens for controlling iron overloading in thalassaemia major. *Br J Haematol* (2017) 178(5):676–88. doi: 10.1111/bjh.14712

145. Ran R, Liao HY, Wang ZQ, Gong CY, Zhou KS, Zhang HH. Mechanisms and functions of long noncoding RNAs in intervertebral disc degeneration. *Pathol Res Pract* (2022) 235:153959. doi: 10.1016/j.prp.2022.153959

146. Bhujel B, Shin HE, Choi DJ, Han I. Mesenchymal stem cell-derived exosomes and intervertebral disc regeneration: Review. *Int J Mol Sci* (2022) 23(13):7306. doi: 10.3390/ijms23137306

147. Lin KH, Kuo JR, Lu WJ, Chung CL, Chou DS, Huang SY, et al. Hinokitiol inhibits platelet activation ex vivo and thrombus formation in vivo. *Biochem Pharmacol* (2013) 85(10):1478–85. doi: 10.1016/j.bcp.2013.02.027

148. Xi J, Zhang Z, Wang Z, Wu Q, He Y, Xu Y, et al. Hinokitiol functions as a ferroptosis inhibitor to confer neuroprotection. *Free Radic Biol Med* (2022) 190:202–15. doi: 10.1016/j.freeradbiomed.2022.08.011

149. Wang YM, Gong FC, Qi X, Zheng YJ, Zheng XT, Chen Y, et al. Mucin 1 inhibits ferroptosis and sensitizes vitamin e to alleviate sepsis-induced acute lung injury through GSK3β/Keap1-Nrf2-GPX4 pathway. *Oxid Med Cell Longev* (2022) 2022:2405943. doi: 10.1155/2022/2405943

150. Mishima E, Ito J, Wu Z, Nakamura T, Wahida A, Doll S, et al. A non-canonical vitamin K cycle is a potent ferroptosis suppressor. *Nature* (2022) 608(7924):778–83. doi: 10.1038/s41586-022-05022-3

151. Wei Z, Shaohuan Q, Pinfang K, Chao S. Curcumin attenuates ferroptosis-induced myocardial injury in diabetic cardiomyopathy through the Nrf2 pathway. *Cardiovasc Ther* (2022) 2022:3159717. doi: 10.1155/2022/3159717

152. Hirata Y, Okazaki R, Sato M, Oh-Hashi K, Takemori H, Furuta K. Effect of ferroptosis inhibitors oxindole-curcumin hybrid compound and N,N-dimethylaniline derivatives on rotenone-induced oxidative stress. *Eur J Pharmacol* (2022) 928:175119. doi: 10.1016/j.ejphar.2022.175119

153. Jing X, Du T, Chen K, Guo J, Xiang W, Yao X, et al. Icariin protects against iron overload-induced bone loss *via* suppressing oxidative stress. *J Cell Physiol* (2019) 234(7):10123–37. doi: 10.1002/jcp.27678

154. Zuo S, Zou W, Wu RM, Yang J, Fan JN, Zhao XK, et al. Icariin alleviates IL-1β-Induced matrix degradation by activating the Nrf2/ARE pathway in human chondrocytes. *Drug Des Devel Ther* (2019) 13:3949–61. doi: 10.2147/dddt.S203094

155. Zhao L, Wang Y, Wang Z, Xu Z, Zhang Q, Yin M. Effects of dietary resveratrol on excess-iron-induced bone loss *via* antioxidative character. *J Nutr Biochem* (2015) 26(11):1174–82. doi: 10.1016/j.jnutbio.2015.05.009

156. Tian Q, Wu S, Dai Z, Yang J, Zheng J, Zheng Q, et al. Iron overload induced death of osteoblasts *in vitro*: involvement of the mitochondrial apoptotic pathway. *PeerJ* (2016) 4:e2611. doi: 10.7717/peerj.2611

157. Wang X, Ma H, Sun J, Zheng T, Zhao P, Li H, et al. Mitochondrial ferritin deficiency promotes osteoblastic ferroptosis *Via* mitophagy in type 2 diabetic osteoporosis. *Biol Trace Elem Res* (2022) 200(1):298–307. doi: 10.1007/s12011-021-02627-z

158. Yang RZ, Xu WN, Zheng HL, Zheng XF, Li B, Jiang LS, et al. Exosomes derived from vascular endothelial cells antagonize glucocorticoid-induced osteoporosis by inhibiting ferritinophagy with resultant limited ferroptosis of osteoblasts. *J Cell Physiol* (2021) 236(9):6691–705. doi: 10.1002/jcp.30331

159. Lu J, Yang J, Zheng Y, Chen X, Fang S. Extracellular vesicles from endothelial progenitor cells prevent steroid-induced osteoporosis by suppressing the ferroptotic pathway in mouse osteoblasts based on bioinformatics evidence. *Sci Rep* (2019) 9(1):16130. doi: 10.1038/s41598-019-52513-x

frontiers | Frontiers in Endocrinology

TYPE Original Research
PUBLISHED 22 November 2022
DOI 10.3389/fendo.2022.1080033

OPEN ACCESS

EDITED BY
Shibao Lu,
Xuanwu Hospital, Capital Medical University, China

REVIEWED BY
Yukun Zhang,
Huazhong University of Science and Technology, China
Cao Yang,
Huazhong University of Science and Technology, China
Haiying Liu,
Peking University People's Hospital, China

*CORRESPONDENCE
Weishi Li
puh3liweishi@163.com

SPECIALTY SECTION
This article was submitted to Bone Research, a section of the journal Frontiers in Endocrinology

RECEIVED 25 October 2022
ACCEPTED 08 November 2022
PUBLISHED 22 November 2022

CITATION
Wang W, Guo Y, Li W and Chen Z (2022) The difference of paraspinal muscle between patients with lumbar spinal stenosis and normal middle-aged and elderly people, studying by propensity score matching. *Front. Endocrinol.* 13:1080033. doi: 10.3389/fendo.2022.1080033

The difference of paraspinal muscle between patients with lumbar spinal stenosis and normal middle-aged and elderly people, studying by propensity score matching

Wei Wang[1], Yang Guo[1], Weishi Li[2,3,4]* and Zhongqiang Chen[2,3,4]

[1]Department of Orthopaedics, Tianjin Hospital, Tianjin, China, [2]Department of Orthopaedics, Peking University Third Hospital, Beijing, China, [3]Beijing Key Laboratory of Spinal Disease Research, Beijing, China, [4]Engineering Research Center of Bone and Joint Precision Medicine, Ministry of Education, Beijing, China

Objective: The purpose of this study was to elaborate the characteristics of paraspinal muscles in lower lumbar, to compare the differences of paraspinal muscle between patients with lumbar spinal stenosis and normal people and to explore the influencing factors of paraspinal muscle degeneration in patients with lumbar spinal stenosis.

Method: The 39 pairs of patients and normal people were selected by propensity score matching. The differences of multifidus muscle and erection spine muscle parameters between the two groups were compared by independent-samples t-test and the relationship between age, paraspinal muscle degeneration and other factors in patients with lumbar spinal stenosis was analyzed by Pearson or Spearman correlation analysis.

Result: The general conditions of the two groups (patients with lumbar spinal stenosis and normal people) were well matched. There were significant differences in the relative fatty cross sectional area, fatty infiltration and relative signal intensity of multifidus muscle at L3 level. The fatty infiltration and relative signal intensity of multifidus muscle at L4 level and the relative signal intensity of multifidus muscle at L5 level were also significantly different. For male, the relative fatty cross sectional area, the fatty infiltration and relative signal intensity of multifidus muscle in patients were higher than those in healthy peers. For female, the relative signal intensity of multifidus muscle in patients was higher, too. In patients group, age was significantly correlated with the relative fatty cross sectional area, fatty infiltration and relative signal intensity of multifidus muscle and erector spinae muscle. Weight and BMI were significantly correlated with the relative total cross-sectional area of erector spinae muscle. The fatty infiltration increased more significantly with age in patients than that in normal people.

10.3389/fendo.2022.1080033

Conclusion: The change rules of paraspinal muscles in patients with lumbar spinal stenosis are similar to those in normal people. The degeneration of paraspinal muscle in patients with lumbar spinal stenosis was more severe than that in normal people, mostly in multifidus muscle. The paraspinal muscle degeneration was related to age in patients, and the effect of age on atrophy of paraspinal muscle was greater than that of normal people.

KEYWORDS

multifidus, erector spinae muscle, paraspinal muscle degeneration, normal people, lumbar spinal stenosis

Introduction

With the aging of the population, the incidence of lumbar degenerative diseases is gradually increasing. Recently, many studies focused on the degeneration of paraspinal muscle in lumbar degenerative diseases (1–6), because paraspinal muscle plays an important role in maintaining stability. Ogon studied the degeneration of paraspinal muscles in 40 pairs of patients with chronic nonspecific low back pain and lumbar spinal stenosis (7). Other studies also investigated the degeneration of paraspinal muscle in patients with low back pain (8, 9) and lumbar degenerative kyphosis (3, 10).

Lumbar spinal stenosis (LSS) is one of the most common lumbar degenerative diseases (11), which is associated with high social and economic burden (12). Many researches also explored the degeneration of paraspinal muscle in patients with LSS (5, 13, 14). Yagi investigated the degeneration of paraspinal muscle in patients with both simple LSS and degenerative scoliosis combined with LSS. By analyzing the data of 60 pairs of female patients, they found that the cross-sectional area of multifidus muscle was significantly smaller in patients with degenerative scoliosis combined with LSS than that in patients with simple LSS (15). Another study found that the decrease of cross-sectional area and atrophy in multifidus muscle was associated with poorer outcome in patients with LSS (16), while it only measured the parameters of multifidus muscle. Although these researches investigated the degeneration of paraspinal muscle in patients with LSS, the difference of paraspinal muscle between normal people and patients with lumbar spinal stenosis was unclear.

Previous studies focused on the degeneration of paraspinal muscles, especially in lower lumbar, while their results were not comparable due to the differences of measurements (17–20). Some studies measured paraspinal muscle parameters at single level of lumbar (13, 14, 21), while others measured at multi-levels (4, 10, 17). The parameters they measured were also different from each other. There lacked a study detailing paraspinal muscle parameters.

So the purpose of this study was to elaborate the characteristics of paraspinal muscles in lower lumbar, to compare the differences of paraspinal muscle between patients with LSS and normal people and to explore the influencing factors of paraspinal muscle degeneration in patients with LSS.

Method

General information

This study was approved by the Ethics Committee of Peking University Third Hospital. There were 93 patients in our study, who were diagnosed as lumbar spinal stenosis and underwent posterior lumbar decompression and fusion surgery from October 2018 to June 2019. The inclusion criteria were (i) age was from 50 to 80 years old, (ii) diagnosed as lumbar spinal stenosis, (iii) undertook lumbar MRI test. The exclusion criteria were (i) with other spinal diseases, (ii) with a history of spinal surgery, (iii) with neuromuscular diseases, (iiii) lumbar MRI was uncomplete. Control group included 45 normal middle-aged and elderly people, who were prospectively recruited from February 2020 to November 2020. The inclusion criteria were (i) age was from 50 to 80 years old, (ii) without spinal diseases, (iii) without spinal surgery, (iiii) without low back pain and trauma in past 3 months. The exclusion criteria were (i) with neuromuscular diseases, (ii) with MRI contraindications. All the normal people signed the informed consent forms.

Clinical measurements

The data of both patients and normal people was recorded, including the age, gender, height, weight and history of hypertension or diabetes. All patients underwent lumbar magnetic resonance imaging (MRI) within 1 month before surgery. All normal people underwent lumbar MRI within 1 month before we measured the parameters.

Measurements of the multifidus (MF) and erector spinae muscle (ES) were obtained from T2-weighted images by Image J software. MRIs were required with Signa HDxt 3.0T (General Electric Company, USA). Patients were placed in the supine position, with their legs straight and the lumbar spine in a neutral posture. Axial MRI was parallel to the inferior endplate of the vertebral body. All muscles were measured bilaterally at the inferior vertebral endplate of L3 to L5. The mean value of left and right paraspinal muscle was calculated. Region of interest was used to measure muscular parameters, including: total cross-sectional area (tCSA), fatty cross-sectional area (fCSA), fatty infiltration (FI) and signal intensity (SI). The fCSA was defined as the area of fatty tissue in muscle, which was measured by the thresholding technique. The FI was defined as the ratio of fCSA to tCSA. They reflected the degeneration of paraspinal muscles.

In order to reduce the influence of height, weight and body size on paraspinal muscle parameters, we calculated the relative cross-sectional area (rCSA) and relative signal intensity (rSI). The relative total cross-sectional area (rtCSA) was defined as the ratio of cross-sectional area of paraspinal muscle to cross-sectional area of vertebral body. The relative fatty cross-sectional area (rfCSA) was defined as the ratio of cross-sectional area of fatty tissue to cross-sectional area of vertebral body. The relative signal intensity (rSI) was defined as the ratio of signal intensity of paraspinal muscle to signal intensity of subcutaneous fat.

Statistical analysis

SPSS version 22.0 (IBM company, USA) was used to analyze the collected data. By using propensity score matching, we matched 93 patients with LSS and 45 normal people at a ratio of 1:1. The matching model we used was logistic regression model. To get a good matching score, the influencing factors such as age, gender, height, weight and body mass index (BMI) were used as matching indexes. The values were expressed as mean ± standard deviation. Age, BMI and paraspinal muscle parameters were continuous variable while gender was categorical variable. We measured the paraspinal muscle parameters at a level of L3 to L5 and analyzed the change rule of paraspinal muscle parameters. The differences of paraspinal muscle parameters between patients with LSS and normal people were compared. The independent sample t-test or rank sum test were used to explore the difference of continuous variables between the two groups, while the chi-square test was used to analyze the difference of categorical variables. Correlations between measurements of paraspinal muscle and other factors were investigated by Pearson correlation analysis or Spearman correlation analysis. Statistical significance was set at p-value < 0.05.

Results

By using propensity score matching, we matched 39 pairs of patients with LSS and normal middle-age and elderly people well. As showed in Table 1, there were 18 males and 21 females in patients group. The average age of patients was 62.9 ± 7.8 years. 10 patients were diagnosed as hypertension and 4 patients were diagnosed as diabetes. In normal middle-age and elderly people group (normal group), there were 16 males and 23 females. The average age of normal people was 62.1 ± 7.3 years. 10 patients were diagnosed as hypertension and 6 patients were diagnosed as diabetes. There was no significant difference in age, gender, height, weight, BMI and comorbidities between the two groups, indicating that the two groups were matched well.

To explore the differences in paraspinal muscles between patients with LSS and normal middle-aged and elderly people, we measured the praspinal muscle parameters, including rtCSA, rfCSA, FI and rSI. The results were recorded in Table 2. Compared with the normal group, the change rules of paraspinal muscle in the patient group were similar. From top to bottom of the spinal axis, the relative cross-sectional area of MF increases, while that of ES decreases. The FI and rSI of MF and ES increased gradually.

For paraspinal muscle parameters at L3 level, there were significant differences in the rfCSA, FI, rSI of MF and rSI of ES (P<0.05). The FI and rSI of MF at L4 level and the rSI of MF at L5 level were also significantly different (P<0.05). Although there was no significant difference in rfCSA of MF and rSI of ES at L4 level and rfCSA, FI of MF, and rSI of ES at L5 level, those parameters of

TABLE 1 The basic information of two groups.

Parameters	Patients group	Normal group	P-value
Age (years)	62.9 ± 7.8	62.1 ± 7.3	0.666
Gender (M/F)	18/21	16/23	0.648
Height (cm)	163.7 ± 8.7	163.2 ± 9.1	0.767
Weight (kg)	68.2 ± 10.3	66.1 ± 11.8	0.502
BMI (kg/m^2)	25.4 ± 2.9	24.7 ± 2.9	0.298
Hypertension (Y/N)	10/29	10/29	1.00
Diabetes (Y/N)	4/35	6/33	0.735

BMI, body mass index.

10.3389/fendo.2022.1080033

TABLE 2 The comparison of paraspinal muscle parameters at L3 to L5 levels.

Parameters	Patients group	Normal group	P-value
L3			
MF rtCSA	0.96 ± 0.30	0.94 ± 0.17	0.731
MF rfCSA	0.32 ± 0.17	0.27 ± 0.15	0.042*
ES rtCSA	2.60 ± 0.62	2.71 ± 0.43	0.385
ES rfCSA	0.56 ± 0.24	0.59 ± 0.22	0.415
MF FI	0.34 ± 0.14	0.28 ± 0.11	0.013*
ES FI	0.22 ± 0.08	0.22 ± 0.08	0.948
MF rSI	0.49 ± 0.13	0.40 ± 0.09	<0.01**
ES rSI	0.41 ± 0.09	0.37 ± 0.08	0.030*
L4			
MF rtCSA	1.29 ± 0.32	1.29 ± 0.24	0.946
MF rfCSA	0.48 ± 0.23	0.41 ± 0.19	0.062
ES rtCSA	2.20 ± 0.52	2.38 ± 0.40	0.083
ES rfCSA	0.66 ± 0.29	0.71 ± 0.23	0.412
MF FI	0.37 ± 0.15	0.31 ± 0.11	0.044*
ES FI	0.29 ± 0.10	0.30 ± 0.09	0.964
MF rSI	0.53 ± 0.13	0.44 ± 0.11	0.002**
ES rSI	0.47 ± 0.11	0.43 ± 0.10	0.116
L5			
MF rtCSA	1.52 ± 0.36	1.55 ± 0.32	0.630
MF rfCSA	0.55 ± 0.20	0.50 ± 0.23	0.102
ES rtCSA	1.39 ± 0.41	1.55 ± 0.42	0.088
ES rfCSA	0.57 ± 0.26	0.63 ± 0.25	0.143
MF FI	0.37 ± 0.15	0.32 ± 0.11	0.087
ES FI	0.42 ± 0.14	0.40 ± 0.12	0.653
MF rSI	0.54 ± 0.13	0.47 ± 0.11	0.014*
ES rSI	0.56 ± 0.11	0.51 ± 0.10	0.070

MF, multifidus; ES, erector spinae; FI, fatty infiltration; rtCSA, relative total cross sectional area; rfCSA, relative fatty cross sectional area; rSI, relative signal intensity *means P value < 0.05; **means P value < 0.01.

patients were higher than those of normal people. The results reflected that the overall degeneration of paraspinal muscle in patients with LSS was worse than that in normal people.

We further compared the mean values of paraspinal muscle parameters from L3 to L5 level between the two groups (The mean value was used in the following analyses) and found that the rfCSA, FI, rSI of MF and rSI of ES in patients group were significantly higher than those in normal group (Table 3). The degeneration of paraspinal muscle in patients with LSS was significantly severer than that in normal people, which was mainly manifested in multifidus muscle (Figures 1, 2).

These patients were divided into two groups according to the gender. There was no significant difference in paraspinal muscle parameters between the two groups. But compared with males, the rfCSA and FI of MF and ES were higher in females (Table 4).

Then we compared the differences of paraspinal muscle parameters between patients and normal people under different gender. As the results showed in Table 5, for males, the rfCSA, FI and rSI of MF were higher in patients than those in normal peers ($p<0.05$). For females, the rSI of MF was higher in patients than that in normal peers ($p<0.05$). Although there was no significant difference in the rfCSA and FI of MF between female patients and normal peers, the rfCSA and FI of MF were also higher in female patients.

We used correlation analysis to explore the relationship between paraspinal muscle parameters and other factors, such as age, height, weight and BMI in patients with LSS and the results were recorded in Table 6. Age was significantly correlated with the rfCSA, FI and rSI of both MF and ES ($p<0.05$). Weight and BMI were significantly correlated with the rtCSA of ES ($p<0.05$).

The linear regression analysis was used to evaluate the relationship between age and the FI of MF. As showed in Figure 3, the slope of fitted linear was higher in patients than that in normal people, indicating that with the increase of age, the fatty infiltration increased more significantly in patients than that in normal people.

10.3389/fendo.2022.1080033

TABLE 3 The mean values of paraspinal muscle parameters.

Parameters	Patients group	Normal group	P-value
MF rtCSA	1.25 ± 0.28	1.26 ± 0.22	0.897
MF rfCSA	0.45 ± 0.18	0.39 ± 0.18	0.013*
ES rtCSA	2.06 ± 0.38	2.21 ± 0.35	0.072
ES rfCSA	0.60 ± 0.20	0.64 ± 0.21	0.404
MF FI	0.36 ± 0.14	0.30 ± 0.10	0.014*
ES FI	0.31 ± 0.09	0.31 ± 0.09	0.671
MF rSI	0.52 ± 0.12	0.44 ± 0.10	0.001**
ES rSI	0.48 ± 0.09	0.44 ± 0.09	0.038*

MF, multifidus; ES, erector spinae; FI, fatty infiltration; rtCSA, relative total cross sectional area; rfCSA, relative fatty cross sectional area; rSI, relative signal intensity *means P value < 0.05; **means P value < 0.01.

Discussion

With the aging of population, the incidence of lumbar degenerative diseases is gradually increasing. Lumbar spinal stenosis is one of the common lumbar diseases and many researches focused on the degeneration of paraspinal muscle in lumbar spinal stenosis. Zotti found that the decrease of cross-sectional area of MF was correlated to the outcome in patients with LSS (16). But this study only measured the MF and lacked the data of normal people. In this study, we found that the degeneration of paraspinal muscle was worse in patients with LSS compared with that in normal people, especially in the multifidus.

Previous studies found that age, gender and BMI may influence the degeneration of paraspinal muscle (2, 18, 21). In order to increase the comparability, we used propensity score matching to minimize the differences in general conditions between the two groups. As the results showed in Table 1, there was no significant difference in general conditions, indicating the two groups were matched well.

The change rule of paraspinal muscle in patients with LSS was similar to that in normal people. From top to bottom of the spinal axis, the relative cross-sectional area of MF increased, while that of ES decreased. The FI and the rSI of MF and ES increased gradually. Another research measured the volume of paraspinal muscle in patients with LSS and found that the volume of paraspinal muscle was the largest at L3-4 level and gradually decreased toward the caudal end (22). They measured the volume of paraspinal muscle rather than parameters of both MF and ES, which was different with our study, but the change rule of paraspinal muscle was similar to our finding.

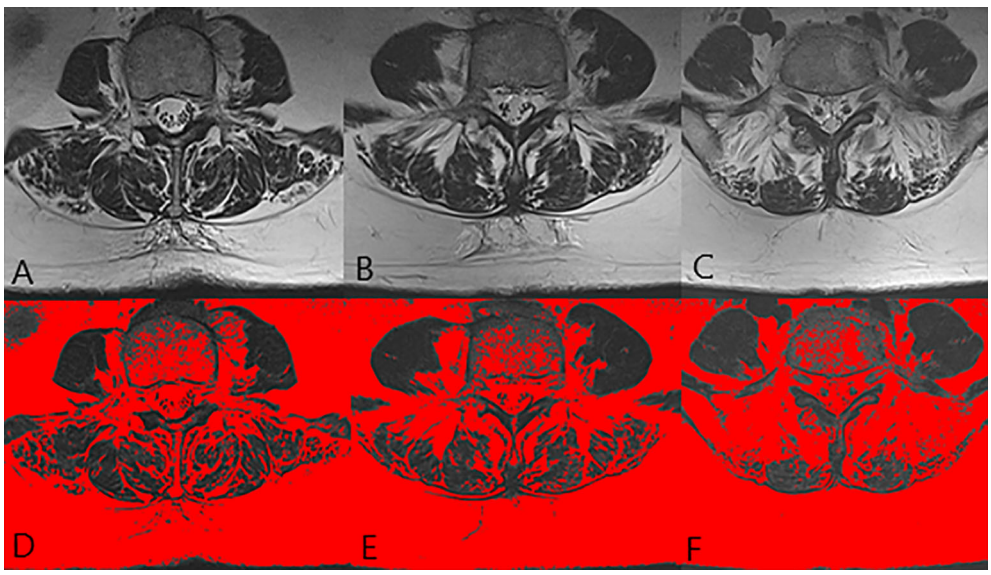

FIGURE 1
The images of paraspinal muscle in a 71 years old normal female. **(A, D)** were at L3 level. **(B, E)** were at L4 level. **(C, F)** were at L5 level. The FI of MF was 36.8% and the FI of ES was 48.2%.

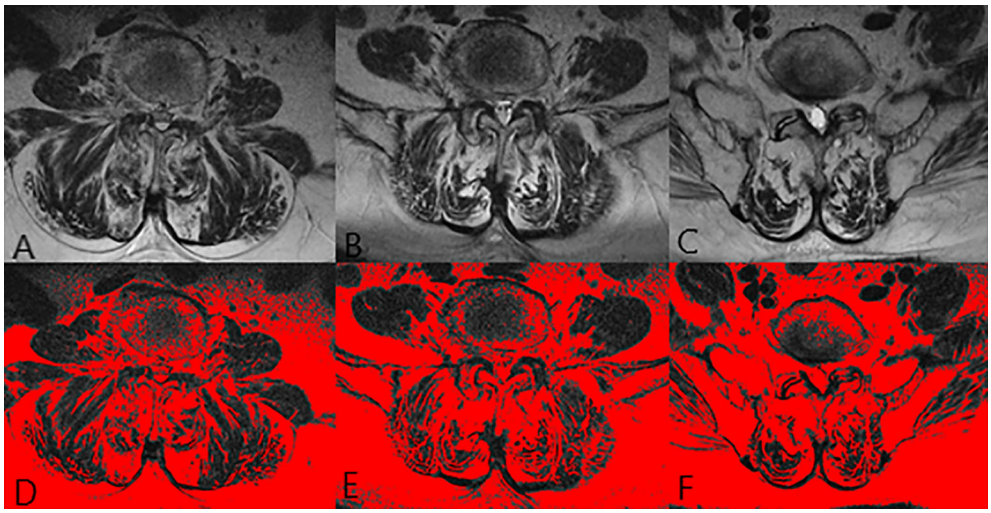

FIGURE 2
The images of paraspinal muscle in a 70 years old female patient. **(A, D)** were at L3 level. **(B, E)** were at L4 level. **(C, F)** were at L5 level. The FI of MF was 57.6% and the FI of ES was 43.0%.

Recently many studies focused on the degeneration of paraspinal muscle in patients with chronic nonspecific low back pain and lumbar degenerative diseases. Ogon found that intracellular lipid content in multifidus muscle cells was higher in patients with chronic nonspecific low back pain than that in patients with LSS (7). Yagi found that the cross-sectional area of multiuse muscle was significantly smaller in patients with degenerative scoliosis combined with LSS than that in patients with single LSS (15). Liu found that FI in multifidus muscle at L5-S1 could be a predictor of functional improvement after surgery in patients with L4-5 single-segment LSS (14). But few studies investigated the differences of paraspinal muscle between patients with LSS and normal people.

By comparing the paraspinal muscle parameters between the two groups, the degeneration of paraspinal muscle was worse in patients with LSS than that in normal people. For parameters at L3 level, the rfCSA, FI, rSI of MF and rSI of ES were higher in patients group than those in normal group. Besides, the FI and rSI of MF at L4 level and the rSI of MF at L5 level were also higher in patients group. Moreover, the mean value of

TABLE 4 Comparison of paraspinal muscle parameters between genders in patients.

Parameter	Male	Female	P-value
Age (yrs)	62.2 ± 8.0	63.5 ± 7.9	0.610
Height (cm)	170.1 ± 7.3	158.3 ± 5.7	<0.01**
Weight (kg)	72.6 ± 10.0	64.4 ± 9.1	0.011*
BMI (kg/m^2)	25.0 ± 2.6	25.7 ± 3.1	0.568
MF rtCSA	1.22 ± 0.30	1.29 ± 0.27	0.452
MF rfCSA	0.43 ± 0.16	0.47 ± 0.19	0.477
ES rtCSA	2.16 ± 0.38	1.98 ± 0.36	0.122
ES rfCSA	0.59 ± 0.18	0.61 ± 0.21	0.786
MF FI	0.36 ± 0.16	0.37 ± 0.12	0.832
ES FI	0.30 ± 0.11	0.32 ± 0.08	0.692
MF rSI	0.52 ± 0.15	0.52 ± 0.09	0.957
ES rSI	0.48 ± 0.10	0.48 ± 0.07	0.796

BMI, body mass index; MF, multifidus; ES, erector spinae; FI, fatty infiltration; rtCSA, relative total cross sectional area; rfCSA, relative fatty cross sectional area; rSI, relative signal intensity
*means P value < 0.05; **means P value < 0.01.

TABLE 5 Comparison of paraspinal muscle parameters between patients and normal peers under different gender.

Parameter	Male			Female		
	Patients	Normal peers	P-value	Patients	Normal peers	P-value
Age (yrs)	62.2 ± 8.0	60.8 ± 7.2	0.592	63.5 ± 7.9	63.1 ± 7.4	0.991
Height (cm)	170.1 ± 7.3	171.6 ± 5.7	0.508	158.3 ± 5.7	157.4 ± 5.8	0.579
Weight (kg)	72.6 ± 10.0	74.6 ± 10.7	0.577	64.4 ± 9.1	60.3 ± 8.5	0.128
BMI(kg/m^2)	25.0 ± 2.6	25.2 ± 2.5	0.817	25.7 ± 3.1	24.3 ± 3.1	0.154
MF rtCSA	1.22 ± 0.30	1.25 ± 0.21	0.721	1.29 ± 0.27	1.27 ± 0.23	0.835
MF rfCSA	0.43 ± 0.16	0.32 ± 0.09	0.020*	0.47 ± 0.19	0.44 ± 0.21	0.184
ES rtCSA	2.16 ± 0.38	2.31 ± 0.41	0.273	1.98 ± 0.36	2.14 ± 0.30	0.098
ES rfCSA	0.59 ± 0.18	0.56 ± 0.12	0.623	0.61 ± 0.21	0.70 ± 0.24	0.192
MF FI	0.36 ± 0.16	0.25 ± 0.05	0.025*	0.37 ± 0.12	0.34 ± 0.12	0.275
ES FI	0.30 ± 0.11	0.27 ± 0.06	0.198	0.32 ± 0.08	0.34 ± 0.10	0.613
MF rSI	0.52 ± 0.15	0.40 ± 0.10	0.009**	0.52 ± 0.09	0.46 ± 0.10	0.045*
ES rSI	0.48 ± 0.10	0.41 ± 0.09	0.059	0.48 ± 0.07	0.46 ± 0.09	0.273

BMI, body mass index; MF, multifidus; ES, erector spinae; FI, fatty infiltration; rtCSA, relative total cross sectional area; rfCSA, relative fatty cross sectional area; rSI, relative signal intensity
*means P value < 0.05; **means P value < 0.01.

parameters from L3 to L5 level, such as rfCSA, FI, rSI of MF and rSI of ES were also significantly higher in patients group than those in normal group. Paraspinal muscle is important to maintain the spinal stability. The atrophy of paraspinal muscle led to the increase of fatty cross-sectional area and decrease of functional cross-sectional area, which was associated with the decrease in muscle strength (23), resulting in weakness in maintaining spinal stability. So we should pay attention to the degeneration of paraspinal muscle in LSS.

The degeneration of MF was significantly worse in patients than that in normal people, which may relate to the denervation of muscle fibers and differences in muscle stress. Yoshihara found that the denervation caused by compression of nerve root may lead to the degeneration of type I and type II fibers, causing structural changes of multifidus muscle (24). So nerve compression in patients with LSS may cause more degeneration of multifidus muscle.

In addition, the degeneration of MF was significantly different between the two groups, while there was no significant difference in degeneration of ES. While maintaining the spinal stability, the paraspinal muscle also bears the stress from the body or activities. The stress within physiological range is help to the exercise of muscle, but the overlord stress will cause muscle injury or degeneration. Previous studies reported that the MF bear more stress than the ES (25, 26), which may explain the degeneration of MF was worse rather than the ES. However, there also existed different conclusions. Lee measured the paraspinal muscle parameters of 650 patients from CT test and found that the atrophy of ES appeared earlier and more severe than the MF, which may relate to the difference of anatomical structure (27). Our conclusion was different with Lee's, which may be associated with the difference of paraspinal muscle measurements and characteristics of population. In this study, we measured paraspinal muscle parameters from T2-weighted MRI, while Lee measured those from CT. All patients in this study were diagnosed as LSS, while the subject in Lee' study was patient without spinal surgery, deformity and neuromuscular diseases. The inclusion criteria were broader than those in this study. The differences of paraspinal muscle degeneration need to be further explored.

In normal people, we found that the rfCSA and FI of MF, rfCSA and FI of ES and rSI of MF were significantly greater in

TABLE 6 Relationships between paraspinal muscle parameters and other factors in patients.

Parameter	MF rtCSA	MF rfCSA	ES rtCSA	ES rfCSA	MF FI	ES FI	MF rSI	ES rSI
Age	-0.056	0.427**	-0.053	0.354*	0.499**	0.415**	0.498**	0.390*
Height	-0.100	-0.195	0.183	-0.100	-0.181	-0.216	-0.217	-0.228
Weight	0.150	0.094	0.378*	0.055	-0.148	-0.108	-0.171	-0.122
BMI	0.246	0.283	0.364*	0.289	0.038	0.145	0.077	0.118

BMI, body mass index; MF, multifidus; ES, erector spinae; FI, fatty infiltration; rtCSA, relative total cross sectional area; rfCSA, relative fatty cross sectional area; rSI, relative signal intensity
*means P value < 0.05; **means P value < 0.01.

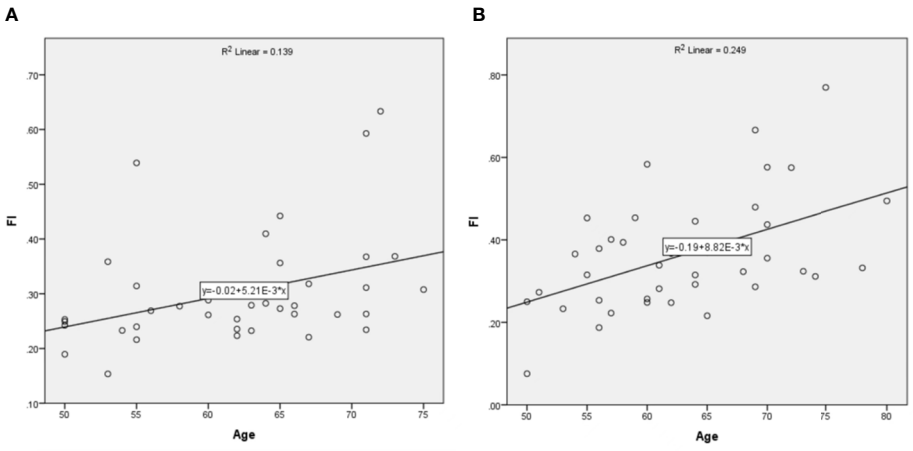

FIGURE 3
The relationship between age and FI of MF. **(A)** was in normal people and **(B)** was in patients.

females than those in males. In patients with lumbar disease, the FI of MF was also higher in females than that in males (18, 28). Compared to above results, there was no significant difference in paraspinal muscle parameter between different genders in patients with LSS, but the atrophy of paraspinal muscle was more severe in female than that in male. In addition, compared with normal people, the degeneration of multifidus muscle was higher in patients with lumbar spinal stenosis under different genders.

Age was an important factor for the degeneration of paraspinal muscle in patients with LSS and it was positively correlated with the rfCSA, FI and rSI of MF and ES, indicating that the degeneration of paraspinal muscle increased gradually with age. This result was consistent with previous studies (16, 18, 28, 29). We used the linear regression analysis to evaluate the relationship between age and FI of MF. The slope of fitted linear was higher in patients than that in normal people, indicating that with the increase of age, the degeneration of MF increased more significantly in patients than that in normal people. Shahidi analyzed the data of 199 patients who were between 18 and 80 years old. They found that the FI of MF and ES increased with age. They further compared paraspinal muscle parameters with the data of healthy people from Crawford's study and found that the age-fat infiltration rate fitted line had a higher slope in female patients (18). Their results were consistent with this study. Except for age, weight and BMI were significantly correlated with the rtCSA of ES rather than the rtCSA of MF, suggesting that weight mainly affected the quantity of erector spinae.

In this study, propensity score matching was used to ensure the comparability between patients with lumbar spinal stenosis and normal people and reduce the influence of individual factors on the results. Paraspinal muscle parameters from L3 to L5 and the mean value of parameters were compared between the two groups and the differences in paraspinal muscle parameters were comprehensively analyzed. Patients with lumbar spinal stenosis are mainly middle-aged and elderly people, so this study focused on middle-aged and elderly people over 50 years old. However, there are some shortcomings in this study. Firstly, this study is a single-center study, which may have selection bias. Secondly, the number of people included in this study was small and the study with a larger sample size is needed to verify our results in the future.

Conclusion

The change rules of paraspinal muscle in patients with lumbar spinal stenosis were similar to those in normal people. The degeneration of paraspinal muscle was more severe in patients with lumbar spinal stenosis than that in normal people, especially in multifidus. The degeneration of paraspinal muscle in patients with lumbar spinal stenosis was mainly related to age and the effect of age on atrophy of paraspinal muscle was greater than that of normal people.

Data availability statement

The raw data supporting the conclusions of this article will be made available by the authors, without undue reservation.

Ethics statement

The studies involving human participants were reviewed and approved by the Ethics Committee of Peking University Third

Hospital. The patients/participants provided their written informed consent to participate in this study.

Author contributions

WW conceived the project and analyzed the data. All authors contributed towards the interpretation and the collection of the data. All authors contributed to the article and approved the submitted version.

Funding

This study was funded by Tianjin Key Medical Discipline (Specialty) Construction Project (TJYXZDXK-026A).

Conflict of interest

The authors declare that the research was conducted in the absence of any commercial or financial relationships that could be construed as a potential conflict of interest.

Publisher's note

References

1. Stanuszek A, Jedrzejek A, Gancarczyk-Urlik E, Kolodziej I, Pisarska-Adamczyk M, Milczarek O, et al. Preoperative paraspinal and psoas major muscle atrophy and paraspinal muscle fatty degeneration as factors influencing the results of surgical treatment of lumbar disc disease. *Arch Orthop Trauma Surg* (2022) 142(7):1375–84. doi: 10.1007/s00402-021-03754-x

2. Hida T, Eastlack RK, Kanemura T, Mundis GJ, Imagama S, Akbarnia BA, et al. Effect of race, age, and gender on lumbar muscle volume and fat infiltration in the degenerative spine. *J Orthop Sci* (2021) 26(1):69–74. doi: 10.1016/j.jos.2019.09.006

3. Ding JZ, Kong C, Li XY, Sun XY, Lu SB, Zhao GG, et al. Different degeneration patterns of paraspinal muscles in degenerative lumbar diseases: a MRI analysis of 154 patients. *Eur Spine J* (2022) 31(3):764–73. doi: 10.1007/s00586-021-07053-2

4. Leng J, Han G, Zeng Y, Chen Z, Li W. The effect of paraspinal muscle degeneration on distal pedicle screw loosening following corrective surgery for degenerative lumbar scoliosis. *Spine (Phila Pa 1976)* (2020) 45(9):590–8. doi: 10.1097/BRS.0000000000003336

5. Hiyama A, Katoh H, Sakai D, Tanaka M, Sato M, Watanabe M. The correlation analysis between sagittal alignment and cross-sectional area of paraspinal muscle in patients with lumbar spinal stenosis and degenerative spondylolisthesis. *BMC Musculoskelet Disord* (2019) 20(1):352. doi: 10.1186/s12891-019-2733-7

6. Xia W, Fu H, Zhu Z, Liu C, Wang K, Xu S, et al. Association between back muscle degeneration and spinal-pelvic parameters in patients with degenerative spinal kyphosis. *BMC Musculoskelet Disord* (2019) 20(1):454. doi: 10.1186/s12891-019-2837-0

7. Ogon I, Takebayashi T, Takashima H, Morita T, Yoshimoto M, Terashima Y, et al. Magnetic resonance spectroscopic analysis of multifidus muscles lipid content and association with spinopelvic malalignment in chronic low back pain. *Br J Radiol* (2017) 90(1073), 20160753. doi: 10.1259/bjr.20160753

8. Kalichman L, Hodges P, Li L, Guermazi A, Hunter DJ. Changes in paraspinal muscles and their association with low back pain and spinal degeneration: CT study. *Eur Spine J* (2010) 19(7):1136–44. doi: 10.1007/s00586-009-1257-5

9. Jermy JE, Copley PC, Poon M, Demetriades AK. Does pre-operative multifidus morphology on MRI predict clinical outcomes in adults following surgical treatment for degenerative lumbar spine disease? A systematic review. *Eur Spine J* (2020) 29(6):1318–27. doi: 10.1007/s00586-020-06423-6

10. Hyun SJ, Bae CW, Lee SH, Rhim SC. Fatty degeneration of the paraspinal muscle in patients with degenerative lumbar kyphosis: A new evaluation method of quantitative digital analysis using MRI and CT scan. *Clin Spine Surg* (2016) 29 (10):441–7. doi: 10.1097/BSD.0b013e3182aa28b0

11. Kim CH, Chung CK, Park CS, Choi B, Hahn S, Kim MJ. Reoperation rate after surgery for lumbar spinal stenosis without spondylolisthesis: a nationwide cohort study. *Spine J* (2013) 13(10):1230–7. doi: 10.1016/j.spinee.2013.06.069

12. Waldrop R, Cheng J, Devin C, McGirt M, Fehlings M, Berven S. The burden of spinal disorders in the elderly. *Neurosurgery* (2015) 77Suppl 4:S46–50. doi: 10.1227/NEU.0000000000000950

13. Miki T, Naoki F, Takashima H, Takebayashi T. Associations between paraspinal muscle morphology, disc degeneration, and clinical features in patients with lumbar spinal stenosis. *Prog Rehabil Med* (2020) 5:20200015. doi: 10.2490/prm.20200015

14. Liu Y, Liu Y, Hai Y, Liu T, Guan L, Chen X. Fat infiltration in the multifidus muscle as a predictor of prognosis after decompression and fusion in patients with single-segment degenerative lumbar spinal stenosis: An ambispective cohort study based on propensity score matching. *World Neurosurg* (2019) 128:e989–e1001. doi: 10.1016/j.wneu.2019.05.055

15. Yagi M, Hosogane N, Watanabe K, Asazuma T, Matsumoto M. The paravertebral muscle and psoas for the maintenance of global spinal alignment in patient with degenerative lumbar scoliosis. *Spine J* (2016) 16(4):451–8. doi: 10.1016/j.spinee.2015.07.001

16. Zotti M, Boas FV, Clifton T, Piche M, Yoon WW, Freeman B. Does pre-operative magnetic resonance imaging of the lumbar multifidus muscle predict clinical outcomes following lumbar spinal decompression for symptomatic spinal stenosis? *Eur Spine J* (2017) 26(10):2589–97. doi: 10.1007/s00586-017-4986-x

17. Sun D, Liu P, Cheng J, Ma Z, Liu J, Qin T. Correlation between intervertebral disc degeneration, paraspinal muscle atrophy, and lumbar facet joints degeneration in patients with lumbar disc herniation. *BMC Musculoskelet Disord* (2017) 18(1):167. doi: 10.1186/s12891-017-1522-4

18. Shahidi B, Parra CL, Berry DB, Hubbard JC, Gombatto S, Zlomislic V, et al. Contribution of lumbar spine pathology and age to paraspinal muscle size and fatty infiltration. *Spine (Phila Pa 1976)* (2017) 42(8):616–23. doi: 10.1097/BRS.0000000000001848

19. Hu ZJ, He J, Zhao FD, Fang XQ, Zhou LN, Fan SW. An assessment of the intra- and inter-reliability of the lumbar paraspinal muscle parameters using CT scan and magnetic resonance imaging. *Spine (Phila Pa 1976)* (2011) 36(13):E868–74. doi: 10.1097/BRS.0b013e3181ef6b51

20. Ranson CA, Burnett AF, Kerslake R, Batt ME, O'Sullivan PB. An investigation into the use of MR imaging to determine the functional cross sectional area of lumbar paraspinal muscles. *Eur Spine J* (2006) 15(6):764–73. doi: 10.1007/s00586-005-0909-3

21. Peng X, Li X, Xu Z, Wang L, Cai W, Yang S, et al. Age-related fatty infiltration of lumbar paraspinal muscles: a normative reference database study in 516 Chinese females. *Quant Imaging Med Surg* (2020) 10(8):1590–601. doi: 10.21037/qims-19-835

22. Boissiere L, Moal B, Gille O, De-Roquefeuil E, Durieux M, Obeid I, et al. Lumbar spinal muscles and spinal canal study by MRI three-dimensional reconstruction in adult lumbar spinal stenosis. *Orthop Traumatol Surg Res* (2017) 103(2):279–83. doi: 10.1016/j.otsr.2016.10.025

23. Fortin M, Wilk N, Dobrescu O, Martel P, Santaguida C, Weber MH. Relationship between cervical muscle morphology evaluated by MRI, cervical muscle strength and functional outcomes in patients with degenerative cervical myelopathy. *Musculoskelet Sci Pract* (2018) 38:1–7. doi: 10.1016/j.msksp.2018.07.003

24. Okada Y. Histochemical study on the atrophy of the quadriceps femoris muscle caused by knee joint injuries of rats. *Hiroshima J Med Sci* (1989) 38(1):13–21.

25. Mayer JM, Graves JE, Clark BC, Formikell M, Ploutz-Snyder LL. The use of magnetic resonance imaging to evaluate lumbar muscle activity during trunk extension exercise at varying intensities. *Spine (Phila Pa 1976)* (2005) 30(22):2556–63. doi: 10.1097/01.brs.0000186321.24370.4b

26. Ng J, Richardson C. EMG study of erector spinae and multifidus in two isometric back extension exercises. *Aust J Physiother* (1994) 40(2):115–21. doi: 10.1016/S0004-9514(14)60458-X

27. Lee SH, Park SW, Kim YB, Nam TK, Lee YS. The fatty degeneration of lumbar paraspinal muscles on computed tomography scan according to age and disc level. *Spine J* (2017) 17(1):81–7. doi: 10.1016/j.spinee.2016.08.001

28. Takayama K, Kita T, Nakamura H, Kanematsu F, Yasunami T, Sakanaka H, et al. New predictive index for lumbar paraspinal muscle degeneration associated with aging. *Spine (Phila Pa 1976)* (2016) 41(2):E84–90. doi: 10.1097/BRS.0000000000001154

29. Crawford RJ, Filli L, Elliott JM, Nanz D, Fischer MA, Marcon M, et al. Age- and level-dependence of fatty infiltration in lumbar paravertebral muscles of healthy volunteers. *AJNR Am J Neuroradiol* (2016) 37(4):742–8. doi: 10.3174/ajnr.A4596

frontiers | Frontiers in Endocrinology

TYPE Review
PUBLISHED 06 December 2022
DOI 10.3389/fendo.2022.1038171

OPEN ACCESS

EDITED BY
Baoshan Xu,
Tianjin Hospital, China

REVIEWED BY
Farasat Zaman,
Karolinska University Hospital, Sweden
Zhen Sun,
Fourth Military Medical University, China
Jiandong Song,
Hubei Xinhua Hospital, China

*CORRESPONDENCE
Yuzeng Liu
beijingspine2010@163.com
Yong Hai
yong.hai@ccmu.edu.cn;
prof.haiyong@outlook.com
Yangpu Zhang
zhangyp223@163.com

†These authors have contributed equally to this work and share first authorship

SPECIALTY SECTION
This article was submitted to Bone Research, a section of the journal Frontiers in Endocrinology

RECEIVED 06 September 2022
ACCEPTED 18 November 2022
PUBLISHED 06 December 2022

CITATION
Cheng F, Yang H, Cheng Y, Liu Y, Hai Y and Zhang Y (2022) The role of oxidative stress in intervertebral disc cellular senescence. *Front. Endocrinol.* 13:1038171. doi: 10.3389/fendo.2022.1038171

The role of oxidative stress in intervertebral disc cellular senescence

Fengqi Cheng†, Honghao Yang†, Yunzhong Cheng†, Yuzeng Liu*, Yong Hai* and Yangpu Zhang*

Department of Orthopedic Surgery, Beijing Chao-Yang Hospital, Capital Medical University, Beijing, China

With the aggravation of social aging and the increase in work intensity, the prevalence of spinal degenerative diseases caused by intervertebral disc degeneration(IDD)has increased yearly, which has driven a heavy economic burden on patients and society. It is well known that IDD is associated with cell damage and degradation of the extracellular matrix. In recent years, it has been found that IDD is induced by various mechanisms (e.g., genetic, mechanical, and exposure). Increasing evidence shows that oxidative stress is a vital activation mechanism of IDD. Reactive oxygen species (ROS) and reactive nitrogen species (RNS) could regulate matrix metabolism, proinflammatory phenotype, apoptosis, autophagy, and aging of intervertebral disc cells. However, up to now, our understanding of a series of pathophysiological mechanisms of oxidative stress involved in the occurrence, development, and treatment of IDD is still limited. In this review, we discussed the oxidative stress through its mechanisms in accelerating IDD and some antioxidant treatment measures for IDD.

KEYWORDS

oxidative stress, intervertebral disc, cellular senescence, signaling pathway, degenerative disc diseases

Introduction

With the aging population, the incidence of spinal degenerative diseases caused by disc degeneration is increasing year by year (1). Degenerative disc diseases, including disc herniation, spinal stenosis, vertebral instability, and other symptoms, can cause severe low back pain and even nerve compression symptoms, resulting in a substantial mental and economic pressure on patients and a heavy burden on the health-care system (2–4). Up to now, the pathogenesis of intervertebral disc degeneration (IDD) is not clear. Studies have found that IDD occurs in various mechanisms (genetic, mechanical, and exposure). Each mechanism exerts *via* a series of pathways leading to the ultimate common outcome of disc cell senescence. There are many therapies for IDD, including therapeutic protein

injection, stem cell injection, gene therapy, and tissue engineering, besides the most commonly used surgical treatment. However, there is no effective drug intervention (5).

With the development of molecular biology, epigenetics, and immune technology, people have a more comprehensive and in-depth understanding of the pathogenic factors of IDD. Studies have found that IDD is caused by the senescence of disc cells, and cellular senescence is a process of gradual activation resulting from a variety of initiating factors, among which oxidative stress is an important initiating factor leading to the senescence of disc cells (6). Vitro experiments have demonstrated that the rate of intervertebral disc (IVD) cell senescence is associated with high levels of reactive oxygen species (ROS) and reactive nitrogen species (RNS) production. Still, the specific mechanism of oxidative stress-induced IVD cell senescence still need to be explored (7).

Current researches have focused on identifying the mechanisms by which oxidative stress leads to cell senescence in the IVD. In this review, we focus on the role of oxidative stress in the pathogenesis of IDD and highlight the research advances in the pathways through which oxidative stress leads to the senescence of disc IVD cells and important senescence-related factors. Through studying oxidative stress in the pathogenesis of IDD, we optimize the current therapeutic schemes and try to find new therapeutic interventions with strong specificity, safety, and high efficiency to prevent and treat the disease (5).

Intervertebral disc

IVD is the largest non-vascularized tissue in the human body. It consists of four parts: central nucleus pulposus (NP), annulus fibrosus (AF), cartilage endplate (EP), and bone endplate (BP). Intervertebral disc cells mainly absorb nutrients by diffusion through the EP, so the cell division of the intervertebral disc is inactive, and the repair ability is poor, which is the potential cause of IDD (8).

The gelatinous NP, located in the center of the intervertebral disc, is rich in the extracellular matrix (ECM) and is composed of water (70-90%), proteoglycans (PGS), and type II collagen (Col). PGS and type II Col play an important role in resisting and alleviating the axial pressure of the spine. With the increase of age, the hardening of the NP is gradually aggravated, and the effect of decompression and cushioning is weakened, which is an important reason why the IVD is vulnerable to external force injury (9).

The fiber ring is a unique structure composed of 15-25 concentric rings. It looks like a Nylon Mesh pocket and has strong ductility and toughness. The fibrous ring surrounds the NP and bears the pressure from all directions, which plays a protective role in the NP. Each lamina is composed of parallel Col fibers (type I and type II). The fibrous rings are arranged in layers on the cross-section, and the posterolateral part is weak, which is also the reason why IVD herniation tends to occur in the posterolateral part (Figure 1) (2, 10).

The endochondral EP is a thin layer of hyaline cartilage, which fixes the IVD on the adjacent vertebrae and acts as a barrier between NP and its upper and lower cancellous bones (11). Endochondral EP cells are distributed in the hyaline cartilage matrix and bind the cartilage disc to the covered vertebrae (12).The cartilage EP is the main contact mode between the IVD and vascular supply: small capillaries penetrate the cartilage EP and make contact with the NP and AP. In the process of IDD, the number of small capillaries decreases, and the bone marrow cavity and cartilage EP calcify, which leads to the reduction of AF and NP blood supply and aggravates the degeneration of the lumbar intervertebral disc (13).

Intervertebral disc degeneration

During IDD, the degenerative processes at different cellular, molecular, and tissue degeneration levels and their effects on IDD have been a hot topic of research. The different levels of degeneration are causal and contribute to each other, leading to degenerative changes in the intervertebral disc (Table 1). For example, IVD cellular senescence is a fundamental cellular program, a multi-linked programmed change influenced by multiple factors involving all aspects of cellular morphology and function. Senescent cells stop responding to mitotic stimuli and undergo significant changes in chromatin structure and gene expression. Cell proliferation, differentiation, and material metabolism are ultimately hindered (14). With the disruption of normal cell structure and function, the secretion of relevant cytokines and degradative enzymes increases, affecting the microenvironment of IVD cell proliferation, differentiation, and material metabolism. These changes further lead to functional and morphological disruption of IVD cells and even apoptosis and autophagy, ultimately leading to IDD development and exacerbation (15, 16).

At the cellular level, apoptosis and autophagy play a key role in IDD. There are two types of programmed cell death, apoptosis, and autophagy (17). Apoptosis occurs in IVD cells in response to oxidative stress, abnormal mechanical stress, and inflammatory factors. Apoptosis occurs through the mitochondrial pathway, the death receptor pathway, and the endoplasmic reticulum pathway (18).When apoptosis occurs, important intracellular organelles and contents are destroyed and degraded, such as causing damage to mitochondria (19).Therefore, apoptosis is an essential factor in oxidative stress leading to degenerative changes in the IVD.

There is a close relationship between cellular autophagy and apoptosis. Autophagy is a protective mechanism of the cell itself. The activation pathways of cellular autophagy include the Mammalian Target of Rapamycin (mTOR)-dependent pathway and the non mTOR-dependent pathway. mTOR-

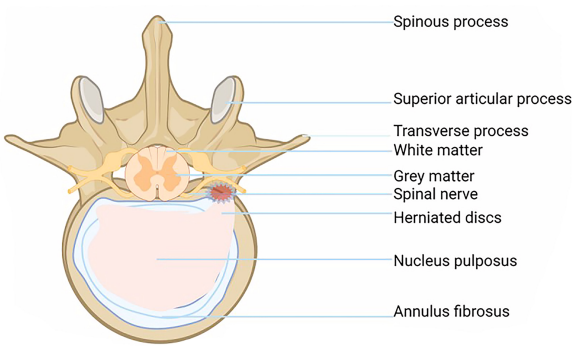

FIGURE 1
Shows a disc pathology with a horizontal view of a herniated disc and bulging disc above.

dependent ways include the AMPK/mTOR pathway and the PI3K/Akt/mTOR pathway (20).It was found that basal levels of cellular autophagy were present in normal rat NP cells. However, cellular autophagy levels were significantly increased or decreased in NP tissues that underwent degenerative lesions. Low levels of autophagy induced by mild oxidative stress can inhibit apoptosis and have a protective effect on the cells. Severe oxidative stress or abnormal mechanical stress, resulting in high cellular autophagy levels, caused organelle damage and led to increased apoptosis in myeloid cells (21). In IDD caused by oxidative stress, cellular autophagy plays a different role depends on the degree of disc degeneration changes (22).

In the process of IDD, an imbalance between the anabolic and catabolic metabolism of IVD cells due to a combination of abnormal factors causes the loss of tissue repair capacity, resulting in IDD (23). For example, the ability of articular chondrocytes to proliferate and synthesize decreases, but matrix-degrading enzymes in the cells retain high activity, leading to the destruction and loss of articular cartilage. In addition, the reduction of collagen (Col) and PGS in IVD is an essential indicator of IDD. The synthesis and quality of Col and PGS are also decreased in IVD cells (24, 25).

In addition, protease is also involved in the senescence of IVD cells. As a marker enzyme of cell aging, the positive rate of senescence-associated b-galactosidase (SA-b-Gal). SA-b-Gal increases with the severity of IDD. The results showed that the number of SA-b-Gal positive cells in IVD herniation tissue increased significantly, and the positive rate accounted for 8.5% of the total cells (26). In degenerative IVD, the positive rate of SA-b-Gal in NP cells is higher than that in AP cells, and the proportion of positive cells is as high as 25.5%. This indicates that the aging degree of NP cells in the degenerated IVD is more serious than that in the AP (27).

At the same time, the study found that in degenerated human IVD, not only the expression of SA-b-Gal increased, but also telomerase activity decreased and telomere length shortened (28). Telomere length determines the ability of cell division and proliferation to a certain extent, and telomere length is maintained by telomerase. With the decrease in telomerase activity, the telomere length of cells gradually shortens, and the cell senescence and even apoptosis would occur (29, 30).

Due to the decrease in the production of matrix components and the increase in the expression of degradation enzymes, the dynamic balance between the synthesis and degradation of ECM is disturbed. The reduction of the ECM level of the IVD is a characteristic of IDD. The abnormally high levels of many enzymes, such as matrix metalloproteinase, lectin, and cathepsin, accelerate the catabolism of the ECM. Among them, matrix metalloproteinase-3 (MMP-3) and matrix metalloproteinase-13 (MMP-13) are the key enzymes of ECM degradation in IVD, and interleukin (IL) and tumor necrosis factor (TNF) are important regulators. *In vitro* experiments showed that the activities of MMP-3 and MMP-13 increased significantly in aging IVD (31, 32).

TABLE 1 Mechanisms and manifestations of intervertebral disc degeneration at different levels.

Level	Degeneration mechanism	Degeneration performance
molecular	DNA is blocked in the g0/g1 phase and could not progress to the next phase.	Cells lose the ability to respond to mitogens and synthesize DNA.
	Abnormal accumulation of inflammation-related factors in the intervertebral disc, such as TNF, IL, NO and leukotrienes.	Inflammatory response and injury.
cellular	Decreased production of extracellular matrix components and increased expression of degradative enzymes	Decrease in extracellular matrix levels.
	Decrease in telomerase activity	The telomere length is gradually shortened.
	Decreased proliferation of articular chondrocytes.	(1) Destruction and reduction of articular cartilage occurs. (2) The lumbar intervertebral disc loses its ability to repair.
organizational	Calcification of cartilage plates.	Decreased exchange of nutrients and metabolites in IVD
	Vascular infiltration can be observed in degenerative disc tissue.	(1) Lymphocytes and macrophages are distributed around the neovascularization, inducing an inflammatory response. (2) Neovascularization delivers more oxygen to degenerated tissues, thus exacerbating oxidative stress.

Because the IVD is an avascular tissue, the EP is the key nutritional pathway, and nutrients nourish the NP and AP through the cartilage plate by diffusion. Calcification of the EP reduces the exchange of nutrients and metabolites in IVD, thereby inhibiting the production of an ECM. The imbalance between anabolism and catabolism in the ECM of the IVD leads to the decline of the ECM, thereby accelerating the IDD (33).

At the tissue level, calcification of EP and vascular infiltration interfere with the usual exchange of nutrients and metabolites in the IVD, thereby inhibiting cell proliferation, differentiation, and ECM production. Since the IVD is an avascular tissue, EP is a critical nutrient pathway. Nutrients nourish the NP and AP by diffusion through the cartilage plate, and calcification of the EP disrupts the normal pathway of material exchange (33). In addition, vascular infiltration is an essential factor in promoting IDD. In normal adult IVD, there is no angiogenesis (34). However, vascular infiltration can be observed in degenerative disc tissue. Most neovascularization is located at the edge of the disc and is formed by a single or a few endothelial cells with a very narrow lumen. Vascular endothelial growth factor and p53 may be jointly involved in the process of neo-capillary formation. Coordinated expression of VEGF and p53 was demonstrated in degenerated IVD tissue. In rat degenerative IVD tissues with capillary infiltration, the positive expression of VEGF and p53 was higher than that in the non-infiltrated group. The experimental results suggest that both VEGF and p53 are involved in the process of neovascular infiltration, which accelerates the degeneration of rat IVD tissues (35). Microscopically, lymphocytes and macrophages were distributed around the neovascularization, which could induce an inflammatory response and promote IDD (36).In addition, neovascularization in degenerated discs delivers more oxygen to the degenerated tissue, thus exacerbating the damage to the discs from oxidative stress.

At the molecular level, it was found that the DNA of aging cells was blocked in G0/G1 phase and could not enter the next stage. Cells lose the ability to react with mitogen and synthesize DNA. The content of DNA in cells cannot alter with the normal periodic changes of cells (37). In addition, in the early stage of IDD, due to inflammatory injury, abnormal accumulation of inflammatory-related factors occurred in the IVD, such as TNF, IL, NO, and leukotriene. Among them, IL-8 not only accelerates the degeneration of IVD but also leads to the neuroinflammation infiltration of the nerve root, resulting in low back pain (38–40).

Modeling of intervertebral disc degeneration

An appropriate model of IDD is the most important step for subsequent mechanism research. The production of animal models of IDD can be broadly divided into natural-induced models, genetic technology-induced models, physical-induced models, chemical-induced models, and biomechanical-induced models.

Natural-induced models

The spontaneous model refers to the selection of special breeds of animals, such as rhesus monkeys, dogs, and baboons, without human interference, which can naturally develop IDD similar to humans during the growth and development of the experimental animal.

Genetic technology-induced models

Gene therapy models are designed to induce IDD by genetically suppressing or promoting the expression of genes in experimental animals, resulting in an imbalance between IVD cell anabolism and catabolism. For example, knocking out the Chsy3 gene in mice induces the development of IDD models. The experimental conditions for gene technology are demanding, complex, and limited in studying specific genes (41).

Physical-induced models

Direct surgical incision of the fibrous ring can form a model of severe IDD, but it is so destructive to the fibrous ring that it is rarely used. Microscopic removal of the NP of the IVD in mice using a tiny scalpel can also successfully create a model of IDD. Alternatively, the NP, the lamina, and the AF can be damaged by puncture (42). Shi et al. successfully established an IDD model by puncturing the rabbit AF with a thicker needle and extracting the NP under a microscope. The IDD model was also induced by puncturing the cartilage EP and blocking the regular nutrient supply by injecting drugs or bone cement (43). Puncture-induced method is the most commonly used method due to the short model construction period and less damage to the spine of experimental animals.

Chemical-induced models

D-galactose can be injected into the circulatory system of experimental animals, which leads to abnormal metabolism of the whole body, and then leads to structural and functional damage of various organs. The IVD structure and function of the experimental animals will also change, leading to apoptosis of the IVD cells and finally obtaining a IDD model (44). This systemic chemical induction method is highly damaging to the experimental animals, and the degeneration of the systemic system interferes with the experimental results, which ultimately affects the accuracy and reliability of the experiment.

In addition, chemicals such as Papain Chymotrypsin(PC) and Chondroitinase ABC can be injected into the IVD, forming an IDD in the injected segment (45). Experimental studies showed that PC and Chondroitinase ABC were injected into the IVD of rabbits and goats, respectively, and the degree of IDD was exacerbated with increasing doses. Moreover, the proteoglycan and type II collagen expression levels in IVD were much lower than those in the control group (46). The local chemical induction method has few systemic side effects on experimental animals and no apparent interference with the experimental results. However, the quality of injected chemicals is not easy to control, and the puncture sites are prone to infection and bone destruction.

Biomechanical model

The normal stresses on the disc are altered by the mechanical application of force, unusual behavior, and intervertebral fusion to induce the development of degenerative changes in the IVD. The current compression tests performed in the rat and goat lumbar spine are very effective in constructing degenerative lumbar spine models. The method is feasible and less damaging to the experimental animals; however, it is prone to local infection and spinal cord injury when external forces are applied. Disruption of the connection between the IVDs can impact the balance of forces in the spine and thus alter the normal intervertebral stresses. For example, the removal of the lumbar interspinous ligaments or synovial joints can alter the static balance, and stripping the sacrospinous or severing the erector spinal muscles can alter the dynamic balance (47–49). Special behavioral models, such as the construction of a double hind limb upright rat model, in which young rats have their forelimbs amputated and are forced to stand and walk using both hind limbs or are placed in an upright tube for 4-12 weeks (50). Dissection of the vertebrae of the experimental animals showed that the degeneration of the lumbar spine was very obvious, the height of the intervertebral space and the proteoglycan of the NP were significantly reduced, the laminar arrangement of the fibrous ring was disturbed, and the EP was fractured. The particular behavioral pattern-induced method could resemble the human lumbar spine stresses more closely, but the strategy is ethically controversial and only applicable to small animals.

Oxidative stress and IDD

Oxidative stress is caused by the imbalance between the production of free radicals and active metabolites (known as oxidants or ROS) and the elimination of this protective mechanism of antioxidants (51). ROS is a series of incompletely reduced oxidation molecules, which generally contain oxygen free radicals, such as superoxide anion (O2-), hydrogen peroxide (H2O2), hydroxyl radical (OH-), and hypochlorite ion (OCL-), with high chemical activity and a relatively short half-life. Highly active oxidation molecules always have harmful effects on living cells, and mitochondria are the main place for the production of oxygen free radicals. In addition to ROS, RNS are also considered to be members of the ROS family, such as nitric oxide (NO) and its oxidized derivatives such as $N0_2$, N_2O_3, and GSNO, etc. Their chemical properties are as active as ROS, and they can also be used as key regulatory signals during various cell reactions (52).

Relatively excessive accumulation of ROS will lead to mitochondrial dysfunction and the destruction of cellular homeostasis through the oxidative stress pathway. At the same time, oxidative stress can promote the formation of autophagy through transcriptional regulation and post-transcriptional regulation. These include the following molecular signaling pathways, such as ROS-FOXO3-LC3/BNIP3-autophagy, ROS-NRF2-P62-autophagy, ROS-HIF1-BNIP3/NIX-Autophagy, and ROS-Tigar- Autophagy (53).

The levels of oxidative stress biomarkers, including NO, superoxide dismutase (SOD), malondialdehyde (MDA), and advanced oxidative protein products (AOPPs) in the IVD of Wistar rats were evaluated by histological analysis. The experiment showed that with the increase of age, the concentration of NO in IVD significantly increased, and the levels of MDA and AOPP in serum and IVD gradually increased. However, with the increase of age, the SOD activity of serum and IVD gradually decreased. Experiments show that with age, the production of ROS in IVD is excessive, and antioxidants are reduced, indicating that oxidative stress is related to the degenerative changes of IVD (54).

Oxidative stress plays a key role in the occurrence and development of IDD. Oxidative stress destroys DNA, lipids, protein, and ECM in IVD cells through metabolic regulation mechanisms and inflammatory pathways, thereby damaging the microenvironment balance and mechanical function of IVD. For example, increased NO production causes DNA strand breaks and base modifications through the IL-1 pathway, resulting in increased DNA damage (55).

It also promotes apoptosis and autophagy through a variety of mechanisms, reducing the number of living and functional cells in the IVD micro-environment. Studies have shown that oxidative stress increases the apoptosis and subsequent calcification of cartilage EP cells through Ros/P38/Erk/P65 pathway, thereby reducing the nutritional supply to the IVD and accelerating the degeneration of the IVD (56).

In conclusion, oxidative stress participates in the occurrence and development of IDD through a series of pathophysiological mechanisms.

Oxidative stress signaling pathway

Micro-RNA signaling pathway

Micro-RNA is an endogenous non-transcriptional micro-RNA, which is produced by DNA transcription and plays an important regulatory role in the process of transcription and translation after gene expression. Micro-RNA can directly bind to the target mRNA, reducing the expression of the protein encoded by the mRNA. In addition, Micro-RNA can also be used as a specific sequence guide of functional Ribonucleo-protein (RNP) to the target RNA so as to change the secondary structure of mRNA and regulate its translation level. Micro-RNA plays an important role in immune regulation, cell differentiation, and proliferation (57, 58).

The MiR-106b family in Micro-RNA is associated with gene expression that regulates the cell cycle. P21 is the direct target of MiR-106b, and p21 silencing plays a key role in the cell cycle phenotype induced by MiR-106b. In addition, MiR-106b covers the DNA damage checkpoint induced by Adriamycin, thereby promoting cell proliferation. Oxidative stress can reduce the expression level of MiR-106b and promote the aging and death of IVD cells. Experiments have proved that in human fibroblasts and trabecular meshwork cells cultured *in vitro*, oxidative stress can lead to the continuous reduction of MiR-106b, thus promoting the expression of the p21 gene, revealing DNA damage checkpoints, thereby blocking the cell cycle and promoting cell death (59).

Additionally, multiple mi-RNA families pass through the p53 pathway, causing the arrest of the cell cycle. P53 is a transcriptional regulator that can regulate the levels of micro-RNA (mi-RNA). MicroRNA-34a (miR-34a) is a direct transcriptional target of p53 in promoting apoptosis. It was experimentally demonstrated that p53 could induce miR-34a expression in cultured cells, and increased expression levels of miR-34a can mildly increase cell apoptosis (60).Under the induction of p53 activation, the expression levels of miR-192 and miR-215 were also increased. MiR-192 and MiR-215 target transcripts of the G (1) and G (2) checkpoints as direct targets, causing the arrest of the cell cycle and leading to apoptosis through regulatory actions between these genes by miRNAs (61).

NF-κB signaling pathway

NF-κB regulates the expression of many genes, such as genes related to immunity, inflammation, and cell cycle. NF-κB and IK-Bs binding exists in the cytoplasm as an inactive form. NF-κB is rapidly activated by cytokines, infectious factors, and oxidative factors (e.g., ROS) (62). For example, ROS can activate IK-Bs Kinase (IKK) through ROS-Hsp27-Ikkbeta mediated signal pathway, promoting phosphorylation of IK-Bs, and then IK-Bs is recognized by ubiquitinase and degraded, releasing NF-κB bound by IK-Bs and activating NF-κB signaling pathway (63).

The activation of NF- κB through the NF- κB/p65 pathway promotes the expression of the downstream signal molecule–p65 in the nucleus (64). Experiments showed that compared with normal NP cells, NP cells isolated from IDD patients contained less cytoplasm, and the expression level of p65 in the cytoplasm was higher than that in the nucleus of healthy NP cells treated with PDTC. In addition, the level of p65 increased with the prolonged exposure of cells to peroxynitrite (65, 66).NF-κB/p65 pathway can change the expression levels of mRNA or protein of key transcription factors (such as c-Fos and NFATc1) in osteoclast differentiation, leading to the senescence of NP cells. For example, TCF7L2 is expressed in the nucleus of NP cells and promotes the degradation of cell-matrix and the senescence of intervertebral disc cells through p65/NF-κB signaling pathway (67).

In addition, the activation of the NF-κB/p53 signaling pathway is another pathway of disc cellular senescence. Studies have shown that compared with normal NP cells, the expression of p65 and p53 in IDD cells is significantly increased. Moreover, the expression level of p53 was significantly reduced after the transfection of Sip53 (65).In addition, TNF- α can induce apoptosis of NP cells. Experiments show that TNF-α can increase the expression of TRIM14 and the activity of NF-κB/P65, thereby reducing the viability of human NP cells and inducing apoptosis (68). The activation of NF- κB can also promote the release of proteolytic enzymes such as MMPs and ADAMTs, accelerate the degradation of ECM and aggravate IDD by triggering transcription and translation (69, 70).

PHD2 forms a regulatory loop with TNF-α *via* NF-κB, thereby enhancing its own response to the activation of TNF-α. In the aging NP cells, the expression of both PHD2 and catabolic markers induced by TNF-α increase, accelerating the senescence of IVD cells (71).

ROS activates NLRP3 in NP cells and promotes the release of intracellular inflammatory factors *via* the NF-κB pathway. For example, the NF-κB signaling pathway stimulates the expression of IL-8, thereby promoting cell aging and apoptosis (63). Research shows that Piezo1 passes the Ca^{2+}/NF-κB pathway and activates NLRP3, thereby accelerating the production and maturation of IL-1β and promoting the senescence of IVD (72). The oxidative stress signaling pathways were illustrated in Figures 2, 3.

MAPK-ERK signaling pathway

Mitogen-activated protein kinases (MAPK) are conserved serine/threonine protein kinases. It also plays an important role in the proliferation, differentiation, and apoptosis of eukaryotic cells. MAPK pathway includes three main kinases: MAPK Kinase, MAPK Kinase, and mitogen-activated protein kinase.

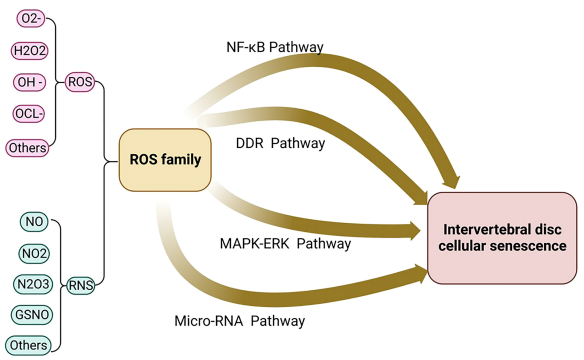

FIGURE 2
The oxidative stress signaling pathway includes the four major signaling pathways: micro-RNA signaling pathway, NF-kB signaling pathway, MAPK-ERK signaling pathway, and DDR signaling pathway.

They are activated step by step and phosphorylate downstream molecules to complete the transmission of a variety of signals. MAPK can trigger the adaptive response of cells according to the changes in physical and chemical levels of cells. MAPK can regulate the levels and functions of many proteins, including pro-inflammatory factors and factors in p21/p53 and p16/RB pathways so that cells are in a state of infinite growth arrest (73).

Extracellular regulated kinase 1/2 (ERK1/2) is the main type of MAPK kinase. ERK1/2 is essential to maintain the normal physiological function of cells and constitutes a key signaling pathway in various stress-induced apoptosis. Apoptosis signal-regulated kinase 1 (ASK1) is a member of the mitogen-activated protein kinase family. It activates ERK1/2 through MKK4/MKK7-JNK and MKK3/MKK6-p38 MAPKs pathways. ROS/RNS triggers the oxidation of TRX interacting proteins, activates JNK and p38MAPK pathways through the polymerization of ASK, and finally activates the ERK1/2 pathway, resulting in the continuous activation of ERK1/2 (74).Experiments have confirmed that ROS can activate the p38MAPK pathway to regulate the expression of p16 and pl9ARF, limit the self-renewal ability of mouse hematopoietic stem cells, and thus affect the life span of mice (75).

The increased expression of pro-inflammatory cytokines is an important pathological feature of IVD cellular senescence. Endoplasmic reticulum stress regulates the release of inflammatory factors through p38 MAPKs and CHOP pathways. Studies have shown that endoplasmic reticulum stress inducer-thapsigargin (TG) induces the phosphorylation of p38 MAPKs, and p38 MAPKs signal pathway transmits

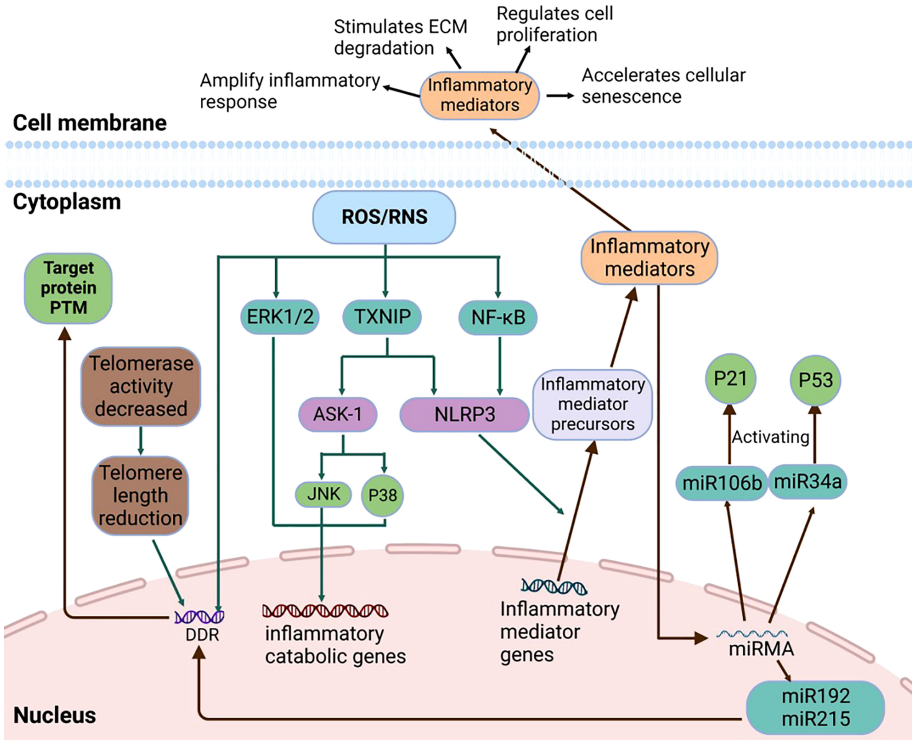

FIGURE 3
The details of Micro-RNA Signaling Pathway, NF-κB signaling pathway, MAPK signaling pathway, and DDR signaling pathway.

extracellular signals to the nucleus through three-stage cascade amplification, thereby activating the gene expression of IL-6 (76, 77).H_2O_2 stimulates autophagy of the IVD through ERK/mTOR signaling pathway and the AMPK/mTOR signaling pathway. In addition, the AMPK/mTOR pathway could also induce neuroinflammation, causing low back pain (78, 79).

Mitogen-activated protein kinase activated protein kinase (Mapkapk) is a protein composed of hundreds of amino acids. It exists uniformly in the cytoplasm and nucleus and can be phosphorylated by ERK and P38MAPKs. Mapkapk5 and PRKCZ pathways have been considered to have the ability to regulate multiple catabolism and are associated with oxidative stress-induced gene methylation (80, 81).

Integrin-β3 is significantly upregulated with cell aging, and p38 MAPK, a key downstream molecule in the senescence pathway mediated by Integrin-β3, is hyperactivated in senescent cells. Retinoic acid-inducible gene-I (RIG-I) is a cytosolic pattern recognition receptor that can alleviate cell senescence, so Rig-I-deficient cells can cause cell senescence *via* integrinβ3/p38 MAPK signal pathway. Studies have shown that compared with wild-type mice, Rig-I-deficient mice have faster hair shedding, and embryonic fibroblasts (MEFs) are more prone to continuous passage related to replicative senescence. Therefore, the p38 MAPK signaling pathway, as a key regulatory pathway of cell senescence, is a regulator of the expression of integrinβ3 in Rig-I-deficient cells (82).

Senescent cells can secrete inflammatory factors, proteases, and transcription factors, known as senescence-related secretory phenotype (SASP) (83).Studies have shown that the expression level of p38 MAPK is upregulated in senescent cells, and p38 MAPK increases NF-κB transcriptional activity and induces SASP. P38 MAPK promoting the SASP pathway is independent of DNA damage response. P53 can inhibit p38 MAPK activation and SASP expression, alleviating apoptosis (84).

DNA damage response

DNA damage response (DDR) is a signaling pathway that originates from DNA damage and prevents cell proliferation. DNA damage caused by ROS plays an important role in inducing cellular senescence. Nucleotides in DNA molecules are the key targets of ROS. ROS can rapidly induce cell senescence through DDR signaling pathway. In severe cases, the most serious type of DNA damage-DNA double-strand break (DSB) can be formed (85).The DDR pathway is composed of a complex regulatory network, and DDR transmits signals to downstream effector molecules through post-translational modification (PTM) of target proteins and their interactions. Post-translational modifications to target proteins include phosphorylation, ubiquitination, sumoylation, and acetylation, of which phosphorylation is the most common PTM that regulates DDR (86).

In addition, small non-coding RNAs(nc-RNAs) also play an important role in the DDR pathway. miRNAs associated with inflammation and aging (miR-146, miR-155, and miR-21), participating in the DDR pathway through the regulation of nc-RNAs gene expression. Nc-RNAs are processed by Dicer and Drosha RNases to generate small RNAs. Small RNAs produce RNA interference in a Mre11-Rad50-NBS1 complex-dependent manner, causing DNA damage. MiRNA can affect the expression of enzyme proteins and inflammatory factors, and link the inflammatory response with the DDR (87, 88).

The shortening of telomere length is a key signal to trigger the DDR pathway. Since most normal cells cannot fully replicate the linear genome, and the length of chromosome telomeres in cells gradually shortens with cell division (89). When the telomere length is shortened to a certain extent, the DDR pathway is triggered to activate the DNA damage checkpoint kinases CHK1 and CHK2, causing cell cycle arrest (90).

Oxidative stress can cause DSB and other DNA damage. Ataxia telangiectasia mutant kinase (ATM) is a protein kinase induced by DNA damage. ATM is a major regulator of stress response after DSB. It can promote the phosphorylation of DNA damage reaction substrate, up-regulate the activity of p53/p21, stimulate the p19ARF/p53/p21 pathway, and trigger cell senescence (91, 92).

Cell senescence related factors

P16 and cell senescence

P16 is a cell cycle inhibitor associated with cellular senescence. INK4a, the gene encoding p16, is located on chromosome 9p21. The p16 protein was able to promote the binding of Rb protein to E2F, thereby inhibiting the phosphorylation of Rb protein. In addition, E2F binding to the Rb protein fails to stimulate the expression of genes related to cell proliferation downstream. Activation of the p16/RB signaling pathway, which can arrest the cell cycle at the G1/S checkpoint, leads to the inhibition of normal cell proliferation or induction of apoptosis (93, 94).

Expression levels of p16 within the cell are regulated by multiple factors. MiRNAs can regulate the transcription of p16. In mouse MEFs, a tight link exists between genes associated with MEF senescence (p19ARF, p16, p21) and the miRNA family (miR-20a, miR-21, mir-28, miR-290). For example, miR-20a can upregulate the transcriptional activity of INK4a/ARF, leading to cell senescence (95, 96). In addition, acetylation of intracellular proteins can elevate the expression of p16. For example, the acetylation modification of histones can promote the activity of INK4A, activating the expression of p16. Acetylation of the transcription factor HBP1 by p300/CBP, which also enhances the expression of p16, accelerates cellular senescence (97, 98).

Loss and methylation of the promoter in the gene encoding INK4a can inhibit the expression of p16, thereby delaying cellular senescence (99). A-U-rich elements at the 3' untranscribed end can bind to the 3' untranscribed end of the mRNA of p16, and the binding of AUF1 to the 3'UTR of p16 promotes the degradation of p16 and has a significant anti-aging effect. Experimentally, HeLa cells overexpressing AUF1 are resistant to cellular senescence induced by H_2O_2 (100).

ARF/P53/P21 and cell senescence

P53 encoded by the p53 gene is a tumor suppressor protein; P21 encoded by the p21 gene is a cell cycle-associated inhibitory protein (101, 102). ARF regulates the expression of p53 and p21, and the gene encoding ARF is located on chromosome 9p21. The ARF/p53/p21 pathway is an important regulatory pathway of cellular senescence (Figure 4) (103).

Compared with the p16 pathway, the ARF/p53/p21 pathway is relatively complex. P53 can cause cell senescence by activating p21, and in addition, p53 itself promotes the expression of apoptotic factors Puma and Bax, among others, to induce apoptosis (104).ARF renders MDM2 unable to bind E3 by binding to the ubiquitin ligase MDM2. MDM2, which is not bound to E3, has lost the ability to degrade the p53 protein, thereby increasing the expression level of p53 in cells and promoting the expression of p21. P21 can inhibit the activity of the CDK2/cyclinE complex and keep pRb in a hypophosphorylated or dephosphorylated state. The inactive state of PRB can bind to E2F and arrest the normal cell cycle (105, 106).

The expression level of p53 in cells is regulated by multiple pathways. Damaged DNA in senescent cells induces the expression of p53 through the ATM pathway (107).In response to DNA damage and oxidative stress, the acetylation of p53 is also essential for regulating the transcriptional activity of p53 (108).As a multifunctional phosphoprotein, Artemis is also a key protein of non-homologous terminal junction (NHEJ). Under oxidative stress, Artemis and DNA PKC participate in the negative regulation of p53 (109). P19ARF/p53/p21 is one of the major signaling pathways of senescence responses in cells. When DNA is damaged, p53 can activate the expression of a variety of related genes to arrest the cell cycle in G1 and G2 phases, thereby preventing cell proliferation and inducing cell senescence (110).

Experiments have shown that elevating the expression levels of p53 or p21 in cells can induce a cellular senescence response. The expression levels of ARF, p53, and p21 were elevated in senescent MEFs cells and during senescence induced by the oncogenic signal H-ras. Mouse fibroblasts with humanized p53 (Hupki cells, derived from a human p53 knock-in mouse model) first senesce (111, 112).In addition, telomeres become progressively shorter in length, and once the length reaches a critical threshold, the telomeres signal to p53 for growth arrest *via* the ATM pathway, and upregulate p21 to lead to G1 arrest *via* the p19ARF/p53/p21 pathway, ultimately leading to cell senescence (113, 114).

Therapy

Inhibition of the NF- κB signaling pathway activation

Spartolonin B can significantly inhibit toll-like receptor 4 (TLR4) and NF- κ B protein expression through the TLR4/MyD88/NF- κB pathway. In the rat lumbar model, Spartolonin B effectively reduced the histological score of disc degeneration and alleviated disc cell death (115). The selective NF- κ b-

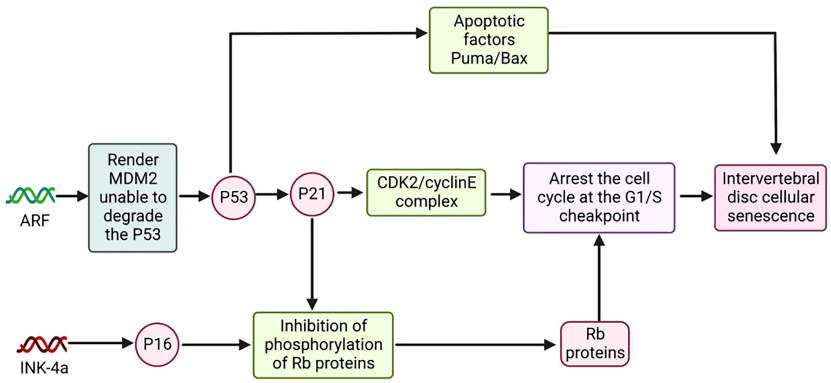

FIGURE 4
The Model of P16 and Cell Senescence and ARF/P53/P21 and Cell Senescence.

pathway inhibitor –JSH-23 can inhibit senescence and apoptosis of NPCs, as well as ECM degeneration induced by oxidative stress and inflammatory responses. The experiments showed that deficiency of ARG-2 produced similar results to JSH-23. Deficiency of ARG2, therefore, suppresses NF- κ B pathways to prevent DDD (116).

Additionally, the experiments showed that the expression of collagen 2 and aggrecan gradually decreased along with the expression levels of TFEB (Transcription factor EB) and QNZ (Quinazoline) as the degree of DDD increased. After over-expression of TFEB and QNZ, in NP cells, NF- κ B and ROS levels decreased, antioxidant enzymes upregulated, and inflammatory factors decreased. Studies have shown that both TFEB and QNZ inhibit inflammatory response and degradation of the ECM *via* NF- κ B signaling pathway, thereby slowing down degenerative changes of intervertebral discs (117, 118).

The findings showed that Celastrol decreased the expression levels of catabolic genes (MMP-3, 9, 13, ADAMTS-4, 5), oxidative stress factors (COX-2, iNOS), and pro-inflammatory factors (IL-6, TNF- α). Celastrol also inhibited NF- κ B pathways, thereby reducing I κ B α and phosphorylation of p65. Moreover, mangiferin antagonized the activation of the NF-κB signaling pathway induced by TNF- α, thereby reducing mitochondrial ROS activity and ameliorating mitochondrial damage. In conclusion, our study showed that celastrol and mangiferin could act on NF- κ B signaling pathway that reduces inflammatory factor-induced matrix catabolism and inflammatory response in NP cells and attenuates disc degeneration. In addition, Vitamin D and Naringin could inhibit the activation of the NF- κB signaling pathway *in vitro* and *in vivo* experiments, thereby suppressing the expression of p65 and Iκ B kinases α in NP cells (119–122).

Inhibition of the ERK/MAPK pathway activation

AAPH induced oxidative stress and subsequent degenerative changes in NP cells *via* the ERK/MAPK pathway. PBN (N-tert-butyl-α-phenylnitrone) inhibited the activation of the ERK/MAPK pathway induced by AAPH(2,2'-azobis (2-amidinopropane) dihydrochloride) and attenuated the expression of matrix-degrading proteases and cell apoptosis. We preliminarily identified the underlying mechanism of the protective effect of PBN, which could protect IVD from oxidative stress damage and slow down the catabolism of cell-matrix and cell apoptosis. Additionally, Exenatide regulates ECM anabolic balance and restores disc degeneration by inhibiting MAPK activation and its downstream AP-1 activity. As potent drugs inhibiting the ERK/MAPK pathway, PBN and Exenatide provide therapeutic targets for the treatment of DDD (123, 124).

Both STS (Sodium tanshinone IIA sulfonate) and AQP-3 (aquaporin-3) inhibited the p38 MAPK pathway. In the experiment, STS could significantly reverse the lower level of Col2 and aggrecan as well as the higher level of MMP-3/13, IL-1β, IL-6, and TNF- α in the IDD group, and increased antioxidant enzyme activities, reducing the level of oxidative stress caused by acupuncture. AQP-3 could inhibit the expression of Bax and caspase-3 genes and alleviate NP cells' apoptosis under oxidative damage. The inhibition of the p38 MAPK pathway by STS and AQP-3 has implications in further applications for alleviating the development of DDD (125, 126).

Additionally, we found that Que (Quercetin) inhibited the p38 MAPK signaling pathway through the p38 MAPK autophagy pathway. Que significantly reduced intracellular ROS levels by decreasing Bax and increasing Bcl-2 expression. Que also promotes ECM stability by increasing collagen II and aggrecan and decreasing MMP13 levels. Our results also showed that Que promoted the expression of autophagy markers Beclin-1, LC3-II/I and decreased p62. In a rat tail puncture-induced IVDD model, Que inhibited NPCs from undergoing apoptosis by regulating the p38 MAPK-mediated autophagy pathway (127).

In vitro studies have shown that Sirt3(sirtuin3) expression is reduced in degenerating NP tissue and that the activation of the AMPK/PGC-1 α pathway may partially alleviate NPC senescence caused by Sirt3 reduction. Therefore, the activation of AMPK/PGC-1α by up-regulating Sirt3 pathways delaying aging and NPC senescence is a potential therapeutic strategy for the treatment of IVDD (128).

Inhibition of the P53-P21-RB/P16-RB pathway activation

Studies have shown that expression of Sirt1(sirtuin1) and Sirt2(sirtuin2) is significantly reduced in severely degenerated disc tissues. In degenerative disc disease, the inflammatory factor IL-1 β and ROS significantly contribute to DDD progression. However, the over-expression of Sirt1 and Sirt2 can reverse the IL-1 β effect and increase the production of the antioxidant SOD1/2. In addition, the p53 and p21 signaling pathways could be significantly inhibited by the over-expression of Sirt1 and Sirt2. These results suggest that Sirt1 and Sirt2 alleviate NP cell death by suppressing oxidative stress and inflammation *via* repression of the p53/p21 pathway. Sirt1 and Sirt2 can be novel targets for DDD therapy in the future (129).

Restoration of mitochondrial function

Antioxidant administration and restoration of mitochondrial function may be as strategies for the treatment of IDD (122).BMSCs-exos were shown to dramatically decrease

ROS and MDA levels, alleviating oxidative stress of NP cells. Meanwhile, mitochondrial membrane potential could be enhanced and the mitochondrial damage could be prevented by BMSCs-exos, then the proliferation and cytoactive of NP cells were stimulated (130).H2O2 and tert-butyl hydroperoxide (TBHP) were commonly used to stimulate the oxidative stress microenvironment. Bari et al. reported that MSCs-exos at the doses of 5 and 50 mg/ml could play a protective role for NP cells, against the H2O2-induced oxidative stress damage (131).In a mice model, platelet-rich plasma (PRP)-derived exosomal miR-141-3p suppressed the cytotoxicity of H2O2 on NP cells and slowed down senescence process of IVD through the activation of Keap1/Nrf2 pathway (132).Also, MSCs-derived exosomal miR-31-5p could inhibit the apoptosis and calcification of TBHB-induced endplate chondrocyte by reducing ATF6-related ER stress (133).

Mitochondria, including genome or other components, plays an important role in intercellular communication (134).Exosomes also participants in the process of mitochondrial transfer. MSCs-exos may deliver mitochondria-related proteins to NP cells and repair the mitochondrial malfunction (135).In a rabbit model, MSCs-derived exosome could preserve the proteoglycan in IVD and block the oxidative stress-induced ECM degradation (136).Additionally, owing to the inhibited formation of ROS and NLRP3 inflammasome by MSC-exos, the apoptosis of NPCs could be alleviated and the deterioration of IDD could be halted.

Humanin (HN), a mitochondria-related peptide translated by the open reading frame of mitochondrial 16S rRNA, plays a role in resisting cellular oxidative damage and inhibiting apoptosis in response to oxidative stress. Experimentally, exogenous HN was shown to reduce intracellular ROS content and the extent of cellular damage and to enhance cellular anabolism and mitochondrial function; this anti-oxidative effect was lost in a cellular model in which HN expression was inhibited (137).In treating age-related cataracts and macular degeneration, HN exerts a positive antioxidant effect. In oxidatively stressed human lens epithelial cells (HLECs) and retinal pigment epithelial cells (hRPE): HN protects cells by upregulating GSH expression levels in mitochondria, thereby resisting the impairment of mitochondrial function by oxidative stress and activating caspase 3 and caspase 4 expression (138, 139).

In ischemia-reperfusion injury, humanin (HN) and its analogs (HNG) also play an anti-oxidative stress role. HNG-treated rat cardiomyocytes (H9C2 cells) were placed in a hydrogen peroxide (H2O2) solution. The level of reactive oxygen species (ROS) expression in cells treated with HNG was significantly lower than in the control group. The structure, membrane potential, and ATP levels of mitochondria were maintained as usual (140).HNG induced activation of catalase and glutathione peroxidase (GPx) within 5 min and reduced the ratio of oxidized to reduced glutathione within 30 min. Red-eared turtles can withstand prolonged hypoxia without causing cellular damage in the presence of rapid oxygen reperfusion. In red-eared turtles, the presence of humanin homolog (TSE-humanin) was confirmed by ELISA and western immunoblotting. TSE-humanin induced catalase and glutathione peroxidase (GPx) activation to produce antioxidant effects in the presence of blood reperfusion (141).

Interestingly, humanin (HN) inhibits apoptosis and promotes the proliferation of growth plate chondrocytes. It was demonstrated that GCs-induced bone growth impairment and chondrocyte apoptosis were inhibited in bones of mice overexpressed with HN or treated with HN. Still, HN did not interfere with the expected anti-inflammatory effects of GCs (142). Further, HN protected chondrocytes even in inflammation (143). Altogether, these data from chondrocytes may also provide a new strategy for treating lumbar degenerative diseases.

Polymeric biomaterials

The process of IDD could not be slowed down or reversed by the therapies that are now available. On the basis of this, polymeric biomaterials are now being developed, which have the potential to stimulate the regeneration and repair of the IVD. There were various advantages of polymeric biomaterials, including appropriate biomechanical characteristics and plasticity to restore the disc height and volume, and sustain the mechanical stress and segmental movement; excellent biocompatibility with no significant harmful effects on either autologous tissues or injected cells; good biodegradability, which indicated the ability to be metabolized and regenerated together with IVD (144, 145). These properties has brought forth fresh hope for the treatment of spinal degenerative illnesses.

Numerous experiments have confirmed that polymeric biomaterial therapy is essential for intervertebral disc repair at the molecular and cellular levels. Clinical investigations have demonstrated the ability of polymer-peptide hydrogels to promote the transformation of adult myeloid cells from a degenerative fibroblast-like state to a juvenile myeloid phenotype. *In vitro* three-dimensional culture, encapsulation of adult degenerative NP cells in a rigid formulation of hydrogels with laminin-mimetic peptides IKVAV and AG73 promotes the biosynthetic capacity of NP cells. In animal experiments, rabbit NP cells were inoculated on biodegradable nanofiber (NF) scaffolds and regenerated NP-like tissues *in vitro* and a subcutaneous implantation model. Extracellular matrix (ECM) (glycosaminoglycan and type II collagen) production was significantly higher on NF scaffolds than on control SW scaffolds. ASC-loaded collagen hydrogels were additionally implanted into the degenerated lumbar spine tissue, and the height of the degenerated discs was analyzed at 6 and 12 months of implantation. The size of the degenerated disc remained

TABLE 2 Therapeutic effects of therapeutic drugs on intervertebral disc cellular senescence.

Drugs	Drug properties	Therapeutic effects
Spartolonin B	Antagonist of both TLR2 and TLR4	Inhibited the expression of the Toll Like Receptor 4 (TLR4) and NF-KB
JSH-23	Inhibitor of NF-κB	Inhibited senescence, apoptosis and ECM degeneration
TFEB	A transcription factor	Inhibited inflammatory response and degradation of extracellular matrix
QNZ	Inhibitor of NF-κB	Inhibited inflammatory response and degradation of extracellular matrix
Celastrol	Inhibitor of proteasome	Downregulates the expression of catabolic genes, oxidative stress factor and pro-inflammatory factors
Vitamin D	Fat soluble vitamins	Inhibition of the NF- κB signalling pathway activation
Naringin	Inhibitor of NF-κB	Inhibition of the NF- κB signalling pathway activation
Mangiferin	Nrf2 activator and inhibitor of NF-κB	Inhibition of the NF- κB signalling pathway activation
PBN	A free-radical scavenger	Inhibition of the ERK/MAPK pathway activation Downregulates the expression of matrix degrading proteases
Exenatide	A glucagon-like peptide-1 receptor agonist	Inhibition of the MAPK pathway activation and AP-1 activation.
STS	A water-soluble derivate of tanshinone IIA (Tan IIA)	Upregulation the expression of Col2 and aggrecan Promoted the activation of antioxidant enzyme
AQP-3	An intrinsic membrane protein	Downregulates the expression of Bax and caspase-3 gene
Que	A natural flavonoid	Upregulation the expression of Bcl-2 aggrecan and type II collagen Downregulates the expression of Bax, MMP-3 and MMP-13
SIRT3	A deacetylase class	Promoted the activation of AMPK/PGC-1α
Sirt1 and Sirt2	A deacetylase class	Suppressing oxidative stress and inflammation
BMSCs-exos	Small membrane vesicles containing complex RNAs and proteins	Scavenging of intracellular reactive oxygen species Recovery of mitochondrial function Inhibition of apoptosis Promotes cell proliferation and differentiation
MSCs-exos	Small membrane vesicles containing complex RNAs and proteins	Recovery of mitochondrial function Inhibits degradation of extracellular matrix Inhibition of apoptosis Inhibition of calcification at the EP Promotes cell proliferation and differentiation
Humanin (HN)	mitochondria-related peptide	Reducing intracellular ROS content Enhanced cellular anabolism Recovery of mitochondrial function Inhibition of apoptosis
Polymeric Biomaterials (PB)	Biopolymers	Induce regeneration and repair of IVD.
Hyaluronic acid(HA)	water-soluble polysaccharide	Controls and alleviates oxidative stress processes and inflammatory responses
Silk Fibroin (SF)	natural high-molecular-weight fibre protein	Removes the active oxygen species aspect in the IVD. Controls and alleviates oxidative stress processes and inflammatory responses

stable, without significant loss, but did not fully recover. As a therapeutic strategy to address degenerative disc degeneration, polymeric biomaterial therapy can deliver nutrients, growth-promoting factors, and active cells to the degenerative disc, effectively combating lumbar disc degeneration and lumbar spine cellular aging.

Additionally, the role of antioxidant was also found in some polymeric biomaterials. Chitosan is a naturally occurring amino polysaccharide that is produced by the deacetylation of chitin. Chitin is the precursor to chitosan. Research on tissue engineering has made extensive use of chitosan because of its low cytotoxicity, excellent biocompatibility, *in-vivo* biodegradability, and antibacterial characteristics (146). Chitosan hydrogels could be as carriers of BMSCs, fibroblast growth factor, or diclofenac, which indeed improve the versatility of this polymeric biomaterial, including antioxidant effects (147).

Hyaluronic acid (HA) is a polymer that is made up of D-glucuronic acid and N-acetylglucosamine. It is a water-soluble polysaccharide that is often found in the epithelium and connective tissue of animals. Hyaluronic acid is also the principal component of the extracellular matrix in humans (ECM) (148). Additionally, HA has beneficial characteristics as an anti-inflammatory and an antioxidant. This effect was favorable to IDD that was followed by local oxidative stress and was exerted by high molecular weight HA *via* the classical IFN- signaling pathway, which was reported by Kazezian et al. (149).

The issue of immunogenicity may be sidestepped by using fibrin gel since it is already present in blood. It is advantageous in that it consists of basic materials, can be prepared quickly, has a reasonable level of toughness, and has good application prospects in the field of IVD disc tissue engineering (150). Silk fibroin (SF) is a natural high-molecular-weight fibre protein that is derived from silk. It has the same 18 amino acids that are found in the human body (151). The β-folding structure that is present in the crystallization region of the protein is associated with the greatly increased mechanical capabilities that SF hydrogels display (145). Bari et al. produced a microglue using a combination of silk protein, platelet-poor plasma, and regenerated platelet lysate. The IVD could be protected against apoptosis attributed to the anti-oxidant properties of the composite hydrogel, which played a role in cleaning the reactive oxygen species in IVD while also controlling the oxidative stress process and reducing inflammation. The properties and therapeutic effects of several therapies were summarized in Table 2 (152).

Conclusion and future directions

IDD is a significant risk factor causing low back pain and nerve compression in the lower extremities, which imposes a heavy economic burden on patients and society. With aging and in the role of multiple related factors, ROS accumulate in the IVD, leading to senescence and apoptosis of the disc cells through various mechanisms of action and eventually leading to IDD. The main pathways and targets of oxidative stress that inhibit normal cell proliferation and differentiation and induce cellular senescence and apoptosis remain to be verified. However, based on the current research on the mechanism of action, we summarized four signaling pathways and related cytokines for oxidative stress-induced senescence and apoptosis in IVD cells. Oxidative stress regulates the transcription and translation of downstream target genes through the aforementioned cellular signaling pathways and cytokines, leading to pathological changes such as the release of inflammatory factors, methylation of DNA structures, and cellular autophagy. Antioxidant therapy is considered the most promising therapeutic tool for the treatment and prevention of IDD. This article presents preclinical and clinical therapeutic strategies against oxidative stress to find therapeutic drug targets for the different molecular mechanisms of oxidative stress-induced IDD so that more effective and safer drugs can be applied to prevent and treat IDD. We still need to track cutting-edge basic research experiments and clinical trials to develop new therapeutic agents for the treatment and prevention of IDD and mitigate the burden on patients and society.

Author contributions

HY, YC, and YZ contributed to conception and design of the study. FC, HY, and YC collected the documents and wrote the first draft of the manuscript. YZ wrote sections of the manuscript. FC, HY and YZ designed the figures. HY, YC, YL, YH, and YZ critically revised the manuscript. YL, YH, and YZ supervised the manuscript. All authors have read and approved the submitted version.

Funding

This study was supported by the Golden Seed Program of Beijing Chaoyang Hospital (CYJZ202104).

Conflict of interest

The authors declare that the research was conducted in the absence of any commercial or financial relationships that could be construed as a potential conflict of interest.

Publisher's note

References

1. Han B, Ding H, Hai Y, Liu Y, Guan L, Pan A, et al. May the midline lumbar interbody fusion (MIDLIF) prevent the early radiographic adjacent segment degeneration? a minimum 3-year follow-up comparative study of MIDLIF in L4/5 with cortical bone trajectory screw versus traditional pedicle screw fixation. *BMC Musculoskelet Disord* (2022) 23(1):480. doi: 10.1186/s12891-022-05363-0

2. Kos N, Gradisnik L, Velnar T. A brief review of the degenerative intervertebral disc disease. *Med Arch* (2019) 73(6):421–4. doi: 10.5455/medarh.2019.73.421-424

3. Hartvigsen J, Hancock MJ, Kongsted A, Louw Q, Ferreira ML, Genevay S, et al. What low back pain is and why we need to pay attention. *Lancet* (2018) 391 (10137):2356–67. doi: 10.1016/S0140-6736(18)30480-X

4. Rothenfluh DA, Mueller DA, Rothenfluh E, Min K. Pelvic incidence-lumbar lordosis mismatch predisposes to adjacent segment disease after lumbar spinal fusion. *Eur Spine J* (2015) 24(6):1251–8. doi: 10.1007/s00586-014-3454-0

5. Dowdell J, Erwin M, Choma T, Vaccaro A, Iatridis J, Cho SK. Intervertebral disk degeneration and repair. *Neurosurgery* (2017) 80(3S):S46–54. doi: 10.1093/neuros/nyw078

6. Durackova Z. Some current insights into oxidative stress. *Physiol Res* (2010) 59(4):459–69. doi: 10.33549/physiolres.931844

7. Vo N, Niedernhofer LJ, Nasto LA, Jacobs L, Robbins PD, Kang J, et al. An overview of underlying causes and animal models for the study of age-related degenerative disorders of the spine and synovial joints. *J Orthop Res* (2013) 31 (6):831–7. doi: 10.1002/jor.22204

8. Giers MB, Munter BT, Eyster KJ, Ide GD, Newcomb A, Lehrman JN, et al. Biomechanical and endplate effects on nutrient transport in the intervertebral disc. *World Neurosurg* (2017) 99:395–402. doi: 10.1016/j.wneu.2016.12.041

9. Molladavoodi S, McMorran J, Gregory D. Mechanobiology of annulus fibrosus and nucleus pulposus cells in intervertebral discs. *Cell Tissue Res* (2020) 379(3):429–44. doi: 10.1007/s00441-019-03136-1

10. Erwin WM, Hood KE. The cellular and molecular biology of the intervertebral disc: A clinician's primer. *J Can Chiropr Assoc* (2014) 58(3):246–57.

11. Waxenbaum JA, Reddy V, Futterman B. *Anatomy, back, intervertebral discs*. Treasure Island (FL: StatPearls) (2022).

12. Hayes AJ, Benjamin M, Ralphs JR. Extracellular matrix in development of the intervertebral disc. *Matrix Biol* (2001) 20(2):107–21. doi: 10.1016/S0945-053X (01)00125-1

13. Huang YC, Urban JP, Luk KD. Intervertebral disc regeneration: do nutrients lead the way? *Nat Rev Rheumatol* (2014) 10(9):561–6. doi: 10.1038/nrrheum.2014.91

14. Ben-Porath I, Weinberg RA. The signals and pathways activating cellular senescence. *Int J Biochem Cell Biol* (2005) 37(5):961–76. doi: 10.1016/j.biocel.2004.10.013

15. Kirnaz S, Capadona C, Lintz M, Kim B, Yerden R, Goldberg JL, et al. Pathomechanism and biomechanics of degenerative disc disease: Features of healthy and degenerated discs. *Int J Spine Surg* (2021) 15(s1):10–25. doi: 10.14444/8052

16. Vergroesen PP, Kingma I, Emanuel KS, Hoogendoorn RJ, Welting TJ, van Royen BJ, et al. Mechanics and biology in intervertebral disc degeneration: a vicious circle. *Osteoarthritis Cartilage* (2015) 23(7):1057–70. doi: 10.1016/j.joca.2015.03.028

17. Ma KG, Shao ZW, Yang SH, Wang J, Wang BC, Xiong LM, et al. Autophagy is activated in compression-induced cell degeneration and is mediated by reactive oxygen species in nucleus pulposus cells exposed to compression. *Osteoarthritis Cartilage* (2013) 21(12):2030–8. doi: 10.1016/j.joca.2013.10.002

18. Tschoeke SK, Hellmuth M, Hostmann A, Robinson Y, Ertel W, Oberholzer A, et al. Apoptosis of human intervertebral discs after trauma compares to degenerated discs involving both receptor-mediated and mitochondrial-dependent pathways. *J Orthop Res* (2008) 26(7):999–1006. doi: 10.1002/jor.20601

19. Rannou F, Lee TS, Zhou RH, Chin J, Lotz JC, Mayoux-Benhamou MA, et al. Intervertebral disc degeneration: the role of the mitochondrial pathway in annulus fibrosus cell apoptosis induced by overload. *Am J Pathol* (2004) 164(3):915–24. doi: 10.1016/S0002-9440(10)63179-3

20. Xue JF, Shi ZM, Zou J, Li XL. Inhibition of PI3K/AKT/mTOR signaling pathway promotes autophagy of articular chondrocytes and attenuates inflammatory response in rats with osteoarthritis. *BioMed Pharmacother* (2017) 89:1252–61. doi: 10.1016/j.biopha.2017.01.130

21. Chang H, Cai F, Zhang Y, Xue M, Liu L, Yang A, et al. Early-stage autophagy protects nucleus pulposus cells from glucose deprivation-induced degeneration via the p-eIF2alpha/ATF4 pathway. *BioMed Pharmacother* (2017) 89:529–35. doi: 10.1016/j.biopha.2017.02.074

22. Miyazaki S, Kakutani K, Yurube T, Maeno K, Takada T, Zhang Z, et al. Recombinant human SIRT1 protects against nutrient deprivation-induced mitochondrial apoptosis through autophagy induction in human intervertebral disc nucleus pulposus cells. *Arthritis Res Ther* (2015) 17:253. doi: 10.1186/s13075-015-0763-6

23. Martin JA, Klingelhutz AJ, Moussavi-Harami F, Buckwalter JA. Effects of oxidative damage and telomerase activity on human articular cartilage chondrocyte senescence. *J Gerontol A Biol Sci Med Sci* (2004) 59(4):324–37. doi: 10.1093/gerona/59.4.B324

24. Park JB, Chang H, Kim KW. Expression of fas ligand and apoptosis of disc cells in herniated lumbar disc tissue. *Spine (Phila Pa 1976)* (2001) 26(6):618–21. doi: 10.1097/00007632-200103150-00011

25. Laagland LT, Bach FC, Creemers LB, Le Maitre CL, Poramba-Liyanage DW, Tryfonidou MA. Hyperosmolar expansion medium improves nucleus pulposus cell phenotype. *JOR Spine* (2022) 5(3):e1219. doi: 10.1002/jsp2.1219

26. Roberts S, Evans EH, Kletsas D, Jaffray DC, Eisenstein SM. Senescence in human intervertebral discs. *Eur Spine J* (2006) 15 Suppl 3:S312–6. doi: 10.1007/s00586-006-0126-8

27. Gruber HE, Ingram JA, Norton HJ, Hanley EN Jr. Senescence in cells of the aging and degenerating intervertebral disc: immunolocalization of senescence-associated beta-galactosidase in human and sand rat discs. *Spine (Phila Pa 1976)* (2007) 32(3):321–7. doi: 10.1097/01.brs.0000253960.57051.de

28. Kim KW , Chung HN, Ha KY, Lee JS, Kim YY. Senescence mechanisms of nucleus pulposus chondrocytes in human intervertebral discs. *Spine J* (2009) 9 (8):658–66. doi: 10.1016/j.spinee.2009.04.018

29. Wang YT, Wu XT, Wang F. Regeneration potential and mechanism of bone marrow mesenchymal stem cell transplantation for treating intervertebral disc degeneration. *J Orthop Sci* (2010) 15(6):707–19. doi: 10.1007/s00776-010-1536-3

30. Ju Z, Jiang H, Jaworski M, Rathinam C, Gompf A, Klein C, et al. Telomere dysfunction induces environmental alterations limiting hematopoietic stem cell function and engraftment. *Nat Med* (2007) 13(6):742–7. doi: 10.1038/nm1578

31. Mavrogonatou E, Angelopoulou MT, Kletsas D. The catabolic effect of TNFalpha on bovine nucleus pulposus intervertebral disc cells and the restraining role of glucosamine sulfate in the TNFalpha-mediated up-regulation of MMP-3. *J Orthop Res* (2014) 32(12):1701–7. doi: 10.1002/jor.22725

32. Yao Z, Nie L, Zhao Y, Zhang Y, Liu Y, Li J, et al. Salubrinal suppresses IL-17-Induced upregulation of MMP-13 and extracellular matrix degradation through the NF-kB pathway in human nucleus pulposus cells. *Inflammation* (2016) 39 (6):1997–2007. doi: 10.1007/s10753-016-0435-y

33. Townsend DM, Tew KD, Tapiero H. The importance of glutathione in human disease. *BioMed Pharmacother* (2003) 57(3-4):145–55. doi: 10.1016/S0753-3322(03)00043-X

34. Fan J, Wang L, Jiang GN, He WX, Ding JA. The role of survivin on overall survival of non-small cell lung cancer, a meta-analysis of published literatures. *Lung Cancer* (2008) 61(1):91–6. doi: 10.1016/j.lungcan.2007.11.011

35. Liu XW, Kang J, Fan XD, Sun LF. Expression and significance of VEGF and p53 in rat degenerated intervertebral disc tissues. *Asian Pac J Trop Med* (2013) 6 (5):404–6. doi: 10.1016/S1995-7645(13)60047-4

36. Lu XY, Ding XH, Zhong LJ, Xia H, Chen XD, Huang H, et al. Expression and significance of VEGF and p53 in degenerate intervertebral disc tissue. *Asian Pac J Trop Med* (2013) 6(1):79–81. doi: 10.1016/S1995-7645(12)60206-5

37. Rajasekaran S, Babu JN, Arun R, Armstrong BR, Shetty AP, Murugan S, et al. ISSLS prize winner: A study of diffusion in human lumbar discs: a serial magnetic resonance imaging study documenting the influence of the endplate on diffusion in normal and degenerate discs. *Spine (Phila Pa 1976)* (2004) 29 (23):2654–67. doi: 10.1097/01.brs.0000148014.15210.64

38. Ahn SH, Cho YW, Ahn MW, Jang SH, Sohn YK, Kim HS, et al. mRNA expression of cytokines and chemokines in herniated lumbar intervertebral discs. *Spine (Phila Pa 1976)* (2002) 27(9):911–7. doi: 10.1097/00007632-200205010-00005

39. Fujii K, Yamazaki M, Kang JD, Risbud MV, Cho SK, Qureshi SA, et al. Discogenic back pain: Literature review of definition, diagnosis, and treatment. *JBMR Plus* (2019) 3(5):e10180. doi: 10.1002/jbm4.10180

40. Risbud MV, Shapiro IM. Role of cytokines in intervertebral disc degeneration: pain and disc content. *Nat Rev Rheumatol* (2014) 10(1):44–56. doi: 10.1038/nrrheum.2013.160

41. Wei L, Cao P, Xu C, Zhong H, Wang X, Bai M, et al. Chondroitin synthase-3 regulates nucleus pulposus degeneration through actin-induced YAP signaling. *FASEB J* (2020) 34(12):16581–600. doi: 10.1096/fj.202001021R

42. Shi C, Das V, Li X, KC R, Qiu S, o-Sullivan I, et al. Development of an in vivo mouse model of discogenic low back pain. *J Cell Physiol* (2018) 233(10):6589–602. doi: 10.1002/jcp.26280

43. Yin S, Du H, Zhao W, Ma S, Zhang M, Guan M, et al. Inhibition of both endplate nutritional pathways results in intervertebral disc degeneration in a goat model. *J Orthop Surg Res* (2019) 14(1):138. doi: 10.1186/s13018-019-1188-8

44. Azman KF, Zakaria R. D-galactose-induced accelerated aging model: an overview. *Biogerontology* (2019) 20(6):763–82. doi: 10.1007/s10522-019-09837-y

45. Gullbrand SE, Ashinsky BG, Martin JT, Pickup S, Smith LJ, Mauck RL, et al. Correlations between quantitative T2 and T1rho MRI, mechanical properties and biochemical composition in a rabbit lumbar intervertebral disc degeneration model. *J Orthop Res* (2016) 34(8):1382–8. doi: 10.1002/jor.23269

46. Gullbrand SE, Malhotra NR, Schaer TP, Zawacki Z, Martin JT, Bendigo JR, et al. A large animal model that recapitulates the spectrum of human intervertebral disc degeneration. *Osteoarthritis Cartilage* (2017) 25(1):146–56. doi: 10.1016/j.joca.2016.08.006

47. Stokes IA, Counts DF, Frymoyer JW. Experimental instability in the rabbit lumbar spine. *Spine (Phila Pa 1976)* (1989) 14(1):68–72. doi: 10.1097/00007632-198901000-00014

48. Wada E, Ebara S, Saito S, Ono K. Experimental spondylosis in the rabbit spine. overuse could accelerate the spondylosis. *Spine (Phila Pa 1976)* (1992) 17(3 Suppl):S1–6. doi: 10.1097/00007632-199203001-00001

49. Nagano T , Yonenobu K, Miyamoto S, Tohyama M, Ono K. Distribution of the basic fibroblast growth factor and its receptor gene expression in normal and

degenerated rat intervertebral discs. *Spine (Phila Pa 1976)* (1995) 20(18):1972–8. doi: 10.1097/00007632-199509150-00002

50. Cassidy JD, Yong-Hing K, Kirkaldy-Willis WH, Wilkinson AA. A study of the effects of bipedism and upright posture on the lumbosacral spine and paravertebral muscles of the wistar rat. *Spine (Phila Pa 1976)* (1988) 13(3):301–8. doi: 10.1097/00007632-198803000-00013

51. Xian D, Guo M, Xu J, Yang Y, Zhao Y, Zhong J. Current evidence to support the therapeutic potential of flavonoids in oxidative stress-related dermatoses. *Redox Rep* (2021) 26(1):134–46. doi: 10.1080/13510002.2021.1962094

52. Qi J, Song CP, Wang B, Zhou J, Kangasjärvi J, Zhu JK, et al. Reactive oxygen species signaling and stomatal movement in plant responses to drought stress and pathogen attack. *J Integr Plant Biol* (2018) 60(9):805–26. doi: 10.1111/jipb.12654

53. Li L, Tan J, Miao Y, Lei P, Zhang Q. ROS and autophagy: Interactions and molecular regulatory mechanisms. *Cell Mol Neurobiol* (2015) 35(5):615–21. doi: 10.1007/s10571-015-0166-x

54. Hou G, Lu H, Chen M, Yao H, Zhao H. Oxidative stress participates in age-related changes in rat lumbar intervertebral discs. *Arch Gerontol Geriatr* (2014) 59 (3):665–9. doi: 10.1016/j.archger.2014.07.002

55. Davies CM, Guilak F, Weinberg JB, Fermor B. Reactive nitrogen and oxygen species in interleukin-1-mediated DNA damage associated with osteoarthritis. *Osteoarthritis Cartilage* (2008) 16(5):624–30. doi: 10.1016/j.joca.2007.09.012

56. Han Y, Li X, Yan M, Yang M, Wang S, Pan J, et al. Oxidative damage induces apoptosis and promotes calcification in disc cartilage endplate cell through ROS/MAPK/NF-kappaB pathway: Implications for disc degeneration. *Biochem Biophys Res Commun* (2019) 516(3):1026–32. doi: 10.1016/j.bbrc.2017.03.111

57. Bushati N, Cohen SM. microRNA functions. *Annu Rev Cell Dev Biol* (2007) 23:175–205. doi: 10.1146/annurev.cellbio.23.090506.123406

58. Mohr AM, Mott JL. Overview of microRNA biology. *Semin Liver Dis* (2015) 35(1):3–11. doi: 10.1055/s-0034-1397344

59. Ivanovska I, Ball AS, Diaz RL, Magnus JF, Kibukawa M, Schelter JM, et al. MicroRNAs in the miR-106b family regulate p21/CDKN1A and promote cell cycle progression. *Mol Cell Biol* (2008) 28(7):2167–74. doi: 10.1128/MCB.01977-07

60. Raver-Shapira N, Marciano E, Meiri E, Spector Y, Rosenfeld N, Moskovits N, et al. Transcriptional activation of miR-34a contributes to p53-mediated apoptosis. *Mol Cell* (2007) 26(5):731–43. doi: 10.1016/j.molcel.2007.05.017

61. Georges SA, Biery MC, Kim SY, Schelter JM, Guo J, Chang AN, et al. Coordinated regulation of cell cycle transcripts by p53-inducible microRNAs, miR-192 and miR-215. *Cancer Res* (2008) 68(24):10105–12. doi: 10.1158/0008-5472.CAN-08-1846

62. Hacker H, Karin M. Regulation and function of IKK and IKK-related kinases. *Sci STKE* (2006) 2006(357):re13. doi: 10.1126/stke.3572006re13

63. Bhattacharyya S, Dudeja PK, Tobacman JK. ROS, Hsp27, and IKKbeta mediate dextran sodium sulfate (DSS) activation of IkappaBa, NFkappaB, and IL-8. *Inflammation Bowel Dis* (2009) 15(5):673–83. doi: 10.1002/ibd.20821

64. Liu M, Liu S, Zhang Q, Fang Y, Yu Y, Zhu L, et al. Curculigoside attenuates oxidative stress and osteoclastogenesis via modulating Nrf2/NF-kappaB signaling pathway in RAW264.7 cells. *J Ethnopharmacol* (2021) 275:114129. doi: 10.1016/j.jep.2021.114129

65. Zhang L, Li X, Kong X, Jin H, Han Y, Xie Y. Effects of the NFkappaB/p53 signaling pathway on intervertebral disc nucleus pulposus degeneration. *Mol Med Rep* (2020) 22(3):1821–30. doi: 10.3892/mmr.2020.11288

66. Rai P, Onder TT, Young JJ, McFaline JL, Pang B, Dedon PC, et al. Continuous elimination of oxidized nucleotides is necessary to prevent rapid onset of cellular senescence. *Proc Natl Acad Sci U.S.A.* (2009) 106(1):69–74. doi: 10.1073/pnas.0809834106

67. Sun J, Hong J, Sun S, Wang X, Peng Y, Zhou J, et al. Transcription factor 7-like 2 controls matrix degradation through nuclear factor kappaB signaling and is repressed by microRNA-155 in nucleus pulposus cells. *BioMed Pharmacother* (2018) 108:646–55. doi: 10.1016/j.biopha.2018.09.076

68. Zhu H, Sun B, Shen Q. TNF-alpha induces apoptosis of human nucleus pulposus cells via activating the TRIM14/NF-kappaB signalling pathway. *Artif Cells Nanomed Biotechnol* (2019) 47(1):3004–12. doi: 10.1080/21691401.2019.1643733

69. Ma C, Wu L, Song L, He Y, Adel Abdo Moqbel S, Yan S, et al. The pro-inflammatory effect of NR4A3 in osteoarthritis. *J Cell Mol Med* (2020) 24(1):930–40. doi: 10.1111/jcmm.14804

70. Nerlich AG, Bachmeier BE, Schleicher E, Rohrbach H, Paesold G, Boos N, et al. Immunomorphological analysis of RAGE receptor expression and NF-kappaB activation in tissue samples from normal and degenerated intervertebral discs of various ages. *Ann N Y Acad Sci 2007* (1096) p:239–48. doi: 10.1196/annals.1397.090

71. Li J, Yuan W, Jiang S, Ye W, Yang H, Shapiro IM, et al. Prolyl-4-hydroxylase domain protein 2 controls NF-kappaB/p65 transactivation and enhances the catabolic effects of inflammatory cytokines on cells of the nucleus pulposus. *J Biol Chem* (2015) 290(11):7195–207. doi: 10.1074/jbc.M114.611483

72. Sun Y, Leng P, Song M, Li D, Guo P, Xu X, et al. Piezo1 activates the NLRP3 inflammasome in nucleus pulposus cell-mediated by Ca(2+)/NF-kappaB pathway. *Int Immunopharmacol* (2020) 85:106681. doi: 10.1016/j.intimp.2020.106681

73. Anerillas C, Abdelmohsen K, Gorospe M. Regulation of senescence traits by MAPKs. *Geroscience* (2020) 42(2):397–408. doi: 10.1007/s11357-020-00183-3

74. Liang YJ, Yang WX. Kinesins in MAPK cascade: How kinesin motors are involved in the MAPK pathway? *Gene* (2019) 684:1–9. doi: 10.1016/j.gene.2018.10.042

75. Ito K, Hirao A, Arai F, Takubo K, Matsuoka S, Miyamoto K, et al. Reactive oxygen species act through p38 MAPK to limit the lifespan of hematopoietic stem cells. *Nat Med* (2006) 12(4):446–51. doi: 10.1038/nm1388

76. Wang YM, Gao FJ, Lin SQ, Yi ZX, Zhang JM, Wu HX, et al. Activation of p38MAPK in spinal microglia contributes to autologous nucleus pulposus-induced mechanical hyperalgesia in a modified rat model of lumbar disk herniation. *Brain Res* (2020) 1742:146881. doi: 10.1016/j.brainres.2020.146881

77. Krupkova O, Sadowska A, Kameda T, Hitzl W, Hausmann ON, Klasen J, et al. p38 MAPK facilitates crosstalk between endoplasmic reticulum stress and IL-6 release in the intervertebral disc. *Front Immunol* (2018) 9:1706. doi: 10.3389/fimmu.2018.01706

78. Ni B, Shen H, Wang W, Lu H, Jiang Lc . TGF-beta1 reduces the oxidative stress-induced autophagy and apoptosis in rat annulus fibrosus cells through the ERK signaling pathway. *J Orthop Surg Res* (2019) 14(1):241. doi: 10.1186/s13018-019-1260-4

79. Liu Y, Li J, Li H, Shang Y, Guo Y, Li Z, et al. AMP-activated protein kinase activation in dorsal root ganglion suppresses mTOR/p70S6K signaling and alleviates painful radiculopathies in lumbar disc herniation rat model. *Spine (Phila Pa 1976)* (2019) 44(15):E865–72. doi: 10.1097/BRS.0000000000003005

80. Tanoue T, Moriguchi T, Nishida E. Molecular cloning and characterization of a novel dual specificity phosphatase, MKP-5. *J Biol Chem* (1999) 274(28):19949–56. doi: 10.1074/jbc.274.28.19949

81. Namour F, Vanhoutte FP, Beetens J, Blockhuys S, De Weer M, Wigerinck P. Pharmacokinetics, safety, and tolerability of GLPG0259, a mitogen-activated protein kinase-activated protein kinase 5 (MAPKAPK5) inhibitor, given as single and multiple doses to healthy male subjects. *Drugs R D* (2012) 12(3):141–63. doi: 10.2165/11633120-000000000-00000

82. Zhao J, Jiang X, Yan L, Lin J, Guo H, Yu S, et al. Retinoic acid inducible gene-I slows down cellular senescence through negatively regulating the integrin beta3/p38 MAPK pathway. *Cell Cycle* (2019) 18(23):3378–92. doi: 10.1080/15384101.2019.1677074

83. Cuollo L, Antonangeli F, Santoni A, Soriani A. The senescence-associated secretory phenotype (SASP) in the challenging future of cancer therapy and age-related diseases. *Biol (Basel)* (2020) 9(12):485. doi: 10.3390/biology9120485

84. Freund A, Patil CK, Campisi J. p38MAPK is a novel DNA damage response-independent regulator of the senescence-associated secretory phenotype. *EMBO J* (2011) 30(8):1536–48. doi: 10.1038/emboj.2011.69

85. Ou HL, Schumacher B. DNA Damage responses and p53 in the aging process. *Blood* (2018) 131(5):488–95. doi: 10.1182/blood-2017-07-746396

86. Durdikova K, Chovanec M. Regulation of non-homologous end joining via post-translational modifications of components of the ligation step. *Curr Genet* (2017) 63(4):591–605. doi: 10.1007/s00294-016-0670-7

87. Francia S, Michelini F, Saxena A, Tang D, de Hoon M, Anelli V, et al. Site-specific DICER and DROSHA RNA products control the DNA-damage response. *Nature* (2012) 488(7410):231–5. doi: 10.1038/nature11179

88. Olivieri F, Albertini MC, Orciani M, Ceka A, Cricca M, Procopio AD, et al. DNA Damage response (DDR) and senescence: shuttled inflamma-miRNAs on the stage of inflamm-aging. *Oncotarget* (2015) 6(34):35509–21. doi: 10.18632/oncotarget.5899

89. Rossiello F, Herbig U, Longhese MP, Fumagalli M, d'Adda di Fagagna F, et al. Irreparable telomeric DNA damage and persistent DDR signalling as a shared causative mechanism of cellular senescence and ageing. *Curr Opin Genet Dev* (2014) 26:89–95. doi: 10.1016/j.gde.2014.06.009

90. d'Adda di Fagagna F, Reaper PM, Clay-Farrace L, Fiegler H, Carr P, Von Zglinicki T, et al. A DNA damage checkpoint response in telomere-initiated senescence. *Nature* (2003) 426(6963):194–8. doi: 10.1038/nature02118

91. Lee JH, Paull TT. Cellular functions of the protein kinase ATM and their relevance to human disease. *Nat Rev Mol Cell Biol* (2021) 22(12):796–814. doi: 10.1038/s41580-021-00394-2

92. Tichy A, Vávrová J, Pejchal J, Rezácová M, et al. Ataxia-telangiectasia mutated kinase (ATM) as a central regulator of radiation-induced DNA damage response. *Acta Med (Hradec Kralove)* (2010) 53(1):13–7. doi: 10.14712/18059694.2016.57

93. Rayess H, Wang MB, Srivatsan ES. Cellular senescence and tumor suppressor gene p16. *Int J Cancer* (2012) 130(8):1715–25. doi: 10.1002/ijc.27316

94. Chen L, Yang R, Qiao W, Zhang W, Chen J, Mao L, et al. 1,25-dihydroxyvitamin d exerts an antiaging role by activation of Nrf2-antioxidant signaling and inactivation of p16/p53-senescence signaling. *Aging Cell* (2019) 18 (3):e12951. doi: 10.1111/acel.12951

95. Rizzo M, Evangelista M, Simili M, Mariani L, Pitto L, Rainaldi G. Immortalization of MEF is characterized by the deregulation of specific miRNAs with potential tumor suppressor activity. *Aging (Albany NY)* (2011) 3(7):665–71. doi: 10.18632/aging.100353

96. Chen H, Gu X, Su IH, Bottino R, Contreras JL, Tarakhovsky A, et al. Polycomb protein Ezh2 regulates pancreatic beta-cell Ink4a/Arf expression and regeneration in diabetes mellitus. *Genes Dev* (2009) 23(8):975–85. doi: 10.1101/gad.1742509

97. Zhou R, Han L, Li G, Tong T. Senescence delay and repression of p16INK4a by lsh via recruitment of histone deacetylases in human diploid fibroblasts. *Nucleic Acids Res* (2009) 37(15):5183–96. doi: 10.1093/nar/gkp533

98. Wang W, Pan K, Chen Y, Huang C, Zhang X. The acetylation of transcription factor HBP1 by p300/CBP enhances p16INK4A expression. *Nucleic Acids Res* (2012) 40(3):981–95. doi: 10.1093/nar/gkr818

99. Liggett WHJr., Sidransky D. Role of the p16 tumor suppressor gene in cancer. *J Clin Oncol* (1998) 16(3):1197–206. doi: 10.1200/JCO.1998.16.3.1197

100. Guo GE, Ma LW, Jiang B, Yi J, Tong TJ, Wang WG. Hydrogen peroxide induces p16(INK4a) through an AUF1-dependent manner. *J Cell Biochem* (2010) 109(5):1000–5. doi: 10.1002/jcb.22474

101. Sabapathy K, Lane DP. Understanding p53 functions through p53 antibodies. *J Mol Cell Biol* (2019) 11(4):317–29. doi: 10.1093/jmcb/mjz010

102. Georgakilas AG, Martin OA, Bonner WM. p21: A two-faced genome guardian. *Trends Mol Med* (2017) 23(4):310–9. doi: 10.1016/j.molmed.2017.02.001

103. Zhou X, Zhang L, Fu SJ, Liu G, Guo XG, Yi G, et al. [Shaoyangzhugu formula regulates p19(Arf)-p53-p21(Cip1) signaling pathway to ameliorate cartilage degeneration in aged cynomolgus monkeys with knee osteoarthritis]. *Nan Fang Yi Ke Da Xue Xue Bao* (2018) 38(3):346–52. doi: 10.3969/j.issn.1673-4254.2018.03.17

104. Kim EM, Jung CH, Kim J, Hwang SG, Park JK, Um HD. The p53/p21 complex regulates cancer cell invasion and apoptosis by targeting bcl-2 family proteins. *Cancer Res* (2017) 77(11):3092–100. doi: 10.1158/0008-5472.CAN-16-2098

105. He G, Siddik ZH, Huang Z, Wang R, Koomen J, Kobayashi R, et al. Induction of p21 by p53 following DNA damage inhibits both Cdk4 and Cdk2 activities. *Oncogene* (2005) 24(18):2929–43. doi: 10.1038/sj.onc.1208474

106. Heo SY, Jeong MS, Lee HS, Park WS, Choi IW, Yi M, et al. Dieckol induces cell cycle arrest by down-regulating CDK2/cyclin e in response to p21/p53 activation in human tracheal fibroblasts. *Cell Biochem Funct* (2022) 40(1):71–8. doi: 10.1002/cbf.3675

107. Hafner A, Bulyk ML, Jambhekar A, Lahav G. The multiple mechanisms that regulate p53 activity and cell fate. *Nat Rev Mol Cell Biol* (2019) 20(4):199–210. doi: 10.1038/s41580-019-0110-x

108. Brooks CL, Gu W. The impact of acetylation and deacetylation on the p53 pathway. *Protein Cell* (2011) 2(6):456–62. doi: 10.1007/s13238-011-1063-9

109. Zhang X, Zhu Y, Geng L, Wang H, Legerski RJ. Artemis Is a negative regulator of p53 in response to oxidative stress. *Oncogene* (2009) 28(22):2196–204. doi: 10.1038/onc.2009.100

110. Duan J, Duan J, Zhang Z, Tong T. Irreversible cellular senescence induced by prolonged exposure to H2O2 involves DNA-damage-and-repair genes and telomere shortening. *Int J Biochem Cell Biol* (2005) 37(7):1407–20. doi: 10.1016/j.biocel.2005.01.010

111. Shimazaki K, Uchida T, Komine A, Takahashi K. p53 retards cell-growth and suppresses etoposide-induced apoptosis in Pin1-deficient mouse embryonic fibroblasts. *Biochem Biophys Res Commun* (2012) 422(1):133–8. doi: 10.1016/j.bbrc.2012.04.121

112. Odell A, Askham J, Whibley C, Hollstein M. How to become immortal: let MEFs count the ways. *Aging (Albany NY)* (2010) 2(3):160–5. doi: 10.18632/aging.100129

113. Westin ER, Aykin-Burns N, Buckingham EM, Spitz DR, Goldman FD, Klingelhutz AJ. The p53/p21(WAF/CIP) pathway mediates oxidative stress and senescence in dyskeratosis congenita cells with telomerase insufficiency. *Antioxid Redox Signal* (2011) 14(6):985–97. doi: 10.1089/ars.2010.3444

114. Herbig U, Jobling WA, Chen BP, Chen DJ, Sedivy JM. Telomere shortening triggers senescence of human cells through a pathway involving ATM, p53, and p21(CIP1), but not p16(INK4a). *Mol Cell* (2004) 14(4):501–13. doi: 10.1016/S1097-2765(04)00256-4

115. Ge J, Chen L, Yang Y, Lu X, Xiang Z. Sparstolonin b prevents lumbar intervertebral disc degeneration through toll like receptor 4, NADPH oxidase activation and the protein kinase b signaling pathway. *Mol Med Rep* (2018) 17 (1):1347–53. doi: 10.3892/mmr.2017.7966

116. Li F, Sun X, Zheng B, Sun K, Zhu J, Ji C, et al. Arginase II promotes intervertebral disc degeneration through exacerbating senescence and apoptosis caused by oxidative stress and inflammation via the NF-kappaB pathway. *Front Cell Dev Biol* (2021) 9:737809. doi: 10.3389/fcell.2021.737809

117. Liang H, Liu Z, Wang Y, Wang D, Tian J. Transcription factor EB mediates oxidative stress-induced intervertebral disc degeneration via the NF-kappaB signaling pathway. *Ann Transl Med* (2021) 9(17):1385. doi: 10.21037/atm-21-3756

118. Chen ZB, Yu YB, Wa QB, Zhou JW, He M, Cen Y. The role of quinazoline in ameliorating intervertebral disc degeneration by inhibiting oxidative stress and anti-inflammation via NF-kappaB/MAPKs signaling pathway. *Eur Rev Med Pharmacol Sci* (2020) 24(4):2077–86. doi: 10.26355/eurrev_202002_20387

119. Yu H, Hou G, Cao J, Yin Y, Zhao Y, Cheng L. Mangiferin alleviates mitochondrial ROS in nucleus pulposus cells and protects against intervertebral disc degeneration via suppression of NF-kappaB signaling pathway. *Oxid Med Cell Longev* (2021) 2021:6632786. doi: 10.1155/2021/6632786

120. Chen J, Xuan J, Gu YT, Shi KS, Xie JJ, Chen JX, et al. Celastrol reduces IL-1beta induced matrix catabolism, oxidative stress and inflammation in human nucleus pulposus cells and attenuates rat intervertebral disc degeneration in vivo. *BioMed Pharmacother* (2017) 91:208–19. doi: 10.1016/j.biopha.2017.04.093

121. Huang H, Cheng S, Zheng T, Ye Y, Ye A, Zhu S. Vitamin d retards intervertebral disc degeneration through inactivation of the NF-kappaB pathway in mice. *Am J Transl Res* (2019) 11(4):2496–506.

122. Zhang YH, Shangguan WJ, Zhao ZJ, Zhou FC, Liu HT, Liang ZHc, et al. Naringin inhibits apoptosis induced by cyclic stretch in rat annular cells and partially attenuates disc degeneration by inhibiting the ROS/NF-kappaB pathway. *Oxid Med Cell Longev* (2022) 2022:6179444. doi: 10.1155/2022/6179444

123. Zhou Z, Wang Y, Liu H, Wang L, Liu Z, Yuan H, et al. PBN protects NP cells from AAPH-induced degenerative changes by inhibiting the ERK1/2 pathway. *Connect Tissue Res* (2021) 62(4):359–68. doi: 10.1080/03008207.2020.1743697

124. Wu Q, Wang Y, Li Q. Matairesinol exerts anti-inflammatory and antioxidant effects in sepsis-mediated brain injury by repressing the MAPK and NF-kappaB pathways through up-regulating AMPK. *Aging (Albany NY)* (2021) 13 (20):23780–95. doi: 10.18632/aging.203649

125. Dai S, Shi X, Qin R, Zhang X, Xu F, Yang H. Sodium tanshinone IIA sulfonate ameliorates injury-induced oxidative stress and intervertebral disc degeneration in rats by inhibiting p38 MAPK signaling pathway. *Oxid Med Cell Longev* (2021) 2021:5556122. doi: 10.1155/2021/5556122

126. Xu Y, Yao H, Wang Q, Xu W, Liu K, Zhang J, et al. Aquaporin-3 attenuates oxidative stress-induced nucleus pulposus cell apoptosis through regulating the P38 MAPK pathway. *Cell Physiol Biochem* (2018) 50(5):1687–97. doi: 10.1159/000494788

127. Zhang S, Liang W, Abulizi Y, Xu T, Cao R, Xun C, et al. Quercetin alleviates intervertebral disc degeneration by modulating p38 MAPK-mediated autophagy. *BioMed Res Int 2021* (2021) 2021:6631562. doi: 10.1155/2021/6631562

128. Lin J, Du J, Wu X, Xu C, Liu J, Jiang L, et al. SIRT3 mitigates intervertebral disc degeneration by delaying oxidative stress-induced senescence of nucleus pulposus cells. *J Cell Physiol* (2021) 236(9):6441–56. doi: 10.1002/jcp.30319

129. Yang M, Peng Y, Liu W, Zhou M, Meng Q, Yuan C. Sirtuin 2 expression suppresses oxidative stress and senescence of nucleus pulposus cells through inhibition of the p53/p21 pathway. *Biochem Biophys Res Commun* (2019) 513 (3):616–22. doi: 10.1016/j.bbrc.2019.03.200

130. Hu Y, Tao R, Wang L, Chen L, Lin Z. Exosomes derived from bone mesenchymal stem cells alleviate compression-induced nucleus pulposus cell apoptosis by inhibiting oxidative stress. *Oxid Med Cell Longev 2021* (2021) 2021:2310025. doi: 10.1155/2021/2310025

131. Bari E, Perteghella S, Di Silvestre D, Sorlini M, Catenacci L, Sorrenti M, et al. Pilot production of mesenchymal Stem/Stromal freeze-dried secretome for cell-free regenerative nanomedicine: A validated GMP-compliant process. *Cells* (2018) 7(11):190. doi: 10.3390/cells7110190

132. Xu J, Xie G, Yang W, Wang W, Zuo Z, Wang W. Platelet-rich plasma attenuates intervertebral disc degeneration via delivering miR-141-3p-containing exosomes. *Cell Cycle* (2021) 20(15):1487–99. doi: 10.1080/15384101.2021.1949839

133. Xie L, Chen Z, Liu M, Huang W, Zou F, Ma X, et al. MSC-derived exosomes protect vertebral endplate chondrocytes against apoptosis and calcification via the miR-31-5p/ATF6 axis. *Mol Ther Nucleic Acids* (2020) 22:601–14. doi: 10.1016/j.omtn.2020.09.026

134. Torralba D, Baixauli F, Sanchez-Madrid F. Mitochondria know no boundaries: Mechanisms and functions of intercellular mitochondrial transfer. *Front Cell Dev Biol* (2016) 4:107. doi: 10.3389/fcell.2016.00107

135. Valenti D, Vacca RA, Moro L, Atlante A. Mitochondria can cross cell boundaries: An overview of the biological relevance, pathophysiological implications and therapeutic perspectives of intercellular mitochondrial transfer. *Int J Mol Sci* (2021) 22(15):8312. doi: 10.3390/ijms22158312

136. Xia C, Zeng Z, Fang B, Tao M, Gu C, Zheng L. Mesenchymal stem cell-derived exosomes ameliorate intervertebral disc degeneration via anti-oxidant and anti-inflammatory effects. *Free Radic Biol Med* (2019) 143:1–15. doi: 10.1016/j.freeradbiomed.2019.07.026

137. Yang H, Cui Y, Tang Y, Tang X, Yu X, Zhou J. Cytoprotective role of humanin in lens epithelial cell oxidative stressinduced injury. *Mol Med Rep* (2020) 22(2):1467–79. doi: 10.3892/mmr.2020.11202

138. Sreekumar PG, Ishikawa K, Spee C, Mehta HH, Wan J, Yen K, et al. The mitochondrial-derived peptide humanin protects RPE cells from oxidative stress, senescence, and mitochondrial dysfunction. *Invest Ophthalmol Vis Sci* (2016) 57 (3):1238–53. doi: 10.1167/iovs.15-17053

139. Minasyan L, Sreekumar PG, Hinton DR, Kannan R. Protective mechanisms of the mitochondrial-derived peptide humanin in oxidative and endoplasmic reticulum stress in RPE cells. *Oxid Med Cell Longev 2017* (2017) p:1675230. doi: 10.1155/2017/1675230

140. Klein LE, Cui L, Gong Z, Su K, Muzumdar R, et al. A humanin analog decreases oxidative stress and preserves mitochondrial integrity in cardiac myoblasts. *Biochem Biophys Res Commun* (2013) 440(2):197–203. doi: 10.1016/j.bbrc.2013.08.055

141. Wijenayake S, Storey KB. Oxidative damage? not a problem! the characterization of humanin-like mitochondrial peptide in anoxia tolerant freshwater turtles. *Protein J* (2021) 40(1):87–107. doi: 10.1007/s10930-020-09944-7

142. Zaman F, Zhao Y, Celvin B, Mehta HH, Wan J, Chrysis D, et al. Humanin is a novel regulator of hedgehog signaling and prevents glucocorticoid-induced bone growth impairment. *FASEB J* (2019) 33(4):4962–74. doi: 10.1096/fj.201801741R

143. Celvin B, Zaman F, Aulin C, Sävendahl L. Humanin prevents undesired apoptosis of chondrocytes without interfering with the anti-inflammatory effect of dexamethasone in collagen-induced arthritis. *Clin Exp Rheumatol* (2020) 38(1):129–35.

144. Huang YC, Hu Y, Li Z, Luk KDK. Biomaterials for intervertebral disc regeneration: Current status and looming challenges. *J Tissue Eng Regener Med* (2018) 12(11):2188–202. doi: 10.1002/term.2750

145. Zhao X, Ma H, Han H, Zhang L, Tian J, Lei B, et al. Precision medicine strategies for spinal degenerative diseases: Injectable biomaterials with in situ repair and regeneration. *Mater Today Bio* (2022) 16:100336. doi: 10.1016/j.mtbio.2022.100336

146. Islam MM, Shahruzzaman M, Biswas S, Nurus Sakib M, Rashid TU, et al. Chitosan based bioactive materials in tissue engineering applications-a review. *Bioact Mater* (2020) 5(1):164–83. doi: 10.1016/j.bioactmat.2020.01.012

147. Jiang C, Li DP, Zhang ZJ, Shu HM, Hu L, Li ZN, et al. [Effect of basic fibroblast growth factor and transforming growth factor-B1 combined with bone marrow mesenchymal stem cells on the repair of degenerated intervertebral discs in rat models]. *Zhongguo Yi Xue Ke Xue Yuan Xue Bao* (2015) 37(4):456–65. doi: 10.3881/j.issn.1000-503X.2015.04.016

148. Wang Y, Niu W, Qu X, Lei B. Bioactive anti-inflammatory thermocatalytic nanometal-polyphenol polypeptide scaffolds for MRSA-Infection/Tumor postsurgical tissue repair. *ACS Appl Mater Interfaces* (2022) 14(4):4946–58. doi: 10.1021/acsami.1c21082

149. Kazezian Z, Sakai D, Pandit A. Hyaluronic acid microgels modulate inflammation and key matrix molecules toward a regenerative signature in the injured annulus fibrosus. *Adv Biosyst* (2017) 1(10):e1700077. doi: 10.1002/adbi.201700077

150. Growney Kalaf EA, Liu J, Wang J, Wang T, Jiang Y, Hu J, et al. Characterization of slow-gelling alginate hydrogels for intervertebral disc tissue-engineering applications. *Mater Sci Eng C Mater Biol Appl* (2016) 63:198–210. doi: 10.1016/j.msec.2016.02.067

151. Liu X, Liu J, Wang J, Wang T, Jiang Y, Hu J, et al. Bioinspired, microstructured silk fibroin adhesives for flexible skin sensors. *ACS Appl Mater Interfaces* (2020) 12(5):5601–9. doi: 10.1021/acsami.9b21197

152. Bari E, Perteghella S, Marrubini G, Sorrenti M, Catenacci L, Tripodo G, et al. In vitro efficacy of silk sericin microparticles and platelet lysate for intervertebral disk regeneration. *Int J Biol Macromol* (2018) 118(Pt A):792–9. doi: 10.1016/j.ijbiomac.2018.06.135

frontiers | Frontiers in Endocrinology

TYPE Review
PUBLISHED 07 December 2022
DOI 10.3389/fendo.2022.1067373

OPEN ACCESS

EDITED BY
Baoshan Xu,
Tianjin Hospital, China

REVIEWED BY
Esther POTIER,
Centre National de la Recherche Scientifique (CNRS), France
Murat Eksi,
Acıbadem University, Turkey

*CORRESPONDENCE
Yongning Li
liyongning@pumch.cn
Jun Gao
gaojpumch@hotmail.com

SPECIALTY SECTION
This article was submitted to Bone Research, a section of the journal Frontiers in Endocrinology

RECEIVED 11 October 2022
ACCEPTED 24 November 2022
PUBLISHED 07 December 2022

CITATION
Wang Z, Zhao Z, Han S, Hu X, Ye L, Li Y and Gao J (2022) Advances in research on fat infiltration and lumbar intervertebral disc degeneration. *Front. Endocrinol.* 13:1067373. doi: 10.3389/fendo.2022.1067373

Advances in research on fat infiltration and lumbar intervertebral disc degeneration

Zairan Wang[1], Zijun Zhao[2], Shiyuan Han[1], Xianghui Hu[1], Liguo Ye[1], Yongning Li[1,3]* and Jun Gao[1]*

[1]Department of Neurosurgery, Peking Union Medical College Hospital, Chinese Academy of Medical Sciences, Beijing, China, [2]Spine Center, Sanbo Brain Hospital, Capital Medical University, Beijing, China, [3]Department of International Medical Services, Peking Union Medical College Hospital, Chinese Academy of Medical Sciences, Beijing, China

Low back pain (LBP) is a disabling condition with no available cure, severely affecting patients' quality of life. Intervertebral disc degeneration (IVDD) is the leading cause of chronic low back pain (CLBP). IVDD is a common and recurrent condition in spine surgery. Disc degeneration is closely associated with intervertebral disc inflammation. The intervertebral disc is an avascular tissue in the human body. Transitioning from hematopoietic bone marrow to bone marrow fat may initiate an inflammatory response as we age, resulting in bone marrow lesions in vertebrae. In addition, the development of LBP is closely associated with spinal stability imbalance. An excellent functional state of paraspinal muscles (PSMs) plays a vital role in maintaining spinal stability. Studies have shown that the diminished function of PSMs is mainly associated with increased fat content, but whether the fat content of PSMs is related to the degree of disc degeneration is still under study. Given the vital role of PSMs lesions in CLBP, it is crucial to elucidate the interaction between PSMs changes and CLBP. Therefore, this article reviews the advances in the relationship and the underlying mechanisms between IVDD and PSMs fatty infiltration in patients with CLBP.

KEYWORDS

low back pain, intervertebral disc degeneration, paraspinal muscles, fatty infiltration, Modic changes, inflammation

Introduction

Low back pain (LBP) is a disabling condition with no available cure, often caused by a sedentary lifestyle and reduced exercise (1), severely affecting patients' quality of life. Chronic low back pain (CLBP) accounts for approximately 23% of LBP (2). Intervertebral disc degeneration (IVDD) is the leading cause of CLBP (3). IVDD is a chronic, multifactorial and irreversible process that severely compromises spinal stability and

disc shock absorption (3). Early biochemical changes in IVDD include loss of proteoglycans and water, while late morphological changes include reduced disc height, nucleus pulposus herniation, and annular tears (4). The paraspinal muscles (PSMs) are fundamental determinants of the structural stability and function of the lumbar spine (5). There is a potential mechanism of action between defects in the vertebral endplate and decreased muscle mass of the PSMs during the development of disc degeneration. Previous studies have shown that CLPB induced myoelectric activity and muscle remodeling (e.g., muscle atrophy, fatty infiltration, and altered fiber type) (6–10). At the L4/L5 level, fatty infiltration in PSMs is more severe when damage to the adjacent spinal endplates (11). Thus the formation of IVDD is not an isolated process but a chain reaction that includes vertebral endplate changes and fatty infiltration in the PSMs (12). Given the vital role of PSMs lesions in CLBP, it is crucial to elucidate the interaction between PSMs changes and CLBP. Therefore, this article reviews the advances in the relationship and the underlying mechanisms between IVDD and PSMs fatty infiltration in patients with CLBP.

Fatty infiltration in PSMs

The PSMs are the general term for the muscles surrounding the spine, which include the psoas, multifidus, and erector spinae. An excellent functional state of the PSMs is essential for maintaining the spine structure. A decrease in the function of PSMs can alter the original biomechanical relationships and increase the load on the disc, thus causing IVDD. Conversely, IVDD can also cause PSMs to compensate, leading to an imbalance in loads of PSMs and producing atrophy. Studies have shown that the atrophy of the PSMs is highly correlated with the degree of IVDD. Muscle degeneration is characterized by atrophy of muscle fibers, fiber bundles, and fat infiltration (13, 14). Muscle atrophy and fat replacement are thought to be the main features of PSMs remodeling in patients with CLBP, and fat infiltration may exacerbate CLBP. It is, therefore, crucial to elucidate the relationship between fatty infiltration of PSMs and IVDD.

With the development of medical imaging modalities, the metrics for assessing the atrophy of PSMs have gradually become diverse. Earlier, the degree of atrophy of PSMs was mainly determined by measuring the cross-sectional area (CSA) of PSMs using computed tomography (CT) or real-time ultrasound. In 1994, Goutallier et al. (15) proposed a semi-quantitative assessment of fatty infiltration in PSMs based on CT images, which opened new doors to exploring the mechanisms of IVDD. Using CT images, researchers found that fatty infiltration in PSMs was associated with small joint degeneration, lumbar spondylolisthesis, and narrowing of the vertebral space (16, 17). The degree of fatty infiltration in PSMs is significantly increased in patients with higher degrees of small joint degeneration (16–19). With the advent of high-resolution magnetic resonance imaging (MRI), MRI techniques have become the primary technique for assessing the atrophy of PSMs. Earlier magnetic resonance techniques used axial T2-weighted scans more often. In recent years, MRI has been able to distinguish well between muscle and adipose tissue by threshold segmentation techniques to assess the degree of atrophy of PSMs better. Ekşi et al. (20) proposed a new scoring system that included fatty infiltration in PSMs, Modic changes (MCs), and IVDD. Patients with more intense LBP had a more degenerative spine (20). However, this scoring system did not detail the role fat infiltration of PSMs played in LPB.

In 2015, Teichtahl et al. (21) used the iterative decomposition of water and fat with echo asymmetry and least square estimation-iron quantification (IDEAL-IQ) technique to quantify the fat content of PSMs and to assess the correlation between the fat content of PSMs and IVDD. They found that the fat content of PSMs was associated with reduced disc height. In addition, in 2016, the team found IVDD in all lumbar spine segments was associated with high-fat content in PSMs (22). A more recent study analyzed the correlation between fatty infiltration in different PSMs and IVDD in more detail using the Pfirmann classification (23) to assess the degree of IVDD. The study showed a strong positive correlation between Pfirmann classification and fat infiltration in the multifidus muscle (Rho=0.57, $p<0.001$) and a moderate positive correlation with fat infiltration in the erector spinae (Rho=0.49, $p<0.001$) and psoas major (Rho=0.31, $p<0.001$) (24).

Multifidus

The multifidus is a general term for a group of PSMs that are shorter in cross-section but run almost the entire length of the spine and are, therefore, more susceptible to pathological changes. The multifidus is lateral to the spinous process, covering the corresponding vertebral plate, and is more closely related to the vertebral plate and spinous process than the erector spinae. Sun et al. (25) found that atrophy of the multifidus was significantly and positively correlated with IVDD at the L3/L4 disc level compared to the other PSMs. The exact mechanism of muscle degeneration is unclear. Disuse and denervation are two main mechanisms often mentioned (26). Liu et al. (27) proposed two hypothetical models by studying 264 subjects. One was that degeneration of the multifidus caused lumbar instability, which exacerbated upper lumbar disc degeneration. The other was that a herniated lumbar disc compressed the nerve roots of the corresponding segment, resulting in post-denervated multifidus atrophy. Hodges et al. (28) and Goubert et al. (29) suggested the reduction in multifidus activity due to pain as the leading cause of wasting muscle atrophy. Studies have shown that fatty infiltration in PSMs is strongly associated with high-intensity pain or disability

and structural abnormalities of the lumbar spine (30). However, a study of patients with high-intensity pain and disability, which excluded the effect of physical activity level by adjusting for bias in the results, demonstrated that fatty infiltration in multifidus was an independent influence factor on the degree of disc degeneration (22). The facts about the fatty infiltration in multifidus during disc degeneration are clear. But the opposite conclusion is shown in studies targeting the muscle's CSA. Faur et al. (26) reported that multifidus degeneration occurs mainly in the cross-section of MRI scans. However, the more common view is that muscle CSA does not correlate with IVDD (24, 31). To improve the bias caused by muscle CSA in individual body size, Urrutia et al. (32) calculated the relative CSA (RCSA) by dividing the CSA of the L3 vertebrae by the muscle CSA and showed a stronger correlation between fat signal fraction and IVDD. In addition, muscle symmetry became a perspective that was looked at. It has been suggested that a 10% or more significant asymmetry in the multifidus' CSA be used to indicate potential spinal abnormalities (33). However, it was found that more than 10% of men with no history of LBP also had asymmetry of PSMs (34) and that asymmetry of muscle CSA was not associated with lumbar disc herniation (24). The Atrophy of PSMs is seen mainly in the inner side and deep layers of cross-sectional scans on MRI of the lumbar spine (26). Thus, measuring the CSA of PSMs and the ratio of functional CSA to CSA to assess the degree of fatty infiltration in PSMs can be biased by individual measurement differences. In addition, it may also produce inconsistent results for different lumbar spine segments. Some investigators have suggested that fatty infiltration in PSMs correlates more strongly with pathological changes in the intervertebral disc than muscle CSA (35).

Sarcopenia is defined as systemic muscle mass loss and a decline in physical performance (36), of which back muscle atrophy or fat infiltration may be a component (37). A study has shown that systemic muscle mass loss substantially impacts back muscle atrophy and fatty infiltration more than disc degeneration (37). In other words, the effect of age and gender on systemic muscle mass can further affect back muscle atrophy and fat infiltration. Another study using CT techniques to analyze trunk muscles showed that, in addition to the multifidus, fatty infiltration in the gluteus maximus and transversus abdominis muscles was also associated with IVDD (17). Still, the exact mechanisms involved need to be further explored.

Significant results have been obtained in cross-sectional studies, and experimental animal studies under univariate control are essential. By quantitative MRI, Huang et al. (38) assessed fat infiltration in PSMs of patients with discogenic LBP and rats in a novel discogenic LBP model. It was found that fatty infiltration was present in the PSMs of both LBP patients and rats and that there was a causal relationship between fatty infiltration and IVDD (38). Another study showed that dogs with higher IVDD grades had less fat infiltration in psoas and multifidus than those with lower mean IVDD degrees (39). From this, the authors speculated that the presence or severity of IVDD was not uniquely associated with fat infiltration in these muscles. A study using a porcine model showed that disc and nerve root injury might lead to a CSA reduction of the multifidus and its fatty infiltration (28). However, there was no atrophy of the multifidus following disc injury in sheep (40). This evidence challenges whether IVDD affects the characteristics of PSMs, but we are more skeptical that their relationship may not be purely causal. Özcan-Ekşi et al. (30) found that fatty infiltration in multifidus increased the probability of severe LBP fourfold. Patients with severe lumbar disc herniation were likelier to have increased fatty infiltration of the multifidus and erector spinae muscles (12). Therefore, further investigation is needed to determine whether lack of muscle strength and poor control due to fatty infiltration in the multifidus is the cause of LPB or vice versa.

Erector spinae

Although the role of the erector spinae in the spine's biomechanics is uncertain, its primary function is to be responsible for the flexion movement of the spine and, together with the multifidus, to maintain the stability of the lumbar spine. A cross-sectional study with Japanese subjects showed that fatty infiltration in PSMs correlated with age, and fatty infiltration of the upper lumbar erector spinae was significantly associated with LBP (41). In a separate study, the proton density fat fraction (PDFF) of multifidus and erector spinae at both L4/5 and L5/S1 levels was explored by MR techniques and analyzed the correlation with IVDD. The results showed a significant correlation between the PDFF of the PSMs and the degree of IVDD (42). This correlation also confirms that the two are mutually reinforcing processes, i.e., disc degeneration can also lead to further atrophy of the erector spinae by destabilizing the spine. However, a study on erector spinae in adolescents showed that the more intense the patient's LBP, the less fatty infiltration in erector spinae (43). The investigators suggest that this may be an automatic compensatory mechanism for the lumbar spine during the development of LBP in adolescents and children (43).

Psoas major

The psoas major is an essential flexor muscle of the spine and is the primary connection between the trunk and lower limbs. It contributes to the extension and general stability of the lumbar spine (44). Animal studies point to significant differences in the psoas major in comparing different degrees of disc degeneration (39). But it has also been shown that fatty infiltration in erector spinae and multifidus was significantly

associated with IVDD, whereas in psoas major was not significantly associated with IVDD (12). A study explicitly analyzing degenerative changes in the psoas major and lumbar spine showed that degenerative changes in the lumbar spine, including MCs, do not alter the activity of the psoas major (45). The CSA of the psoas major at the L3/L4 and L4/L5 discs is even greater in patients with LBP compared to the healthy population. The result is inconsistent with the results of previous animal experiments. In addition, Parkkola et al. (46) found that patients with CLBP had smaller psoas major by comparison with volunteers.

In contrast, Danneels et al. (47) showed no difference in CSA of the psoas major between patients with CLBP and healthy controls. Considering that the study by Danneels et al. chose subjects who did not undergo surgery, the author speculates that the difference in results may be related to increased activity of the psoas major during treatment such as surgery. It has been suggested that gender, age, and degree of disc degeneration are independently associated with the PSMs' fat signal fraction (FSF) (32). However, only gender and age affect the FSF of the psoas major, and the degree of disc degeneration does not alter the degree of fat infiltration in the psoas major (32). A study conducted to overcome gender bias concluded that the psoas major becomes more active in female patients with pain to stabilize the lumbar spine due to significant fat infiltration in the multifidus as a compensatory mechanism (15). Although gender is an essential factor influencing PSMs infiltration (42), this does not affect the validity of the conclusions of the above study.

Vertebral endplate changes

MCs refer to MRI signal intensity changes in the spinal endplate and subendplate bone. The characteristics of MCs were systematically described by Modic in 1988, who concluded that MCs are caused by disc degeneration and that their pathological evolution is characterized by disc degeneration → weakening or loss of endplate protection → edema of the adjacent cancellous bone → fatty infiltration of the vertebral body → fibrosis and calcification (48). They described three different Modic types (I, II, and III). Since then, mixed Modic lesions (I/II and II/III) have also been identified, which indirectly suggests that all Modic lesions can progress from one type to another (48–50). Based on the results of previous studies, types I and II are the most common types of the lumbar spine, with the most common distribution at the L4-L5 or L5-S1 levels (48, 51). Studies have concluded that Modic type II changes are less associated with LBP (51–54). The current studies confirm that Modic type II changes are more common than type I changes (48, 49, 51, 55–57) yet remain rare in individuals without degenerative lumbar disc disease (51, 58, 59).

MCs have previously been reported to occur mainly in the lower lumbar segments (L4-L5 and L5-S1) (60, 61). In a recent study, Ekşi et al. (43) found that MCs were predominantly seen at the L1-L4 level rather than the L4-S1 level and were more common in patients with severe IVDD than in those with mild to moderate IVDD. When analyzing this association on a level-by-level basis, the authors found that severe IVDD was significantly associated with MCs at the L1-L2 and L3-L4 disc levels (43). And multifidus' fatty infiltration in the L3-L4 and L4-L5 segments increased the risk of MCs in all lumbar parts by 8.3-fold and 9.1-fold, respectively (43). An MRI study showed that fatty infiltration in PSMs was associated with reduced disc height and MCs (31). In addition, Patients with Modic type I or I/II changes had more fatty degeneration in the lumbar PSMs (62). However, there is still considerable debate as to whether MCs precede lipoatrophy or occur after back pain.

Molecular mechanisms of fat infiltration in PSMs

The lumbar discs and the PSMs are not only adjacent but also interconnected at the molecular and metabolic levels. IVDD is characterized by a progressive decrease in the proteoglycan and water content of the nucleus pulposus and a loss of resistance to compressive loads (63). The above mechanism is one of many, so we have sorted out the possible underlying mechanisms.

Inflammation

Early views suggested that fatty infiltration compromised the mass of the PSMs because the adipose tissue was non-contractible (64, 65). There are currently many hypotheses for the mechanism of the relationship between fatty infiltration of the PSMs and spinal disorders, such as loss of nerve (28), chronic disuse (66), and inflammation (67). Inflammation, in particular, has been extensively studied. An experiment modeled in rats demonstrated that fatty infiltration in PSMs was closely associated with inflammation (38). Inflammation contributes to the development of pain (68) and may contribute to MCs (69). Increased reactive oxygen species (ROS) production has been reported to be associated with the differentiation of preadipocytes to adipocytes and the accumulation of adipose tissue (70). Thus, effectively mitigating cellular oxidative stress in an inflammatory environment would also block ROS-induced adipogenesis (71). In a study by James et al. (72), muscle and fat specimens were collected intraoperatively from patients with herniated discs, and gene expression was detected using a quantitative polymerase chain reaction, dividing the patients into a high-fat infiltration group and a low-fat infiltration group. The results showed high tumor necrosis factor (TNF) expression in the multifidus of subjects in the high-fat infiltration group. Another study addressing the mechanism showed that the expression levels of interleukin (IL)-1β, IL-6, IL-8, nitric oxide

synthase-2 (NOS-2), and transforming growth factor (TGF)-β did not differ in severe IVDD compared to mild IVDD (24). The expression of TNF in lumbar disc tissue was significantly higher in the severe degeneration group than in the mild degeneration group (24). During the inflammatory process, TNF possesses intense pro-inflammatory activity and is closely associated with various pathological processes in IVDD (73). Some researchers have speculated that TNF may not only be a product of adipose tissue but also regulate adipogenesis (72).

Fibroblasts and preadipocytes are found in the connective tissue surrounding muscle fibers and can differentiate in response to inflammation. Adipocytes also increase following sympathetic degeneration, which is likely to occur following nerve injury. On the other hand, the dramatic increase in deoxyribonucleic acid synthesis following injury leads to the secretion of pro-inflammatory cytokines, stimulating fibroblasts, preadipocytes, and muscle precursor cells, ultimately leading to adipocyte proliferation.

Histological analysis shows that patients with LBP primarily display degeneration of the multifidus muscle, which occurs in relation to elevated inflammation, fiber size, and the ratio of fat to connective tissue (74). In addition, it was found that degenerating muscles were predominantly composed of type I fibers with less vascularity (74). Although there was no concurrent sign of atrophy at the individual fiber level, inflammatory cell density and vascular density changed in different muscle groups. In particular, inflammatory cells were significantly increased in normal skeletal muscle cells in the subgroup with 10%-50% fat infiltration, which suggests that regeneration and degeneration were out of balance in that condition (74).

Obesity

Obesity is a pro-inflammatory state that releases cytokines such as TNF-α and IL-6. It is commonly believed that obesity is closely associated with MCs. Albert et al. suggest that it is not obesity but rather its resulting overweight that plays a vital role in the development of MCs (50). Two possible mechanisms explain this effect: 1) When the disc is stressed, matrix synthesis and proteoglycan content are reduced. The load-bearing capacity then gradually decreases. 2) IVDD or disc herniation can increase the shear forces on the vertebral endplates due to loss of the nucleus pulposus. The increased axial and torsional stresses may result in microfractures of the vertebral endplate.

LBP has been reported to be significantly associated with body mass index (BMI) (75). However, it has also been suggested that BMI is not associated with fatty infiltration in PSMs (24). A study of fatty infiltration in PSMs showed no difference in pain scores between obese and non-obese patients (76). Still, obese patients had more severe disc degeneration in the lower lumbar spine, possibly due to the increased load on the vertebral body caused by obesity (76). Subcutaneous fat tissue thickness (SFTT) is a new radiological index for assessing body fat percentage (77). Recent studies have shown that SFTT at L1-L2 level was superior to BMI in predicting severe IVDD and MCs (77, 78). A zoological study showed that a high-calorie diet did not cause disc degeneration in the vertebrae of mice (79). However, advanced glycation end products (AGEs) can lead to IVDD (80, 81). The receptor for advanced glycation end-products (RAGE) deletion inhibits systemic pro-inflammatory cytokine activity. D'Erminio et al. (79) used the RAGE knockout (RAGE-KO) model to control inflammation. They found that the effect of RAGE-KO in improving IVDD was limited and gender-related, suggesting that obesity and other sources of inflammation leading to a biomechanical overload of the lumbar spine may also have an impact (79). Another study showed that diabetes, rather than obesity, reduced the glycosaminoglycan and water content of the discs, and IVDD was associated with increased vertebral endplate thickness, reduced endplate porosity, and increased levels of AGEs (81). Due to their reduced glycosaminoglycan and water content and higher AGEs levels, the discs from diabetic rats became stiffer and had less alteration during compression (81). These findings suggest that endplate sclerosis, increased oxidative stress, and AGE/RAGE-mediated interactions may explain the high incidence of IVDD in patients with type 2 diabetes (81). Cell culture studies have shown increased palmitic acid-induced apoptosis in nucleus pulposus cells and activation of caspases 3, 7, 9, and poly (ADP-ribose) polymerase (PARP) mainly through the mitogen-activated protein kinases (MAPK) pathway, particularly the extracellular-signal-regulated kinases (ERK) pathway (82). Most obese patients have abnormally high blood lipid levels, and hypertriglyceridemia can induce IVDD independent of age and BMI (82). The results do not exclude the possibility of additional direct mechanical influences in the process of disc degeneration in humans (82).

Conversion of hematopoietic bone marrow to fatty bone marrow

The intervertebral disc is an avascular tissue in the human body. Its nutritional supply depends on the transport of capillaries from the adjacent vertebrae. The study of Krug et al. showed that the conversion of hematopoietic bone marrow to fatty bone marrow impairs the supply of adequate nutrients to the disc cells and thus may accelerate disc degeneration (83). The MRI quantitative analysis confirmed that in the early stages of IVDD, IVDD and bone marrow fat interacted to some extent, with the severity of lumbar disc degeneration increasing with the adjacent vertebral fatty conversion (84). The relationship was particularly evident in the L4/5 lumbar segment (84). Focal fat conversion in normal hematopoietic red bone marrow may impede the transport of nutrients from the bone marrow to the end plate (85). IVDD is usually accompanied by osteoporosis, suggesting that the development of osteoporosis and IVDD may be a concomitant

process (86, 87). Adipocytes and osteoblasts are derived from bone marrow mesenchymal stem cells (BMSCs). In BMSCs, there is a balance between osteogenesis and lipogenesis. If this balance is disturbed, it leads to a physiological disturbance, i.e., an increase in adipocytes in the bone marrow and decreased bone formation (79). Focal fatty degeneration of the bone marrow near the disc endplates can lead to disc degeneration by impeding the transport and metabolic exchange of nutrients essential to the disc. In addition, adipocyte growth and inflammatory edema compress the blood vessels in the confined bone cavity, further reducing blood flow (49, 88).

Adipokines

Adipose tissue releases pro-inflammatory cytokines that have a potential role in various tissue pathologies. Cytokines such as leptin, adiponectin, and TNF produced by adipocytes have been shown to be associated with obesity and osteoarthritis (89).

Leptin regulates adipose tissue metabolism and inflammation (90) and can lead to adipocyte hypertrophy (91). Leptin and TNF are components of a positive feedback loop that promotes adipocyte hypertrophy (90). This cascade response could explain the rapid deterioration of adipose infiltration over time. Segar et al. (92) found that leptin acting alone or in concert with TNF-α, IL-1β, or IL-6 in the nucleus pulposus significantly increased nitric oxide (NO) production and promoted inflammatory cytokines and matrix metalloproteinases (MMP). These processes further initiate the degradation of disc cells and the inflammatory cascade response, thereby accelerating the degenerative process (92). Meanwhile, a study by Han et al. (93) confirmed that leptin expression was associated with the calcification of the cartilage endplates.

Adiponectin, mainly produced by lipids, is downregulated in patients with disc degeneration (94). Adiponectin may play an anti-inflammatory role in maintaining the homeostasis of the degenerating disc environment by down-regulating TNF-α production by degenerating nucleus pulposus cells (94). And adiponectin can reduce TNF-α and IL-6 significantly upregulated by IL-1β stimulation in nucleus pulposus cells and annulus fibrosus cells (95). James et al. (72) found increased expression of lipocalin and NOS-2 in epidural fat. And high leptin and low arginase 1 expressions were found in the intramuscular and subcutaneous adipose tissues (72). They speculated that disc disease is associated with a dysregulation of the local inflammatory condition (72).

Resistin is commonly involved in intra-articular angiogenesis and the inflammatory milieu (96, 97). Resistin expression is upregulated in degenerating disc tissue. In nucleus pulposus cells, it binds to Toll-like receptor 4 *via* the p38-MAPK and NF-KB signaling pathways, leading to inflammation (98), further leading to metabolic disturbances in nucleus pulposus cells, and accelerated disc degeneration processes (99).

Visfatin is secreted by visceral adipocytes and is involved in immunity, stress, and inflammation processes. In degenerated disc tissue, visfatin expression levels were progressively upregulated as degeneration progressed (100). In the nucleus pulposus cells, increased visfatin expression was associated with an upregulation of degradation-related proteins (100). In contrast, the knockdown of visfatin expression or the use of inhibitors showed a decrease in cellular autophagy and a downregulation of autophagy-related protein expression (100). Similarly, a study modeled in rats to simulate severe IVDD and performed pathway analysis indicated that inhibition of visfatin protected the nucleus pulposus from degeneration and that focusing on epidural lipids and visfatin would be a potential therapeutic target to control the inflammation associated with IVDD (101).

Conclusion

IVDD is the leading cause of CLBP. IVDD is a chronic, multifactorial, irreversible process that severely compromises spinal stability and disc shock absorption. The PSMs are fundamental determinants of the structural stability and function of the lumbar spine. Studies have confirmed that fatty infiltration in PSMs plays a crucial role in IVDD. Inflammation, obesity, conversion of hematopoietic bone marrow to fatty bone marrow, and adipokines may be potential mechanisms for fat infiltration in PSMs. However, the quantitative methods and determination criteria for fat infiltration in PSMs and the vertebral plate need to be further studied. The biochemical and molecular mechanisms of fat infiltration in IVDD remain to be further investigated. The communication between the two at the molecular level still needs to be confirmed, especially concerning the potential signaling pathways in adipocytokines in IVDD.

Author contributions

All authors listed have made a substantial, direct, and intellectual contribution to the work and approved it for publication.

Funding

This work is supported by National High Level Hospital Clinical Research Funding (2022-PUMCH-B-112).

Conflict of interest

The authors declare that the research was conducted in the absence of any commercial or financial relationships that could be construed as a potential conflict of interest.

Publisher's note

References

1. Chen SM, Liu MF, Cook J, Bass S, Lo SK. Sedentary lifestyle as a risk factor for low back pain: a systematic review. *Int Arch Occup Environ Health* (2009) 82 (7):797–806. doi: 10.1007/s00420-009-0410-0

2. Maher C, Underwood M, Buchbinder R. Non-specific low back pain. *Lancet* (2017) 389(10070):736–47. doi: 10.1016/S0140-6736(16)30970-9

3. Vergroesen PP, Kingma I, Emanuel KS, Hoogendoorn RJ, Welting TJ, van Royen BJ, et al. Mechanics and biology in intervertebral disc degeneration: a vicious circle. *Osteoarthritis Cartilage* (2015) 23(7):1057–70. doi: 10.1016/j.joca.2015.03.028

4. Modic MT, Ross JS. Lumbar degenerative disk disease. *Radiology* (2007) 245 (1):43–61. doi: 10.1148/radiol.2451051706

5. Hodges PW, Danneels L. Changes in structure and function of the back muscles in low back pain: different time points, observations, and mechanisms. *J Orthop Sports Phys Ther* (2019) 49(6):464–76. doi: 10.2519/jospt.2019.8827

6. Geisser ME, Ranavaya M, Haig AJ, Roth RS, Zucker R, Ambroz C, et al. A meta-analytic review of surface electromyography among persons with low back pain and normal, healthy controls. *J Pain* (2005) 6(11):711–26. doi: 10.1016/j.jpain.2005.06.008

7. Solomonow M, Hatipkarasulu S, Zhou BH, Baratta RV, Aghazadeh F. Biomechanics and electromyography of a common idiopathic low back disorder. *Spine* (2003) 28(12):1235–48. doi: 10.1097/01.BRS.0000065568.47818.B9

8. Ranger TA, Cicuttini FM, Jensen TS, Heritier S, Urquhart DM. Paraspinal muscle cross-sectional area predicts low back disability but not pain intensity. *Spine J* (2019) 19(5):862–8. doi: 10.1016/j.spinee.2018.12.004

9. Agten A, Stevens S, Verbrugghe J, Timmermans A, Vandenabeele F. Biopsy samples from the erector spinae of persons with nonspecific chronic low back pain display a decrease in glycolytic muscle fibers. *Spine J* (2020) 20(2):199–206. doi: 10.1016/j.spinee.2019.09.023

10. Kalichman L, Carmeli E, Been E. The association between imaging parameters of the paraspinal muscles, spinal degeneration, and low back pain. *BioMed Res Int* (2017) 2017:2562957. doi: 10.1155/2017/2562957

11. Bailey JF, Fields AJ, Ballatori A, Cohen D, Jain D, Coughlin D, et al. The relationship between endplate pathology and patient-reported symptoms for chronic low back pain depends on lumbar paraspinal muscle quality. *Spine* (2019) 44(14):1010–7. doi: 10.1097/BRS.0000000000003035

12. Özcan-Ekşi EE, Ekşi MŞ, Akçal MA. Severe lumbar intervertebral disc degeneration is associated with modic changes and fatty infiltration in the paraspinal muscles at all lumbar levels, except for L1-L2: a cross-sectional analysis of 50 symptomatic women and 50 age-matched symptomatic men. *World Neurosurg* (2019) 122:e1069–77. doi: 10.1016/j.wneu.2018.10.229

13. Goldspink DF. The influence of immobilization and stretch on protein turnover of rat skeletal muscle. *J Physiol* (1977) 264(1):267–82. doi: 10.1113/jphysiol.1977.sp011667

14. Safran O, Derwin KA, Powell K, Iannotti JP. Changes in rotator cuff muscle volume, fat content, and passive mechanics after chronic detachment in a canine model. *J Bone Joint Surg Am* (2005) 87(12):2662–70. doi: 10.2106/JBJS.D.02421

15. Goutallier D, Postel JM, Bernageau J, Lavau L, Voisin MC. Fatty muscle degeneration in cuff ruptures. pre- and postoperative evaluation by CT scan. *Clin Orthop Relat Res* (1994) 304):78–83.

16. Kalichman L, Klindukhov A, Li L, Linov L. Indices of paraspinal muscles degeneration: reliability and association with facet joint osteoarthritis: feasibility study. *Clin Spine Surg* (2016) 29(9):465–70. doi: 10.1097/BSD.0b013e31828be943

17. Sebro R, O'Brien L, Torriani M, Bredella MA. Assessment of trunk muscle density using CT and its association with degenerative disc and facet joint disease of the lumbar spine. *Skeletal Radiol* (2016) 45(9):1221–6. doi: 10.1007/s00256-016-2405-8

18. Kalichman L, Hodges P, Li L, Guermazi A, Hunter DJ. Changes in paraspinal muscles and their association with low back pain and spinal degeneration: CT study. *Eur Spine J* (2010) 9(7):1136–44. doi: 10.1007/s00586-009-1257-5

19. Kalichman L, Kim DH, Li L, Guermazi A, Hunter DJ. Computed tomography-evaluated features of spinal degeneration: prevalence, intercorrelation, and association with self-reported low back pain. *Spine J* (2010) 10(3):200–8. doi: 10.1016/j.spinee.2009.10.018

20. Ekşi MŞ, Özcan-Ekşi EE, Orhun Ö, Turgut VU, Pamir MN. Proposal for a new scoring system for spinal degeneration: Mo-Fi-Disc. *Clin Neurol Neurosurg* (2020) 198:106120. doi: 10.1016/j.clineuro.2020.106120

21. Teichtahl AJ, Urquhart DM, Wang Y, Wluka AE, O'Sullivan R, Jones G, et al. Physical inactivity is associated with narrower lumbar intervertebral discs, high fat content of paraspinal muscles and low back pain and disability. *Arthritis Res Ther* (2015) 17(1):114. doi: 10.1186/s13075-015-0629-y

22. Teichtahl AJ, Urquhart DM, Wang Y, Wluka AE, O'Sullivan R, Jones G, et al. Lumbar disc degeneration is associated with modic change and high paraspinal fat content - a 3.0T magnetic resonance imaging study. *BMC Musculoskelet Disord* (2016) 17(1):439. doi: 10.1186/s12891-016-1297-z

23. Pfirrmann CW, Metzdorf A, Zanetti M, Hodler J, Boos N. Magnetic resonance classification of lumbar intervertebral disc degeneration. *Spine* (2001) 26(17):1873–8. doi: 10.1097/00007632-200109010-00011

24. Shi L, Yan B, Jiao Y, Chen Z, Zheng Y, Lin Y, et al. Correlation between the fatty infiltration of paraspinal muscles and disc degeneration and the underlying mechanism. *BMC Musculoskelet Disord* (2022) 23(1):509. doi: 10.1186/s12891-022-05466-8

25. Sun D, Liu P, Cheng J, Ma Z, Liu J, Qin T. Correlation between intervertebral disc degeneration, paraspinal muscle atrophy, and lumbar facet joints degeneration in patients with lumbar disc herniation. *BMC Musculoskelet Disord* (2017) 18(1):167. doi: 10.1186/s12891-017-1522-4

26. Faur C, Patrascu JM, Haragus H, Anglitoiu B. Correlation between multifidus fatty atrophy and lumbar disc degeneration in low back pain. *BMC Musculoskelet Disord* (2019) 20(1):414. doi: 10.1186/s12891-019-2786-7

27. Liu C, Xue J, Liu J, Ma G, Moro A, Liang T, et al. Is there a correlation between upper lumbar disc herniation and multifidus muscle degeneration? a retrospective study of MRI morphology. *BMC Musculoskelet Disord* (2021) 22 (1):92. doi: 10.1186/s12891-021-03970-x

28. Hodges P, Holm AK, Hansson T, Holm S. Rapid atrophy of the lumbar multifidus follows experimental disc or nerve root injury. *Spine (Phila Pa 1976)* (2006) 31(25):2926–33. doi: 10.1097/01.brs.0000248453.51165.0b

29. Goubert D, De Pauw R, Meeus M, Willems T, Cagnie B, Schouppe S, et al. Lumbar muscle structure and function in chronic versus recurrent low back pain: a cross-sectional study. *Spine J* (2017) 17(9):1285–96. doi: 10.1016/j.spinee.2017.04.025

30. Özcan-Ekşi EE, Ekşi MŞ, Turgut VU, Canbolat Ç, Pamir MN. Reciprocal relationship between multifidus and psoas at L4-L5 level in women with low back pain. *Br J Neurosurg* (2021) 35(2):220–8. doi: 10.1080/02688697.2020.1783434

31. Teichtahl AJ, Urquhart DM, Wang Y, Wluka AE, Wijethilake P, O'Sullivan R, et al. Fat infiltration of paraspinal muscles is associated with low back pain, disability, and structural abnormalities in community-based adults. *Spine J* (2015) 15(7):1593–601. doi: 10.1016/j.spinee.2015.03.039

32. Urrutia J, Besa P, Lobos D, Campos M, Arrieta C, Andia M, et al. Lumbar paraspinal muscle fat infiltration is independently associated with sex, age, and inter-vertebral disc degeneration in symptomatic patients. *Skeletal Radiol* (2018) 47 (7):955–61. doi: 10.1007/s00256-018-2880-1

33. Hides J, Gilmore C, Stanton W, Bohlscheid E. Multifidus size and symmetry among chronic LBP and healthy asymptomatic subjects. *Man Ther* (2008) 13 (1):43–9. doi: 10.1016/j.math.2006.07.017

34. Niemeläinen R, Briand MM, Battié MC. Substantial asymmetry in paraspinal muscle cross-sectional area in healthy adults questions its value as a marker of low back pain and pathology. *Spine (Phila Pa 1976)* (2011) 36(25):2152–7. doi: 10.1097/BRS.0b013e318204b05a

35. Fortin M, Lazáry À, Varga PP, McCall I, Battié MC. Paraspinal muscle asymmetry and fat infiltration in patients with symptomatic disc herniation. *Eur Spine J* (2016) 25(5):1452–9. doi: 10.1007/s00586-016-4503-7

36. Cruz-Jentoft AJ, Bahat G, Bauer J, Boirie Y, Bruyère O, Cederholm T, et al. Sarcopenia: revised European consensus on definition and diagnosis. *Age Ageing* (2019) 48(1):16–31. doi: 10.1093/ageing/afy169

37. Lee D, Kang M. Correlation between psoas muscle index and degeneration of spinal back muscle in patients with back pain. *Healthcare (Basel)* (2021) 9 (9):1189. doi: 10.3390/healthcare9091189

38. Huang Y, Wang L, Luo B, Yang K, Zeng X, Chen J, et al. Associations of lumber disc degeneration with paraspinal muscles myosteatosis in discogenic low back pain. *Front Endocrinol (Lausanne)* (2022) 13:891088. doi: 10.3389/fendo.2022.891088

39. Lerer A, Nykamp SG, Harriss AB, Gibson TW, Koch TG, Brown SH. MRI-Based relationships between spine pathology, intervertebral disc degeneration, and muscle fatty infiltration in chondrodystrophic and non-chondrodystrophic dogs. *Spine J* (2015) 15(11):2433–9. doi: 10.1016/j.spinee.2015.08.014

40. Hodges PW, James G, Blomster L, Hall L, Schmid A, Shu C, et al. Multifidus muscle changes after back injury are characterized by structural remodeling of muscle, adipose and connective tissue, but not muscle atrophy: molecular and morphological evidence. *Spine* (2015) 40(14):1057–71. doi: 10.1097/BRS.0000000000000972

41. Sasaki T, Yoshimura N, Hashizume H, Yamada H, Oka H, Matsudaira K, et al. MRI-Defined paraspinal muscle morphology in Japanese population: the wakayama spine study. *PloS One* (2017) 12(11):e0187765. doi: 10.1371/journal.pone.0187765

42. Huang Y, Wang L, Zeng X, Chen J, Zhang Z, Jiang Y, et al. Association of paraspinal muscle CSA and PDFF measurements with lumbar intervertebral disk degeneration in patients with chronic low back pain. *Front Endocrinol (Lausanne)* (2022) 13:792819. doi: 10.3389/fendo.2022.792819

43. Ekşi MŞ, Özcan-Ekşi EE, Özmen BB, Turgut VU, Huet SE, Dinç T, et al. Lumbar intervertebral disc degeneration, end-plates and paraspinal muscle changes in children and adolescents with low-back pain. *J Pediatr Orthop B* (2022) 31(1):93–102. doi: 10.1097/BPB.0000000000000833

44. Nachemson A. The possible importance of the psoas muscle for stabilization of the lumbar spine. *Acta Orthop Scand* (1968) 39(1):47–57. doi: 10.3109/17453676808989438

45. Arbanas J, Pavlovic I, Marijancic V, Vlahovic H, Starcevic-Klasan G, Peharec S, et al. MRI Features of the psoas major muscle in patients with low back pain. *Eur Spine J* (2013) 22(9):1965–71. doi: 10.1007/s00586-013-2749-x

46. Parkkola R, Rytökoski U, Kormano M. Magnetic resonance imaging of the discs and trunk muscles in patients with chronic low back pain and healthy control subjects. *Spine (Phila Pa 1976)* (1993) 18(7):830–6. doi: 10.1097/00007632-199306000-00004

47. Danneels LA, Vanderstraeten GG, Cambier DC, Witvrouw EE, De Cuyper HJ. CT imaging of trunk muscles in chronic low back pain patients and healthy control subjects. *Eur Spine J* (2000) 9(4):266–72. doi: 10.1007/s005860000190

48. Modic MT, Steinberg PM, Ross JS, Masaryk TJ, Carter JR. Degenerative disk disease: assessment of changes in vertebral body marrow with MR imaging. *Radiology* (1988) 166(1 Pt 1):193–9. doi: 10.1148/radiology.166.1.3336678

49. de Roos A, Kressel H, Spritzer C, Dalinka M. MR imaging of marrow changes adjacent to end plates in degenerative lumbar disk disease. *AJR Am J Roentgenol* (1987) 149(3):531–4. doi: 10.2214/ajr.149.3.531

50. Albert HB, Kjaer P, Jensen TS, Sorensen JS, Bendix T, Manniche C. Modic changes, possible causes and relation to low back pain. *Med Hypotheses* (2008) 70 (2):361–8. doi: 10.1016/j.mehy.2007.05.014

51. Kuisma M, Karppinen J, Niinimäki J, Ojala R, Haapea M, Heliövaara M, et al. Modic changes in endplates of lumbar vertebral bodies: prevalence and association with low back and sciatic pain among middle-aged male workers. *Spine* (2007) 32(10):1116–22. doi: 10.1097/01.brs.0000261561.12944.ff

52. Toyone T, Takahashi K, Kitahara H, Yamagata M, Murakami M, Moriya H. Vertebral bone-marrow changes in degenerative lumbar disc disease. an MRI study of 74 patients with low back pain. *J Bone Joint Surg Br* (1994) 76(5):757–64.

53. Mitra D, Cassar-Pullicino VN, McCall IW. Longitudinal study of vertebral type-1 end-plate changes on MR of the lumbar spine. *Eur Radiol* (2004) 14 (9):1574–81. doi: 10.1007/s00330-004-2314-4

54. Albert HB, Manniche C. Modic changes following lumbar disc herniation. *Eur Spine J* (2007) 16(7):977–82. doi: 10.1007/s00586-007-0336-8

55. Modic MT, Masaryk TJ, Ross JS, Carter JR. Imaging of degenerative disk disease. *Radiology* (1988) 168(1):177–86. doi: 10.1148/radiology.168.1.3289089

56. Schmid G, Witteler A, Willburger R, Kuhnen C, Jergas M, Koester O. Lumbar disk herniation: correlation of histologic findings with marrow signal intensity changes in vertebral endplates at MR imaging. *Radiology* (2004) 231 (2):352–8. doi: 10.1148/radiol.2312021708

57. Karchevsky M, Schweitzer ME, Carrino JA, Zoga A, Montgomery D, Parker L. Reactive endplate marrow changes: a systematic morphologic and epidemiologic evaluation. *Skeletal Radiol* (2005) 34(3):125–9. doi: 10.1007/s00256-004-0886-3

58. Weishaupt D, Zanetti M, Hodler J, Boos N. MR imaging of the lumbar spine: prevalence of intervertebral disk extrusion and sequestration, nerve root compression, end plate abnormalities, and osteoarthritis of the facet joints in asymptomatic volunteers. *Radiology* (1998) 209(3):661–6. doi: 10.1148/radiology.209.3.9844656

59. Kjaer P, Korsholm L, Bendix T, Sorensen JS, Leboeuf-Yde C. Modic changes and their associations with clinical findings. *Eur Spine J* (2006) 15(9):1312–9. doi: 10.1007/s00586-006-0185-x

60. Tarukado K, Ono T, Tono O, Tanaka H, Ikuta K, Harimaya K, et al. Does modic change progresss with age? *Spine* (2017) 42(23):1805–9. doi: 10.1097/BRS.0000000000002254

61. Mok FP, Samartzis D, Karppinen J, Fong DY, Luk KD, Cheung KM. Modic changes of the lumbar spine: prevalence, risk factors, and association with disc degeneration and low back pain in a large-scale population-based cohort. *Spine J* (2016) 16(1):32–41. doi: 10.1016/j.spinee.2015.09.060

62. Atci IB, Yilmaz H, Samanci MY, Atci AG, Karagoz Y. The prevalence of lumbar paraspinal muscle fatty degeneration in patients with modic type I and I/II end plate changes. *Asian Spine J* (2020) 14(2):185–91. doi: 10.31616/asj.2018.0333

63. Smith LJ, Nerurkar NL, Choi KS, Harfe BD, Elliott DM. Degeneration and regeneration of the intervertebral disc: lessons from development. *Dis Model Mech* (2011) 4(1):31–41. doi: 10.1242/dmm.006403

64. MacDonald D, Moseley GL, Hodges PW. People with recurrent low back pain respond differently to trunk loading despite remission from symptoms. *Spine* (2010) 35(7):818–24. doi: 10.1097/BRS.0b013e3181bc98f1

65. Macdonald DA, Dawson AP, Hodges PW. Behavior of the lumbar multifidus during lower extremity movements in people with recurrent low back pain during symptom remission. *J Orthop Sports Phys Ther* (2011) 41(3):155–64. doi: 10.2519/jospt.2011.3410

66. Pagano AF, Brioche T, Arc-Chagnaud C, Demangel R, Chopard A, Py G. Short-term disuse promotes fatty acid infiltration into skeletal muscle. *J Cachexia Sarcopenia Muscle* (2018) 9(2):335–47. doi: 10.1002/jcsm.12259

67. James G, Sluka KA, Blomster L, Hall L, Schmid AB, Shu CC, et al. Macrophage polarization contributes to local inflammation and structural change in the multifidus muscle after intervertebral disc injury. *Eur Spine J* (2018) 27(8):1744–56. doi: 10.1007/s00586-018-5652-7

68. Ray L, Lipton RB, Zimmerman ME, Katz MJ, Derby CA. Mechanisms of association between obesity and chronic pain in the elderly. *Pain* (2011) 152(1):53–9. doi: 10.1016/j.pain.2010.08.043

69. Ekşi MŞ, Kara M, Özcan-Ekşi EE, Aytar MH, Güngör A, Özgen S, et al. Is diabetes mellitus a risk factor for modic changes?: a novel model to understand the association between intervertebral disc degeneration and end-plate changes. *J Orthop Sci* (2020) 25(4):571–5. doi: 10.1016/j.jos.2019.09.005

70. Furukawa S, Fujita T, Shimabukuro M, Iwaki M, Yamada Y, Nakajima Y, et al. Increased oxidative stress in obesity and its impact on metabolic syndrome. *J Clin Invest* (2004) 114(12):1752–61. doi: 10.1172/JCI21625

71. Xiao L, Aoshima H, Saitoh Y, Miwa N. The effect of squalane-dissolved fullerene-C60 on adipogenesis-accompanied oxidative stress and macrophage activation in a preadipocyte-monocyte co-culture system. *Biomaterials* (2010) 31 (23):5976–85. doi: 10.1016/j.biomaterials.2010.04.032

72. James G, Chen X, Diwan A, Hodges PW. Fat infiltration in the multifidus muscle is related to inflammatory cytokine expression in the muscle and epidural adipose tissue in individuals undergoing surgery for intervertebral disc herniation. *Eur Spine J* (2021) 30(4):837–45. doi: 10.1007/s00586-020-06514-4

73. Wang Y, Che M, Xin J, Zheng Z, Li J, Zhang S. The role of IL-1β and TNF-α in intervertebral disc degeneration. *BioMed Pharmacother* (2020) 131:110660. doi: 10.1016/j.biopha.2020.110660

74. Shahidi B, Hubbard JC, Gibbons MC, Ruoss S, Zlomislic V, Allen RT, et al. Lumbar multifidus muscle degenerates in individuals with chronic degenerative lumbar spine pathology. *J Orthop Res* (2017) 35(12):2700–6. doi: 10.1002/jor.23597

75. Goode A, Cook C, Brown C, Isaacs R, Roman M, Richardson W. Differences in comorbidities on low back pain and low back related leg pain. *Pain Pract* (2011) 11(1):42–7. doi: 10.1111/j.1533-2500.2010.00391.x

76. Özcan-Ekşi EE, Turgut VU, Küçüksüleymanoğlu D, Ekşi MŞ. Obesity could be associated with poor paraspinal muscle quality at upper lumbar levels and degenerated spine at lower lumbar levels: Is this a domino effect? *J Clin Neurosci* (2021) 94:120–7 doi: 10.1016/j.jocn.2021.10.005

77. Özcan-Ekşi EE, Kara M, Berikol G, Orhun Ö, Turgut VU, Ekşi MŞ. A new radiological index for the assessment of higher body fat status and lumbar spine degeneration. *Skeletal Radiol* (2022) 51(6):1261–71 doi: 10.1007/s00256-021-03957-8

78. Berikol G, Ekşi MŞ, Aydın L, Börekci A, Özcan-Ekşi EE. Subcutaneous fat index: a reliable tool for lumbar spine studies. *Eur Radiol* (2022) 32(9):6504–13. doi: 10.1007/s00330-022-08775-7

79. D'Erminio DN, Krishnamoorthy D, Lai A, Hoy RC, Natelson DM, Poeran J, et al. High fat diet causes inferior vertebral structure and function without disc degeneration in RAGE-KO mice. *J Orthop Res* (2022) 40(7):1672–86. doi: 10.1002/jor.25191

80. Illien-Jünger S, Palacio-Mancheno P, Kindschuh WF, Chen X, Sroga GE, Vashishth D, et al. Dietary advanced glycation end products have sex- and age-dependent effects on vertebral bone microstructure and mechanical function in mice. *J Bone Miner Res* (2018) 33(3):437–48. doi: 10.1002/jbmr.3321

81. Fields AJ, Berg-Johansen B, Metz LN, Miller S, La B, Liebenberg EC, et al. Alterations in intervertebral disc composition, matrix homeostasis and biomechanical behavior in the UCD-T2DM rat model of type 2 diabetes. *J Orthop Res* (2015) 33(5):738–46. doi: 10.1002/jor.22807

82. Zhang X, Chen J, Huang B, Wang J, Shan Z, Liu J, et al. Obesity mediates apoptosis and extracellular matrix metabolic imbalances *via* MAPK pathway activation in intervertebral disk degeneration. *Front Physiol* (2019) 10:1284. doi: 10.3389/fphys.2019.01284

83. Krug R, Joseph GB, Han M, Fields A, Cheung J, Mundada M, et al. Associations between vertebral body fat fraction and intervertebral disc biochemical composition as assessed by quantitative MRI. *J Magn Reson Imaging* (2019) 50(4):1219–26. doi: 10.1002/jmri.26675

84. Ji Y, Hong W, Liu M, Liang Y, Deng Y, Ma L. Intervertebral disc degeneration associated with vertebral marrow fat, assessed using quantitative magnetic resonance imaging. *Skeletal Radiol* (2020) 49(11):1753–63. doi: 10.1007/s00256-020-03419-7

85. Urban JP, Smith S, Fairbank JC. Nutrition of the intervertebral disc. *Spine* (2004) 29(23):2700–9. doi: 10.1097/01.brs.0000146499.97948.52

86. Castaño-Betancourt MC, Oei L, Rivadeneira F, de Schepper EI, Hofman A, Bierma-Zeinstra S, et al. Association of lumbar disc degeneration with osteoporotic fractures; the Rotterdam study and meta-analysis from systematic review. *Bone* (2013) 57(1):284–9. doi: 10.1016/j.bone.2013.08.004

87. Fabreguet I, Fechtenbaum J, Briot K, Paternotte S, Roux C. Lumbar disc degeneration in osteoporotic men: prevalence and assessment of the relation with presence of vertebral fracture. *J Rheumatol* (2013) 40(7):1183–90. doi: 10.3899/jrheum.120769

88. Wang GJ, Sweet DE, Reger SI, Thompson RC. Fat-cell changes as a mechanism of avascular necrosis of the femoral head in cortisone-treated rabbits. *J Bone Joint Surg Am* (1977) 59(6):729–35. doi: 10.2106/00004623-197759060-00003

89. de Boer TN, van Spil WE, Huisman AM, Polak AA, Bijlsma JW, Lafeber FP, et al. Serum adipokines in osteoarthritis; comparison with controls and relationship with local parameters of synovial inflammation and cartilage damage. *Osteoarthritis Cartilage* (2012) 20(8):846–53. doi: 10.1016/j.joca.2012.05.002

90. La Cava A. Leptin in inflammation and autoimmunity. *Cytokine* (2017) 98:51–8. doi: 10.1016/j.cyto.2016.10.011

91. Skurk T, Alberti-Huber C, Herder C, Hauner H. Relationship between adipocyte size and adipokine expression and secretion. *J Clin Endocrinol Metab* (2007) 92(3):1023–33. doi: 10.1210/jc.2006-1055

92. Segar AH, Fairbank JCT, Urban J. Leptin and the intervertebral disc: a biochemical link exists between obesity, intervertebral disc degeneration and low back pain-an *in vitro* study in a bovine model. *Eur Spine J* (2019) 28(2):214–23. doi: 10.1007/s00586-018-5778-7

93. Han YC, Ma B, Guo S, Yang M, Li LJ, Wang SJ, et al. Leptin regulates disc cartilage endplate degeneration and ossification through activation of the MAPK-ERK signalling pathway in vivo and in vitro. *J Cell Mol Med* (2018) 22(4):2098–109. doi: 10.1111/jcmm.13398

94. Yuan B, Huang L, Yan M, Zhang S, Zhang Y, Jin B, et al. Adiponectin downregulates TNF-α expression in degenerated intervertebral discs. *Spine* (2018) 43(7):E381–9. doi: 10.1097/BRS.0000000000002364

95. Terashima Y, Kakutani K, Yurube T, Takada T, Maeno K, Hirata H, et al. Expression of adiponectin receptors in human and rat intervertebral disc cells and changes in receptor expression during disc degeneration using a rat tail temporary static compression model. *J Orthop Surg Res* (2016) 11(1):147. doi: 10.1186/s13018-016-0481-z

96. Jamaluddin MS, Weakley SM, Yao Q, Chen C. Resistin: functional roles and therapeutic considerations for cardiovascular disease. *Br J Pharmacol* (2012) 165 (3):622–32. doi: 10.1111/j.1476-5381.2011.01369.x

97. Fang WQ, Zhang Q, Peng YB, Chen M, Lin XP, Wu JH, et al. Resistin level is positively correlated with thrombotic complications in southern Chinese metabolic syndrome patients. *J Endocrinol Invest* (2011) 34(2):e36–42. doi: 10.1007/BF03347059

98. Li Z, Wang X, Pan H, Yang H, Li X, Zhang K, et al. Resistin promotes CCL4 expression through toll-like receptor-4 and activation of the p38-MAPK and NF-κB signaling pathways: implications for intervertebral disc degeneration. *Osteoarthritis Cartilage* (2017) 25(2):341–50. doi: 10.1016/j.joca.2016.10.002

99. Liu C, Yang H, Gao F, Li X, An Y, Wang J, et al. Resistin promotes intervertebral disc degeneration by upregulation of ADAMTS-5 through p38 MAPK signaling pathway. *Spine* (2016) 41(18):1414–20. doi: 10.1097/BRS.0000000000001556

100. Shi C, Wu H, Du D, Im HJ, Zhang Y, Hu B, et al. Nicotinamide phosphoribosyltransferase inhibitor APO866 prevents IL-1β-induced human nucleus pulposus cell degeneration *via* autophagy. *Cell Physiol Biochem* (2018) 49(6):2463–82. doi: 10.1159/000493843

101. Cui H, Du X, Liu C, Chen S, Cui H, Liu H, et al. Visfatin promotes intervertebral disc degeneration by inducing IL-6 expression through the ERK/JNK/p38 signalling pathways. *Adipocyte* (2021) 10(1):201–15. doi: 10.1080/21623945.2021.1910155

frontiers | Frontiers in Endocrinology

TYPE Systematic Review
PUBLISHED 07 December 2022
DOI 10.3389/fendo.2022.1038973

OPEN ACCESS

EDITED BY
Meifeng Zhu,
Nankai University, China

REVIEWED BY
Tianyuan Yu,
Beijing University of Chinese Medicine, China
Elena Amaricai,
Boston Children's Hospital, Harvard Medical School, United States

*CORRESPONDENCE
Min Fang
fm-tn0510@shutcm.edu.cn

†These authors have contributed equally to this work and share first authorship

SPECIALTY SECTION
This article was submitted to Bone Research, a section of the journal Frontiers in Endocrinology

RECEIVED 08 September 2022
ACCEPTED 21 November 2022
PUBLISHED 07 December 2022

CITATION
Ren J, Kong L, Wu Z, Zhou X, Huang Q, He T and Fang M (2022) Benefits on pain and mental health of manual therapy for idiopathic scoliosis: A meta-analysis. *Front. Endocrinol.* 13:1038973. doi: 10.3389/fendo.2022.1038973

Benefits on pain and mental health of manual therapy for idiopathic scoliosis: A meta-analysis

Jun Ren[1†], Lingjun Kong[1,2†], Zhiwei Wu[1,2†], Xin Zhou[1,2], Qian Huang[3], Tianxiang He[1] and Min Fang[1,2,4*]

[1]Yueyang Hospital of Integrated Traditional Chinese and Western Medicine, Shanghai University of Traditional Chinese Medicine, Shanghai, China, [2]Institute of Tuina, Shanghai Institute of Traditional Chinese Medicine, Shanghai, China, [3]Department of Acupuncture and Tuina, Lianyungang Traditional Chinese Medicine Hospital Affiliated to Nanjing University of Chinese Medicine, Lianyungang, China, [4]Shuguang Hospital, Shanghai University of Traditional Chinese Medicine, Shanghai, China

Background: Idiopathic scoliosis (IS) is a common spinal disorder. Although several studies have reported the benefits of manual therapy for patients with IS in improving pain, anxiety, depression, and spinal disorders, the efficacy of manual therapy in the management of IS remain controversial. Therefore, this review was conducted to assess effects of manual therapy in the management of IS, primarily on pain and mental health of the patients and secondarily on their spinal disorders.

Methods: Six electronic databases were searched for randomized controlled trials of manual therapy in the management of IS. The methodological quality of the included studies was assessed using the Physiotherapy Evidence Database (PEDro) Scale. The meta-analysis was conducted depending on different outcomes and control therapies using Review Manager version 5.3 software.

Results: Seventeen studies were included in the present review. The PEDro scores of the included studies ranged from 5-7 points. The aggregated results indicated that Tuina (a traditional Chinese manipulation technique) had valuable improvement effects on pain (standardized mean difference (SMD), 0.92; 95% confidence interval (CI), 0.59 to 1.25; $P<0.00001$), negative emotions (SMD, 0.82; 95% CI, 0.51 to 1.13; $P<0.00001$), and disability (SMD, 1.29; 95% CI, 0.39 to 2.19; $P=0.005$). For the radiographic outcomes including the Cobb angle and vertebral rotation, Tuina, especially when combined with other conservative therapies, showed potential complementary effects for patients with IS.

Conclusions: Tuina, as a complementary and alternative therapy, should be considered for the effective management of patients with IS, especially for the improvement of their pain and mental health. More randomized controlled trials are recommended to validate the current evidence.

10.3389/fendo.2022.1038973

Systematic review registration: https://www.crd.york.ac.uk/prospero/, identifier CRD42020165220.

KEYWORDS

manual therapy, idiopathic scoliosis, complementary and alternative therapy, mental health, pain

Introduction

Idiopathic scoliosis (IS), a common spinal disorder with at least a 10° lateral curve of the spine, affects approximately 2-3% of adolescents worldwide (1, 2). In China, the prevalence of IS is as high as 5.1% among more than 200 thousand adolescent students (3). Patients with IS suffer from muscle pain, depression, anxiety, functional impairments, and poor quality of life (2, 4). Therefore, patients with IS and their families usually bear substantial socioeconomic burden and distress owing to the spinal deformities and their accompanying comorbidities (5).

The management options for IS include surgery and complementary and alternative therapies, including bracing, scoliosis-specific exercises, and manual therapy (4). Most patients with mild to moderate IS (Cobb < 40°) prefer complementary and alternative therapies to prevent and treat scoliosis, especially to improve pain and mental health. These physical and mental abnormalities are usually the main clinical symptoms in patients with mild to moderate IS. Having a good physical and mental health is essential for fulfilling lives, realizing one's full potential, and contributing to the society. The International Society on Scoliosis Orthopaedic and Rehabilitation Treatment (SOSORT) also recommends complementary and alternative therapies to improve back pain, negative emotions, quality of life, and disability (2).

Manual therapy, as a complementary and alternative therapy for IS, is a skilled hand manipulative technique, including massage, chiropractic, osteopathy, and Tuina (traditional Chinese manipulation). It is comprised of soft-tissue manipulations (such as massage) and joint manipulations. Soft-tissue manipulations could restore the range of spinal motion by relieving muscle spasm (6). Joint manipulations (such as chiropractic) involve a manual procedure directed thrust to move a joint past the physiological range of motion, without exceeding the anatomical limit, which could improve stiffness of the spinal joints by adjusting the stress of intervertebral joints surface (7). Manual therapy could intervene the transcription and translation of inflammation-related genes through miRNAs to improve neuroinflammation and alleviate neuropathic pain (8). Although several trials have reported that manual therapy had benefits in improving negative emotions and spinal pain in patients with IS, the efficacy of manual therapy in the management of IS remains controversial (9, 10). In the previous review (11), there was no data synthesis in the meta-analysis due to the small number of eligible studies (12–14). Therefore, there is no positive recommendation for manual therapy in the treatment of IS in the SOSORT guidelines due to the lack of evidence-based results (2). In recent years, however, some randomized controlled trials (RCTs) were conducted to assess the efficacy of manual therapy in the treatment of IS (15–18). Particularly in China, Tuina is used in the management of IS by practitioners. Tuina comprise soft-tissue manipulations and joint manipulations. Compared to its role in correcting spinal abnormalities, it showed better potential effects in improving the pain and mental health of patients with IS.

Consequently, the current systematic review was conducted to examine the benefits of manual therapy in the treatment of IS. The Scoliosis Research Society (SRS) and SOSORT recommended that complementary and alternative therapies should focus primarily on the pain and mental health, and secondarily on spinal disorders (such as Cobb angle and vertebral rotation) in patients with IS (19). Therefore, the systematic review and meta-analysis was performed to evaluate the benefits of manual therapy in the management of IS, primarily in improving pain and mental health and secondarily in improving the spinal disorders.

Methods

Search strategy

A computerized literature search was conducted using the following electronic databases from their inceptions to January 2022: PubMed, Cochrane Library, EMBASE, CNKI, Weipu Database, and Wanfang Data. The key terms were scoliosis,

manual therapy, chiropractic, massage, mobilization, osteopathy, myofascial release, spinal manipulation, Tuina, and shiatsu. Additionally, a manual search was conducted at the library of the Shanghai University of Traditional Chinese Medicine. Literatures were also obtained from the reference lists of related reviews. No restrictions were conducted for the language or publication status.

Study selection

The criteria of the eligible studies were: (1) study design: RCTs as study design, (2) participants diagnosed with IS without any limitations on their gender or nationality, (3) intervention is manual therapy, such as Tuina, massage, chiropractic, mobilization, myofascial release, and shiatsu. The control interventions were any treatments without manual therapy, (4) outcomes are pain evaluated by any valid scale including visual analogue scale (VAS), mental health evaluated by any valid scale including self-rating depression scale (SDS) and self-rating anxiety scale (SAS), disability evaluated by any valid scale including oswestry disability index (ODI), and quality of life evaluated by any valid scale including scoliosis research society-22 (SRS-22), and spinal disorders (Cobb angle and vertebral rotation). Two reviewers independently selected studies. In case of persistent disagreement, a third reviewer will adjudicate and resolve the conflict.

Studies that included scoliosis patients undergoing combined orthopedic surgery were excluded. Likewise, studies involving IS patients with congenital spinal deformities or secondary to spinal organic diseases such as tumor, trauma, tuberculosis and other causes were also excluded.

Data extraction

Data were independently extracted by two reviewers. The extracted information included the basic study information (first author, year, and country), participant information (sample size, mean age, Cobb angle, and main curve location), main outcomes, and intervention information. If disagreements persist, consensus will be adjudicated by the third reviewer.

Quality assessment

Quality assessment of the included studies was conducted independently by the two reviewers using the Physiotherapy Evidence Database (PEDro) scale, which is an available evaluation method for methodological quality of randomized trials of physiotherapy interventions (20, 21). The PEDro scale contains the assessment of criteria regarding eligibility, randomised allocation of participants, concealed allocation, comparison of baselines, blinding (subjects, therapists, assessors), adequate follow-up, intention-to-treat, between-group comparisons, and point estimates and variability data. By scoring each of the last ten criteria, the quality of a paper ranges from low (0 point) to high (10 points), and the cut-off value for high-quality RCTs (6 points). In case of persistent disagreement, a third reviewer will adjudicate and resolve the conflict.

Data synthesis and analysis

For the continuous data, standardized mean difference (SMD) and 95% confidence interval (CI) were used to conduct a meta-analysis using Review Manager version 5.3 software (the Cochrane Collaboration, Oxford, UK). We used a random-effects model for the better heterogeneity in the meta-analysis. The heterogeneity was assessed using the Cochran Q statistic (P value < 0.05 was considered statistically significant) and I^2 (I^2> 75% considerable heterogeneity). Sensitivity analyses were also performed to investigate the impact of individual studies on heterogeneity measures. Subgroup analyses were performed depending on outcomes and control interventions. A comparison adjustment funnel plot was used to test the publication bias, when the number of studies included was larger than 10.

Results

Search and selection

A literature search identified 1716 records. 866 potential studies were found after removing the duplications. After screening titles and abstracts, 810 studies were excluded, and the remaining 56 full texts were screened for inclusion. After detailed full-text screening, 39 studies were excluded. Finally, 17 RCTs were included in the current review (15–18, 22–34). The detailed process of search and selection is presented in Figure 1.

Characteristics of the included studies

Seventeen included studies conducted between 2003 and 2019 in China, USA, and Switzerland, which included a total of 956 participants with the mean Cobb angle 24.47° ± 5.26°. Manual therapy included Tuina, chiropractic, and osteopathic interventions. Ten studies used only manual therapy (Tuina or osteopathic) in the management of IS (15, 16, 18, 22, 26, 27, 31–34). Other studies combined manual therapy and other conservative interventions including bracing, exercise, traction, transcutaneous electrical stimulation, and medication. The control interventions included sham treatment, observation,

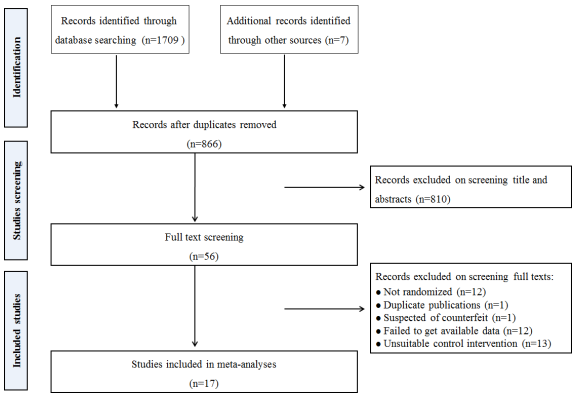

FIGURE 1
Study selection process.

bracing, traction, electroacupuncture, exercise and medication. The duration of the manual therapy ranged from 3-96 weeks. The time of each intervention ranged from 10-45 min. Two studies assessed the long-term effects of manual therapy for IS after the 3 (26) and 12 months (29). The characteristics of the included studies are summarized in Table 1.

Methodological quality

Most studies (88%) of manual therapy for IS, ranging from 5-7 on the PEDro scores, were rated as high quality with the exceeded cut-off PEDro score of 6. The most obvious bias was related to blinding and concealed allocations. Only one study performed concealed allocation (15), and two studies employed blinded assessors (15, 24). Furthermore, an intention-to-treat analysis was not used in three included studies (15, 33, 34). The other items in the included studies were scored as positive. Detailed scores are listed in Table 2.

The effects on patient-centered outcomes

Pain

The aggregated results of three studies reported the beneficial effects of Tuina in relieving pain (SMD, 0.92; 95% CI, 0.59 to 1.25; P < 0.00001; Figure 2) with low heterogeneity (Q=1.17, I^2 = 0%; P=0.56) in patients with IS in comparison with those of medicines, including celecoxib and eperisone (28, 30, 32). Two studies assessed the effects of Tuina in relieving pain in comparison with those of braces (26, 33). However, the aggregated results failed to show that Tuina was more effective than braces in relieving pain (SMD, 1.01; 95% CI, -0.45 to 2.47; P = 0.17; Figure 2) with high heterogeneity (Q=12.70, I^2 = 92%; P=0.0004).

Mental health

Two studies reported the effect of Tuina on depression or anxiety of patients with IS (26, 34). The aggregated result indicated that Tuina showed better effects in alleviating negative emotions including depression and anxiety (SMD, 0.82; 95% CI, 0.51 to 1.13; P<0.00001, Figure 3) with low heterogeneity (Q=2.13, I^2 = 6%; P=0.34) compared with brace.

Disability

Three studies reported the effect of Tuina in improving lumbar disability of patients with IS using the Oswestry disability index (28, 30, 32). The results of meta-analysis indicated that Tuina had beneficial effects in improving the disability (SMD, 1.29; 95% CI, 0.39 to 2.19; P=0.005, Figure 4) with high heterogeneity (Q=12.64, I^2 = 84%; P=0.002) compared with medicine. In sensitivity analysis, exclusion of sun 2016 from the meta-analysis resulted in a bigger SMD of 1.68 (95% CI 1.13 to 2.24) and reduced heterogeneity (Q=1.34, I^2 = 25%, P=0.25).

Quality of life

In the included studies, only one reported the effect on quality of life of Tuina plus bracing for IS patients compared with bracing alone (26). The result showed that Tuina plus bracing have more benefits on domains of function/activity and pain of SRS-22 compared with bracing alone.

The effects on radiographic outcomes

Cobb angles

Two studies reported the effects of Tuina in comparison with those of medicine in the management of Cobb angles in patients with IS (28, 32). The results of meta-analysis indicated that Tuina had better benefits than medicine in Cobb angles (SMD, 0.41; 95% CI, 0.01 to 0.82; P=0.04, Figure 5) with low heterogeneity (Q=0.16, I^2 = 0%; P=0.69). However, five trials assessed the effect of Tuina compared with bracing (16, 23, 31, 33, 34). The aggregated result of the meta-analysis did not support better improvements of Tuina than bracing (SMD, 0.68; 95% CI, -0.09 to 1.45; P=0.08, Figure 5) with high heterogeneity (Q=44.68, I^2 = 91%; P<0.0001). The exclusion of included studies from the analysis had minimal impact on the total estimate or on heterogeneity measures by sensitivity analysis. Wang et al. reported that Tuina had better benefits in Cobb angle of patients with IS compared with traction (27).

To achieve better efficacy, patients with IS usually prefer to combine manual therapy with other conservative therapies. In

10.3389/fendo.2022.1038973

TABLE 1 Randomized controlled trials of manual therapy for idiopathic scoliosis.

Study	Sample size	Mean age (year)	Cobbdegrees	Follow-up	Curve location*	Main outcomes	TCMintervention	Control group intervention
Liu,2003,China (22)	11 11 13 10	9-16	27.50±6.15 26.45±6.35 26.08±4.91 25.63±4.79	—	NR	Cobb, AVR	Tuina (120 sessions, 240 days)	Electroacupuncture (20 min, 120 sessions, 240 days) Tuinn plus electroacupuncture Observation
Quan,2006,China (23)	32 32	11.98±1.92 11.87±2.02	20.00±7.91 20.13±8.04	—	8,20,4 7,22,3	Cobb	Tuina (25 min, 24 sessions, 12 weeks) plus traction (15 min, 84 sessions, 12 weeks)	Brace (Boston) (22h/day, 12 weeks) plus traction (15 min, 84 sessions, 12 weeks)
Rowe,2006,USA (24)	2 3 1	14.50 13 16	21.50 29 18	—	0,1,1 2,1,0 0,0,1	Cobb, QOF	Chiropractic (32 sessions, 24 weeks) plus observation/brace	Observation/brace Sham chiropractic (32 sessions, 24 weeks) plus observation /brace
Hasler, 2010, Switzerland(15)	10 10	16.50 14.70	27.10 31.50	—	5,4,1 4,2,4	Spine flexibility, Trunk morphology	Osteopathic (3 sessions, 5 weeks)	Observation
Wan,2011,China (25)	20 20	14±3	28±11 27±10	—	NR	Cobb	Tuina (30 min/day, 12 weeks) plus traction (30 min/day, 12 weeks) and transcutaneous electrical stimulation and exercise	Traction (30 min/day, 12 weeks) plus transcutaneous electrical stimulation and exercise
Zhang,2011, China(26)	20 20	12.80±1.58 12.67±1.67	30.97±5.00 29.56±5.78	3 months	NR	Cobb, SRS-22, AVR	Tuina (30-45 min, 45 sessions, 12 weeks) plus brace (8 h/day, 12 weeks)	Brace (8 h/day, 12 weeks)
Wang,2014,China (27)	50 50	10~20	10~40	—	NR	Cobb	Tuina (35 sessions, 5 weeks)	Traction (20 min /35 sessions, 5 weeks)
Tian,2015,China (28)	20 18	66.63±7.73 63.51±6.61	17.87±6.23 18.01±5.67	—	NR	Cobb, VAS, ODI	Tuina (30 min, 36 sessions)	Celecoxib (200 mg/bid, 36 days) plus eperisone (50 mg/tid, 36 days)
Yang,2015,China (18)	42 42	11-23 11-22	32.20 31.80	—	NR	Cobb	Tuina (6 weeks)	Brace (23 h/day, 6 weeks) plus exercise (30-60 min/day, 6 weeks)
Lin,2016,China (29)	21 20	12.80±2.10 12.30±2.50	28.30±3.60 27.80±3.80	12 months	NR	Cobb	Tuina (12 sessions, 12 weeks) plus exercise (20-30 min, 6 sessions, 12 weeks)	Exercise (20-30 min, 6 sessions, 12 weeks)
Sun,2016,China (30)	30 30	61.80±6.90 63.60±4.80	18.10±6.40 18.90±5.80	—	NR	Cobb, VAS, ODI	Tuina (30 min, 10 sessions, 3 weeks) plus eperisone (50 mg/tid, 3 weeks)	Eperisone (50 mg/tid, 3 weeks)
Huang,2017, China(31)	20 20	9-15	20.54±5.21 21.51±5.09	—	NR	Cobb	Tuina (20 sessions, 20 days)	Brace (22 h/day, 20 days)
Zhao,2017,China (32)	30 30	64.80±4.90 63.70±4.60	16.83±4.26 16.54±4.32	—	NR	Cobb, VAS, ODI	Tuina (30 min/day, 36 days)	Celecoxib (200 mg/time, 2 time/day, 36 days) plus eperisone

(Continued)

TABLE 1 Continued

Study	Sample size	Mean age (year)	Cobbdegrees	Follow-up	Curve location*	Main outcomes	TCMintervention	Control group intervention
								(50 mg/time, 3 time/day, 36 days)
Chen,2018,China (33)	41 41	NR	29.35±5.23 28.32±6.02	—	NR	Cobb, VAS	Tuina (24 weeks)	Brace (Cheneau) (24 weeks)
Li,2018,China (34)	40 40	11.68±1.69 12.23±2.07	21.85±2.97 22.53±3.19	—	NR	Cobb, EMG, SDS, SAS	Tuina (10-15 min/session, 90 sessions, 96 weeks)	Brace (Milwaukee) (22 h/day, 96 weeks)
Luo,2018,China (17)	37 39	12.68±1.53 12.18±1.59	18.43±6.50 20.87±9.69	—	NR	Cobb	Tuina (30 min, 36 sessions, 12 weeks) plus exercise (36 sessions, 12 weeks)	Exercise (36 sessions, 12 weeks)
Li,2019,China (16)	40 40	11.27±3.02	32.75±8.49 31.75±7.87	—	21,36,23	Cobb, Vertebral rotation	Tuina (8 sessions, 4 weeks)	Brace (23 h/day, 4 weeks) plus exercise (30-60 min/day, 4 weeks)

*Main curve location: participants with thoracic curve, thoracolumbar curve, and lumbar curve.
QOF, Quality of life; VAS, Visual analogue scale; NR, Not reported; SDS=Self-rating depression scale; SAS, Self-rating anxiety scale; ODI, Oswestry disability index; SRS-22, Scoliosis research society-22; AVR, apical vertebral rotation.

the included studies, the combination therapies included Tuina plus exercises, medicine, bracing, traction and transcutaneous electrical stimulation, and chiropractic plus observation/brace. The aggregated results indicated that Tuina plus other conservative therapies showed better complementary effects in improving the Cobb angles in patients with IS (SMD, 0.28; 95% CI, 0.03 to 0.52; P=0.03, Figure 6) (17, 25, 26, 29, 30) with low heterogeneity (Q=3.90, I^2 = 0%; P=0.42). Rowe et al. reported no difference in the Cobb angles between patients tread with chiropractic plus bracing/observation, bracing/observation, and sham chiropractic, but this pilot study confirmed the strength of the existing protocols with amendments for use in a full RCT (24).

Vertebral rotation

Three trials assessed the effects of Tuina on vertebral rotation in patients with IS (16, 22, 26). The aggregated results supported that Tuina showed more benefits in improving vertebral rotation (SMD, 0.45; 95% CI, 0.11 to 0.78; P=0.008, Figure 7) with low heterogeneity (Q=1.66, I^2 = 0%; P=0.44). However, Hasler et al. reported that osteopathic treatment did not show better therapeutic effects on rib hump, plumb line, and sagittal profile of the spine than those by observation (15).

The follow-up effects

Zhang et al. reported that manual therapy plus the brace showed better improvements in vertebral rotation, pain, and negative emotions than those by bracing alone, but no significant difference in Cobb angles was observed after 3 months of follow-up (26). Lin et al. reported that, after 12 months of follow-up, manual therapy plus exercise showed a better decreasing trend in the Cobb angles than that by exercise alone (29).

Publication bias

The risk of publication bias was not assessed, because fewer than 10 studies were included in the meta-analysis. It means that the test power is too low to distinguish chance from real asymmetry (35).

Discussion

To the best of our knowledge, the current study is the first systematic review with data synthesis of RCTs on manual therapy for IS. Subgroup analyses were conducted based on the different outcomes and control interventions. In terms of the patient-centered outcomes of the patients with IS, the current systematic review demonstrated that Tuina has valuable benefits in relieving pain, alleviating negative emotions, and improving lumbar disability. In the management of the Cobb angles, Tuina only showed better improvements than those by medicine, but Tuina plus other conservative therapies showed better effects in improving the Cobb angles in patients with IS than those by the conservative treatments alone. Tuina also has beneficial complementary effects on vertebral rotation in patients with IS. However, there is little evidence regarding follow-up effects of manual therapy for patients with IS.

TABLE 2 PEDro scale of quality for the included trials.

Study	Eligibility criteria	Random allocation	Concealed allocation	Similar at baseline	Subjects blinded	Therapists blinded	Assessors blinded	<15% dropouts	Intention-to-treat analysis	Between-group comparisons	Point measures and variability data	Total
Liu,2003 (22)	1	1	0	1	0	0	0	1	1	1	1	6
Quan,2006 (23)	1	1	0	1	0	0	0	1	1	1	1	6
Rowe,2006 (24)	1	1	0	0	0	0	1	1	1	1	1	6
Hasler, 2010 (15)	1	1	1	1	0	0	1	1	0	1	1	7
Wan,2011 (25)	1	1	0	1	0	0	0	1	1	1	1	6
Zhang, 2011 (26)	1	1	0	1	0	0	0	1	1	1	1	6
Wang,2014 (27)	1	1	0	1	0	0	0	1	1	1	1	6
Tian,2015 (28)	1	1	0	1	0	0	0	1	1	1	1	6
Yang,2015 (18)	1	1	0	1	0	0	0	1	1	1	1	6
Lin,2016 (29)	1	1	0	1	0	0	0	1	1	1	1	6
Sun,2016 (30)	1	1	0	1	0	0	0	1	1	1	1	6
Huang, 2017 (31)	1	1	0	1	0	0	0	1	1	1	1	6
Zhao,2017 (32)	1	1	0	1	0	0	0	1	1	1	1	6
Chen,2018 (33)	1	1	0	0	0	0	0	1	0	1	1	5
Li,2018 (34)	1	1	0	1	0	0	0	1	0	1	1	5
Luo, 2018 (17)	1	1	0	1	0	0	0	1	1	1	1	6
Li, 2019 (16)	1	1	0	1	0	0	0	1	1	1	1	6

Criteria (2–11) were used to calculate the total PEDro score. Each criterion was scored as either 1 or 0 according to whether the criteria was met or not, respectively.

10.3389/fendo.2022.1038973

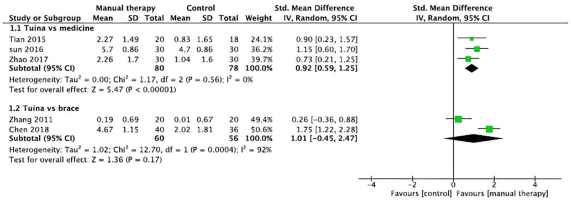

FIGURE 2
Forest plot of the effect of manual therapy for idiopathic scoliosis in pain.

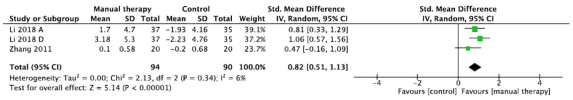

FIGURE 3
Forest plot of the effect of manual therapy for idiopathic scoliosis in mental health.

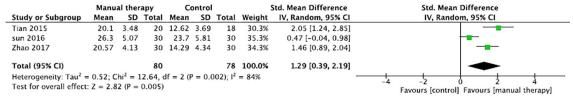

FIGURE 4
Forest plot of the effect of manual therapy for idiopathic scoliosis in disability.

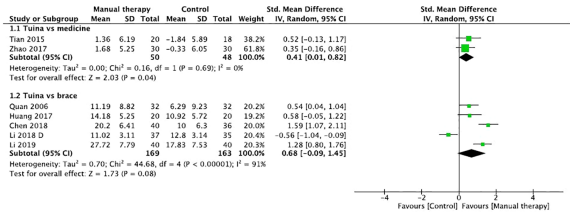

FIGURE 5
Forest plot of the effect of manual therapy for idiopathic scoliosis in Cobb angles.

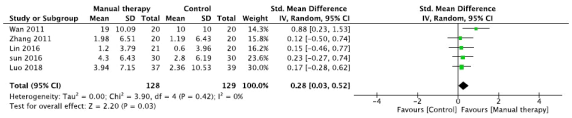

FIGURE 6
Forest plot of the effect of manual therapy plus other conservative therapies for idiopathic scoliosis in Cobb angles.

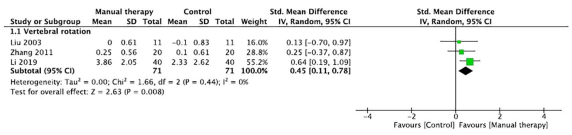

FIGURE 7
Forest plot of the effect of manual therapy for idiopathic scoliosis in vertebral rotation.

Given that pain and negative emotions may be the chief reason for which patients with IS seek treatments, many complementary and alternative therapies may hold value even when they cannot produce radiographic changes of spinal deformity (36). For complementary and alternative therapies, the SOSORT and SRS also recommend that clinical outcomes (such as negative emotion, pain, and disability) relevant to patients with IS should be the primary focus (19). In the current review and meta-analysis, manual therapy, especially Tuina manipulation, showed valuable effects on pain and mental health, including depression and anxiety, which are important for IS treatment. This is usually the main reason why adults with IS visit clinics. In addition, the improvements in depression and anxiety might be beneficial for the long-term adherence to complementary and alternative treatments, and then contribute to halting the curve progression in patients with immature IS (37). These potential benefits should be assessed in the further high-quality clinical trials.

Most of the included studies focused on radiographic outcomes of patients with IS. In our review, Tuina showed beneficial improvements in the management of the Cobb angles and vertebral rotation in patients with IS. The current finding is interesting but insufficient to produce a reliable conclusion/recommendation. The progression of scoliosis differs significantly among the various Risser stages. However, few studies have reported the baseline Risser stage. The initial Risser stage is important for the research on patients with immature IS. For example, a stable Cobb angle from Risser 0 to Risser 3 may have better therapeutic benefits than a 6°curve correction during Risser 4 (13). Furthermore, the included studies did not report the number of patients with Cobb change of 6°or more, which was an improved standard in Cobb angles by the SOSORT and SRS. Several studies have reported that mean changes in the Cobb angles are less than 6°before and after the intervention (22, 28, 32). In addition, a minimum of 5-year follow-up period for adults with IS was recommended by the SOSORT criteria (13). There is little evidence of long-term effects of manual therapy on the Cobb angles. However, for the combined interventions, manual therapy showed beneficial complementary effects in halting/improving the curve progression. Therefore, the current results are interesting for future research.

Limitation

The current study has a few limitations. The reviewers did their best to locate all eligible studies, but the distorting effects of publication and location bias on systematic reviews cannot be avoided. There were some flaws in the blinding methods used in the included studies. Although it was difficult to blind patients and therapists to manual therapy, blinded assessors should compensate for these flaws. Concealed allocation also should be performed to improve the study quality. In the meta-analysis, most studies used Tuina for IS. However, few studies included other manual therapies such as chiropractic, osteopathy, and massage. Moreover, the related studies were mostly conducted in China, and there were limitations in the regional distribution of the trials. Finally, few adverse events were reported in the included studies.

Conclusions

The current review shows valuable evidence in support of Tuina for IS in terms of improving pain and mental health, and disability. The SOSORT and SRS also recommended that clinical studies should focus primarily on patient-centered outcomes, which are more important for IS, and secondarily on the radiographic outcomes. In radiographic outcomes, including the Cobb angle and vertebral rotation, Tuina, especially Tuina plus other conservative therapy including bracing and exercise, showed potential complementary effects for patients with IS. Therefore, manual therapy, especially Tuina, should be considered in management of patients with IS as a complementary and alternative therapy to improve their physical and mental well-being. More RCTs are recommended to validate the current findings.

Data availability statement

The original contributions presented in the study are included in the article/supplementary material. Further inquiries can be directed to the corresponding author.

Author contributions

Study design: LK, JR, and MF; Literature search: QH and JR; Data extract: XZ and JR; Methodological quality assess: XZ and LK; Data analysis: ZW, JR, and LK; Draft manuscript: MF, LK, ZW, and JR. The submitted version has been approved by all authors.

Funding

This work was supported by the Shanghai Pujiang Program (21PJD071), Innovation Team and Talents Cultivation Program of National Administration of Traditional Chinese Medicine (ZYYCXTD-C-202008), Talent development program in Shanghai (2019048), and Shanghai "Science and Technology Innovation Action Plan" Phospherus Cultivation Project (22YF1449900).

Conflict of interest

The authors declare that the research was conducted in the absence of any commercial or financial relationships that could be construed as a potential conflict of interest.

Publisher's note

All claims expressed in this article are solely those of the authors and do not necessarily represent those of their affiliated organizations, or those of the publisher, the editors and the reviewers. Any product that may be evaluated in this article, or claim that may be made by its manufacturer, is not guaranteed or endorsed by the publisher.

References

1. Yaman O, Dalbayrak S. Idiopathic scoliosis. *Turk Neurosurg* (2014) 24 (5):646–57. doi: 10.5137/1019-5149.JTN.8838-13.0

2. Negrini S, Donzelli S, Aulisa AG, Czaprowski D, Schreiber S, de Mauroy JC, et al. 2016 SOSORT guidelines: orthopaedic and rehabilitation treatment of idiopathic scoliosis during growth. *Scoliosis Spinal Disord* (2018) 13:3. doi: 10.1186/s13013-017-0145-8

3. Yi M, Kai K. *The prevalence of scoliosis in guangzhou adolescents is more than 5%* (2015). Available at: https://www.jiankang.com/detail/107789.shtml.

4. Horne JP, Flannery R, Usman S. Adolescent idiopathic scoliosis: Diagnosis and management. *Am Fam Physician* (2014) 89(3):193–8.

5. Campbell M, Matsumoto H, St Hilaire T, Roye BD, Roye DP, Vitale MG. Burden of care in families of patients with early onset scoliosis. *J Pediatr Orthop B* (2020) 29(6):567–71. doi: 10.1097/BPB.0000000000000711

6. Kang T, Kim B. Cervical and scapula-focused resistance exercise program versus trapezius massage in patients with chronic neck pain: A randomized controlled trial. *Med (Baltimore)* (2022) 101(39):e30887. doi: 10.1097/MD.0000000000030887

7. Deng Z, Wang K, Wang H, Lan T, Zhan H, Niu W. A finite element study of traditional Chinese cervical manipulation. *Eur Spine J* (2017) 26(9):2308–17. doi: 10.1007/s00586-017-5193-5

8. Yao C, Ren J, Huang R, Tang C, Cheng Y, Lv Z, et al. Transcriptome profiling of microRNAs reveals potential mechanisms of manual therapy alleviating neuropathic pain through microRNA-547-3p-mediated Map4k4/NF-κb signaling pathway. *J Neuroinflamm* (2022) 19(1):211. doi: 10.1186/s12974-022-02568-x

9. LeBauer A, Brtalik R, Stowe K. The effect of myofascial release (MFR) on an adult with idiopathic scoliosis. *J Bodyw Mov Ther* (2008) 12(4):356–63. doi: 10.1016/j.jbmt.2008.03.008

10. Morningstar MW. Outcomes for adult scoliosis patients receiving chiropractic rehabilitation: a 24-month retrospective analysis. *J Chiropr Med* (2011) 10(3):179–84. doi: 10.1016/j.jcm.2011.01.006

11. Lotan S, Kalichman L. Manual therapy treatment for adolescent idiopathic scoliosis. *J Bodyw Mov Ther* (2019) 23(1):189–93. doi: 10.1016/j.jbmt.2018.01.005

12. Romano M, Negrini S. Manual therapy as a conservative treatment for adolescent idiopathic scoliosis: A systematic review. *Scoliosis* (2008) 3:2. doi: 10.1186/1748-7161-3-2

13. Morningstar MW, Stitzel CJ, Siddiqui A, Dovorany B. Chiropractic treatments for idiopathic scoliosis: A narrative review based on SOSORT outcome criteria. *J Chiropr Med* (2017) 16(1):64–71. doi: 10.1016/j.jcm.2016.10.004

14. Czaprowski D. Manual therapy in the treatment of idiopathic scoliosis. analysis of current knowledge. *Ortop Traumatol Rehabil* (2016) 18(5):409–24. doi: 10.5604/15093492.1224615

15. Hasler C, Schmid C, Enggist A, Neuhaus C, Erb T. No effect of osteopathic treatment on trunk morphology and spine flexibility in young women with adolescent idiopathic scoliosis. *J Child Orthop* (2010) 4(3):219–26. doi: 10.1007/s11832-010-0258-6

16. Li H. Effect of tendon massage combined with orthopedic therapy in the treatment of the adolescent scoliosis. *J Math Med* (2019) 32(2):212–13.

17. Luo X, Huang R, Hu Y, Song Y. Three-dimensional massage therapy for adolescent idiopathic scoliosis. *Chin Manipulation Rehabil Med* (2018) 9(13):32–3. doi: 10.19787/j.issn.1008-1879.2018.13.016

18. Yang YT, Zuo G. Forty-two cases of adolescent scoliosis treated by musculature massage in combination with bone-setting therapy. *Henan Traditional Chin Med* (2015) 35(6):1343–4. doi: 10.16367/j.issn.1003-5028.2015.06.0562

19. Negrini S, Hresko TM, O'Brien JP, Price NSOSORT Boards and SRS Non-Operative Committee. Recommendations for research studies on treatment of idiopathic scoliosis: Consensus 2014 between SOSORT and SRS non-operative management committee. *Scoliosis* (2015) 10:8. doi: 10.1186/s13013-014-0025-4

20. Maher CG, Sherrington C, Herbert RD, Moseley AM, Elkins M. Reliability of the PEDro scale for rating quality of randomized controlled trials. *Phys Ther* (2003) 83(3):713–21. doi: 10.1093/ptj/83.8.713

21. Macedo LG, Elkins MR, Maher CG, Moseley AM, Herbert RD, Sherrington C. There was evidence of convergent and construct validity of physiotherapy evidence database quality scale for physiotherapy trials. *J Clin Epidemiol* (2010) 63 (8):920–5. doi: 10.1016/j.jclinepi.2009.10.005

22. Liu NY, Jin HZ, Li Y, Ma GZ, Ji B. Clinical study on 13 cases of adolescent idiopathic scoliosis treated with tuina plus electroacupuncture. *Jiangsu J Traditional Chin Med* (2003) 24(8):41–2.

23. Quan XB, Chen HJ, Cao DC. Clinical study on 32 cases of adolescent idiopathic scoliosis treated with tuina plus traction. *Zhejiang J Traditional Chin Med* (2006) 41(5):296–7.

24. Rowe DE, Feise RJ, Crowther ER, Grod JP, Menke JM, Goldsmith CH, et al. Chiropractic manipulation in adolescent idiopathic scoliosis: a pilot study. *Chiropr Osteopat* (2006) 14:15. doi: 10.1186/1746-1340-14-15

25. Wan L. Rehabilitation effect of tuina on primary "S" type scoliosis. *Chin J Trauma Disability Med* (2011) 19(1):25–6.

26. Zhang HC. The clinical research on treating adolescent idiopathic scoliosis by tuina plus night used orthotic device for scoliosis. [dissertation/master's thesis]. Harbin: Heilongjiang University of Chinese Medicine (2011).

27. Wang SQ, Zhu QG, Lin YF. Clinical research of sudden-traction manipulation in supine position in treatment of adolescent idiopathic scoliosis. *Hubei J Traditional Chin Med* (2014) 36(2):15–6.

28. Tian G, Shen MR, Jiang WG, Xie FR, Wei WW. Case-control study on spinal leveraging manipulation and medicine for the treatment of degenerative scoliosis. *China J Orthop Trauma* (2015) 28(6):508–11.

29. Lin WF, Zhao JJ, Li L, Tian Q, Li ZB, Wu S. Clinical observation on 21 cases of adolescent idiopathic scoliosis treated by tuina combined with exercise intervention. *J New Chin Med* (2016) 48(2):117–20. doi: 10.13457/j.cnki.jncm.2016.02.044

30. Sun W, Zhu LG, Gao JH, Yang KX, Feng MS, Gao CY. Clinical research on spine manipulation combined with eperisone in the treatment of degenerative scoliosis. *Chin J Trad Med Traum Orthop* (2016) 24(4):18–21.

31. Huang Y, Huang BC. The effect of characteristic tuina on adolescent scoliosis. *Chin J Convalescent Med* (2017) 26(10):1053–4. doi: 10.13517/j.cnki.ccm.2017.10.017

32. Zhao L, Li HR, Li HQ, Zhang SH, Zhang JH, Dong ZY, et al. Comparison of therapeutic effects of tuina and medicine on degenerative scoliosis. *Modern J Integrated Traditional Chin Western Med* (2017) 26(4):399–401.

33. Chen T, Wang ZL, Zhang P, Zuo HF. Three designated tuina in the treatment of adolescent idiopathic scoliosis. *Jilin J Chin Med* (2018) 38:717–9. doi: 10.13463/j.cnki.jlzyy.2018.06.028

34. Li ZX, Zhang HH, Lin BC, Hu CX, Zhang RX, Sun J, et al. The clinical research into adolescent idiopathic scoliosis treated with six dimensional space tuina. *Henan Traditional Chin Med* (2018) 38(7):1089–92. doi: 10.16367/j.issn.1003-5028.2018.07.0292

35. Sterne JA, Sutton AJ, Ioannidis JP, Terrin N, Jones DR, Lau J, et al. Recommendations for examining and interpreting funnel plot asymmetry in meta-analyses of randomised controlled trials. *BMJ* (2011) 343:d4002. doi: 10.1136/bmj.d4002

36. Rigo M. Differential diagnosis of back pain in adult scoliosis (non operated patients). *Scoliosis* (2010) 5(Suppl 1):O44. doi: 10.1186/1748-7161-5-S1-O44

37. Zhao FN, Peng HJ, Huo LT, Dong Q. Investigation on anxiety status and related factors in patients with scoliosis. *For all Health* (2016) 10(04):92–3.

frontiers | Frontiers in Endocrinology

TYPE Review
PUBLISHED 08 December 2022
DOI 10.3389/fendo.2022.1081185

OPEN ACCESS

EDITED BY
Shibao Lu,
Xuanwu Hospital, Capital Medical University, China

REVIEWED BY
Chang Qing Zhao,
Shanghai Jiao Tong University, China
Run-Ze Yu,
Anhui No.2 Provincial People's Hospital, China

*CORRESPONDENCE
Hao Yang
yanghao71_99@yeah.net
Dingjun Hao
haodingjun@mail.xjtu.edu.cn

†These authors have contributed equally to this work

SPECIALTY SECTION
This article was submitted to Bone Research, a section of the journal Frontiers in Endocrinology

RECEIVED 27 October 2022
ACCEPTED 23 November 2022
PUBLISHED 08 December 2022

CITATION
Jiang C, Chen Z, Wang X, Zhang Y, Guo X, Xu Z, Yang H and Hao D (2022) The potential mechanisms and application prospects of non-coding RNAs in intervertebral disc degeneration.
Front. Endocrinol. 13:1081185.
doi: 10.3389/fendo.2022.1081185

The potential mechanisms and application prospects of non-coding RNAs in intervertebral disc degeneration

Chao Jiang[1†], Zhe Chen[1†], Xiaohui Wang[1,2†], Yongyuan Zhang[1], Xinyu Guo[1], Zhengwei Xu[1], Hao Yang[3*] and Dingjun Hao[1*]

[1]Department of Spine Surgery, Hong Hui Hospital, Xi'an Jiaotong University, Xi'an, China, [2]Department of Developmental Genetics, Max Planck Institute for Heart and Lung Research, Bad Nauheim, Germany, [3]Translational Medicine Center, Hong Hui Hospital, Xi'an Jiaotong University, Xi'an, China

Low back pain (LBP) is one of the most common musculoskeletal symptoms and severely affects patient quality of life. The majority of people may suffer from LBP during their life-span, which leading to huge economic burdens to family and society. According to the series of the previous studies, intervertebral disc degeneration (IDD) is considered as the major contributor resulting in LBP. Furthermore, non-coding RNAs (ncRNAs), mainly including microRNAs (miRNAs), long noncoding RNAs (lncRNAs) and circular RNAs (circRNAs), can regulate diverse cellular processes, which have been found to play pivotal roles in the development of IDD. However, the potential mechanisms of action for ncRNAs in the processes of IDD are still completely unrevealed. Therefore, it is challenging to consider ncRNAs to be used as the potential therapeutic targets for IDD. In this paper, we reviewed the current research progress and findings on ncRNAs in IDD: i). ncRNAs mainly participate in the process of IDD through regulating apoptosis of nucleus pulposus (NP) cells, metabolism of extracellular matrix (ECM) and inflammatory response; ii). the roles of miRNAs/lncRNAs/circRNAs are cross-talk in IDD development, which is similar to the network and can modulate each other; iii). ncRNAs have been attempted to combat the degenerative processes and may be promising as an efficient bio-therapeutic strategy in the future. Hence, this review systematically summarizes the principal pathomechanisms of IDD and shed light on the therapeutic potentials of ncRNAs in IDD.

KEYWORDS

non-coding RNAs, microRNAs, long noncoding RNAs, circular RNAs, intervertebral disc degeneration

Introduction

Currently, low back pain (LBP) serves as one of the most prevalent musculoskeletal symptoms and has severe effects on the quality of life of individuals in the worldwide (1–3). Previous studies indicated that almost all people may have suffered from LBP during their life-span, resulting in substantial distress and economic burden (3, 4). With regard to the causes for LBP, it is still not completely unraveled, but intervertebral disc degeneration (IDD) is considered as the major contributor (5). IDD is a series of physiological and pathological changes occurring in the aging and degeneration of the intervertebral disc (IVD). A cross-sectional study indicated that almost 40% individuals suffered from IDD are less than 30 years, which is as high as 90% between 50 and 55 years (6). Nonetheless, there is lack of effective bio-therapeutic strategies for IDD and surgical intervention is hard to avoid in the final stage (7). Therefore, it is greatly necessary to clarify the underlying mechanisms of IDD at a cellular and molecular level.

IDD is a long and chronic process accompanying structural failure and progressive aging of the normal intervertebral disc (IVD), which is attributed to series of factors including lifestyle, aging, genetic predispositions and excessively mechanical loading (8, 9). IVD is the fibrocartilage tissue structure between each two vertebrae and serve as crucial role in maintaining the stability of the spine. In terms of anatomical structure, IVD is composed of nucleus pulposus (NP) cells, annulus fibrosus (AF) and cartilaginous endplate (CEP) (Figure 1). Accumulating evidences demonstrate that genetic and environmental factors contribute to IDD, but the exact molecular mechanisms are still largely unclear (10). The pathophysiological processes of IDD are mainly characterized by cells apoptosis, imbalance of extracellular matrix (ECM) and inflammatory response (Figure 1).

Noncoding RNAs (ncRNAs), primarily including microRNAs (miRNAs), long ncRNAs (lncRNAs) and circular RNAs (circRNAs), have been found to exert extensive effects on biological processes such as cell proliferation, apoptosis and ECM metabolism (4, 11, 12). Furthermore, compelling evidences supported that the expression of ncRNAs are significantly different between IDD and control samples, implicating ncRNAs play crucial roles in the development of IDD (13–15). Notably, novel ncRNAs have been constantly identified through microarray, RNA sequencing and reverse transcription-quantitative PCR (RT-qPCR) (16, 17), which has attracted a large number of interesting researcher's attentions on the functions and specific molecular mechanisms of ncRNAs in IDD. There is no doubt that these works provide excellent value of understanding the precise roles of ncRNAs and display promising future for IDD bio-therapeutic strategy.

In this review, we systematically summarized the literature of past five years on ncRNAs in the pathophysiological processes of IDD, mainly involving miRNAs, lncRNAs and circRNAs. In addition, the application prospects of ncRNAs as bio-therapeutic strategy for effective treatment of IDD are also discussed.

The roles of miRNAs in the development of IDD

MiRNAs, a group of endogenous ncRNAs with 20–24bp nucleotides in length, can regulate gene expression through

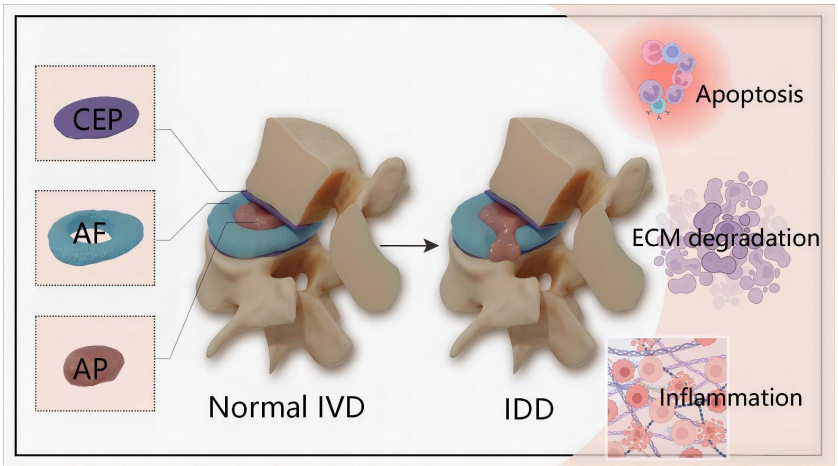

FIGURE 1
Schematic illustration of the anatomical structure of normal IVD and main pathophysiological features of IDD. IVD is composed of the central NP tissue, AF surrounding the NP, and CEP adhering the upper and lower vertebrae.The pathophysiological features of IDD are mainly characterized by cells apoptosis, imbalance of ECM and inflammatory response. IVD, intervertebral disc; IDD, intervertebral disc degeneration; CEP, cartilaginous endplate; AF, annulus fibrosus; NP, nucleus pulposus; ECM, extracellular matrix.

recognizing and targeting the complementary 3′untranslated regions (3′UTRs) of particular mRNAs. Previous studies demonstrated that miRNAs were significantly differentially expressed between IDD and non-IDD, and acted as pivotal roles in the development of IDD (11, 18).

MiRNAs regulate the apoptosis of cells

The apoptosis of NP cells is a typical feature of IDD and a myriad of studies reported that miRNAs mediated the NP cells apoptosis through regulating specific gene expression (18). Previously, Ji et al. firstly confirmed that miR-141 causes spontaneous progression of IDD by means of a study in miR-141 KO and wild-type mice (19). Mechanistically, miR-141 induced NP cell apoptosis and facilitated IDD progress *via* the regulation of downstream SIRT1/NF-κB axis (19). In addition, silencing of miR-141 had a protective effect on IDD mice, while upregulating miR-141 accelerated the development of IDD. Similar to miR-141, a large body of studies demonstrated that miRNAs were up-regulated in DD and aggravated NP cells apoptosis, such as miR-96/FRS2 (20), miR-4478/MTH1 (21) and miR-328-5p/WWP2 (22). On the contrary, there were substantial numbers of miRNAs were down-regulated and most likely exert anti-apoptotic effects in IDD, mainly involving miR-129-5p/BMP2 (23), miR-623/CXCL12 (24) and miR-155-3p/KDM3A/HIF1α (25). Therefore, miRNA-mediated apoptosis of NP cells affected the pathological process of IDD *via* downstream hub proteins or signal pathway. Notably, apart from anti-apoptosis, miR-623/CXCL12 axis inhibited senescence in LPS-induced NP cells (24), which suggested that miRNAs likely play an important role in IDD development by affecting cellular senescence.

Given the particular structure of IVD, CEP is essential for NP cells to acquire nutrition and prevent damaging factors into the disc. Previous studies showed that CEP cells apoptosis or calcification induced CEP degeneration, which resulted in nutrient loss and rendered IDD progress (26, 27). In a previous experiment, overexpression of miR-34a was evidenced to promote Fas-induced CEP cells apoptosis through inhibiting Bcl-2 (28). Additionally, miR-20a/ANKH-mediated stiff matrix enhanced calcification of CEP, whereas suppression of miR-20a alleviated the gene expression of calcification (29). Likewise, miR-221 positively regulated CEP cells apoptosis by targeting estrogen receptor α (ERα) (30). Based on the findings above, miRNAs have been shown to contribute to CEP cells apoptosis and calcification, which is closely pertinent to the development of IDD. However, recent literature demonstrated that miR-142-3p knockdown promoted apoptosis and autophagy of CEP cells by HMGB1 (31), implying that miR-142-3p is likely to have potential in protecting IDD. Apart from the foregoing mechanisms, miR-106a-5p also mediates AF cells apoptosis, which can be suppressed by melatonin (32).

Taken together, miRNAs-mediated cells apoptosis (NP, CEP and AF cells) regulates the onset of IDD, which provides potential targets for intervening IDD. Nevertheless, the roles of miRNAs in NP cells apoptosis attracted more attention. In the future, the related-studies should pay more attention to the effects of miRNAs on CEP and AF cells apoptosis.

MiRNAs regulate the metabolism of ECM

ECM, a non-cellular three-dimensional macromolecular network predominantly composed of collagens and proteoglycan, is indispensable to maintain normal IVD cell function. With regard to the pathological process of IDD, the imbalance of ECM metabolism is a biological hallmark for IDD, which is characterized by synthesis decrease and degradation increase (9, 33). The metabolism of ECM is determined by proteolytic enzymes, such as matrix metalloproteinases (MMPs) and growth differentiation factor 5 (GDF5). miRNAs have been evidenced to play crucial roles in ECM degradation through modulating the activity of essential enzymes.

MMPs have acted as an essential factor for modulating metabolism of ECM. It has been reported that miR-127-5p was downregulated in degenerated NP tissues and inhibited the expression of type II collagen (34). Further experiment confirmed that miR-127-5p mediated the degradation of ECM components through enhancing MMP-13 expression. Another study found that the level of miR-210 remarkably increased in human degenerated NP cells, resulting in suppression of autophagy-related gene 7 (ATG7) and elevation of MMP-13 and MMP-3 (35). Notably, ATG7 knock-down seriously undermined the influences of miR-210 inhibitor on MMP-13 and MMP-3. These findings indicated that miR-210-induced ECM degradation was attributed to the proteolytic activity of upregulated MMP-13 and MMP-3 by directly targeting ATG7. Similarly, Wang et al. (36) also evidenced that miR-21 contributed to ECM catabolism by inhibiting autophagy through PTEN/Akt/mTOR signal pathway and elicited upregulation of MMP-9 and MMP-3 expression. Collectively, miRNAs play critical roles in MMPs-mediated metabolism of ECM *via* modulating autophagy.

GDF5, a crucial member of bone morphogenetic protein family, has been found to exert vital effects in musculoskeletal physiological process (37, 38). More importantly, recent publications also revealed that GDF5 provided protective effects against IDD through inhibiting ECM catabolism and promoting ECM anabolism (39, 40). Specifically, miR-132 contributed to the degradation of ECM by inhibiting GDF5, whereas antagomiR-132 protected ECM from degradation in IDD rats (39). Likewise, upregulation of miR-665 enhanced expression of catabolic genes (MMP13 and ADAMTS4) *via* specifically binding to GDF5, leading to ECM degradation

(40). Consequently, GDF5 is likely to be an important target in ECM degradation caused by miRNAs.

It has been evidenced that SRY-related high mobility group box (SOX) is involved in the process of IDD (41). MiR-30d was found to be upregulated in degenerative NP tissues, and suppression of miR-30d resulted in hypoactive catabolism of ECM *in vitro* (42). Notably, bioinformatics analysis demonstrated that SOX9, an important transcription factor, was a direct target regulated by miR-30d. Interestingly, overexpression of miR-499a-5p is propitious to prevent NP cells apoptosis and ECM decomposition through repressing SOX4 expression (43). Although SOX9 and SOX4 belong to the transcription factors, they show opposite effects on ECM in the development of IDD. In addition, there are some miRNAs mediated ECM metabolism, such as miR-154/FGF14 (44), miR-145/ADAM17 (45) and miR-1260b/TCF7L2 (46) axis. This implicates a wide biofunction of miRNAs in the IDD process.

In summary, ECM metabolism mediated by miRNAs has affected the progress of IDD. Targeting miRNAs may be a promising approach for maintenance of the proper balance of ECM catabolism and anabolism, thereby delaying the pathological change of IDD.

MiRNAs regulate the inflammation

Inflammation is widely envisioned as one of pathological features accompanying with IDD (47, 48). Up to now, accumulating evidence have also shown that multiple miRNAs are involved in regulating the inflammatory response of IDD (49–51).

Nuclear factor κB (NF-κB) is a key signal pathway in inflammatory response. The activation of NF-κB promotes the inflammatory cascade, leading to adverse environment for NP cells and impetus to degeneration of IVD (48). With regard to miRNAs-related to modulating inflammation, miR-16 was confirmed to negatively regulate the inflammation-related genes in LPS-induced NP cells, including COX-2, iNOS and PGE2 (51). Subsequently, target prediction found that TAB3 was directly regulated by miR-16, which was experimentally validated by a miRNA luciferase reporter assay. Besides, miR-16 attenuated the inflammation in LPS-mediated NP cells *via* inhibiting NF-κB and MAPK signal pathway. Likewise, MiR-223 was identified to share similar roles in LPS-treated NP cells through Irak1-mediated suppression of NF-κB (52). Apart from the above-mentioned, miR-15a-5p was found to aggravate the inflammation and apoptosis of NP cells by modulating NF-κB pathway (53). Hence, miRNAs can alleviate inflammation in NP cells by suppressing NF-κB. On the contrary, Dong et al. (54) demonstrated that miR-640 showed overt pro-inflammatory effects by enforcing activation of NF-κB, resulting in NP cells degeneration, conversely, inhibition of miR-640 displayed the opposite effects. Extracellular signal-regulated kinase (ERK) pathway has been evidenced to play key role in inhibiting inflammation (55). MiR-181a suppressed the expression of inflammatory factors through blocking ERK pathway in IDD mice (56), indicating that miR-181a affords protective effects in IDD.

Apart from mediated-apoptosis in IDD process, ERα is reported to a key player in modulating inflammation (57, 58). Specifically, the expression of miR-203-3p was positively correlated with the severity of IDD and negatively with Erα (58). Further evidence showed that ERα was the specific target of miR-203-3p and can be inhibited in LPS-stimulated NP cells, indicating that miR-203-3p was likely to aggravate intervertebral disc inflammation and degeneration through targeting ERα. These findings revealed that the same gene could exert different roles due to different miRNAs, implying the complexity and diversity of miRNA in regulation of IDD.

Additionally, other miRNAs were also demonstrated to link with inflammation in IDD progress. For example, miR-194-5p actively contributed to human IDD by targeting CUL4A and CUL4B and significantly decreased in inflammatory environment of IDD, indicating a negative regulation of miR-194-5p in the progression of IDD (59). In contrast, miR-125b-5p expression was found to be enforced in IL-1β-induced NP cells and human degenerating NP samples, which contributed to inflammation and NP cells apoptosis by monitoring TRIAP1 (60).

In summary, current studies demonstrate that miRNAs are key regulators and have important effects on the pathological cascades of IDD through intervening cells apoptosis, ECM metabolism and inflammation. In fact, the roles of miRNAs in the pathogenesis of IDD are not limited to the above-mentioned aspects. Latest studies indicate that miRNAs-mediated autophagy and ferroptosis are intimately linked with pathological progression of IDD. MiR-202-5p suppressed autophagy in degenerating NP cells through targeting ATG7 (61). Notably, Wu and colleagues (62) provided sufficient evidence that downregulation of miR-130b-3p promoted autophagy in NP cells and ameliorated IDD through ATG14/PRKAA1 *in vivo* and vitro. Ferroptosis, an iron-dependent type of programmed cell death, is associated with the pathogenesis of IDD. Overexpression of miR-10a-5p partially reversed IL-6-mediated ferroptosis in cartilage cells (63). In addition, latest evidence showed that inhibition of miR-874-3p positively modulated ferroptosis in NP cells by targeting activation transcription factor 3 (ATF3) (64). Undoubtedly, increasing studies revealed that miRNAs can mediate the initiation and progress of IDD (Table 1), indicating miRNAs-based therapy for IDD may be a promising strategy.

The roles of lncRNAs in the development of IDD

LncRNAs are a class of long noncoding RNAs whose transcript length exceeds 200 nucleotides in length. In general, lncRNAs are lack of capacity to code proteins, but share

excellent regulation of gene expression through genetic, transcriptional and post-transcriptional modifications (65). Recently, emerging studies indicated that lncRNAs were associated with musculoskeletal degeneration diseases, such as osteoarthritis and IDD (4, 66). LncRNAs have exerted critical effects on the IDD by regulating cellular phenotype (cells proliferation, apoptosis, autophagy and ECM metabolism) through directly targeting hub gene expression and miRNAs.

It is well known that lncRNAs participate in the pathological changes of degenerative diseases by sponging specific miRNAs. LncRNA PART1 was verified to be significantly increased in NP cells isolated from IDD patients, indicating that PART1 probably impacted the degeneration of NP cells (67). Then, the expression of genes responsible for cells apoptosis, proliferation and ECM metabolism were evaluated. Results showed that lncRNA PART1 promoted NP cells apoptosis and ECM degradation, whereas cells proliferation and ECM synthesis were suppressed. Mechanistically, lncRNA PART1 competitively sponged miR-93, causing the degradation of NP cells by MMP2. Based on these findings, it can be inferred that lncRNAs play key role in IDD, albeit lack of *in vivo* evidence to support the potential role of PART1 for IDD. Zhong and team (68) found that lncRNA ADIRF-AS1/miR-214-3p/SERPINA1 pathway was negatively correlated with the severity of IDD, suggesting the protective role of ADIRF-AS1. Specifically, upregulation of ADIRF-AS1 enhanced NP cells viability and suppressed cellular senescence and apoptosis. Strikingly, latest study reported by Yu et al. (69) uncovered that lncRNA GAS5 was a principal contributor to NP cells apoptosis and catabolism of ECM through miR-17-3p/Ang-2 axis, eliciting the occurrence and progress of IDD. In addition, both inhibition of GAS5 and upregulation of miR-17-3p ameliorated IVDD in mice models. Collectively, *in vitro* and vivo studies afforded abundant supports that the lncRNA GAS5 might participate in IDD progress by miR-17-3p/Ang-2-mediated NP cells apoptosis and ECM degradation. Besides, inflammation and oxidative stress destroyed the homeostasis of IVD, enhancing the development of IDD. LncRNA MT1DP was found to mitigate anti-oxidation through miR-365/NRF-2 signal pathway, leading to NP cells apoptosis and IDD (70). Notably, LncRNA FAM83H-AS1 alleviated inflammatory response and promoted NP cells proliferation through miR-22-3p, preventing further deterioration of IDD in rat models caused by advanced glycation end products (71).

LncRNAs play important roles in regulating IDD through direct modulation of hub gene or signal pathway, ultimately triggering downstream cascades. Within the event, nuclear factor E2-related factor 2 (Nrf2) was reported to facilitate protecting NP cells from oxidative injury and preventing IDD deterioration (72, 73). Kang and colleagues (74) evidenced that upregulation of lncRNA ANPODRT attenuated oxidative stress and reduced tert-butyl hydroperoxide-stimulated apoptosis in NP cells, which could be attributed to the activation of Nrf2. As previously mentioned, miRNAs-mediated autophagy influenced the progress of IDD. As a consequence, lncRNAs may affect the process of IDD through autophagic pathway. HOTAIR, a novel lncRNA, was found to associate with autophagy and highly expressed in human NP tissue suffering from IDD (75). Furthermore, upregulation of HOTAIR potentiated autophagy *via* AMPK/mTOR/ULK1 signaling pathway in human NP cells, leading to NP cells apoptosis, senescence, and ECM degradation. More importantly, blocking HOTAIR attenuated the adverse effects in IDD rats. Interestingly, lncRNA HOTAIR could activate Wnt/β-catenin pathway and exert similar functions except for modulating AMPK/mTOR/ULK1 (76), implying lncRNA may act as key regulators of multiple downstream pathways.

At the present, an increasing number of lncRNAs have been found to involve in the pathological process of IDD, such as lncRNA SNHG6/miR-101-3p (77), lncRNA MIR155HG/miR-223-3p (78) and lncRNA H19/miR-139-3p/CXCR4/NF-κB (79) axes. In summary, these important roles of lncRNAs in IDD have been comprehensively verified (Table 2). Helpfully, these findings further elucidate the underlying mechanisms of IDD and shed light on lncRNAs as potential therapeutic target for treatment of IDD.

The roles of circRNAs in the development of IDD

CircRNAs, another particular type of ncRNAs with the covalently closed loops, have attracted substantial attentions because of their excellent biological properties. Currently, there are a series of circRNAs have been evidenced to be pertinent to the underlying mechanisms of IDD (15, 80). As naturally formed endogenous non–coding RNAs, circRNAs serve as a competing endogenous RNAs and modulate the pathological process of IDD, mainly involving in cellular apoptosis, ECM metabolism and inflammation (80).

In the light of pathological mechanism of IDD, NP cells apoptosis is primary factor accelerating the pathological progression of IDD. Cheng and colleagues (81) observed that circVMA21 could depress the expression of apoptotic and catabolic genes, and enhance the collagen II and aggrecan expression in NP cells treated by inflammatory cytokines through miR-200c/XIAP pathway. *In vivo* injection of circVMA21 ameliorated the degeneration of NP tissues in rat model, suggesting the protective role of circVMA21/miR-200c/XIAP against IDD. Subsequently, Guo et al. (82) also verified that circGRB10 provided the beneficial effects in preventing IDD by reducing NP cell apoptosis through miR-328-5p/ERBB2 axis. Similarly, other studies demonstrated that cicrRNAs also afforded protection against IDD development, mainly including circRNA-CIDN/miR-34a-5p/SIRT1 (83), circGLCE/

TABLE 1 The roles of miRNAs in the development of IDD.

MiRNAs	Expression	Target/Pathway	Function	Reference
miR-141	Up	SIRT1/NF-κB	NP cells apoptosis(+)	Ji et al. (19)
miR-96	Up	FRS2	NP cells apoptosis(+)	Yang et al. (20)
miR-4478	Up	MTH1	NP cells apoptosis(+)	Zhang et al. (21)
miR-328-5p	Up	WWP2	NP cells apoptosis(+)	Yan et al. (22)
miR-129-5p	Down	BMP2	NP cells apoptosis(-)	Yang et al. (23)
miR-623	Down	CXCL12	NP cells apoptosis/senescence(-)	Zhong et al. (24)
miR-155-3p	Down	KDM3A/HIF1α	NP cells apoptosis(-)	Zhou et al. (25)
miR-34a	Up	Bcl-2	CEP cells apoptosis(+)	Chen et al. (28)
miR-20a	Up	ANKH	CEP calcification(+)	Liu et al. (29)
miR-221	Up	ERα	CEP cells apoptosis(+)	Sheng et al. (30)
miR-142-3p	Down	HMGB1	CEP cells apoptosis(-)	Wang et al. (31)
miR-106a-5p	Up	ATG7	AF cells apoptosis(+)	Hai et al. (32)
miR-127-5p	Down	MMP-13	ECM anabolism(+)	Hua et al. (34)
miR-210	Up	ATG7/MMP-13/MMP-3	ECM catabolism(+)	Wang et al. (35)
miR-21	Up	PTEN/Akt/mTOR/MMP-9/MMP-3	ECM catabolism(+)	Wang et al. (36)
miR-132	Up	GDF5	ECM catabolism(+)	Liu et al. (39)
miR-665	Up	GDF5	ECM catabolism(+)	Tan et al. (40)
miR-30d	Up	SOX9	NP cells apoptosis/ECM catabolism(+)	Lv et al. (42)
miR-499a-5p	Down	SOX4	NP cells apoptosis/ECM catabolism(-)	Sun et al. (43)
miR-154	Up	FGF14	ECM catabolism(+)	Wang et al. (44)
miR-145	Down	ADAM17	NP cells apoptosis(-)/ECM anabolism(+)	Zhou et al. (45)
miR-1260b	Down	TCF7L2	ECM anabolism(+)	Chen et al. (46)
miR-16	Down	TAB3	Anti-inflammation	Du et al. (51)
miR-223	Down	Irak1	Anti-inflammation	Wang et al. (52)
miR-15a-5p	Up	SOX9/NF-κB	Pro-inflammation/NP cells apoptosis(+)	Zhang et al. (53)
miR-640	Up	NF-κB	Pro-inflammation	Dong et al. (54)
miR-181a	Down	ERK	Anti-inflammation	Sun et al. (56)
miR-203-3p	Up	ERα	Pro-inflammation	Cai et al. (58)
miR-194-5p	Down	CUL4A/CUL4B	Anti-inflammation	Chen et al. (59)
miR-125b-5p	Up	TRIAP1	Pro-inflammation/NP cells apoptosis(+)	Jie et al. (60)
miR-202-5p	Up	ATG7	NP cells autophagy(-)	Chen et al. (61)
miR-130b-3p	Up	ATG14/PRKAA1	NP cells autophagy(-)	Wu et al. (62)
miR-10a-5p	Down	IL-6R	Cartilage cells ferroptosis(-)	Bin et al. (63)
miR-874-3p	Down	ATF3	NP cells ferroptosis(-)	Li et al. (64)

(+), promotion; (-), inhibition.

TABLE 2 The roles of lncRNAs in the development of IDD.

LncRNAs	Expression	Target/Pathway	Function	Reference
lncRNA PART1	Up	miR-93/MMP2	NP cells apoptosis/ECM catabolism(+)	Gao et al. (67)
lncRNA ADIRF-AS1	Down	miR-214-3p/SERPINA1	NP cells apoptosis/senescence(-)	Zhong et al. (68)
lncRNA GAS5	Up	miR-17-3p/Ang-2	NP cells apoptosis/ECM degradation(+)	Yu et al. (69)
lncRNA MT1DP	Up	miR-365/NRF-2	NP cells apoptosis(+)	Liao et al. (70)
lncRNA FAM83H-AS1	Down	miR-22-3p	Anti-inflammation/NP cells growth(+)	Jiang et al. (71)
lncRNA ANPODRT	Down	Nrf2	Anti-inflammation	Kang et al. (74)
lncRNA HOTAIR	Up	AMPK/mTOR/ULK1	NP cells apoptosis/senescence(+)	Zhan et al. (75)
lncRNA HOTAIR	Up	Wnt/β-catenin	NP cells apoptosis/ECM degradation(+)	Zhan et al. (76)
lncRNA SNHG6	Up	miR-101-3p	NP cells apoptosis(+)	Gao et al. (77)
lncRNA MIR155HG	Up	miR-223-3p	NP cells pyroptosis(+)	Yang et al. (78)
lncRNA H19	Up	miR-139-3p/CXCR4/NF-κB	NP cells apoptosis(+)	Sun et al. (79)

(+), promotion; (-), inhibition.

miR-587/STAP1 (84) and circARL15/miR-431-5p/DISC1 (85) pathway. On the contrary, recent studies showed that circRNAs facilitated apoptosis of NP cells. For instance, circ_001653 was significantly upregulated in degenerated NP tissues, which promoted the NP cells apoptosis and ECM degradation by miR-486-3p/CEMIP axis (86). In addition, a series of evidence indicated that circITCH induced apoptosis and mediated IDD through miR-17-5p/SOX4 axis (87).

As is known to all, the imbalance of ECM metabolism is detrimental for IDD. Considering that miRNAs play important role in modulating anabolism and catabolism of ECM, circRNAs also have been reported to associate with ECM metabolism through sponging miRNAs. Upregulation of circ-4099 promoted the ECM (collagen II and aggrecan) synthesis and restricted expression of pro-inflammatory factors (IL-1β, TNF-α, and PGE2) through targeting miR-616-5p/SOX9 (88). Likewise, circSEMA4B could alleviate ECM catabolism in IL-1β-induced NP cells *via* miR-431/GSK-3β/SFRP1 axis (89). Accordingly, these results support that circRNAs can prevent IDD through facilitating the anabolism of ECM. Nevertheless, circRNAs also share unfavorable roles in ECM metabolism and can induce ECM degradation. For instance, growing evidence showed that circRNA_104670 enhanced the expression of MMP-2 known to be associated with ECM catabolism, through miRNA-17-3p/MMP2 pathway, potentiating ECM degradation (90). Furthermore, circRNA_104670 and miRNA-17-3p was found to have excellent diagnostic significance for IDD based on the outcome of the receiver-operating characteristic curve.

Recently, accumulating studies found that circRNAs play vital roles in modulating inflammation response. It is well known that NF-κB is a classical inflammation-related pathway. Guo et al. (91) evidenced that circ-FAM169A mediated inflammatory cytokines (IL-1β and TNF-α) expression through BTRC/NF-κB axis, which induced NP cells apoptosis and ECM degradation. Based on above, there is no doubt that circRNAs play a crucial role in the regulation of miRNAs. Notwithstanding, whether multiple circRNAs can interplay and impact the biological process remain unclear. Strikingly, latest publication showed that circ_0040039 and circ_0004354 competitively regulated miR-345-3p/FAF1/TP73 pathway in IDD, initiating inflammation, ECM catabolism and pro-inflammation in NP cells (92). In detail, circ_0004354 showed stronger capacity to bind miR-345-3p when inflammatory cytokines reached lower level at the early phase of IDD. Subsequently, circ_0004354 was suppressed through negative feedback due to increase of inflammatory cytokines. Meanwhile, increased inflammatory cytokines induced circ_0040039 expression, which in turn inhibited the binding of circ_0004354 with miR-345-3p and augmented circ_0040039 ability to target miR-345-3p. Collectively, circ_0004354 and circ_0040039 showed different capacity to bind miR-345-3p relying on different concentration of inflammatory cytokines, eventually triggering inflammatory cascades and accelerating IDD progression.

Taken together, circRNAs display excellent ability to modulate the development of IDD through cells apoptosis, ECM metabolism and inflammation (Table 3). In addition, circRNAs also take important roles in affecting cellular senescence. For instance, latest research published by Wang et al. (93) reported that circ_7042 could prevent the IDD progression through inhibiting NP cells apoptosis, senescence and ECM degradation by absorption of miR-369-3p/BMP2/PI3K/Akt axis. Apart from sponging miRNAs, the interaction of different circRNAs may have impacts on the downstream

TABLE 3 The roles of circRNAs in the development of IDD.

CircRNAs	Expression	Target/Pathway	Function	Reference
circVMA21	Down	miR-200c/XIAP	NP cells apoptosis(-)/ECM anabolism(+)	Cheng et al. (81)
circGRB10	Down	miR-328-5p/ERBB2	NP cells apoptosis(-)	Guo et al. (82)
circRNA-CIDN	Down	miR-34a-5p/SIRT1	NP cells apoptosis/ECM catabolism(-)	Xiang et al. (83)
circGLCE	Down	miR-587/STAP1	NP cells apoptosis/ECM catabolism(-)	Chen et al. (84)
circARL15	Down	miR-431-5p/DISC1	NP cells apoptosis(-)	Wang et al. (85)
circ_001653	Up	miR-486-3p/CEMIP	NP cells apoptosis/ECM catabolism(+)	Cui et al. (86)
circITCH	Up	miR-17-5p/SOX4	NP cells apoptosis/ECM catabolism(+)	Zhang et al. (87)
circ-4099	Down	miR-616-5p/SOX9	ECM anabolism(+)	Wang et al. (88)
circSEMA4B	Down	miR-431/GSK-3β/SFRP1	ECM anabolism(+)	Wang et al. (89)
circRNA_104670	Up	miRNA-17-3p/MMP2	ECM catabolism(+)	Song et al. (90)
circ-FAM169A	Up	miR-583/BTRC/NF-κB	ECM catabolism(+)	Guo et al. (91)
circ_0040039/circ_0004354	Up	miR-345-3p/FAF1/TP73	Inflammation/ECM catabolism(+)	Li et al. (92)
circ_7042	Down	miR-369-3p/BMP2/PI3K/Akt	NP cells apoptosis/senescence/ECM degradation	Wang et al. (93)

(+), promotion; (-), inhibition.

pathway, which urgently needs more evidence to further verify.

Interactions of miRNAs, lncRNAs, and circRNAs

In terms of current findings, dysregulation of ncRNAs mediates the onset and progression of IDD. More importantly, the exertion of functions regarding ncRNAs appears to be not completely independent of modulating the pathological process of IDD. LncRNAs and circRNAs, as particular ncRNAs, can directly sponge miRNAs and initiate a series of gene expression to regulate cells apoptosis, ECM metabolism and inflammation. Furthermore, there is a competitive relationship to bind miRNAs among multiple circRNAs. Collectively, the cross-talk of miRNAs/lncRNAs/circRNAs orchestrates IDD development (Figure 2), which is similar to the network and can modulate each other.

Therapeutic strategies for IDD based on ncRNAs

On the basis of understanding functions of ncRNAs, emerging evidence demonstrate that multiple strategies show excellent efficacy on treatment IDD through ncRNAs, mainly including stem cell therapy, exosomes, biomaterials and pharmacologic strategy (Figure 3).

Stem cell

With more profound studies on stem cells, stem cell therapy is considered as a promising approach to intervene IDD owing to their capacity to release ncRNAs (94, 95). Shi and colleagues (96) found that bone marrow mesenchymal stem cells (BMSCs) enhanced the expression of autophagy-related genes and suppressed apoptosis-related genes in OGD NP cells through secreting miR-155, reducing NP cells apoptosis. Although they indicated that miRNA-derived from BMSCs probably afforded protective effects on NP cells *in vitro*, there is currently no *in vivo* evidence. Therefore, whether stem cells can improve IDD by ncRNAs needs further study. Intriguingly, a recent study demonstrated that BMSC-derived extracellular vesicles (BMSC-EVs) supported survival of NP cells and reduced ECM catabolism through circ_0050205/miR-665/GPX4 pathway in IDD mice (97). Hence, stem cell therapy may also be an effective strategy for treatment of IDD through ncRNAs.

Exosome

Exosome, a kind of extracellular vesicles secreted by the majority of cell types, contains numerous bioactive components involved in intercellular communication. Accumulating studies have paid attention to the role of exosomal ncRNAs in treatment of IDD (98, 99). For instance, Cheng and colleagues (100) demonstrated that MSC-derived exosomes (MSC-exosomes) could be taken by NP cells and exerted cytoprotective effects

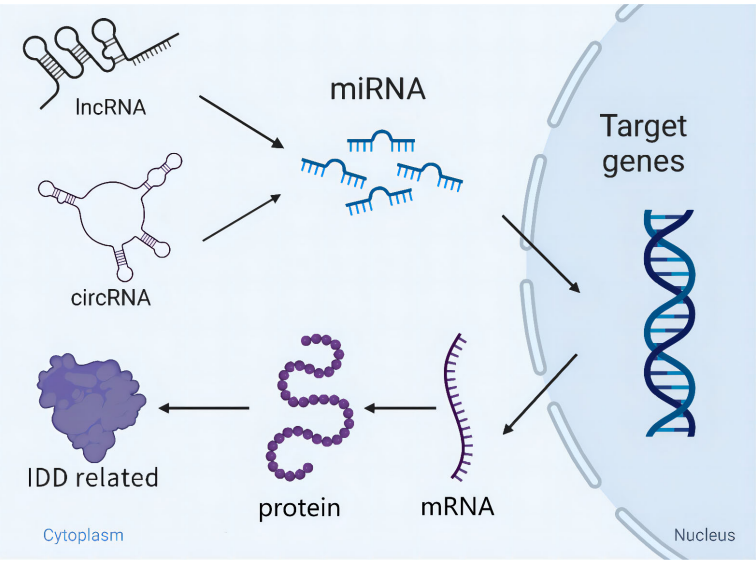

FIGURE 2
Schematic diagram of the cross-talk of miRNAs/lncRNAs/circRNAs orchestrating IDD development. LncRNAs/circRNAs directly sponge miRNAs and initiate a series of gene expression relating to IDD. Besides, miRNAs are able to modulate IDD independently through targeting key genes.

against NP cells apoptosis. This was likely to be mainly ascribed to activation of miR-21/PI3K/Akt signal pathway. In rat IDD model, the injection of MSC-exosomes reduced NP cells apoptosis and delayed IDD deterioration, showing the therapeutic potential of MSC exosomes in IDD. Recently, Chen et al. (101) also extracted exosomes from cartilage endplate stem cells (CESC-exosomes) and found that CESC-exosomes can suppress NP cells apoptosis and ECM degradation through delivery of miR-125-5p. Although exosomal ncRNAs show greatly therapeutic potential in treatment of IDD, obtaining highly purified exosomes in large quantities still requires further investigation. Hence, further study needs to be conducted to bail out current dilemma for clinical application.

Biomaterial

Biomaterial-based strategies have attracted increasing attention in the field of disc pro-regeneration (102, 103). Existing studies indicate that biomaterials have shown remarkable potential to arrest IDD owing to their unique biological properties including excellent biocompatibility and mechanical properties (103). Hydrogel, a particular biomaterial, is similar to the natural extracellular matrix and has been widely used to clinical trials. Feng and colleagues (104) designed a kind of polyplex micelle-encapsulated hydrogel that could encapsulate miR-29a and prevent miR-29a from spillage and degradation *in vivo*. In rabbit IDD models, the injection of miR-29a/polyplex reversed IDD through the suppression of MMP-2/β-catenin signal pathway. Lipid nanocapsules (LNC), as a particular carrier, can load and release certain miRNAs into cells. Regarding the point, miR-155-loaded LNC (miR-155 LNC) has been devised to evaluate the potential for treatment of IDD *in vitro* and *in vivo* (105). Intriguingly, their results showed that miR-155 LNC could be internalized in NP cells and maintain bioactivity. Moreover, *in vivo* experiments, injection of miR-155 LNC was proven to be safe and feasible. Unfortunately, they didn't further investigate the specific effects of miR-155 LNC on IDD progress. Collectively, biomaterials show great potential for treatment of IDD through delivery of ncRNAs.

Pharmacologic

At the present, pharmacological intervention is also considered as adjuvant therapy alternatives for IDD, such as traditional Chinese medicine (TCM) and natural products (106, 107). Notably, Yang et al. (108) found that aucubin, an active ingredient of eucommia ulmoides, could prevent the ECM degradation in human NP cells treated by IL-1β or TNF-α. Concomitantly, further experiments verified that miR-140/CREB1 signal pathway participated in aucubin-mediated

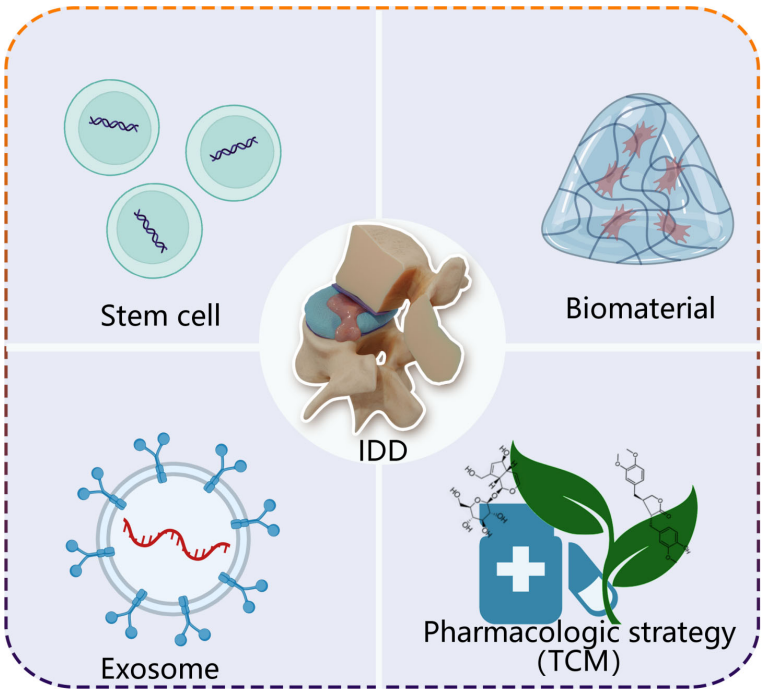

FIGURE 3
A simplified scheme of ncRNA-based therapeutics for treatment of IDD. Stem cell, exosome, biomaterial and pharmacologic strategy, as carries, deliver loading endogenous and exogenous ncRNAs to degenerative intervertebral disc tissue. TCM, traditional Chinese medicine.

protection against IDD (108). In addition, latest study demonstrated that arctigenin shared multiple roles in anti-IDD through up-regulating miR-483-3p, including reduction of NP cells apoptosis, ECM catabolism and inflammation-related genes expression (109). Consequently, these vitro findings afford a novel pharmacological strategy based on ncRNAs for treatment IDD. Although ncRNAs can be envisioned as pharmacological targets for the management of IDD, whether pharmacologic strategy-linked with ncRNAs exerts positive effects *in vivo* due to the complicated internal environment. Therefore, future study should focus on the *in vivo* effects and screen the determined ncRNAs for potential treatment of IDD.

Up to now, ncRNA-based therapeutics have made enormous progress, but present studies focused only on NP cells or rodents with IDD models. In fact, the biomechanical properties of intervertebral disc are obviously different between human and rodents. Therefore, it is essential to investigate the efficacy of ncRNA-based therapy in the IDD models conforming to the human biomechanical properties.

Prospects

Intervertebral disc degeneration is a main contributor to chronic low back pain. With regard to the pathological features, many factors involved in the progression of IDD, mainly focused on cells apoptosis, ECM metabolism and inflammation (9, 11). Increasing evidence have indicated that ncRNAs involve in the initiation and development of IDD, which hints the important potential of ncRNAs for IDD of treatment (110). In present review, we summarized the functions of ncRNAs in IDD and found that ncRNAs acted as pivotal regulators in the pathological process of IDD. On one hand, ncRNAs play positive roles in delaying or reversing IDD progression through inhibiting cells apoptosis, ECM catabolism and inflammatory cascades. On the other hand, ncRNAs also cause IDD deterioration by promoting cells apoptosis, ECM degradation and pro-inflammatory cytokines secretion. In addition, ncRNAs have exerted effects on IDD by regulating autophagy and ferroptosis. In fact, the ncRNAs to IDD is a double-edge sword, which depends on the downstream hub gene or signal pathway. Critically, multiple ncRNAs can regulate the same target genes or the different targets can be modulated by the same ncRNAs, like network, which jointly participates in IDD. Based on the existing evidence, ncRNAs have been attempted to manage the degenerative processes and shown positive efficacy though delivery of ncRNAs.

To our best knowledge, it is requisite for clinical application to develop drug targeting ncRNAs and conduct large-scale studies. Current studies demonstrate that a variety of ncRNAs are involved in the process of IDD (15, 80), but the decisive ncRNAs in IDD remain unclear. Furthermore, most studies still focused on the NP cells or IDD models. Therefore, ncRNAs-based therapy is still in the preclinical stage. Apart from clinical treatment, whether ncRNAs can be considered as clinical biomarkers for diagnosis is not fully elucidated, diagnosis of IDD at early stage is still challenging. In the future, research should pay more attention to the following aspects: i). the roles of ncRNAs should be explored in depth to better understand the underlying mechanisms of IDD; ii). screening of the ncRNAs with diagnostic value; iii). design of the IDD models that are similar to human biomechanical properties.

In conclusion, the present studies have demonstrated that ncRNAs are hub regulators mediating the onset and progression of IDD. In this review, we have systematically reviewed recent advances in related fields and summarized the role of ncRNAs in IDD. Further, we have discussed the ncRNAs-based strategy for treatment of IDD, which sheds light on the preface of switching theoretical strategy toward actually clinical application. Lastly, considering the current research advance in ncRNAs for treatment of IDD, we have analyzed the issues that need to be paid more attention in future research, producing meaningful ideas for next studies. Based on the aforementioned, ncRNAs, as novel therapeutic targets for IDD, may possess an excellent prospect. Comprehensive understanding the function of ncRNAs in IDD is critical for exploring biological therapies for treatment of IDD.

Author contributions

HY and DH conceived of the review and supervised the project. CJ, ZC and XW wrote the manuscript and drew figures. YZ and XG contributed to literature review and editing. ZX contributed to compiled table. All authors contributed to the article and approved the submitted version.

Funding

This work was supported by the National Natural Science Foundation of China (Grants No. 82071551 and 81830077).

Conflict of interest

The authors declare that the research was conducted in the absence of any commercial or financial relationships that could be construed as a potential conflict of interest.

Publisher's note

References

1. Suman A, Schaafsma F, Elders P, van Tulder M, Anema J. Cost-effectiveness of a multifaceted implementation strategy for the Dutch multidisciplinary guideline for nonspecific low back pain: Design of a stepped-wedge cluster randomised controlled trial. *BMC Public Health* (2015) 15:522. doi: 10.1186/s12889-015-1876-1

2. Vos T, Abajobir AA, Abbafati C, Abbas KM, Abate KH, Abd-Allah F, et al. Global, regional, and national incidence, prevalence, and years lived with disability for 328 diseases and injuries for 195 countries, 1990-2016: A systematic analysis for the global burden of disease study 2016. *Lancet* (2017) 390(10100):1211–59. doi: 10.1016/s0140-6736(17)32154-2

3. Guo H, Guo M, Wan Z, Song F, Wang H. Emerging evidence on noncoding-rna regulatory machinery in intervertebral disc degeneration: A narrative review. *Arthritis Res Ther* (2020) 22(1):270. doi: 10.1186/s13075-020-02353-2

4. Li Z, Li X, Chen C, Li S, Shen J, Tse G, et al. Long non-coding rnas in nucleus pulposus cell function and intervertebral disc degeneration. *Cell proliferation* (2018) 51(5):e12483. doi: 10.1111/cpr.12483

5. Luoma K, Riihimäki H, Luukkonen R, Raininko R, Viikari-Juntura E, Lamminen A. Low back pain in relation to lumbar disc degeneration. *Spine* (2000) 25(4):487–92. doi: 10.1097/00007632-200002150-00016

6. Cheung K, Karppinen J, Chan D, Ho D, Song Y, Sham P, et al. Prevalence and pattern of lumbar magnetic resonance imaging changes in a population study of one thousand forty-three individuals. *Spine* (2009) 34(9):934–40. doi: 10.1097/BRS.0b013e3181a01b3f

7. Jiang C, Yin S, Wei J, Zhao W, Wang X, Zhang Y, et al. Full-endoscopic posterior lumbar interbody fusion with epidural anesthesia: Technical note and initial clinical experience with one-year follow-up. *J Pain Res* (2021) 14:3815–26. doi: 10.2147/jpr.S338027

8. Setton L, Chen J. Mechanobiology of the intervertebral disc and relevance to disc degeneration. *J Bone Joint Surg Am volume* (2006) 88-A (Suppl 2):52–7. doi: 10.2106/jbjs.F.00001

9. Cazzanelli P, Wuertz-Kozak K. Micrornas in intervertebral disc degeneration, apoptosis, inflammation, and mechanobiology. *Int J Mol Sci* (2020) 21(10):3601. doi: 10.3390/ijms21103601

10. Kadow T, Sowa G, Vo N, Kang J. Molecular basis of intervertebral disc degeneration and herniations: What are the important translational questions? *Clin orthopaedics related Res* (2015) 473(6):1903–12. doi: 10.1007/s11999-014-3774-8

11. Wang C, Wang WJ, Yan YG, Xiang YX, Zhang J, Tang ZH, et al. Micrornas: New players in intervertebral disc degeneration. *Clin Chim Acta* (2015) 450:333–41. doi: 10.1016/j.cca.2015.09.011

12. Li Z, Chen X, Xu D, Li S, Chan M, Wu W. Circular rnas in nucleus pulposus cell function and intervertebral disc degeneration. *Cell proliferation* (2019) 52(6):e12704. doi: 10.1111/cpr.12704

13. Li Y, Zhou S, Peng P, Wang X, Du L, Huo Z, et al. Emerging role of circular rna in intervertebral disc degeneration: Knowns and unknowns (Review). *Mol Med Rep* (2020) 22(4):3057–65. doi: 10.3892/mmr.2020.11437

14. Zheng Y, Song G, Guo J, Su X, Chen Y, Yang Z, et al. Interactions among Lncrna/Circrna, mirna, and mrna in musculoskeletal degenerative diseases. *Front Cell Dev Biol* (2021) 9:753931. doi: 10.3389/fcell.2021.753931

15. Zou F, Ding Z, Jiang J, Lu F, Xia X, Ma X. Confirmation and preliminary analysis of circrnas potentially involved in human intervertebral disc degeneration. *Mol Med Rep* (2017) 16(6):9173–80. doi: 10.3892/mmr.2017.7718

16. Beermann J, Piccoli MT, Viereck J, Thum T. Non-coding rnas in development and disease: Background, mechanisms, and therapeutic approaches. *Physiol Rev* (2016) 96(4):1297–325. doi: 10.1152/physrev.00041.2015

17. Yao R-W, Wang Y, Chen L-L. Cellular functions of long noncoding rnas. *Nat Cell Biol* (2019) 21(5):542–51. doi: 10.1038/s41556-019-0311-8

18. Sherafatian M, Abdollahpour HR, Ghaffarpasand F, Yaghmaei S, Azadegan M, Heidari M. Microrna expression profiles, target genes, and pathways in intervertebral disk degeneration: A meta-analysis of 3 microarray studies. *World Neurosurg* (2019) 126:389–97. doi: 10.1016/j.wneu.2019.03.120

19. Ji ML, Jiang H, Zhang XJ, Shi PL, Li C, Wu H, et al. Preclinical development of a microrna-based therapy for intervertebral disc degeneration. *Nat Commun* (2018) 9(1):5051. doi: 10.1038/s41467-018-07360-1

20. Yang X, Liu H, Zhang Q, Liu K, Yu D, Zhang Y, et al. Mir-96 promotes apoptosis of nucleus pulpous cells by targeting Frs2. *Hum Cell* (2020) 33(4):1017–25. doi: 10.1007/s13577-020-00389-9

21. Zhang J, Liu R, Mo L, Liu C, Jiang J. Mir-4478 accelerates nucleus pulposus cells apoptosis induced by oxidative stress by targeting Mth1. *Spine* (2022). doi: 10.1097/brs.0000000000004486

22. Yan J, Wu LG, Zhang M, Fang T, Pan W, Zhao JL, et al. Mir-328-5p induces human intervertebral disc degeneration by targeting Wwp2. *Oxid Med Cell Longev* (2022) 2022:3511967. doi: 10.1155/2022/3511967

23. Yang W, Sun P. Downregulation of microrna-129-5p increases the risk of intervertebral disc degeneration by promoting the apoptosis of nucleus pulposus cells *Via* targeting Bmp2. *J Cell Biochem* (2019) 120(12):19684–90. doi: 10.1002/jcb.29274

24. Zhong H, Zhou Z, Guo L, Liu F, Zheng B, Bi S, et al. The mir-623/Cxcl12 axis inhibits lps-induced nucleus pulposus cell apoptosis and senescence. *Mech Ageing Dev* (2021) 194:111417. doi: 10.1016/j.mad.2020.111417

25. Zhou X, Li J, Teng J, Liu Y, Zhang D, Liu L, et al. Microrna-155-3p attenuates intervertebral disc degeneration *Via* inhibition of Kdm3a and Hif1α. *Inflammation Res* (2021) 70(3):297–308. doi: 10.1007/s00011-021-01434-5

26. Zhao X, Xu B, Duan W, Chang L, Tan R, Sun Z, et al. Insights into exosome in the intervertebral disc: Emerging role for disc homeostasis and normal function. *Int J Med Sci* (2022) 19(11):1695–705. doi: 10.7150/ijms.75285

27. Grant MP, Epure LM, Bokhari R, Roughley P, Antoniou J, Mwale F. Human cartilaginous endplate degeneration is induced by calcium and the extracellular calcium-sensing receptor in the intervertebral disc. *Eur Cell Mater* (2016) 32:137–51. doi: 10.22203/ecm.v032a09

28. Chen H, Wang J, Hu B, Wu X, Chen Y, Li R, et al. Mir-34a promotes fas-mediated cartilage endplate chondrocyte apoptosis by targeting bcl-2. *Mol Cell Biochem* (2015) 406(1-2):21–30. doi: 10.1007/s11010-015-2420-4

29. Liu MH, Sun C, Yao Y, Fan X, Liu H, Cui YH, et al. Matrix stiffness promotes cartilage endplate chondrocyte calcification in disc degeneration *Via* mir-20a targeting ankh expression. *Sci Rep* (2016) 6:25401. doi: 10.1038/srep25401

30. Sheng B, Yuan Y, Liu X, Zhang Y, Liu H, Shen X, et al. Protective effect of estrogen against intervertebral disc degeneration is attenuated by mir-221 through targeting estrogen receptor α. *Acta Biochim Biophys Sin (Shanghai)* (2018) 50(4):345–54. doi: 10.1093/abbs/gmy017

31. Wang B, Ji D, Xing W, Li F, Huang Z, Zheng W, et al. Mir-142-3p and Hmgb1 are negatively regulated in proliferation, apoptosis, migration, and autophagy of cartilage endplate cells. *Cartilage* (2021) 13(2_suppl):592s–603s. doi: 10.1177/19476035211012444

32. Hai B, Ma Y, Pan X, Yong L, Liang C, He G, et al. Melatonin benefits to the growth of human annulus fibrosus cells through inhibiting mir-106a-5p/Atg7 signaling pathway. *Clin Interv Aging* (2019) 14:621–30. doi: 10.2147/cia.S193765

33. Wang XQ, Tu WZ, Guo JB, Song G, Zhang J, Chen CC, et al. A bioinformatic analysis of micrornas' role in human intervertebral disc degeneration. *Pain Med* (2019) 20(12):2459–71. doi: 10.1093/pm/pnz015

34. Hua WB, Wu XH, Zhang YK, Song Y, Tu J, Kang L, et al. Dysregulated mir-127-5p contributes to type ii collagen degradation by targeting matrix metalloproteinase-13 in human intervertebral disc degeneration. *Biochimie* (2017) 139:74–80. doi: 10.1016/j.biochi.2017.05.018

35. Wang C, Zhang ZZ, Yang W, Ouyang ZH, Xue JB, Li XL, et al. Mir-210 facilitates ecm degradation by suppressing autophagy *Via* silencing of Atg7 in human degenerated Np cells. *BioMed Pharmacother* (2017) 93:470–9. doi: 10.1016/j.biopha.2017.06.048

36. Wang WJ, Yang W, Ouyang ZH, Xue JB, Li XL, Zhang J, et al. Mir-21 promotes ecm degradation through inhibiting autophagy *Via* the Pten/Akt/Mtor signaling pathway in human degenerated Np cells. *BioMed Pharmacother* (2018) 99:725–34. doi: 10.1016/j.biopha.2018.01.154

37. Chujo T, An HS, Akeda K, Miyamoto K, Muehleman C, Attawia M, et al. Effects of growth differentiation factor-5 on the intervertebral disc–*in vitro* bovine study and in vivo rabbit disc degeneration model study. *Spine (Phila Pa 1976)* (2006) 31(25):2909–17. doi: 10.1097/01.brs.0000248428.22823.86

38. Lv B, Gan W, Cheng Z, Wu J, Chen Y, Zhao K, et al. Current insights into the maintenance of structure and function of intervertebral disc: A review of the regulatory role of growth and differentiation factor-5. *Front Pharmacol* (2022) 13:842525. doi: 10.3389/fphar.2022.842525

39. Liu W, Xia P, Feng J, Kang L, Huang M, Wang K, et al. Microrna-132 upregulation promotes matrix degradation in intervertebral disc degeneration. *Exp Cell Res* (2017) 359(1):39–49. doi: 10.1016/j.yexcr.2017.08.011

40. Tan H, Zhao L, Song R, Liu Y, Wang L. Microrna-665 promotes the proliferation and matrix degradation of nucleus pulposus through targeting Gdf5 in intervertebral disc degeneration. *J Cell Biochem* (2018) 119(9):7218–25. doi: 10.1002/jcb.26888

41. Gruber HE, Norton HJ, Ingram JA, Hanley ENJr. The Sox9 transcription factor in the human disc: Decreased immunolocalization with age and disc degeneration *Spine* (2005) 30(6):625–30 doi: 10.1097/01.brs.0000155420.01444.c6

42. Lv J, Li S, Wan T, Yang Y, Cheng Y, Xue R. Inhibition of microrna-30d attenuates the apoptosis and extracellular matrix degradation of degenerative human nucleus pulposus cells by up-regulating Sox9. *Chem Biol Interact* (2018) 296:89–97. doi: 10.1016/j.cbi.2018.09.010

43. Sun JC, Zheng B, Sun RX, Meng YK, Wang SM, Yang HS, et al. Mir-499a-5p suppresses apoptosis of human nucleus pulposus cells and degradation of their extracellular matrix by targeting Sox4. *BioMed Pharmacother* (2019) 113:108652. doi: 10.1016/j.biopha.2019.108652

44. Wang J, Liu X, Sun B, Du W, Zheng Y, Sun Y. Upregulated mir-154 promotes ecm degradation in intervertebral disc degeneration. *J Cell Biochem* (2019). 120(7):11900–11907 doi: 10.1002/jcb.28471

45. Zhou J, Sun J, Markova DZ, Li S, Kepler CK, Hong J, et al. Microrna-145 overexpression attenuates apoptosis and increases matrix synthesis in nucleus pulposus cells. *Life Sci* (2019) 221:274–83. doi: 10.1016/j.lfs.2019.02.041

46. Chen S, Shi G, Zeng J, Li PH, Peng Y, Ding Z, et al. Mir-1260b protects against lps-induced degenerative changes in nucleus pulposus cells through targeting Tcf7l2. *Hum Cell* (2022) 35(3):779–91. doi: 10.1007/s13577-021-00655-4

47. Navone SE, Marfia G, Giannoni A, Beretta M, Guarnaccia L, Gualtierotti R, et al. Inflammatory mediators and signalling pathways controlling intervertebral disc degeneration. *Histol Histopathol* (2017) 32(6):523–42. doi: 10.14670/hh-11-846

48. Wuertz K, Vo N, Kletsas D, Boos N. Inflammatory and catabolic signalling in intervertebral discs: The roles of nf-κb and map kinases. *Eur Cell Mater* (2012) 23:103–19. doi: 10.22203/ecm.v023a08

49. O'Connell RM, Rao DS, Baltimore D. Microrna regulation of inflammatory responses. *Annu Rev Immunol* (2012) 30:295–312. doi: 10.1146/annurev-immunol-020711-075013

50. Liang H, Yang X, Liu C, Sun Z, Wang X. Effect of nf-kb signaling pathway on the expression of mif, tnf-α, il-6 in the regulation of intervertebral disc degeneration. *J Musculoskelet Neuronal Interact* (2018) 18(4):551–6.

51. Du K, He X, Deng J. Microrna-16 inhibits the lipopolysaccharide-induced inflammatory response in nucleus pulposus cells of the intervertebral disc by targeting Tab3. *Arch Med Sci* (2021) 17(2):500–13. doi: 10.5114/aoms.2018.74950

52. Wang H, Hao P, Zhang H, Xu C, Zhao J. Microrna-223 inhibits lipopolysaccharide-induced inflammatory response by directly targeting Irak1 in the nucleus pulposus cells of intervertebral disc. *IUBMB Life* (2018) 70(6):479–90. doi: 10.1002/iub.1747

53. Zhang S, Song S, Zhuang Y, Hu J, Cui W, Wang X, et al. Role of microrna-15a-5p/Sox9/Nf-κb axis in inflammatory factors and apoptosis of murine nucleus pulposus cells in intervertebral disc degeneration. *Life Sci* (2021) 277:119408. doi: 10.1016/j.lfs.2021.119408

54. Dong W, Liu J, Lv Y, Wang F, Liu T, Sun S, et al. Mir-640 aggravates intervertebral disc degeneration *Via* nf-κb and wnt signalling pathway. *Cell Prolif* (2019) 52(5):e12664. doi: 10.1111/cpr.12664

55. Zhang HJ, Liao HY, Bai DY, Wang ZQ, Xie XW. Mapk /Erk signaling pathway: A potential target for the treatment of intervertebral disc degeneration. *BioMed Pharmacother* (2021) 143:112170. doi: 10.1016/j.biopha.2021.112170

56. Sun Y, Shi X, Peng X, Li Y, Ma H, Li D, et al. Microrna-181a exerts anti-inflammatory effects *Via* inhibition of the erk pathway in mice with intervertebral disc degeneration. *J Cell Physiol* (2020) 235(3):2676–86. doi: 10.1002/jcp.29171

57. Jia M, Dahlman-Wright K, Gustafsson J. Estrogen receptor alpha and beta in health and disease. *Best Pract Res Clin Endocrinol Metab* (2015) 29(4):557–68. doi: 10.1016/j.beem.2015.04.008

58. Cai Z, Li K, Yang K, Luo D, Xu H. Suppression of mir-203-3p inhibits lipopolysaccharide induced human intervertebral disc inflammation and degeneration through upregulating estrogen receptor α. *Gene Ther* (2020) 27 (9):417–26. doi: 10.1038/s41434-019-0118-z

59. Chen Z, Han Y, Deng C, Chen W, Jin L, Chen H, et al. Inflammation-dependent downregulation of mir-194-5p contributes to human intervertebral disc degeneration by targeting Cul4a and Cul4b. *J Cell Physiol* (2019) 234(11):19977–89. doi: 10.1002/jcp.28595

60. Jie J, Xu X, Li W, Wang G. Regulation of apoptosis and inflammatory response in interleukin-1β-Induced nucleus pulposus cells by mir-125b-5p *Via* targeting Triap1. *Biochem Genet* (2021) 59(2):475–90. doi: 10.1007/s10528-020-10009-8

61. Chen J, Sun Q, Liu GZ, Zhang F, Liu CY, Yuan QM, et al. Effect of mir-202-5p-Mediated Atg7 on autophagy and apoptosis of degenerative nucleus pulposus cells. *Eur Rev Med Pharmacol Sci* (2020) 24(2):517–25. doi: 10.26355/eurrev_202001_20027

62. Wu T, Jia X, Zhu Z, Guo K, Wang Q, Gao Z, et al. Inhibition of mir-130b-3p restores autophagy and attenuates intervertebral disc degeneration through mediating Atg14 and Prkaa1. *Apoptosis* (2022) 27(5-6):409–25. doi: 10.1007/s10495-022-01725-0

63. Bin S, Xin L, Lin Z, Jinhua Z, Rui G, Xiang Z. Targeting mir-10a-5p/Il-6r axis for reducing il-6-Induced cartilage cell ferroptosis. *Exp Mol Pathol* (2021) 118:104570. doi: 10.1016/j.yexmp.2020.104570

64. Li Y, Pan D, Wang X, Huo Z, Wu X, Li J, et al. Silencing Atf3 might delay tbhp-induced intervertebral disc degeneration by repressing npc ferroptosis, apoptosis, and ecm degradation. *Oxid Med Cell Longev* (2022) 2022:4235126. doi: 10.1155/2022/4235126

65. Brosnan CA, Voinnet O. The long and the short of noncoding rnas. *Curr Opin Cell Biol* (2009) 21(3):416–25. doi: 10.1016/j.ceb.2009.04.001

66. Zhao B, Lu M, Wang D, Li H, He X. Genome-wide identification of long noncoding rnas in human intervertebral disc degeneration by rna sequencing. *BioMed Res Int* (2016) 2016:3684875. doi: 10.1155/2016/3684875

67. Gao D, Hao L, Zhao Z. Long non-coding rna Part1 promotes intervertebral disc degeneration through regulating the mir–93/Mmp2 pathway in nucleus pulposus cells. *Int J Mol Med* (2020) 46(1):289–99. doi: 10.3892/ijmm.2020.4580

68. Zhong H, Zhou Z, Guo L, Liu FS, Wang X, Li J, et al. Serpina1 is a hub gene associated with intervertebral disc degeneration grade and affects the nucleus pulposus cell phenotype through the adirf-As1/Mir-214-3p axis. *Transl Res* (2022) 245:99–116. doi: 10.1016/j.trsl.2022.02.006

69. Yu X, Liu Q, Wang Y, Bao Y, Jiang Y, Li M, et al. Depleted long noncoding rna Gas5 relieves intervertebral disc degeneration *Via* microrna-17-3p/Ang-2. *Oxid Med Cell Longev* (2022) 2022:1792412. doi: 10.1155/2022/1792412

70. Liao ZW, Fan ZW, Huang Y, Liang CY, Liu C, Huang S, et al. Long non-coding rna Mt1dp interacts with mir-365 and induces apoptosis of nucleus pulposus cells by repressing nrf-2-Induced anti-oxidation in lumbar disc herniation. *Ann Transl Med* (2021) 9(2):151. doi: 10.21037/atm-20-8123

71. Jiang X, Chen D. Lncrna Fam83h-As1 maintains intervertebral disc tissue homeostasis and attenuates inflammation-related pain *Via* promoting nucleus pulposus cell growth through mir-22-3p inhibition. *Ann Transl Med* (2020) 8 (22):1518. doi: 10.21037/atm-20-7056

72. Zhang CY, Hu XC, Zhang GZ, Liu MQ, Chen HW, Kang XW. Role of Nrf2 and ho-1 in intervertebral disc degeneration. *Connect Tissue Res* (2022) 63(6):559–76. doi: 10.1080/03008207.2022.2089565

73. Xiang Q, Zhao Y, Lin J, Jiang S, Li W. The Nrf2 antioxidant defense system in intervertebral disc degeneration: Molecular insights. *Exp Mol Med* (2022) 54 (8):1067–75. doi: 10.1038/s12276-022-00829-6

74. Kang L, Tian Y, Guo X, Chu X, Xue Y. Long noncoding rna anpodrt overexpression protects nucleus pulposus cells from oxidative stress and apoptosis by activating Keap1-Nrf2 signaling. *Oxid Med Cell Longev* (2021) 2021:6645005. doi: 10.1155/2021/6645005

75. Zhan S, Wang K, Xiang Q, Song Y, Li S, Liang H, et al. Lncrna hotair upregulates autophagy to promote apoptosis and senescence of nucleus pulposus cells. *J Cell Physiol* (2020) 235(3):2195–208. doi: 10.1002/jcp.29129

76. Zhan S, Wang K, Song Y, Li S, Yin H, Luo R, et al. Long non-coding rna hotair modulates intervertebral disc degenerative changes *Via* Wnt/β-catenin pathway. *Arthritis Res Ther* (2019) 21(1):201. doi: 10.1186/s13075-019-1986-8

77. Gao ZX, Lin YC, Wu ZP, Zhang P, Cheng QH, Ye LH, et al. Lncrna Snhg6 can regulate the proliferation and apoptosis of rat degenerate nucleus pulposus cells *Via* regulating the expression of mir-101-3p. *Eur Rev Med Pharmacol Sci* (2020) 24 (16):8251–62. doi: 10.26355/eurrev_202008_22621

78. Yang W, Huang XD, Zhang T, Zhou YB, Zou YC, Zhang J. Lncrna Mir155hg functions as a cerna of mir-223-3p to promote cell pyroptosis in human degenerative Np cells. *Clin Exp Immunol* (2022) 207(2):241–52. doi: 10.1093/cei/uxab030

79. Sun Z, Tang X, Wang H, Sun H, Chu P, Sun L, et al. Lncrna H19 aggravates intervertebral disc degeneration by promoting the autophagy and apoptosis of nucleus pulposus cells through the mir-139/Cxcr4/Nf-κb axis. *Stem Cells Dev* (2021) 30(14):736–48. doi: 10.1089/scd.2021.0009

80. Xu D, Ma X, Sun C, Han J, Zhou C, Wong SH, et al. Circular rnas in intervertebral disc degeneration: An updated review. *Front Mol Biosci* (2021) 8:781424. doi: 10.3389/fmolb.2021.781424

81. Cheng X, Zhang L, Zhang K, Zhang G, Hu Y, Sun X, et al. Circular rna Vma21 protects against intervertebral disc degeneration through targeting mir-200c and X linked inhibitor-of-Apoptosis protein. *Ann Rheum Dis* (2018) 77 (5):770–9. doi: 10.1136/annrheumdis-2017-212056

82. Guo W, Zhang B, Mu K, Feng SQ, Dong ZY, Ning GZ, et al. Circular rna Grb10 as a competitive endogenous rna regulating nucleus pulposus cells death in degenerative intervertebral disk. *Cell Death Dis* (2018) 9(3):319. doi: 10.1038/s41419-017-0232-z

83. Xiang Q, Kang L, Wang J, Liao Z, Song Y, Zhao K, et al. Circrna-cidn mitigated compression loading-induced damage in human nucleus pulposus cells *Via* mir-34a-5p/Sirt1 axis. *EBioMedicine* (2020) 53:102679. doi: 10.1016/j.ebiom.2020.102679

84. Chen Z, Zhang W, Deng M, Li Y, Zhou Y. Circglce alleviates intervertebral disc degeneration by regulating apoptosis and matrix degradation through the targeting of mir-587/Stap1. *Aging (Albany NY)* (2020) 12(21):21971–91. doi: 10.18632/aging.104035

85. Wang H, Zhu Y, Cao L, Guo Z, Sun K, Qiu W, et al. Circarl15 plays a critical role in intervertebral disc degeneration by modulating mir-431-5p/Disc1. *Front Genet* (2021) 12:669598. doi: 10.3389/fgene.2021.669598

86. Cui S, Zhang L. Circ_001653 silencing promotes the proliferation and ecm synthesis of npcs in idd by downregulating mir-486-3p-Mediated cemip. *Mol Ther Nucleic Acids* (2020) 20:385–99. doi: 10.1016/j.omtn.2020.01.026

87. Zhang F, Lin F, Xu Z, Huang Z. Circular rna itch promotes extracellular matrix degradation *Via* activating Wnt/β-catenin signaling in intervertebral disc degeneration. *Aging* (2021) 13(10):14185–97. doi: 10.18632/aging.203036

88. Wang H, He P, Pan H, Long J, Wang J, Li Z, et al. Circular rna circ-4099 is induced by tnf-α and regulates ecm synthesis by blocking mir-616-5p inhibition of Sox9 in intervertebral disc degeneration. *Exp Mol Med* (2018) 50(4):1–14. doi: 10.1038/s12276-018-0056-7

89. Wang X, Wang B, Zou M, Li J, Lü G, Zhang Q, et al. Circsema4b targets mir-431 modulating il-1β-Induced degradative changes in nucleus pulposus cells in intervertebral disc degeneration *Via* wnt pathway. *Biochim Biophys Acta Mol Basis Dis* (2018) 1864(11):3754–68. doi: 10.1016/j.bbadis.2018.08.033

90. Song J, Wang HL, Song KH, Ding ZW, Wang HL, Ma XS, et al. Circularrna_104670 plays a critical role in intervertebral disc degeneration by functioning as a cerna. *Exp Mol Med* (2018) 50(8):1–12. doi: 10.1038/s12276-018-0125-y

91. Guo W, Mu K, Zhang B, Sun C, Zhao L, Dong ZY, et al. The circular rna Fam169a functions as a competitive endogenous rna and regulates intervertebral disc degeneration by targeting mir-583 and btrc. *Cell Death Dis* (2020) 11(5):315. doi: 10.1038/s41419-020-2543-8

92. Li Y, Wu X, Li J, Du L, Wang X, Cao J, et al. Circ_0004354 might compete with Circ_0040039 to induce npcs death and inflammatory response by targeting mir-345-3p-Faf1/Tp73 axis in intervertebral disc degeneration. *Oxid Med Cell Longev* (2022) 2022:2776440. doi: 10.1155/2022/2776440

93. Wang Z, Zhao Y, Liu Y, Qu Z, Zhuang X, Song Q, et al. Circ0007042 alleviates intervertebral disc degeneration by adsorbing mir-369 to upregulate Bmp2 and activate the Pi3k/Akt pathway. *Arthritis Res Ther* (2022) 24(1):214. doi: 10.1186/s13075-022-02895-7

94. Vadalà G, Ambrosio L, Russo F, Papalia R, Denaro V. Interaction between mesenchymal stem cells and intervertebral disc microenvironment: From cell therapy to tissue engineering. *Stem Cells Int* (2019) 2019:2376172. doi: 10.1155/2019/2376172

95. Zhang W, Sun T, Li Y, Yang M, Zhao Y, Liu J, et al. Application of stem cells in the repair of intervertebral disc degeneration. *Stem Cell Res Ther* (2022) 13(1):70. doi: 10.1186/s13287-022-02745-y

96. Shi M, Zhao Y, Sun Y, Xin D, Xu W, Zhou B. Therapeutic effect of Co-culture of rat bone marrow mesenchymal stem cells and degenerated nucleus pulposus cells on intervertebral disc degeneration. *Spine J* (2021) 21(9):1567–79. doi: 10.1016/j.spinee.2021.05.007

97. Yu XJ, Liu QK, Lu R, Wang SX, Xu HR, Wang YG, et al. Bone marrow mesenchymal stem cell-derived extracellular vesicles carrying Circ_0050205 attenuate intervertebral disc degeneration. *Oxid Med Cell Longev* (2022) 2022:8983667. doi: 10.1155/2022/8983667

98. Widjaja G, Jalil AT, Budi HS, Abdelbasset WK, Efendi S, Suksatan W, et al. Mesenchymal Stromal/Stem cells and their exosomes application in the treatment of intervertebral disc disease: A promising frontier. *Int Immunopharmacol* (2022) 105:108537. doi: 10.1016/j.intimp.2022.108537

99. Li Z, Wu Y, Tan G, Xu Z, Xue H. Exosomes and exosomal mirnas: A new therapy for intervertebral disc degeneration. *Front Pharmacol* (2022) 13:992476. doi: 10.3389/fphar.2022.992476

100. Cheng X, Zhang G, Zhang L, Hu Y, Zhang K, Sun X, et al. Mesenchymal stem cells deliver exogenous mir-21 *Via* exosomes to inhibit nucleus pulposus cell apoptosis and reduce intervertebral disc degeneration. *J Cell Mol Med* (2018) 22 (1):261–76. doi: 10.1111/jcmm.13316

101. Chen D, Jiang X. Exosomes-derived mir-125-5p from cartilage endplate stem cells regulates autophagy and ecm metabolism in nucleus pulposus by targeting Suv38h1. *Exp Cell Res* (2022) 414(1):113066. doi: 10.1016/j.yexcr.2022.113066

102. Bowles RD, Setton LA. Biomaterials for intervertebral disc regeneration and repair. *Biomaterials* (2017) 129:54–67. doi: 10.1016/j.biomaterials.2017.03.013

103. Li C, Bai Q, Lai Y, Tian J, Li J, Sun X, et al. Advances and prospects in biomaterials for intervertebral disk regeneration. *Front Bioeng Biotechnol* (2021) 9:766087. doi: 10.3389/fbioe.2021.766087

104. Feng G, Zha Z, Huang Y, Li J, Wang Y, Ke W, et al. Sustained and bioresponsive two-stage delivery of therapeutic mirna *Via* polyplex micelle-loaded injectable hydrogels for inhibition of intervertebral disc fibrosis. *Adv Healthc Mater* (2018) 7(21):e1800623. doi: 10.1002/adhm.201800623

105. Le Moal B, Lepeltier É, Rouleau D, Le Visage C, Benoit JP, Passirani C, et al. Lipid nanocapsules for intracellular delivery of microrna: A first step towards intervertebral disc degeneration therapy. *Int J Pharm* (2022) 624:121941. doi: 10.1016/j.ijpharm.2022.121941

106. Zhu L, Yu C, Zhang X, Yu Z, Zhan F, Yu X, et al. The treatment of intervertebral disc degeneration using traditional Chinese medicine. *J Ethnopharmacol* (2020) 263:113117. doi: 10.1016/j.jep.2020.113117

107. Chen HW, Zhang GZ, Liu MQ, Zhang LJ, Kang JH, Wang ZH, et al. Natural products of pharmacology and mechanisms in nucleus pulposus cells and intervertebral disc degeneration. *Evid Based Complement Alternat Med* (2021) 2021:9963677. doi: 10.1155/2021/9963677

108. Yang S, Li L, Zhu L, Zhang C, Li Z, Guo Y, et al. Aucubin inhibits il-1β- or tnf-α-Induced extracellular matrix degradation in nucleus pulposus cell through blocking the mir-140-5p/Creb1 axis. *J Cell Physiol* (2019) 234(8):13639–48. doi: 10.1002/jcp.28044

109. Ji Z, Guo R, Ma Z, Li H. Arctigenin inhibits apoptosis, extracellular matrix degradation, and inflammation in human nucleus pulposus cells by up-regulating mir-483-3p. *J Clin Lab Anal* (2022) 36(7):e24508. doi: 10.1002/jcla.24508

110. Zhang H, Zhang M, Meng L, Guo M, Piao M, Huang Z, et al. Investigation of key mirnas and their target genes involved in cell apoptosis during intervertebral disc degeneration development using bioinformatics methods. *J Neurosurg Sci* (2022) 66(2):125–32. doi: 10.23736/s0390-5616.20.04773-6

frontiers | Frontiers in Endocrinology

TYPE Original Research
PUBLISHED 06 February 2023
DOI 10.3389/fendo.2023.1089796

OPEN ACCESS

EDITED BY
Shibao Lu,
Xuanwu Hospital, Capital Medical University, China

REVIEWED BY
Chensheng Qiu,
Medical College of Wisconsin, United States
Yuan Xue,
Tianjin Medical University General Hospital, China

*CORRESPONDENCE
Weishi Li
puh3liweishi@bjmu.edu.cn

†These authors have contributed equally to this work

SPECIALTY SECTION
This article was submitted to Bone Research, a section of the journal Frontiers in Endocrinology

RECEIVED 04 November 2022
ACCEPTED 04 January 2023
PUBLISHED 06 February 2023

CITATION
Xiang Q, Zhao Y and Li W (2023) Identification and validation of ferroptosis-related gene signature in intervertebral disc degeneration.
Front. Endocrinol. 14:1089796.
doi: 10.3389/fendo.2023.1089796

Identification and validation of ferroptosis-related gene signature in intervertebral disc degeneration

Qian Xiang[1,2,3†], Yongzhao Zhao[1,2,3†] and Weishi Li[1,2,3*]

[1]Department of Orthopaedics, Peking University Third Hospital, Beijing, China, [2]Beijing Key Laboratory of Spinal Disease Research, Beijing, China, [3]Engineering Research Center of Bone and Joint Precision Medicine, Ministry of Education, Beijing, China

Lower back pain (LBP) is a leading cause of disability in the elderly and intervertebral disc degeneration (IDD) is the major contributor to LBP. Ferroptosis is a newly discovered programmed cell death, characterized by iron-dependent lethal lipid peroxidation. Growing evidence has shown that ferroptosis plays important roles in various human diseases. However, the underlying mechanism of ferroptosis in IDD remains elusive. This study is aimed to uncover the key roles of ferroptosis in the pathogenesis and progression of IDD comprehensively. To investigate the ferroptosis related differentially expressed genes (FRDEGs) in IDD, we analyzed the microarray data from the Gene Expression Omnibus (GEO) database. Then we performed functional enrichment analysis and protein-protein interaction (PPI) network analysis, and screened out the hub FRDEGs. To further evaluate the predictive value of these hub FRDEGs, we performed ROC analysis based on the GSE124272 dataset. A total of 80 FRDEGs were identified, including 20 downregulated and 60 upregulated FRDEGs. The FRDEGs were primarily involved in the biological processes of response to chemical, and response to stress. KEGG pathway enrichment analysis showed that the FRDEGs were mainly involved in ferroptosis, TNF signaling pathway, HIF-1 signaling pathway, NOD-like receptor signaling pathway, and IL-17 signaling pathway. Ten hub OSRDEGs were obtained according to the PPI analysis, including *HMOX1, KEAP1, MAPK1, HSPA5, TXNRD1, IL6, PPARA, JUN, HIF1A, DUSP1*. The ROC analysis and RT-qPCR validation results suggested that most of the hub FRDEGs might be potential signature genes for IDD. This study reveals that ferroptosis might provide promising strategy for the diagnosis and treatment of IDD.

KEYWORDS

lower back pain, intervertebral disc degeneration, nucleus pulposus, ferroptosis, oxidative stress

1 Introduction

Lower back pain (LBP), a common musculoskeletal problem, is one of the leading causes of disability in the elderly worldwide (1, 2). It is acknowledged by a number of reports that the major contributor to LBP is intervertebral disc degeneration (IDD) (3, 4). Physiologically, the intervertebral disc (IVD) is an avascular structure of the human body in adults. The IVD is composed of three distinct regions, including the internal nucleus pulposus (NP), the peripheral annulus fibrosus (AF), and the inferior and superior cartilaginous endplates (CEP), with characterized cell types in each region respectively. Pathologically, the pathogenesis and progression of IDD is promoted by various and complicated factors, including aging, oxidative stress, inflammation, and mechanical stress, *etc.* The IDD process is characterized of degeneration of the NP, rapture of the AF, and calcification of the CEP (5, 6). However, the specific molecular mechanisms of disc degeneration remain elusive currently.

Ferroptosis is a newly discovered mode of regulated cell death, which differs from apoptosis, necrosis, and autophagy in morphological, biochemical, and genetic aspects (7). The cells that undergo ferroptosis have distinctive morphological characteristics, including cell membrane disruption and vesiculation, mitochondrial shrinkage with lessened cristae, mitochondrial membrane condensation and outer membrane rupture (8). In mechanism, ferroptosis is typified by intracellular iron-dependent lipid peroxidation and reactive oxygen species (ROS) accumulation to lethal levels (8, 9). Ferroptosis is implicated in various biological activities, including iron homeostasis, lipid peroxidation metabolism, glutathione (GSH) metabolism (10). Ferroptosis is negatively regulated by glutathione peroxidase 4 (GPX4), which is responsible for scavenging intracellular lipid peroxide through GSH (7, 11). It has been reported that the suppression of GPX4 or inhibition of GSH can effectively induce ferroptosis (11). Ferroptosis is also regulated by some other critical pathways, such as p53 signaling, Nrf2 signaling, Hippo signaling as well as mitochondrial signaling pathway (12).

Growing evidence has suggested that ferroptosis is interrelated with multiple pathophysiological contexts, including cancer, degenerative diseases, diabetes, cardiovascular diseases, *etc* (13, 14). Moreover, it has been demonstrated that ferroptosis might be also associated with some skeletal diseases, including osteoarthritis, osteoporosis, as well as rheumatoid arthritis (15). Osteoarthritis (OA) is a common degenerative joint disorder worldwide, and ferroptosis has been shown to play regulating roles in the pathogenesis and progression of OA. Recently, Miao et al. found that ferroptosis existed in OA, during which the key regulator GPX4 played critical roles in the chondrocyte cell death and extracellular matrix (ECM) degradation (16). Furthermore, by using single cell RNA sequencing analysis, Lv et al. (17) identified an important ferroptosis-associated target named TRPV1 in OA. And TRPV1 activation could protect chondrocytes from ferroptosis and mitigate the development of OA *via* modulating GPX4. A recent study revealed that some specific ferroptosis-related genes could be promising biomarkers for osteoporosis diagnosis and interventions, including the *ER*, *VDR*, *IL-6*, *COL1A1*, *COL1A2*, and *PTH* (18). Besides, growing evidence has also found the involvement of ferroptosis in the pathogenesis of rheumatoid arthritis, and targeting ferroptosis could be a promising therapeutic strategy for inflammatory arthritis.

Growing evidence has demonstrated that iron overload, closely associated with ferroptosis, is a common phenomenon in the aging process (19, 20). Unexpectedly, recent studies have revealed that this special type of cell death might also be related to IDD, a very common degenerative musculoskeletal disease that progresses with age. In 2021, Zhang et al. (21) established the IDD animal models and found that the levels of iron and Heme Oxygenase 1 (HO-1) were obviously elevated, and the levels of ferritin light chain markedly decreased in IDD compared to control. More recently, a study reported that iron overload could be an independent risk factor for IDD and it promoted endplate degeneration and calcification through oxidative stress and ferroptosis (22). However, the underlying mechanism of ferroptosis in IDD remains elusive and still needs further investigations. In the current research work, we aimed to explore the key roles of ferroptosis in the pathogenesis and progression of IDD comprehensively by using mature and recognized bioinformatic analysis methods, and hope to provide novel diagnostic and therapeutic targets for IDD.

2 Materials and methods

2.1 Data collection

The data used in this study is available in the Gene Expression Omnibus (GEO) repository (https://www.ncbi.nlm.nih.gov/geo/), with an accession number of GSE56081 for the differentially expressed genes (DGEs) identification dataset. The GEO dataset GSE124272 was used as a validation analysis dataset. The GSE56081 dataset contained five degenerated disc NP tissues and five control NP tissues (23). The GSE124272 dataset contained whole blood samples obtained from eight patients with IDD and eight healthy controls (24). The ferroptosis related genes, including ferroptosis markers, ferroptosis drivers, ferroptosis suppressors and unclassified genes, were acquired from the FerrDb online database (http://www.zhounan.org/ferrdb/current/). This study was approved by the Ethics Committee of Peking University Third Hospital.

2.2 Determination of DEGs and ferroptosis related DEGs

The DGEs in IDD were acquired by using the R package "limma", and the criterions of identifying the DEGs were set as the fold change > 2 and the adjusted p value < 0.05. The FRDEGs were acquired by the intersection of DGEs based on GSE56081 and ferroptosis related genes based on FerrDb database by using the Venn diagram. Volcano plot of the DEGs, and hierarchical cluster heatmap of the FRDEGs were obtained by the R package "ggplot2".

2.3 Functional enrichment analysis

The Gene Ontology (GO) analysis and Kyoto Encyclopedia of Genes and Genomes (KEGG) analysis were conducted for the

FRDEGs and hub FRDEGs. The GO is an international standardized gene function classification system which is composed of three categories: biological process (BP), cell component (CC), as well as molecular function (MF). The GO analysis was conducted by the R package "clusterProfiler" (version 3.14.3) based on the GO annotations in R package "org.hs.eg.db" (version 3.1.0). The KEGG analysis was applied to determine related signaling pathways for FRDEGs. The KEGG analysis was conducted by the R package "clusterProfiler" (version 3.14.3) based on the latest KEGG pathway genes annotations, which were obtained from the KEGG rest API (https://www.kegg.jp/kegg/rest/keggapi.html). The corresponding item with a p value < 0.05 was considered statistically significant. The enriched items were plotted by using the R package "ggplot2".

2.4 Protein-protein interaction network analysis

The PPI network analysis of the FRDEGs was conducted based on the STRING database v11.5 (https://cn.string-db.org/), a commonly used tool to evaluate the protein-protein interactions. The protein interaction pairs with score > 0.40 were further imported to the Cytoscape software v3.2 (https://cytoscape.org/) to establish PPI network. In the PPI network, the nodes represented the FRDEGs enriched in the STRING database, and the edges (connections between nodes) represented the interactions between different FRDEGs. The PPI score was obtained by using the degree analysis method in the CytoHubba plug-in, and the top ten significantly connected nodes were selected as the hub FRDEGs for further analysis.

2.5 Correlation analysis among the hub FRDEGs

To evaluate the relationships among these hub FRDEGs, the correlations among the hub FRDEGs were conducted by using Pearson correlation analysis. In the Pearson's correlation analysis, the r value refers the correlation coefficient and was used to evaluate the effect size. And then the correlation matrix heatmap and the scatter plots were mapped by using the R package "ggplot2".

2.6 ROC analysis of the hub FRDEGs

Receiver operating characteristics (ROC) analysis was applied to obtain the area under the curve (AUC) values by using the R software package "pROC" (version 1.17.0.1). In brief, the gene expression of the corresponding hub FRDEGs was obtained according to the GEO dataset GSE124272. Then the roc function of "pROC" was applied for ROC analysis, and the ci function of "pROC" was used to evaluate AUC and confidence interval. In the ROC curve, the sensitivity values were plotted on the Y-axis, and the false positive rates (1-specificity) values were plotted on the X-axis. The ROC curve with an AUC value >= 0.70 was considered to indicate an adequate predictive value.

2.7 Cell viability analysis

The rat NP cells were treated with different concentrations (0, 25, 50, 75 μM) of tert-butyl hydroperoxide (TBHP, Sigma-Aldrich, St. Louis, MO, USA) for 24 h to establish an *in vitro* IDD cell model, as reported previously (25, 26). The cell viability of the rat NP cells was evaluated by the cell counting kit- (CCK-) 8 assay (Dojindo, Japan). In brief, the cells were seeded in 24-well plates and incubated for 24 h, and then treated with TBHP with different concentrations. Subsequently, 20 μL of CCK-8 solution was added to each well with 200 μL culture medium. The cells were then incubated at 37°C for 2 h, and then the absorbance signal at 450 nm was detected using the SpectraMax iD3 spectrophotometer (Molecular Devices).

2.8 RNA extraction and RT-qPCR

Total RNA from the rat NP cells in each group was isolated by the SteadyPure Universal RNA Extraction Kit (AG21017, Accurate Biology, China) following the manufacturer's instructions. RNA purity and concentration were determined by the DHS NanoPro 2020 spectrophotometer. Then the RNA was reverse-transcribed to cDNA by the Evo M-MLV Mix Kit with gDNA Clean for qPCR (AG11728, Accurate Biology, China). The qPCR assay was performed by using a SYBR Green Premix Pro Taq HS qPCR Kit (ROX Plus) (AG11718, Accurate Biology, China) with the QuantStudio 3 Real-Time PCR System (Applied Biosystems, USA). The qPCR conditions were set as follows: 95°C for 30 s, 40 cycles of 95°C for 5 s, and 60°C for 30 s; followed by a melt curve stage of 95°C for 15 s, 60°C for 1 min and 95°C for 15 s. Relative expression levels of genes was calculated by using the $2^{-\Delta\Delta CT}$ method and normalized to GAPDH. The primers used in the present study are listed as follows (5'-3'). HMOX1 FORWARD: GGGTCAGGTGTCCAGGGAAGG; HMOX1 REVERSE: TGGGTTCTGCTTGTTTCGCTCTATC; KEAP1 FORWARD: TGCTCAACCGCTTGCTGTATGC; KEAP1 REVERSE: TCATCCGCCACTCATTCCTCTCC; MAPK1 FORWARD: TGAAGACACAGCACCTCAGCAATG; MAPK1 REVERSE: GGTGTTCAGCAGGAGGTTGGAAG; HSPA5 FORWARD: CGGAGGAGGAGGACAAGAAGGAG; HSPA5 REVERSE: ATACGACGGTGTGATGCGGTTG; TXNRD1 FORWARD: CACGGATGAGGAGCAGACCAATG; TXNRD1 REVERSE: CATACAGCCTCTGAGCCAGCAATC; IL6 FORWARD: ACTTCCAGCCAGTTGCCTTCTTG; IL6 REVERSE: TGGTCTGTTGTGGGTGGTATCCTC; PPARA FORWARD: ACGATGCTGTCCTCCTTGATGAAC; PPARA REVERSE: ATGATGTCGCAGAATGGCTTCCTC; JUN FORWARD: GGAAACGACCTTCTACGACGATGC; JUN REVERSE: GGAGGTGCGGCTTCAGATTGC; HIF1A FORWARD: CCGCCACCACCACTGATGAATC; HIF1A REVERSE: GTGAGTACCACTGTATGCTGATGCC; DUSP1 FORWARD: GCCACCATCTGCCTTGCTTACC; DUSP1 REVERSE: GATAATACTCCGCCTCTGCTTCACG; GAPDH FORWARD: GACATGCCGCCTGGAGAAAC; GAPDH REVERSE: AGCCCAGGATGCCCTTTAGT.

2.9 Statistical analysis

The data in IDD cell model were analyzed by GraphPad Prism software and were presented as means ± standard deviation of three independent experiments. The difference between groups was analyzed by unpaired Student's t test. The correlation analysis among the hub FRDEGs was performed by Pearson analysis. A p value of less than 0.05 was considered to be statistically significant.

3 Results

3.1 Determination of the ferroptosis related differentially expressed genes

First, we screened out the differentially expressed genes (DGEs) in IDD compared to control based on GSE56081 dataset. The volcano plot showed there are 2269 DGEs in total, including 847 downregulated and 1422 upregulated genes (Figure 1A). Subsequently, we intersected the DGEs in IDD with the ferroptosis-related genes based on FerrDb database. A total of 80 ferroptosis related differentially expressed genes (FRDEGs) were determined, as presented in the Venn diagram (Figure 1B). Among these 80 FRDEGs, 20 were downregulated and 60 were upregulated, as shown in Table 1. The hierarchical cluster heatmap demonstrated that the expression of ferroptosis-related genes in IDD group was obviously different from that in control group (Figure 2).

3.2 GO and KEGG function analysis of the FRDEGs

The Gene Ontology (GO) is an international standardized gene function classification system which is commonly used to classify the predicted genes function. There are three main GO categories: biological process (BP), cellular component (CC), and molecular function (MF). As for the GO enrichment analysis for biological process, these FRDEGs are mainly involved in response to chemical, response to stress, and cellular response to chemical stimulus (Figure 3A). As shown in Figure 3B, the most significantly enriched GO items for cellular component are endomembrane system, vesicle, and extracellular region part. As for the molecular function, these FRDEGs are mainly involved in enzyme binding, transition metal ion binding, and oxidoreductase activity (Figure 3C). And then, we conducted the Kyoto Encyclopedia of Genes and Genomes (KEGG) analysis for the 80 FRDEGs. As indicated in Figure 3D, results show that the FRDEGs are primarily involved in the following significant pathways: Ferroptosis, TNF signaling pathway, HIF-1 signaling pathway, NOD-like receptor signaling pathway, and IL-17 signaling pathway, *etc.*

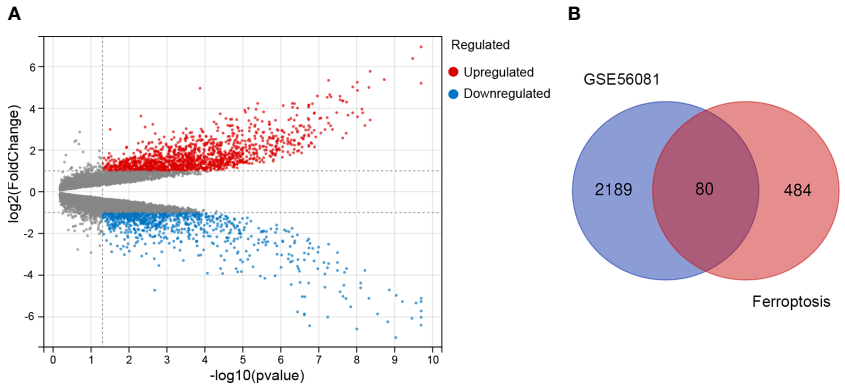

FIGURE 1
Identification of the differentially expressed genes between IDD and control groups. **(A)** The volcano plot of the differentially expressed genes in GSE56081 microarray data from the GEO database, in which the X-axis refers to the -$\log_{10}$(p value) and the Y-axis refers to the $\log_2$(fold change). The red dots represent the upregulated genes, and the blue dots represent the downregulated genes; the gray dots represent the genes without significant differential expression. **(B)** Venn diagram of the differentially expressed genes analyzed according to GSE56081 and the ferroptosis-related genes based on FerrDb database.

TABLE 1 A list of the 80 ferroptosis related differentially expressed genes (FRDEGs).

Gene symbols	Expression	Number
FADS2, PARP16, LGMN, MT1G, CXCL2, CDKN1A, CAMKK2, IL6, AQP8, KEAP1, PEBP1, ULK2, MMP13, FXN, PRR5, IFNA14, ENPP2, MGST1, TFAP2A, CS	Downregulated	20
HBA1, TXNRD1, ZFP36, CEBPG, CP, KLF2, TFR2, ATF4, TMBIM4, TGFB1, INTS2, NUPR1, TIMP1, SLC2A3, JUN, TRIB3, PRDX6, ATF2, MPC1, SNCA, MTDH, ARRDC3, HSPA5, MDM4, MAPK1, HMOX1, ECH1, CIRBP, ALOX15B, PDSS2, CHP1, ADAMTS13, FADS1, NR1D1, BLOC1S5-TXNDC5, EMC2, PML, FTH1, CA9, TNFAIP3, CYP4F8, COPZ1, KDM6B, HIF1A, MAP3K11, MLLT1, ANO6, DUOX1, YWHAE, ALDH3A2, PPARA, PHF21A, XBP1, DUSP1, TRIB2, VDAC2, SLC1A5, PCK2, CAPG, PRDX1	Upregulated	60

3.3 PPI analysis of the FRDEGs

The PPI network analysis was performed based on the STRING database and visualized by Cytoscape software (Figure 4A). Then we determined the top ten hub FRDEGs based on the PPI score, including HMOX1, KEAP1, MAPK1, HSPA5, TXNRD1, IL6, PPARA, JUN, HIF1A, and DUSP1, as shown in Figure 4B. Detailed information of these hub FRDEGs was presented in Table 2. Among these hub FRDEGs, KEAP1 and IL6 were downregulated in IDD, and the rest six hub genes were obviously upregulated. Most of these hub genes had either promoting or inhibiting effects on ferroptosis, and the potential roles of TXNRD1 on ferroptosis was not fully understand. Next, we performed Pearson correlation analysis to evaluate the relationships among these hub FRDEGs (Figure 4C). The most negatively related pair was KEAP1-MAPK1, and the most positively related pairs were HSPA5-JUN, HSPA5-TXNRD1, HSPA5-DUSP1, and DUSP1-JUN. The correlation analysis of HSPA5-JUN pair was presented in Figure 4D, with a r value of 0.99 and p value < 0.01. The correlation analysis of KEAP1-MAPK1 pair was shown in Figure 4E, with a r value of -0.93 and p value < 0.01.

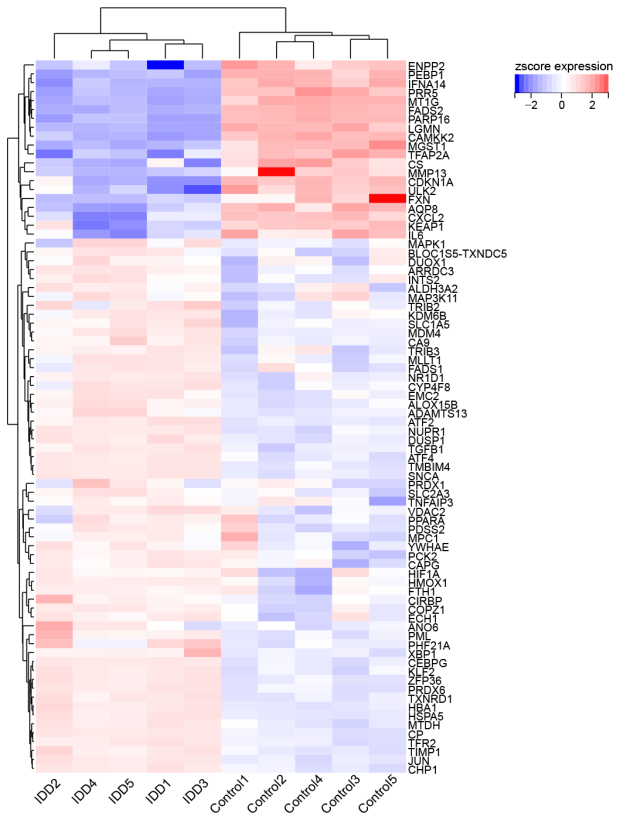

FIGURE 2
The hierarchical cluster heatmap of the 80 ferroptosis related differentially expressed genes (FRDEGs). The color scale indicates the relative gene expression of each sample. The red represents upregulated genes in IDD group compared to control, and the blue represents downregulated genes in IDD group. Among these FRDEGs, 20 FRDEGs are downregulated and 60 FRDEGs are upregulated.

3.4 Function analysis of the hub FRDEGs

To further investigate the potential molecular functions of the top ten hub FRDEGs, we performed functional and pathway enrichment analysis. As for the GO enrichment analysis in the category of biological process, these hub FRDEGs are mainly involved in response to oxidative stress, response to toxic substance, response to inorganic substance, and cellular response to oxidative stress (Figure 5A). In the category of cellular component, the most significantly enriched GO items include nuclear part, caveola, neuron projection cytoplasm, and plasma membrane raft (Figure 5B). In the molecular function, the FRDEGs are mainly associated with transcription factor binding, protein domain specific binding, enzyme binding, and ubiquitin protein ligase binding (Figure 5C). Subsequently, we performed KEGG pathway enrichment analysis for the ten hub genes. As shown in Figure 5D, it is suggested that the most meaningful and significantly enriched pathways include Th17 cell differentiation and HIF-1 signaling pathway.

3.5 The validation of hub FRDEGs in GSE124272 dataset

To evaluate the predictive value of these hub FRDEGs, we performed ROC analysis based on the GSE124272 dataset. The ROC curve reveals that the AUC values of six hub genes are greater than or equal to 0.70, including *KEAP1, MAPK1, HSPA5, TXNRD1, JUN*, and *HIF1A* (Figures 6A–J). The above data suggested that these six hub FRDEGs have potential predictive values for IDD.

3.6 Expression validation of hub FRDEGs in IDD cell model

To further validate the expression of theses hub FRDEGs in IDD, we established the IDD cell model by treating rat disc NP cells with TBHP. As shown in Figure 7A, the TBHP treatment for 24 h obviously inhibited the cell viability of rat NP cells in a dose-dependent manner, and the concentration of 75 μM was selected for subsequent experiments. Then we performed validation experiments for theses hub FRDEGs in the IDD cell model by RT-qPCR assay. As shown in Figures 7B–K, TBHP had significant effects on the mRNA expression levels of the hub FRDEGs. Compared to control group, the expression levels of HMOX1, KEAP1 and HSPA5 were downregulated in TBHP group, and the expression levels of IL6 and DUSP1 were upregulated in TBHP group.

4 Discussion

IDD is the one of the leading causes of LBP, which is a very common musculoskeletal disease and has brought a heavy healthcare burden and great socioeconomic cost globally (1–3). Ferroptosis is a newly discovered type of programmed cell death which is distinct from other types of cell death. More and more studies have demonstrated that ferroptosis is closely associated with multiple

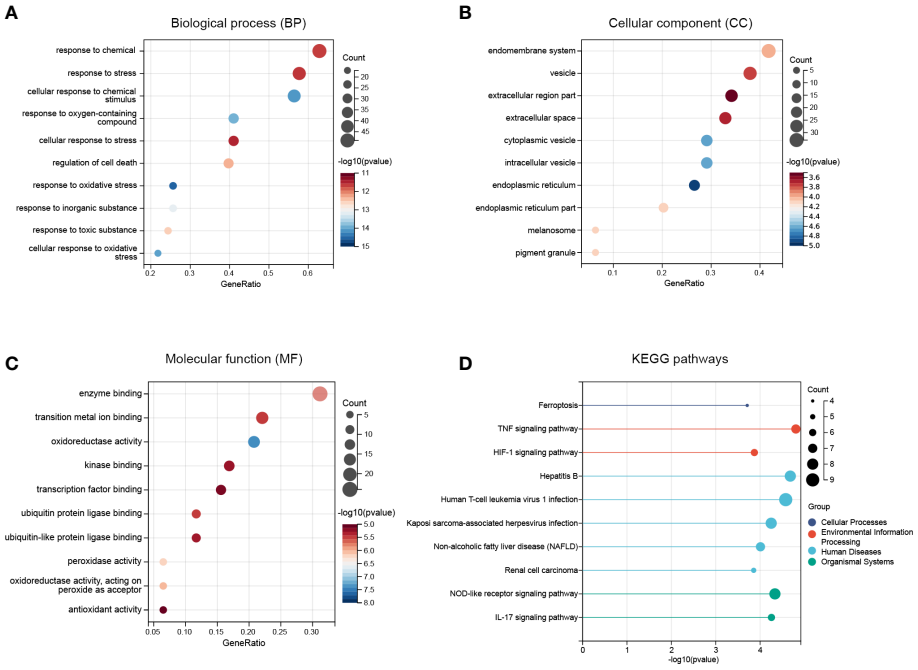

FIGURE 3
Functional enrichment analysis of the FRDEGs. **(A)** The top 10 significantly enriched GO terms in the category of biological process (BP) for the FRDEGs. **(B)** The top 10 significantly enriched GO terms in the category of cellular component (CC). **(C)** The top 10 significantly enriched GO terms in the category of molecular function (MF). **(D)** Kyoto Encyclopedia of Genes and Genomes (KEGG) pathway enrichment analysis for the FRDEGs.

human diseases, especially degenerative skeletal diseases, including osteoarthritis, osteoporosis, and inflammatory arthritis (15). Interestingly, ferroptosis might also be interrelated with the pathogenesis and progression of IDD. In the present research, we performed comprehensive bioinformatic analysis to uncover the significant roles of ferroptosis in IDD. Firstly, we screened out the DGEs in IDD according to the public datasets, including 847 downregulated genes and 1422 upregulated genes. Then we found that the expression of ferroptosis-related DGEs in IDD group was different from that in control group. We have identified 80 FRDEGs, including 20 downregulated FRDEGs and 60 upregulated FRDEGs.

In this research work, we conducted functional enrichment analysis to investigate the enriched GO items and significant pathways based on these FRDEGs. These FRDEGs are mainly related to response to chemical, response to stress, and cellular response to chemical stimulus, *etc.* It is worth noting that the FRDEGs are closely associated with several important pathways in IDD, including TNF signaling pathway, HIF-1 signaling pathway, and IL-17 signaling pathway. TNF-α, a member of the tumor necrosis factor (TNF) superfamily, was reported to be dysregulated in degenerated IVDs (27). Moreover, TNF signaling is deeply involved in various pathological process during IDD, including extracellular matrix (ECM) degradation, apoptosis, autophagy inflammatory responses (27). Hypoxia-inducible factors (HIFs) are transcription factors that that plays essential roles in the cellular response to low oxygen (28). The hypoxia inducible factor 1 subunit alpha (*HIF1A*), one of the key FRDEGs identified in this study, was reported to be decreased with the disc degeneration and participated in the IDD process through interacting with autophagy (29). However, another research work by Wang et al. (30) demonstrated that HIF1A expression was dysregulated in cartilaginous endplate and annulus fibrosus tissues of IDD patients and mouse models. They also found that aberrant activation of HIF1A in EP and AF tissues was a pathological factor for DDD, and inhibition of its aberrant activation prevented the IDD development in animal models. Interleukin-17 (IL-17), namely IL-17A, is a key cytokine of IL-17 family and is primarily secreted by T helper 17 (Th17) cells. IL-17 can trigger various signal pathways to exert regulating effects on mammalian cells (31, 32). Importantly, the expression of IL-17 was positively correlated the degree of IDD, and it could promote the IDD progression by regulating ECM metabolism, inflammatory responses, neo-angiogenesis, and NP cell autophagy and proliferation (33). It is suggested that the FRDEGs might play roles in regulating these critical signaling pathways during IDD initiation and progression, which needs further investigations in the future.

Moreover, we conducted the PPI network analysis to further identify the key and hub genes among these FRDEGs. We determined ten most important hub FRDEGs, as follows: *HMOX1, KEAP1, MAPK1, HSPA5, TXNRD1, IL6, PPARA, JUN, HIF1A*, and *DUSP1*. Then we performed functional and pathway enrichment analysis to further explore the potential molecular functions of the ten hub genes. Importantly, these hub FRDEGs are primarily involved in response to oxidative stress and cellular response to oxidative stress. It is suggested that these hub FRDEGs are closely related to oxidative stress. Oxidative stress has played key roles in the pathogenesis and development of IDD, as reported in previous studies from ours and others (34–37). Interestingly, oxidative stress is closely associated with ferroptosis. In 2009, Reardon et al. (38) reported that iron injections could upregulate skeletal muscle iron content and promote oxidative stress in mice. Recently, researchers have found that iron overload

10.3389/fendo.2023.1089796

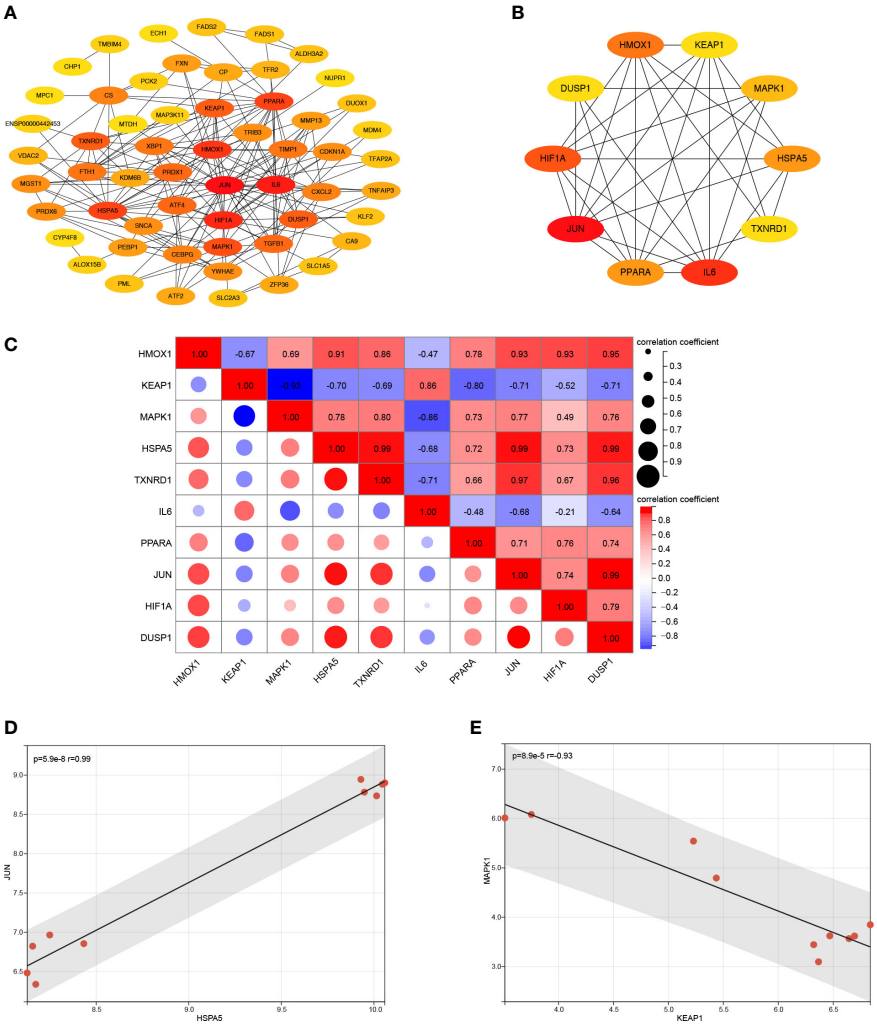

FIGURE 4
PPI analysis of the FRDEGs. **(A)** PPI analysis of these FRDEGs. **(B)** The top 10 hub FRDEGs. **(C)** Correlation analysis among the top 10 hub FRDEGs by Pearson analysis. **(D)** Correlation analysis between *HSPA5* and *JUN* by Pearson analysis. **(E)** Correlation analysis between *KEAP1* and *MAPK1* by Pearson analysis.

TABLE 2 Detailed information of the top 10 hub FRDEGs.

Gene symbols	Gene full names	Expression	Log2(fold change)	P value	Ferroptosis regulation
HMOX1	Heme oxygenase 1	Upregulated	1.60	<0.01	Driver, Suppressor
KEAP1	Kelch like ECH associated protein 1	Downregulated	-1.60	<0.01	Driver
MAPK1	Mitogen-activated protein kinase 1	Upregulated	1.69	<0.01	Driver
HSPA5	Heat shock protein family A (Hsp70) member 5	Upregulated	1.77	<0.01	Suppressor
TXNRD1	Thioredoxin reductase 1	Upregulated	3.56	<0.01	Unclassified
IL6	Interleukin 6	Downregulated	-1.64	<0.01	Driver, Suppressor
PPARA	Peroxisome proliferator activated receptor alpha	Upregulated	1.06	<0.01	Suppressor
JUN	Jun proto-oncogene	Upregulated	2.16	<0.01	Suppressor
HIF1A	Hypoxia inducible factor 1 subunit alpha	Upregulated	1.22	<0.01	Driver, Suppressor
DUSP1	Dual specificity phosphatase 1	Upregulated	1.04	<0.01	Unclassified

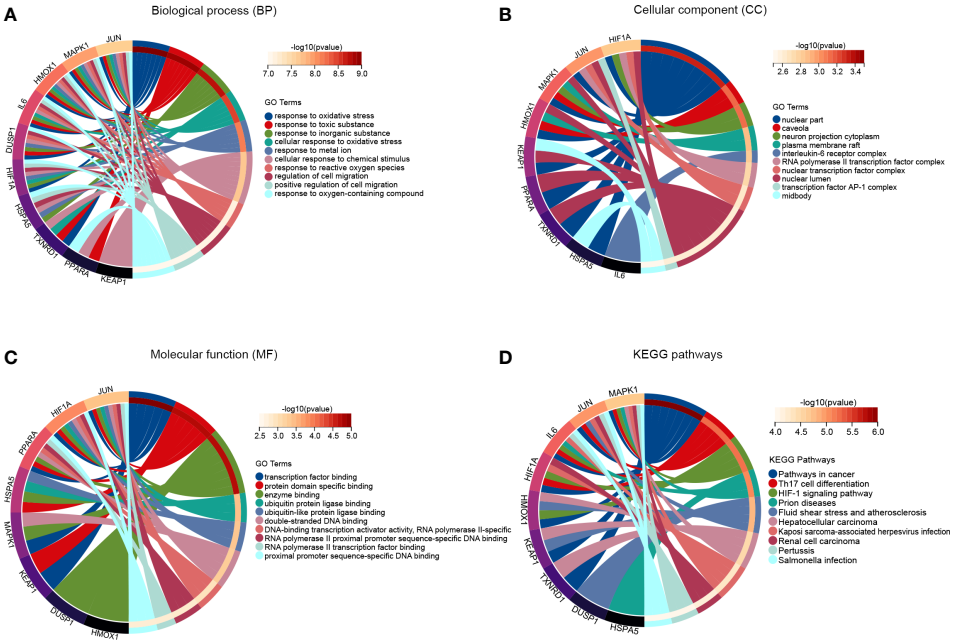

FIGURE 5
Function analysis of the hub FRDEGs. **(A)** The top 10 significantly enriched GO terms in the category of biological process for these hub FRDEGs. **(B)** The top 10 significantly enriched GO terms in the category of cellular component. **(C)** The top 10 significantly enriched GO terms in the category of molecular function. **(D)** KEGG pathway analysis for these hub FRDEGs.

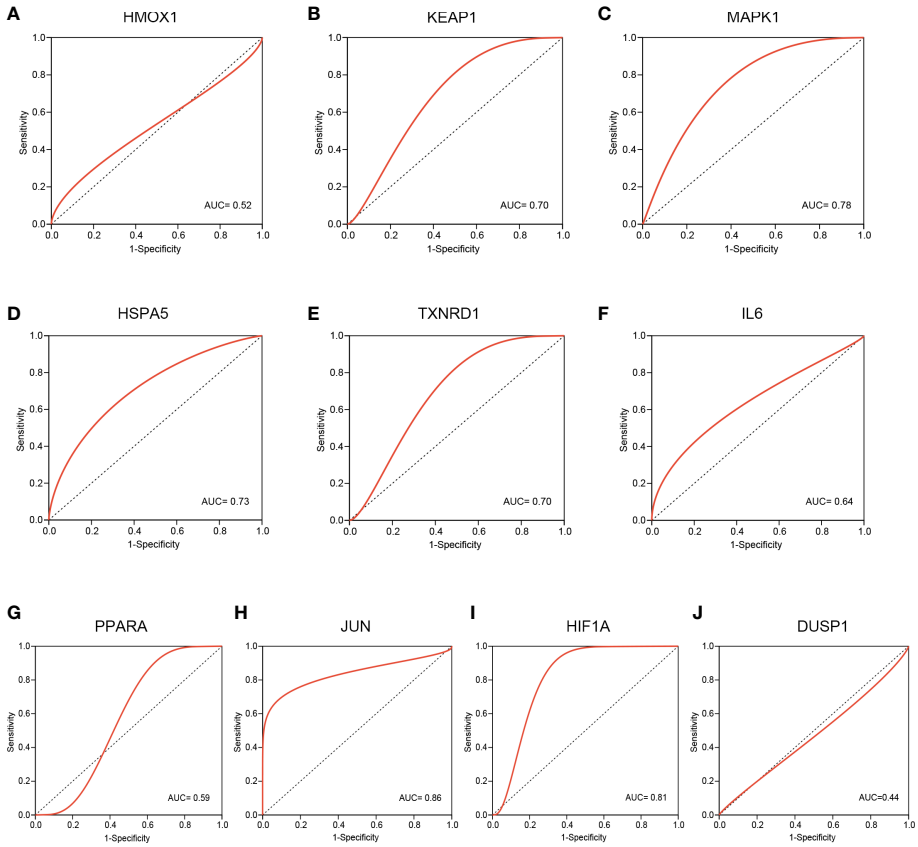

FIGURE 6
Validation of these hub FRDEGs based on the GSE124272 dataset. **(A–J)** ROC analysis of the ten hub FRDEGs, including *HMOX1, KEAP1, MAPK1, HSPA5, TXNRD1, IL6, PPARA, JUN, HIF1A*, and *DUSP1*. The X-axis represents the (1-Specificity), and the Y-axis represents the Sensitivity.

10.3389/fendo.2023.1089796

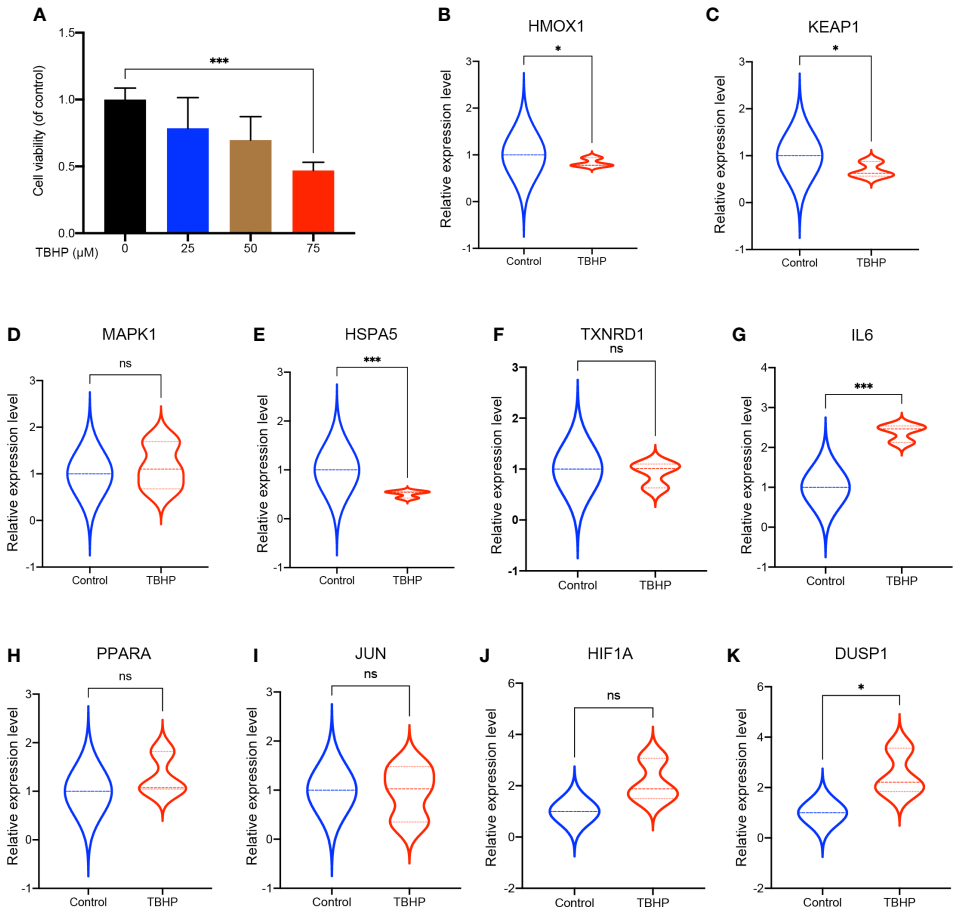

FIGURE 7
Validation of these hub FRDEGs in IDD cell model. **(A)** The cell viability of the rat NP cells treated with different concentrations of TBHP for 24 h was determined by the CCK-8 analysis. **(B–K)** The mRNA expression levels of these ten hub FRDEGs in the rat NP cells with or without TBHP treatment were determined by RT-qPCR assay. ns, not significant. $^{*}p < 0.05$, $^{***}p < 0.001$, n = 3.

was an independent risk factor for IDD and it accelerated IDD development *via* oxidative stress and ferroptosis in endplate chondrocytes (22). Besides, oxidative stress could induce ferroptosis in AF cells and NP cells in an autophagy-dependent way during IDD process (39). Therefore, the interaction between oxidative stress and ferroptosis has significantly contributed to the disc degeneration. In the pathway enrichment analysis, the most meaningful and significantly enriched pathways include Th17 cell differentiation and HIF-1 signaling pathway, and related contents have been discussed above.

We further performed ROC analysis to evaluate the predictive value of the hub FRDEGs, and also established IDD cell model to validate these genes expression in the current study. Results of ROC analysis showed that six out of the ten hub FRDEGs might be potential signature genes for IDD, including *KEAP1, MAPK1, HSPA5, TXNRD1, JUN*, and *HIF1A*. KEAP1, the Kelch like ECH associated protein 1, has been found to exert promoting functions on ferroptosis (40). KEAP1 is a redox sensor for ROS and electrophiles and negatively modulates the activation of nuclear factor E2-related factor 2 (NRF2) signaling (41). In fact, the KEAP1-NRF2 complex is a redox-sensitive transcriptional regulatory system to protect cells against oxidative stress injury (42). In our previous review article, we have comprehensively discussed the roles of KEAP1-NRF2 system in IDD progression (4). This crucial antioxidant defense system could regulate the NP cell apoptosis, senescence, extracellular matrix (ECM) metabolism, inflammatory responses, and EP calcification in IDD. MAPK1, mitogen-activated protein kinase 1, is a core signal transductor of the MAPK/ERK signaling pathway, and it could facilitate ferroptosis through regulating ROS production (43). Evidence has shown that the MAPK1 expression was increased in the degenerated disc tissues and it could accelerate the development of disc degeneration (44). HSPA5, heat shock protein family A (Hsp70) member 5, was found to resist ferroptosis in cancer cells (45). Mechanistically, HSPA5 can bind to GPX4 protein and suppress the degradation of GPX4, which is a vital suppressor of intracellular lipid peroxidation and ferroptosis as described above. However, whether and how HSPA5 participates in IDD process is unclear so far. Though the effects of TXNRD1 (thioredoxin reductase 1) on ferroptosis is not fully understood, accumulating evidence has shown that TXNRD1 might also take part in the lipid peroxidation and ferroptosis (46, 47). The roles of TXNRD1 in IDD is not so clear either. JUN, namely Jun proto-oncogene, was demonstrated to inhibit erastin-induced ferroptosis in Schwann cells (48). A previous work has revealed that the c-Jun could alleviate IDD by modulating TGF-β (49). Previous studies have reported that HIF1A could exert promoting or inhibiting effects in regulating ferroptosis (50, 51). Moreover, as mentioned above, HIF1A has exerted critical regulatory functions in the disc degeneration process, and it could be also an important target to prevent the IDD development (29, 30, 52).

Therefore, these key FRDEGs might be closely involved in the initiation and progression of IDD.

Accumulating studies have attempted to explore the underlying mechanisms of IDD by bioinformatic analysis, including inflammatory response, immune infiltration, mitochondrial dysfunction, etc (53, 54). The present study focused on the association between ferroptosis with IDD, and provided novel insights into the pathogenesis of IDD. However, certain limitations should be noted when interpreting our findings. First, we did not perform microarrays or RNA sequencing in this study. The gene expression data was obtained from the GEO database, and especially, the validation dataset was from blood samples of IDD patients and healthy controls. Second, the IDD cell model used in our study could not reflect the intact IDD microenvironment *in vivo*, which was far more complexed than *in vitro* models. And this may be part of the cause for some hub FRDEGs with different expression patterns in the microarray analysis and in the IDD cell model results. Lastly, the cellular and molecular biology experiments did not unveil specific mechanisms of ferroptosis in IDD, which needed more in-depth research to explore in the future.

5 Conclusion

In summary, this study illuminated that the expression pattern of ferroptosis related genes in IDD was distinct from controls. We have determined 80 FRDEGs dysregulated in IDD. Furthermore, ten most important OSRDEGs were identified and validated, including *HMOX1, KEAP1, MAPK1, HSPA5, TXNRD1, IL6, PPARA, JUN, HIF1A, DUSP1*. These hub FRDEGs had close relationships with oxidative stress and some other crucial signaling pathway, which were deeply involved in IDD initiation and development. These identified hub FRDEGs might be potential signature genes for IDD. This work reveals that ferroptosis might provide a novel and promising strategy for the diagnosis and treatment of the disc degeneration.

Data availability statement

The original contributions presented in the study are included in the article/supplementary material. Further inquiries can be directed to the corresponding author.

Author contributions

WL designed and supervised the study. QX and YZ performed the experiments, analyzed the data, and wrote the manuscript. All authors contributed to the article and approved the submitted version.

Funding

This study was supported by the National Natural Science Foundation of China (Grant No. 82172480).

Conflict of interest

The authors declare that the research was conducted in the absence of any commercial or financial relationships that could be construed as a potential conflict of interest.

Publisher's note

References

1. Maher C, Underwood M, Buchbinder R. Non-specific low back pain. *Lancet* (2017) 389(10070):736–47. doi: 10.1016/s0140-6736(16)30970-9

2. Zhou Z, Hui ES, Kranz GS, Chang JR, de Luca K, Pinto SM, et al. Potential mechanisms underlying the accelerated cognitive decline in people with chronic low back pain: A scoping review. *Ageing Res Rev* (2022), 82:101767. doi: 10.1016/j.arr.2022.101767

3. Binch ALA, Fitzgerald JC, Growney EA, Barry F. Cell-based strategies for ivd repair: Clinical progress and translational obstacles. *Nat Rev Rheumatol* (2021) 17(3):158–75. doi: 10.1038/s41584-020-00568-w

4. Xiang Q, Zhao Y, Lin J, Jiang S, Li W. The Nrf2 antioxidant defense system in intervertebral disc degeneration: Molecular insights. *Exp Mol Med* (2022) 54(8):1067–75. doi: 10.1038/s12276-022-00829-6

5. Sakai D, Grad S. Advancing the cellular and molecular therapy for intervertebral disc disease. *Adv Drug Delivery Rev* (2015) 84:159–71. doi: 10.1016/j.addr.2014.06.009

6. Sampara P, Banala RR, Vemuri SK, Av GR, Gpv S. Understanding the molecular biology of intervertebral disc degeneration and potential gene therapy strategies for regeneration: A review. *Gene Ther* (2018) 25(2):67–82. doi: 10.1038/s41434-018-0004-0

7. Dixon SJ, Lemberg KM, Lamprecht MR, Skouta R, Zaitsev EM, Gleason CE, et al. Ferroptosis: An iron-dependent form of nonapoptotic cell death. *Cell* (2012) 149(5):1060–72. doi: 10.1016/j.cell.2012.03.042

8. Stockwell BR, Friedmann Angeli JP, Bayir H, Bush AI, Conrad M, Dixon SJ, et al. Ferroptosis: A regulated cell death nexus linking metabolism, redox biology, and disease. *Cell* (2017) 171(2):273–85. doi: 10.1016/j.cell.2017.09.021

9. Dixon SJ, Stockwell BR. The role of iron and reactive oxygen species in cell death. *Nat Chem Biol* (2014) 10(1):9–17. doi: 10.1038/nchembio.1416

10. Wu S, Zhu C, Tang D, Dou QP, Shen J, Chen X. The role of ferroptosis in lung cancer. *biomark Res* (2021) 9(1):82. doi: 10.1186/s40364-021-00338-0

11. Yang WS, SriRamaratnam R, Welsch ME, Shimada K, Skouta R, Viswanathan VS, et al. Regulation of ferroptotic cancer cell death by Gpx4. *Cell* (2014) 156(1-2):317–31. doi: 10.1016/j.cell.2013.12.010

12. Ge C, Zhang S, Mu H, Zheng S, Tan Z, Huang X, et al. Emerging mechanisms and disease implications of ferroptosis: Potential applications of natural products. *Front Cell Dev Biol* (2021) 9:774957. doi: 10.3389/fcell.2021.774957

13. Toyokuni S, Ito F, Yamashita K, Okazaki Y, Akatsuka S. Iron and thiol redox signaling in cancer: An exquisite balance to escape ferroptosis. *Free Radic Biol Med* (2017) 108:610–26. doi: 10.1016/j.freeradbiomed.2017.04.024

14. Conrad M, Angeli JP, Vandenabeele P, Stockwell BR. Regulated necrosis: Disease relevance and therapeutic opportunities. *Nat Rev Drug Discovery* (2016) 15(5):348–66. doi: 10.1038/nrd.2015.6

15. Liu X, Wang T, Wang W, Liang X, Mu Y, Xu Y, et al. Emerging potential therapeutic targets of ferroptosis in skeletal diseases. *Oxid Med Cell Longev* (2022) 2022:3112388. doi: 10.1155/2022/3112388

16. Miao Y, Chen Y, Xue F, Liu K, Zhu B, Gao J, et al. Contribution of ferroptosis and Gpx4's dual functions to osteoarthritis progression. *EBioMedicine* (2022) 76:103847. doi: 10.1016/j.ebiom.2022.103847

17. Lv Z, Han J, Li J, Guo H, Fei Y, Sun Z, et al. Single cell rna-seq analysis identifies ferroptotic chondrocyte cluster and reveals Trpv1 as an anti-ferroptotic target in osteoarthritis. *EBioMedicine* (2022) 84:104258. doi: 10.1016/j.ebiom.2022.104258

18. Hu Y, Han J, Ding S, Liu S, Wang H. Identification of ferroptosis-associated biomarkers for the potential diagnosis and treatment of postmenopausal osteoporosis. *Front Endocrinol (Lausanne)* (2022) 13:986384. doi: 10.3389/fendo.2022.986384

19. DeRuisseau KC, Park YM, DeRuisseau LR, Cowley PM, Fazen CH, Doyle RP. Aging-related changes in the iron status of skeletal muscle. *Exp Gerontol* (2013) 48 (11):1294–302. doi: 10.1016/j.exger.2013.08.011

20. Kim BJ, Ahn SH, Bae SJ, Kim EH, Lee SH, Kim HK, et al. Iron overload accelerates bone loss in healthy postmenopausal women and middle-aged men: A 3-year retrospective longitudinal study. *J Bone Miner Res* (2012) 27(11):2279–90. doi: 10.1002/jbmr.1692

21. Zhang Y, Han S, Kong M, Tu Q, Zhang L, Ma X. Single-cell rna-seq analysis identifies unique chondrocyte subsets and reveals involvement of ferroptosis in human intervertebral disc degeneration. *Osteoarthr Cartilage* (2021) 29(9):1324–34. doi: 10.1016/j.joca.2021.06.010

22. Wang W, Jing X, Du T, Ren J, Liu X, Chen F, et al. Iron overload promotes intervertebral disc degeneration *Via* inducing oxidative stress and ferroptosis in endplate chondrocytes. *Free Radical Biol Med* (2022) 190:234–46. doi: 10.1016/j.freeradbiomed.2022.08.018

23. Wan ZY, Song F, Sun Z, Chen YF, Zhang WL, Samartzis D, et al. Aberrantly expressed long noncoding rnas in human intervertebral disc degeneration: A microarray related study. *Arthritis Res Ther* (2014) 16(5):465. doi: 10.1186/s13075-014-0465-5

24. Wang Y, Dai G, Li L, Liu L, Jiang L, Li S, et al. Transcriptome signatures reveal candidate key genes in the whole blood of patients with lumbar disc prolapse. *Exp Ther Med* (2019) 18(6):4591–602. doi: 10.3892/etm.2019.8137

25. Li Y, Pan D, Wang X, Huo Z, Wu X, Li J, et al. Silencing Atf3 might delay tbhp-induced intervertebral disc degeneration by repressing npc ferroptosis, apoptosis, and ecm degradation. *Oxid Med Cell Longev* (2022) 2022:4235126. doi: 10.1155/2022/4235126

26. Kang L, Xiang Q, Zhan S, Song Y, Wang K, Zhao K, et al. Restoration of autophagic flux rescues oxidative damage and mitochondrial dysfunction to protect against intervertebral disc degeneration. *Oxid Med Cell Longev* (2019) 2019:7810320. doi: 10.1155/2019/7810320

27. Wang C, Yu X, Yan Y, Yang W, Zhang S, Xiang Y, et al. Tumor necrosis factor-A: A key contributor to intervertebral disc degeneration. *Acta Biochim Biophys Sin* (2017) 49 (1):1–13. doi: 10.1093/abbs/gmw112

28. McGettrick AF, O'Neill LAJ. The role of hif in immunity and inflammation. *Cell Metab* (2020) 32(4):524–36. doi: 10.1016/j.cmet.2020.08.002

29. He R, Wang Z, Cui M, Liu S, Wu W, Chen M, et al. Hif1a alleviates compression-induced apoptosis of nucleus pulposus derived stem cells *Via* upregulating autophagy. *Autophagy* (2021) 17(11):3338–60. doi: 10.1080/15548627.2021.1872227

30. Wang Z, Chen H, Tan Q, Huang J, Zhou S, Luo F, et al. Inhibition of aberrant Hif1α activation delays intervertebral disc degeneration in adult mice. *Bone Res* (2022) 10 (1):2. doi: 10.1038/s41413-021-00165-x

31. Konieczny P, Xing Y, Sidhu I, Subudhi I, Mansfield KP, Hsieh B, et al. Interleukin-17 governs hypoxic adaptation of injured epithelium. *Science* (2022) 377(6602):eabg9302. doi: 10.1126/science.abg9302

32. Mimpen JY, Baldwin MJ, Cribbs AP, Philpott M, Carr AJ, Dakin SG, et al. Interleukin-17a causes osteoarthritis-like transcriptional changes in human osteoarthritis-derived chondrocytes and synovial fibroblasts in vitro. *Front Immunol* (2021) 12:676173. doi: 10.3389/fimmu.2021.676173

33. Tan JH, Li ZP, Liu LL, Liu H, Xue JB. Il-17 in intervertebral disc degeneration: Mechanistic insights and therapeutic implications. *Cell Biol Int* (2022) 46(4):535–47. doi: 10.1002/cbin.11767

34. Zhao Y, Xiang Q, Lin J, Jiang S, Li W. Oxidative stress in intervertebral disc degeneration: New insights from bioinformatic strategies. *Oxid Med Cell Longev* (2022) 2022:2239770. doi: 10.1155/2022/2239770

35. Song Y, Li S, Geng W, Luo R, Liu W, Tu J, et al. Sirtuin 3-dependent mitochondrial redox homeostasis protects against ages-induced intervertebral disc degeneration. *Redox Biol* (2018) 19:339–53. doi: 10.1016/j.redox.2018.09.006

36. Li Y, Chen L, Gao Y, Zou X, Wei F. Oxidative stress and intervertebral disc degeneration: Pathophysiology, signaling pathway, and therapy. *Oxid Med Cell Longev* (2022) 2022:1984742. doi: 10.1155/2022/1984742

37. Kang L, Liu S, Li J, Tian Y, Xue Y, Liu X. The mitochondria-targeted anti-oxidant mitoq protects against intervertebral disc degeneration by ameliorating mitochondrial dysfunction and redox imbalance. *Cell Prolif* (2020) 53(3):e12779. doi: 10.1111/cpr.12779

38. Reardon TF, Allen DG. Iron injections in mice increase skeletal muscle iron content, induce oxidative stress and reduce exercise performance. *Exp Physiol* (2009) 94 (6):720–30. doi: 10.1113/expphysiol.2008.046045

39. Yang RZ, Xu WN, Zheng HL, Zheng XF, Li B, Jiang LS, et al. Involvement of oxidative stress-induced annulus fibrosus cell and nucleus pulposus cell ferroptosis in intervertebral disc degeneration pathogenesis. *J Cell Physiol* (2021) 236(4):2725–39. doi: 10.1002/jcp.30039

40. Fan Z, Wirth AK, Chen D, Wruck CJ, Rauh M, Buchfelder M, et al. Nrf2-Keap1 pathway promotes cell proliferation and diminishes ferroptosis. *Oncogenesis* (2017) 6(8): e371. doi: 10.1038/oncsis.2017.65

41. Itoh K, Wakabayashi N, Katoh Y, Ishii T, Igarashi K, Engel JD, et al. Keap1 represses nuclear activation of antioxidant responsive elements by Nrf2 through binding to the amino-terminal Neh2 domain. *Genes Dev* (1999) 13(1):76–86. doi: 10.1101/gad.13.1.76

42. Yamamoto M, Kensler TW, Motohashi H. The Keap1-Nrf2 system: A thiol-based sensor-effector apparatus for maintaining redox homeostasis. *Physiol Rev* (2018) 98 (3):1169–203. doi: 10.1152/physrev.00023.2017

43. Su L, Jiang X, Yang C, Zhang J, Chen B, Li Y, et al. Pannexin 1 mediates ferroptosis that contributes to renal Ischemia/Reperfusion injury. *J Biol Chem* (2019) 294(50):19395–404. doi: 10.1074/jbc.RA119.010949

44. Zhou M, He SJ, Liu W, Yang MJ, Hou ZY, Meng Q, et al. Ezh2 upregulates the expression of Mapk1 to promote intervertebral disc degeneration *Via* suppression of mir-129-5p. *J Gene Med* (2022) 24(3):e3395. doi: 10.1002/jgm.3395

45. Zhu S, Zhang Q, Sun X, Zeh HJ3rd, Lotze MT, Kang R, et al. Hspa5 regulates ferroptotic cell death in cancer cells. *Cancer Res* (2017) 77(8):2064–77. doi: 10.1158/0008-5472.Can-16-1979

46. Tang D, Chen X, Kang R, Kroemer G. Ferroptosis: Molecular mechanisms and health implications. *Cell Res* (2021) 31(2):107–25. doi: 10.1038/s41422-020-00441-1

47. Guo W, Wu Z, Chen J, Guo S, You W, Wang S, et al. Nanoparticle delivery of mir-21-3p sensitizes melanoma to anti-Pd-1 immunotherapy by promoting ferroptosis. *J Immunother Cancer* (2022) 10(6). doi: 10.1136/jitc-2021-004381

48. Gao D, Huang Y, Sun X, Yang J, Chen J, He J. Overexpression of c-jun inhibits erastin-induced ferroptosis in schwann cells and promotes repair of facial nerve function. *J Cell Mol Med* (2022) 26(8):2191–204. doi: 10.1111/jcmm.17241

49. Lei M, Wang K, Li S, Zhao K, Hua W, Wu X, et al. The c-jun signaling pathway has a protective effect on nucleus pulposus cells in patients with intervertebral disc degeneration. *Exp Ther Med* (2020) 20(5):123. doi: 10.3892/etm.2020.9251

50. Yang YC, Zhang MY, Liu JY, Jiang YY, Ji XL, Qu YQ. Identification of ferroptosis-related hub genes and their association with immune infiltration in chronic obstructive pulmonary disease by bioinformatics analysis. *Int J Chron Obstruct Pulmon Dis* (2022) 17:1219–36. doi: 10.2147/copd.S348569

51. Yang M, Chen P, Liu J, Zhu S, Kroemer G, Klionsky DJ, et al. Clockophagy is a novel selective autophagy process favoring ferroptosis. *Sci Adv* (2019) 5(7):eaaw2238. doi: 10.1126/sciadv.aaw2238

52. Li Y, Liu S, Pan D, Xu B, Xing X, Zhou H, et al. The potential role and trend of Hif −1α in intervertebral disc degeneration: Friend or foe? (Review). *Mol Med Rep* (2021) 23 (4). doi: 10.3892/mmr.2021.11878

53. Lan T, Hu Z, Guo W, Yan B, Zhang Y. Development of a novel inflammatory-associated gene signature and immune infiltration patterns in intervertebral disc degeneration. *Oxid Med Cell Longev* (2022) 2022:2481071. doi: 10.1155/2022/2481071

54. Zhu Z, He Z, Tang T, Wang F, Chen H, Li B, et al. Integrative bioinformatics analysis revealed mitochondrial dysfunction-related genes underlying intervertebral disc degeneration. *Oxid Med Cell Longev* (2022) 2022:1372483. doi: 10.1155/2022/1372483

frontiers | Frontiers in Endocrinology

TYPE Review
PUBLISHED 15 March 2023
DOI 10.3389/fendo.2023.1138255

OPEN ACCESS

EDITED BY
Meifeng Zhu,
Nankai University, China

REVIEWED BY
Esther Potier,
Centre National de la Recherche Scientifique (CNRS), France
Joanna K. Filipowska,
City of Hope National Medical Center, United States

*CORRESPONDENCE
Changfeng Fu
fucf@jlu.edu.cn

SPECIALTY SECTION
This article was submitted to Bone Research, a section of the journal Frontiers in Endocrinology

RECEIVED 05 January 2023
ACCEPTED 27 February 2023
PUBLISHED 15 March 2023

CITATION
Wang H, Zhu J, Xia Y, Li Y and Fu C (2023) Application of platelet-rich plasma in spinal surgery.
Front. Endocrinol. 14:1138255.
doi: 10.3389/fendo.2023.1138255

Application of platelet-rich plasma in spinal surgery

Hengyi Wang, Jianshu Zhu, Yuanliang Xia, Yuehong Li and Changfeng Fu*

Department of Spinal Surgery, The First Hospital of Jilin University, Changchun, China

With the aging of the population and changes in lifestyle, the incidence of spine-related diseases is increasing, which has become a major global public health problem; this results in a huge economic burden on the family and society. Spinal diseases and complications can lead to loss of motor, sensory, and autonomic functions. Therefore, it is necessary to identify effective treatment strategies. Currently, the treatment of spine-related diseases includes conservative, surgical, and minimally invasive interventional therapies. However, these treatment methods have several drawbacks such as drug tolerance and dependence, adjacent spondylosis, secondary surgery, infection, nerve injury, dural rupture, nonunion, and pseudoarthrosis. Further, it is more challenging to promote the regeneration of the interstitial disc and restore its biomechanical properties. Therefore, clinicians urgently need to identify methods that can limit disease progression or cure diseases at the etiological level. Platelet-rich plasma (PRP), a platelet-rich form of plasma extracted from venous blood, is a blood-derived product. Alpha granules contain a large number of cytokines, such as platelet-derived growth factor (PDGF), vascular endothelial growth factor (VEGF), epidermal growth factor, platelet factor 4 (PF-4), insulin-like growth factor-1 (IGF-1), and transforming growth factor-β (TGF-β). These growth factors allow stem cell proliferation and angiogenesis, promote bone regeneration, improve the local microenvironment, and enhance tissue regeneration capacity and functional recovery. This review describes the application of PRP in the treatment of spine-related diseases and discusses the clinical application of PRP in spinal surgery.

KEYWORDS

platelet-rich plasma, spinal diseases, cytokines, osteogenesis, facilitated repair

1 Introduction

Spine-related diseases place a heavy financial and psychological burden on the general population (1). These diseases include discogenic low back pain (DLBP) (2), lumbar disc herniation (3), lumbar disc degeneration (4), spinal cord injury (5), ligament injury (6), and sacroiliac joint disease (7). The complexity of spine-related diseases depends on numerous

factors such as age, sex, occupation, and lifestyle. Since 1990, there has been a sharp increase in the prevalence of spine-related diseases, which has become one of the main causes of disability in the world (8). At present, treatment options for these diseases can be divided into conservative, surgical, and minimally invasive interventional treatments. However, these treatment methods have several drawbacks such as adjacent segment disorder, pseudarthrosis, postoperative recurrence, secondary operation, drug dependence and tolerance, infection, dural rupture, nerve injury, and expensive treatment, among others. Moreover, the above treatment schemes are not satisfactory in promoting intervertebral disc regeneration and restoring its biomechanical properties such as damping and vibration reduction. Therefore, finding an effective and fundamental treatment plan has become a new research direction to resolve these issues, and can be beneficial for the development of spine surgery. As a natural cytokine pool (Table 1), platelet-rich plasma (PRP) promotes endogenous healing and may be an effective treatment for spine-related diseases (Scheme 1).

2 Current understanding of PRP

2.1 Definition and origin of PRP

As a biological product, PRP is a platelet concentrate obtained by centrifugation of autologous peripheral blood (16). PRP releases high concentrations of bioactive molecules. Numerous growth factors, cytokines, and chemokines are present in their alpha granules, which play an integral role in regulating the extracellular matrix (ECM), promoting angiogenesis and accelerating cell recruitment, proliferation, and differentiation (17). PRP has been used in maxillofacial surgery because of its positive anti-inflammatory and cell proliferation properties (18). Furthermore, with the advancement and development of technology, the application of PRP appeared in the field of sports injuries (19). Additionally, PRP has been used in the fields of urology, gynecology, orthopedics, cardiology, and ophthalmology (20–24). In recent years, in spine surgery, the application of PRP has gradually become a new therapeutic tool for the treatment of spine-related diseases.

2.2 Preparation of PRP

PRP can be prepared in several ways, and different PRP can be produced according to different parameters (centrifugal force, centrifugation time, and temperature) (25). At present, PRP preparation technology is generally divided into two types: one-time and two-time centrifugation. The platelet concentration and PRP activity obtained using different centrifugation times, number of centrifugation cycles, and centrifugal force are different, and the recommendations by various researchers are also different. At present, most researchers believe that PRP obtained by secondary centrifugation has a higher platelet recovery rate. Mazzucco et al. compared the two PRP preparation methods and found that platelet and growth factor concentrations were significantly higher in the two-time centrifugation method than in the one-time centrifugation method (26). Harrison et al. found that a single centrifugation method, although capable of extracting PRP, was not optimal because it resulted in decreased platelet production (27). The IADVL Dermatology Association recommends the use of the manual double-spin method for the preparation of PRP. The recommended centrifuge parameters are 100–300 $\times g$ for 5–10 min for the first centrifugation and 400–700 $\times g$ for the second centrifugation for 10–17 min. The PRP obtained using this method is optimal for various dermatological indications (28). Similar studies have also found that the double-spin method is more helpful for treatment of female hair loss (29). Currently, commercial equipment or kit extractions for PRP have become a trend. Different brands have developed different separation methods, and the content of the extracted PRP component is also different. Therefore, the best kit can be selected for extraction according to different therapeutic requirements (30).

2.3 Different types of PRP

Owing to the lack of uniform standards in the preparation methods and quality control, the prepared PRP components are different. This leads to the difficulty in comparative analysis of clinical results, and is also part of the reason for the difference in clinical efficacy. Therefore, it is urgently necessary to develop a

TABLE 1 Cytokines in platelet-rich plasma.

Cytokines	Function
PDGF (9)	Stimulating chemotaxis of macrophages and neutrophils; Regulate collagenase secretion and collagen synthesis; Stimulate mitosis of mesenchymal cells and osteoblasts; Stimulate chemotaxis and mitosis of fibroblasts/glia/smooth muscle cells.
VEGF (10)	Promote angiogenesis and increase vascular permeability; Promote endothelial cell migration and proliferation; Promote granulation tissue formation.
TGF-β (11)	Promote angiogenesis; Increased proliferation of fibroblasts and keratinocytes; Metalloproteinase inhibitors; Mediate extracellular matrix and collagen production; Regulating mitosis of other growth factors; Inhibit macrophage and lymphocyte proliferation.
EGF (12)	Increase the proliferation and migration of keratinocytes and fibroblasts; Stimulate endothelial cell mitosis; Promote granulation tissue formation.
FGF (13)	Promote mitosis, growth and differentiation of mesenchymal cells, chondrocytes and osteoblasts; Promote fibroblast migration; Initial stimulation of angiogenesis.
PF-4 (14)	Calls leucocytes and regulates their activation. Microbiocidal activities.
IGF-1 (15)	Increases chemotaxis of fibroblasts and stimulates protein synthesis; enhances bone formation through proliferation and differentiation of osteoblasts.

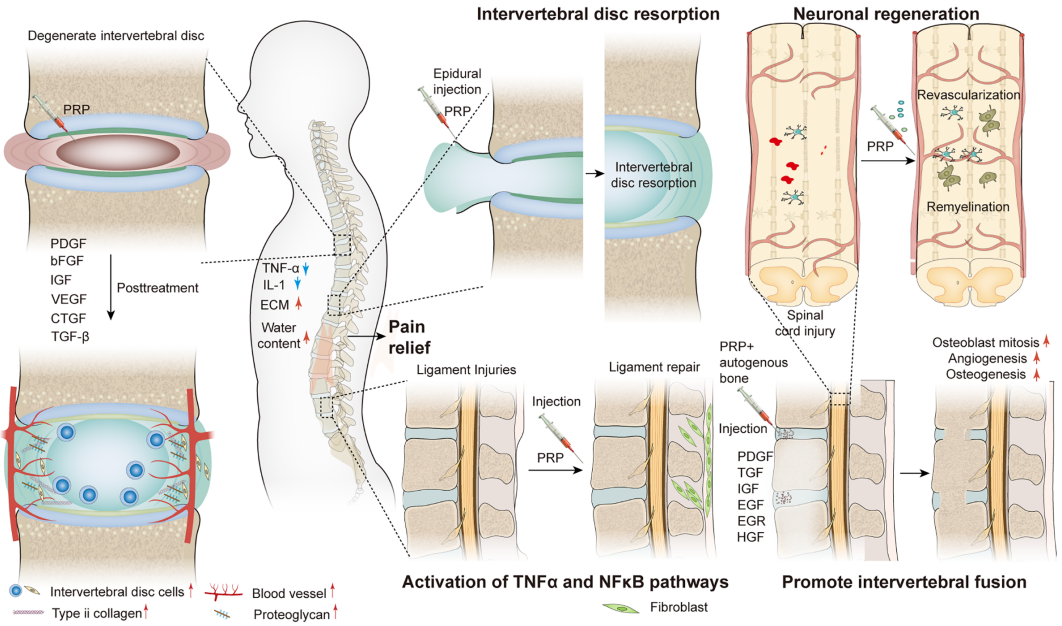

SCHEME 1
Schematic diagram of PRP in the treatment of spine-related diseases.

method to unify the production standard of PRP. In 2009, Ehrenfest et al. first proposed a classification method for platelet concentrates that combines three main variables—platelet, leukocyte, and fibrin content—and divided many PRP products into four categories: pure PRP (P-PRP), leukocyte-rich PRP (L-PRP), pure platelet-rich fibrin (PRF, P-PRF), and leukocyte-rich PRF (L-PRF) (31). In 2016, Magalon et al. proposed a more comprehensive classification method, the DEPA (Dose, Efficiency, Purity, Activation) classification, which is based on four different parameters: injection dose, production efficiency, purity, and activation process. However, the DEPA classification method also has shortcomings, such as a lack of clinical correlation (32). To standardize PRP, the ISTH Science and Standardization Committee established an expert working group to reach a series of consensus recommendations and develop a new PRP classification system (33). The above classification methods aim to establish a common unified standard to achieve the standardization of PRP and lay a foundation for the further clinical application of PRP.

2.4 Mechanism of action and main components of platelet-rich plasma

The secretion of growth factors in PRP must be initiated by blood coagulation; therefore, anticoagulants should be used during treatment to prevent coagulation and maintain a stable state to ensure that they are not activated prior to use (34). This process inhibits clotting by disabling calcium ions, which are required in the coagulation cascade (35). This disabling step can be performed using citrate ions, which can combine with calcium ions to form calcium citrate and deactivate it (36). This is an indispensable and important condition for PRP preparation.

For downstream use, PRP must be reactivated. Exogenous calcium activators can be added to PRP to promote the release of biologically active proteins such as growth factors (37). This step can be accomplished with calcium activators such as calcium chloride, calcium gluconate, or thrombin (38). Calcium previously bound to anticoagulants can be replenished in this manner.

PRP preparation contains a variety of cytokines, growth factors, cell adhesion molecules, and chemokines. These factors participate in the process of tissue healing and proliferation, as well as the activation and synthesis of essential products through interaction and mutual regulation (39). When PRP is activated, a large number of growth factors, such as transforming growth factor-β (TGF-β), platelet-derived growth factor (PDGF), fibroblast growth factor (FGF), hepatocyte growth factor (HGF), and vascular endothelial growth factor (VEGF), can be released. PDGF can stimulate endothelial cell growth, promote capillary angiogenesis, and stimulate mononuclear macrophage chemotaxis to increase collagen synthesis. Both TGF-β and PDGF can increase the proliferation of various cells involved in wound repair, stimulate collagen synthesis, and activate the interaction between macrophages and other cytokines. VEGF is a strong vascular growth factor, which can bind to the corresponding receptors on the surface of vascular endothelial cells, stimulate the proliferation of endothelial cells, induce the formation of new blood vessels, and increase the permeability of blood vessels, especially small blood vessels. It provides nutrients for cell growth and the establishment of new capillary networks, plays an important role in wound healing and vascularization, and is a key promoter in the early stage of angiogenesis (40). In addition to growth factors, PRP also contains

fibrin, fibronectin, and hypolenin, which form a fiber network and can perform the scaffold function of tissue-repairing cells, promoting cell adhesion and preventing cell loss (39). Owing to the coaction of bioactive factors in PRP, it plays a powerful role in tissue regeneration and repair.

3 Application of PRP in spine surgery

3.1 PRP for treatment of discogenic back pain

One of the most common diseases of the spine is low back pain, which can be experienced at different degrees in different stages of life. Lumbar muscle strain, intervertebral disc herniation, isthmus, spinal deformity, and lumbar spondylolisthesis are all causes of low back pain, and these factors can exist alone or in combination (41). Discogenic back pain referred to in this article is chronic low back pain caused by stimulation of the pain receptors in the intervertebral disc due to intraductal disorders, such as degeneration, intraductal fissure, and discitis, without root symptoms, nerve root compression, or excessive displacement of vertebral body segments (42). This can be described as chemically mediated discogenic pain. Increased levels of leukotriene, nitric oxide, lactic acid, and prostaglandin E in early intervertebral disc degeneration (IVD) are considered strong chemical injurious stimuli (43). The mechanism of pain is caused by the growth of vascularized granulation tissue and pain nerve fibers into annulus fibrosus or even nucleus pulposus along the annulus fibrosus of degenerative intervertebral disc. In addition, these granulation tissues and nerves are easily affected by interstitial changes and inflammatory mediators, thus causing pain (2). Mechanical compression of nerve roots was previously considered the main cause of low back pain. However, in actual clinical practice, for a vast majority of patients, low back pain was caused by non-nerve root compression, while DLBP was one of the main causes of non-nerve root compression (44).

Currently, the treatment methods for DLBP include non-surgical treatment (drug therapy, physical therapy), surgical treatment (intervertebral fusion, disc replacement), and minimally invasive interventional treatment (intervertebral disc injection therapy and epidural injection) (45–50). However, many of these treatments have disadvantages such as adjacent segment disorder after fusion, secondary surgery, drug dependence and tolerance, infection, dural rupture, and nerve injury. Therefore, safer PRP injection therapy, which is dedicated to repair the intervertebral disc itself, has been proposed.

With the development of experimental research, PRP has been used in the treatment of DLBP and has achieved good results. In a preliminary clinical trial to determine the efficacy and safety of autologous PRP releasers in patients with DLBP, Akeda et al. included 14 patients with certain inclusion criteria and evaluated the results using a visual analog scale (VAS), Roland-Morris Disability Questionnaire (RDQ), and X-ray and magnetic resonance imaging (MRI) (T2-quantification) for data analysis. During the 10-month follow-up period, the patient VAS and RDQ scores decreased significantly in the first month and continued throughout the observation period (Figures 1A, B).

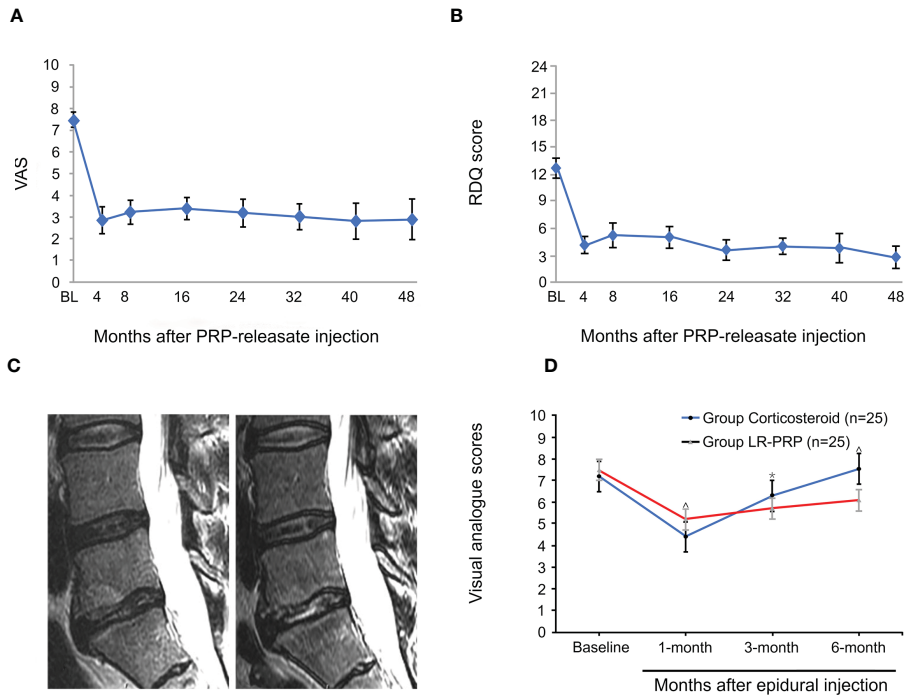

FIGURE 1
PRP for treatment of discogenic low back pain. Mean Visual Analogue Scale (VAS) score **(A)** and mean Roland-Morris Disability Questionnaire (RDQ) score **(B)** of patients after intradiscal injection of PRP. **(C)** Sagittal MRI one year before the caudal epidural and intraductal PRP injection showed increased T2 nuclear signal intensity and decreased type I Modic change in the L5-S1 disc compared to pre-injection. **(D)** Mean VAS scores were significantly lower at 3 and 6 months in patients who received LR-PRP injection. Reproduced with permission from (51–53). *P < 0.05 and ^P < 0.01.

However, MRI quantitative analysis did not observe that this method had a significant effect on the repair of intervertebral disc, but it did not have a negative effect on the height of intervertebral disc. Furthermore, no adverse effects were observed during follow-up (51). In a case report, MRI examination was performed 1 year after PRP injection, and the results showed that the nuclear T2 signal intensity increased (Figure 1C), notably, and pain and function were also significantly improved (52). However, only one patient was described in this report, and a clear correlation between disc improvement and PRP injection could not be determined. Therefore, it is necessary to expand the sample size and carefully design future prospective studies. In order to prove the efficacy of PRP, Zhang et al. showed that intradiscal injection of PRP can significantly relieve pain and improve lumbar function in patients with DLBP (54). In another randomized, double-blind controlled trial, Ricardo et al. included 50 eligible patients with low back pain. All patients were randomized 1:1 to corticosteroids and leukocyte-rich PRP (LR-PRP) groups and were treated by tail epidural injection. Pain levels and quality of life were evaluated using the VAS and the Short Form 36-Item Health Survey (SF-36) at 1, 3, and 6 months after treatment. The results showed that the VAS scores of both groups were significantly lower than those before treatment. The corticosteroid group had lower VAS scores at 1 month, whereas the LR-PRP group had lower scores at 3 and 6 months (Figure 1D). SF-36 at 6 months showed a significant improvement in all domains in the LR-PRP group. Both groups showed good therapeutic effects in pain relief, but LR-PRP was superior to corticosteroids in improving the quality of life (53). Tuakli-Wosornu et al. reported that in a randomized controlled trial of 72 patients, compared to those of a control group that received contrast media alone, the functional rating index, the numeric rating scale (NRS), and the North American Spine Society satisfaction scores of the PRP group were significantly improved (55). But in a recent trial, Zielenskietal's findings confirmed that PRP did not work as well in DLBP, with only 17% of patients showing significant improvement in clinical symptoms. This may be due to patient demographic differences, sensitivity to outcome measurements, or misalignment of statistical analysis (56).

3.2 PRP for treatment of lumbar disc herniation

Lumbar disc herniation (LDH) is one of the most common causes of low back pain (57). LDH is a disease caused by a combination of genetic, aging, biomechanical, and environmental factors (58). In terms of pathophysiology, LDH is usually due to IVD degeneration, which tends to develop with age. Disc lesions can develop in young adulthood. Subsequently, due to the gradual decrease in water content in the annulus fibrosus (AF) and nucleus pulposus (NP), the tension decreases, and the height of the intervertebral disc decreases, resulting in narrowing of the intervertebral space, loss of elasticity of the NP, and relaxation of the structure of the intervertebral disc. Dehydration may further aggravate cracks in AF. Subsequently, degenerated NP can highlight fissures or weaknesses in AF due to injury or trauma. Prominent NP can become ischemic and cause nerve root symptoms through mechanical compression, chemical stimulation, and activation of the inflammatory cascade (59).

Clinical symptoms often determine treatment options for LDH, including conservative and surgical treatment. However, the latter treatment only temporarily relieves pain or removes the NP of nerve root compression and prevents reherniation, which only partially solves problems associated with low back pain, and does not promote disc regeneration or restore its biomechanical properties such as damping and vibration reduction. Therefore, PRP with endogenous healing effects may be an effective treatment for LDH.

This treatment has been reported in clinical practice. Benjamin described a case report of two patients with symptomatic disc herniation who showed almost complete disc absorption on MRI after two epidural injections of PRP (Figures 2A, B) (60). Furthermore, the clinical symptoms and function of both patients improved significantly. In another prospective, randomized, controlled trial involving 60 patients, Jiang et al. randomized patients to receive transforaminal endoscopic lumbar discectomy combined with injection of PRP and without injection of PRP. During the postoperative follow-up period, VAS for lower back and leg pain and Oswestry disability index were lower in the PRP group than in the control group. Furthermore, quantitative MRI analysis showed that in the PRP group, values were 5% higher than those in the control group after treatment (Figure 2D). Similarly, the spinal cross-section of the PRP group was 9% higher than that of the control group (Figure 2C) (61). Similar results were also confirmed by Rohan et al. (62). Through clinical trials, Xu et al. found that during the 1-year follow-up period after transforaminal injection of PRP and steroids in the treatment of LDH, VAS, pressure pain thresholds (PPTs), Oswestry disability index (ODI), and SF-36 scores improved significantly compared to those before treatment, but there were no significant differences between the two groups. This suggests that the two treatments achieved similar results, but PRP may serve as a safer alternative treatment (63). No adverse events were reported during treatment in these studies.

3.3 PRP for treatment of spinal cord injury

Spinal cord injury (SCI) is a devastating pathological condition of the central nervous system that causes sensory, motor, and autonomic nervous dysfunction in the limbs below the injured segment (5). This intractable disease causes unavoidable physical, psychological, and economic burden on patients and their families (64). Due to the complex pathophysiological processes after SCI, such as a series of cascades of ischemia, inflammation, oxidative stress, and apoptosis, successful cure of SCI remains a great challenge for clinical workers (65).

Currently, SCI treatment includes early drug and surgical treatment. The former includes methylprednisolone (66), gangliosides (67), calcium antagonists (68), and dehydrating agents (69). Drugs play a key role in inhibiting lipid peroxidation, maintaining ion balance, improving circulation, alleviating edema, inhibiting the release of toxic substances, promoting axon growth, and improving functional recovery of patients with SCI. However,

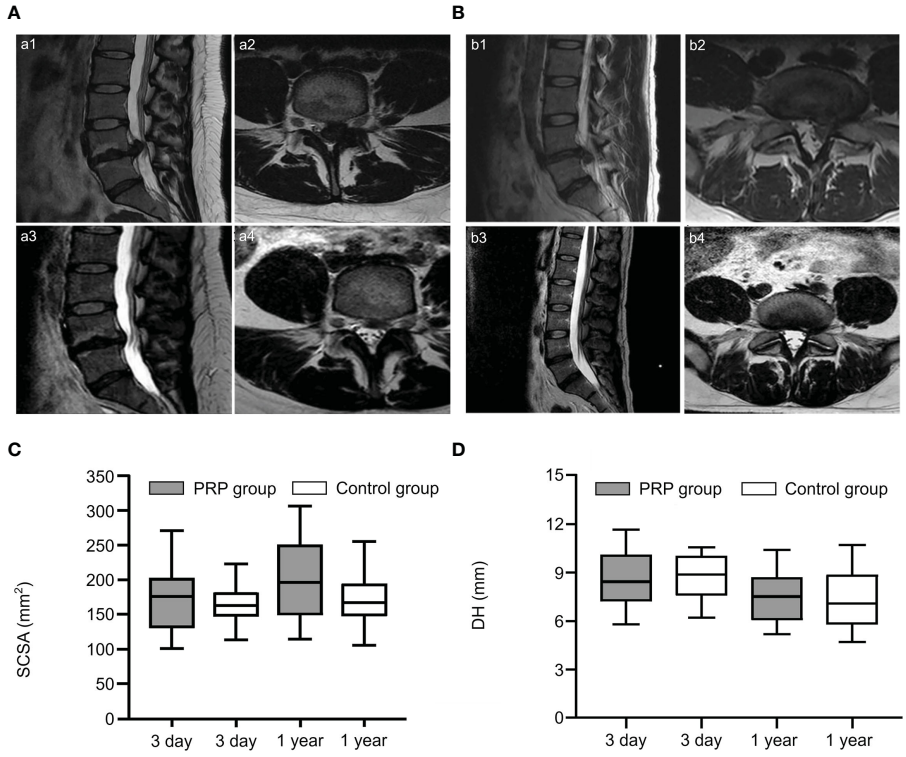

FIGURE 2
PRP treatment of lumbar disc herniation. **(A, B)** Sagittal and axial slices showed significant disc resorption before and after epidural injection of PRP in two patients. Sagittal (a1, b1) and axial (a2, b2) MRI images showed lumbar disc herniation in two patients before treatment; Sagittal (a3, b3) and axial (a4, b4) images showed significant disc resorption after treatment. **(C, D)** Comparison of spinal cord cross-sectional area (SCSA) and disc height (DH) on MRI at 3 and 1 years after treatment. Reproduced with permission from (60, 61).

only hormones and gangliosides have been confirmed in laboratory and clinical trials of neurotherapy and rehabilitation. Further, hormone therapy also has drawbacks and remains controversial due to many systemic adverse reactions (70). Early surgical treatment of SCI includes fracture reduction, orthopedics, spinal canal decompression or dilation, fixation, and bone graft fusion. The aims of surgical intervention include: (1) reconstruction of the stability of the spine, enabling patients to move early, which is conducive to more meticulous nursing, and reducing early complications and mortality; (2) prevention of secondary injury of the spinal cord caused by spinal instability; and (3) after decompression, spinal cord compression is relieved to create a relaxed internal environment for spinal nerve recovery (71–73). These methods have played a certain role in alleviating secondary nerve injury and reducing the mortality of patients after SCI, but their role in promoting functional recovery is limited because the nonregenerative nature of neurons renders SCI treatment more challenging. Preclinical trials on SCI repair are being continuously developed and some therapeutic results have been achieved. Examples include cell therapy (74) and neural tissue engineering (75). The treatment of SCI with PRP is also being investigated.

In an *in vitro* trial, Michiko et al. co-cultured human PRP with the cortex and spinal cord of 3-day-old Sprague-Dawley rats and added neutralizing antibodies against different growth factors. They found that PRP promotes spinal cord axon growth through mechanisms related to IGF-1 and VEGF, while inhibition of TGF-β1 had a negative effect on axon growth (76). In another trial, PRP was combined with BDNF-overexpressing BMSCs in a rat model of spinal cord hemisection. In the treatment group, the neuronal gene markers NF-200, GFAP, and MAP2 were highly expressed in the presence of PRP, thus promoting axonal myelin sheath regeneration (Figures 3E–G) (77). Baklaushev et al. designed a novel two-component matrix (SPRPix) that contained spider silk proteins and PRP. This complex promoted the proliferation of directly reprogrammed human neural precursor cells (drNPC) in neurons, astrocytes, and other neural support cells, and allowed these β III-tubulin- and MAP2-positive nerve cells to grow oriented along the spider protein microfibers (Figures 3A–C). In contrast, there was almost no directional growth in the hydrogels when PRP was removed (Figure 3D). Quantitative analysis of cells using the NIS Elements software (Nikon) showed that the absolute number of neuronal progenitor cells in the PRP group was five times higher than that of the blank group in the same volume. In *in vivo* experiments, drNPCs and the complex were implanted in the brain and spinal cord of rhesus monkeys, which showed good biocompatibility and successful differentiation into MAP2 positive neurons (78). Injury to the dorsal spinal cord can lead to a loss of transmission of proprioceptive information and affect motor behavior. Baklaushev et al. conducted research on dorsal spinal cord repair. The research team injected human PRP into the

10.3389/fendo.2023.1138255

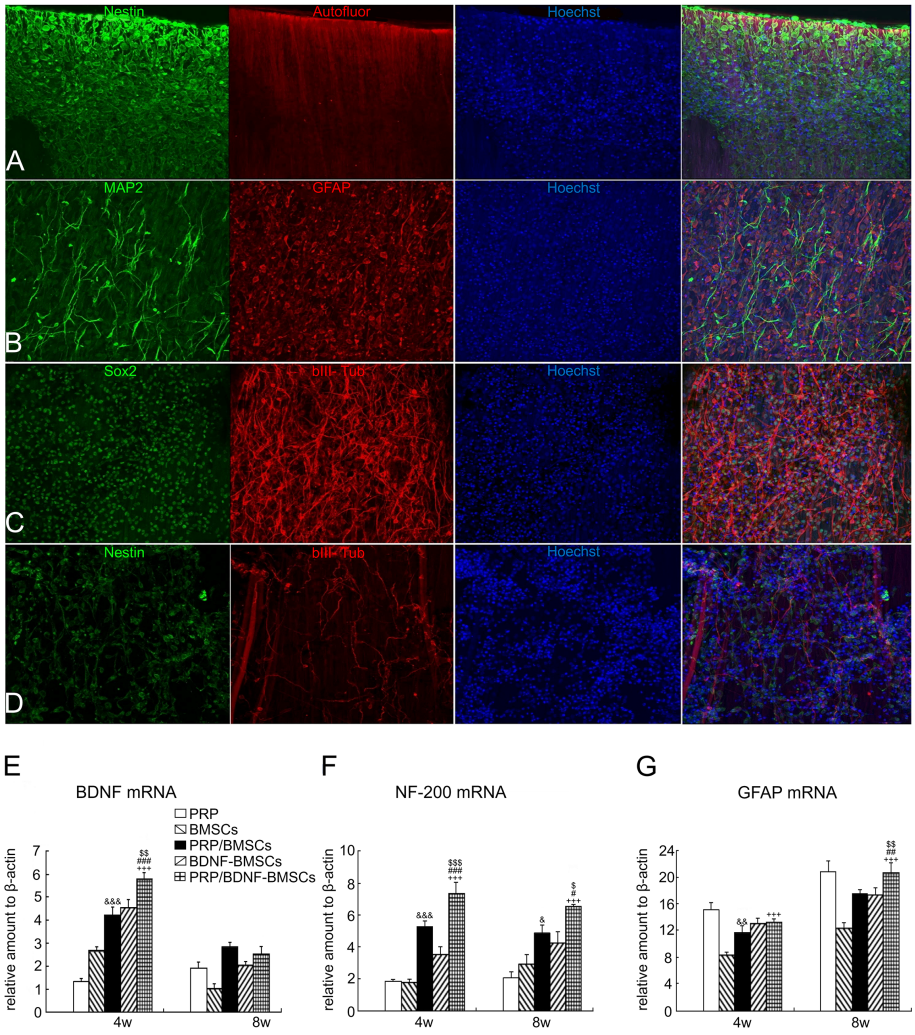

FIGURE 3
PRP treatment of spinal cord injury. **(A-C)** drNPC cultured on the two component SPRPix matrix (PRP hydrogel embedded into the rSS-PCL scaffold) demonstrated a high level of adhesion and neuronal differentiation: drNPC completely covered the entire SPRPix matrix surface and formed long βIII-tubulin- and MAP2- positive processes oriented along the spidroin microfibrils. **(D)** No directional growth was observed in scaffolds without PRP. **(E–G)** The expression of BDNF, NF-200 and GFAP genes was significantly increased after PRP and BMSCs were used together. Reproduced with permission from (77, 78). $ or $$ or $$$ P< 0.05 or P< 0.01 or P< 0.001 (PRP/BDNF-BMSCs vs. BDNF-BMSCs), # or ## or ### P< 0.05 or P< 0.01 or P< 0.001 (PRP/BDNF-BMSCs vs. PRP/BMSCs), +++ P < 0.001 (PRP/BDNF-BMSCs vs. BMSCs alone),& or && or &&&P < 0.05 or P < 0.01 or P < 0.001 (PRP/ BMSCs vs. BMSCs alone).

unilateral spinal cord dorsal root injury model and evaluated the recovery of reflex arc by electronic von Frey weekly. The arc recovered and the paw withdrawal reflex was partially restored as the treatment progressed. Intermediate filaments (nerve filaments) were observed throughout the reimplantation area (Figure 4A), indicating nerve regeneration. Furthermore, this treatment has immunomodulatory properties that can effectively improve regeneration and reduce inflammatory responses (79). In another study, researchers injected PRP directly into the injured spinal cord of rats and examined the effects of PRP on spinal cord repair. The results showed that PRP could protect white matter, improve motor recovery, promote neuronal regeneration and angiogenesis, and regulate its size (81). These experiments indicated that PRP could be used as a promising therapeutic agent for SCI.

3.4 Treatment of spinal fusion

As a mature surgical technique in spinal surgery, spinal fusion aims at achieving mid- and long-term stability of the spine, which is crucial for maintaining normal spinal function. This can be achieved using different surgical methods, implants, and grafts (82). Spinal fusion has been widely used in the treatment of various spinal malformations and diseases, including spondylolisthesis, fractures, lateral curvature, and lumbar disc diseases (83–88).

However, surgical complications, especially failure of postoperative bone formation, connection, or reshaping, results in the formation of a nonunion or pseudoarthrosis. This condition is significantly more frequent in multisegmental and osteoporotic

10.3389/fendo.2023.1138255

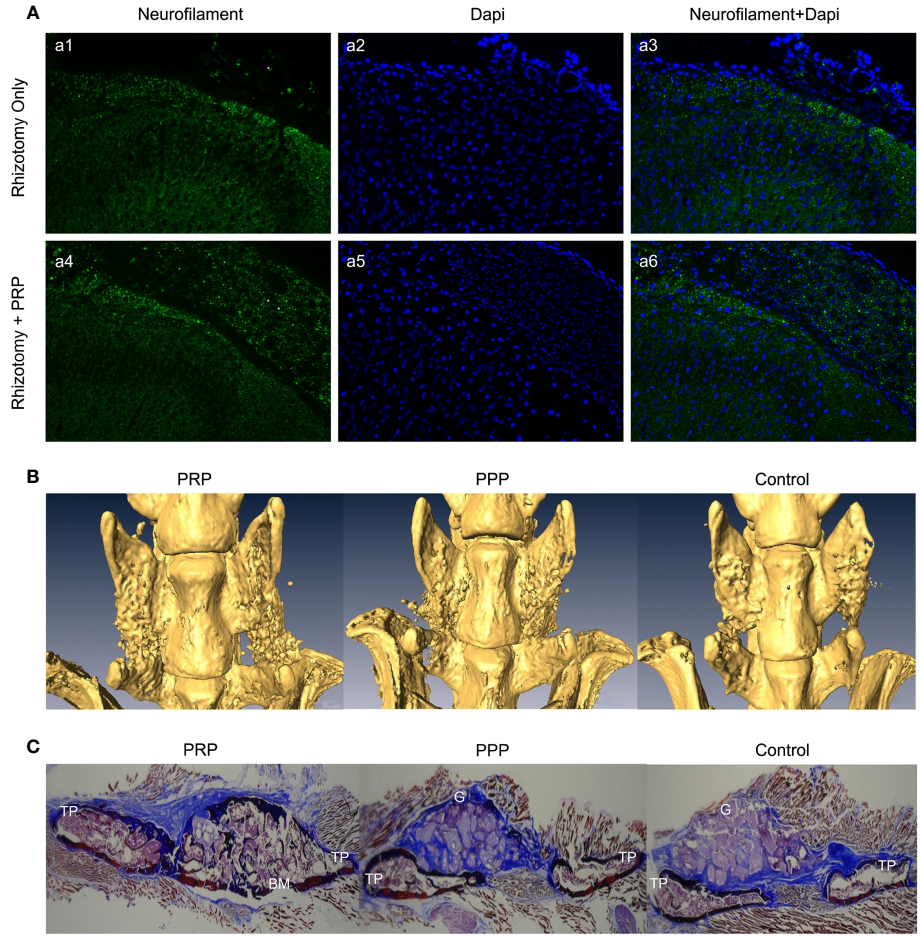

FIGURE 4
(A) Immunofluorescence analysis of neurofilament in the spinal cord dorsal horn and roots 8 weeks following dorsal rhizotomy and repair. (a1-a3) The Rhizotomy Only group showed obvious dorsal root degeneration. (a4-a6) Rhizotomy + PRP group showed obvious dorsal root repair. Degenerated dorsal roots are indicated by (*), and repaired dorsal roots are indicated by (**). **(B)** Microscopic CT scans of each group. PRP group had better fusion quality between transverse processes. **(C)** Masson's trichrome staining showed more new bone formation in the PRP group with mature fusion masses between transverse processes. TP transverse process, BM bone marrow, G granules of mineral carrier. Reproduced with permission from (79, 80).

cases (89). Currently, various materials have been used in clinical practice to improve the rate of bone fusion. The most used products include autologous, allograft, and bone graft replacement materials. Autografts have long been considered the gold standard bone graft material and have significantly improved bone fusion rate (90). However, autologous bone grafting presents associated safety issues such as donor site-related complications (especially at the iliac crest), limited bone harvesting, increased blood loss, and increased operative time (91). In other studies, allografts have proven to be promising materials that can promote bone formation. However, allografts have also been questioned as therapeutic options and are considered less successful than autografts (92). In recent years, the application of various alternative bone grafting materials combined with mesenchymal stem cells and osteogenic induction factors, such as bone transplantation, has a bright prospect. These biomaterials exhibit good biocompatibility and are beneficial for cell attachment, migration, and osteogenic matrix deposition. Good porosity is suitable for the development of the vascular network and the diffusion of nutrients (93). PRP, a natural growth factor library, has also been used for spinal fusion.

Related studies have shown that TGF- β and PDGF contained in PRP can attract osteoblast progenitor cells to the desired site for value-added differentiation and promote bone formation. Simultaneously, VEGF in PRP can induce angiogenesis and provide sufficient nutrients for the osteogenic process to promote bone fusion (94, 95). The application of PRP, alone or in combination with composite materials, has been reported in animal models and clinical trials. In a rat lumbar posterolateral fusion model, PRP derived from rat peripheral blood was combined with collagen-mineral scaffolds for treatment. After 12 weeks, micro-computed tomography (CT) and manual palpation showed a more efficient fusion rate than the control group (Figure 4B), and Masson's trichrome staining showed mature bone fusion blocks and more new bone formation between the transverse processes in the PRP group (Figure 4C) (80). However, no further studies have been conducted on the mechanisms promoting integration. This has

been explained in a previous study. Jeffrey et al. constructed composite scaffolds based on a combination of hydroxyapatite/type I collagen (MHA/Coll) and PRP. *In vivo*, the composite group produced more trabecular and cortical bone than did the stent group alone, and the fusion rate was better than that of the control group. Quantitative analysis of the expression of key osteogenic genes showed that RUNX2, SPARC, and SPP1 were significantly up-regulated compared to the control group (Figures 5B–D) (96). This appears to be the key to the promotion of bone fusion. With the advent of the aging society, the spinal fusion rate of elderly patients with degenerative spinal diseases due to osteoporosis is not satisfactory (99). To this end, researchers have combined collagen-binding bone morphogenetic protein-2 (CBD-BMP-2), which has good biological activity and slow-release function, with PRP to treat osteopenia in an elderly rat model. Through comparative analysis, the fusion rate, area, volume, and number of bone trabeculae were significantly better than those of the control group; however, PRP alone did not show satisfactory fusion efficiency (100). This finding is similar to that of a meta-analysis of clinical cases (101). The study concluded that additional use of PRP did not lead to further significant improvement in patients compared to traditional graft techniques and that PRP may have a limited role in enhancing spinal fusion. However, several other retrospective and meta-analyses have confirmed the role of PRP in promoting new bone formation and bone fusion (102, 103). In a prospective randomized controlled trial to evaluate PRP efficacy after posterolateral lumbar fusion surgery, Kubota et al. randomly divided 62 patients into PRP and control groups; the final bone union rate, fusion area, and mean union time in the PRP group were significantly better than those of the control group at the end of follow-up period (104). In another retrospective analysis, 20 patients underwent single-level transforaminal lumbar interbody fusion (TLIF) surgery for L4 spondylolisthesis, among which, 11 patients received PRP combination therapy. Postoperative CT analysis showed that the bone fusion effect was significantly better in the PRP group than in the control group (Figure 5E); however, there was no significant difference in healing time (97). The differences in the above experiments may be related to the preparation method,

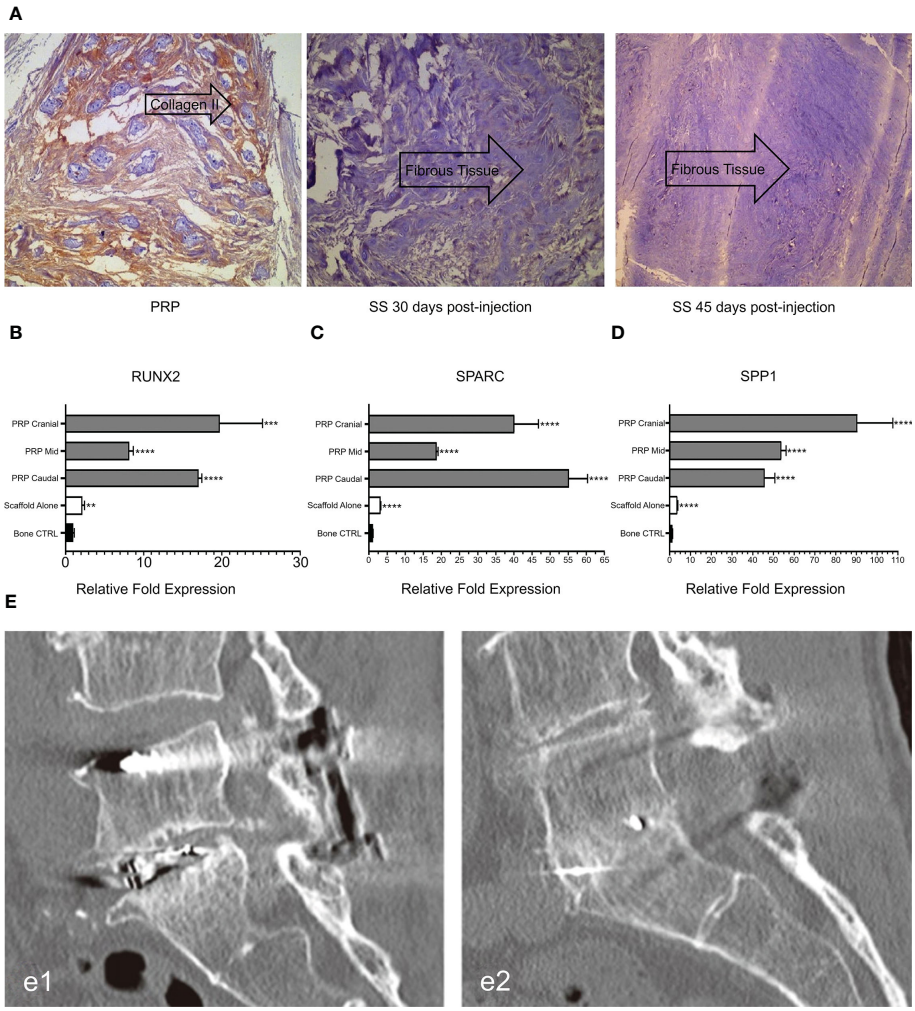

FIGURE 5
(A) Immunohistochemical expression of type II collagen in intervertebral disc tissues at different time points after injection. **(B-D)** Analysis of osteogenic gene expression. **(E)** CT evaluation of spinal fusion in different groups. Reproduced with permission from (96–98). **P = 0.0034, ***p = 0.0002, ****p < 0.0001. e1: Control group. e2: PRP group.

composition, concentration, and injection dosage of PRP, which should be further studied.

3.5 Promotion of degenerative disc regeneration

IVD degeneration (IVDD) is a serious global health concern. In 2019 alone, the global prevalence rate exceeded 60%, with a higher prevalence among men and the elderly, resulting in high healthcare costs for families and societies (4). The pathophysiological process of IVDD involves dehydration of the NP, tearing of the AF, rupture of the cartilage endplate, and inflammatory factors (105). These cascade reactions are often the root of discogenic pain and LDH, which can affect the extension and flexion of the spine and, in severe cases, lead to disability or even loss of work force (106). Due to the avascular tissue structure of the IVD, its self-healing ability is extremely poor and common drug therapy is generally ineffective. Currently, IVDD treatment methods include mainly bed rest, epidural injection, physical therapy, surgical decompression, disc fusion, and disc replacement (107).

However, clinical treatment (including conservative and surgical methods) is still aimed at alleviating symptoms rather than limiting disease progression or preventing disease according to etiology. Therefore, it is necessary to develop new treatment strategies. In recent years, regenerative biotherapy targeting IVD regeneration, including gene therapy, stem cell injection, and growth factor tissue engineering, has become the focus of recent research (108). PRP is also being investigated for this purpose. Related studies have shown that growth factors (TGF- β 1, VEGF, PDGF, and EGF) and adhesive proteins (fibrin, fibronectin, and vitronectin) in PRP can stimulate NP cell proliferation and extracellular matrix regeneration. This is helpful for intervertebral disc repair and symptom relief in early IDD patients (4).

Gelalis et al. injected autologous PRP into a rabbit IVDD model and found that the degree of degeneration of AF and NP was significantly lower in the PRP group than in the control group during the 6-week follow-up period. Notably, the histological analysis of hematoxylin-eosin staining in the treated group showed a significant increase in type II collagen expression (Figure 5A), which resulted in significant reversal and regeneration of the affected disc (98). In the artificial simulation of NP, alginate, a highly customizable biocompatible polymer whose properties can be adjusted, is used. Growney et al. combined PRP with alginate chemistry using carbondiimine chemistry, and the obtained a hydrogel that had good biocompatibility and mechanical properties. After 14 days of co-culture with human nucleus pulposus cells (hNPC), quantitative analysis of glycoaminoglycan showed that the complex allowed ECM expression, suggesting that PRP-modified alginate could stimulate matrix synthesis and repair (109). PRP also restored glycosaminoglycan levels in another study (110). In a cell therapy trial, the researchers combined PRP with adipose tissue-derived stromal cells (ADSC) to treat a New Zealand rabbit model of early disc degeneration. After 4 weeks, the signal strength and disc height on T2-weighted MRI were assessed. The disc signal in the ADSC combined with PRP group showed higher intensity than that in the other groups (Figure 6A) and was statistically significant in reversing disc degeneration (Figure 6B) (111). Similar therapies based on the combination of PRP and stem cells have been reported in many studies (113–116), and the biological efficacy of PRP has been confirmed in the experimental results. With the addition of PRP, many types of stem cells can differentiate into NP cell phenotype, and the diseased intervertebral disc can be reversed and regenerated to a certain extent, which provides a potential feasible scheme for future clinical treatment.

3.6 Promotion of ligament injury repair

The spine ligaments carry most of the tension load on the spine and their carrying capacity is the strongest when the load direction is in line with the direction of the fibers. When the spinal segment is in motion, the corresponding ligaments are stretched and stabilize the spine (6). The spinal ligaments have many functions. First, spinal ligaments provide sufficient physical activity between the two vertebral bodies to maintain a certain posture. Second, they protect the spinal cord by limiting movement, maintaining it within the proper physiological range, and absorbing energy. Third, by limiting displacement, they absorb high load and highspeed energy to protect the spinal cord from injury (117, 118). Therefore, the treatment of ligament injuries plays a vital role in maintaining spinal stability. Autologous PRP was administered to a rabbit model mimicking spinal ligament injury and compared with a saline-injected control group. Better healing was observed in the morphology and histology of the treated ligaments, which was determined to be achieved through activation of inflammatory pathways (IL-17 and TNF) (119), by pathway analysis. This idea was partly supported by another animal study. Hudgens et al. analyzed the effect of PRP on gene expression changes in tendon fibroblasts by microarray and analyzed multiple changes in gene expression using the Ingenuity Pathway Analysis software. They concluded that PRP induced a large number of inflammatory responses and oxidative stress in fibroblasts through activation of the TNF-α and NFκB signaling pathways, leading to tissue regeneration responses (Figures 6C–E) (112). The supraspinal ligament (SSL) and interspinous ligament (ISL), as part of the posterior ligament complex, play an indispensable role in spinal stability. A case report described two cases of SSL and ISL injury, in which, ultrasound-guided ligament-targeted injection of LR-PRP leukocyte-rich plasma was successful, with almost 100% pain improvement 6 and 9 months after treatment, respectively (120).

3.7 PRP for treatment of sacroiliac joint disease

Another common cause of lower back pain is sacroiliac joint (SIJ) disease, which is considered the most likely source of lower

10.3389/fendo.2023.1138255

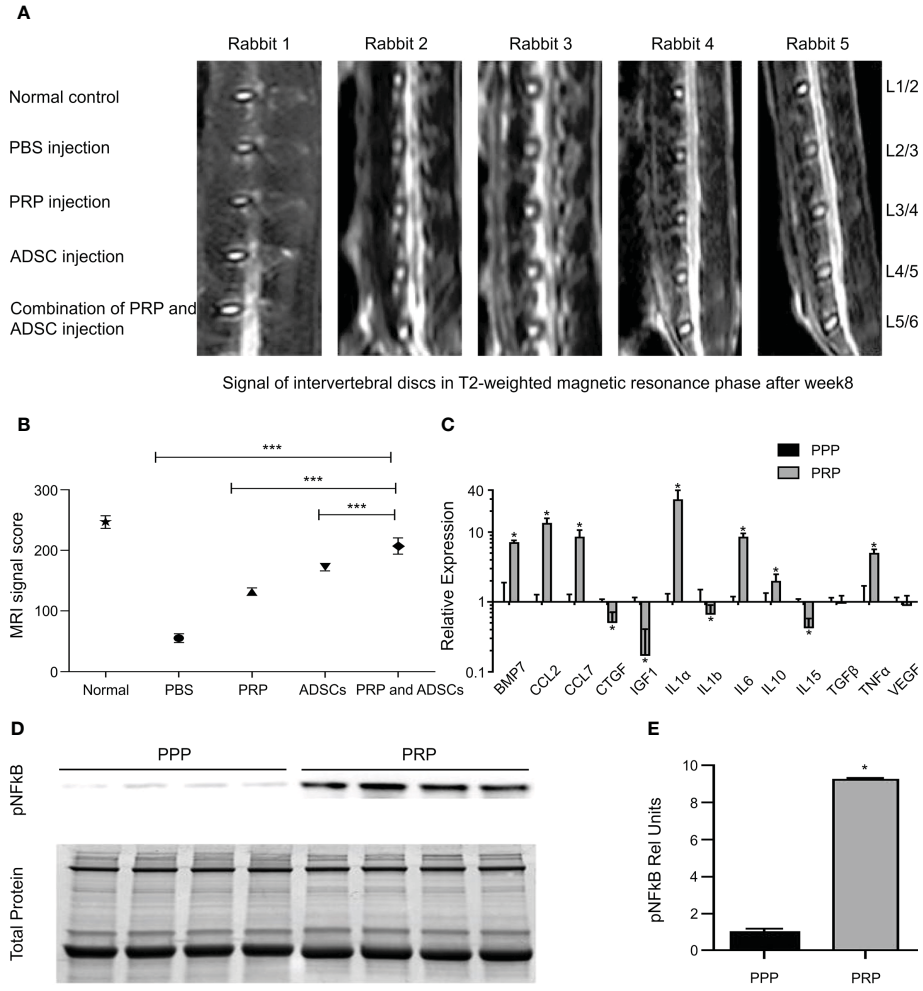

FIGURE 6
(A) The disc signals in magnetic resonance T2-weighted image in the group of ADSC-combined PRP showed higher signal strength than the other groups. **(B)** PRP combination with ADSCs has the best effect in reversing degeneration. **(C)** Gene expression of growth factor and cytokine transcripts from PPP or PRP treated tendon fibroblasts. **(D)** Immunoblots for phospho NFκB activation from tendon fibroblasts treated with PRP or PPP. **(E)** Band densitometry analysis for phospho NFκB blots. Reproduced with permission from (111, 112). * P< 0.05, *** P<0.001.

back pain in patients after lumbosacral or lumbar fusion surgery (121). Initial treatment of SIJ disease is usually conservative and includes physical therapy, massage therapy, and drug therapy. However, these treatments are often aimed at pain relief, rather than eradication. Other treatment options, such as periarticular injection, intraarticular injection, or nerve block, are generally administered if there is no improvement in symptoms after 6 weeks of conservative treatment. Surgery is considered when all treatments fail (7). PRP can be used as a new treatment modality for the treatment of SIJ disease.

This concept has been tested in several clinical trials. In a prospective randomized trial, Singla et al. found that PRP efficacy was maintained over a 3-month follow-up period, with VAS scores reduced to 90%, while efficacy in the steroid group was reduced to only 25% over the same time period. The results of Modified Oswestry Disability Questionnaire (MODQ) and SF-12 also confirmed the efficacy of PRP (122). Patrick et al. reported similar results (123). This may be due to the abundance of growth factors in PRP, which enhances the biological environment and contributes to tissue homeostasis. Notably, in one case report, the efficacy of PRP maintained improvement in joint stability and low back pain after 4 years of treatment (124). Therefore, according to clinical trials, it can be concluded that ultrasound-guided PRP injection is a safe and effective treatment for SIJ disease and can reduce dysfunction and low back pain.

3.8 PRP for treatment of related complications

Related complications of spinal disease also plague healthcare professionals and pose a significant risk to patient outcomes, including shoulder pain, deep surgical site infections, pressure ulcers, and epidural fibrosis. Therefore, treatment of complications is of great importance for the good prognosis of patients with spinal diseases.

Shoulder pain is one of the most common complaints in patients with spinal cord injuries in wheelchairs. The common causes include

shoulder tendinopathy and other musculoskeletal disorders. In a prospective trial of six patients with chronic shoulder pain due to rotator cuff disease, Dyson-Hudson et al. treated the lesion with ultrasound-guided injection of PRP. During the 24-week follow-up period, the wheelchair user shoulder pain index, pain NRS, and the physical examination scores showed a downward trend. The overall condition of the patient improved and no adverse events were reported (125). The efficacy of PRP has also been demonstrated in shoulder pain caused by biceps tendinopathy (126).

Deep surgical site infections (dSSI) undoubtedly pose significant therapeutic challenges for spinal surgeons, with post-infection treatment typically focused on surgical debridement, wound drainage, and long-term antibiotic therapy. Vasilikos added PRF to 12 patients at the time of the second surgical revision. All patients achieved complete wound healing between 14 and 21 days, and no recurrence of dSSI or complications were observed during follow-up (127).

Pressure ulcers (PrU) is one of the main complications of SCI. PrU may be more difficult to heal in patients with SCI because such patients often require intensive care around the clock. This is certainly a daunting challenge for patients and caregivers. PrU often does not heal and leads to progressive chronic inflammation, which is the root cause of death in SCI patients (128). PrU healing is a dynamic and complex process, and many growth factors in platelets can regulate this complex event and improve the quality of life and prognosis of patients. In a pilot study of 15 patients with SCI and chronic PrU who developed fistulas, the authors observed a decrease in fistula secretion levels after 1 week of PRP treatment, no fistulas at 2 weeks, and complete disappearance of fistulas at 3 weeks on MRI (129). Gurpreet et al. demonstrated in comparative tests that PRP significantly improved ulcer area, volume, and pressure ulcer healing scale scores compared to hydrogel dressings (Figures 7A–C), and had significant advantages in granulation, epithelial formation, and vascular formation (130). Similar experiments have also demonstrated the feasibility of PRP in the treatment of PrU (128, 132, 133). PRP may be a better alternative to traditional dressings for the treatment of PrU.

Lower back pain after laminectomy is a recurrent clinical condition that has attracted the attention of spinal surgeons. This is caused by epidural fibrosis, which occurs naturally after laminectomy. Excessive scarring produces adhesion between tissues or stress on surrounding anatomical structures, leading to clinically significant sequelae. Therefore, effective prevention of epidural fibrosis is conducive to patient prognosis. In an animal study, Guler et al. performed laminectomy in male rats and covered the exposed dura with fat pads, collagenous dura matrix, and PRP. At the end of the week 4, the three groups of rats were sacrificed and the samples were histologically analyzed. Epidural fibrosis (grade 3, 43%) was more common and presented the largest area of fibrotic scar tissue in the collagen-dural matrix group, while no fibroblast activity was detected in PRP group (grade 1, 71%; grade 0, grade 2, 14%). The PRP group prevented epidural fibrosis more efficiently than the fat pad group (grade 1, 71%; grade 2, 28%) and also showed better results (Figure 7D) (131). Another study investigated the barrier functions of hyaluronic acid (HAS), activated polyethylene glycol, polyethylene imine (PEG), and PRP. Histopathological results showed that PRP could improve tissue integrity and reduce scar tissue level, histopathological grade, Masson's trichrome staining (MTS) grade, and fibroblast numbers. Real-time polymerase chain reaction showed that PRP reduced the levels of type I collagen, type III collagen, TGF-1β, and TNF-α compared to the control group. These results indicated that PRP could significantly reduce the level of peridural fibrosis in a rat model (134).

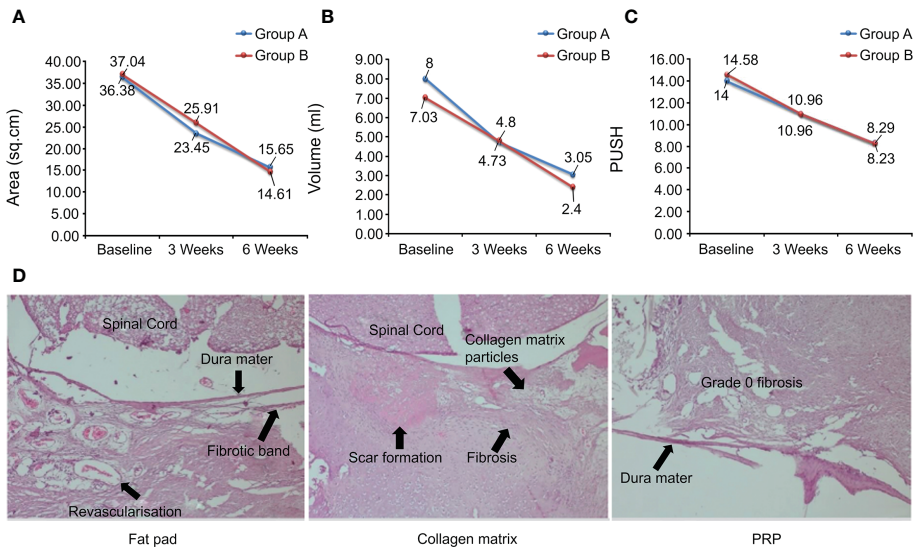

FIGURE 7
(A–C) Ulcer area, ulcer volume, and PUSH score over time. **(D)** Scar and fibrotic tissue staining in different groups. Reproduced with permission from (130, 131).

4 Safety study of PRP therapy

The safety of biological agents is very important for patients, and only when safety is guaranteed can better efficacy be achieved. In a systematic review of PRP for the treatment of skin aging, PRP accelerated skin healing and reduced signs of skin aging after laser surgery with no reported serious adverse events (135). In the field of dermatology, Shen et al. applied PRP to the treatment of skin ulcers and concluded that PRP was superior to traditional treatments owing to its high healing rate, high percentage of area loss, and smaller vascular ulcers. However, while PRP showed fewer adverse events in the short term, it showed a higher rate of adverse events in the long term (136). In a study by Nassar et al., the PRP group showed greater side effects and no significant improvement in the treatment of atrophic scars compared with patients receiving carboxyl therapy (137). In burn departments, PRP has played an important role in the repair of severe burn wounds and its safety has also been affirmed (138). In the orthopedic field, Taisuke et al. applied PRP for the treatment of ankle osteoarthritis. During the 24 weeks of treatment and follow-up, PRP did not cause any serious adverse reactions and significantly reduced pain, demonstrating the safety and efficacy of the treatment with PRP (139). PRP has also been shown to be safe and effective in similar studies on knee osteoarthritis (140).

Based on the above studies, overall PRP presents good efficacy in different fields, and most studies have shown that its safety can be guaranteed. However, some studies have also found side effects that cannot be ignored. Few in-depth studies and reports on the safety of PRP in spine surgery have been published. If PRP is to be used in spinal surgery, a large number of studies are needed to confirm its safety.

5 Conclusions and prospects

As an indispensable part of the skeletal system controlling body movements, the spine plays an important role in uploading and distribution. On being affected by a serious disease, it results in immeasurable serious consequences. Spine-related diseases are of great concern owing to their increasing annual incidence. Although the medical community has developed a variety of treatment methods, including surgical, conservative, and interventional treatment, there is no specific treatment for common diseases in spinal surgery. At present, several problems need to be addressed. For example, (1) bone nonunion and pseudarthrosis after spinal fusion, (2) accelerated degeneration of intervertebral disc, (3) how to promote intervertebral disc regeneration and restore its biomechanical properties after minimally invasive surgery, (4) how to promote nerve growth and reconnection after spinal cord injury, (5) how to avoid recurrent attacks of low back pain, (6) how to treat various complications caused by spinal column-related diseases and improve patients' prognosis and survival rate. All these are the key problems that need to be solved in this field.

This article reviewed the applications of PRP in the treatment of spinal diseases. PRP is an autologous product with platelet concentrations much higher than baseline. The therapeutic principle of PRP is that injection of PRP at the site of injury or surgery can initiate tissue repair by releasing a variety of bioactive factors (PDGF, TGF-β, VEGF, and IGF-1) and adhesive proteins in α particles, promoting revascularization and the generation of new connective tissue. This accelerates the healing of chronic injuries and repair of acute injuries. This process is attributed to the synergistic activity of various growth factors, cytokines, and local regulators *via* paracrine, endocrine, and autocrine mechanisms. PRP preparations are becoming increasingly popular due to their widespread use in different medical fields. The main advantages of PRP include its safety and the superior technology of commercial equipment for the preparation of PRP biologics that can be widely used. Most importantly, PRP is an autologous product with no known side effects and shows promising therapeutic efficacy in a wide range of medical fields.

However, there is still considerable work to be done to achieve widespread application in the field of spine-related diseases. For example, (1) standard procedures for PRP production are lacking. Currently, there are many formulations and techniques to produce PRP, but there is no standard for these parameters, including initial whole blood volume, platelet concentration, and PRP composition. (2) Individual differences. For example, age differences can lead to differences in growth factors and the overall composition of PRP. Osteoporosis can lead to differences in treatment effects. (3) Insufficient number of experiments. In both clinical trials and animal experiments, there is a low level of evidence, insufficient sample size, confusion in nomenclature, lack of standardization of preparation methods, and lack of in-depth research on basic science. (4) There is no clear consensus on indications, and (5) the cost of treatment remains controversial. Some researchers believe that short-term use of PRP is more expensive than steroid injection, while long-term treatment may be economical. Finally, the (6) lack of safety studies. Moreover, there is no uniform standard for safety assessment. Faced with these issues, spinal surgeons should conduct more clinical, randomized, controlled, and unbiased trials and a large number of animal trials with more in-depth investigation to reach a consensus on the standardized classification of PRP. Formulation of a more systematic and authoritative production and treatment standards is required. The treatment of spine-related diseases still in its early stages; however, with further understanding of PRP and the advancement of manufacturing technology, it is possible to achieve a standardized treatment plan for spine surgery in the future.

Author contributions

HW wrote the initial manuscript. CF and YX contributed new ideas. HW and YL created the figures. YX and JZ created

Table 1 HW, JZ, YX, and YL revised the manuscript. All authors contributed to the article and approved the submitted version.

Funding

This work was supported by the National Natural Science Foundation of China (Grant Nos. 82071391), the "13th Five-Y ear" Science and Technology Research Planning Project of Jilin Province (Grant No. JLKHJJKH20190042KJ), and the Achievement Transformation Fund of the First Hospital of Jilin University (Grant No. JDYYZH-2102052).

Acknowledgments

We would like to express our appreciation to everyone who was involved in the drafting and preparation of the manuscript. We would like to thank Editage (www.editage.cn) for English language editing.

Conflict of interest

The authors declare that the research was conducted in the absence of any commercial or financial relationships that could be construed as a potential conflict of interest.

Publisher's note

References

1. Yurube T, Han I, Sakai D. Concepts of regeneration for spinal diseases in 2021. *Int J Mol Sci* (2021) 22(16):8356. doi: 10.3390/ijms22168356

2. Zhao L, Manchikanti L, Kaye AD, Abd-Elsayed A. Treatment of discogenic low back pain: Current treatment strategies and future options-a literature review. *Curr Pain Headache Rep* (2019) 23(11):86. doi: 10.1007/s11916-019-0821-x

3. Ruschel LG, Agnoletto GJ, Aragao A, Duarte JS, de Oliveira MF, Teles AR. Lumbar disc herniation with contralateral radiculopathy: a systematic review on pathophysiology and surgical strategies. *Neurosurg Rev* (2021) 44(2):1071–81. doi: 10.1007/s10143-020-01294-3

4. Chang Y, Yang M, Ke S, Zhang Y, Xu G, Li Z. Effect of platelet-rich plasma on intervertebral disc degeneration. *In Vivo In Vitro: A Crit Review Oxid Med Cell Longev* (2020) 2020:8893819. doi: 10.1155/2020/8893819

5. Anjum A, Yazid MD, Fauzi Daud M, Idris J, Ng AMH, Selvi Naicker A, et al. Spinal cord injury: Pathophysiology, multimolecular interactions, and underlying recovery mechanisms. *Int J Mol Sci* (2020) 21(20):7533. doi: 10.3390/ijms21207533

6. Oxland TR. Fundamental biomechanics of the spine–what we have learned in the past 25 years and future directions. *J Biomech* (2016) 49(6):817–32. doi: 10.1016/j.jbiomech.2015.10.035

7. Gartenberg A, Nessim A, Cho W. Sacroiliac joint dysfunction: pathophysiology, diagnosis, and treatment. *Eur Spine J* (2021) 30(10):2936–43. doi: 10.1007/s00586-021-06927-9

8. Green BN, Johnson CD, Haldeman S, Griffith E, Clay MB, Kane EJ, et al. A scoping review of biopsychosocial risk factors and co-morbidities for common spinal disorders. *PloS One* (2018) 13(6):e0197987. doi: 10.1371/journal.pone.0197987

9. Bowen-Pope DF, Raines EW. History of discovery: Platelet-derived growth factor. *Arterioscler Thromb Vasc Biol* (2011) 31(11):2397–401. doi: 10.1161/ATVBAHA.108.179556

10. Ballmer-Hofer K. Vascular endothelial growth factor, from basic research to clinical applications. *Int J Mol Sci* (2018) 19(12):3750. doi: 10.3390/ijms19123750

11. Morikawa M, Derynck R, Miyazono K. TGF-beta and the TGF-beta family: Context-dependent roles in cell and tissue physiology. *Cold Spring Harb Perspect Biol* (2016) 8(5):a021873. doi: 10.1101/cshperspect.a021873

12. Wroblewski OM, Vega-Soto EE, Nguyen MH, Cederna PS, Larkin LM. Impact of human epidermal growth factor on tissue-engineered skeletal muscle structure and function. *Tissue Eng Part A* (2021) 27(17-18):1151–9. doi: 10.1089/ten.tea.2020.0255

13. Maddaluno L, Urwyler C, Werner S. Fibroblast growth factors: key players in regeneration and tissue repair. *Development* (2017) 144(22):4047–60. doi: 10.1242/dev.152587

14. Field DJ, Aggrey-Amable AA, Blick SK, Ture SK, Johanson A, Cameron SJ, et al. Platelet factor 4 increases bone marrow b cell development and differentiation. *Immunol Res* (2017) 65(5):1089–94. doi: 10.1007/s12026-017-8951-x

15. Yoshida T, Delafontaine P. Mechanisms of IGF-1-Mediated regulation of skeletal muscle hypertrophy and atrophy. *Cells* (2020) 9(9):1970. doi: 10.3390/cells9091970

16. Andia I, Abate M. Platelet-rich plasma: underlying biology and clinical correlates. *Regenerative Med* (2013) 8(5):645–58. doi: 10.2217/rme.13.59

17. Zhang W, Guo Y, Kuss M, Shi W, Aldrich AL, Untrauer J, et al. Platelet-rich plasma for the treatment of tissue infection: Preparation and clinical evaluation. *Tissue engineering Part B Rev* (2019) 25(3):225–36. doi: 10.1089/ten.teb.2018.0309

18. Anitua E. Plasma rich in growth factors: preliminary results of use in the preparation of future sites for implants. *Int J Oral Maxillofac implants* (1999) 14 (4):529–35.

19. Lim WB, Park SH, Moon YL. Platelet-rich plasma: Applications in sports medicine. *Sports Orthopaedics Traumatology Sport-Orthopädie - Sport-Traumatologie* (2015) 31(3):206–14. doi: 10.1016/j.orthtr.2015.07.003

20. Belk JW, Kraeutler MJ, Houck DA, Goodrich JA, Dragoo JL, McCarty EC. Platelet-rich plasma versus hyaluronic acid for knee osteoarthritis: A systematic review and meta-analysis of randomized controlled trials. *Am J Sports Med* (2021) 49(1):249–60. doi: 10.1177/0363546520909397

21. Mouanness M, Ali-Bynom S, Jackman J, Seckin S, Merhi Z. Use of intra-uterine injection of platelet-rich plasma (PRP) for endometrial receptivity and thickness: a literature review of the mechanisms of action. *Reprod Sci* (2021) 28(6):1659–70. doi: 10.1007/s43032-021-00579-2

22. Streit-Cieckiewicz D, Futyma K, Miotla P, Grzybowska ME, Rechberger T. Platelet-rich plasma as adjuvant therapy for recurrent vesicovaginal fistula: A prospective case series. *J Clin Med* (2019) 8(12):2122. doi: 10.3390/jcm8122122

23. Zhai Q, Wang Y, Yuan Z, Zhang R, Tian A. Effects of platelet-rich plasmapheresis during cardiovascular surgery: A meta-analysis of randomized controlled clinical trials. *J Clin Anesth* (2019) 56:88–97. doi: 10.1016/j.jclinane.2019.01.018

24. Arnalich F, Rodriguez AE, Luque-Rio A, Alio JL. Solid platelet rich plasma in corneal surgery. *Ophthalmol Ther* (2016) 5(1):31–45. doi: 10.1007/s40123-016-0051-9

25. Cao Y, Zhu X, Zhou R, He Y, Wu Z, Chen Y. A narrative review of the research progress and clinical application of platelet-rich plasma. *Ann Palliat Med* (2021) 10 (4):4823–9. doi: 10.21037/apm-20-2223

26. Mazzucco L, Balbo V, Cattana E, Guaschino R, Borzini P. Not every PRP-gel is born equal. evaluation of growth factor availability for tissues through four PRP-gel preparations: Fibrinet, RegenPRP-kit, plateltex and one manual procedure. *Vox Sang* (2009) 97(2):110–8. doi: 10.1111/j.1423-0410.2009.01188.x

27. Harrison TE, Bowler J, Levins TN, Cheng AL, Reeves KD. Platelet yield and yield consistency for six single-spin methods of platelet rich plasma preparation. *Platelets* (2020) 31(5):661–6. doi: 10.1080/09537104.2019.1663808

28. Dashore S, Chouhan K, Nanda S, Sharma A. Preparation of platelet-rich plasma: National IADVL PRP taskforce recommendations. *Indian Dermatol Online J* (2021) 12 (Suppl 1):S12–23. doi: 10.4103/idoj.idoj_269_21

29. El-Husseiny RM, Saleh HM, Moustafa AA, Salem SA. Comparison between single- versus double-spin prepared platelet-rich plasma injection in treatment of female pattern hair loss: clinical effect and relation to vascular

endothelial growth factor. *Arch Dermatol Res* (2021) 313(7):557–66. doi: 10.1007/s00403-020-02134-6

30. Prysak MH, Kyriakides CP, Zukofsky TA, Reutter SE, Cheng J, Lutz GE. A retrospective analysis of a commercially available platelet-rich plasma kit during clinical use. *PM R* (2021) 13(12):1410–7. doi: 10.1002/pmrj.12569

31. Dohan Ehrenfest DM, Rasmusson L, Albrektsson T. Classification of platelet concentrates: from pure platelet-rich plasma (P-PRP) to leucocyte- and platelet-rich fibrin (L-PRF). *Trends Biotechnol* (2009) 27(3):158–67. doi: 10.1016/j.tibtech.2008.11.009

32. Magalon J, Chateau AL, Bertrand B, Louis ML, Silvestre A, Giraudo L, et al. DEPA classification: A proposal for standardising PRP use and a retrospective application of available devices. *BMJ Open Sport Exerc Med* (2016) 2(1):e000060. doi: 10.1136/bmjsem-2015-000060

33. Harrison P. Subcommittee on platelet physiology, the use of platelets in regenerative medicine and proposal for a new classification system: Guidance from the SSC of the ISTH. *J Thromb Haemost* (2018) 16(9):1895–900. doi: 10.1111/jth.14223

34. Marx RE. Platelet-rich plasma: Evidence to support its use. *J Oral Maxillofac Surg* (2004) 62(4):489–96. doi: 10.1016/j.joms.2003.12.003

35. Kholmukhamedov A, Janecke R, Choo HJ, Jobe SM. The mitochondrial calcium uniporter regulates procoagulant platelet formation. *J Thromb Haemost* (2018) 16(11):2315–21. doi: 10.1111/jth.14284

36. Boer W, van Tornout M, Solmi F, Willaert X, Schetz M, Oudemans-van Straaten H. Determinants of total/ionized calcium in patients undergoing citrate CVVH: A retrospective observational study. *J Crit Care* (2020) 59:16–22. doi: 10.1016/j.jcrc.2020.05.005

37. Pensato R, La Padula S. The use of platelet-rich plasma in aesthetic and regenerative medicine: A comprehensive review. *Aesthetic Plast Surg* (2022). doi: 10.1007/s00266-022-02781-2

38. Cavallo C, Roffi A, Grigolo B, Mariani E, Pratelli L, Merli G, et al. Platelet-rich plasma: The choice of activation method affects the release of bioactive molecules. *BioMed Res Int* (2016) 2016:6591717. doi: 10.1155/2016/6591717

39. Pachito DV, Bagattini AM, de Almeida AM, Mendrone-Junior A, Riera R. Technical procedures for preparation and administration of platelet-rich plasma and related products: A scoping review. *Front Cell Dev Biol* (2020) 8:598816. doi: 10.3389/fcell.2020.598816

40. Alves R, Grimalt R. A review of platelet-rich plasma: History, biology, mechanism of action, and classification. *Skin Appendage Disord* (2018) 4(1):18–24. doi: 10.1159/000477353

41. Knezevic NN, Candido KD, Vlaeyen JWS, Van Zundert J, Cohen SP. Low back pain. *Lancet* (2021) 398(10294):78–92. doi: 10.1016/S0140-6736(21)00733-9

42. Bogduk N, Aprill C, Derby R. Lumbar discogenic pain: State-of-the-Art review. *Pain Med* (2013) 14(6):813–36. doi: 10.1111/pme.12082

43. Fujii K, Yamazaki M, Kang JD, Risbud MV, Cho SK, Qureshi SA, et al. Discogenic back pain: Literature review of definition, diagnosis, and treatment. *JBMR Plus* (2019) 3(5):e10180. doi: 10.1002/jbm4.10180

44. Yang G, Liao W, Shen M, Mei H. Insight into neural mechanisms underlying discogenic back pain. *J Int Med Res* (2018) 46(11):4427–36. doi: 10.1177/0300060518799902

45. Enthoven WT, Roelofs PD, Deyo RA, van Tulder MW, Koes BW. Non-steroidal anti-inflammatory drugs for chronic low back pain. *Cochrane Database Syst Rev* (2016) 2:CD012087. doi: 10.1002/14651858.CD012087

46. Liu J, He Y, Huang B, Zhang X, Shan Z, Chen J, et al. Reoccurring discogenic low back pain (LBP) after discoblock treated by oblique lumbar interbody fusion (OLIF). *J Orthop Surg Res* (2020) 15(1):22. doi: 10.1186/s13018-020-1554-6

47. Lu S, Sun S, Kong C, Sun W, Hu H, Wang Q, et al. Long-term clinical results following charite III lumbar total disc replacement. *Spine J* (2018) 18(6):917–25. doi: 10.1016/j.spinee.2017.08.252

48. Michalik AJ, Patel RK. Evaluation of transforaminal epidural steroid injections for discogenic axial lumbosacral back pain utilizing PROMIS as an outcome measure. *Spine J* (2021) 21(2):202–11. doi: 10.1016/j.spinee.2020.10.018

49. Owen PJ, Miller CT, Mundell NL, Verswijveren S, Tagliaferri SD, Brisby H, et al. Which specific modes of exercise training are most effective for treating low back pain? Network meta-analysis. *Br J Sports Med* (2020) 54(21):1279–87. doi: 10.1136/bjsports-2019-100886

50. Sainoh T, Orita S, Miyagi M, Inoue G, Kamoda H, Ishikawa T, et al. Single intradiscal administration of the tumor necrosis factor-alpha inhibitor, etanercept, for patients with discogenic low back pain. *Pain Med* (2016) 17(1):40–5. doi: 10.1111/pme.12892

51. Akeda K, Ohishi K, Masuda K, Bae WC, Takegami N, Yamada J, et al. Intradiscal injection of autologous platelet-rich plasma releasate to treat discogenic low back pain: A preliminary clinical trial. *Asian Spine J* (2017) 11(3):380–9. doi: 10.4184/asj.2017.11.3.380

52. Lutz GE. Increased nuclear T2 signal intensity and improved function and pain in a patient one year after an intradiscal platelet-rich plasma injection. *Pain Med* (2017) 18(6):1197–9. doi: 10.1093/pm/pnw299

53. Ruiz-Lopez R, Tsai YC, Randomized Double-Blind Controlled Pilot Study Comparing Leucocyte-Rich Platelet-Rich Plasma A. And corticosteroid in caudal epidural injection for complex chronic degenerative spinal pain. *Pain Pract* (2020) 20(6):639–46. doi: 10.1111/papr.12893

54. Zhang J, Liu D, Gong Q, Chen J, Wan L. Intradiscal autologous platelet-rich plasma injection for discogenic low back pain: A clinical trial. *BioMed Res Int* (2022) 2022:9563693. doi: 10.1155/2022/9563693

55. Tuakli-Wosornu YA, Terry A, Boachie-Adjei K, Harrison JR, Gribbin CK, LaSalle EE, et al. Lumbar intradiskal platelet-rich plasma (PRP) injections: A prospective, double-blind, randomized controlled study. *PM R* (2016) 8(1):1–10. doi: 10.1016/j.pmrj.2015.08.010

56. Zielinski MA, Evans NE, Bae H, Kamrava E, Calodney A, Remley K, et al. P; Jordan, s., safety and efficacy of platelet rich plasma for treatment of lumbar discogenic pain: A prospective, multicenter, randomized, double-blind study. *Pain Physician* (2022) 25(1):29–34.

57. Amin RM, Andrade NS, Neuman, B. J. Lumbar disc herniation. *Curr Rev Musculoskelet Med* (2017) 10(4):507–16. doi: 10.1007/s12178-017-9441-4

58. Frapin L, Clouet J, Delplace V, Fusellier M, Guicheux J, Le Visage C. Lessons learned from intervertebral disc pathophysiology to guide rational design of sequential delivery systems for therapeutic biological factors. *Advanced Drug Delivery Rev* (2019) 149-150:49–71. doi: 10.1016/j.addr.2019.08.007

59. Schroeder GD, Guyre CA, Vaccaro AR. The epidemiology and pathophysiology of lumbar disc herniations. *Semin Spine Surg* (2016) 28(1):2–7. doi: 10.1053/j.semss.2015.08.003

60. Rawson B. Platelet-rich plasma and epidural platelet lysate: Novel treatment for lumbar disk herniation. *J Am Osteopath Assoc* (2020) 120(3):201–7. doi: 10.7556/jaoa.2020.032

61. Jiang Y, Zuo R, Yuan S, et al. Clinical outcomes of transforaminal endoscopic lumbar discectomy with or without platelet-rich plasma injection in the treatment of lumbar disc herniation: A prospective, randomized, controlled pilot study. *Res Sq (2020)* [Preprint]. doi: 10.21203/rs.3.rs-86541/v1

62. Bhatia R, Chopra G. Efficacy of platelet rich plasma via lumbar epidural route in chronic prolapsed intervertebral disc patients-a pilot study. *J Clin Diagn Res* (2016) 10(9):UC05–7. doi: 10.7860/JCDR/2016/21863.8482

63. Xu Z, Wu S, Li X, Liu C, Fan S, Ma C, et al. Ultrasound-guided transforaminal injections of platelet-rich plasma compared with steroid in lumbar disc herniation: A prospective, randomized, controlled study. *Neural Plasticity* (2021) 2021:1–11. doi: 10.1155/2021/5558138

64. Jeong HJ, Yun Y, Lee SJ, Ha Y, Gwak SJ. Biomaterials and strategies for repairing spinal cord lesions. *Neurochem Int* (2021) 144:104973. doi: 10.1016/j.neuint.2021.104973

65. Ahuja CS, Mothe A, Khazaei M, Badhiwala JH, Gilbert EA, van der Kooy D, et al. The leading edge: Emerging neuroprotective and neuroregenerative cell-based therapies for spinal cord injury. *Stem Cells Transl Med* (2020) 9(12):1509–30. doi: 10.1002/sctm.19-0135

66. Baltin ME, Sabirova DE, Kiseleva EI, Kamalov MI, Abdullin TI, Petrova NV, et al. Comparison of systemic and localized carrier-mediated delivery of methylprednisolone succinate for treatment of acute spinal cord injury. *Exp Brain Res* (2021) 239(2):627–38. doi: 10.1007/s00221-020-05974-w

67. Joaquim AF, Daniel JW, Schroeder GD, Vaccaro AR. Neuroprotective agents as an adjuvant treatment in patients with acute spinal cord injuries: A qualitative systematic review of randomized trials. *Clin Spine Surg* (2020) 33(2):65–75. doi: 10.1097/BSD.0000000000000861

68. Huebner EA, Budel S, Jiang Z, Omura T, Ho TS-Y, Barrett L, et al. Diltiazem promotes regenerative axon growth. *Mol Neurobiol* (2018) 56(6):3948–57. doi: 10.1007/s12035-018-1349-5

69. Li HX, Cui J, Fan JS, Tong JZ. An observation of the clinical efficacy of combining riluzole with mannitol and hyperbaric oxygen in treating acute spinal cord injury. *Pak J Med Sci* (2021) 37(2):320–4. doi: 10.12669/pjms.37.2.3418

70. Canseco JA, Karamian BA, Bowles DR, Markowitz MP, DiMaria SL, Semenza NC, et al. Updated review: The steroid controversy for management of spinal cord injury. *World Neurosurg* (2021) 150:1–8. doi: 10.1016/j.wneu.2021.02.116

71. Badhiwala JH, Wilson JR, Witiw CD, Harrop JS, Vaccaro AR, Aarabi B, et al. The influence of timing of surgical decompression for acute spinal cord injury: a pooled analysis of individual patient data. *Lancet Neurol* (2021) 20(2):117–26. doi: 10.1016/S1474-4422(20)30406-3

72. Behroozi Z, Ramezani F, Janzadeh A, Rahimi B, Nasirinezhad F. Platelet-rich plasma in umbilical cord blood reduces neuropathic pain in spinal cord injury by altering the expression of ATP receptors. *Physiol Behav* (2021) 228:113186. doi: 10.1016/j.physbeh.2020.113186

73. Lee DY, Park YJ, Song SY, Hwang SC, Kim KT, Kim DH. The importance of early surgical decompression for acute traumatic spinal cord injury. *Clin Orthop Surg* (2018) 10(4):448–54. doi: 10.4055/cios.2018.10.4.448

74. Kajikawa K, Imaizumi K, Shinozaki M, Shibata S, Shindo T, Kitagawa T, et al. Cell therapy for spinal cord injury by using human iPSC-derived region-specific neural progenitor cells. *Mol Brain* (2020) 13(1):120. doi: 10.1186/s13041-020-00662-w

75. Chen BK, Madigan NN, Hakim JS, Dadsetan M, McMahon SS, Yaszemski MJ, et al. GDNF schwann cells in hydrogel scaffolds promote regional axon regeneration, remyelination and functional improvement after spinal cord

transection in rats. *J Tissue Eng Regenerative Med* (2018) 12(1):e398–407. doi: 10.1002/term.2431

76. Takeuchi M, Kamei N, Shinomiya R, Sunagawa T, Suzuki O, Kamoda H, et al. Human platelet-rich plasma promotes axon growth in brain-spinal cord coculture. *Neuroreport* (2012) 23(12):712–6. doi: 10.1097/WNR.0b013e3283567196

77. Zhao T, Yan W, Xu K, Qi Y, Dai X, Shi Z. Combined treatment with platelet-rich plasma and brain-derived neurotrophic factor-overexpressing bone marrow stromal cells supports axonal remyelination in a rat spinal cord hemi-section model. *Cytotherapy* (2013) 15(7):792–804. doi: 10.1016/j.jcyt.2013.04.004

78. Baklaushev VP, Bogush VG, Kalsin VA, Sovetnikov NN, Samoilova EM, Revkova VA, et al. Tissue engineered neural constructs composed of neural precursor cells, recombinant spidroin and PRP for neural tissue regeneration. *Sci Rep* (2019) 9(1):3161. doi: 10.1038/s41598-019-39341-9

79. Castro MV, Silva M, Chiarotto GB, Volpe BB, Santana MH, Malheiros Luzo AC, et al. Reflex arc recovery after spinal cord dorsal root repair with platelet rich plasma (PRP). *Brain Res Bull* (2019) 152:212–24. doi: 10.1016/j.brainresbull.2019.07.024

80. Liao J-C. Positive effect on spinal fusion by the combination of platelet-rich plasma and collagen-mineral scaffold using lumbar posterolateral fusion model in rats. *J Orthopaedic Surg Res* (2019) 14(1):39. doi: 10.1186/s13018-019-1076-2

81. Chen NF, Sung CS, Wen ZH, Chen CH, Feng CW, Hung HC, et al. Therapeutic effect of platelet-rich plasma in rat spinal cord injuries. *Front Neurosci* (2018) 12:252. doi: 10.3389/fnins.2018.00252

82. Umale S, Yoganandan N, Baisden JL, Choi H, Kurpad SN. A biomechanical investigation of lumbar interbody fusion techniques. *J Mech Behav BioMed Mater* (2022) 125:104961. doi: 10.1016/j.jmbbm.2021.104961

83. Endler P, Ekman P, Berglund I, Möller H, Gerdhem P. Long-term outcome of fusion for degenerative disc disease in the lumbar spine. *Bone Joint J* (2019) 101-B (12):1526–33. doi: 10.1302/0301-620X.101B12.BJJ-2019-0427.R1

84. Kurucan E, Bernstein DN, Thirukumaran C, Jain A, Menga EN, Rubery PT, et al. National trends in spinal fusion surgery for neurofibromatosis. *Spine Deform* (2018) 6(6):712–8. doi: 10.1016/j.jspd.2018.03.012

85. Rothrock RJ, McNeill IT, Yaeger K, Oermann EK, Cho SK, Caridi JM. Lumbar lordosis correction with interbody fusion: Systematic literature review and analysis. *World Neurosurg* (2018) 118:21–31. doi: 10.1016/j.wneu.2018.06.216

86. Uehara M, Takahashi J, Kuraishi S, Ikegami S, Futatsugi T, Oba H, et al. Two-stage posterior spinal fusion for early-onset scoliosis: Two case reports. *Med (Baltimore)* (2019) 98(9):e14728. doi: 10.1097/MD.0000000000014728

87. Watanabe K, Katsumi K, Ohashi M, Shibuya Y, Hirano T, Endo N, et al. Surgical outcomes of spinal fusion for osteoporotic vertebral fracture in the thoracolumbar spine: Comprehensive evaluations of 5 typical surgical fusion techniques. *J Orthop Sci* (2019) 24(6):1020–6. doi: 10.1016/j.jos.2019.07.018

88. Yang LH, Liu W, Li J, Zhu WY, An LK, Yuan S, et al. Lumbar decompression and lumbar interbody fusion in the treatment of lumbar spinal stenosis: A systematic review and meta-analysis. *Med (Baltimore)* (2020) 99(27):e20323. doi: 10.1097/MD.0000000000020323

89. Meng B, Bunch J, Burton D, Wang J. Lumbar interbody fusion: recent advances in surgical techniques and bone healing strategies. *Eur Spine J* (2021) 30(1):22–33. doi: 10.1007/s00586-020-06596-0

90. Salamanna F, Tschon M, Borsari V, Pagani S, Martini L, Fini M. Spinal fusion procedures in the adult and young population: a systematic review on allogenic bone and synthetic grafts when compared to autologous bone. *J Mater Sci Mater Med* (2020) 31(6):51. doi: 10.1007/s10856-020-06389-3

91. Letchuman V, Ampie L, Choy W, DiDomenico JD, Syed HR, Buchholz AL. Bone grafting and biologics for spinal fusion in the pediatric population: current understanding and future perspective. *Neurosurgical Focus* (2021) 50(6):e8. doi: 10.3171/2021.3.FOCUS2148

92. Tuchman A, Brodke DS, Youssef JA, Meisel HJ, Dettori JR, Park JB, et al. Iliac crest bone graft versus local autograft or allograft for lumbar spinal fusion: A systematic review. *Global Spine J* (2016) 6(6):592–606. doi: 10.1055/s-0035-1570749

93. Duarte RM, Varanda P, Reis RL, Duarte ARC, Correia-Pinto J. Biomaterials and bioactive agents in spinal fusion. *Tissue engineering Part B Rev* (2017) 23(6):540–51. doi: 10.1089/ten.teb.2017.0072

94. Iqbal J, Pepkowitz SH, Klapper E. Platelet-rich plasma for the replenishment of bone. *Curr Osteoporos Rep* (2011) 9(4):258–63. doi: 10.1007/s11914-011-0080-1

95. Han J, Gao F, Li Y, Ma J, Sun W, Shi L, et al. The use of platelet-rich plasma for the treatment of osteonecrosis of the femoral head: A systematic review. *BioMed Res Int* (2020) 2020:2642439. doi: 10.1155/2020/2642439

96. Van Eps JL, Fernandez-Moure JS, Cabrera FJ, Taraballi F, Paradiso F, Minardi S, et al. Improved posterolateral lumbar spinal fusion using a biomimetic, nanocomposite scaffold augmented by autologous platelet-rich plasma. *Front Bioeng Biotechnol* (2021) 9:622099. doi: 10.3389/fbioe.2021.622099

97. Kubota G, Kamoda H, Orita S, Inage K, Ito M, Yamashita M, et al. Efficacy of platelet-rich plasma for bone fusion in transforaminal lumbar interbody fusion. *Asian Spine J* (2018) 12(1):112–8. doi: 10.4184/asj.2018.12.1.112

98. Gelalis ID, Christoforou G, Charchanti A, Gkiatas I, Pakos E, Papadopoulos D, et al. Autologous platelet-rich plasma (PRP) effect on intervertebral disc restoration: an experimental rabbit model. *Eur J Orthop Surg Traumatol* (2019) 29(3):545–51. doi: 10.1007/s00590-018-2337-1

99. Bjerke BT, Zarrabian M, Aleem IS, Fogelson JL, Currier BL, Freedman BA, et al. Incidence of osteoporosis-related complications following posterior lumbar fusion. *Global Spine J* (2018) 8(6):563–9. doi: 10.1177/2192568217743727

100. Zhu W, Kong C, Pan F, Ouyang M, Sun K, Lu S. Engineered collagen-binding bone morphogenetic protein-2 incorporated with platelet-rich plasma accelerates lumbar fusion in aged rats with osteopenia. *Exp Biol Med (Maywood)* (2021) 246 (14):1577–85. doi: 10.1177/15353702211001039

101. Yolcu YU, Wahood W, Eissa AT, Alvi MA, Freedman BA, Elder BD, et al. (2020). The impact of platelet-rich plasma on postoperative outcomes after spinal fusion: A systematic review and meta-analysis. *J. Neurosurg.: Spine SPI*. 33(4), 540–7. doi: 10.3171/2020.3.SPINE2046

102. Manini DR, Shega FD, Guo C, Wang Y. Role of platelet-rich plasma in spinal fusion surgery: Systematic review and meta-analysis. *Adv Orthop* (2020) 2020:8361798. doi: 10.1155/2020/8361798

103. Pairuchvej S, Muljadi JA, Arirachakaran A, Kongtharvonskul J. Efficacy of platelet-rich plasma in posterior lumbar interbody fusion: systematic review and meta-analysis. *Eur J Orthop Surg Traumatol* (2020) 30(4):583–93. doi: 10.1007/s00590-019-02603-3

104. Kubota G, Kamoda H, Orita S, Yamauchi K, Sakuma Y, Oikawa Y, et al. Platelet-rich plasma enhances bone union in posterolateral lumbar fusion: A prospective randomized controlled trial. *Spine J* (2019) 19(2):e34–40. doi: 10.1016/j.spinee.2017.07.167

105. Kirnaz S, Capadona C, Wong T, Goldberg JL, Medary B, Sommer F, et al. Fundamentals of intervertebral disc degeneration. *World Neurosurg* (2022) 157:264–73. doi: 10.1016/j.wneu.2021.09.066

106. Roh EJ, Darai A, Kyung JW, Choi H, Kwon SY, Bhujel B, et al. Genetic therapy for intervertebral disc degeneration. *Int J Mol Sci* (2021) 22(4):1579. doi: 10.3390/ijms22041579

107. Zhang XB, Hu YC, Cheng P, Zhou HY, Chen XY, Wu D, et al. Targeted therapy for intervertebral disc degeneration: inhibiting apoptosis is a promising treatment strategy. *Int J Med Sci* (2021) 18(13):2799–813. doi: 10.7150/ijms.59171

108. Kirnaz S, Singh S, Capadona C, Lintz M, Goldberg JL, McGrath LBJr., et al. Innovative biological treatment methods for degenerative disc disease. *World Neurosurg* (2022) 157:282–99. doi: 10.1016/j.wneu.2021.09.068

109. Growney EA, Linder HR, Garg K, Bledsoe JG, Sell SA. Bio-conjugation of platelet-rich plasma and alginate through carbodiimide chemistry for injectable hydrogel therapies. *J BioMed Mater Res B Appl Biomater* (2020) 108(5):1972–84. doi: 10.1002/jbm.b.34538

110. Nikkhoo M, Wang JL, Abdollahi M, Hsu YC, Parnianpour M, Khalaf K. A regenerative approach towards recovering the mechanical properties of degenerated intervertebral discs: Genipin and platelet-rich plasma therapies. *Proc Inst Mech Eng H* (2017) 231(2):127–37. doi: 10.1177/0954411916681597

111. Ma C, Wang R, Zhao D, Wang N, Han Y, Wang S, et al. Efficacy of platelet-rich plasma containing xenogenic adipose tissue-derived stromal cells on restoring intervertebral disc degeneration: A preclinical study in a rabbit model. *Pain Res Manag* (2019) 2019:6372356. doi: 10.1155/2019/6372356

112. Hudgens JL, Sugg KB, Grekin JA, Gumucio JP, Bedi A, Mendias CL. Platelet-rich plasma activates proinflammatory signaling pathways and induces oxidative stress in tendon fibroblasts. *Am J Sports Med* (2016) 44(8):1931–40. doi: 10.1177/0363546516637176

113. Russo F, Ambrosio L, Peroglio M, Guo W, Wangler S, Gewiess J, et al. And platelet-rich plasma hydrogel for mesenchymal stem cell delivery in the intervertebral disc: An organ culture study. *Int J Mol Sci* (2021) 22(6):2963. doi: 10.3390/ijms22062963

114. Wang SZ, Jin JY, Guo YD, Ma LY, Chang Q, Peng XG, et al. Intervertebral disc regeneration using plateletrich plasmacontaining bone marrowderived mesenchymal stem cells: A preliminary investigation. *Mol Med Rep* (2016) 13(4):3475–81. doi: 10.3892/mmr.2016.4983

115. Zhang Z, Ma J, Ren D, Li F. A possible injectable tissue engineered nucleus pulposus constructed with platelet-rich plasma and ADSCs. *vitro J Orthop Surg Res* (2020) 15(1):311. doi: 10.1186/s13018-020-01840-1

116. Zhao C, Xu X, Hu J, Lu H. Histological observation of a gelatin sponge transplant loaded with bone marrow-derived mesenchymal stem cells combined with platelet-rich plasma in repairing an annulus defect. *PloS One* (2017) 12(2):e0171500. doi: 10.1371/journal.pone.0171500

117. Zander T, Rohlmann A, Bergmann G. Influence of ligament stiffness on the mechanical behavior of a functional spinal unit. *J Biomech* (2004) 37(7):1107–11. doi: 10.1016/j.jbiomech.2003.11.019

118. Chazal J, Tanguy A, Bourges M, Gaurel G, Escande G, Guillot M, et al. Biomechanical properties of spinal ligaments and a histological study of the supraspinal ligament in traction. *J biomechanics* (1985) 18(3):167–76. doi: 10.1016/0021-9290(85)90202-7

119. Liu W, Xie X, Wu J. Platelet-rich plasma promotes spinal ligament healing after injury. *Clin Lab* (2020) 66(7). doi: 10.7754/Clin.Lab.2019.191154

120. Creighton A, Sanguino RA, Cheng J, Wyss JF. Successful treatment of supraspinous and interspinous ligament injury with ultrasound-guided platelet-rich plasma injection: Case series. *HSS J* (2021) 17(2):227–30. doi: 10.1177/1556331621992312

121. Buchanan P, Vodapally S, Lee DW, Hagedorn JM, Bovinet C, Strand N, et al. Successful diagnosis of sacroiliac joint dysfunction. *J Pain Res* (2021) 14:3135–43. doi: 10.2147/JPR.S327351

122. Singla V, Batra YK, Bharti N, Goni VG, Marwaha N. Steroid vs. platelet-rich plasma in ultrasound-guided sacroiliac joint injection for chronic low back pain. *Pain Pract* (2017) 17(6):782–91. doi: 10.1111/papr.12526

123. Wallace P, Bezjian Wallace L, Tamura S, Prochnio K, Morgan K, Hemler D. Effectiveness of ultrasound-guided platelet-rich plasma injections in relieving sacroiliac joint dysfunction. *Am J Phys Med Rehabil* (2020) 99(8):689–93. doi: 10.1097/PHM.0000000000001389

124. Ko GD, Mindra S, Lawson GE, Whitmore S, Arseneau L. Case series of ultrasound-guided platelet-rich plasma injections for sacroiliac joint dysfunction. *J Back Musculoskelet Rehabil* (2017) 30(2):363–70. doi: 10.3233/BMR-160734

125. Dyson-Hudson TA, Hogaboom NS, Nakamura R, Terry A, Malanga GA. Ultrasound-guided platelet-rich plasma injection for the treatment of recalcitrant rotator cuff disease in wheelchair users with spinal cord injury: A pilot study. *J Spinal Cord Med* (2022) 45(1):42–8. doi: 10.1080/10790268.2020.1754676

126. Ibrahim VM, Groah SL, Libin A, Ljungberg IH. Use of platelet rich plasma for the treatment of bicipital tendinopathy in spinal cord injury:: a pilot study. *Top Spinal Cord Inj Rehabil* (2012) 18(1):77–8. doi: 10.1310/sci1801-77

127. Vasilikos I, Roelz R, Scholz C, Mizaikoff B, Argiti K, Ralf W, et al. Autologous platelet-rich fibrin (PRF) augmentation as an add-on therapy in deep surgical site infections (dSSIs) after instrumented spinal surgery: preliminary results of a single institution case series. *Acta Neurochir (Wien)* (2021) 163(10):2761–7. doi: 10.1007/s00701-021-04952-7

128. Singh R, Rohilla RK, Dhayal RK, Sen R, Sehgal PK. Role of local application of autologous platelet-rich plasma in the management of pressure ulcers in spinal cord injury patients. *Spinal Cord* (2014) 52(11):809–16. doi: 10.1038/sc.2014.144

129. Biglari B, Reitzel T, Swing T, Büchler A, Gerner HJ, Schmidmaier G, et al. A pilot study on the effectiveness of platelet-rich plasma and debridement for the treatment of nonhealing fistulas in spinal cord-injured patients. *Adv skin Wound Care* (2015) 28(3):123–8. doi: 10.1097/01.ASW.0000459845.95441.1a

130. Singh G, Borah D, Khanna G, Jain S. Efficacy of local autologous platelet-rich plasma in the treatment of pressure ulcer in spinal cord injury patients. *Cureus* (2021) 13(10):e18668. doi: 10.7759/cureus.18668

131. Guler S, Akcali O, Sen B, Micili SC, Sanli NK, Cankaya D. Effect of platelet-rich plasma, fat pad and dural matrix in preventing epidural fibrosis. *Acta Ortop Bras* (2020) 28(1):31–5. doi: 10.1590/1413-785220202801218823

132. Rappl LM. Effect of platelet rich plasma gel in a physiologically relevant platelet concentration on wounds in persons with spinal cord injury. *Int Wound J* (2011) 8(2):187–95. doi: 10.1111/j.1742-481X.2011.00770.x

133. Sell SA, Ericksen JJ, Reis TW, Droste LR, Bhuiyan MB, Gater DR. A case report on the use of sustained release platelet-rich plasma for the treatment of chronic pressure ulcers. *J Spinal Cord Med* (2011) 34(1):122–7. doi: 10.1179/107902610X12923394765616

134. Akkurt I, Bakar B, Dincel GC, Yildiran FAB, Ogden M, Nursoy E, et al. Effectiveness of the biophysical barriers to the peridural fibrosis in rat laminectomy model. *J Invest Surg* (2019) 32(4):361–8. doi: 10.1080/08941939.2017.1423422

135. Maisel-Campbell AL, Ismail A, Reynolds KA, Poon E, Serrano L, Grushchak S, et al. A systematic review of the safety and effectiveness of platelet-rich plasma (PRP) for skin aging. *Arch Dermatol Res* (2020) 312(5):301–15. doi: 10.1007/s00403-019-01999-6

136. Shen Z, Zheng S, Chen G, Li D, Jiang Z, Li Y, et al. Efficacy and safety of platelet-rich plasma in treating cutaneous ulceration: A meta-analysis of randomized controlled trials. *J Cosmet Dermatol* (2019) 18(2):495–507. doi: 10.1111/jocd.12853

137. Nassar SO, Eltatawy RAR, Hassan GFR. Safety and efficacy of platelet-rich plasma vs carboxytherapy in the treatment of atrophic scars: A comparative clinical and histopathological study. *Dermatol Ther* (2020) 33(6):e13942. doi: 10.1111/dth.13942

138. Chen Z, Wu Y, Turxun N, Shen Y, Zhang X. Efficacy and safety of platelet-rich plasma in the treatment of severe burns: A protocol for systematic review and meta analysis. *Med (Baltimore)* (2020) 99(45):e23001. doi: 10.1097/MD.0000000000023001

139. Fukawa T, Yamaguchi S, Akatsu Y, Yamamoto Y, Akagi R, Sasho T. Safety and efficacy of intra-articular injection of platelet-rich plasma in patients with ankle osteoarthritis. *Foot Ankle Int* (2017) 38(6):596–604. doi: 10.1177/1071100717700377

140. Cook CS, Smith PA. Clinical update: Why PRP should be your first choice for injection therapy in treating osteoarthritis of the knee. *Curr Rev Musculoskelet Med* (2018) 11(4):583–92. doi: 10.1007/s12178-018-9524-x

frontiers | Frontiers in Endocrinology

TYPE Original Research
PUBLISHED 23 March 2023
DOI 10.3389/fendo.2023.1131880

OPEN ACCESS

EDITED BY
Baoshan Xu,
Tianjin Hospital, China

REVIEWED BY
Yunzhong Cheng,
Department of Orthopedic Surgery, Capital Medical University, China
Changfeng Lu,
Zhejiang University School of Medicine, China
Di Wu,
Shanghai Jiao Tong University, China

*CORRESPONDENCE
Bo Li
libo_career@163.com;
libo83@mail.sysu.edu.cn
Xumin Hu
Huxumin3@mail.sysu.edu.cn
Liangbin Gao
gaolb@mail.sysu.edu.cn
Peng Wang
wangp57@mail.sysu.edu.cn

†These authors have contributed equally to this work

SPECIALTY SECTION
This article was submitted to Bone Research, a section of the journal Frontiers in Endocrinology

RECEIVED 26 December 2022
ACCEPTED 27 February 2023
PUBLISHED 23 March 2023

CITATION
Yang C, Zeng Z, Yan H, Wu J, Lv X, Zhang D, Zhang Z, Jiang X, Zhang C, Fu G, Peng X, Wang Z, Zhao Q, Li W, Huang R, Wang Q, Li B, Hu X, Wang P and Gao L (2023) Application of vertebral body compression osteotomy in pedicle subtraction osteotomy on ankylosing spondylitis kyphosis: Finite element analysis and retrospective study.
Front. Endocrinol. 14:1131880.
doi: 10.3389/fendo.2023.1131880

Application of vertebral body compression osteotomy in pedicle subtraction osteotomy on ankylosing spondylitis kyphosis: Finite element analysis and retrospective study

Canchun Yang[1†], Ziliang Zeng[1†], Haolin Yan[1†], Jionglin Wu[1†], Xin Lv[1], Di Zhang[1], Zhilei Zhang[1], Xu Jiang[1], Chi Zhang[1], Guo Fu[1], Xiaoshuai Peng[1], Zheyu Wang[1], Qiancheng Zhao[1], Wenpeng Li[1], Renyuan Huang[1], Qiwei Wang[1], Bo Li[1*], Xumin Hu[1*], Peng Wang[2*] and Liangbin Gao[1*]

[1]Department of Orthopedics, Sun Yat-sen Memorial Hospital of Sun Yat-sen University, Guangzhou, China, [2]Department of Orthopedics, The Eighth Affiliated Hospital of Sun Yat-sen University, Shenzhen, China

Background: Ankylosing spondylitis (AS) is a chronic inflammatory rheumatic disease, with pathological characteristics of bone erosion, inflammation of attachment point, and bone ankylosis. Due to the ossified intervertebral disc and ligament, pedicle subtraction osteotomy (PSO) is one of the mainstream surgeries of AS-related thoracolumbar kyphosis, but the large amount of blood loss and high risk of instrumental instability limit its clinical application. The purpose of our study is to propose a new transpedicular vertebral body compression osteotomy (VBCO) in PSO to reduce blood loss and improve stability.

Methods: A retrospective analysis was performed on patients with AS-related thoracolumbar kyphosis who underwent one-level PSO in our hospital from February 2009 to May 2019. A total of 31 patients were included in this study; 6 received VBCO and 25 received eggshell vertebral body osteotomy. We collected demographic data containing gender and age at diagnosis. Surgical data contained operation time, estimated blood loss (EBL), and complications. Radiographic data contained pre-operative and follow-up sagittal parameters including chin brow-vertical angle (CBVA), global kyphosis (GK), thoracic kyphosis (TK), and lumbar lordosis (LL). A typical case with L2-PSO was used to establish a finite element model. The mechanical characteristics of the internal fixation device, vertebral body, and osteotomy plane of the two osteotomy models were analyzed under different working conditions.

Results: The VBCO could provide comparable restoring of CBVA, GK, TK, and LL in the eggshell osteotomy procedure (all $p > 0.05$). The VBCO significantly reduced EBL compared to those with eggshell osteotomy [800.0 ml (500.0–1,439.5 ml) *vs.* 1,455.5 ml (1,410.5–1,497.8 ml), $p = 0.033$]. Compared with the

eggshell osteotomy, VBCO showed better mechanical property. For the intrapedicular screw fixation, the VBCO group had a more average distributed and lower stress condition on both nails and connecting rod. VBCO had a flattened osteotomy plane than the pitted osteotomy plane of the eggshell group, showing a lower and more average distributed maximum stress and displacement of osteotomy plane.

Conclusion: In our study, we introduced VBCO as an improved method in PSO, with advantages in reducing blood loss and providing greater stability. Further investigation should focus on clinical research and biomechanical analysis for the application of VBCO.

KEYWORDS

ankylosing spondylitis (AS), kyphosis, pedicle subtraction osteotomy (PSO), finite element analysis (FEA), estimated blood loss (EBL), vertebral body compression osteotomy (VBCO)

1 Introduction

Ankylosing spondylitis (AS) is a chronic inflammatory rheumatic disease, with pathological characteristics of bone erosion, inflammation of attachment point, and bone ankylosis. Due to the pathophysiological process, the AS intervertebral disc and ligament are seriously ossified and develop progressively upward from sacroiliac joint rigidity, then lumbar, thoracic, and cervical spine ossification. The early symptoms are not typical and patients with late-stage AS suffer from high risk of spinal deformity, including thoracolumbar kyphosis (TLK). Severe TLK disturbs patients' balance of spinal sagittal plane and seriously affects their quality of life due to severe low back pain or severe neurological dysfunction (1). For AS patients with severe TLK, spinal osteotomy and orthopedics are usually the only effective treatment.

In 1945, Smith-Petersen invented the V-shaped osteotomy of the lumbar appendage, which created the first surgical method for the treatment of kyphosis of ankylosing spondylitis (2). The orthopedic correction is achieved by removing the lumbar appendages and pressing the intervertebral disc and ligament. However, due to the ossified intervertebral disc and ligament, the large blood vessels in front of the vertebral body bear a large tensile force, and the blood vessels are easy to tear and cause fatal massive bleeding. Pedicle subtraction osteotomy (PSO) is widely accepted as one of mainstream treatments of AS-related TLK and is effective in restoring patients' sagittal balance (3, 4). The surgical technique in PSO can be summarized as transpedicular wedge-shaped osteotomy following closed osteotomy space using the anterior cortex of the vertebral body as a hinge (5). Its clinical application is restricted by multiple factors. On the one hand, the large amount of blood loss (mean 2,132 ml, range 1.400–1,915 ml) is one of the main limiting factors for the use of this technique (3). Clinical observation showed that vertebral body osteotomy contributes to dramatic blood loss during posterior spinal surgery, which makes it difficult to ensure optimal visualization during surgery and is accompanied by a risk of intraoperative tearing of the sclerotic large vessels and other important organs (6, 7). On the other hand, since we know that AS-related TLK often comes with spinal osteopenia, the over-removal of cancellous bone during the osteotomy procedure can further reduce the bone mass in the affected vertebral body (8). Together, it increases the risk of nonunions and instability of the internal fixation. Therefore, modifying the surgical process to improve its performance poses a new challenge for researchers.

Clinical observation showed that using bone chisel to squeeze and compact the vertebral cancellous bone can reduce local bleeding from bone marrow cavity. A similar phenomenon was also reported; increasing bone mass density could reduce the amount of blood loss during spinal deformity surgery and the risk of instrumental failure (9). Therefore, we propose a new wedge-shaped osteotomy in PSO achieved by transpedicular vertebral body compression.

Finite element analysis (FEA) is one of the most commonly used theoretical biomechanical research methods to simulate the physical system by using mathematical approximation and has been widely used in spine biomechanical analysis (10, 11). Compared with experimental biomechanical research, FEA has the advantages of revealing the mechanical data of the internal structure of the spine (12, 13). Additionally, the FEA model can be examined from various angles and repeatedly examined, thus substantially lowering expenses. This study aims to describe our procedure for transpedicular VBCO and compare its clinical performance and theoretical biomechanical characteristics in PSO with eggshell osteotomy.

2 Materials and methods

2.1 Patients

A retrospective analysis was performed on patients with AS and associated TLK who underwent spinal PSO in our hospital from February 2009 to May 2019. Inclusion criteria were as follows: (1) patients diagnosed with AS and TLK (maximum sagittal kyphosis angle >40° and Cobb angle of the coronal plane <10°) (14) and (2) patients who underwent PSO at a single vertebral level in the thoracolumbar region with eggshell osteotomy or VBCO. Exclusion criteria were as follows: (1) patients with pathological fractures or pseudarthrosis, (2) patients with a history of other spine lesions and surgery, (3) combined hip and knee joint movement limitation or ankylosis, and (4) incomplete radiological data. Thirty-one patients were included in this study, of whom 6 received VBCO and 25 received eggshell vertebral body osteotomy.

2.2 Data collection

Data were collected for three main categories, namely, demographic data, surgical data, and radiographic data. Demographic data contained patients' gender and age at diagnosis. Surgical data contained operation time, estimated blood loss (EBL) during operation, and complications. Radiographic data contained pre-operative and follow-up sagittal parameters including chin brow-vertical angle (CBVA), global kyphosis (GK), thoracic kyphosis (TK), and lumbar lordosis (LL). The lateral full-length x ray radiographs of whole spine, pelvis, and fully extended hips and knee were obtained before surgery, 2 weeks after surgery, and at final follow-up for all patients. CBVA was the angle between the straight line from the forehead to the chin and the vertical line on the ground. GK was formed by the upper endplate of the most inclined upper vertebra and the lower endplate of the most inclined lower vertebra. TK was formed by the upper endplate of T4 and the lower endplate of T12. LL was formed by the upper endplate of L1 and the upper endplate of S1. The correction of sagittal parameters was defined as the improvement between final follow-up and pre-operative parameters.

2.3 Surgical technique

PSO was generally divided into pre-osteotomy instrumentation, vertebral body osteotomy, and post-osteotomy instrumentation. The main differences between VBCO (the VBCO workflow displayed in Figure 1) and eggshell procedures can be found in the vertebral osteotomy section.

2.3.1 Pre-osteotomy instrumentation

The surgery followed the standard midline approach. At least two levels above and two levels below the osteotomized segment were subperiosteally exposed. The spinous process, ossified ligamentum flavum, lamina of intended vertebrae, and bilateral superior and inferior articular processes were removed, and the dural sac was released. Bilateral pedicle screw and rod were inserted into two levels above and two levels below the osteotomized segment to provide temporary control after vertebral body osteotomy. The lateral wall of the pedicle was then excised to the posterior vertebral body to expose the pedicle root.

2.3.2 Vertebral body osteotomy

Vertebral body osteotomy aims to create a wedge space, which is higher posteriorly than anteriorly, to shorten the middle and posterior columns. This process was achieved by VBCO and eggshell osteotomy.

2.3.3 Eggshell procedure

A high-speed turbine drill or ultrasonic osteotome was utilized to create the wedge space. The cutting bit resected the cancellous bone, and the fragment was removed through the bilateral pedicle. Cancellous bone was greatly removed from posterior and medial vertebral body and less from anterior vertebral body to excavate a V shape capacity.

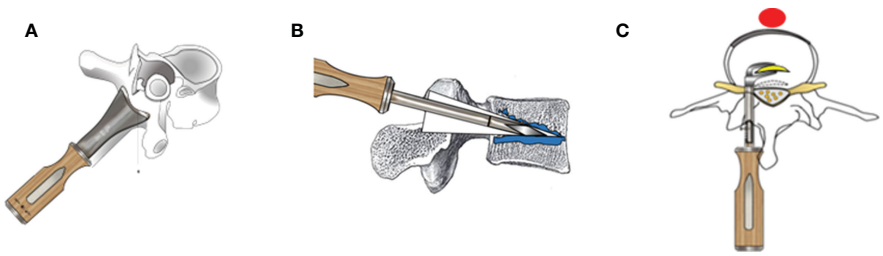

FIGURE 1
The schematic diagram of PSO with the VBCO procedure. **(A)** The spinous process, ossified ligamentum flavum, lamina of intended vertebrae, and bilateral superior and inferior articular processes were removed. **(B)** An extrusion-type bone osteotome was inserted into the treated pedicle. The wedge-shaped cutting bit was carefully advanced along the pedicle into vertebral body. Then, the osteotome was swung up and down to squeeze surrounding cancellous bone. The fragmented bone was gently compacted toward the floor and ceiling, so as to gradually expand capacity among the vertebral body. During this procedure, we took caution to avoid penetration of any vertebral cortices and inferior and superior osseous endplates, and the neural elements should be gently protected. **(C)** After VBCO, the posterior medial cortex of the wedge space was also resected before closure of the osteotomy surface.

2.3.4 VBCO procedure

An extrusion type bone osteotome was inserted into the treated pedicle. The wedge-shaped cutting bit was carefully advanced along the pedicle into vertebral body. The osteotome was then swung up and down to squeeze the surrounding cancellous bone. The fragmented bone was gently compacted toward the floor and ceiling to gradually expand the capacity throughout the vertebral body. During this procedure, caution was taken to avoid penetrating any vertebral cortices, and inferior and superior osseous endplates.

2.3.5 Post-osteotomy instrumentation

The posterior medial cortex of the wedge space was also resected bilaterally. The remnant cancellous bone and anterior cortex acted as a hinge to close the osteotomy surface (15). Controlled correction was achieved with a flexion operation table. A lateral C-arm fluoroscopy was utilized to prevent anterior and posterior displacement on the osteotomy surface. The pedicle screw and permanent rods were then locked side by side. Finally, the depression of neural elements and hemostasis were checked before the incision was closed with a standard layered closure.

2.4 Establishment and verification of the FEA model

2.4.1 Establishment of the FEA model

A case was selected to establish the FEA model of his spine. The patient chosen was a 30-year-old man, 165 cm tall and weighing 65 kg. He had been complaining of low back and hip pain for more than 10 years, conforming to the diagnosis standards for AS with TLK. He experienced an increasing severity of scoliosis, making him unable to maintain a normal life. The patient received full-length anteroposterior and lateral x-ray films, with CBVA −11.6°, GK 72.5°, TK 57.4°, LL 45.1°, coronal Cobb angle 0°, and T10 being apical vertebral body. A PSO with VBCO was applied on L2 with intra-pedicular screw fixation from T12 to L4. After the surgery, the patients were able to walk upright and look at the front again, leading to an improvement in quality of life with imaging correction with CBVA −6.1°, GK 76.6°, TK 50.6°, and LL 31.0°.

The patient received 64-row spiral CT (Siemens, Germany) scanning the whole spine. The scanning slice thickness was 1 mm, and the reconstruction slice thickness was 0.5 mm. The 2D tomographic software extracts 3D images of the patient's cervical, thoracic, lumbar, and sacral vertebrae through Mimics 21.0. Geomagic studio 2017 was utilized to generate continuous non-uniform rational B-spline (NURBS) surface models. Ansys 17.0 was used to mesh the FEA element model. The material properties were adopted from literature (16, 17). The facet joints were set to fusion state, in which the nucleus pulposus was assigned according to the attributes of the fibrous ring, and the fibrous ring was assigned according to the attributes of the cortical bone with a thickness of 0.4 cm (18–20). The geometric models of pedicle screws (Shanghai Sanyou pedicle screws, screw diameter 65 mm, screw length 450 mm) and rods (diameter 5.5 mm) were generated and assigned using the same method. The rod was shaped along the position of the pedicle screw to fit it with the latter, and the contact type between the rod and screw was set as the binding mode (21). The FEA parameters are listed in Table 1 (19).

A simulation of the biomechanical properties of the model was conducted for verification. The above model was introduced into Ansys Workbench 17.0 to constrain the degrees of freedom of the sacrum in all directions. A 150-N axial load was applied on the T4 vertebral body as the basis load, and 7.5 Nm load was applied forward, backward, and during left and right lateral bending and rotation to simulate spinal activity. The relative displacement and angle changes of thoracolumbar vertebrae were determined.

2.4.2 Construction of PSO models

According to eggshell osteotomy and VBCO osteotomy, the spinal model after L2 vertebral osteotomy was simulated. The mechanical characteristics of the internal fixation device, vertebral body, and osteotomy plane of the two osteotomy models were analyzed under different working conditions.

In SolidWorks 2017, two osteotomy models were constructed by simulating osteotomy on the verified spinal model. Model 1 was a single-segment eggshell osteotomy. The osteotomy site was L2 vertebral body, and the osteotomy angle was 30°. Modeling tools were used on the osteotomy surface to dig holes of different sizes to simulate the uneven osteotomy surface after PSO osteotomy. The pedicle screws were placed in T12, L1, L3, and L4 vertebral bodies. After the osteotomy end closed, it was fixed with a rod with a diameter of 5.5 mm. Model 2 was a single-segment VBCO osteotomy. The osteotomy site was L2 vertebral body, and the osteotomy angle was 30°. Modeling tools were used on the osteotomy surface to make a flat osteotomy surface, and 1/3 of the upper and lower parts of the osteotomy vertebral body were compressed to simulate the flat and compressed osteotomy surface after compression osteotomy. The pedicle screws were placed in T12, L1, L3, and L4 vertebral bodies. After the osteotomy end was closed, it was fixed with a rod with a diameter of 5.5 mm.

In SolidWorks 2017, the PSO models were constructed on the verified FEA spinal model with eggshell osteotomy (model 1) and VBCO (model 2). The osteotomy site was at L2 vertebral body, and the osteotomy angle was 30°. The pedicle screws were placed in T12, L1, L3, and L4 vertebral bodies with 5.5-mm connecting rods. In model 1, the osteotomy surface was set as uneven

TABLE 1 FEA mechanical parameters in the PSO model.

Material	Young's elastic modulus	Poisson's ratio
Cortical bone	12,000	0.3
Cancellous bone	100	0.2
Annulus fibrosus	4.2	0.45
Nucleus pulposus	0.2	0.49
Ligament	12,000	0.3
Internal fixation†	110,000	0.3

† including Shanghai Sanyou pedicle screws (screw diameter, 65 mm; screw length, 450 mm) and rods (diameter, 5.5 mm).

osteotomy surface and the bone was removed after eggshell osteotomy. In model 2, the osteotomy was set as a flat osteotomy surface and 1/3 of the upper and lower parts of the removed vertebral body were compressed to simulate the flat and compressed osteotomy surface after VBCO.

2.4.3 Biomechanical analysis of PSO models

The PSO model was imported into Ansys Workbench 17.0. The degree of freedom of sacrum was constrained in all directions, and its *X*, *Y*, and *Z* directions were set to 0 as the boundary condition. Stress on internal fixation, osteotomy plane, and displacement of plane was measured under various workloads, including stand forward flexion and backward extension, left and right flexion, and rotation. A 424.7-N axial load was applied on the T1 vertebral body, and bending, extension, and rotation were achieved with additional 10-Nm moment of force (22) (Table 2).

Overall stress distribution and displacement were measured on each internal fixation model and osteotomy planes, and the mechanical distribution of PSO models was compared under different workloads using numerical comparison.

2.5 Statistical analysis

Radiographic data were measured using DICOM by orthopedic spine surgeons. Demographic and surgical data were collected from outpatients' and inpatients' records.

Gender, osteotomy vertebral segment, and complication were labeled as categorical variables. The χ^2 test was used for intergroup analysis, and Fisher's precision probability test was applied when existing components in crosstab was less than 5. Age, EBL, operative time, sagittal parameters, and operative correction were labeled as continuous numerical variables. Firstly, Shapiro–Wilk test was utilized to filter the variables in normal distribution from variables in skewness distribution ($p< 0.05$). Secondly, parametric and nonparametric tests were applied depending on whether variables were in normal or skewness distribution. For variables in normal distribution, the value was displayed as *Mean* ($\bar{x}$) ± *Standard deviation* (σ) and intergroup analysis was conducted using unpaired *t*-test. For variables in skewness distribution, the value was displayed as *Median* (*M*) ± *Interquartile range* (*IQR*) and intergroup analysis was conducted using unpaired Wilcoxon signed-rank test. The statistical significance of operative correction was determined by paired test. For all statistical tests, $p< 0.05$ was defined as rejecting null hypothesis with statistical significance. All statistical analyses were performed using SPSS software (24.0 IBM) and Excel software.

TABLE 2 Additional load on T1 vertebrae under various workloads†.

Workload	Additional load
Standing condition	None
Antexion–extension condition	The sagittal bending force of 10 Nm is loaded forward or backward
Side bending condition	The coronal bending force of 10 Nm is loaded on the left or right side
Rotating condition	The horizontal torsional force of 10 Nm is loaded

† We applied a basis 424.7 N axial load on the T1 vertebral body.

3 Results

3.1 Surgical procedure

Among the 31 patients with AS-related TLK, 22 received PSO with eggshell osteotomy and 9 received PSO with VBCO. Among the continuous numerical variables, age, follow-up time, and TK were in normal distribution and CBVA, LL, EBL, and EBL were in skewness distribution (Table 3). The demographic and surgical information is displayed in Table 4. The follow-up duration of the compression group was not statistically different from that of the eggshell group (76.2 ± 28.6 months *vs*. 89.8 ± 42.9 months, $p = 0.39$).

Single-level PSO was performed between L1 and L3, mostly in L2–3. The EBL under compression was significantly reduced compared to that under eggshell procedure [800.0 ml (500.0–1,439.5 ml) vs. 1,455.5 ml (1,410.5–1,497.8 ml), $p = 0.033$]. The compression group had a shorter operation time than the eggshell group, but the difference was not statistically significant [354.0 min (250.0–374.1 min) *vs*. 359.0 min (341.1–368.4 min), $p = 0.68$].

The baseline pre-operative and post-operative follow-up radiographic parameters are displayed in Table 5. The spinal deformity in two groups was balanced on baseline [no significant difference in pre-operative CBVA, GK, TK, and LL (all *p*-value > 0.05)]. Correction in sagittal parameters is displayed in Table 6. The median CBVA changed from 22.2° to 13.0° after surgery, with no significant difference between the two groups [−8.8° (−13.5° to −2.2°) vs. −9.9° (−13.6° to −5.0°), $p = 0.72$]. It also restored and provided consistent performance in correction among GK, LL, and TK, which showed no difference in correction between two groups (all *p*-value > 0.05). Together, comparison of the baseline and correction of radiographic parameters between the two groups revealed that VBCO could provide comparable correction for sagittal parameters as eggshell osteotomy for patients with AS-related TLK to PSO.

3.2 Establishment of the FEA model of administration of PSO on AS

We established a 3D FEA model of the AS spine with 663,054 nodes and 349,832 elements. Under a vertical load of 150 N and a torque of 7.5 Nm, the T5–L5 mobility of the AS model was 1.84° of flexion, 2.19° of extension, 0.96° of left flexion, and 0.56° of right flexion. Our model of mobility was comparable to the existing AS finite element models, and much restricted than those based on normal subjects (23, 24).

PSO with eggshell osteotomy and VBCO were then applied on the FEA model (Figures 2A–C). Compared with the eggshell osteotomy, VBCO showed better mechanical property with lower stress on nails and rods and lower stress and displacement on the

TABLE 3 Normal test of continuous variables.

	Value	*p*-value†
Variables in normal distribution		
Age (years)	40.7 ± 11.8	0.18
Follow up (months)	85.8 ± 39.3	0.08
TK (°)	41.9 ± 13.2	0.39
Variables in skewness distribution		
CBVA (°)	21.7 (11.9–29.0)	<0.001***
GK (°)	66.8 (60.6–72.8)	0.009**
LL (°)	6.0 (−2.2–8.7)	0.010*
EBL (ml)	1,441.0 (600.0–1,474.0)	0.001**
Operation time (min)	358.3 (331.0–368.0)	0.002**

CBVA, chin brow-vertical angle; GK, global kyphosis, TK, thoracic kyphosis; LL, lumbar lordosis; TPA, T1 pelvic angle; SVA, sagittal vertical axis; EBL, estimated blood loss.
† Normal test was applied by the Shapiro–Wilk test, in which p > 0.05 means variables are in normal distribution and p< 0.05 means variables are in skewness distribution.
*:p<0.05; **:p<0.01; ***:p<0.001.

osteotomy plane (Figure 3). For the intra-pedicular screw fixation, the VBCO group (model 2) had a more average distributed and lower stress condition on both nails and connecting rod than in the eggshell group (model 1). Compared with the VBCO group (model 2), the eggshell group (model 1) had a more variable high stress in lateral bending, especially left side bending and rotation than in other conditions and the stress was aggregated centrally on the middle of the connecting rod, mainly distributed in the osteotomy area. The VBCO group (model 2) had a flattened osteotomy plane compared to the pitted osteotomy plane of the eggshell group (model 1). It made the VBCO group (model 2) show a lower and more average distributed maximum stress and displacement of the osteotomy plane than the eggshell group (model 1). Overall, the compression model obtained better FEA mechanics stability than the eggshell model.

4 Discussion

Due to the AS-ossified intervertebral disc and ligament, Smith-Petersen appendage osteotomy on AS with TLK was limited by the high risk of tearing blood vessels that may cause fatal massive bleeding (2). The process could cause spinal spondylolisthesis and damage the spinal cord and nerve root, with many serious complications and high mortality. In PSO, vertebral body osteotomy is conducted using the eggshell procedure, which fragments and resects the cancellous bone to create the wedge space in intended vertebrae (25). The surgical procedure was applied transpedicularly, without affecting the ossified intervertebral disc and the adjacent vertebral bodies. However, the application of this method is still restricted by the massive hemorrhage and a risk of instrumental failure by bone loss. Our

TABLE 4 Demographic and surgical information of patients.

	Eggshell	VBCO	*p*-value
	(*n* = 22)	(*n* = 9)	
Age (years)			0.42
Mean ± SD	41.8 ± 12.1	37.9 ± 11.3	
Follow up (months)			0.39
Mean ± SD	89.8 ± 42.9	76.2 ± 28.6	
Sex			0.86
Male	18 (81.8%)	7 (77.8%)	
Female	4 (18.2%)	2 (22.2%)	
Operation time (min)			0.68
Median (IQR)	359.0 (341.1–368.4)	354.0 (250.0–374.1)	
EBL (ml)			0.033*
Median (IQR)	1,455.5 (1,410.5–1,497.8)	800.0 (500.0–1,439.5)	

VBCO, vertebral body compression osteotomy; EBL, estimated blood loss; IQR, interquartile range; SD, standard deviation.

TABLE 5 Preoperative and follow-up radiographic parameters.

	Eggshell			VBCO			*p*-value†
	Preoperation	Follow-up	*p*-value	Preoperation	Follow-up	*p*-value	
CBVA (°)			0.004**			0.008**	0.25
Median (IQR)	20.2 (11.0–29.6)	12.7 (8.8–14.7)		25.2 (19.8–29.4)	14.7 (11.3–20.3)		
GK (°)			<0.001***			0.018*	0.12
Median (IQR)	68.5 (62.7–77.0)	52.4 (43.6–58.9)		64.1 (56.1–67.1)	50.0 (45.0–51.4)		
TK (°)			<0.001***			0.003**	0.84
Mean ± SD	42.2 ± 13.7	37.6 ± 8.7		41.1 ± 12.6	37.2 ± 9.1		
LL (°)			<0.001***			0.008**	0.40
Median (IQR)	7.6 (−2.9–27.7)	25.7 (19.5–31.9)		5.3 (−0.3–6.8)	24.9 (19.1–28.7)		

VBCO, vertebral body compression osteotomy; CBVA, chin brow-vertical angle; GK, global kyphosis, TK, thoracic kyphosis; LL, lumbar lordosis; IQR, interquartile range; SD, standard deviation.
† p-value of intergroup comparison of preoperative sagittal parameters between two osteotomy procedures.
*:p<0.05; **:p<0.01; ***:p<0.001.

research aimed to improve PSO by proposing a novel method of VBCO, which can reduce hemorrhage, preserve bone mass, and strengthen internal fixation.

Patients with AS-related kyphosis have a long-term course of ankylosis and immobility, leading to the osteopenia of thoracolumbar vertebra (8). Osteopenia is an important risk factors in spinal instrumental failure (26). Approximately 30% of patients with AS-related kyphosis could develop vertebral compression fractures, and the risk is even higher in patients suffering from reduced bone mass and long course of disease (27–29). Our previous research revealed that imbalanced redox played an important role in the pathogenesis of AS-related osteopenia (30). During the operation, the operator noticed that we could effortlessly resect the bone using bone chisel on patients with AS-related kyphosis. Combined with the above results, this realization reminded us of the compressible space in the cancellous bone of patients with late-stage AS-related kyphosis. Additionally, previous biomechanical studies showed that the yield strength of cancellous bone decreased significantly in the stress–strain curve, and the stress conduction of trabecular bone in cancellous bone was attenuated and poorly conductive (31, 32). This finding suggests that vertebral body osteotomy by compressing the cancellous bone can avoid rupturing the surrounding structure due to poor compression. VBCO could preserve bone fragments to a large extent with a flat osteotomy plane and reduce further bone loss of the vertebral body. On the one hand, the vascular supply of cancellous bone presents a rich anastomosing vascular sinusoidal bed (33). The vascular sinusoidal bed is a semi-open circulation and lacks soft tissue coverage, which is the histological basis of the difficulty of hemostasis on vertebral body osteotomy (33, 34). Compared with eggshell osteotomy, VBCO reduces the destruction of cancellous bone sinusoidal bed. The compacted fragmented cancellous bone also closes the wound surface and relatively reduces blood loss. Increasing bone mass and flat

TABLE 6 Comparison of sagittal parameter correction after follow-up.

	Eggshell	VBCO	*p*-value
ΔCBVA (°)			0.72
Median (IQR)	−8.8 (−13.5 to −2.2)	−9.9 (−13.6 to −5.0)	
ΔGK (°)			0.48
Median (IQR)	−17.1 (−29.9 to −8.6)	−15.6 (−22.6 to −5.4)	
ΔTK (°)			0.69
Mean ± SD	−4.6 ± 8.5	−4.0 ± 6.8	
ΔLL (°)			0.88
Median (IQR)	18.2 (13.6 to 25.3)	19.0 (14.8 to 27.1)	

VBCO, vertebral body compression osteotomy; CBVA, chin brow-vertical angle; GK, global kyphosis, TK, thoracic kyphosis; LL, lumbar lordosis; Δ, comparison of sagittal parameters; IQR, interquartile range; SD, standard deviation.

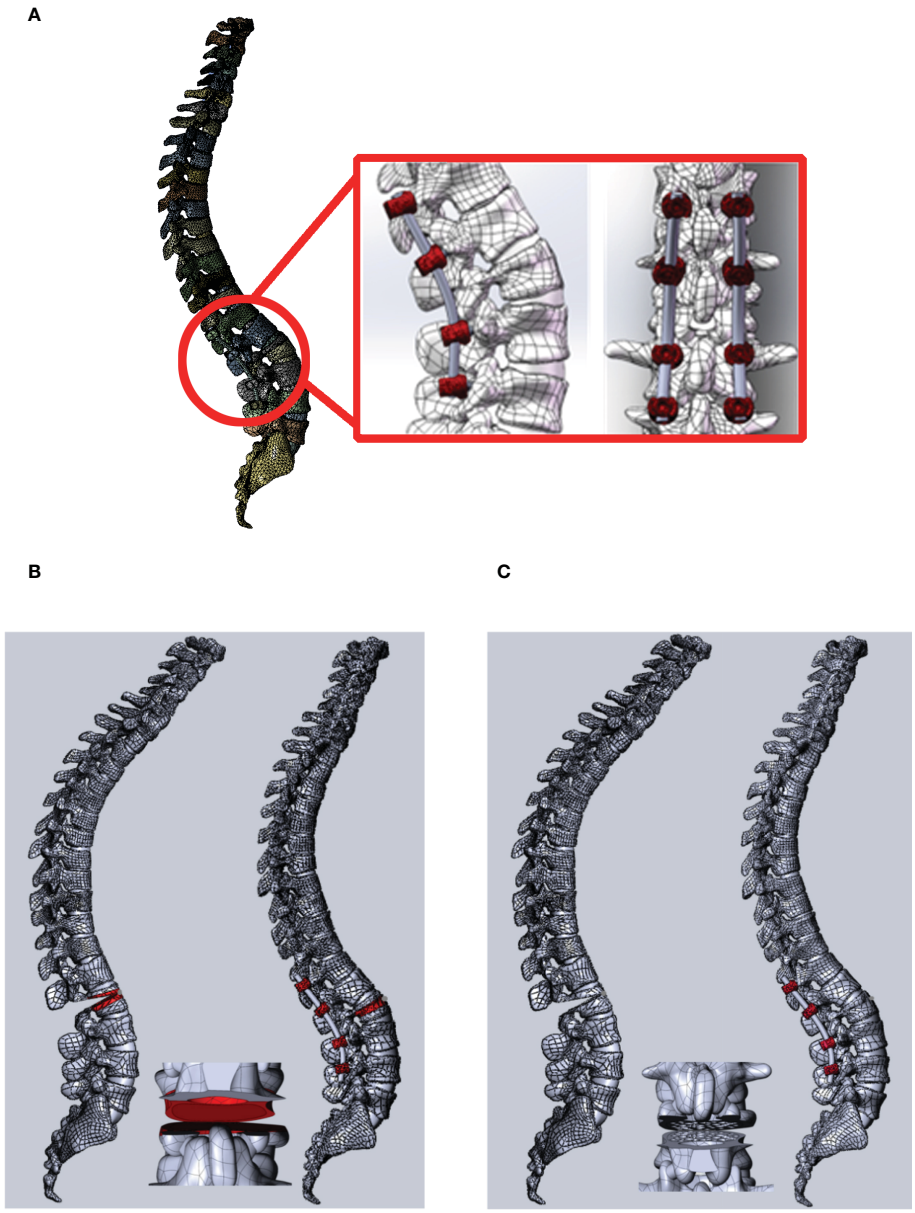

FIGURE 2
The PSO operation FEA model on the AS kyphosis model with VBCO and eggshell osteotomy. **(A)** The view of PSO operation on L2 with intra-pedicular screw fixation from T12 to L4. The red box shows the local detailed structure of intra-pedicular screw fixation and the osteotomy plane. **(B, C)** PSO operation with eggshell osteotomy (model 1, **B**) and VBCO (model 2, **C**) on the FEA model.

osteotomy plane could improve the strength of internal fixation. Together, VBCO could largely save bone fragments and reduce further bone mass loss of vertebral body. It can enhance the local stability of the osteotomy segment and promote the bone integration after PSO. Additionally, our center previously conducted an anatomical study of the blood supply of the spine and spinal cord through vascular casting and spinal cord angiography. It found that the nerves and blood vessels enter and exit the vertebral canal from the upper and lower intervertebral foramen of the vertebral arch, suggesting that the posterior approach osteotomy through the middle of the vertebral arch and vertebral body could reduce the EBL (35).

FEA provides a feasible research method for the design of spinal osteotomy. Compared with eggshell osteotomy, the PSO models showed that VBCO improved mechanical stability in the following aspects: the load on nails and rod was smaller and in more equal distribution, which reduced locally aggregating stress on the middle of connecting rod near the osteotomy plane and the stress and displacement on the osteotomy plane were smaller. Both properties are beneficial for postoperative stability, which reduces the risk of bone

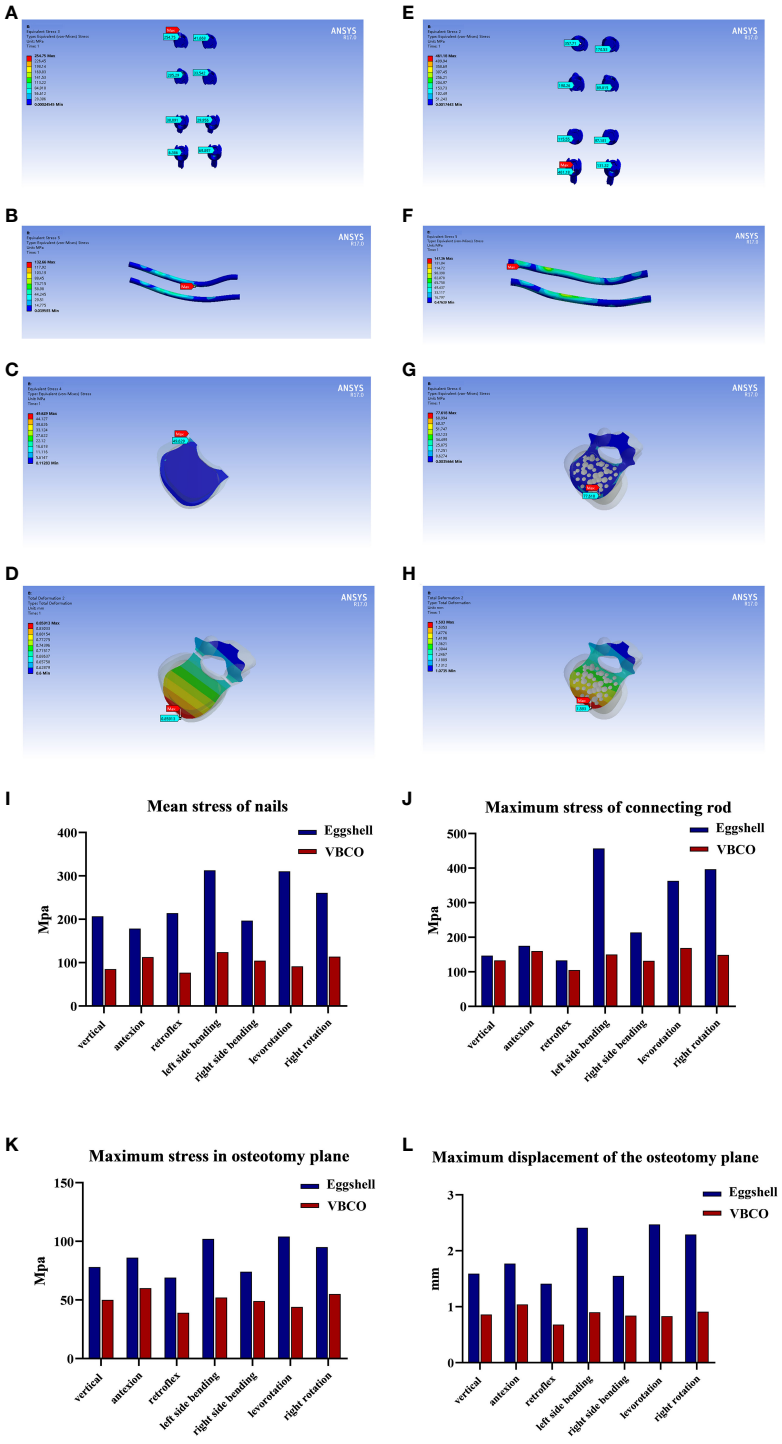

FIGURE 3
FEA of two PSO models with VBCO and eggshell osteotomy. **(A–C)** Stress distribution of eggshell osteotomy (model 1) nails **(A)**, connecting rod **(B)**, and osteotomy plane **(C)** under different workloads. **(D)** Displacement distance distribution on the osteotomy plane of eggshell osteotomy (model 1). **(E–G)**. Stress distribution of VBCO (model 2) nails **(E)**, connecting rod **(F)**, and osteotomy plane **(G)** under different workloads. **(H)** Displacement distance distribution on the osteotomy plane of VBCO (model2). **(I)** Comparison of average force on nails of two models under different working conditions. **(J, K)** Comparison of the maximum force on the rods **(J)** and osteotomy plane **(K)** of the two models under different working conditions. **(L)** Comparison of the maximum displacement of the osteotomy plane of two models under different working conditions.

nonunion, intra-pedicular screw fixation rupture, and the loss of correction angle during follow-up. Overall, vertebral body compression–osteotomy is theoretically advantageous than eggshell osteotomy by reducing hemorrhage and mechanical stability.

The operator applied PSO with VBCO in patients with AS-related kyphosis. We reviewed the data of 31 patients with AS-related TLK who underwent single-level PSO with VBCO or eggshell osteotomy. Firstly, VBCO could achieve comparable

correction of sagittal parameters to eggshell osteotomy. The compression group exhibited similarly restored spinal sagittal balance with the eggshell group (all p-value > 0.05 on intergroup comparison of correction among CBVA, GK, LL, and TK). This result supported previous biomechanical analysis and confirmed the feasibility of compression osteotomy in patients with AS-related kyphosis. Compared with eggshell osteotomy, compression osteotomy could reduce the amount of blood loss [800.0 ml (500.0–1,439.5 ml) vs. 1,455.5 ml (1,410.5–1,497.8 ml), $p = 0.033$] and tended to shorten the operation time [354.0 min (250.0–374.1 min) vs. 359.0 min (341.1–368.4 min), $p = 0.68$]. Thus, compression osteotomy can enhance the local stability of osteotomy segments and promote bone integration after PSO. In summary, VBCO has three main technical advantages over eggshell osteotomy in PSO. It reduces the operation difficulty by significantly reducing blood loss. The compacted bone fragments help in local hemostasis by compressing the vascular sinusoidal bed of cancellous bone. Additionally, it creates a flat surface and could reduce the bone mass loss of vertebral body to provide stability and fusion. Further investigation is ongoing for the following objectives: modifying the design of extrusion type bone osteotome according to vertebral body structure, modifying the slope and size of cutting bit to fit the osteotomy angle and designing mechanical experimentation to validate FEA studies on compression osteotomy for the application of force analysis and stability in compression osteotomy segments.

Our report has several limitations. Firstly, the sample size in our retrospective design was small. An adequate sample size is necessary to ensure statistical power and for the comparison of low probability events, including operative compliance. Further investigation is in progress with standard sample size calculation and persuasive statistical data analysis. Secondly, the modeling case was picked without a standard random method, which increased sampling bias. Thirdly, a verification with biomechanical analysis and long-term clinical follow-up is required to support the results. Future studies should examine the difference in life quality and treatment costs between two surgical procedures.

5 Conclusion

In our study, we introduced VBCO as an improved method in PSO for patients with AS-related kyphosis. Compared with eggshell osteotomy, VBCO has advantages in reducing blood loss, creating flat and aligned wedge-shape capacity with largely preserved bone mass in the vertebral body, showing better mechanical property and providing greater stability and better fusion. For the intra-pedicular screw fixation, the VBCO group had a more average distributed and lower stress condition on both nails and connecting rod than the eggshell group. The VBCO group had a flattened osteotomy plane than the pitted osteotomy plane of the eggshell group, showing a lower and more average distributed maximum stress and displacement of osteotomy plane than the eggshell group. This study served as a reference for the improved vertebral body osteotomy in PSO on patients with AS kyphosis. Further investigation should focus on clinical research and biomechanical analysis for the application of VBCO.

Data availability statement

The original contributions presented in the study are included in the article/supplementary material. Further inquiries can be directed to the corresponding authors.

Ethics statement

The studies involving human participants were reviewed and approved by The Institute Ethics committee of the Sun Yat-sen Memorial Hospital (SYSKY-2022-451-01). The patients/participants provided their written informed consent to participate in this study.

Author contributions

LG, BL, PW, and XH conceived the studies. CY, ZZe, JW, and HY designed the research process and were major contributors in writing the manuscript. XL, DZ and ZZh collected and assembled the data. XJ, CZ, GF, XP, ZW, QZ, WL, RH and QW participated in software support and data analysis. All authors contributed to the article and approved the submitted version.

Funding

The study was supported by the Medical Scientific Research Foundation of Guangdong Province of China (A2021044 and A2021371), the Guangzhou Municipal Science and Technology Bureau (202102020096), the Basic and Applied Basic Research Foundation of Guangdong Province (2021A1515111216), and the Guangzhou Science and Technology Planning Project (202201011042).

Conflict of interest

The authors declare that the research was conducted in the absence of any commercial or financial relationships that could be construed as a potential conflict of interest.

Publisher's note

References

1. Zhang Y, Qian B, Qiu Y, Qu Z, Mao S, Jiang J, et al. Sagittal vertical axias, spinosacral angle, spinopelvic angle, and T1 pelvic angle: Which parameters may effectively predict the quality of life in ankylosing spondylitis patients with thoracolumbar kyphosis? *Clin Spine Surg* (2017) 30:E871–6. doi: 10.1097/BSD.0000000000000463

2. Cho K, Bridwell K, Lenke L, Berra A, Baldus C. Comparison of smith-petersen versus pedicle subtraction osteotomy for the correction of fixed sagittal imbalance. *Spine* (2005) 30:2030–7. doi: 10.1097/01.brs.0000179085.92998.ee

3. Hu X, Thapa AJ, Cai Z, Wang P, Huang L, Tang Y, et al. Comparison of smith-petersen osteotomy, pedicular subtraction osteotomy, and poly-segmental wedge osteotomy in treating rigid thoracolumbar kyphotic deformity in ankylosing spondylitis a systematic review and meta-analysis. *BMC Surg* (2016) 16:4. doi: 10.1186/s12893-015-0118-x

4. Liu H, Yang C, Zheng Z, Ding W, Wang J, Wang H, et al. Comparison of smith-petersen osteotomy and pedicle subtraction osteotomy for the correction of thoracolumbar kyphotic deformity in ankylosing spondylitis: A systematic review and meta-analysis. *Spine (Phila Pa 1976)* (2015) 40:570–9. doi: 10.1097/BRS.0000000000000815

5. Thomasen E. Vertebral osteotomy for correction of kyphosis in ankylosing spondylitis. *Clin orthopaedics related Res* (1985) 194:142–52. doi: 10.1097/00003086-198504000-00019

6. Postacchini R, Cinotti G, Postacchini F. Injury to major abdominal vessels during posterior lumbar interbody fusion. *A Case Rep Rev lit Spine J* (2013) 13:e7–11. doi: 10.1016/j.spinee.2012.11.016

7. Chiu C, Chan C, Aziz I, Hasan M, Kwan M. Assessment of intraoperative blood loss at different surgical stages during posterior spinal fusion surgery in the treatment of adolescent idiopathic scoliosis. *Spine* (2016) 41:E566–73. doi: 10.1097/BRS.0000000000001304

8. Boonen A, van der Linden S. The burden of ankylosing spondylitis. *J Rheumatol* (2006) 78:4–11.

9. Modi H, Suh S, Hong J, Song S, Yang J. Intraoperative blood loss during different stages of scoliosis surgery: A prospective study. *Scoliosis* (2010) 5:16. doi: 10.1186/1748-7161-5-16

10. Zhizhong T, Bin X, Kai Y, Yonggang X, Yanbin Z. Biomechanical evaluation of the transcortical and transpedicular trajectories for pedicle screw insertion in thoracolumbar fracture fixation for ankylosing spondylitis. *Front Surg 8* (2021) 13. doi: 10.3389/fsurg.2021.706597

11. Haroon NN, Szabo E, Raboud JM, Mcdonald-Blumer H, Fung L, Josse RG, et al. Alterations of bone mineral density, bone microarchitecture and strength in patients with ankylosing spondylitis: A cross-sectional study using high-resolution peripheral quantitative computerized tomography and finite element analysis. *Arthritis Res Ther* (2015) 17:377. doi: 10.1186/s13075-015-0873-1

12. Zhiqiang G, Zixian C, Zhenzhou F, Yuanwu C, Chun J, Xiaoxing J. Finite element analysis of 3 posterior fixation techniques in the lumbar spine. *Orthopedics* (2014) 37(5):e441–8. doi: 10.3928/01477447-20140430-54

13. Belytschko. TB, Andriacchi. TP, Schultz. AB, Galante. JO. Analog studies of forces in the human spine: Computational techniques. *J Biomech* (1973) 6(4):361–71. doi: 10.1016/0021-9290(73)90096-1

14. van der Linden S, Valkenburg H, Cats A. Evaluation of diagnostic criteria for ankylosing spondylitis. A proposal for modification of the new York criteria. *Arthritis rheum* (1984) 27:361–8. doi: 10.1002/art.1780270401

15. Heary R, Bono C. Pedicle subtraction osteotomy in the treatment of chronic, posttraumatic kyphotic deformity. *J neurosurg Spine* (2006) 5:1–8. doi: 10.3171/spi.2006.5.1.1

16. Jones AC, Wilcox RK. Finite element analysis of the spine: Towards a framework of verification, validation and sensitivity analysis. *Med Eng Phys* (2008) 30(10):1287–304 doi: 10.1016/j.medengphy.2008.09.006

17. Burstein. AH, Reilly DT, Martens. M. Aging of bone tissue: Mechanical properties. *J Bone Joint surg Am vol* (1976) 58:19. doi: 10.2106/00004623-197658010-00015

18. Sovira T, Jianhua Y, Flynn. JA, Yao. L, Ward. MM. Zygapophyseal joint fusion in ankylosing spondylitis assessed by computed tomography: Associations with syndesmophytes and spinal motion. *J Rheumatol* (2017) 44(7):1004–1010. doi: 10.3899/jrheum.161462.

19. Robinson Y, Almkvist VL, Olerud C, Halldin P, Fahlstedt M. Finite element analysis of long posterior transpedicular instrumentation for cervicothoracic fractures related to ankylosing spondylitis. *Global Spine J* (2018) 8(6):570–578. doi: 10.1177/2192568217745068

20. Aikeremujiang M, Hui L, Junyi M, Yong M, Yuan M. Establishment of a three-dimensional finite element model of severe kyphotic deformity secondary to ankylosing spondylitis. *J Int Med Res* (2017) 45(2):639–646. doi: 10.1177/0300060517699303.

21. Lu T, Lu Y. Comparison of biomechanical performance among posterolateral fusion and transforaminal, extreme, and oblique lumbar interbody fusion: A finite element analysis. *World Neurosurg* (2019) 129:e890–e899. doi: 10.1016/j.wneu.2019.06.074

22. Nachemson. A, Elfstrom. G. Intravital dynamic pressure measurements in lumbar discs. A study of common movements, maneuvers and exercises. *Scand J Rehabil Med* (1970) 1:1–40.

23. Tianyu Z, Yanhua W, Peixun Z, Feng X, Dianying Z, Baoguo J. Different fixation pattern for thoracolumbar fracture of ankylosing spondylitis: A finite element analysis. *PloS One* (2021) 16(4):e0250009. doi: 10.1371/journal.pone.0250009

24. Robert P, Philipp S, Jan S, Matti S, Kathrin L, Cyrus K-K, et al. Biomechanical comparison of expandable cages for vertebral body replacement in the thoracolumbar spine. *Spine* (2004) 29.(13):1413–9. doi: 10.1097/01.brs.0000129895.90939.1e

25. Murrey D, Brigham C, Kiebzak G, Finger F, Chewning S. Transpedicular decompression and pedicle subtraction osteotomy (eggshell procedure): A retrospective review of 59 patients. *Spine* (2002) 27:2338–45. doi: 10.1097/00007632-200211010-00006

26. Wang T, Zhao Y, Cai Z, Wang W, Xia Y, Zheng G, et al. Effect of osteoporosis on internal fixation after spinal osteotomy: A finite element analysis. *Clin biomech (Bristol Avon)* (2019) 69:178–83. doi: 10.1016/j.clinbiomech.2019.07.032

27. Pray C, Feroz N, Nigil Haroon N. Bone mineral density and fracture risk in ankylosing spondylitis: A meta-analysis. *Calcified Tissue Int* (2017) 101:182–92. doi: 10.1007/s00223-017-0274-3

28. Ralston S, Urquhart G, Brzeski M, Sturrock R. Prevalence of vertebral compression fractures due to osteoporosis in ankylosing spondylitis. *BMJ (Clin Res ed)* (1990) 300:563–5. doi: 10.1136/bmj.300.6724.563

29. Ulu M, Batmaz İ, Dilek B, Çevik R. Prevalence of osteoporosis and vertebral fractures and related factors in patients with ankylosing spondylitis. *Chin Med J* (2014) 127:2740–7.

30. Wang L, Gao L, Jin D, Wang P, Yang B, Deng W, et al. The relationship of bone mineral density to Oxidant/Antioxidant status and inflammatory and bone turnover markers in a multicenter cross-sectional study of young men with ankylosing spondylitis. *Calcified Tissue Int* (2015) 97:12–22. doi: 10.1007/s00223-015-0001-x

31. Soltanihafshejani N, Bitter T, Janssen D, Verdonschot N. Development of a crushable foam model for human trabecular bone. *Med Eng Phys* (2021) 96:53–63. doi: 10.1016/j.medengphy.2021.08.009

32. Mondal A, Nguyen C, Ma X, Elbanna A, Carlson J. Network models for characterization of trabecular bone. *Phys rev E* (2019) 99:042406. doi: 10.1103/PhysRevE.99.042406

33. Zamboni L, Pease DC. The vascular bed of red bone marrow. *J Ultrastruct Res* (1961) 5:65–85. doi: 10.1016/S0022-5320(61)80006-3

34. De Bruyn PP, Michelson S, Thomas TB. The migration of blood cells of the bone marrow through the sinusoidal wall. *J Morphol* (1971) 133:417–37. doi: 10.1002/jmor.1051330406

35. Gao L, Wang L, Su B, Wang P, Ye J, Shen H. The vascular supply to the spinal cord and its relationship to anterior spine surgical approaches. *Spine J* (2013) 13:966–73. doi: 10.1016/j.spinee.2013.03.017

frontiers | Frontiers in Endocrinology

TYPE Original Research
PUBLISHED 20 June 2023
DOI 10.3389/fendo.2023.1089414

OPEN ACCESS

EDITED BY
Jeff M. P. Holly,
University of Bristol, United Kingdom

REVIEWED BY
Mojgan Yazdanpanah,
University of Montreal, Canada
Jean Claude De Mauroy,
Independent Researcher, Lyon, France

*CORRESPONDENCE
Chikashi Terao
chikashi.terao@riken.jp

RECEIVED 04 November 2022
ACCEPTED 17 May 2023
PUBLISHED 20 June 2023

CITATION
Otomo N, Khanshour AM, Koido M, Takeda K, Momozawa Y, Kubo M, Kamatani Y, Herring JA, Ogura Y, Takahashi Y, Minami S, Uno K, Kawakami N, Ito M, Sato T, Watanabe K, Kaito T, Yanagida H, Taneichi H, Harimaya K, Taniguchi Y, Shigematsu H, Iida T, Demura S, Sugawara R, Fujita N, Yagi M, Okada E, Hosogane N, Kono K, Nakamura M, Chiba K, Kotani T, Sakuma T, Akazawa T, Suzuki T, Nishida K, Kakutani K, Tsuji T, Sudo H, Iwata A, Inami S, Wise CA, Kochi Y, Matsumoto M, Ikegawa S, Watanabe K and Terao C (2023) Evidence of causality of low body mass index on risk of adolescent idiopathic scoliosis: a Mendelian randomization study. *Front. Endocrinol.* 14:1089414. doi: 10.3389/fendo.2023.1089414

Evidence of causality of low body mass index on risk of adolescent idiopathic scoliosis: a Mendelian randomization study

Nao Otomo[1,2,3], Anas M. Khanshour[4], Masaru Koido[1,5], Kazuki Takeda[2], Yukihide Momozawa[6], Michiaki Kubo[6], Yoichiro Kamatani[5,7], John A. Herring[8,9], Yoji Ogura[2], Yohei Takahashi[2], Shohei Minami[10], Koki Uno[11], Noriaki Kawakami[12], Manabu Ito[13], Tatsuya Sato[14], Kei Watanabe[15], Takashi Kaito[16], Haruhisa Yanagida[17], Hiroshi Taneichi[18], Katsumi Harimaya[19], Yuki Taniguchi[20], Hideki Shigematsu[21], Takahiro Iida[22,23], Satoru Demura[24], Ryo Sugawara[25], Nobuyuki Fujita[2,26], Mitsuru Yagi[2,27], Eijiro Okada[2], Naobumi Hosogane[2,28], Katsuki Kono[2,29], Masaya Nakamura[2], Kazuhiro Chiba[2,26], Toshiaki Kotani[10], Tsuyoshi Sakuma[10], Tsutomu Akazawa[10], Teppei Suzuki[11], Kotaro Nishida[30], Kenichiro Kakutani[30], Taichi Tsuji[12], Hideki Sudo[31], Akira Iwata[32], Satoshi Inami[18], Carol A. Wise[4,9,33], Yuta Kochi[34], Morio Matsumoto[2], Shiro Ikegawa[3], Kota Watanabe[2] and Chikashi Terao[1,35,36]*

[1]Laboratory for Statistical and Translational Genetics, RIKEN Center for Integrative Medical Sciences, RIKEN, Yokohama, Japan, [2]Department of Orthopaedic Surgery, Keio University School of Medicine, Tokyo, Japan, [3]Laboratory for Bone and Joint Diseases, RIKEN Center for Integrative Medical Sciences, Tokyo, Japan, [4]Center for Translational Research, Scottish Rite for Children, Dallas, TX, United States, [5]Division of Molecular Pathology, Institute of Medical Science, The University of Tokyo, Tokyo, Japan, [6]Laboratory for Genotyping Development, RIKEN Center for Integrative Medical Sciences, Yokohama, Japan, [7]Laboratory of Complex Trait Genomics, Graduate School of Frontier Science, The University of Tokyo, Tokyo, Japan, [8]Department of Orthopaedic Surgery , Scottish Rite for Children, Dallas, TX, United States, [9]Department of Orthopaedic Surgery and Pediatric, University of Texas Southwestern Medical Center, Dallas, TX, United States, [10]Department of Orthopaedic Surgery, Seirei Sakura Citizen Hospital, Sakura, Japan, [11]Department of Orthopaedic Surgery, National Hospital Organization, Kobe Medical Center, Kobe, Japan, [12]Department of Orthopaedic Surgery, Meijo Hospital, Nagoya, Japan, [13]Department of Orthopaedic Surgery, National Hospital Organization, Hokkaido Medical Center, Sapporo, Japan, [14]Department of Orthopaedic Surgery, Juntendo University School of Medicine, Tokyo, Japan, [15]Department of Orthopaedic Surgery, Niigata University Medical and Dental General Hospital, Niigata, Japan, [16]Department of Orthopaedic Surgery, Osaka University Graduate School of Medicine, Suita, Japan, [17]Department of Orthopaedic and Spine Surgery, Fukuoka Children's Hospital, Fukuoka, Japan, [18]Department of Orthopaedic Surgery, Dokkyo Medical University School of Medicine, Mibu, Japan, [19]Department of Orthopaedic Surgery, Kyushu University Beppu Hospital, Beppu, Japan, [20]Department of Orthopaedic Surgery, Faculty of Medicine, The University of Tokyo, Tokyo, Japan, [21]Department of Orthopaedic Surgery, Nara Medical University, Kashihara, Japan, [22]Department of Orthopaedic Surgery, Dokkyo Medical University Saitama Medical Center, Koshigaya, Japan, [23]Department of Orthopaedic Surgery, Teine Keijinkai Hospital, Sapporo, Japan, [24]Department of Orthopaedic Surgery Graduated School of Medical Science, Kanazawa University, Kanazawa, Japan, [25]Department of Orthopaedic Surgery, Jichi Medical University, Shimotsuke, Japan, [26]Department of Orthopaedic Surgery, Fujita Health University, Toyoake, Japan, [27]Department of Orthopaedic Surgery, International University of Health and Welfare School of Medicine, Narita, Japan, [28]Department of Orthopaedic Surgery, National Defense Medical College, Tokorozawa, Japan, [29]Department of Orthopaedic Surgery, Kono Orthopaedic Clinic, Tokyo, Japan, [30]Department of Orthopaedic Surgery, Kobe University Graduate School of Medicine, Kobe, Japan, [31]Department of Advanced Medicine for Spine and Spinal Cord Disorders, Hokkaido

University Graduate School of Medicine, Sapporo, Japan, [32]Department of Preventive and Therapeutic Research for Metastatic Bone Tumor, Faculty of Medicine and Graduate School of Medicine, Hokkaido University, Sapporo, Japan, [33]McDermott Center for Human Growth and Development, University of Texas Southwestern Medical Center, Dallas, TX, United States, [34]Department of Genomic Function and Diversity, Medical Research Institute, Tokyo Medical and Dental and University, Tokyo, Japan, [35]Clinical Research Center, Shizuoka General Hospital, Shizuoka, Japan, [36]Department of Applied Genetics, The School of Pharmaceutical Sciences, University of Shizuoka, Shizuoka, Japan

Introduction: Adolescent idiopathic scoliosis (AIS) is a disorder with a three-dimensional spinal deformity and is a common disease affecting 1-5% of adolescents. AIS is also known as a complex disease involved in environmental and genetic factors. A relation between AIS and body mass index (BMI) has been epidemiologically and genetically suggested. However, the causal relationship between AIS and BMI remains to be elucidated.

Material and methods: Mendelian randomization (MR) analysis was performed using summary statistics from genome-wide association studies (GWASs) of AIS (Japanese cohort, 5,327 cases, 73,884 controls; US cohort: 1,468 cases, 20,158 controls) and BMI (Biobank Japan: 173430 individual; meta-analysis of genetic investigation of anthropometric traits and UK Biobank: 806334 individuals; European Children cohort: 39620 individuals; Population Architecture using Genomics and Epidemiology: 49335 individuals). In MR analyses evaluating the effect of BMI on AIS, the association between BMI and AIS summary statistics was evaluated using the inverse-variance weighted (IVW) method, weighted median method, and Egger regression (MR-Egger) methods in Japanese.

Results: Significant causality of genetically decreased BMI on risk of AIS was estimated: IVW method (Estimate (beta) [SE] = -0.56 [0.16], $p = 1.8 \times 10^{-3}$), weighted median method (beta = -0.56 [0.18], $p = 8.5 \times 10^{-3}$) and MR-Egger method (beta = -1.50 [0.43], $p = 4.7 \times 10^{-3}$), respectively. Consistent results were also observed when using the US AIS summary statistic in three MR methods; however, no significant causality was observed when evaluating the effect of AIS on BMI.

Conclusions: Our Mendelian randomization analysis using large studies of AIS and GWAS for BMI summary statistics revealed that genetic variants contributing to low BMI have a causal effect on the onset of AIS. This result was consistent with those of epidemiological studies and would contribute to the early detection of AIS.

KEYWORDS

adolescent idiopathic scoliosis, body mass index, Mendelian randomization (MR), genetic study, genome-wide association study

Introduction

AIS is a problem

Adolescent idiopathic scoliosis (AIS) is a disorder with a three-dimensional spinal deformity. AIS is defined as scoliosis that develops during adolescence with a Cobb angle (CA) of 10 degrees or more on plain radiographs in the standing position (1, 2). AIS is a common disease affecting 1-5% of adolescents (3), progressing rapidly during periods of rapid growth (4), and is associated with physical (5), mental (6), and respiratory problems (7). To prevent these problems, identification of the cause of the onset of AIS is demanded. In Japan, AIS has been adopted as one of the screening factors for adolescents and is considered an important adolescent health problem.

Etiology of AIS

AIS is also known as a complex disease involved in environmental and genetic factors. In twin's studies, he

concordance of AIS between twins in monozygotic pair is as high as 0.73 to 0.92 and its heritability is estimated as 87.5% (8–11), suggesting that genetic factors account for a large fraction of AIS onset. Research groups including us have identified 20 GWAS significant loci in AIS (12).

AIS and BMI

BMI is also known as a highly polygenic trait with 670 GWAS significant loci identified so far (13). A relationship between AIS and body mass index (BMI) has been epidemiologically (12) suggested. A clinical study has reported that AIS patients had a significantly lower BMI in comparison with those healthy adolescents (14, 15). We showed a negative genetic correlation between AIS and BMI, which indicates that AIS and BMI share genetic backgrounds or polygenicity with opposing directions of effects (12, 16). This is in line with the epidemiological association between the onset of AIS and low BMI. However, the causal relationship between AIS and BMI remains to be elucidated.

Mendelian randomization

Using genetic data is becoming popular to resolve those phenotypic relationships (17). Mendelian randomization (MR) is an approach to summarize causal inference between phenotypes using the genome-wide association study (GWAS) results (18, 19). The genetically determined phenotypic profiles are robust for lifelong confounding factors, which can be interpreted as ideal randomization of the subject. Because of the development of MR analytic methods (20) and the achievement of large-scale GWASs of various human phenotypes with publicly available data, MR is one of the best methods to infer causality. Here we conducted MR analysis to investigate the causal inference between BMI and the onset of AIS (Figure 1).

Materials and methods

Subjects

The ethical committees at all collaborating institutions and RIKEN approved the study. Informed consent was obtained from subjects and/or parents. The details about collecting samples and inclusion criteria have been shown in the previous studies (12, 21–24). In the Japanese AIS cohort, the age of the case (93% of female ratio) was 10 -18 years, and the age of the controls (46% of female ratio) was 18 -100 years. To evaluate the causal relationship in a trans-ethnic manner, we also used another GWAS for AIS summary statistic derived from European ancestry. The age of the case (86% of female ratio) was 12.2 -17 years and the age of the control (55% of female ratio) was 44 -88 years for control.

GWAS of European ancestry

We used AIS GWAS summary statistics derived from two US cohorts of European ancestry: Missouri (MO1) described in a previous study (25) and Texas (TX). The cases in the TX cohort (n=1,358) were recruited at Texas Scottish Rite Hospital for Children as approved by the Institute Review Board of the University Texas Southwestern

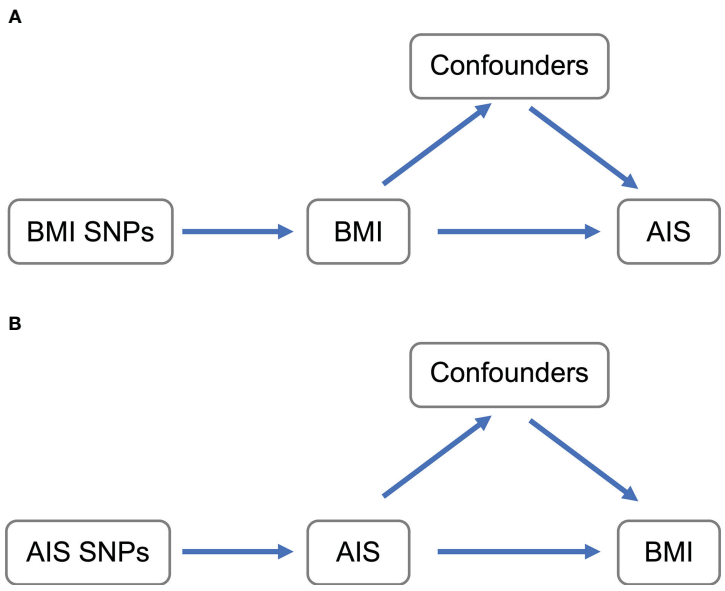

FIGURE 1
Schematic representation of MR analyses. **(A)** BMI SNPs were used as instrumental variables to investigate the causal effect of BMI upon AIS. **(B)** AIS SNPs were used as instrumental variables to investigate the causal effect of genetic risk of AIS upon BMI. Arrows indicate MR assumption such that the instrumental variable is associated with the exposure—not associated with confounders—and only affects the outcome via the exposure. AIS, adolescent idiopathic scoliosis; BMI, body mass index; MR, mendelian randomization; SNP, single-nucleotide polymorphism.

Medical Center as previously described (26) and genotyped on the Illumina HumanCoreExome BeadChip. For controls in the TX cohort, we utilized 12,507 non-AMD GRU (non-age related macular degeneration general research use) subjects of European ancestry, downloaded from dbGaP website (https://www.ncbi.nlm.nih.gov/gap) from the International Age-Related Macular Degeneration Genomics Consortium study (IAMDGC: phs001039.v1.p1.c1). Cases and controls genotypes were merged and imputed as described in a previous study (25). Then only bi-allelic common (MAF>0.01) SNPs with imputation quality Rsq >=0.3 were included for further analysis. Genetic association for the imputed allele dosages was performed in Mach2dat (27) using logistic regression with gender and 10 principal components as covariates. The major histocompatibility complex (MHC) region was excluded form analysis.

Instrumental variables

For AIS, we used published summary statistics of Japanese AIS (12). For summary statistics of European AIS, a new GWAS was performed, the details of which are described above.

For BMI, we used published summary statistics derived from Japanese populations based on the Biobank Japan project (range of 18 -100 years, 46% of female ratio) (16). For European ancestry, we used two published summary statistics derived from European populations; a meta-analysis of GWAS on BMI in UK biobank (range of 40 -69 years, 54% of female ratio) and genetic investigation of anthropometric traits (GIANT) (range of 40 -75 years, 55% of female ratio) (13), and a result of GWAS for BMI of European children (range of 2 -10 years, 51% of female ratio) (28). In addition, summary statistics from the population architecture using genomics and epidemiology (PAGE) consortium (range of 18 -79 years, 50% of female ratio), including African American, Asian, Hispanic, Native American, and Native Hawaiian populations quantities were also used (29). In the above three BMI GWASs, age and sex were added as covariates for the analysis.

The overlapped significant SNPs between BMI and AIS GWAS were used for the analysis (Table 1). The Analyses were performed for each population. In the above three BMI GWASs, age and sex were added as covariates for the analysis.

We also evaluated the F-statistics metric to include the strength of genetic instruments for all instruments in different populations. Based on the previous studies, the F-statistic metric was calculated by using the formula: $F = (R2/k)/([1 - R2]/[n - k - 1])$. R2 represents the proportion of variance explained by the exposure SNP-instruments, k represents the number of instruments, and N represents the exposure GWAS sample size (30, 31).

Mendelian randomization analysis for the association between AIS and BMI

MR is a method for evaluating the causal effect of a risk factor on an outcome from observational data using genetic variants (32, 33). We adopted two-sample MR which is one of the MR analysis approaches. Two sample MR in which SNP exposure and SNP outcome associations are estimated handling GWAS summary statistics derived from independent studies was applied to the analysis. In this study, we focused on the causality of BMI to AIS using this method implemented in the R software "TwoSampleMR" which is composed of the R language (19). The instruction of this software also provides source codes for analysis. The association between BMI and AIS was evaluated using the inverse-variance weighted (IVW) method, a typical and conventional method in MR, to obtain a weighted average of the effect estimates.

Sensitivity analysis

If SNPs act through a pleiotropic pathway, it would violate the MR assumption that the instrumental variable affects the outcome only via exposure and bias the causal estimate (that is, the effect of a genetic variant on the outcome acts entirely through the exposure of interest.). Because testing the validity of these assumptions is difficult in indeed, therefore, we conducted additional two MR methods in addition to IVW, namely Egger regression method (MR-Egger) and the weighted median estimator method (Weighted median), to check for the robustness of the estimates for IVW. MR-Egger is similar to IVW other than that the intercept is not limited to passing through the origin, and the nonlinear intercept indicates the possibility of

TABLE 1 The characteristics and source of genetic instruments used in MR analyses.

Population of AIS	Instruments form of BMI	Sample size	Number of SNPs		Reference
			Used in MR	Used in reverse MR	
Japanese	Japanese (Biobank Japan)	173,430	70	13	Akiyama et al., 2017 (16)
US	European (UK biobank + GIANT)	806,334	537	NA	Pulit et al., 2019 (13)
	European child	39,620	31	NA	Vogelezang et al., 2020 (28)
	PAGE (Non-European)	49,335	61	NA	Wojcik et al., 2019 (29)

MR, mendelian randomization; AIS, adolescent idiopathic scoliosis; BMI, body mass index; SNP, single nucleotide polymorphism; GIANT, Genetic Investigation of Anthropometric Traits; PAGE, Population Architecture using Genomics and Epidemiology.
Number of SNPs used in MR analysis represent the overlapped BMI associated SNPs between BMI GWAS and AIS GWAS.
Number of SNPs used in reverse MR analysis represent the overlapped AIS associated SNPs between BMI GWAS and AIS GWAS.
NA, not available.

directional pleiotropy (20, 34). MR-Egger is statistically less powerful but can adjust the pleiotropy. The Weighted median method works even when at least half of the subset of genetic variants of the instrumental variables are valid and provides a valid causal estimate (35). The number of SNPs used in each analysis is described in Table 1. In Japanese, we also evaluated potential bias in the results of MR analyses by sensitivity analyses including leave-one-out analysis, intercept test for MR-Egger followed in the R software "TwoSampleMR" which also provides source codes for these analyses and global test followed in the R software "MR-PRESSO" (36).

We performed the reverse-direction MR analysis inferring the causality of AIS on BMI. For Japanese overlapped significant SNPs reported in Japanese GWAS for AIS were used as instrumental variables (Table 2) (12). Unfortunately, the number of independent SNPs passing the genome-wide significant threshold ($p<5\times10^{-8}$) was too small to be analyzed using US AIS summary statistics.

Trans-ethnic genetic correlation

To estimate the genetic correlation of GWAS SNPs from different populations, the python package, popcorn (version 0.9.9; https://github.com/brielin/popcorn), was used (37). East Asian and European data of the 1000 Genomes Project (1KG) were used to compute cross-population scores considering each linkage disequilibrium (LD) structure (38). Consequently, a high genetic correlation of AIS between Japanese and Europeans (rho:0.87 (SE:0.11)) was observed.

Power calculation for mendelian randomization analysis

We performed power calculations for MR regarding the previous study (39). Using the GWAS data of the Japanese cohort as a reference, we set input parameters including sample size (79,211), the proportion of cases in the study (0.067), type I error rate (0.05), and true odds ratio of the outcome variable per standard deviation of the exposure variable calculated from the estimate of MR analysis with Japanese BMI and AIS GWAS result.

Polygenic assessment for shared common variants between BMI and AIS

Since MR analysis using summary statistics with different populations is not recommended, we assessed genetic backgrounds between BMI and AIS. The correlation of the odds ratios of the genome-wide SNPs, excluding the BMI and AIS-associated loci, were estimated for sets of SNPs stratified by p-values of GWAS thresholds in each trait. For the shared SNPs between the two traits, LD pruning of the SNPs (r2<0.3) was adopted at first. When stratifying the SNPs

TABLE 2 Results of the MR analyses and the reverse direction MR analyses.

Population of AIS	Instruments form of BMI			Method	MR			Revers MR		
	Cohort	R2	F statistics		Estimate	SE	P-value	Estimate	SE	P-value
Japanese	Japanese (Biobank Japan)	2.80	71.34	IVW	-0.56	0.16	1.1×10^{-3}	-0.01	0.03	0.62
				Weighted median	-0.56	0.18	5.1×10^{-3}	0.00	0.01	0.61
				MR Egger	-1.50	0.43	2.8×10^{-3}	0.02	0.07	0.77
US	European (UK biobank + GIANT)	3.91	60.90	IVW	0.17	0.14	0.22	NA		
				Weighted median	-0.20	0.24	0.42			
				MR Egger	-0.48	0.36	0.18			
	European child	2.92	38.14	IVW	-0.31	0.20	0.12	NA		
				Weighted median	-0.51	0.23	0.03			
				MR Egger	-0.71	0.59	0.24			
	PAGE (Non-European)	7.21	62.67	IVW	-0.79	0.12	9.1×10^{-12}	NA		
				Weighted median	-0.91	0.16	1.5×10^{-8}			
				MR Egger	-1.74	0.40	4.8×10^{-5}			

BMI, body mass index; AIS, adolescent idiopathic scoliosis; MR, mendelian randomization; SE, standard error; GIANT, Genetic Investigation of Anthropometric Traits; PAGE, Population Architecture using Genomics and Epidemiology; R2, variance explained; IVW, inverse variance-weighted; NA, not available.
MR analyses infer causality of the BMI on AIS. Reverse MR analyses infer causality of the AIS on BMI. P value means false discovery rate by Boneferroni's correction.

10.3389/fendo.2023.1089414

based on the p-values in each GWAS, the correlation of odds ratios of the SNPs between BMI and AIS was evaluated by Pearson's correlation coefficient. This approach has been established to assess the direction of genetic risk between traits or populations as a previous study reported (40).

Results

Mendelian randomization analyses of the association between BMI and AIS risk

The primary analyses included 83 SNPs in the Japanese GWAS as instruments for BMI (16). We found significant causality of genetically decreased BMI on the risk of AIS (estimate=-0.56, $P=1.110^{-3}$ in IVW) (Figure 2; Table 2). The significant causality was also supported in the weighted median method (estimate=-0.56, $P=5.110^{-3}$) and the MR-Egger method (estimate=-1.50, $P=22.8\times10^{-3}$) (Table 2). The direction of estimates was consistent across all results, indicating that the risk SNPs of increased BMI had suppressive effects on the onset of AIS. These results are consistent with that of an epidemiological study (14). We conducted sensitivity analyses, intercept tests of MR-Egger and MR-PRESSO to evaluate potential bias in the results of MR analysis. According to the MR-Egger intercept test and MR-PRESSO, we did not observe obvious horizontal pleiotropy (Table 3).

Next, we addressed whether the causal inference could be generalizable regardless of the selection of instruments. BMI GWASs have been mainly conducted in European populations. In US GWAS, we observed the analysis was conducted without any problems (λ_{GC}=1.03) and three genome-wide significant signals were observed. Since US GWAS has a small sample size, we conducted a trans-ethnic genetic correlation of AIS between Japanese and Europeans using the Popcorn program (37) and observed a high genetic correlation of AIS (rho:0.87 (SE:0.11)). Therefore, to address the generalizability of this inference on AIS and to confirm this trend in different populations, we conducted MR analysis using summary statistics of GWAS for AIS from the US population (European ancestry) and analyzed in three methods (IVW, weighted median method, and MR-Egger) as in the Japanese AIS analysis. We repeated the analyses, using 537 of the 640 BMI-associated SNPs identified by the meta-analysis of the UK biobank and GIANT consortium, 31 of 43 BMI-associated SNPs identified by GWAS for BMI derived from European children, and 61 of the 63 BMI-associated SNPs identified by PAGE consortium (Table 1).

Before the analysis, the power calculation was performed to evaluate the results more conservatively. This calculation is based on each variant, not summary statistics. Therefore, we selected two variants, rs11642015 and rs633715, showing the highest association in the Japanese analysis. The power for MR analysis was 0.63 for rs11642015 and 0.36 for rs633715. On the other hand, when we tried to obtain the same results with the US cohort as those of the

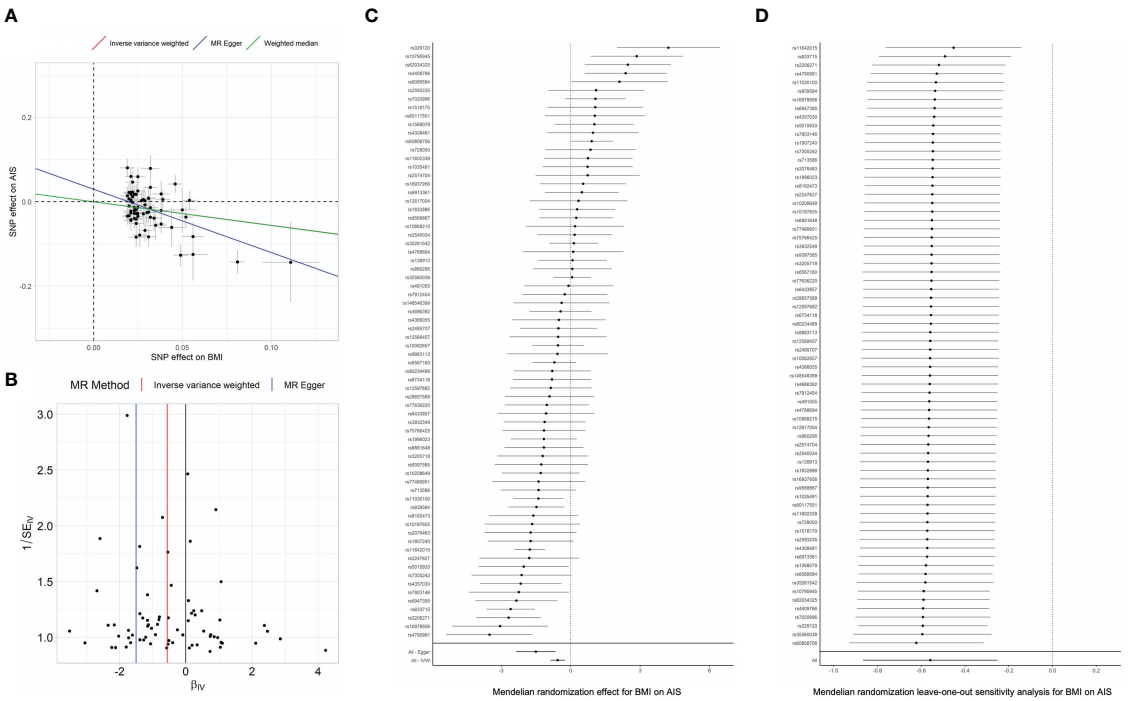

FIGURE 2
MR analyses and sensitivity analyses in Japanese. **(A)** Regression plot of MR analyses. Dots represent the BMI-associated SNPs plotted along with effect size estimates on BMI (x-axis) and psoriasis risk (y-axis) with 95% confidence intervals in the Japanese population. Regression lines obtained from the MR analyses are plotted in red (by IVW), blue (by MR-Egger) and purple (by Weighted median). BMI, body mass index; IVW, inverse variance weighted; MR, Mendelian randomization; SNP, single nucleotide polymorphism. Sensitivity analysis results evaluating the MR causal relationships of BMI on the risk of Adolescent idiopathic scoliosis. Panels indicate funnel plot **(B)**, heterogeneity test **(C)** and leave-one-out analysis **(D)** in Japanese population.

Japan cohort, the power was 0.23 for rs11642015 and 0.17 for rs633715. There is no significant difference in the case ratios between the Japanese and US cohorts, indicating that the sample size has a pure effect. Additionally, the total sample size was calculated to be 80,918 for rs11642015 and 80,515 for rs633715 to obtain the same power as in Japan with the same cohort ratio. These results indicate that the results of this MR analysis are mainly due to the small sample size of the US cohort.

According to the result of power calculation for MR analysis, a small sample size of the US GWAS lowered statistical power. However, even though most of the results were not significant, but showed consistent trends with those using summary statistics of Japanese GWAS for AIS were observed (Table 2). We also repeated the sensitivity analyses, intercept test and MR-PRESSO for each BMI instrument using both of AIS instruments (Table 3). We did not find apparent bias by sensitivity analyses, and similar trends like MR analyses were observed between Japanese and US instruments. Finally, we applied the reverse MR analysis inferring the causality of AIS on BMI (Table 1). We did not observe evidence of the causality of AIS on BMI in any MR methods (Table 2). Since the number of independent SNPs passing genome-wide significant threshold ($p<5\times10^{-8}$) were too small (3 SNPs) for reverse MR to be analyzed using US AIS summary statistic.

Polygenic assessment for shared common variants between BMI and AIS

We further tried to provide evidence to support the causal relationship between low BMI on the development of AIS (and not vice versa). We conducted polygenic assessment for common variants shared between GWAS summary statistics for AIS and BMI to compare genetic backgrounds between BMI and AIS. We stratified the SNPs based on the p-values of GWAS (P) in each summary statistic and evaluated the correlation of odds ratios of the SNPs between the two traits. We observed significant negative correlations of odds ratios for the SNPs related to BMI, even for those showing modest association (P<0.0001 in the GWAS for BMI of Biobank Japan; r=-0.65~-0.18 for each P value range, p-value<0.005 for each correlation test) (Figure 3), confirming agreement in direction of genetic risk in a polygenic manner (40, 41). Observed correlations (r) of odds ratios indicate substantial overlap of the genetic risk (with opposing directions of effects) between the two traits, not only in the identified BMI susceptibility loci exceeding the GWAS significant level but also at the loci showing nonsignificant associations. These findings are consistent with the negative relationship between AIS with BMI reported in the previous studies (12, 16). When repeating these analyses using other BMI summary statistics from other populations, similar trends of correlation of odds ratios were observed in the analyses using the BMI summary statistics of transethnic analysis (PAGE) and European child. On the other hand, we did not observe modest correlations of odds ratios for the SNPs in p-value based on GWAS for AIS (Figure 3).

Discussion

Previous epidemiological studies have reported an association low BMI with AIS (14, 15) in several populations. However, the causality has been proven by the previous epidemiological studies because BMI may be correlated with other factors. MR is a method based on genetic study and estimates causal inferences between traits. And one of the characteristics of genetic studies is basically independent of the environment, which differentiates MR from epidemiological studies and is its advantage. Therefore, we conducted MR analyses using summary statistics from the largest GWAS meta-analyses of BMI and AIS. We found significant evidence of genetically low BMI having a causal effect on onset of AIS. Our results are consistent with those of epidemiological studies showing the correlation AIS with low BMI (our previous GWAS for AIS was only able to show a genetic correlation, considering polygenic effect based GWAS summary statistics, between AIS and BMI in Japanese). Therefore, this is the first study revealing the causality between the two in genetic aspect.

Our study also showed the direction of effect: the variants having decreasing effects on BMI could be risk of onset of AIS,

TABLE 3 Result of MR Egger intercept test and MR-PRESSO for horizontal pleiotropy.

AIS cohort	BMI cohort	MR				Reverse MR			
		MR Egger			MR-PRESSO	MR Egger			MR-PRESSO
		Intercept	SE	P-value	Global test P-value	Intercept	SE	P-value	Global test P-value
Japanese	Japanese (Biobank Japan)	0.03	0.01	0.07	0.52	0.00	0.01	0.58	0.06
US	European (UK biobank + GIANT)	0.01	0.01	0.235	0.12	NA			
	European child	0.02	0.03	0.48	0.08				
	PAGE	0.05	0.02	0.07	0.81				

BMI, body mass index; AIS, adolescent idiopathic scoliosis; MR, mendelian radomization; SE, standard error; GIANT, Genetic Investigation of Anthropometric Traits; PAGE, Population Architecture using Genomics and Epidemiology.
MR analyses infer causality of the BMI on AIS. Reverse MR analyses infer causality of the AIS on BMI.
P value means false discovery rate by Boneferroni's correction.

10.3389/fendo.2023.1089414

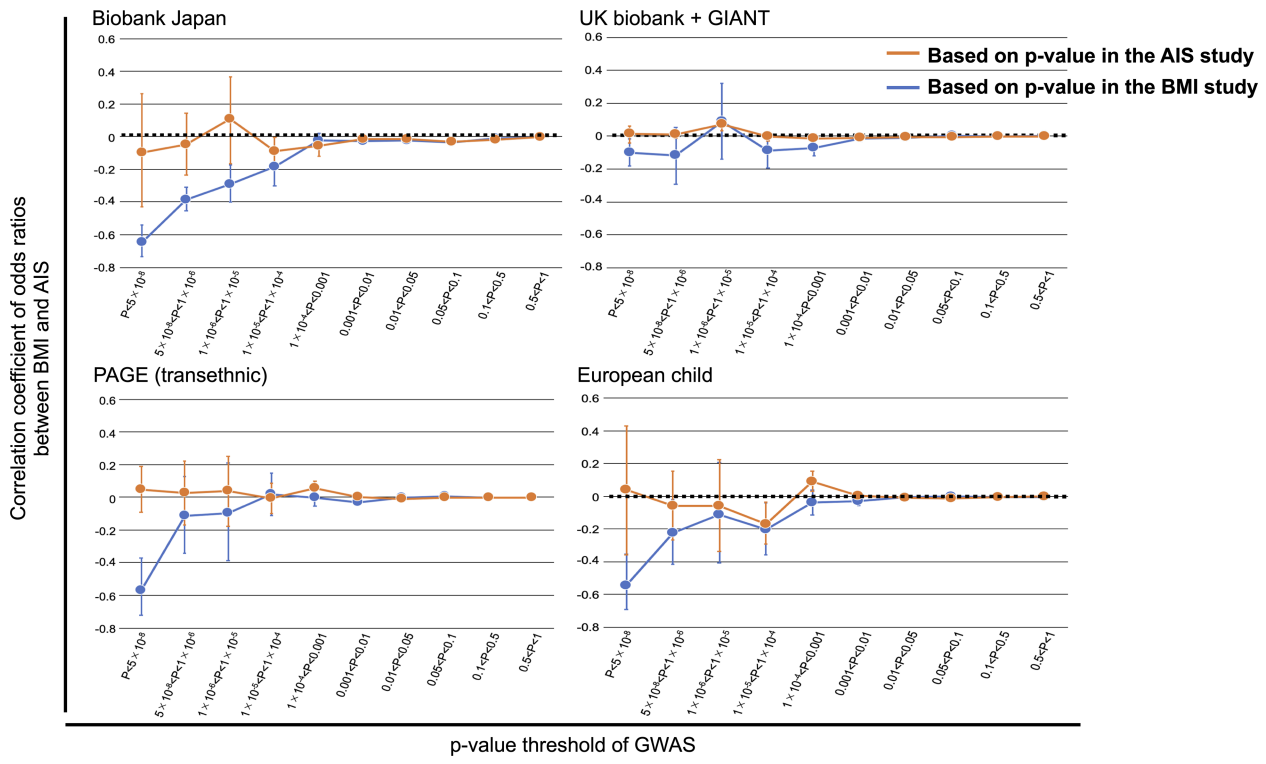

FIGURE 3
Overlap of the association with BMI and AIS. Correlations were evaluated for sets of SNPs stratified by the thresholds based on the *P* values of GWAS in each study after pruning the SNPs by LD ($r2 < 0.3$). For genome-wide SNPs, BMI or AIS susceptibility loci were excluded. The correlation coefficient and 95% CI are shown on the y-axis. Significant negative correlations of odds ratios for the SNPs related to BMI were observed, even for those showing modest association (P<0.0001 in the GWAS for BMI of BBJ). Similar trends of correlation were also observed using the BMI summary statistics of PAGE and European children. On the other hand, no modest correlations for the SNPs in p-value based on GWAS for AIS. GIANT, Genetic Investigation of Anthropometric Traits; PAGE, Population Architecture using Genomics and Epidemiology.

but the risk variants of AIS would not be risk for low BMI. This finding is consistent with epidemiological knowledge in relation AIS with BMI (14).

Previous studies have reported that AIS patients generally have a low BMI, with 25% having BMI scores in the anorexia region (42, 43). Low BMI may indicate eating disorders, excessive exercise, bone loss, and hormonal imbalances. And all of these may be associated with AIS trough lowering BMI. However, it is important to note that the distribution of BMI in the Japanese population is different from that of Western populations. According to the previous study, the non-Asian population has a higher a higher BMI than Asians (44). Since the distribution of BMI varies by population, it would be important to treat BMI as a continuous variable and estimate the risk of developing AIS, rather than uniformly applying a BMI threshold to individuals with different ratios across the distribution.

Since the relation of AIS with low BMI has been observed in Japanese as well as other populations (15), we repeated MR analyses using another summary statistic of GWAS for AIS derived from US cohort (European ancestry) and using summary statistics of GWAS for BMI derived from mainly European ancestry. GWAS summary statistics showed a significant correlation between Japanese and Caucasian in AIS. This result indicates that the genetic architecture of the AIS has a large portion in common among these populations. Therefore, based on the hypothesis that causal variants are common, MR was performed for each population. Even though the power calculation for MR analyses showed low statistical power of the US AIS cohort due to the sample size, the consistent trends with those of Japanese GWAS for AIS were replicated. This finding indicates that low BMI is a common risk factor for onset of AIS could among Japanese and European ancestry. Since most of GWAS for BMI are based on the BMI after becoming adults, the best GWAS data for BMI to be used together with GWAS for AIS is the results based on BMI measured in adolescents. In order to address this issue, we performed MR analyses using summary statistics of GWAS for BMI based on European children's data. Consequently, the results were consistent with those of using adult's results. These indicate the variants affecting BMI are shared between adults and children, and strengthens the results using BMI summary statistics derived from adults.

The US GWAS results of AIS contained a small sample size which led to low statistical power and our Japanese AIS GWAS is the largest one which means summary statistics are more accurate. On the contrary, BMI GWASs has been mainly reported based on Caucasians. Since MR using summary statistics from different populations is not recommended due to differences in LD, we take polygenic assessment for shared common variants between BMI and AIS. In addition, since it has been reported that Japanese

lead variants in AIS have similar odds ratios to those of Caucasians and East Asians (25), we consider that the effect of LD differences is small. To take BMI results in the European and apply them to AIS results in Japanese would decrease power to detect negative relationship of BMI on AIS. However, we observed similar trends in various summary statistics. This indicates that even in the conservative approach, we could observe supportive relationship between BMI on AIS. There are indeed differences in genetic structure in the population due to LD structure, however, we consider that applying the instrumental variable to different populations is a rather conservative approach considering LD structure.

To make these findings more robust, further study with larger sample size is needed. Although it is difficult to improve the results in the current situation, it is expected that the results can be sufficiently improved by continuing the research and increasing the sample size. On the other hand, the estimate of MR analysis using European population (UK biobank and GIANT) summary statistic of BMI was relatively higher in comparison with the other instruments of BMI. These results suggest the possibility of pleiotropy. This is particularly remarkable in the European data and may reflect the results of epidemiological studies showing a positive correlation between AIS and BMI (45).

We conducted reverse MR to investigate the effect of AIS on the risk of low BMI. While less independent SNPs used for analyses compared to those of GWASs for BMI, the consistent results that the estimate of AIS instruments was around 0 in contrast to those of MR analyses were observed. These findings support that the risk variants of AIS would not be a risk of low BMI. And this study shows that genetically low BMI is a risk for onset of AIS, which suggests that children with low BMI should be screened for scoliosis at an early stage to potentiate early detection and intervention of AIS.

The Scoliosis Study Group recommends that all children between the ages of 10 and 14 have an examination for scoliosis once a year (46). This is because early scoliosis screening in children is beneficial for the early detection and prevention of spinal deformities and is associated with a better prognosis (46). Several developed nations, including the United States, Japan, and some European countries, have recognized the importance of scoliosis screening in children and have implemented scoliosis screening at the national level. With screening, these nations try to prevent and proactively manage spinal deformities and scoliosis in children (47–49). It is important to use various information, including epidemiology and genetic background, to detect scoliosis in its early stages. Further research is also needed to discover whether or not growing weight through diet can help prevent the onset and progression of scoliosis.

There are some limitations in this study. In a previous study, no major differences in genetic architecture between rare and common variants have been observed in Japanese AIS (12). Therefore, we do not consider it problematic to evaluate only the common variant for our study. However, the rare variant has not been evaluated among Caucasians. Future study is needed to confirm whether the trend is similar to that of the Japanese. Since sample size and number of significant SNPs of GWAS for AIS has been much smaller in comparison with GWAS for BMI. Unfortunately, we could not conduct reverse-MR analyses using AIS summary statistic of U.S cohort due to lack of significant SNPs. Recruiting samples and further studies are needed to deny the reverse causation (AIS on BMI) more convincingly and to develop insight of AIS. Especially, as our GWAS results are based on Asian population, replication using other population's GWAS results are favorable. Since AIS is a disease caused by multiple factors, it is important to recognize that low BMI is one of the factors affecting the onset of AIS. And the identification of other factors involved in the onset of AIS is also necessary. While the results of MR-Egger intercept test and MR-PRESSO did not show any obvious pleiotropy, the possibility of pleiotropy cannot be completely ruled out at this time. Because previous studies reported the association of onset of AIS with low bone mineral density (BMD) (50) or low muscle mass (51). Considering the results of weighted median method, which use half of variants for analyses, there could be a mixture of variants in BMI associated SNPs that affect BMI directly and variants that affect BMI through other pathways. Further studies are demanded to clarify the variants which directly affect BMI. Then, we could evaluate the causality more precisely.

Conclusions

This is a first study conducting MR analysis between AIS and BMI. We showed the possibility that genetically low BMI has a causal effect on onset of AIS. This result was consistent with those of epidemiological study and would contribute the early detection of AIS.

Scottish Rite Hospital Clinical Group (SRHCG)

Lori A. Karol[1], Karl E. Rathjen[1], Daniel J. Sucato[1], John G. Birch[1], Charles E. Johnston III[1], B. Stephens Richards[1], Brandon A. Ramo[1], Amy L. McIntosh[1], John A. Herring[1], Todd A. Milbrandt[2], Vishwas R. Talwakar[3], Henry J. Iwinski[3], Ryan D. Muchow[3], J. Channing Tassone[4], X. -C. Liu[4], Richard Shindell[5], William Schrader[6], Craig Eberson[7], Anthony Lapinsky[8], Randall Loder[9] and Joseph Davey[10]

1. Department of Orthopaedic Surgery, Texas Scottish Rite Hospital for Children, Dallas, Texas, USA.

2. Department of Orthopaedic Surgery, Mayo Clinic, Rochester, Minnesota, US

3. Department of Orthopaedic Surgery, Shriners Hospitals for Children, Lexington, Kentucky, USA.

4. Department of Orthopaedic Surgery, Children's Hospital of Wisconsin, Milwaukee, Wisconsin, USA.

5. OrthoArizona, Phoenix, Arizona, USA.

6. Departments of Orthopaedics, Sports Medicine, and Surgical Services, Akron Children's Hospital, Akron, Ohio, USA.

7. Pediatric Orthopaedics and Scoliosis, Hasbro Children's Hospital, Providence, Rhode Island, USA.

8. University of Massachusetts Memorial Medical Center, Worcester, Massachusetts, USA.

9. Indiana University-Purdue University Indianapolis, Indianapolis, Indiana, USA.

10. University of Oklahoma Health Sciences Center, Oklahoma City, Oklahoma, USA.

Data availability statement

Publicly available datasets were analyzed in this study. This data can be found here: http://jenger.riken.jp/.

Ethics statement

All genomic DNA from patients were examined after obtaining informed consent. The Medical Ethics Committee of the Keio university hospital, Tokyo, approved the study protocol (20080129). We have obtained written informed consent for publication of clinical details of the patients.

Author contributions

CT, SI, KW, and CW supervised the project. NO and CT designed the project and provided overall project management. NO and CT drafted the manuscript. YM and MiK performed the genotyping for the GWAS. CT, NO, YK, Yuk, MaK and AK analyzed the GWAS data and performed integrative analyses. NO, KT, YO, YoT, SM, NK, KU, MI, TaS, KeW, TaK, HY, HT, KH, YuT, ToK, TT, TS, HSh, AI, SaI, TS, NF, MY, MN, KC, KaK, TsS, TA, KN, KeK, HSu, TI, SD, RS, NH, EO, MM, KW, and JH collected and managed clinical data. All authors contributed to the article and approved the submitted version.

Funding

This work was supported by JSPS KAKENHI Grant (No. 16H05453 to MM, 22H03207 to SI), Scoliosis Research Society and NIH (NICHD P01 HD084387 to CAW).

Acknowledgments

We thank all participating subjects. We also thank Y. Takahashi, T. Oguma, T. Kusadokoro, H. Takuwa, and H. Suetsugu for technical assistance, and K. Sasada and Y. Yukawa for statistical analysis assistance. We are grateful to the clinical investigators who referred patients into the study from Scottish Rite Hospital Clinical Group (SRHCG). We thank Dr. Julia Kozlitina from the McDermott Center for Human Growth and Development at UT Southwestern Medical Center, Dallas, Texas, for helpful statistical advice and reviewing the manuscript. We acknowledge the Texas Advanced Computing Center (TACC, URL: http://www.tacc.utexas.edu) at The University of Texas at Austin for providing computing resources that have contributed to the research results reported within this paper related to the GWAS of European ancestry section. We thank the submitters of the dbGap study (phs001039.v1.p1.c1), all contributing sites and additional funding information are acknowledged here: Fritsche et al. (2016) Nature Genetics 48 134–143, (doi:10.1038/ng.3448); The International AMD Genomics consortium's web page is: http://eaglep.case.edu/iamdgc_web/, and additional information is available on: http://csg.sph.umich.edu/abecasis/public/amd2015/.

Conflict of interest

The authors declare that the research was conducted in the absence of any commercial or financial relationships that could be construed as a potential conflict of interest.

Publisher's note

References

1. Levine DB. The hospital for special surgery 1955 to 1972: t. Campbell Thompson serves as sixth surgeon-in-Chief 1955-1963 followed by Robert Lee Patterson, jr. @ the seventh surgeon-in-Chief 1963-1972. *Hss J* (2010) 6(1):1–13. doi: 10.1007/s11420-009-9136-5

2. Kim H, Kim HS, Moon ES, Yoon CS, Chung TS, Song HT, et al. Scoliosis imaging: what radiologists should know. *Radiographics* (2010) 30(7):1823–42. doi: 10.1148/rg.307105061

3. Weinstein SL. Natural history. *Spine (Phila Pa 1976).* (1999) 24(24):2592–600. doi: 10.1097/00007632-199912150-00006

4. Ueno M, Takaso M, Nakazawa T, Imura T, Saito W, Shintani R, et al. A 5-year epidemiological study on the prevalence rate of idiopathic scoliosis in Tokyo: school screening of more than 250,000 children. *J Orthop Sci* (2011) 16(1):1–6. doi: 10.1007/s00776-010-0009-z

5. Pratt RK, Burwell RG, Cole AA, Webb JK. Patient and parental perception of adolescent idiopathic scoliosis before and after surgery in comparison with surface and radiographic measurements. *Spine (Phila Pa 1976)* (2002) 27(14):1543–50. doi: 10.1097/00007632-200207150-00012

6. Kahanovitz N, Weiser S. The psychological impact of idiopathic scoliosis on the adolescent female. a preliminary multi-center study. *Spine (Phila Pa 1976).* (1989) 14(5):483–5. doi: 10.1097/00007632-198905000-00001

7. Weinstein SL, Zavala DC, Ponseti IV. Idiopathic scoliosis: long-term follow-up and prognosis in untreated patients. *J Bone Joint Surg Am* (1981) 63(5):702–12. doi: 10.2106/00004623-198163050-00003

8. Kesling KL, Reinker KA. Scoliosis in twins. a meta-analysis of the literature and report of six cases. *Spine (Phila Pa 1976)* (1997) 22(17):2009–14. doi: 10.1097/00007632-199709010-00014

9. Inoue M, Minami S, Kitahara H, Otsuka Y, Nakata Y, Takaso M, et al. Idiopathic scoliosis in twins studied by DNA fingerprinting: the incidence and type of scoliosis. *J Bone Joint Surg Br* (1998) 80(2):212–7. doi: 10.1302/0301-620X.80B2.0800212

10. Miller NH. Genetics of familial idiopathic scoliosis. *Clin Orthop Relat Res* (2007) 462:6–10. doi: 10.1097/BLO.0b013e318126c062

11. Tang NL, Yeung HY, Hung VW, Di Liao C, Lam TP, Yeung HM, et al. Genetic epidemiology and heritability of AIS: a study of 415 Chinese female patients. *J Orthop Res* (2012) 30(9):1464–9. doi: 10.1002/jor.22090

12. Kou I, Otomo N, Takeda K, Momozawa Y, Lu HF, Kubo M, et al. Genome-wide association study identifies 14 previously unreported susceptibility loci for adolescent idiopathic scoliosis in Japanese. *Nat Commun* (2019) 10(1):3685. doi: 10.1038/s41467-019-11596-w

13. Pulit SL, Stoneman C, Morris AP, Wood AR, Glastonbury CA, Tyrrell J, et al. Meta-analysis of genome-wide association studies for body fat distribution in 694 649 individuals of European ancestry. *Hum Mol Genet* (2019) 28(1):166–74. doi: 10.1093/hmg/ddy327

14. Watanabe K, Michikawa T, Yonezawa I, Takaso M, Minami S, Soshi S, et al. Physical activities and lifestyle factors related to adolescent idiopathic scoliosis. *J Bone Joint Surg Am volume* (2017) 99(4):284–94. doi: 10.2106/JBJS.16.00459

15. Clark EM, Taylor HJ, Harding I, Hutchinson J, Nelson I, Deanfield JE, et al. Association between components of body composition and scoliosis: a prospective cohort study reporting differences identifiable before the onset of scoliosis. *J Bone Miner Res* (2014) 29(8):1729–36. doi: 10.1002/jbmr.2207

16. Akiyama M, Okada Y, Kanai M, Takahashi A, Momozawa Y, Ikeda M, et al. Genome-wide association study identifies 112 new loci for body mass index in the Japanese population. *Nat Genet* (2017) 49(10):1458–67. doi: 10.1038/ng.3951

17. Pingault JB, O'Reilly PF, Schoeler T, Ploubidis GB, Rijsdijk F, Dudbridge F. Using genetic data to strengthen causal inference in observational research. *Nat Rev Genet* (2018) 19(9):566–80. doi: 10.1038/s41576-018-0020-3

18. Holmes MV, Ala-Korpela M, Smith GD. Mendelian randomization in cardiometabolic disease: challenges in evaluating causality. *Nat Rev Cardiol* (2017) 14(10):577–90. doi: 10.1038/nrcardio.2017.78

19. Hemani G, Zheng J, Elsworth B, Wade KH, Haberland V, Baird D, et al. The MR-base platform supports systematic causal inference across the human phenome. *Elife* (2018) 7. doi: 10.7554/eLife.34408

20. Burgess S, Thompson SG. Interpreting findings from mendelian randomization using the MR-egger method. *Eur J Epidemiol* (2017) 32(5):377–89. doi: 10.1007/s10654-017-0255-x

21. Takahashi Y, Kou I, Takahashi A, Johnson TA, Kono K, Kawakami N, et al. A genome-wide association study identifies common variants near LBX1 associated with adolescent idiopathic scoliosis. *Nat Genet* (2011) 43(12):1237–40. doi: 10.1038/ng.974

22. Kou I, Takahashi Y, Johnson TA, Takahashi A, Guo L, Dai J, et al. Genetic variants in GPR126 are associated with adolescent idiopathic scoliosis. *Nat Genet* (2013) 45(6):676–9. doi: 10.1038/ng.2639

23. Ogura Y, Kou I, Miura S, Takahashi A, Xu L, Takeda K, et al. A functional SNP in BNC2 is associated with adolescent idiopathic scoliosis. *Am J Hum Genet* (2015) 97(2):337–42. doi: 10.1016/j.ajhg.2015.06.012

24. Nakamura Y. The BioBank Japan project. *Clin Adv Hematol Oncol* (2007) 5(9):696–7.

25. Khanshour AM, Kou I, Fan Y, Einarsdottir E, Makki N, Kidane YH, et al. Genome-wide meta-analysis and replication studies in multiple ethnicities identify novel adolescent idiopathic scoliosis susceptibility loci. *Hum Mol Genet* (2018) 27(22):3986–98. doi: 10.1093/hmg/ddy306

26. Sharma S, Gao X, Londono D, Devroy SE, Mauldin KN, Frankel JT, et al. Genome-wide association studies of adolescent idiopathic scoliosis suggest candidate susceptibility genes. *Hum Mol Genet* (2011) 20(7):1456–66. doi: 10.1093/hmg/ddq571

27. Li Y, Willer C, Sanna S, Abecasis G. Genotype imputation. *Annu Rev Genomics Hum Genet* (2009) 10:387–406. doi: 10.1146/annurev.genom.9.081307.164242

28. Vogelezang S, Bradfield JP, Ahluwalia TS, Curtin JA, Lakka TA, Grarup N, et al. Novel loci for childhood body mass index and shared heritability with adult cardiometabolic traits. *PloS Genet* (2020) 16(10):e1008718. doi: 10.1371/journal.pgen.1008718

29. Wojcik GL, Graff M, Nishimura KK, Tao R, Haessler J, Gignoux CR, et al. Genetic analyses of diverse populations improves discovery for complex traits. *Nature* (2019) 570(7762):514–8. doi: 10.1038/s41586-019-1310-4

30. Palmer TM, Lawlor DA, Harbord RM, Sheehan NA, Tobias JH, Timpson NJ, et al. Using multiple genetic variants as instrumental variables for modifiable risk factors. *Stat Methods Med Res* (2012) 21(3):223–42. doi: 10.1177/0962280210394459

31. Park JH, Wacholder S, Gail MH, Peters U, Jacobs KB, Chanock SJ, et al. Estimation of effect size distribution from genome-wide association studies and implications for future discoveries. *Nat Genet* (2010) 42(7):570–5. doi: 10.1038/ng.610

32. Lawlor DA, Harbord RM, Sterne JA, Timpson N, Davey Smith G. Mendelian randomization: using genes as instruments for making causal inferences in epidemiology. *Stat Med* (2008) 27(8):1133–63. doi: 10.1002/sim.3034

33. Evans DM, Davey Smith G. Mendelian randomization: new applications in the coming age of hypothesis-free causality. *Annu Rev Genomics Hum Genet* (2015) 16:327–50. doi: 10.1146/annurev-genom-090314-050016

34. Bowden J, Davey Smith G, Burgess S. Mendelian randomization with invalid instruments: effect estimation and bias detection through egger regression. *Int J Epidemiol* (2015) 44(2):512–25. doi: 10.1093/ije/dyv080

35. Bowden J, Davey Smith G, Haycock PC, Burgess S. Consistent estimation in mendelian randomization with some invalid instruments using a weighted median estimator. *Genet Epidemiol* (2016) 40(4):304–14. doi: 10.1002/gepi.21965

36. Verbanck M, Chen CY, Neale B, Do R. Detection of widespread horizontal pleiotropy in causal relationships inferred from mendelian randomization between complex traits and diseases. *Nat Genet* (2018) 50(5):693–8. doi: 10.1038/s41588-018-0099-7

37. Brown BC, Ye CJ, Price AL, Zaitlen N. Transethnic genetic-correlation estimates from summary statistics. *Am J Hum Genet* (2016) 99(1):76–88. doi: 10.1016/j.ajhg.2016.05.001

38. Auton A, Brooks LD, Durbin RM, Garrison EP, Kang HM, Korbel JO, et al. A global reference for human genetic variation. *Nature* (2015) 526(7571):68–74. doi: 10.1038/nature15393

39. Brion MJ, Shakhbazov K, Visscher PM. Calculating statistical power in mendelian randomization studies. *Int J Epidemiol* (2013) 42(5):1497–501. doi: 10.1093/ije/dyt179

40. Okada Y, Terao C, Ikari K, Kochi Y, Ohmura K, Suzuki A, et al. Meta-analysis identifies nine new loci associated with rheumatoid arthritis in the Japanese population. *Nat Genet* (2012) 44(5):511–6. doi: 10.1038/ng.2231

41. Stranger BE, Stahl EA, Raj T. Progress and promise of genome-wide association studies for human complex trait genetics. *Genetics* (2011) 187(2):367–83. doi: 10.1534/genetics.110.120907

42. Smith FM, Latchford GJ, Hall RM, Dickson RA. Do chronic medical conditions increase the risk of eating disorder? a cross-sectional investigation of eating pathology in adolescent females with scoliosis and diabetes. *J Adolesc Health* (2008) 42(1):58–63. doi: 10.1016/j.jadohealth.2007.08.008

43. Ramírez M, Martínez-Llorens J, Sanchez JF, Bagó J, Molina A, Gea J, et al. Body composition in adolescent idiopathic scoliosis. *Eur Spine J* (2013) 22(2):324–9. doi: 10.1007/s00586-012-2465-y

44. Ogden CL, Fryar CD, Hales CM, Carroll MD, Aoki Y, Freedman DS. Differences in obesity prevalence by demographics and urbanization in US children and adolescents, 2013-2016. *Jama* (2018) 319(23):2410–8. doi: 10.1001/jama.2018.5158

45. Gilbert SR, Savage AJ, Whitesell R, Conklin MJ, Fineberg NS. BMI and magnitude of scoliosis at presentation to a specialty clinic. *Pediatrics* (2015) 135(6):e1417–24. doi: 10.1542/peds.2014-2000

46. Janicki JA, Alman B. Scoliosis: review of diagnosis and treatment. *Paediatr Child Health* (2007) 12(9):771–6. doi: 10.1093/pch/12.9.771

47. Lonstein JE, Bjorklund S, Wanninger MH, Nelson RP. Voluntary school screening for scoliosis in Minnesota. *J Bone Joint Surg Am volume* (1982) 64(4):481–8. doi: 10.2106/00004623-198264040-00002

48. Ohtsuka Y, Yamagata M, Arai S, Kitahara H, Minami S. School screening for scoliosis by the Chiba university medical school screening program. results of 1.24 million students over an 8-year period. *Spine* (1988) 13(11):1251–7. doi: 10.1097/00007632-198811000-00008

49. Willner S, Udén A. A prospective prevalence study of scoliosis in southern Sweden. *Acta orthopaedica Scandinavica* (1982) 53(2):233–7. doi: 10.3109/17453678208992208

50. Li X, Hung VWY, Yu FWP, Hung ALH, Ng BKW, Cheng JCY, et al. Persistent low-normal bone mineral density in adolescent idiopathic scoliosis with different curve severity: a longitudinal study from presentation to beyond skeletal maturity and peak bone mass. *Bone* (2020) 133:115217. doi: 10.1016/j.bone.2019.115217

51. Tam EMS, Liu Z, Lam TP, Ting T, Cheung G, Ng BKW, et al. Lower muscle mass and body fat in adolescent idiopathic scoliosis are associated with abnormal leptin bioavailability. *Spine* (2016) 41(11):940–6. doi: 10.1097/BRS.0000000000001376

Frontiers in Endocrinology

Explores the endocrine system to find new therapies for key health issues

The second most-cited endocrinology and metabolism journal, which advances our understanding of the endocrine system. It uncovers new therapies for prevalent health issues such as obesity, diabetes, reproduction, and aging.

Discover the latest Research Topics

See more →

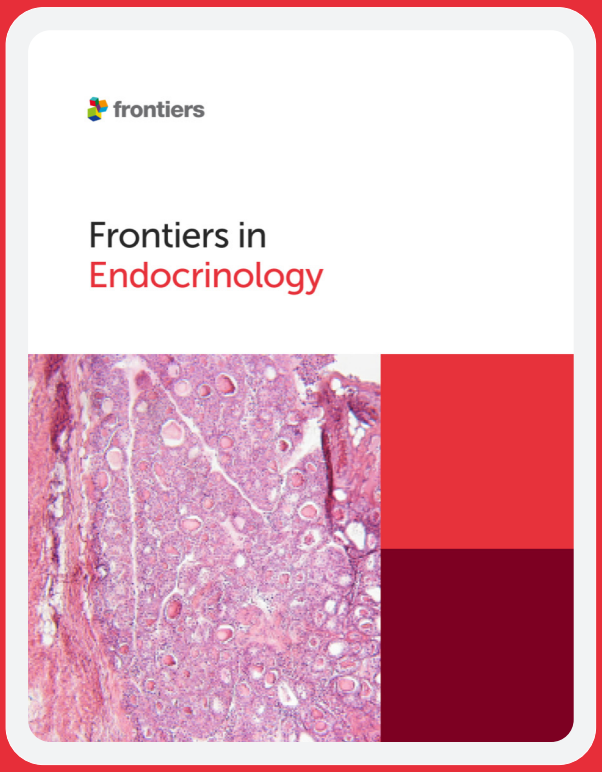

Frontiers

Avenue du Tribunal-Fédéral 34
1005 Lausanne, Switzerland
frontiersin.org

Contact us

+41 (0)21 510 17 00
frontiersin.org/about/contact